

Reconstruction of manual behaviours in fossil hominins: functional inferences from cortical bone structure of extant hominid phalanges



Samar Masud Syeda

School of Anthropology and Conservation
University of Kent

A thesis submitted in fulfilment of the requirements for the degree of Doctor of Philosophy in Anthropology at the University of Kent, October, 2023

“The hand at rest is beautiful in its tranquillity,
but is infinitely more appealing in the flow of action”.

John Napier

Acknowledgements

First and foremost, I would like to thank my supervisors Tracy Kivell and Matt Skinner. Your support, encouragement, patience, and kind words throughout this process have helped me grow immensely and has made me a better scientist. I am truly grateful to have had the opportunity to be a part of such an incredible and supportive team you have created, with research that has excited me from the start and continues to do so. I am also very thankful to all the members of the Kivell/Skinner lab group, who have not just provided lively discussions and constructive criticism but friendship as well, without which this experience would not have been as enjoyable. In particular, I am grateful to Chris Dunmore and Mykolas Imbrasas for technical training and support, as well as Andrea Lukova for thought provoking discussions, lending her ears to my frustrations, encouraging me to have a healthy work-life balance, and her friendship. Finally, within the lab, I would like to extend my gratitude to Marine Cazenave and Zewdi Tsegai. Beyond the tireless technical training and discussions they have provided me, I am grateful to have met two strong, impressive, female mentors (alongside my supervisor) that have guided me throughout the last few years. Outside of the Kivell/Skinner lab group, I would like to thank Kristian Allman-Varty for his constant care and support and knowing when to pull me away from my computer. Last, but not least, I would like to express my deepest gratitude to my family, and particularly my abbu and ammi, Syed Masud Khaver and Aisha Masud – without your sacrifices I would not be where I am today.

Contents

Acknowledgements.....	iii
Contents.....	iv
List of Figures.....	vii
List of Tables.....	x
Abbreviations.....	xiii
1. Introduction.....	1
1.1. The scientific problem.....	1
1.2. Aims of the thesis.....	2
1.3. Chapter summaries.....	2
1.4. Hominid behaviour: locomotion, posture, and manual behaviours.....	3
1.5. Phalangeal external morphology and anatomy.....	12
1.6. Bone functional adaptation.....	22
1.7. Evolution of the hominin hand: fossil evidence.....	25
2. Methods and materials.....	31
2.1. Materials.....	31
2.2. Methods.....	37
3. Cortical bone distribution of the proximal phalanges in great apes and implications for reconstructing manual behaviours.....	56
3.1. Abstract.....	56
3.2. Introduction.....	56
3.3. Methods.....	62
3.4. Results and Discussion.....	66
3.5. Conclusions.....	83
4. Cortical bone architecture of hominid intermediate phalanges reveals functional signals of locomotion and manipulation.....	84
4.1. Abstract.....	84
4.2. Introduction.....	84
4.3. Methods.....	90

4.4. Results.....	96
4.5. Discussion.....	108
4.6. Conclusion.....	115
5. Hand use in fossil hominins: reconstruction of manual behaviours via phalangeal cortical bone morphology.....	116
5.1. Abstract.....	116
5.2. Introduction.....	116
5.3. Methods.....	126
5.4. Results.....	129
5.5. Discussion.....	148
5.6. Conclusion.....	156
6. Discussion and conclusions.....	158
6.1. Functional morphology of phalangeal cortical bone in extant hominids.....	158
6.2. Insights into phalangeal external form and internal structure.....	164
6.3. Phalangeal curvature of <i>Homo sapiens</i>	165
6.4. African ape phalangeal cortical thickness in relation to cross-sectional properties.....	166
6.5. Extant non-human great ape sample.....	167
6.6. Implications for fossil hominin behaviours.....	167
6.7. Developmental plasticity of the hand in relation to variation of phalangeal shape.....	170
6.8. Conclusions.....	172
6.9. Limitations and future directions.....	172
7. References.....	178
8. Appendix.....	210
8.1. Curatorial institutions of the study sample.....	210
8.2. Supplementary materials: Cortical bone distribution of the proximal phalanges in great apes and implications for reconstructing manual behaviours.....	214
8.3. Supplementary materials: Cortical bone architecture of hominid intermediate phalanges reveals functional signals of locomotion and manipulation.....	247

8.4. Supplementary materials: Hand use in fossil hominins: reconstruction of manual behaviours via phalangeal cortical bone morphology.....	288
8.5. Supplementary materials: Discussion and conclusions.....	289
8.6. Published works.....	291

List of Figures

Figure 1.1 Diagram representing phalangeal posture of the <i>Pongo</i> hand during suspensory behaviours.....	4
Figure 1.2: Diagram representing phalangeal posture of the African ape hand during knuckle-walking.	6
Figure 1.3: Example of human precision and power grip.....	10
Figure 1.4: Common hand grips employed during stone tool use.....	11
Figure 1.5: Comparative anatomy of proximal and intermediate phalanges of digits 2-5.....	13
Figure 1.6: Soft tissue anatomy of the finger.....	17
Figure 2.1: Surface models of proximal and intermediate phalanges of fossil hominins.....	33
Figure 2.2: Surface models of proximal and intermediate phalanges of different Neanderthal populations.....	35
Figure 2.3: Surface models of proximal and intermediate phalanges of El Sidron Neanderthals....	36
Figure 2.4: Image depicting reorientation of a <i>Gorilla</i> third proximal phalanx.....	37
Figure 2.5: MIA segmentation steps.....	39
Figure 2.6: Example of segmentation protocol used on fossil hominin phalanges.....	40
Figure 2.7: <i>A. afarensis</i> micro-CT scan showing mineralization of the bone.....	41
Figure 2.8: Medtool protocol used to create external and internal surfaces for data collection in <i>Morphomap</i>	42
Figure 2.9: Data acquisition in <i>Morphomap</i>	44
Figure 2.10: Example of a specimen with a closed medullary cavity.....	46
Figure 2.11: <i>Morphomap</i> output of cortical bone distribution maps.....	47
Figure 2.12: Measurements of phalangeal external morphology.....	49
Figure 3.1: Representative 3D surfaces of proximal phalanges of extant hominids.....	60
Figure 3.2: Steps taken to create surfaces for cortical thickness analysis.....	64
Figure 3.3: Representative 3D maps of cortical bone distribution of proximal phalanges.....	68
Figure 3.4: Average scaled cortical bone thickness across the phalangeal shaft.....	70
Figure 3.5: PC1 and PC2 for cortical bone distribution of proximal phalanges.....	72
Figure 3.6: Ratio of dorsal/palmar cortical bone thickness plotted from the proximal end to the distal end of the phalangeal shaft.....	74

Figure 3.7: Boxplots representing cortical area for digits 2-5.....	76
Figure 3.8: Boxplots representing polar section modulus (Z_{pol}) for digits 2-5.....	78
Figure 3.9: Boxplots representing polar second moment of area (J) for digits 2-5.....	80
Figure 4.1: Surface models derived from micro-CT scans of proximal and intermediate phalanges of digits 2-5 of extant hominins.....	86
Figure 4.2: Images showing the steps taken in <i>Morphomap</i> for cortical bone analysis in a human third intermediate phalanx.....	92
Figure 4.3: Cross-sections at 35%, 50% and 65% of a third intermediate phalanx for each taxon. Cross-sections are scaled to relative size.....	93
Figure 4.4: 3D maps of cortical bone distribution across the intermediate phalanges in a representative individual of each taxon.....	95
Figure 4.5: PC1 and PC2 for cortical bone distribution of intermediate phalanges.....	98
Figure 4.6: Average cortical bone thickness plotted across the intermediate phalangeal shaft.....	100
Figure 4.7: Cortical area (CA) for intermediate phalanges of digits 2-5 of extant taxa.....	102
Figure 4.8: Polar section modulus (Z_{pol}) for intermediate phalanges of digits 2-5 of extant taxa.....	103
Figure 4.9: Polar second moment of area (J) for intermediate phalanges of digits 2-5 of extant taxa.....	104
Figure 4.10: Scaled cortical thickness of the proximal and intermediate phalanges across digits 2-5.....	106
Figure 4.11: Absolute cortical thickness of the proximal and intermediate phalanges across digits 2-5.....	107
Figure 5.1: Cortical bone distribution maps of the Australopiths.....	129
Figure 5.2: Results of the principal component analysis (PCA) of the proximal phalanges in 3D, showing separation among the extant taxa and fossil hominins.....	130
Figure 5.3: Cortical thickness of the proximal and intermediate phalanges plotted across the shaft in extant taxa and fossil hominins.....	131
Figure 5.4: Boxplots of the scaled average cortical thickness of extant great ape and fossil hominin phalanges.....	132
Figure 5.5: Boxplots representing scaled values of cortical area of extant great ape and fossil hominin phalanges.....	134
Figure 5.6: Boxplots representing scaled values of maximum bending strength (Z_{pol}) of extant great ape and fossil hominin phalanges.....	135
Figure 5.7: Boxplots representing scaled values of bending and torsional rigidity (J) of extant great ape and fossil hominin phalanges.	136

Figure 5.8: Boxplots representing the phalangeal curvature (measured via Included Angle) of extant great ape and fossil hominin phalanges.	137
Figure 5.9: Results of the principal component analysis (PCA) of the intermediate phalanges in 3D, showing separation among the extant taxa and fossil hominins.....	139
Figure 5.10: Cortical bone distribution maps of <i>Homo habilis</i> specimen OH 7.....	140
Figure 5.11: Cortical bone distribution maps of phalanges from Swartkrans.....	141
Figure 5.12: Cortical bone distribution maps of <i>Homo naledi</i> (Hand 1).....	142
Figure 5.13: Cortical bone distribution maps of <i>Homo floresiensis</i> phalanges.....	144
Figure 5.14: Cortical bone distribution maps of Neanderthal populations.....	145
Figure 5.15: Boxplots representing the scaled average cortical thickness of Pre-industrial, post-industrial humans and Neanderthals.....	147
Figure 5.16: Illustration depicting rock-climbing hand postures.....	153
Supplementary figures	
Supplementary Figure 3.1: Individual cortical thickness distribution maps of each PP.....	225
Supplementary Figure 3.2: 3D PCAs for cortical bone distribution of PPs.....	240
Supplementary Figure 3.3: Boxplots representing the mean cortical thickness across the shaft of the PPs.....	241
Supplementary Figure 3.4: Boxplots representing the mean cortical thickness across the shaft within the PPs for each taxon.....	242
Supplementary Figure 3.5: Average CA plotted across the shaft of the PPs.....	243
Supplementary Figure 3.6: Average Z_{pol} plotted across the shaft of the PPs.....	244
Supplementary Figure 3.7: Average J plotted across the shaft of the PPs.....	245
Supplementary Figure 3.8: Scatterplot of phalangeal curvature and cortical thickness of PPs....	246
Supplementary Figure 4.1: Individual cortical thickness distribution maps of each IP.....	269
Supplementary Figure 4.2: 3D PCAs of cortical bone distribution of IPs.....	284
Supplementary Figure 4.3: Mean cortical thickness across the digits of each taxon.....	285
Supplementary Figure 4.4: Ratio of dorsal/palmar cortical bone thickness in the IPs.....	286
Supplementary Figure 4.5: Relationship between phalangeal curvature and cortical thickness of the IPs.....	287

List of Tables

Table 2.1: Details of study sample.....	51
Table 3.1: Summary of study sample included in the study.....	62
Table 3.2: Summary statistics of raw (mm) and standardised (dimensionless) cortical thickness measurements of the phalangeal shaft.....	69
Table 3.3: Paired samples t-tests on scaled palmar vs. dorsal cortical thickness across species.....	75
Table 4.1: Summary of the hypotheses and predictions of this study.....	89
Table 4.2: Summary of the sample included in the study.....	90
Table 4.3: Summary statistics of raw (mm) and standardised (dimensionless) cortical thickness measurements of the phalangeal shaft.....	97
Table 4.4: Significance values for post hoc comparisons of cortical thickness among species.....	99
Table 4.5: Paired samples t-tests palmar vs. dorsal thickness across species.....	101
Table 5.1: Predictions of fossil hominin cortical bone morphlgy.....	125
Table 5.2: Fossil specimens included in the study.....	127
Table 6.1: Summary of cortical bone morphology patterns of fossil hominins.....	177
Table 81: Curatorial institutions of the study sample.....	211

Supplementary Tables

Supplementary Table 3.1: Detailed specimen information of the PPs.....	215
Supplementary Table 3.2: PERMANOVA and subsequent pairwise one-way permutational multivariate analysis of variance test statistics on the first 3 PC scores in the PPs.....	218
Supplementary Table 3.3: Mean values of CSG properties of the PPs.....	219
Supplementary Table 3.4: Test statistics for the Kruskal-Wallis tests of cross-sectional properties across species at 35%, 50%, and 65% of the phalanx.....	221
Supplementary Table 3.5: Significance values for post hoc comparisons of CSG properties across species of the PPs.....	222
Supplementary Table 3.6: Test statistics for the Kruskal-Wallis tests of cross-sectional properties within species, across the digits at 35%, 50%, and 65% of the phalanx.....	223
Supplementary Table 3.7: Significance values for post hoc comparisons of cross-sectional properties within species, across the digits at 35%, 50% and 65% of the phalanx.....	224

Supplementary Table 4.1: Detailed specimen information of the IPs.....	250
Supplementary Table 4.2: PERMANOVA and subsequent pairwise one-way permutational multivariate analysis of variance test statistics on the first 3 PC scores in the IPs.....	251
Supplementary Table 4.3: Mean values of standardised cross-sectional properties across species at 35%, 50%, and 65% of the phalanx.....	252
Supplementary Table 4.4: Test statistics for the Kruskal-Wallis tests of cross-sectional properties across species at 35%, 50%, and 65% of the phalanx.....	254
Supplementary Table 4.5: Significance values for post hoc comparisons of cross sectional properties across species at 35%, 50%, and 65% of the phalanx.....	255
Supplementary Table 4.6: Test statistics for the Kruskal-Wallis tests of cross-sectional properties within species, across the digits at 35%, 50%, and 65% of the phalanx.....	256
Supplementary Table 4.7: Significance values for post hoc comparisons of cross-sectional properties within species, across the digits at 35%, 50% and 65% of the phalanx.....	257
Supplementary Table 4.8: Significance values for post hoc comparisons of cross-sectional properties within a phalanx.....	258
Supplementary Table 4.9: Correlation statistics testing the relationship between phalangeal curvature and cortical thickness of the phalangeal shaft within species.....	260
Supplementary Table 4.10: Correlation statistics testing the relationship between median bar and cortical thickness of the phalangeal shaft for IP3.....	260
Supplementary Table 4.11: Correlation statistics testing the relationship between FSR depth and cortical thickness of the phalangeal shaft for IP3.....	261
Supplementary Table 4.12: Correlation statistics testing the relationship between FSR length and cortical thickness of the phalangeal shaft for IP3.....	261
Supplementary Table 4.13: Correlation statistics testing the relationship between median bar and FSR length of the phalangeal shaft for IP3.....	261
Supplementary Table 4.14: Correlation statistics testing the relationship between median bar and FSR depth of the phalangeal shaft for IP3.....	262
Supplementary Table 4.15: Wilcoxon signed rank tests of scaled proximal phalanx vs. intermediate phalanx CA across species.....	263
Supplementary Table 4.16: Wilcoxon signed rank tests of scaled proximal phalanx vs. intermediate phalanx Z_{POL} across species.....	265
Supplementary Table 4.17: Wilcoxon signed rank tests of scaled proximal phalanx vs. intermediate phalanx J across species.....	267
Supplementary Table 5.1: Comparisons of fossil taxa and extant taxa.....	288

Supplementary Table 6.1: Correlation statistics testing the relationship between phalangeal length and cortical thickness.....289

Abbreviations

μ CT	Micro-computed tomography (Micro-CT)
A2	Second annular pulley
A4	Fourth annular pulley
CA	Cortical area
CSG	Cross-sectional geometry
DIP joint	Distal interphalangeal joint
FDP	Flexor digitorum profundus
FDS	Flexor digitorum superficialis
FSRs	Flexor sheath ridges
IA	Included angle
IPs	Intermediate phalanges
IP2	Second intermediate phalanx
IP3	Third intermediate phalanx
IP4	Fourth intermediate phalanx
IP5	Fifth intermediate phalanx
J	Polar moment of area
Kya	Thousands of years ago
McP joint	Metacarpophalangeal joint
MC	Metacarpal
MC3	Third metacarpal
MIA	Medical imaging analysis
Micro-FE	Micro finite element
Mya	Millions of years ago
PC	Principal component
PCA	Principle component analysis
PIP joint	Proximal interphalangeal joint
PPs	Proximal phalanges
PP2	Second proximal phalanx
PP3	Third proximal phalanx
PP4	Fourth proximal phalanx
PP5	Fifth proximal phalanx
ROI	Region of interest
Z_{POL}	Polar section modulus

1 – Introduction

1.1. The scientific problem

Primates use their hands to navigate their environment as a first point of contact with the substrate during locomotion, or object during manipulation. The hand is also used for a number of important social behaviours, such as feeding, grooming, and communication. Thus, the musculoskeletal elements of the hand hold functionally important information regarding the behaviour of an individual across their lifetime. The functional role of the hominin hand has received a great deal of attention and continues to be intensely debated within palaeoanthropology. The primary debate revolves around when and how the transition from a hand primarily used for locomotion, to a dexterous hand occurred within the hominin lineage.

Traditionally, it has been thought that through evolutionary time, reliance on arboreal substrates decreased, which freed the hand from the functional constraints of locomotion, allowing the hominin hand to adapt and specialise for manipulation (Kivell, 2015; Tocheri et al., 2008; Richmond et al., 2016). The increasingly dexterous hand has been associated with key behaviours that define the human lineages, such as habitual and (later) obligate bipedalism and sophisticated tool production and use, that were intrinsically linked to increased brain size and advanced cognition (Napier, 1962b; 1993; Washburn, 1959; 1960). However, with increasing evidence from the palaeontological and archaeological records, as well as behavioural observations and experimental studies of living primates over the last few decades (Vereecke & Wunderlich, 2016 and references therein), it is clear the evolution of the hominin hand is much more complex than traditionally believed. For example, stone tool use and production was considered a uniquely human trait despite all primates having a grasping, dexterous hand and all genera of living great apes (e.g., Breuer et al., 2005; Byrne, 2004; Fontaine et al., 1995; Inoue-Nakamura & Matsuzawa, 1997; Matsuzawa, 2001; Meulman & van Schaik, 2013, plus several monkeys (e.g., Falótico et al., 2019; Haslam et al., 2017; Malaivijitnond et al., 2007; Ottoni, 2015) show the ability to use stone tools or manufacture tools from organic materials (Bandini et al., 2022; Koops et al., 2014; Pal & Sinha, 2022; Shea, 2016). However, the forceful precision grips of human manipulation distinguish humans from extant and fossil hominids (Marzke, 1997). The unique dexterous ability of modern humans has led to detailed studies on the functional morphology of the human hand in relation to great apes (see details below) (e.g., Almecija et al., 2015; Lemelin & Schmitt, 1998; Patel, 2010; Patel & Maiolino, 2016; Susman, 1979; Tocheri et al., 2005; Tuttle, 1969b). These studies have established that the behavioural diversity of the extant hominids is reflected in their diverse external phalangeal morphology, establishing a relationship between phalangeal form and hand use.

Establishing a form–function link between extant hominid phalanges and their behaviours provides paleoanthropologists with a comparative framework from which they can reconstruct fossil hominin hand use. Within this comparative framework, the long, curved phalanges with prominent muscle markings represent ‘great ape-like’ morphology, while humans are distinguished by their short, relatively straight phalanges with broad fingertips (Susman, 1979; Patel & Maiolino, 2016). Within the fossil record, many paleoanthropologists interpret curved phalanges of early fossil hominins, such as *Orrorin* and *Australopithecus*, as functional adaptations to arboreal locomotion (Kivell et al., 2015; 2018; 2020; Richmond & Jungers, 2008; Stern & Susman, 1983; Susman & Creel, 1979; Ward et al., 2012). However, using morphological distinctions in external skeletal form to infer

behaviour is challenging because of the potential 'evolutionary' or 'phylogenetic lag' in external morphology (Lieberman, 1997; Tocheri, 2008; Ward, 2002). It is difficult to distinguish which morphologies are retentions from an ancestor that are no longer functionally 'useful' from those that are functionally adaptive (Ward, 2002; Tocheri, 2007). Bone is a living tissue that can adapt to reflect the mechanical loads it experiences throughout life. Thus, the study of internal bone structure of the skeleton can help differentiate whether certain morphologies are functional or not. Throughout the skeleton, the relationship between the structural properties of bone and behaviour has been established (e.g., Barak et al., 2011; Burr, 1980; Goodship et al., 1979; Ryan & Shaw, 2013; Schaffler & Burr, 1984; Tsegai et al., 2017b; Weatherholt et al., 2013; Webster et al., 2012). Furthermore, within the internal bone structure of the hand, behavioural signals have been detected, linking internal structure with habitual manual behaviours of extant hominids. The study of internal structure aids and enhances the behavioural inferences made from external morphology alone, and within fossils the study of this behaviourally sensitive morphology allows paleoanthropologists to identify morphology that is functionally adaptive. In this thesis, I study the internal cortical structure of the manual proximal and intermediate phalanges, which have remained largely understudied, to establish the form-function relationship of phalangeal internal form and manual behaviours in hominids.

1.2. Aims of the thesis

This thesis aims to explore variation of internal phalangeal form in relation to extant and fossil hominid manual behaviours. The external morphology of hominid phalanges has been studied in detail, with certain features successfully linked to their locomotion and manual abilities (e.g., Patel & Maiolino, 2016; Rein & McCarty, 2012; Richmond, 2007; Stern et al., 1995; Susman, 1979), but the form-function relationship has not yet been established in such detail within the internal bone structure. The initial goal of this thesis is to detect whether the cortical bone structure of the phalangeal shaft differs between extant hominids (*Pongo*, *Gorilla*, *Pan* and humans) in relation to their habitual manual postures. This relationship is first explored in the proximal phalanges (Chapter 3) and then in the intermediate phalanges (Chapter 4) of digits 2-5. Both of these chapters also explore the relationship between phalangeal curvature and cortical bone, with Chapter 4 also investigating the shape and size of the flexor sheath ridges and the palmar median of the intermediate phalanges. This comparative context is then used to infer the manual behaviours from the phalangeal remains of the following fossil hominins: *Australopithecus afarensis*, *Australopithecus africanus*, *Australopithecus sediba*, *Homo habilis*, *Homo naledi*, *Homo floresiensis*, and *Homo neanderthalensis* (Chapter 5).

1.3. Chapter summaries

Chapter 1: Introduction

The remainder of this introductory chapter discusses hominid habitual locomotor, postural, and manual behaviours. The manual behaviours outlined cover what is known about the position and loading of the hand during locomotion as well as grips employed during tool-using behaviours. The review of hominid behaviour is followed by a detailed anatomical description of proximal and intermediate phalanges, including the morphology and biomechanics of phalangeal curvature and the flexor sheath ridges, as well as the soft tissue anatomy of the phalangeal joints. This is followed by a review of bone functional adaptation in relation to external morphology and internal

morphology. Finally, the locomotor repertoire and functional anatomy of the fossil hominins studied in this thesis are reviewed.

Chapter 2: Materials and methods

The materials and methods chapter details the sample and methodology employed in the analysis of the proximal and intermediate phalanges. This chapter includes more detail than could be provided in the published/submitted manuscripts for Chapters 3 and 4, but this also means there is some repetition across these chapters.

Chapter 3: Cortical bone distribution of the proximal phalanges in great apes: implications for reconstructing manual behaviours

Chapter 3 investigates the cortical bone structure of extant hominid proximal phalanges and has already been published in the *Journal of Anatomy* (Syeda et al., 2023). The results demonstrate that the proximal phalangeal cortical bone structure can distinguish the habitual manual postures employed by extant hominids.

Chapter 4: Cortical bone architecture of hominid intermediate phalanges reveals functional signals of locomotion and manipulation

Chapter 4 investigates the cortical bone structure of extant hominid intermediate phalanges and has already been published in the *American Journal of Biological Anthropology* (Syeda et al., 2024). The results demonstrate that intermediate phalangeal cortical bone structure can distinguish the habitual manual postures employed by extant hominids, with the patterns observed in the proximal and intermediate phalanges being similar.

Chapter 5: Cortical bone distribution of fossil hominin phalanges

Chapter 5 presents the results of the cortical bone analyses of all the fossil hominin phalanges included in this thesis. Hand functional morphology of each species is discussed first, followed by the results of each species. Then, based on the results, this chapter infers the potential hand postures and manual behaviours of each fossil taxon.

Chapter 6: Discussion and conclusions

Chapter 6 discusses how the results presented in this thesis contribute to the scientific problem outlined above. I discuss what we can infer about the overall locomotor and manual behaviours of fossil hominins and, more generally, the evolution of the hominin hand. This chapter also acknowledges the limitations associated with the sample and the methodological approach taken in this thesis. Furthermore, I discuss what further work needs to be undertaken to gain a more holistic understanding of hominin hand evolution and accurately reconstruct fossil hominin behaviours.

1.4. Hominid behaviour: locomotion, posture, and manual behaviours

1.4.1. *Pongo*

Orangutan (*Pongo pygmaeus* and *Pongo abelii*) locomotor repertoire is described as highly arboreal, typically using its limbs in variable ways to move within and between trees (Cant, 1987; Thorpe & Crompton, 2006). Within the orangutan locomotor repertoire, torso-orthograde

suspension is employed most often but vertical climbing, quadrumanous clambering, tree swinging and, occasionally, terrestrial behaviours, also characterise their highly complex positional behaviours (Manduell et al., 2011; Tuttle, 1967; Thorpe & Crompton, 2006; Thorpe et al., 2007; 2009). While *P. pygmaeus* and *P. abelii* are broadly described as having a similar locomotor repertoire, Manduell and colleagues (2012) reveal differences in the frequency of certain behaviours within the two species. Torso-orthograde suspensory behaviours and vertical scrambling are observed more frequently in Bornean orangutans (*P. pygmaeus*), while torso-pronograde suspension, climbing, and bipedalism are observed more frequently in Sumatran orangutans (*P. abelii*) (Manduell et al., 2012). Further differences observed among orangutan populations were due to environmental differences. For example, bridging between trees and quadrupedalism was more frequent in a dry lowland forest environment and tree sway was more commonly observed in a peat swamp environment (Manduell et al., 2012). Within the orangutan populations studied by Manduell and colleagues (2012), all species preferred larger substrates when available. Substrate size and overall locomotor frequencies were not impacted by sex and age.

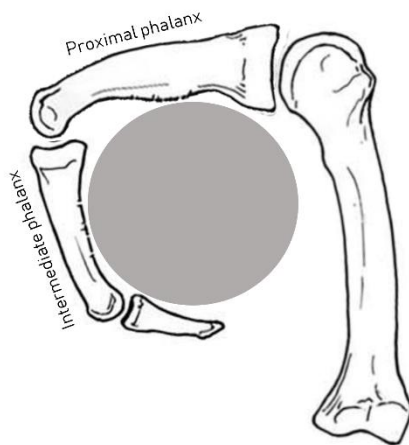


Figure 1.1: Diagram representing phalangeal posture of the *Pongo* hand during suspensory behaviours. Image adapted from Simpson et al., 2018.

During suspensory behaviours, which dominate the orangutan locomotor repertoire, the hand is thought to be positioned like a hook around the substrate (commonly known as the hook grip) (Susman, 1974; Rose, 1988) (Fig. 1.1), with the proximal phalanges positioned above the support, and the intermediate and distal phalanges grasping around the substrate (Rose, 1988; Jungers et al., 1997; Richmond, 2007). The metacarpals have no contact with the substrate in this posture and, as such, the metacarpophalangeal (McP) joint is in a neutral position, while the proximal interphalangeal (PIP) and the distal interphalangeal (DIP) joints are flexed (Rose, 1988). When grasping thin branches or other small substrates, orangutans use the double-locked grip in which all joints of the finger are in flexion, including the MCP joint (Napier, 1960; Rose, 1988). In this grip, the long, curved proximal phalanges are over the substrate with the intermediate phalanges wrapping under it, and distal phalanges locking in with the metacarpal heads. This hook-like position of the hand helps in mitigating bending stresses associated with suspensory manual postures, as the phalanges are being pulled palmarly from gravitational and digital flexor muscle

forces, while the dorsal surface of the phalanges is being loaded in compression through joint reaction forces at the articular ends of the proximal and intermediate phalanges (Carlson & Patel, 2006; Richmond, 2007; Schmitt et al., 2016). However, it is important to note that depending on the size of the substrate, the metacarpals and/or the thumb may be recruited by using a power grip (Alexander, 1994; McClure et al., 2012). This would flex the McP joint to varying degrees, as is observed by the adaptation of the double-locked grip when grasping small substrates (Napier, 1960). Our understanding of orangutan manual behaviours is not as comprehensive compared to that of the other great apes given the logistical challenges of collecting these data in dense tree canopies; however, a preliminary study observing the recruitment of the thumb during locomotion (McClure et al., 2012) points to more diverse behaviours than previously thought.

Manduell and colleagues' (2012) observations of wild orangutans revealed that differences in local environments led to differing frequencies of locomotor behaviours, and as the local environment of orangutans is rapidly changing due to human deforestation, they have also been observed to locomote terrestrially. Terrestrial locomotion in orangutans has also been observed in zoo-housed individuals (Susman, 1974; Tuttle, 1967), in which fist-walking and palmigrady have been noted most frequently (Richmond et al., 2001; Sarmiento, 1988; Tuttle, 1967), along with a singular observation of facultative knuckle-walking (Susman, 1974; Tuttle & Beck, 1972). During fist-walking, the hand is curled like a fist through the flexion of the McP, PIP, and DIP joints and depending on whether the wrist is radially or ulnarly deviated, the proximal phalanges of the ulnar or radial side of the hand are the primary weight-bearing element (Tuttle, 1967). Orangutans appear to easily adapt their locomotor repertoire to the environment around them (Manduell et al., 2012) and given the rapidly occurring changes to their natural habitat, this will ultimately lead to changes in their locomotor behaviour (and manual postures). Detailed studies of orangutan hand postures are needed to get a better understanding of their natural locomotor and manual behaviours rather than behaviour resulting from human habitat destruction.

The challenges associated with wild orangutan observational studies have led to limited reports of tool use in this species (Fox & Bin'Muhammad, 2002; Fox et al., 1999; 2004; van Schaik et al., 2003), but the manipulation capabilities of *Pongo* have been studied in zoo-housed individuals. Experimental studies by Bardo and colleagues (2017; 2018) have shown that orangutans use power grips more frequently than any other apes during variable manual tasks. In the wild, tool use has been primarily observed during feeding behaviours, with an instance of tool use to aid locomotion (Fox & Bin'Muhammad, 2002; Fox et al., 2004).

1.4.2. Gorilla

The genus *Gorilla* consists of western gorillas (*Gorilla gorilla*) and eastern/mountain gorillas (*Gorilla beringei*), both of which primarily locomote terrestrially through knuckle-walking (Doran, 1996; 1997; Remis, 1994; Tuttle & Watts, 1985; Schaller, 1963). Knuckle-walking accounts for ~90% of gorilla locomotion, (Crompton et al., 2010; Doran, 1996) with the hand typically described as being in a palm-back (pronated) position (Inouye, 1994; Matarazzo, 2013). However, locomotor studies of wild gorillas are limited and, until recently (Thompson et al., 2018), all of our information about manual postures came from observations of zoo-housed individuals in unnatural settings. As such, the natural locomotor and postural diversity is likely under-represented in the current literature. Recently, Thompson and colleagues (2018) observed the terrestrial locomotion of mountain gorillas (*G. beringei*) in their natural habitat and found that there is greater variation in

knuckle-walking hand postures than previously thought and that they also frequently use non-knuckle-walking hand postures (e.g. fist-walking, dorsal-metacarpus; see below).

While gorilla locomotion is dominated by terrestrial behaviours, frequencies of arboreal behaviours within gorilla species are variable. Western gorillas are thought to be more arboreal than eastern gorillas, with the former spending an estimated 20% of their time participating in arboreal behaviours and the latter an estimated 2-7% (Crompton et al., 2010; Doran, 1996; Remis, 1995). When comparing arboreality within the African apes, both species of *Gorilla* spend considerably less time in the tress compared to chimpanzees and bonobos (Doran, 1996). This may be due to their larger body mass, as, generally, larger animals tend to spend more time terrestrially than arboreally. This is evidenced in comparisons of female gorilla and male gorilla arboreality. Female gorillas have been observed to spend more time arboreally than their male counterparts (7% in females compared to 2% in males), with males on average being 1.6 times bigger than females (Doran, 1996; Remis, 1999). Differences in arboreal behaviours are also present between the gorilla species (Tuttle & Watts, 1985). Western gorillas regularly climb up and down trees during feeding and move between trees as well (Doran, 1996; Remis, 1994). Both species of gorillas tend to spend most of their time in arboreal settings in postural sitting or lying down (Doran, 1996; Remis, 1994; 1998). Regarding arboreal locomotion, eastern gorillas spend relatively equal time engaging in arboreal quadrupedalism and climbing, while western gorillas spend the majority of their time climbing (Doran 1996; Remis 1994; 1998). Data on the arboreal capacities of gorillas comes primarily only from two gorilla populations/sites (Doran, 1996; Schaller, 1963; Remis, 1994) and therefore it is likely that the current literature does not accurately reflect the actual frequency or diversity of gorilla arboreality.



Figure 1.2: Diagram representing the phalangeal posture of the African ape hand during knuckle-walking. The phalangeal joints are flexed with the dorsal surface of the intermediate phalanges touching down. Image adapted from Simpson et al., 2018.

Just as gorillas arboreal behaviours are not well understood, there is also a lack of knowledge on the hand postures employed during those behaviours. Comparatively, much more is known about hand postures and kinematics of gorilla terrestrial knuckle-walking. During knuckle-walking, the intermediate phalanx contacts the substrate while the proximal phalanx and palm is elevated above it (Fig. 1.2). In this position, the phalangeal joints (PIP joint and DIP joint) are flexed and the McP joint is hyperextended (Tuttle, 1967; 1969a; Wunderlich & Jungers, 2009). *Gorilla* places even pressure across digits 2-5, most likely due to the similar lengths of their metacarpals (Inouye, 1994; Susman, 1979; Matarazzo, 2013). A study of zoo-housed western gorillas revealed that during knuckle-walking pressure moves radially, with digit 5 touching down first and digit 2 experiencing peak pressures (Matarazzo, 2013). Overall pressure was evenly distributed across digits 2-5, which contrasts with the *Pan* pattern, in which digit 5 rarely touches down. However, this data results from a single study of 7 zoo-housed western gorilla individuals and, coupled with the recently described locomotor diversity of eastern gorillas (Thompson et al., 2018), elements of the hand likely experience varying loads and pressure patterns in a natural environment. For example, in 77 counts of eastern gorilla terrestrial locomotor observations, 39% of those were non-knuckle-walking hand postures that load the wrist, metacarpals, and phalanges variably (Thompson et al., 2018). Within the non-knuckle-walking hand postures, fist-walking, in which the dorsal aspect of the proximal phalanges act as the weight-bearing element, was employed most frequently. Fist-walking was followed by 'dorsal metacarpal weight bearing', in which the wrist is hyper-flexed and the dorsal aspect of the hand and wrist is the weight-bearing element. Finally, modified palmigrady, in which the interphalangeal joints are flexed, the wrist extended, and the palm is the main weight-bearing element was also employed. These variable hand postures reported by Thompson and colleagues (2018) result in clear differences in the degree of flexion and extension in the different elements of the hand, which will lead to the proximal and intermediate phalanges being loaded differently.

Hand postures employed during arboreal behaviours also load elements of the hand differently and uniquely from terrestrial hand postures. In the past, gorillas have been broadly described as using power grips during vertical climbing (Sarmiento, 1994). This preliminary observation has been expanded on in wild eastern gorillas by Neufuss and colleagues (2017), in which they describe variation in hand postures during vertical climbing based on substrate size. Neufuss and colleagues (2017) find that on larger substrates (11 cm – 50 cm diameter) a power grip is employed while on medium-sized substrates (6 – 10 cm) a diagonal power grip is used. Power grips for larger substrates used all five digits in flexion and the palm, in which the thumb was either abducted or adducted, while power diagonal grips on medium-sized substrates used all five digits and the palm with the substrate diagonal across them and the thumb opposed to the index finger and either wrapped around the substrate or in line with the axis of the substrate (Neufuss et al., 2017). The wrist is ulnarly deviated in the power diagonal grip and the weight is distributed across digits 2-4 due to the inability of the joints of digit 5 to be in flexion in this hand posture (Neufuss et al., 2017). Although arboreal locomotor behaviours are likely a relatively small component of the overall locomotor repertoire of gorillas, additional data is needed to understand how gorillas move arboreally and in arboreal substrates.

Gorillas have also been observed to employ variable hand postures during food processing and tool use in the wild and in zoos (Bardo et al., 2017; Breuer et al., 2005; Byrne & Byrne, 1991; Byrne et al., 2001; Kinani & Zimmerman, 2015; Masi et al., 2022; Neufuss et al., 2019; Pouydebat et

al., 2005). In the wild, gorilla generally employ power grips with an adducted or opposed thumb during tool-using behaviours (Breuer et al., 2005), while power pad-to-side, transverse hook, precision interdigital, and palm grips were employed during food processing (Byrne et al., 2001; Neufuss et al., 2019). Experimental studies on zoo-housed individuals have shed further light on the ability of gorillas to employ power and precision grips during variable manual tasks (Bardo et al., 2017; Pouydebat et al., 2005).

1.4.3. *Pan*

Knuckle-walking is the predominant form of locomotion of both species of *Pan*, *Pan troglodytes* (chimpanzees) and *Pan paniscus* (bonobos). However, *Pan* is thought to be more arboreal and to generally have a more variable locomotor repertoire than that of *Gorilla*. (Doran, 1996; Doran & Hunt, 1996; Hunt, 1992; Sarringhaus et al., 2014). This variation is present in the way the different species and subspecies of *Pan* locomote terrestrially and arboreally, due to differences in their local environments, food availability, sex, and group differences (Doran, 1996; Doran & Hunt, 1996; Ramos, 2014; Susman et al., 1980; van Lawick-Goodall, 1968). Studies of zoo-housed chimpanzees and bonobos show that their hand postures during knuckle-walking are more variable than that of zoo-housed *Gorilla* (Doran, 1993a; d'Aout et al., 2004; Inouye, 1994; Matarazzo, 2013; Tuttle, 1969a). This difference in *Gorilla* and *Pan* knuckle-walking may in part be attributed to differences in hand morphology; *Pan* rays 2-5 are more variable in length than the relatively similar length observed in *Gorilla* rays 2-5 (Inouye, 1992; Susman, 1979). *Pan* has also been observed to use both 'palm-in' and 'palm-back' postures during knuckle-walking (Matarazzo, 2013; Wunderlich & Jungers, 2009). Palm-in knuckle-walking results in a 'rolling method' in which the intermediate phalanges of the ulnar digits (digit 5 or digit 4) touch down first, followed sequentially by the intermediate phalanges of the radial digits. This places greatest pressure on the radial side of the hand (digit 2 or 3) (Matarazzo, 2013; Wunderlich & Jungers, 2009). In palm-back hand postures, the third digit touches off last as it is placed in front of the other digits (Matarazzo, 2013). Pressure studies of zoo-housed chimpanzees have shown digits 3 and 4 typically experience the highest loads during knuckle-walking, while in some bouts of knuckle-walking digit 5 does not touch down or experiences significantly less loading than the radial three digits (Matarazzo, 2013; Wunderlich & Jungers, 2009).

An experimental study on arboreal knuckle-walking in zoo-housed bonobos also showed digit 5 rarely touched down (Samuel et al., 2018). However, the hand postures of the zoo-housed bonobos differed from those of the chimpanzees, in that the rolling palm-in method was not observed (Matarazzo, 2013; Samuel et al., 2018; Wunderlich & Jungers, 2009). Instead, the third and fourth digits touched down first and peak pressures were experienced around the third digit in the zoo-housed bonobos (Samuel et al., 2018). These experimental studies reveal that peak pressures associated with *Pan* arboreal and terrestrial knuckle-walking are much more variable than what has been observed in (more limited samples of) gorillas (Matarazzo, 2013; Samuel et al., 2018; Wunderlich & Jungers, 2009). However, a recent 3D kinematic study of two subadult chimpanzees reveals knuckle-walking hand kinematics in gorillas and chimpanzees may be more similar than previously thought (Thompson, 2020). Recent kinematic explorations and wild observational data of African apes are increasingly showing that the way in which we describe

knuckle-walking postures, within and across African apes is an oversimplification and does not accurately capture the variation of these great apes.

The degree of arboreality in *Pan* has been comparatively well documented and varies greatly across (sub)species and populations (van Lawick-Goodall, 1968; Hunt, 1992; Doran & Hunt, 1996; Doran, 1996; Sarringhaus et al., 2014; Susman et al., 1980; Drummond-Clarke et al., 2022). Reports on the locomotor repertoire of different *Pan* populations have revealed that around 30–80% of the locomotor time is spent arboreally (Doran, 1996), with bonobos hypothesized to be more arboreal than chimpanzees (Badrian & Badrian, 1977; Doran, 1993a; Hunt 1991a; Susman et al., 1980; Susman, 1984). Along with the purported differences in the degree of arboreality within the species of *Pan*, there are well-noted differences in the locomotor activities performed arboreally (Doran, 1996; Doran & Hunt, 1996; Remis, 1994). For example, chimpanzees spend majority of their arboreal locomotor time climbing (58%–76%), followed by quadrupedal behaviours (11%–31%), then suspensory behaviours (5%–7%), and lastly bipedal behaviours (0.8%–6%), while bonobos are generally more suspensory (Doran, 1993b; 1996; Doran & Hunt, 1996; Remis, 1994). Male bonobos follow a similar pattern as the chimpanzees but are relatively more suspensory and participate in greater leaping behaviours, while female bonobos spend more time quadrupedally and less time climbing (Doran, 1996). This greater degree of arboreality in bonobos may potentially be a consequence of a lack of habituation in the bonobo population studied relative to the chimpanzee populations (Doran, 1993a). The relationship between habituation and degree of arboreality hypothesized by Doran (1993a) has been confirmed by a recent study on a group of habituated bonobos, who did not display a greater degree of arboreality when compared to some chimpanzee populations (Ramos, 2014). Ramos (2014) observed that the arboreal locomotor behaviours of bonobos from Lui Kotale (Democratic Republic of Congo) consisted of less than 1% of their overall arboreal behaviours, with the majority of their time spent arboreally in sitting postures (Ramos, 2014).

Hand postures during these arboreal activities are characterised as employing hook grips, power grips, and diagonal power grips, which all require the fingers to be flexed at the MCP, PIP and DIP joints to various degrees with variably digital loading (Hunt, 2020; Jenkins & Fleagle, 1975; Marzke & Wullstein, 1996; Neufuss et al., 2017; Ramos, 2014; Samuel et al., 2018; Tuttle, 1967; Wunderlich & Jungers, 2009). Specifically, during vertical climbing chimpanzees have been observed to use power grips and diagonal power grips in their natural habitats (Neufuss et al., 2017) and pressure studies on zoo-housed bonobos showed similar flexed-finger power grips during arboreal behaviours (Samuel et al., 2018). While the overall locomotor repertoire of chimpanzees and bonobos is similar, bonobos display greater sex differences, different hand postures, and significantly greater palmigrady in their arboreal behaviours (Doran, 1993a; 1996).

Within the great apes, tool use has been observed most frequently in chimpanzees (e.g., Boesch, 1993; 1995; Boesch & Boesch, 1990; 1993; Marzke et al., 2015; Sanz & Morgan, 2007). Multiple chimpanzee communities were observed using variable grips for tool production, use, and food processing. Tai National Park (Ivory Coast) chimpanzees have been observed to use variations of power and precision grips during nut-cracking based on the size of the object being handled (Boesch & Boesch, 1993). Pad-to-side grips are the most common precision grips employed by wild chimpanzees from Mahale (Tanzania), with transverse hook grips and grips including the second digit and thumb being commonly observed as well (Marzke et al., 2015). In contrast, bonobos

have only rarely been observed using tools in the wild and, thus far, not in the context of food foraging (Samuni et al. 2022).

Experimental studies on zoo-housed chimpanzees and bonobos expand further on the power and precision grip categorization, with detailed information on the particular grips employed (Bardo et al., 2016; Cebeiro & Key, 2023). Experimental studies show power grips are most frequently employed on larger objects, while precision grips with an opposed thumb are used to manipulate smaller objects (Jones-Engel & Bard, 1996; Pouyedebat et al., 2011). Precision handling, an ability previously only observed in humans, has also been observed in zoo-housed chimpanzees (Craat et al., 2009; Marzke, 1997). Although wild bonobo tool use is considered rare, zoo-housed bonobos have been observed to be as dexterous as chimpanzees (Bardo et al., 2016; Neufuss et al., 2017)

1.4.4. *Homo sapiens*

Modern humans are unique among hominids in that they are obligate terrestrial bipeds and mainly use their hands for manipulation rather than locomotion. However, there many modern hunter-gatherer groups habitually climb trees, often unassisted (Kraft et al., 2014) and many modern humans that climb rocks, cliffs and mountains as a sport. A combination of derived morphological features, such as a long robust thumb, a broad facet on the trapeziometacarpal joint, broad apical tufts on the distal phalanges, the orientations of carpal bones, and a mobile fifth digit, allow the human hand to participate in enhanced manipulatory activities (Marzke, 1997; Tocheri et al., 2008; Marzke, 2013; Kivell, 2015) and use our hands for locomotion when required. These features are thought to evolve in the context of fossil hominin tool use and tool manufacturing.

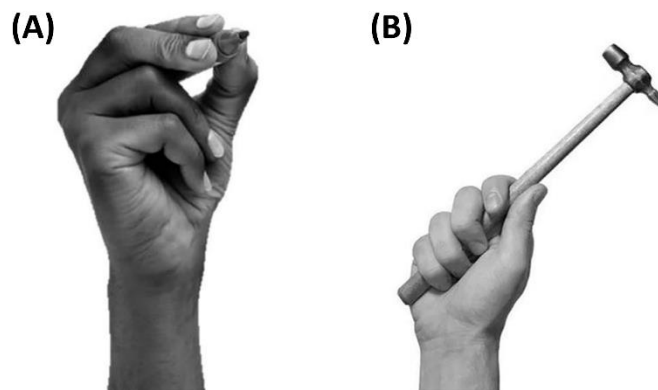


Figure 1.3: Example of a (A) precision grip (specifically tripod precision grip) and a (B) power squeeze grip. Images from Kivell et al., 2022.

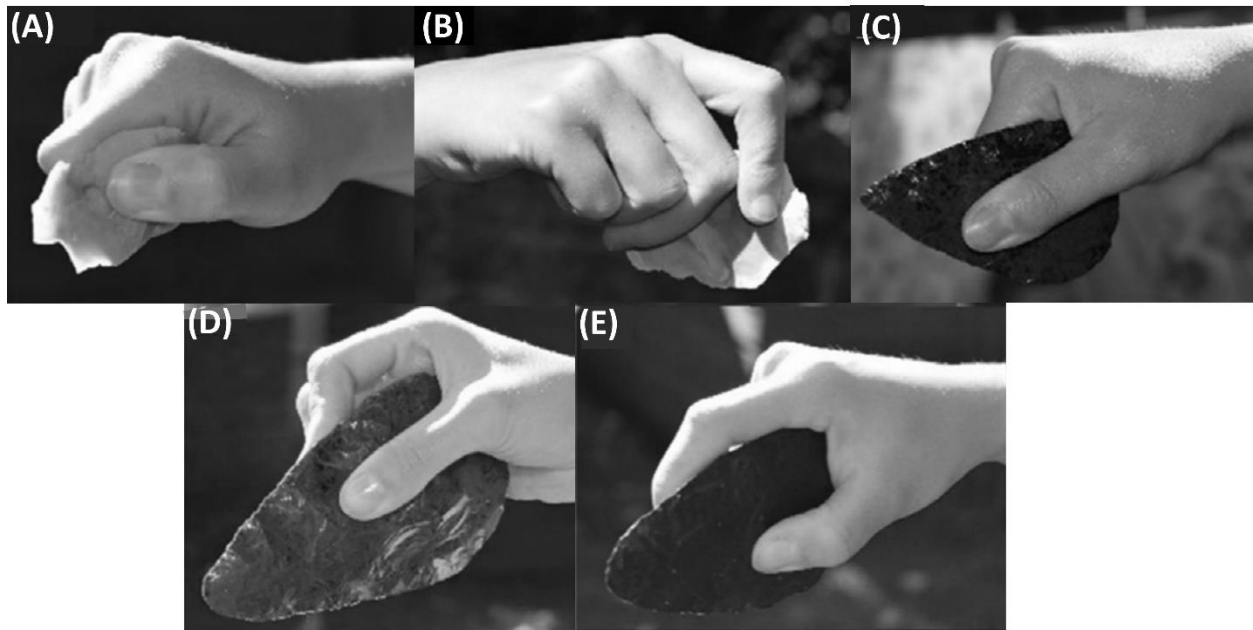


Figure 1.4: Common hand grips employed during stone tool use. (A) Two-jaw chuck pad-to-side; (B) three-jaw chuck pad-to-side; (C) two-jaw buttressed pad-to-side; (D) cradle grip; (E) three-jaw buttressed pad-to-side. Images from Key et al., 2018.

Hand use is divided into two main categories: non-prehensile and prehensile hand use (Napier, 1956). During prehensile hand use, an object is grasped using more than one digit or between the digit(s) and the palm (Napier, 1956), which all primates are capable of doing. Prehensile hand use can then be further divided into two types of grips: power and precision grips (Fig. 1.3). These grip types have been the basis of understanding primate hand use and function, as well as studies on grip strength and diversity in the context of stone tool use and manufacturing (Key et al., 2018; Marzke, 1997; Rolian et al., 2011). During power grips, an object is held against the palm as the fingers are flexed around, with the thumb variably involved as a stabiliser (Napier, 1956; Marzke et al., 1992; Marzke, 1997). During precision grips, an object is held between an opposed thumb and one or more fingers (Napier, 1956; Marzke, 1997). This basic classification has been divided into further subcategories based on the variation observed in grasping activities in modern humans and non-human great apes (Bardo et al., 2017; Key et al., 2018; Marzke, 1997; Marzke et al., 1992; 2015; Neufuss et al., 2017; 2019). Within these subcategories, forceful precision grips, power squeeze grips, and precise in-hand manipulation are important in stone tool making and use and are thought to distinguish modern humans from the manipulatory abilities of other hominids (Marzke, 1992; 1997; Williams-Hatala, 2016). In forceful precision grips, an object is held between the palmar pad of the thumb and one or more fingers with a large amount of force exerted on to the object (Marzke, 1997). There are several types of forceful precision grips that are used frequently by modern humans, as the hand is able to withstand loads from high reaction forces when forceful precision grips are employed (Key et al., 2018; Marzke, 1997). The most frequently employed forceful precision grips in the context of stone tool use are the cradle grip, the two jaw chuck pad-to-side, the three jaw chuck pad-to-side, the two jaw buttressed pad-to-side, and the three jaw buttressed pad-to-side (see Key et al., 2018 for descriptions of these grips and a comprehensive review of

hand grip diversity; Fig. 1.4). During power squeeze grips an object is held in place through the flexion of the fingers and supported by an adducted thumb as it lies diagonally across the palm (Marzke et al., 1992; Marzke, 1997). Finally, precise in-hand manipulation allows humans to adjust an object or their grip on the object just using their fingertips, which has been thought to be beneficial for tool manufacturing (Marzke, 1997).

Precision grips have been observed in many non-human primates (e.g., Bardo et al., 2017; Jones-Engel & Bard, 1996; Neufuss et al., 2019; Pouyedebat et al., 2005; 2011), but the high degree of force that humans exert on to an object during precision grips is thought to be uniquely human (but see Marzke et al., 2015). Described above are the grips most commonly used during modern human stone tool use, but grips used during daily modern human activities differ from those. The most commonly used grips are pinch grips between the pads of one or more fingers and the thumb, power grips using all the digits and the palm with the thumb opposed to the fingers, and power squeeze grips (Dollar, 2014; Feix et al., 2015), with power grips being most frequent (Zheng et al., 2011). Many of these grips require the fingers to be in flexion, with flexion and abduction/adduction at the MCP joint and flexion at the PIP and DIP joints. Experimental research shows that digits 2 and/or 3, and less so digit 5, experience the highest loads during stone tool production and use (Williams et al., 2012, Williams-Hatala et al., 2018; Key et al., 2019). Experimental studies quantifying the biomechanics of power grips show that joint forces increase disto-proximally within digits 2-5, with digit 2 experiencing the greatest loads followed by digits 3, 4, and 5 (Chao et al., 1976; Vigouroux et al. 2011; de Monsabert et al., 2012; Sancho-Bru et al. 2014) and have emphasized the importance of extensor muscles of the hand in these hand grips (Snijders et al., 1987; Keir & Wells, 2002; de Monsabert et al., 2012).

1.5. Phalangeal external morphology and anatomy

The primate hand consists of several bones within the carpus (wrist), metacarpus (palm), and digits (fingers). The metacarpus and digits form the digital rays of the hand, consisting of the metacarpals (MC), proximal phalanges (PP), intermediate phalanges (IP), and distal phalanges (DP). There are five rays within the hand, and within primates, the first ray is referred to as the pollex (thumb) and the fingers are ulnar rays two to five. Each finger has a PP, an IP, and a DP, while the thumb only has a PP and a DP (referred to as the pollical proximal and distal phalanx). The focus of this thesis will be on the proximal and intermediate phalanges of the four ulnar rays (fingers), as they are regularly loaded during locomotion and/or manipulatory behaviours. Below I describe the general anatomy of the proximal and intermediate phalanges (**Fig. 1.5**) that applies to all extant hominids, followed by a description of functionally informative aspects of phalangeal morphology, then discuss the soft tissue anatomy of the fingers, and finally I discuss specific aspects of how external morphology varies between the extant great ape taxa.

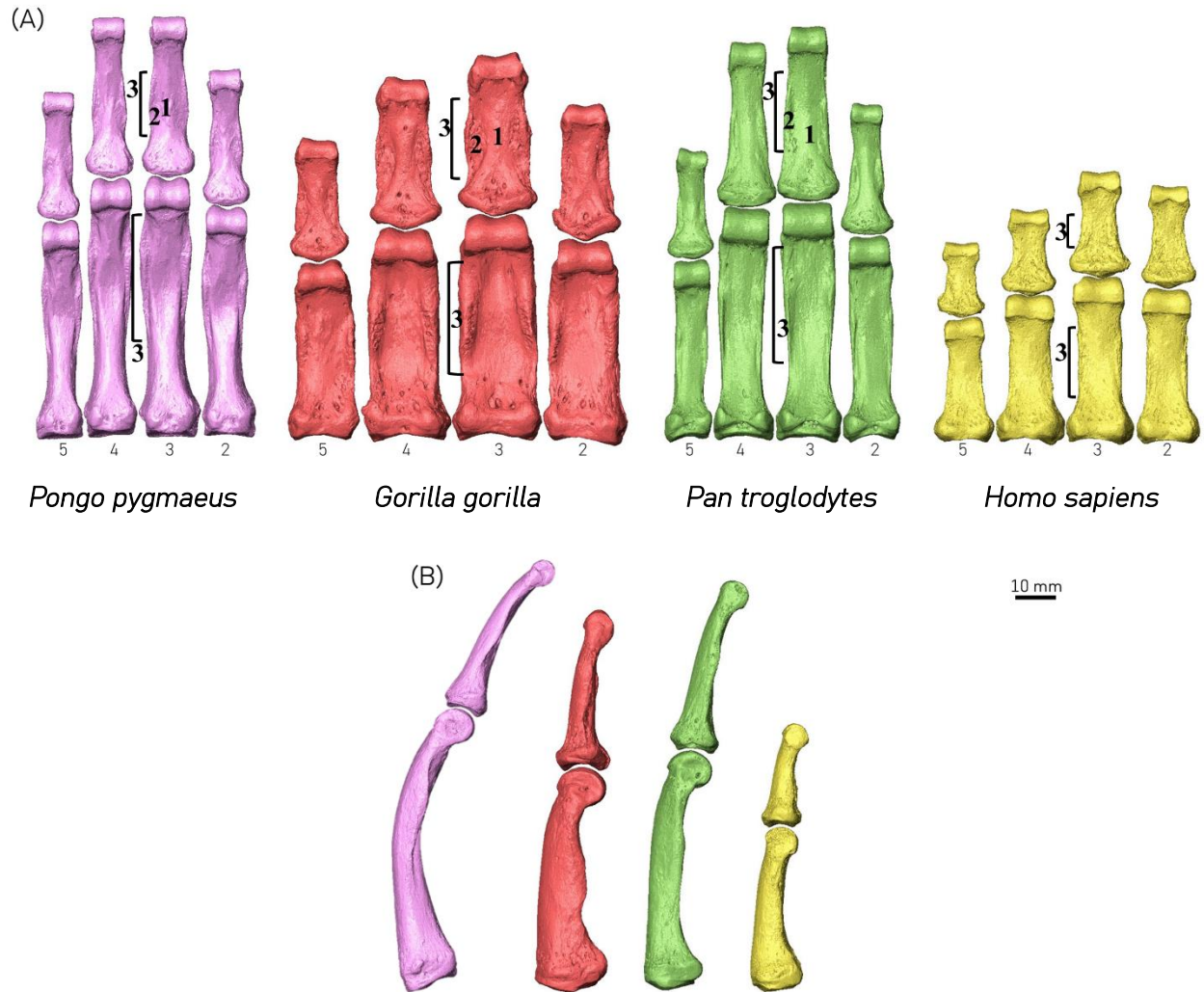


Figure 1.5: Comparative anatomy of proximal and intermediate phalanges of digits 2-5. (A) Depicts the palmar surface of the phalanges. 1: Median bar; 2: Lateral fossae; 3: Flexor sheath ridges. (B) Depicts variation in phalangeal curvature across the hominid third digit.

1.5.1. Proximal phalanges

Both proximal and intermediate phalanges all have a base, a shaft, and a head. Proximal phalanges have a radioulnarly wide base, which is also the dorsopalmarly tallest part of the bone. The base articulates with the corresponding metacarpal head to form the metacarpophalangeal (McP) joint in all primates. Palmarly there are two tubercles on the base, which serve as attachment sites for ligaments of the MCP joint capsule and guide the digital flexor tendons to their distal insertion points (see below for details on the soft tissue anatomy). The shaft of the bone widens radioulnarly at the midshaft before narrowing in close to the head of the bone. The dorsal surface of the shaft is relatively smooth, while the palmar surface shows sites of muscle attachments and has a degree of concavity to it (Patel & Maiolino, 2016). The radial and ulnar sides of the palmar shaft have flexor sheath ridges (FSRs), which are lateral ridges that are thought to be attachment sites for flexor sheaths and hold the digital flexor tendons in place (Susman, 1979; Patel & Maiolino,

2016). Within the extant great apes the FSRs are most developed in *Gorilla* and least developed in *Homo*, with *Pongo* and *Pan* displaying FSR morphology that is intermediate between the two (Syeda et al., 2021). Patel and Maiolino (2016) report the FSRs are often most developed in the proximal phalanges of digits 3 and 4 within hominids. The head of the proximal phalanges is shaped like a trochlea, with asymmetrical radial and ulnar sides. There is a concavity in the middle of the two halves of the trochlea on the dorsal aspect for the proximal beak of the corresponding intermediate phalanx. There are concavities on the radial and ulnar sides immediately below the trochlea, which are attachment sites for the collateral ligaments that stabilize the DIP joint (Ayhan & Ayhan, 2020). Extant hominid PPs also display varying degrees of dorsopalmar curvature (discussed in more detail below). Within hominids, the length formulas of the digits are usually similar such that the third digit is the longest and the fifth is the smallest. Sometimes the fourth digit is longer than the second and at other times the second is longer than the fourth, but in general, the pattern most commonly observed has been digit 3>4>2>5 (Susman, 1979; Patel & Maiolino, 2016).

1.5.2. Intermediate phalanges

The intermediate phalanges are the least studied primate hand bones, apart from the distal phalanges. Similar to the general morphology of the proximal phalanx, each intermediate phalanx has a base, shaft and head. Proximally, the base has two elliptical articular facets which are separated by a vertical keel for articulation with the corresponding proximal phalanx. On the dorsal aspect of the proximal end, the base has a dorsal beak which extends proximally and locks into place with the distal end of the proximal phalanx during extension (Patel & Maiolino, 2016). The shaft of the intermediate phalanges is radioulnarly wide but narrows distally, as observed in the proximal phalanges. The dorsal surface of the shaft is relatively smooth as it lacks any strong insertions of the digital extensor complex (Ayhan & Ayhan, 2020). The palmar surface of the shaft has a suite of morphological features, which are variable among primates but their function is unclear (Marzke et al., 2007). These morphological features are a palmar median bar, depressions on the radial and ulnar side of the palmar shaft known as the lateral fossae, and the FSRs. The palmar median bar runs along the length of the palmar shaft and, in most cases, is bounded by the lateral fossae that vary in depth and are both bounded by FSRs on the radial and ulnar aspects of the bone (Susman, 2004; Marzke et al., 2007). These morphological features are thought to be attachment sites for the tendon of the flexor digitorum superficialis (FDS) muscle, although Marzke and colleagues (2007) demonstrate the size and shape of these morphological features do not represent the size of the muscle or its tendons. The tendons of the FDS muscle still attaches to the palmar surface of the shaft, but there is no association between the morphology of this skeletal area and the size and recruitment of the FDS muscle.

Similar to the proximal phalanges, the head of the intermediate phalanges have a trochlea, but it is not as bulbous and asymmetrical in the intermediate phalanges. The palmar aspect of the trochlea extends proximally which results in a V-shaped morphology (Patel & Maiolino, 2016). On the radial and ulnar sides of the head, there are concavities that are attachment sites for the collateral ligaments of the DIP joints. These concavities are less developed compared to the ones on the head of the proximal phalanges (Patel & Maiolino, 2016). The intermediate phalanges also have a degree of dorsopalmar curvature, but the curvature observed in the intermediate phalanges never exceeds that of the corresponding proximal phalanx (Matarazzo, 2008).

1.5.3. Phalangeal curvature

Phalangeal curvature is a widely discussed and well-studied topic within palaeoanthropology and primate functional morphology. The degree of phalangeal curvature correlates well with the frequency of arboreality across primates (Matarazzo, 2008; Rein, 2011; Richmond, 1998; Stern et al., 1995; Susman, 1979). Therefore phalangeal curvature is traditionally considered a 'plastic' feature and thus a strong functional indicator of arboreal locomotor grasping, which is used to reconstruct posture and locomotion in fossil primates (Begun, 1993; Deane & Begun, 2008; Deane et al., 2005; Hamrick et al., 1995; Jungers et al., 1997; Matarazzo, 2008; Preuschoft, 1973; 1974; Rein, 2011; Richmond, 1998; Stern & Susman, 1983; Stern et al., 1995; Susman, 1979; Susman et al., 1984; Susman, 2004). When grasping curved substrates, the phalanges experience high levels of stress and strain because they are subjected to substrate reaction forces from the branch, muscle forces from the contraction of the digital flexors, and joint reaction forces from the contraction of the MCP, PIP, and DIP joints (Marzke et al., 2007; Patel & Maiolino, 2016; Preuschoft, 1973; Richmond, 1998; 2007). Dorsopalmarly curved phalanges experience lower bending moments and can perform more efficiently than straight phalanges during flexed-finger postures (Oxnard, 1973; Preuschoft, 1973). Bending moments are reduced in a curved phalanx because the curvature aligns the long axis of the phalanx more closely with the joint reaction force during flexed-finger postures. However, this leads to the phalanges experiencing higher compressive forces, which consequently means a curved phalanx would have a higher ratio of compressive to tensile strain (Preuschoft, 1973; Richmond, 2007). Arboreal primates with longer phalanges experience proportionally higher bending stresses, with a high degree of phalangeal curvature being advantageous during arboreal locomotion (Richmond, 2007). This biomechanical function of phalangeal curvature has been validated using finite-element modelling techniques that test for differences in strain distribution in a curved phalanx and a mathematically straight version (Richmond, 2007; Nguyen et al., 2014). Richmond (2007) first tested this and revealed curved phalanges experience roughly half the strain than their mathematically straightened versions and experience a higher ratio of compressive to tensile strain. Nguyen and colleagues (2014) expanded on Richmond (2007) via a 3D micro-finite element analysis that modelled both the external morphology and internal structure of the bone, further confirming the role of curvature in reducing the overall strain experienced by the phalanx in a flexed position. When variation in external and internal morphology was taken into account, the compression-to-tension ratio did not always increase – in some cases, it decreased the ratio (Nguyen et al., 2014). These results confirm the adaptive role of phalangeal curvature and offer a biomechanical explanation as to why there is an association between phalangeal curvature and the frequency of arboreal locomotion in primates.

This association between the degree of finger flexion and strain distribution is further validated as ontogenetic studies have also shown that phalangeal curvature is plastic and subject to change throughout an animal's life depending on mechanical loading (Richmond, 1998; 2007; Jungers et al., 2002 but see Wallace et al., 2020). For example, chimpanzees and gorillas have been observed to locomote arboreally in greater frequency as juveniles (Doran, 1997) and data suggests there is an increase in the degree of curvature from birth up until adulthood, where the degree of arboreality decreases significantly (Richmond, 1998; 2003; 2007; Jungers et al., 2002; Congdon, 2012). This suggests a strong functional link between locomotor behaviour and the degree of phalangeal curvature (but see discussion on Wallace et al., 2020 below)..

1.5.4. Flexor sheath ridges

The radial and ulnar aspects of the palmar shaft of the proximal and intermediate phalanges typically have two raised ridges running proximodistally called the flexor sheath ridges (FSRs). In the proximal phalanges, they are thought to serve as attachment points for the bifurcated tendon of the FDS muscle as it passes through to attach to the intermediate phalanges. Since these ridges extend from the palmar surface of the phalanx, the palmar shaft is concave, and the degree of this concavity depends on how far the ridges extend from the shaft. In the intermediate phalanges, the FSRs also run proximo-distally but instead of a concave shaft, there are lateral fossae on the palmar shaft which are separated by the palmar median bar (described above). These lateral fossae on the radial and ulnar aspect of the palmar shaft of the intermediate phalanges of digits two to five have been attributed as the attachment site for the tendons of the FDS muscle (Marzke et al., 2007). Within primates, the size and shape of the lateral fossae and the associated palmar median bar are quite variable (Susman, 1979; personal observations) and this variation is also observed in the fossil hominin record. The relative size and overall morphology of these fossae have been used to make functional inferences regarding the locomotion of fossil hominins (detailed in Section 1.7 and Chapter 6), and while FSR morphology has been linked to the size and excursion of the FDS muscles, there is a lack of evidence supporting the relationship between the morphology of muscle attachment sites and the size of the muscle in different hand bones (Shrewsbury et al., 2003; Williams-Hatala et al., 2016; but see Karakostis et al., 2018). Furthermore, the functional implications of the variation observed in FSR, lateral fossae and palmar median bar morphology in the intermediate phalanges remained relatively unexplored (Marzke et al., 2007; Patel & Maiolino, 2016).

To date, Marzke and colleagues (2007) are the only ones who have explored the biomechanical and behavioural implications of intermediate phalanx morphology. Marzke and colleagues (2007) predicted the location and length of the lateral fossae are indicators of the size of the FDS tendons and their attachment point in primates. However, using a comparative sample of anthropoid intermediate phalanges they showed that the FDS tendon does not exclusively insert onto the lateral fossae, instead the tendon variably inserts at the FSRs, with the fibres running towards different aspects of the palmar shaft (Marzke et al., 2007). The length of the lateral fossae also does not predict the cross-sectional area or length of the FDS tendon, so the development of FSR morphology cannot be explained by the FDS tendon attachments or the stresses associated with FDS muscle activity. Alternative explanations as to why these fossae develop and why they are so variable have been posited using the palmar median bar. Lateral fossae are, in most cases, accompanied by a palmar median bar so these fossae could just be a by-product of the median bar thickening and developing anteriorly in response to loading (Marzke et al., 2007). Begun and colleagues (1994) studied the pedal intermediate phalanges of *Proconsul*, a purported early Miocene ape, and have hypothesized the palmar median bar reflects dorsopalmarly directed bending stresses which accompany the contraction of the digital flexor muscles and substrate reaction forces. On the other hand, the palmar median bar could form as a result of the lateral fossae excavations (Walker & Leakey, 1993), but this theory would require an explanation other than the lateral fossae serving as attachment sites for FDS tendons to explain why there is a hollowing out of the palmar phalangeal shaft.

While Marzke and colleague's work focused on the shape and size of the lateral fossae (and thus the length of FSRs), they did not explicitly explain or address the role and morphology of FSRs. Nguyen and colleagues' (2014) 3D micro-FE study sheds light on the biomechanical importance of the FSRs. Models detailing the external and internal morphology of a siamang third proximal phalanx were created to investigate how variation in these features affects the biomechanical behaviour of the phalanx under varying loading configurations. Their analyses demonstrated that peak strain occurs along the FSR rather than the palmar shaft (Nguyen et al., 2014). Across all the phalanges that were modelled, the average peak strain on the FSR was higher than the average peak strain on the palmar shaft, reflecting the fact that the FSRs were helping reduce the strain experienced by the shaft. Variation in FSR morphology further confirms the role of the FSR in reducing strain on the shaft such that, the taller the ridge was the higher the tension it experienced and the lower the tension experienced by the rest of the palmar shaft (Nguyen et al., 2014). These results provide biomechanically backed data regarding the functional importance of the FSR.

The variability observed in external phalangeal form, especially in regard to phalangeal curvature and FSR morphology, indicates that there must be a complicated interrelationship of genetic and environmental factors involved in the development of these bones. Different variations and combinations of morphological features may act together to efficiently function and reduce strains on the phalanx.

1.5.5. Joints of the phalanges

Detailed below are the soft tissue anatomy and morphology associated with the phalangeal joints. The following review is based on human joint morphology, as it is the most studied, and the information here largely derives from Ayhan & Ayhan (2020) and Gilroy and colleagues (2016). Where appropriate, additional sources are indicated within the text.

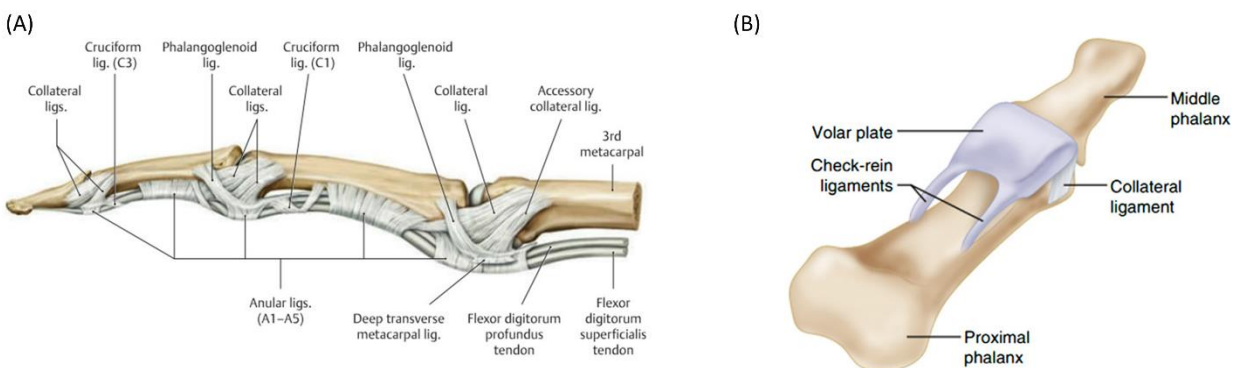


Figure 1.6: Soft tissue anatomy of the finger. (A) Depicts the pulleys and ligaments of the finger. Adapted from Gilroy et al., (2016); (B) Depicts check-rein ligaments that stabilise the PIP joint. Adapted from Ayhan & Ayhan (2020).

1.5.5.a. Metacarpophalangeal (McP) joint

The articulations of the proximal and intermediate phalanges create three joints. The proximal-most joint is the metacarpophalangeal joint (McP), which is between the metacarpal head and the base of the corresponding proximal phalanx. The MCP joint can be defined as a biaxial synovial joint with two planes of movement: flexion/extension and abduction/adduction. The MCP joint is supported by the joint capsule, collateral ligaments, the palmar plate, the transverse intermetacarpal ligament, accessory collateral ligaments, and surrounding tendons and soft tissues. The shape of the joint articulation allows for some axial rotation of the proximal phalanx. The joint capsule is supported by the palmar plate, which is a strong fibrocartilaginous structure that includes the synovial sheaths of the flexor tendons. The dorsal aspect of the joint capsule is thin, weak and contributes minimally to the stability of the joint. The MCP joint is linked by the deep transverse palmar ligament that spans the head of the second to fourth metacarpals and blends in with the palmar MCP ligaments. Along with strengthening the MCP joint, the deep transverse palmar ligaments prevent the corresponding metacarpals from abducting at the carpometacarpal joint. The palmar plate is a fibrocartilaginous covering for the articular surfaces, which increases joint congruence and dorsopalmar stability by limiting hyperextension. The palmar plate also protects the surface of the metacarpal heads from abrasion during grasping. The palmar plate attaches strongly to the base of the proximal phalanx distally and loosely to the metacarpal head proximally. The palmar plates blend with the deep transverse ligament, which holds together the heads of the metacarpals and palmar plates together. Sagittal bands lie dorsal to the deep transverse ligament and connect each palmar plate (through the capsule and deep transverse metacarpal ligament) to the extensor hood. Fibrous sheaths attach superficially to the anterior side of the palmar plates.

Flexion and extension of the MCP joint occurs in the sagittal plane, with the joint being able to flex about 90 degrees and extend 20–30 degrees within humans. While the joint is in flexion, some rotation and deviation may also occur. Abduction and adduction of the MCP joint occur in the coronal plane and the degree of abduction/adduction depends on the digit but ranges from 10–40 degrees in humans (Ayhan & Ayhan, 2020). Great ape MCP flexion (~ 170 degrees) and extension is generally higher when compared to humans (~ 90 degrees), with extension in the African apes around 50 degrees and 19 degrees in orangutans (Bardo et al., 2018; Napier, 1960; Patel & Maiolino, 2016; Rose, 1988; Susman, 1979; Tuttle, 1960)

1.5.5.b. Interphalangeal joints

Distal to the MCP joint is the proximal interphalangeal joint (PIP), which is formed by the articulation of the head of the proximal phalanx and the base of the corresponding intermediate phalanx. The distal most joint of the fingers is the distal interphalangeal joint (DIP), which is formed between the head of the intermediate phalanx and the corresponding base of the distal phalanx (Patel & Maiolino, 2016). There are four PIP and DIP joints in the hand, one of each in digits 2–5. The thumb has a single interphalangeal joint as it does not have an intermediate phalanx. The PIP and DIP joints are synovial hinge joints which are covered by an articular cartilage and are restricted just to the flexion–extension plane (Ayhan & Ayhan, 2020; Pang & Yao, 2018). Similar to the MCP joint, the PIP and DIP joints are supported by the joint capsule, collateral ligaments, and a palmar plate. The collateral ligaments provide lateral stability to the joint, as in the MCP joint, but for the PIP and DIP joints they do not allow for abduction or adduction (Bailie et al., 1996; Stollwerck et al., 2010). Extension is also limited at these joints because of the dorsal proximally-projecting

beaks of the distal articulating element (Patel & Maiolino, 2016). The palmar plates stabilize the joint dorsopalmarly by limiting hyperextension and protecting the palmar surface of the head of the phalanx. The palmar plates of the PIP are thicker than those of the DIP, although they function in the same way as they do in the McP joint. Differing from the McP joint, the PIP and DIP joint palmar plates lack a ligament which attaches the palmar plates together. However, the PIP joint does have another set of ligaments to stabilize the palmar plate. The palmar check-rein ligaments attach on the base of the intermediate phalanx from the lateral aspects of the palmar surface of the proximal phalanx. Since there are no check-rein ligaments for the DIP joints, the DIP joints are less stable than the PIP joints (Stollwerck et al., 2010; Pang & Yao, 2018), but that allows the DIP to hyperextend more compared to the PIP joint. Overall, the interphalangeal joints are also stabilized by the flexor and extensor tendons which surround them (Shrewsbury & Johnson, 1980; Dyson et al. 2008; Ayhan & Ayhan, 2020).

The PIP joints of the fingers have a greater range of flexion than the McP and DIP joints across all taxa. Within humans, there is minimal hyperextension at the PIP joints, but the DIP joint can hyperextend around 30 degrees. Across the extant taxa, great apes have a greater degree of flexion compared to humans (Bardo et al., 2018; Napier, 1960; Rose, 1988; Tuttle, 1969a). While both interphalangeal joints have one plane of movement (flexion/extension), there is slight ulnar deviation and rotation at these joints during flexion and grasping (Ayhan & Ayhan, 2020). These accessory movements are important in directing the fingers toward the thumb during grasping or manipulatory behaviours. The variation in phalangeal morphology of the different digits results in differing patterns of flexion across the fingers. For example, the PIP and DIP joints of the ulnar digits have a greater range of flexion than the radial digits. The asymmetrical trochlea of the proximal phalanges also tilts the flexion/extension axis of motion relative to the long axis of the digit. With respect to the fourth and fifth digits, the flexion/extension movement at these digits allows for axial rotation to occur, which helps the fingers converge toward the thumb towards the thenar eminence during finger flexion. These slight tilts in the movement axis and slight rotation are not observed in the DIP joints due to the symmetry of the articular surfaces of these joints, which allow movement to occur parallel to the long axis of the fingers.

1.5.5.c. Collateral ligaments of the McP and Interphalangeal joints

The collateral ligaments, accessory collateral ligaments, and interosseous-lumbrical muscles provide axial stability to the McP and interphalangeal joints. Collateral ligaments arise from the posterior tubercle on the lateral sides of the metacarpal heads and then run obliquely to the proximal phalanx and insert onto the palmar side of the lateral surface of the base of the proximal phalanx. The radial and ulnar collateral ligaments have broad attachments on the sides of the metacarpal heads and base of the proximal phalanges and thus provide lateral stability to the McP joint. Compared to the ulnar collateral ligaments, the radial collateral ligaments are thicker and wider. The collateral ligaments consist of the collateral ligament proper and the accessory collateral ligament. The collateral ligament proper is dorsal to the flexion/extension axis of the joint and it tightens as the joint gets flexed. This tightening of the collateral ligaments, as the joint goes from extension to flexion, prevents abduction and adduction of the McP joint. Abduction and adduction are further limited at the McP joint because of the partially flattened metacarpal heads. Metacarpal heads are overall round in shape but the anterior portion of the metacarpal head is flattened, which acts as a bony blocker for the base of the proximal phalanx when the McP joint is

in flexion – resulting in reduced ability for the joint to abduct or adduct (Werner et al., 2003; Lutsky et al., 2014). The accessory collateral ligament is palmar relative to the flexion/extension axis of the joint so the ligament gets stretched during extension but dorsal dislocation is resisted because of the presence of the palmar plate.

1.5.6. Hominid phalangeal morphology

1.5.6.a. *Pongo*

The phalanges of orangutans are radioulnarly thin, highly curved, and widen distally, with the shaft radioulnarly widest at the FSRs. The phalangeal length formula of orangutan phalanges differs based on sex; males tend to display a pattern of digit 4>3>2>5 and females have a bone length pattern of digit 3>4>2>5 (Susman, 1979; Patel & Maiolino, 2016). This length formula is variable compared to the African apes, with the female orangutan pattern being similar to the other great apes. The degree and variability of asymmetry of the proximal phalangeal base is similar to what has been observed in PP2 and PP5 of the other great apes, but the asymmetry observed on PP3 and PP4 is variable. PP4 is usually asymmetric, in that it is angled towards the third digit (personal observations); however, in individuals with PP4s that are longer than PP3s, the PP4 tends to be more symmetrical. In those instances, the morphology of PP3 resembles PP2, resulting in a tubercle that is enlarged for the insertion of the pennate portion of the second interosseous muscle and the ipsilateral FSR extending more distally. However, regardless of the longer length of PP4, PP3 is always more robust (Susman, 1979). The shaft of *Pongo* PPs differs from those of the African apes as the radioulnar concavity on the palmar surface of the shaft is lacking. Instead, the palmar surface of the shaft is convex, often raised above the height of the FSRs (similar to what has been observed in bonobos). Distally, the trochlea of the PPs is characterized by a deep sulcus. *Pongo* PPs are the most longitudinally curved among the great apes, which would facilitate the grasping of arboreal substrates with flexed fingers. The FSRs on the palmar surface are not particularly prominent as the palmar surface of the shaft is often raised above the height of the FSRs (Susman, 1979; Patel & Maiolino, 2016; Syeda et al., 2021), but they are located opposite the point of the maximum arc of dorsal curvature, which increases the flexor sheath's ability to prevent bowstringing of the long flexor tendon (Ayhan & Ayhan, 2020; Susman, 1979). These external morphological features are assumed to be advantageous for frequent flexed finger grasping of arboreal substrates of differing diameters in *Pongo*.

The *Pongo* IPs have a high degree of curvature as well and constrict distal to the base and widen at the FSRs. The length patterns of the IPs are variable and deviate from the pattern of the PPs, such that in some cases it can be either 3>4>2>5, or 3=4>2>5, or 4>3>2>5. IP4 has been observed to be more robust than IP3 and, in those cases, the second and third digits are inclined towards the midline (Susman, 1979).

1.5.6.b. *Gorilla*

Gorilla phalanges, both proximal and intermediate, are radio-ulnarly wide, stout, and relatively flat compared to *Pan* and *Pongo*, which is thought to reflect frequent knuckle-walking hand postures. They display a length pattern of digit 3>4>2>5 for both the proximal and intermediates. Overall, the bases of the PPs have marked tubercles for attachment of collateral ligaments and digits 2, 4 and 5 display asymmetrical bases (Susman, 1979; personal observations). On the base of PP2, the radial tubercle on the palmar surface extends proximally and serves as the

insertion point of the pennate portion of the first dorsal interosseous muscle, expanding the radial side and making the base asymmetrical (Susman, 1979). The base of PP4 is asymmetrical due to the insertion of the interosseous muscle, and the base of PP5 is small and asymmetrical because the ulnar side of the base protrudes to serve as the insertion site for the abductor and flexor digit minimi muscle. The palmar surface of the proximal phalangeal base projects above the palmar shaft, which serves to increase the moment arm of the long flexor tendons as they cross over the McP joint, making *Gorilla* locomotion efficient (Susman, 1979; Inouye, 1994; Matarazzo, 2008). The bases of the IPs are broad and well developed as the collateral ligaments for the PIP joint attach there. In the PPs and IPs, the FSRs span the majority of the length of the shaft and greatly extend from the palmar surface across digits 2-4. While the fifth digit is considerably smaller and more asymmetric than the radial three digits, the FSRs of digit 5 are still particularly prominent when compared to the other great apes. These pronounced FSRs may be a functional response that allows *Gorilla* to engage in arboreal behaviours (Susman, 1979). The trochlea of IP2 and IP4-5 are twisted towards the third digit (Susman, 1979).

1.5.6.c. *Pan*

Within the great apes, the phalanges of *Pan* show a greater degree of dorsopalmar curvature relative to *Gorilla*. The phalanges are longer, narrower, and have FSRs that are less prominent than *Gorilla*. They generally display a length pattern of digit 3>4>2>5 for the proximal and intermediate phalanges, although it is difficult to determine a length pattern for the intermediate phalanges as there are not many distinguishing features on the phalanges to accurately assign each to a specific digit, unless the hand is articulated (Susman, 1979; Patel & Maiolino, 2016). Chimpanzees and bonobos share most of these phalangeal morphological features, although there are subtle ways in which bonobos differ. The FSRs on bonobo phalanges are faint, if not absent and the trochlear sulcus on the head of the phalanges is also deeper than in chimpanzees (Susman, 1979). The greater degree of phalangeal curvature in *Pan* relative to *Gorilla* may reflect an increased degree of arboreality in their locomotor repertoire (Susman, 1979; but see Wallace et al., 2020). Interestingly, instead of the palmar surface of the shaft being concave due to the FSRs, the palmar shaft is actually raised above where the fibrous flexor sheaths insert (Patel & Maiolino, 2016).

1.5.6.d. *Homo sapiens*

Human proximal phalanges are typically gracile and lack dorsopalmar curvature and strong muscle markings (Susman, 1979; Patel & Maiolino, 2016). All these morphological features account for the reduced flexion of human fingers. The length pattern of human phalanges is similar to what has been observed in African apes, digit 3>4>2>5 (Susman, 1979). The human second and fourth digits can differ in length based on developmental conditions but can be distinguished. PP2 and PP4 both have a relatively robust body, but PP2 has an enlarged radial tubercle to accommodate the first dorsal interossei muscle on its dorsal aspect. PP4 does not have this basal asymmetry, but it does have more distinct FSRs on PP4. PP5 is the smallest human proximal phalanx, but the PP5 base has a robust appearance compared to its shaft because it is the insertion site for hypothenar muscles. The intermediate phalanges of humans follow a similar pattern to the proximal and have broad bases and variably defined insertions for the FDS.

1.6. Bone functional adaptation

1.6.1. Reconstruction of behaviour via external morphology

Despite numerous studies documenting the association between longitudinal phalangeal curvature and arboreal behaviours (Jungers et al., 1997; Matarazzo, 2008; Rein, 2011; Stern & Susman, 1983), the functional morphology of phalangeal curvature is still not fully understood. Interpreting this morphological feature is complicated by the fact that 'primitive' characteristics can be retained without the continuation of 'primitive' behaviour (Richmond et al., 2016; Ward, 2002). Furthermore, reconstructing behaviour using phalangeal curvature must also be considered within the context of other phalangeal morphological features (e.g., FSRs, median bar) and internal bony architecture (Marzke et al., 2007; Nguyen et al., 2014). For example, gibbons are highly suspensory yet they have lower levels of proximal phalangeal curvature than orangutans, while orangutans have thick cortices despite being highly curved (Richmond et al., 2016; Susman, 1979). The variation observed in the external phalangeal form is evidence that there are multiple ways in which an animal can optimize the strains incurred by their bones (Nguyen et al., 2014). Size and scaling might explain at least some of this variation, especially in regard to how substrate size and hand size influence finger flexion during locomotion. For example, primates with smaller hands might not use as highly flexed finger postures during locomotion as primates with absolutely larger hands because the size of the substrate is large relative to their hands (Richmond et al., 2016). Other hypotheses which try to explain the association between phalangeal curvature and locomotion state that curvature increases the surface area over which the palmar skin can contact the substrate, which would reduce muscular strains and allow the fingers to hold on to larger and more stable substrates (Hunt, 1991b). All of these hypotheses are centred around a functional link between the degree of curvature and suspensory locomotion. However, a recent study revealed the role genetic factors might play in the development of phalangeal curvature (Wallace et al., 2020). Wallace and colleagues (2020) measured the degree of curvature on the manual and pedal phalanges of a chimpanzee who was raised with little to no arboreal activity during its lifetime, and found that its curvature was indistinguishable from those of wild chimpanzees. While these results might lend some support to the hypothesis that phalangeal curvature is a primitive retention, this single individual does not refute the hypothesis that there is a biomechanical advantage to having curved phalanges. However, these results do suggest that phalangeal curvature should not be solely used to assess the importance and frequency of arboreal locomotion of fossil specimens.

1.6.2. Reconstruction of behaviour via internal morphology

Internal bone architecture can be divided into cortical and trabecular bone. Cortical (compact) bone encases the rest of the bony architecture and is responsible for providing structural support to the skeleton as it is relatively stiff due to its composition mainly consisting of inorganic hydroxyapatite (Currey, 2003, 2012). Trabecular (cancellous/spongy) bone has a sponge-like appearance and is located in the epiphyses of long bones and throughout short and flat bones (Currey, 2003). Both these types of bones are subject to changes that result from the external and internal loads experienced by the bone (Frost, 1987; Pearson & Lieberman, 2004; Ruff et al., 2006). The changes in bone microstructure in response to mechanical loading are commonly known as 'bone functional adaptation.' It is worth clarifying here that although bone functional adaptation is used throughout the literature and this thesis, in this instance, the word adaptation should not be confused with the biological definition of the word. In biology, adaptation refers to heritable traits that

natural selection acts upon, while bone functional adaptation is a response to an individual's environment and not a heritable trait. The differing use of the word adaptation may require some nuance to understand what is meant by 'bone functional adaptation'; however, this term accurately and entirely captures what is meant by changes in bone structure due to its mechanical environment, that other terms have failed to do so. Traditionally, this concept has been referred to as Wolff's Law, which was first conceptualized as a strict relationship between bone loading and deformation (Wolff, 1892). However, Wolff (1892) did not take into account the ability of bone to remodel throughout its life, which bone functional adaptation considers (Cowin, 2001; Cowin et al., 1985; Currey, 2003; 2012; Kivell et al., 2016; Lanyon & Rubin, 1985; 2006). Cortical bone adapts to the functional demands placed upon it by adjusting its thickness to provide better resistance against bending forces (Currey, 2003). Trabecular structure changes in regards to its thickness, orientation, and overall volume to optimize the transfer of kinetic energy away from joint surfaces (Barak et al., 2013a; Cowin et al., 1985; Currey, 2011; Keaveny et al., 2001; Reznikov et al., 2015; Sugiyama et al., 2010). Essentially both cortical and trabecular bone act in response to the stress in their mechanical environment by removing bone in skeletal areas where stress is low and adding bone where stress is high (Pearson & Lieberman 2004; Ruff et al., 2006; Tsegai et al., 2013).

Trabecular bone is porous, has a greater surface area, and increased number of bone cells which makes it more active than densely packed cortical bone (Currey, 2003; Jacobs, 2000). As such, trabecular bone remodels at a faster rate (25% turnover rate in adult humans) than cortical bone (2-3% turnover rate; Clarke, 2008; Eriksen, 1986; 2010). Therefore, trabecular bone is thought to reflect the variations in magnitude and direction of loading, and thus reflecting behaviour and function, more clearly than cortical bone (Barak et al., 2011; Jacobs, 2000; Kivell et al., 2016; Martin et al., 2010; Pontzer et al., 2006; Rubin et al., 2002; 2003). Experimental studies on trabecular remodelling (see Barak, 2019 for a discussion on bone modelling vs. remodelling) have revealed how trabecular bone is affected by changes in loading configuration and/or habitual behaviours (Barak et al., 2011; Biewener, 1996; Pontzer et al., 2006; Ryan & Walker, 2010; Ryan & Shaw, 2012). Investigation of variation in trabecular structure across individuals or species can reveal functional (and thus, behavioural) differences in how bones and/or joints of the individual/species were being loaded during its life (Kivell et al., 2016). Understanding the variation in trabecular bone can reveal novel functional information that cannot be understood from external morphology alone.

The hand, and in particular the fingers, make direct contact with the substrate during locomotion so their trabecular structure should provide a clearer functional signal than the trabecular architecture of skeletal elements that are further removed from the substrate. However, comparative studies of trabecular architecture of the hand are limited compared with studies of the femur and humerus (Fajardo et al., 2002; 2007; Ryan & Ketcham 2002a; 2002b; 2005; Ryan & Shaw 2012; Ryan & Walker, 2010; Scherf et al., 2016). Trabecular studies of the hand have focused on the metacarpals and carpals (Barak et al., 2017; Bird et al., 2022; Dunmore et al., 2019; Kivell et al., 2011b; Lazenby et al., 2008a; 2008b; 2010; 2011; Schilling et al. 2014; Skinner et al., 2015a; Stephens et al., 2016), with a particular focus on the third metacarpal (Chirchir et al., 2017; Matarazzo, 2015; Tsegai et al., 2013; Zeininger et al., 2011). The trabecular architecture in the MC3 head has shown a clear link between trabecular structure and locomotor manual postures in extant hominids. The dorsal and palmar loading and hyperextension of the McP joint during knuckle-walking, along with the flexed-finger postures during climbing in African apes results in high trabecular bone volume on the dorsal surface of the MC heads and anisotropic patterning of the trabeculae (Chirchir et al.,

2017; Matarazzo, 2015; Tsegai et al., 2013). In contrast, humans show overall low trabecular bone volume, consistent with loading the hands during manipulation only, and a lower degree of anisotropy suggesting variable loading during manipulation (Stephens et al., 2018; Tsegai et al., 2013). The trabecular bone variables for the suspensory Asian apes fall in between those of the knuckle-walking African apes and the bipedal humans (Chirchir et al., 2017; Tsegai et al., 2013). Dunmore and colleagues (2019) confirmed the results of these studies and expanded on them by revealing the trabecular structure of all metacarpals varies in relation to the habitual locomotor repertoire of extant hominids.

In comparison, the trabecular structure of the manual phalanges remains understudied. To date, there have only been two studies that have explored the trabecular architecture in manual proximal and intermediate phalanges (Matarazzo, 2015; Stephens et al., 2018). Matarazzo (2015) analysed the trabecular architecture at the epiphysis of metacarpals, proximal phalanges, and intermediate phalanges of the third ray in extant hominoids and macaques, the results of which are summarised here. The pattern of trabecular orientation at the proximal ends of the three bones varied in relation to the habitual locomotor repertoire of the study sample (suspension, quadrupedalism, and knuckle-walking). The suspensory primates had a proximodistal alignment of trabecular bone, predicted to mitigate the tensile forces placed upon the digits during suspension. For the knuckle-walking African apes, it was predicted that the proximal and distal end of the phalanges would have a palmo-dorsal alignment of the trabeculae to resist the high compressive forces that are placed upon them during knuckle-walking. However, the trabeculae at the proximal end of the proximal and intermediate phalanges are oriented proximo-distally and the trabeculae at the distal end are oriented palmo-dorsally (Matarazzo, 2015). Measures of pressure outputs during knuckle-walking have revealed the intermediate phalanges experience increased pressure throughout the bone, so it is unclear as to why the orientation of the trabeculae is different at the two ends (Matarazzo, 2013). An explanation of this variation in trabecular orientation could be that in instances in which these apes participate in suspensory behaviors, the phalanges experience strong enough tensile force that the trabecular bone on the proximal ends is remodelled. Since the external morphology of the phalanges has adaptations for knuckle-walking (Susman, 1979; Matarazzo, 2008; Patel & Maiolino 2016), this adjustment in the trabeculae might be needed so that these apes are able to participate in suspensory behaviours as well. While Matarazzo (2015) demonstrated the effectiveness of trabecular orientation in differentiating different locomotor behaviours in the phalanges of the third digit, other variables of trabecular bone in the phalanges failed to distinguish between locomotor behaviours.

Understanding how trabecular bone is structured in human proximal and intermediate phalanges will allow us to understand how the bone (re-)models itself under the biomechanical demands of manipulatory behaviours and help us recognize signals of manipulation in fossil hominins. Stephens and colleagues (2018) documented the variation in the structure of trabecular bone in the human hand. Results from their analyses revealed the distal portions of the phalanges and the distal segments of digits had a greater volume of trabecular bone (e.g., trabecular bone volume was higher in the intermediate phalanx compared to the proximal phalanx and the trabecular bone volume is higher in the head than in the base of the same phalanx; Stephens et al., 2018). These results are contradictory because they confirm previous biomechanical studies on the phalanges, which have revealed the distal portion of the phalanges experience higher forces and contact pressures during manipulation and power grasping (Kargov et al., 2004; Stephens et al.,

2018; Williams et al., 2012), but conflict with results from biomechanical modelling and validation studies. Biomechanical models show higher internal joint forces in the proximal regions of the phalanges due to the larger soft tissue structures and joint surfaces relative to the distal end (An et al., 1983; 1985; Stephens et al., 2018). This inconsistency in the distribution of trabecular bone in the phalanges could be attributed to variation in hand postures during manipulation (Diogo et al., 2012; Marzke, 2013; Rafferty & Ruff, 1994; Ruff, 2000; Stephens et al., 2018). The work of Matarazzo (2015) and Stephens and colleagues (2018) are important initial forays into phalangeal trabecular structure but use different methods, further work on hominid phalangeal trabecular bone using the same methods needs to be conducted to understand (re-)modelling of trabecular architecture in the fingers under different locomotor modes and manipulatory behaviours.

Just as trabecular bone provides us with information regarding the loading patterns on the skeleton and its joints, analysis of cortical bone can do the same. The compressive strength of cortical bone is determined by how dense it is (Currey, 2003). Variation in cortical thickness arises as a response to how the joints are being loaded and the magnitude of habitual loading (Currey, 2003; Frost, 1987; Ruff et al., 2006), since cortical bone is also able to (re-)model during life in response to mechanical load (Pearson & Lieberman 2004; Ruff et al., 2006). Studies evaluating patterns of habitual loading in relation to cortical bone have revealed that regions that are most heavily loaded typically have thickened cortex (Carlson & Patel, 2006; Carlson et al., 2013; Hoobergen et al., 2002; Lewis et al., 2005; Patel & Carlson, 2007). Cortical bone adapts to changes in loading through changes in mineralisation to adapt its stiffness, changes in overall shape to resist loads, or by increasing its thickness (Currey, 2003). These changes in cortical bone are dependent upon the location of the skeletal element, systemic factors, and the magnitude and frequency of strain placed upon the bone cells (Frost, 1987; Pearson & Lieberman, 2004; Ruff et al., 2006). Cortical bone in the diaphysis of long bones can withstand a greater amount of force before deformation compared to the trabecular bone, which has a more dynamic response to loading (Currey, 2003). This dynamic (re-)modelling of trabecular bone works to support cortical bone as it resists fractures during loading (Currey, 2003; Pearson & Lieberman, 2004). The directionality of the stress on the diaphysis results in bone deposition in the same direction, changing the overall shape of the bone in the region being loaded (Pearson & Lieberman, 2004; Ruff et al., 2006). Cortical bone is usually studied through analysis of cross-sectional geometric properties as they are good measures of the strength and rigidity of a bone (Patel et al., 2020; Ruff & Runstead, 1992; Schaffler et al., 1985). There have been a great number of studies on the cross-sectional geometry in several different skeletal elements (Carlson, 2005; Carlson et al., 2006; Marchi, 2005; Ruff, 2000; 2002; 2003; Ruff et al., 2013; Sarringhaus et al., 2005; Shaw & Ryan, 2012; Shaw & Stock, 2013), but studies on the phalanges remain relatively rare. An early study by Doden (1993) on the cortical structure of gibbon and human phalanges noted a functional relationship between manual behaviours and the shape and density of cortical bone. Although studies of cortical and trabecular bone are rare for manual phalanges, there is enough evidence for the functional adaptation of internal bone structure to incurred loads so it needs to be explored in primate fingers to provide a clear functional link between hand use and morphology.

1.7. Evolution of the hominin hand: fossil evidence

Hominin hands are represented in the fossil record from at least six million years ago (mya) but these fossils are typically found in isolation, making it difficult to reconstruct the evolution of

modern human dexterity. While the fossil record is relatively sparse, it is clear that the hominin hand evolved in a complex and mosaic manner (Kivell, 2015; 2016; Kivell et al., 2022). Human hand evolution is characterized by a functional shift from a hand being used primarily for locomotion to an increasing degree of dexterous manipulation. This transition was not a linear process and most likely occurred with the gradual abandonment of arboreal locomotion and the rise of manipulatory behaviours. Despite the limited amount of hand fossils, hominin hand fossils display an astounding amount of morphological variation, suggesting that different hominin species had different locomotor repertoires and manipulative abilities.

Within the fossil record of the hominin hand, the phalangeal remains also show a great degree of variation and a combination of primitive and derived features. Understanding the functional implications of this variability and unique combinations of morphology will help us reconstruct fossil behaviours and provide a finer overview of hominin evolution. Thus, below I review the current knowledge on the overall locomotor repertoire and manual behaviours and morphology of the fossil hominins studied in this thesis. Detailed analysis of hand morphology and function of each species is reviewed in Chapter 6.

1.7.1. *Australopithecus afarensis*

The locomotor repertoire of *Australopithecus afarensis*, an East African hominin dated to around 4.2 – 2.9 mya, is characterised by habitual bipedalism alongside arboreal behaviours (Alemseged, 2023; Ward, 2002). Features of the lower limb, such as the presence of lumbar lordosis, large femoral heads, valgus angle of the knee, and a short, broad and sagittal-oriented pelvis, as well as fossilised footprint, are evidence of bipedality in this fossil hominin. However, features of the upper limbs, including their relatively long length, a superiorly oriented glenoid fossa of the scapula, large supraspinous fossa, and curved phalanges demonstrate the arboreal capabilities of *A. afarensis* (Green & Alemseged, 2012; Green et al., 2007; Ward et al., 2012). Regarding, *A. afarensis* hand morphology, the estimated intrinsic portions (from several isolated elements) have been argued to be human-like and capable of forceful precision grips, which would have facilitated tool use (Alba et al., 2003; Marzke, 2013), but others have estimated gorilla-like proportions with a limited ability to produce precision grips (Rolian & Gordon, 2013). The orientation of the carpometacarpal articulations provides further evidence for the dissipation of loads associated with forceful precision grips (Marzke, 1997; Tocheri et al., 2008). This morphology is concomitant with a relatively gracile first metacarpal, strong FSRs, and African ape-like phalangeal curvature (Bush et al., 1982; Jungers et al., 1997; Susman, 1979; Susman, 1994; but see Wallace et al., 2020). The mosaic external features of the *A. afarensis* hand show affinities with both great apes and humans, indicating a hand capable of dextrous manipulation but also arboreality (Alba et al., 2003; Gebo, 1996; Stern, 2000; Stern & Susman, 1983; Ward, 2002). The contemporaneous presence of stone tools (Harmand et al., 2015; Lewis & Harmand, 2016; McPherron et al., 2010) suggests some level of dexterous, manipulative abilities, but musculoskeletal modelling from a singular study has shown *A. afarensis* carpometacarpal morphology of the fifth digit would have made this difficult (Domalain et al., 2017).

1.7.2. *Australopithecus africanus*

A. africanus is a Southern African australopith dated to around 3.3 – 2.1 mya (Alemseged, 2023). The *A. africanus* bauplan is largely similar to what has been observed in *A. afarensis*, with

the upper limb showing external morphology associated with arboreal behaviours and the lower limb indicating habitual bipedality. The limb proportions and size of limb joints of *A. africanus* have revealed the relatively more ape-like morphology of the *A. africanus* skeleton compared to *A. afarensis* (Green et al., 2007). Furthermore, studies of the internal structure of the humerus in *A. africanus* have shown evidence for arboreal adaptations (Kivell et al., 2018c). Within the lower limb, studies of the *A. africanus* femoral head and distal tibia show human-like hip loading and an extended lower limb bipedal gait, respectively (Barak et al., 2013b; Ryan et al., 2018). The hand remains also demonstrate these mosaic morphologies (Kivell et al., 2020; Pickering et al., 2018). The wrist and metacarpals show external morphology that is intermediate between modern humans and great apes (Green & Gordon, 2008; McHenry, 1983), while overall hand proportions from isolated remains have been estimated to be more human-like than ape-like (Ostrowsky & Richmond, 2015). The internal structure of the metacarpals reveals a human-like pattern of trabecular bone distribution suggesting *A. africanus* was capable of forceful human-like precision grips (Kivell et al., 2020; Ostrowsky & Richmond, 2015; Skinner et al., 2015). The phalanges, however, are ape-like in their external morphology, with robust shafts and an intermediate degree of curvature (Kivell et al., 2020).

1.7.3. *Australopithecus sediba*

A. sediba is a late Pliocene Southern African australopith represented primarily by two individuals, Malapa Hominin 1 (MH1) and Malapa Hominin 2 (MH2), dated to around 1.98 mya (Dirks et al., 2010). MH1 is considered a juvenile male and MH2 a female adult (Berger et al., 2010). The upper limb possesses primarily primitive morphology, while the lower limb displays a mix of primitive and derived morphology (Berger et al., 2010; Churchill et al., 2013; 2018; DeSilva et al., 2018; Zipfel et al., 2011). Similar to other australopiths, the pelvis and lower limb of *A. sediba* indicate bipedality but the ape-like morphology of the foot indicates some ability for climbing and a bipedal gait distinct from that of humans (DeSilva et al., 2018; Zipfel et al., 2011). The upper limb has relatively long forearms and a superiorly oriented glenoid fossa that are advantageous for arboreal behaviours (Berger et al., 2010; Churchill et al., 2013; 2018). However, the hand displays a mixture of primitive and derived features (Kivell et al., 2011; 2018). The nearly complete right hand of MH2 shows a mix of ape-like and human-like morphology of the wrist, gracile metacarpals that suggest limited force production, curved phalanges with prominent FSRs, but also modern human-like hand proportions that would have facilitated human-like precision grips (Kivell et al., 2011; 2018). The internal structure of the wrist and the metacarpals also provides us with mosaic signals, with the wrist and thumb suggesting modern human-like loading, while the palm suggests habitual use of flexed-finger postures associated with locomotory grasping (Bird et al., 2023; Dunmore et al., 2020b). Evidence of locomotor grasping of the palm is consistent with the external morphology of the phalanges that possess curvature and prominent FSRs (Kivell et al., 2018a). The unique mix of primitive and derived characteristics has not been observed in any other known hominin, with the prominent FSRs and lack of median bar of the curved intermediate phalanges being especially unique. Overall, the morphology of the hand of *A. sediba* reveals that this species was probably capable of using their hands for power grasping during locomotion and for precise manipulation used for tool-related behaviours (Bird et al., 2023; Dunmore et al., 2020b; Kivell et al., 2018a).

1.7.4. *Homo habilis*

Remains of *Homo habilis* are found across East Africa and are dated to around 2.3 – 1.65 mya (Spoor et al., 2015). Olduvai (Oldupai) Gorge in Tanzania, East Turkana in Kenya and the Omo River Valley in Ethiopia have yielded cranial and postcranial remains attributed to *H. habilis* but with limited associated remains (OH 7, Leakey et al., 1964; OH 62, Johanson et al., 1987). The majority of the postcranial remains were found at the Olduvai Gorge site FLK and FLK NN (Leakey et al., 1964). The OH 8 foot, OH 35 lower limb, OH 62 upper and lower limb, and the OH 7 hand represent the postcranial remains associated with *H. habilis*, the morphological variability of which has caused debate regarding the functional abilities and taxonomic attribution of this species (DeSilva et al., 2019; Patel et al., 2018; Susman & Stern, 1982; Susman, 2008). The OH 62 remains reveal the upper limb of *H. habilis* was relatively longer and robust compared to the lower limb, supporting the arboreal abilities of this hominin (Ruff, 2009 but see Haeusler & McHenry, 2004). In contrast, the OH 35 lower limb is most similar to modern humans within the extant great apes, lacking climbing adaptations present in the African ape leg (Susman, 2008; Susman & Stern, 1982). This morphology of the *H. habilis* leg is consistent with the OH 8 foot, as it possesses modern human-like features, such as an adducted hallux and longitudinal arch, but also a unique talus morphology and a distinct loading pattern which indicates a bipedal gait different from what is observed in humans (DeSilva et al., 2019; Patel et al., 2018; Susman & Stern, 1982). The derived morphology of the OH 35 and OH 8 remains have led to some researchers proposing that they belong to the same individual (Susman, 2008; Susman & Stern, 1982), however some contest this due to the differing joint morphology of the remains (Aiello et al., 1998; DeSilva et al., 2019; Wood et al., 1998)

The OH 7 hand belongs to a juvenile individual and is represented by two fragmentary proximal phalanges, four intermediate phalanges lacking their proximal epiphysis, three distal phalanges, the base of the second metacarpal, a trapezium, and a scaphoid (Leakey et al., 1964; Napier, 1962a; Susman & Creel, 1979). The morphology of the wrist bones and the distal phalanges is considered advantageous for precision gripping (Susman, 2008; Susman & Creel, 1979; Trinkaus, 1989), while robust, curved, African ape-like phalanges with prominent lateral fossae and FSRs reflect the capacity for *H. habilis* arboreal behaviours (Susman & Creel, 1979).

As discussed earlier, lateral fossae and FSRs are thought to be insertion sites for the flexor digitorum superficialis (FDS) muscle tendon and as such their prominence is interpreted as evidence of arboreal behaviours (Begun et al., 1994 but see Marzke et al., 2007). These features are generally prominent in great ape adults and not subadults, which is why the prominent lateral fossae and FSRs of the juvenile intermediate phalanges made OH 7 such a remarkable specimen upon its discovery. To interpret the unique morphology of the OH 7 phalanges, Susman and Stern (1979) performed electromyographic studies on a small sample of chimpanzees to explore the role of the long digital flexors in the African ape locomotor repertoire. Results revealed that both the FDS and flexor digitorum profundus (FDP) muscles are not active during knuckle-walking or in other forms of quadrupedal locomotion. There is slight activation of these muscles when quadrupedal locomotion is fast, while they are maximally activated throughout suspension (Susman & Stern, 1979). Thus, the prominent lateral fossae and FSRs in the OH 7 hand could be a result of the suspensory behaviours of *H. habilis*. However, recent studies conflict with the assumption that the morphology of muscle attachment site reflect the size and use of muscle (Marzke et al., 2007; Williams-Hatala et al., 2016). Another possible explanation for the prominent markings of the OH 7 intermediate phalanges could be due to manipulation. The FDS shows signs of activation during manipulatory activities in which the object is held tightly (Susman & Stern, 1979). However,

regardless of whether or not OH 7 was using its fingers for manipulation, it is unlikely that the manipulative capabilities of the OH 7 subadult individual would have surpassed those of modern humans, and modern humans do not show such strong insertions of the FDS muscle (Susman & Creel, 1979). If we couple the strong lateral fossae of the OH 7 intermediate phalanges and the estimated curvature of the proximal phalanges, it would be reasonable to interpret these morphological features as evidence of strong locomotory grasping abilities, with some evidence for manipulation as well.

1.7.5. *Homo naledi*

H. naledi was discovered in the fossiliferous Rising Star Cave system in South Africa, dated to around 300 thousand years ago (kya; Dirks et al., 2017). The 15+ individuals that represent *H. naledi* generally display a derived lower limb and a primitive upper limb (Feuerriegel et al., 2017; 2019; Harcourt-Smith et al., 2015; Marchi et al., 2017; Traynor et al., 2022). Within the lower limb, strong muscular entheses and a valgus knee evidence adaptations to habitual bipedality. Furthermore, the foot shows adaptations to striding, long-distance bipedalism due to an adducted hallux, human-like ankle joint and metatarsal morphology, and a stiff midfoot. However, the pedal phalanges are curved, which allows for greater flexion of the toes potentially related to toe grasping behaviours (Berger et al., 2015; Harcourt-Smith et al., 2015). Within the upper limb, a superiorly oriented glenoid fossa, low humeral torsion, and a wide thorax is interpreted as evidence of the importance of climbing and suspensory behaviours in the locomotor repertoire of *H. naledi* (Berger et al., 2015; Feuerriegel et al., 2017; 2019). The combination of derived and primitive morphology in the upper limb and lower limb of *H. naledi* is also present in Hand 1, a nearly complete, associated right hand. External morphology of the wrist, robust appearance of the first metacarpal, a broad distal pollical phalanx, and modern human-like thumb and finger proportions indicate *H. naledi* possessed a strong thumb and a hand that was able to perform forceful precision grips (Bowland et al., 2021; Kivell et al., 2015). The phalanges, on the other hand, have a high degree of phalangeal curvature, prominent FSRs on the intermediate phalanges, and longer phalanges relative to metacarpals (Kivell et al., 2015). This phalangeal morphology is consistent with features of the upper limb, all of which emphasize the continued importance of climbing behaviours in *H. naledi*.

1.7.6. *Homo floresiensis*

H. floresiensis is a diminutive hominin species from the island of Flores in Indonesia, dated to around 100 – 60 kya (Sutikna et al., 2016). *H. floresiensis* was first represented by a nearly complete skeleton of specimen LB1, with further excavations revealing more individuals attributed to *H. floresiensis*. The overall combination of upper and lower limb morphology is unique within the fossil hominin record. The lower limb morphology clearly marks *H. floresiensis* as an obligate biped, but potentially with unique kinematics and kinetics (Brown et al., 2004; Jungers et al., 2009b). That is due to the relatively long foot compared to the lower limb, relatively longer toes when compared to humans, and a lack of longitudinal arch (Jungers et al., 2009a). There is no clear indication of features associated with arboreal behaviours in the upper limb. The bones of the upper limb are generally robust compared to their length, and the scapula resembles a human-like condition, with a humerus that displays low levels of torsion (Larson et al., 2007; 2009; Morwood et al., 2005), which are all features that would not have allowed for overhead arm movements. The hand of *H. floresiensis* is only represented by elements of the wrist, phalanges, and fragmentary metacarpals (Larson et al., 2009). The external and internal morphology of the *H. floresiensis* carpus reveal a

primitive, ape-like wrist lacking anatomy considered adaptive for efficient, forceful tool use (Bird et al., 2023; Orr et al., 2013; Tocheri et al., 2007; 2008). The phalanges of *H. floresiensis* display phalangeal curvature values ranging from modern human-like to *Gorilla*-like, variably prominent FSRs, and with radioulnarly broad apical tufts on the modern human-like distal phalanges (Larson et al., 2009). The mixture of these morphologies do not paint a clear picture of the manual behaviours of *H. floresiensis*, but there are stone tools found in association with *H. floresiensis* remains which indicate the manipulative abilities of fossil hominin (Brumm et al., 2006). Further analysis on upper limb and manual remains is needed to determine the arboreal capacity, if any, of this fossil hominin.

1.7.7. *Homo neanderthalensis*

The locomotor and behavioural repertoire of *H. neanderthalensis* is largely thought to be similar to modern humans due to morphological similarities in the skeleton of the two species. However, there are subtle morphological differences between the two species and the variable archaeological record associated with each species that warrant discussion of Neanderthal behaviour independent of modern humans. Generally, the Neanderthal skeleton has a wider body with relatively shorter limbs, robust long bones with thick cortices and rugose muscle attachment sites, and a wider pelvis when compared to humans. Explanations for the increased robusticity of the Neanderthal skeleton compared to humans include adaption to different climatic conditions and variable activity patterns (Ocobock et al., 2021; Wore et al., 2018). As Neanderthals span a large geographical range, morphological variability is also observed within different Neanderthal populations (Rosas et al., 2006). As such, coupling the behaviour of Neanderthals and *H. sapiens* in a wider discussion of fossil hominin behaviours is an oversimplification. This is apparent in comparisons of Neanderthal hand morphology to modern human hands. Neanderthal hands are more robust, have differing carpal, metacarpal, and phalangeal morphology, and differing carpometacarpal joint articulations, all of which most likely reflect the differences in manual behaviours. Studies of the external and internal morphology of the Neanderthal hand have provided some support for the preference for power grips compared to the precision grips typically employed by humans (Bardo et al., 2020; Bird et al., 2023 but see Karakostis et al., 2018). However, it is important to acknowledge that fossil *H. sapiens* and Neanderthals produced and used similar tools, which probably involved a mixture of precision and power grips. Thus, any differences in Neanderthal and *H. sapiens* morphology most likely resulted in biomechanical disadvantage of performing certain grips efficiently in Neanderthals, with a preference towards power grips. However, more work on the external and internal morphology is needed to determine whether the differences observed are functional.

2 – Methods and materials

2.1. Materials

2.1.1. Sample

2.1.1.a. Extant sample

This thesis analysed the cortical structure of proximal and intermediate phalanges of digits 2–5 of the hand of extant great apes and fossil hominin species. This was done using micro-computed tomography (micro-CT) scans of individual phalanges from 92 extant great ape individuals (*Pongo* = 9, *Gorilla* = 25, *Pan* = 24, and *Homo* = 33). A full set of associated proximal and intermediate phalanges from the same individual's hand was a rare occurrence in our sample (34%), but a larger percentage (71%) of the individuals preserved all four associated proximal phalanges. In some cases, the missing data for associated phalanges was available but not suitable for the methodological approach (described below). When selecting specimens for data analysis, care was given to ensure sample sizes across the extant great apes were similar but also substantial enough to provide robust statistical power. Consideration was also given to produce a sample that had a well-balanced sex and right-to-left hand ratio. However, since the sample size is limited to what is available and accessible in museum osteological collections, similar sample sizes could not be achieved for all extant species (particularly for *Pongo*).

2.1.1.a.1. Non-human great apes

Data collection includes micro-CT scans of a total of 608 individual hominid phalanges, details of which are available in **Table 2.1**. Below is a general summary of our non-human great ape (hereafter referred to as great apes) sample. The orangutan sample includes two *Pongo abelli* individuals and seven *Pongo pygmaeus* individuals. Six of the *P. pygmaeus* individuals have all associated proximal and intermediate phalanges of digits 2–5, with a pathology on one individual's fifth intermediate phalanx. The remaining three *Pongo* individuals only have associated proximal phalanges, with one *P. pygmaeus* individual missing the fifth proximal phalanx. The *Gorilla* sample includes 25 *Gorilla gorilla* individuals, all of which have associated proximal and intermediate phalanges available except for one individual, which is missing all four proximal phalanges. However, only nine *Gorilla* individuals (34%) have a complete set of eight associated phalanges. Some *Gorilla* specimens were not analysed due to methodological issues (described below). The *Pan* sample includes 24 individuals, with 18 individuals having all eight associated phalanges and, from those, the complete set of phalanges could be analysed in 13 individuals. The remaining five *Pan* individuals have similar methodological constraints as the *Gorilla* specimens. All great apes were wild specimens with no signs of pathology, except for the one *Pongo* individual. Details regarding the institutions where these specimens are curated are listed in Table 8.1 of the Appendix.

2.1.1.a.2. *Homo sapiens*

As modern humans occupy a large spatio-temporal range, with diverse manual behaviours across time and place, our modern human sample includes individuals from a diverse set of populations. These populations are very broadly characterised as pre-industrial and post-industrial, based on the approximate intensity of manual behaviours as those differences could potentially be reflected in the internal structure of the phalanges. Dividing these individuals into

these two broad categories is an oversimplification. However, since there is no individual behavioural information associated with these samples, it is hoped that these broad categorisations will capture general variation in activity levels. The pre-industrial group includes four individuals from 6th – 11th century Nubian Egyptians, three individuals from 19th century Tierra del Fuego, an indigenous Inuit from Greenland and two Aboriginal Australians. This sample also includes four fossil *H. sapiens* individuals, which are described in more detail below. The post-industrial populations include two individuals from 20th century Syracuse, Italy, five individuals from 18th–19th century Inden, Germany, and at least seven individuals from 16th century crewmen of the Mary Rose warship. Details regarding the institutions where these specimens are curated are listed in Table 8.1 of the Appendix. In the subsequent chapters, results and discussions of pre-industrial and post-industrial humans are studied together as they were not significantly differentiated. The only exception is in Chapter 5, where different Neanderthal populations were compared to humans as a whole and separately as pre-industrial and post-industrial populations.

2.1.1.b. Fossil hominin specimens

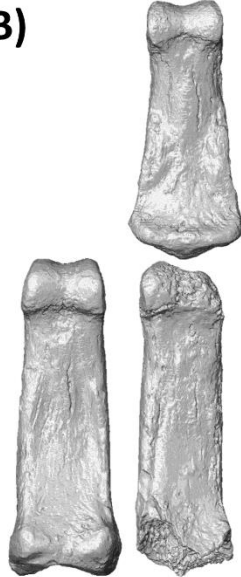
The goal of this thesis is to use the comparative hominid sample to infer the behaviours of fossil hominin specimens. Our sample of fossil hominins includes the following species: *Australopithecus afarensis* (~ 4.2 – 2.9 mya; Alemseged, 2023), *Australopithecus africanus* (~ 3.3 – 2.1 mya; Alemseged, 2023), *Australopithecus sediba* (~ 1.98 mya; Berger et al., 2010), *Homo habilis* (~ 1.8 mya; Leakey et al., 1964), potentially *Paranthropus robustus*/ Early *Homo* specimens from Swartkrans member 1 and 3 (~ 2.2 – 0.95 mya; Gibbon et al., 2014), *Homo naledi* (~ 300 kya; Dirks et al., 2017), *Homo floresiensis* (~ 100 – 60 kya; Sutikna et al., 2016), *Homo neanderthalensis* (~ 400 – 40 kya; Hublin, 2017; Krause et al., 2007), and fossil *Homo sapiens* (**Figs. 2.1-2.3**). The Neanderthal sample includes: the Tabun C1 individual (~ 122 kya; Grun & Stringer, 2000) and the Kebara 2 individual (~ 64 – 59 kya; Rebollo et al., 2011) from Israel, Feldhofer/Neanderthal 1 individual from Germany, and at least two individuals from El Sidron in Spain (~ 49 kya; Wood et al., 2013), and the La Ferrassie 2 individual from France (~ 43 – 45 kya; Guerin et al., 2015) (**Figs. 2.2-2.3**). The fossil *H. sapiens* including Qafzeh 8 and 9 (n=2 individuals, ~ 80 – 130 kya, Israel; Niewoehner, 2001), Ohalo II H2 (n=1, ~ 19 kya, Israel; Hershkovitz et al., 1995), Barma Grande (n=1, ~ 15 – 17 kya, Churchill & Formicola, 1997), Arene Candide (n=1, ~ 12 – 11 kya, Italy; Sparacello et al., 2021), Dolní Věstonice (n=4, ~ 31 – 29 kya, Czech Republic; Fewlass et al., 2019).

(A)



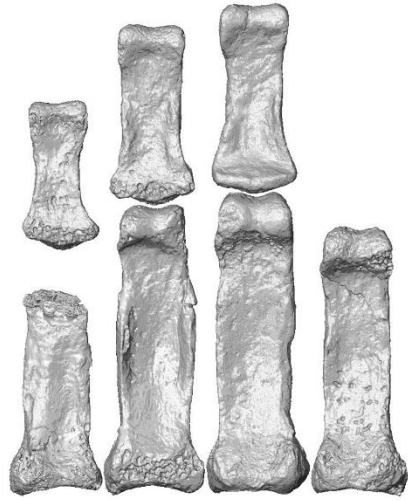
A. afarensis

(B)



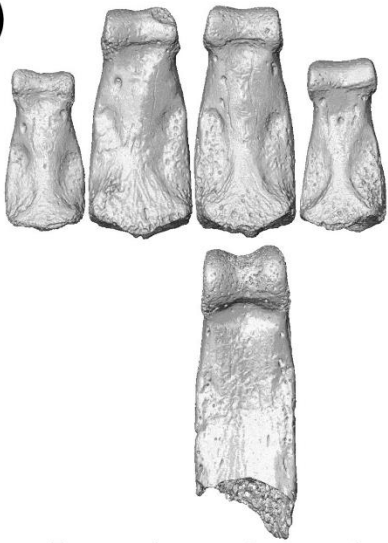
A. africanus

(C)



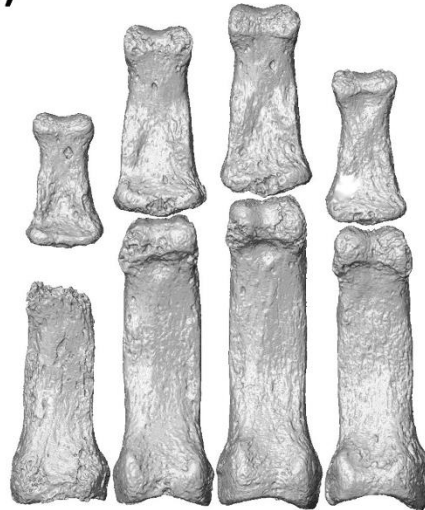
5 4 3 2
A. sediba

(D)



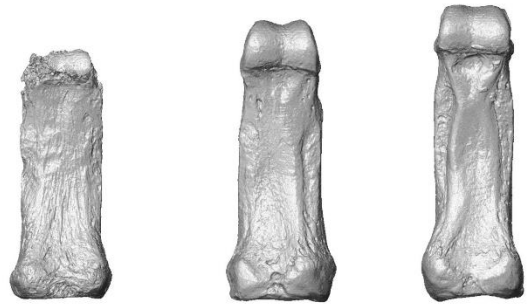
5 4 3 2
H. habilis

(E)



5 4 3 2
H. naledi

(F)



SKX 27431 SKX 5018 SKX 15468

Swartkrans hominins

5 mm

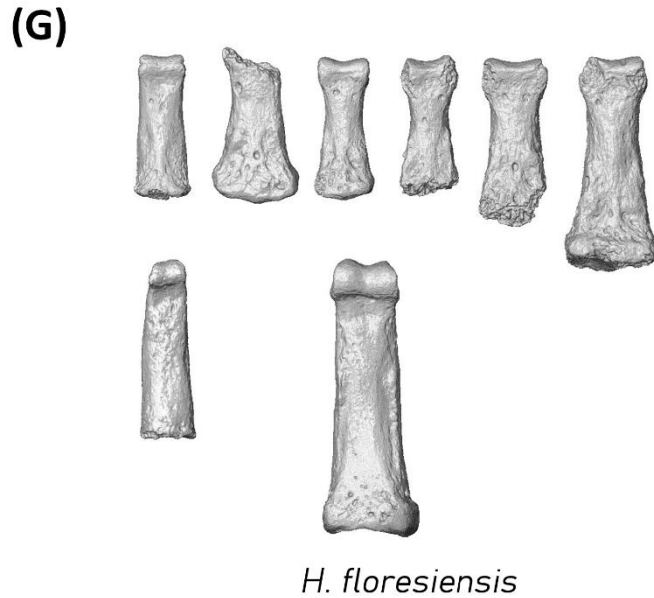


Figure 2.1: Surface models of proximal and intermediate phalanges of (A) *A. afarensis*; (B) *A. africanus*; (C) *A. sediba*; (D) *H. habilis*; (E) *H. naledi*; (F) Swartkrans hominins (either *P. robustus* or early *Homo*); and (G) *Homo floresiensis*. Phalanges of *A. afarensis*, *A. africanus* and Swartkrans hominins are isolated specimens with no digit attributed to them. *A. sediba*, *H. naledi* and *H. habilis* phalanges are associated hand remains, with digit numbers labelled under the phalanges. *H. floresiensis* phalanges are from multiple individuals, with no digit number attributed to them.

Preservation of these fossils is variable, with the majority of the specimens well preserved. Below we describe the fragmentary specimens. *A. africanus* specimen StW 122 is missing all of its proximal base and a portion of the trochlea (Kivell et al., 2020), but preserves enough of the shaft to be included in the analysis. *A. sediba* specimen MH2 includes all eight proximal and intermediate phalanges of a right hand, but the second intermediate phalanx was not included in the analyses because the shaft is fractured and encased in breccia (Kivell et al., 2018a). The proximal and intermediate phalanx of digit 4 of MH2 is complete but is missing cortex on the palmar surface of the base as well as the radial head of the trochlea. The fifth intermediate phalanx of MH2 was also missing some cortex on the palmar surface of the base. The OH 7 hand bones are those of a juvenile represented by four intermediate phalanges and two proximal phalanges (Leakey et al., 1964). The intermediate phalanges are thought to represent digits 2–5 and are complete apart from the (presumably unfused) proximal epiphysis and thus were included in all analyses. The proximal phalanges are thought to be attributed to digits 2 and 3 and are incomplete; specimen FLK NN–H (attributed to digit 3) preserves the distal half of the bone and was included in some analyses (see below), while specimen FLK NN–I (digit 2) preserves the trochlea and approximately 1/3 of the distal shaft and thus was excluded. Out of the three Swartkrans phalanges studied, only specimen SKX 27431 is not completely preserved (Susman, 1988a; 1989). SKX 27431 is missing the dorsal surface of the trochlea, but the shaft is well-preserved and does not impact our analyses. The *H. naledi* Hand 1 preserves almost a complete right hand with all proximal and intermediate phalanges of digits 2–5 (Kivell et al., 2015). The fifth

proximal phalanx was missing its trochlea and the second intermediate phalanx missing cortex on its dorsal surface, which was reconstructed in Geomagic 2015.1.3.

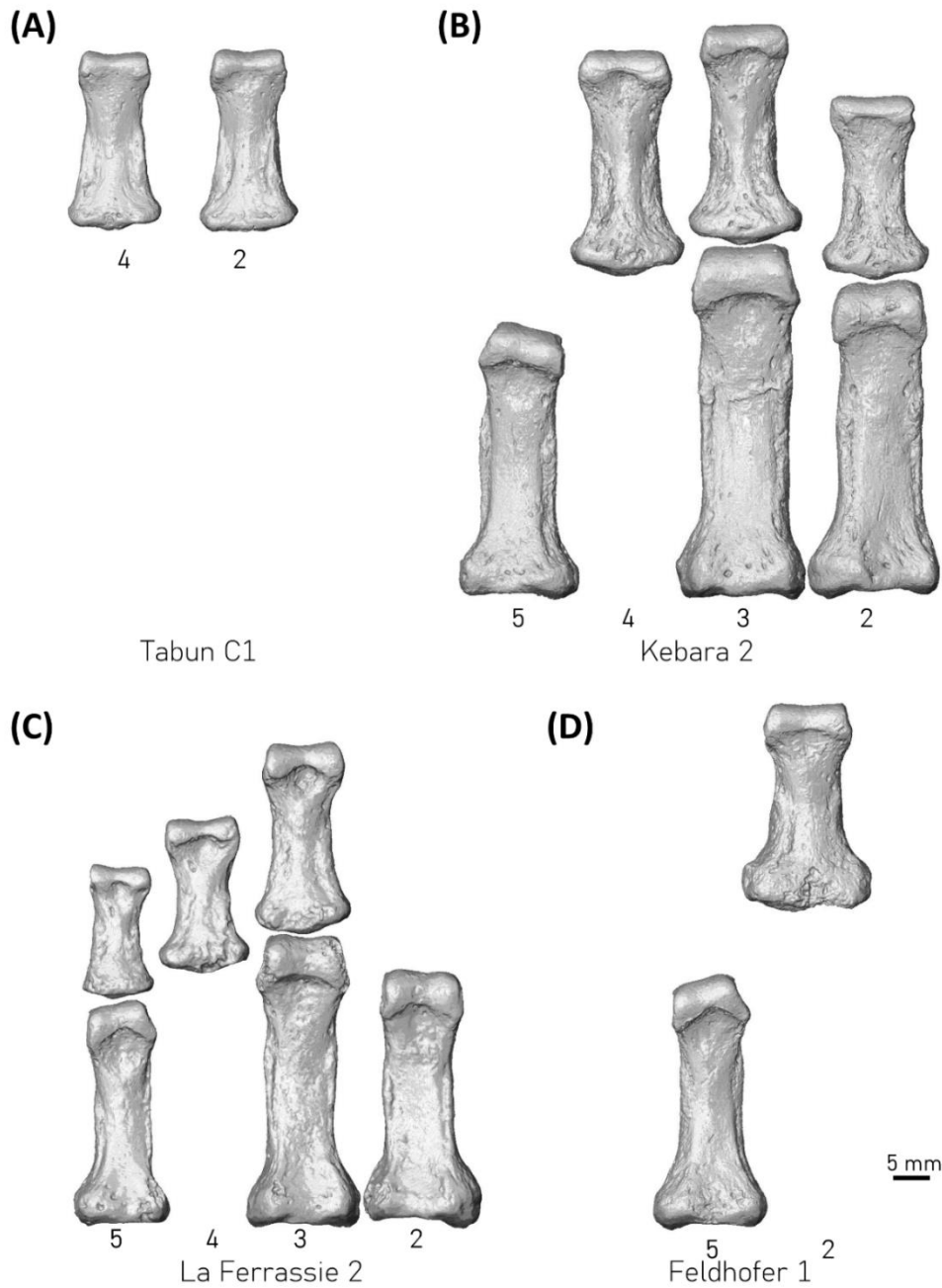


Figure 2.2: Surface models of proximal and intermediate phalanges of different Neanderthal populations (excluding El Sidron). (A) Tabun C1; (B) Kebara 2; (C) La Ferrassie 2; and (D) Feldhofer 1. Phalanges of Tabun C1 are presented by two intermediate phalanges and Feldhofer 1 by one proximal and one intermediate phalanges. Phalanges of Kebara 2 and La Ferrassie 2 are represented by their left- and right-hand phalanges to represent the most complete hand. The digit number assigned to the phalanges is listed under the images.

Within our Neanderthal sample, our El Sidron population was very well preserved. Specimens SD-083, SD-761, SD-777, SD-552, SD-619, SD-084, SD-352a, SD-787, SD-1015, SD-1071, and SD-607 were missing small fragments of bone on the trochlea and base of the phalanges but the missing fragments did not impact the analyses as they were not on the shaft. The remaining populations, which consisted of Kebara 2, Feldhofer 1, and Tabun C1, La Ferrasie 2 were all very well preserved. Unlike the majority of the fossil hominin sample included here, the morphology of the phalangeal remains of the Neanderthals included in this thesis have not been described in the literature but are depicted in **Figures 2.2-2.3**.

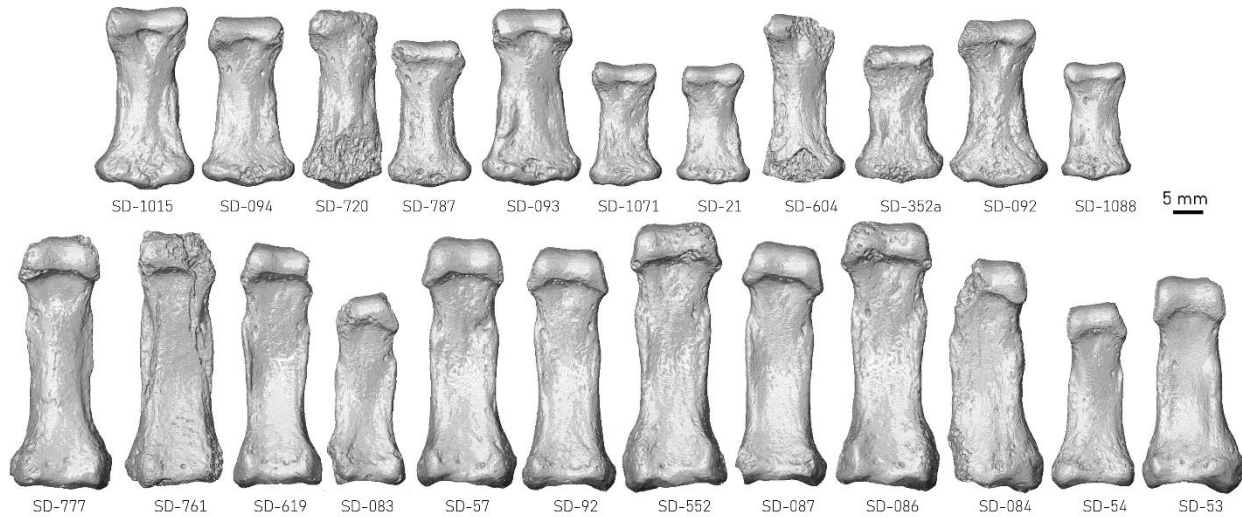


Figure 2.3: Surface models of proximal (bottom row) and intermediate phalanges (top row) of El Sidron Neanderthals.

2.1.2. Assigning isolated phalanges to a digit

Micro-CT scans of great ape individuals that had an associated set of proximal and intermediate phalanges made assigning a digit number to those phalanges straightforward. The external morphology of the phalanges has been well-described and relative length can distinguish which phalanges belong to which digit (Susman, 1979). When a full set of phalanges from digit 2-5 for either the proximal or intermediate phalanges was not present, length and morphological differences make it possible to assign the digit number to phalanges with reasonable certainty (Susman, 1979). These morphological differences are outlined in Chapter 1. Within modern humans, it is challenging to assign digit numbers as the morphological differences across the digits are not as distinct as the great apes. Generally, the third and fifth digits can be distinguished due to differences in size and symmetry of the bone, but the second and fourth digits are more difficult. We used minor variations in basal and trochlear morphology (Case & Heilman, 2006) to assign phalanges to particular digits, although when we could not confidently attribute a digit to the phalanx we did not include those phalanges in digit-specific analyses.

2.2. Methods

2.2.1. Micro-computed tomography

To image the internal structure of the phalanges, we used high-resolution micro-CT. Micro-CT scanning of the sample was conducted on several scanners: a BIR ACTIS 225/300, Diondo D3 or Skyscan 1172 scanner housed at the Department of Human Evolution, Max Planck Institute for Evolutionary Anthropology (Leipzig, Germany); a Nikon 225/XTH scanner at the Cambridge Biotomography Centre, University of Cambridge (Cambridge, UK); or with the Diondo D1 scanner at the Imaging Centre for Life Sciences at the University of Kent (Canterbury, UK). The scan parameters included acceleration voltages of 100–160 kV and 100–140 μ A using a 0.2 to 0.5 mm copper or brass filter. Scan resolution ranged between 0.014 mm to 0.048 mm depending on the size of the bone. Images were reconstructed as 16-bit TIFF stacks and then converted into 8-bit data. The reconstructed 16-bit TIFF stacks of micro-CT data from the Max Planck Institute for Evolutionary Anthropology and the University of Cambridge were readily available, while the micro-CT data from the University of Kent required processing to create the 16-bit TIFF stacks.

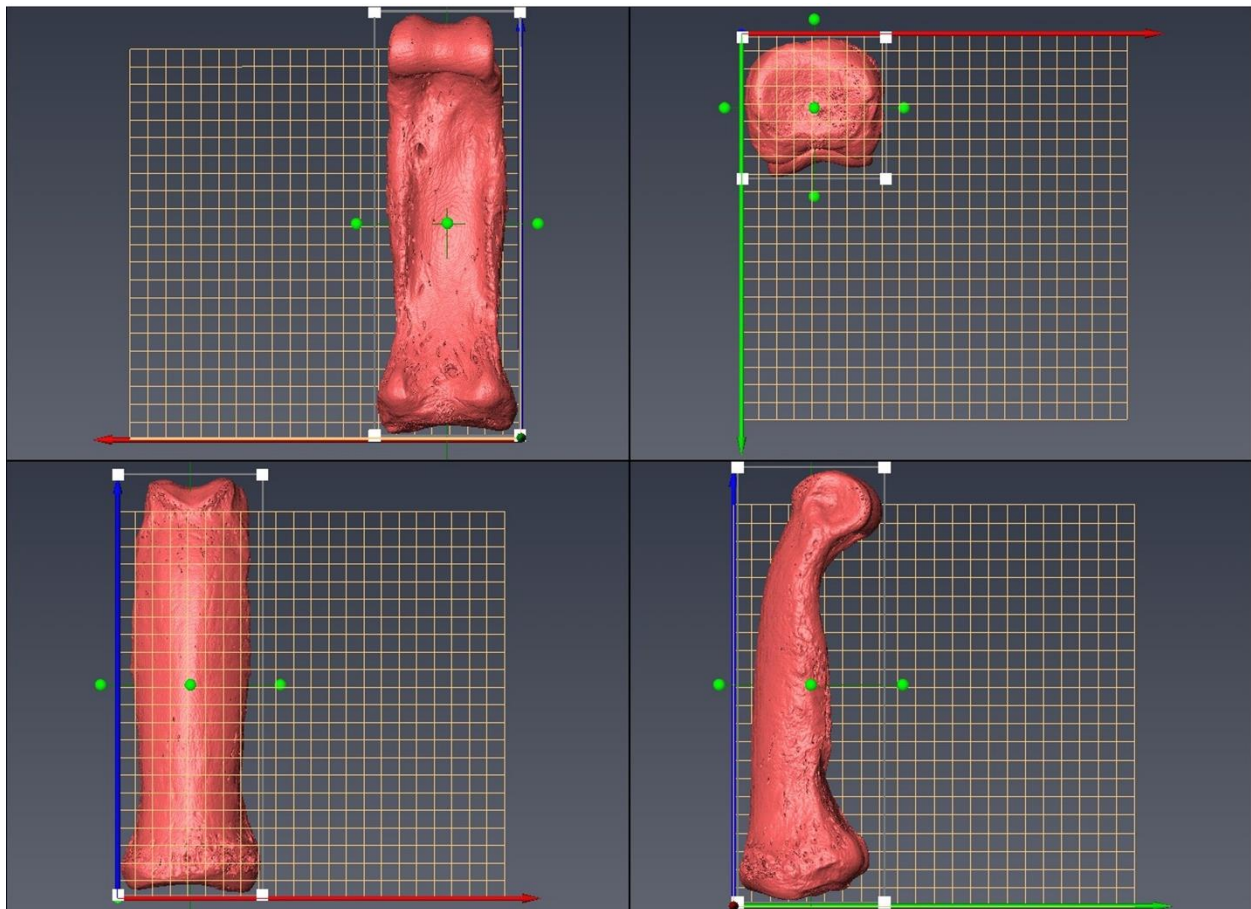


Figure 2.4: Image depicting the reorientation of a *Gorilla* third proximal phalanx.

2.2.2. Reorientation

Each TIFF stack of a phalanx was uploaded into Avizo 9.0.0 (Visualization Sciences Group, SAS) to be reoriented into the same anatomical orientation to ensure comparisons of homologous morphology. The radio-ulnar axis was aligned with the x-axis, the dorso-palmar axis was aligned with the y-axis and the proximo-distal axis was aligned with the z-axis, with the dorsal surface facing the origin (Fig. 2.4). The changes made to the data during reorientation were recorded for repeatability purposes in the future. After reorientation, the scans were cropped as close to the bone as possible to minimize the computing size of the files for further data processing. These files were saved in two formats: a Nifti (.nii) and 3D Raw (.RAW).

2.2.3. Segmentation

The reoriented Nifti files were used to segment these scans into binary files such that the only 'materials' in the scan file are 'bone' voxels and 'air/ background' voxels. Segmentation of the scans is necessary as it removes extraneous materials within the scans, especially within fossil specimens, such as soft tissues, curatorial substances used for preservation, soil matrix, or any other non-bone material included in the bone over time/fossilization process. Segmentation of the data was conducted using medical image analysis (MIA)-clustering algorithm (Dunmore et al., 2018). MIA segments a scan by assigning voxels within the scan to a specified number of classes, i.e. each material in the scan gets assigned to a class, then the probability of each voxel within the image belonging to that class is calculated throughout the scan and each voxel is then assigned to a class. This is done within a grid, where k-means algorithms and fuzzy-c means clustering are applied iteratively. The k-means algorithm assigns the different greyscale values of the scan into a number of groups defined by the user, with fuzzy-c means clustering then using greyscale values of each voxel within the scan to assign them to the groups. The groups are referred to as classes (as mentioned above), in which the assignment of the voxels to each class is dependent upon their probability and similarity to other members of the class. For example, if there is an 80% chance the voxel is white and a 20% chance the voxel is black, the voxel is assigned to the class that includes all the other white voxels (Dunmore et al., 2018). This results in each image being assigned to a class value that can be added/removed/studied separately (Fig. 2.5). This method was used as it is a semi-automated approach that has shown to be efficient, accurate and to reduce subjectivity in the segmentation process. For the extant material, most often 2 classes with a grid size of 15 was used, with slight variations occurring when needed.

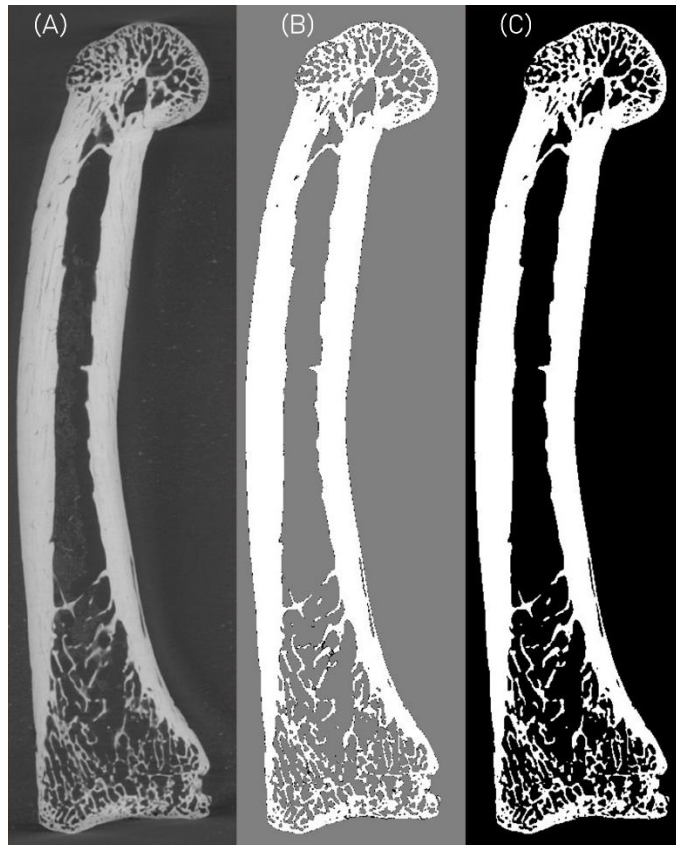


Figure 2.5: MIA segmentation steps. (A) Original micro-CT scan, (B) result of MIA segmentation, (C) Binarized final segmentation used for data collection.

2.2.3.a. Fossil segmentations

As segmentation depends on the greyscale values of materials within the scans, segmentation can become a challenging task when scans have multiple materials with differing density/voxel values; which is often the case for fossilized specimens. Preservation in each fossil specimen can be different due to differing taphonomic conditions. Most fossils were initially segmented within MIA, followed by image filters and manual cleaning within Avizo 6.3. These steps are depicted in **Figure 2.6** for the third proximal phalanx of *H. naledi* as an example. The only fossil which required a slightly different process was the *A. afarensis* specimen (AL 333-19) as it was so mineralised that there was minimal contrast between the 'bone' and included matrix (**Fig. 2.7**). This specimen was segmented using a median filter with a kernel size of 3, followed by a mean of least variance filter with a kernel size of 3 within MIA (Chapelle et al., 2023). This filtered data was further segmented in Avizo 6.3, using a watershed algorithm that helps sharpen the boundaries between materials (Davies et al., 2021). This allowed for the cortex of the shaft to be distinguished from other non-bone materials well enough for external and internal surfaces to be created.

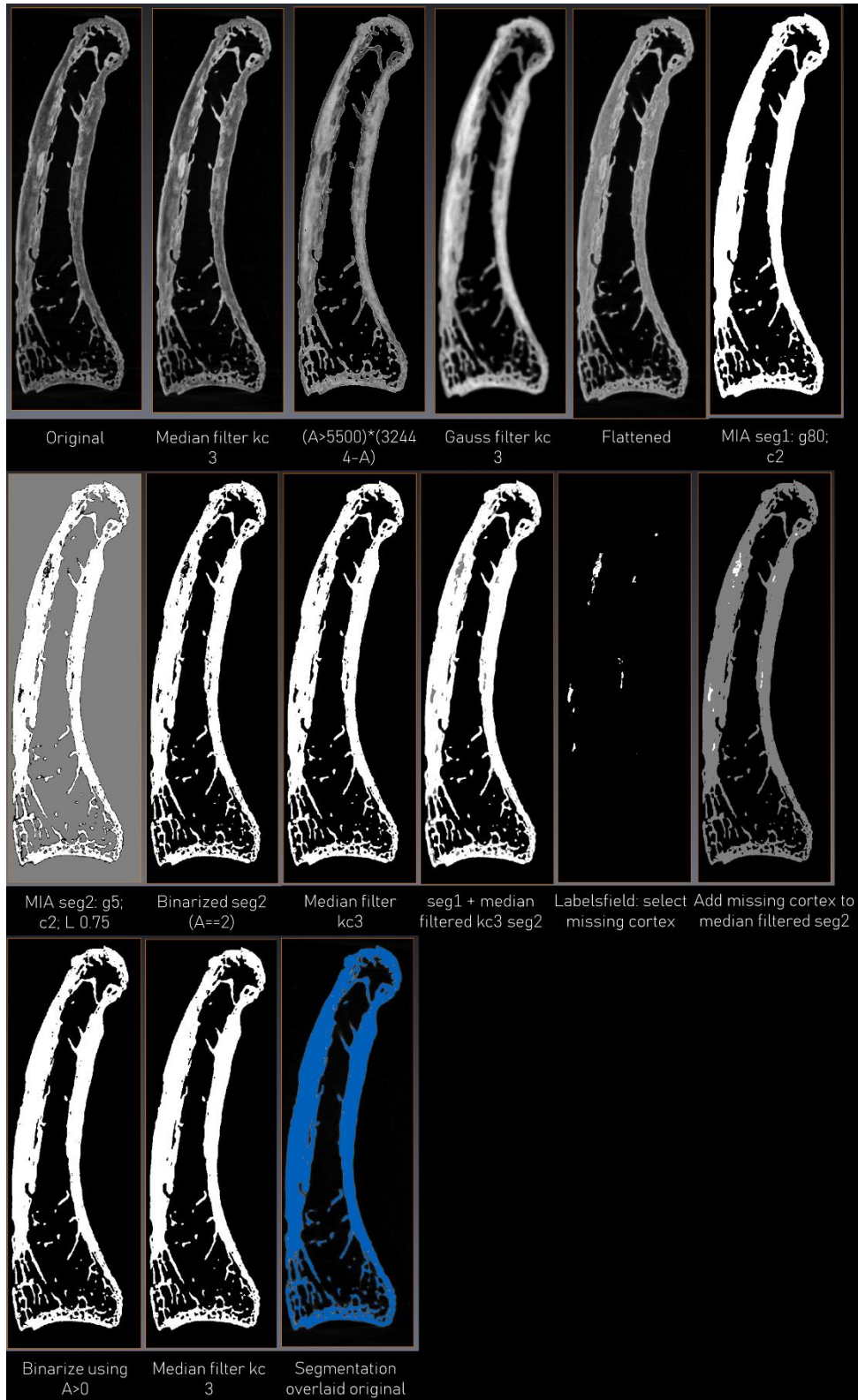


Figure 2.6: Example of segmentation protocol used on fossil hominin phalanges. The specimen depicted here is the third proximal phalanx of *H. naledi*.



Figure 2.7: (A) *A. afarensis* (AL 333-19) fourth proximal phalanx micro-CT scan showing mineralization of the bone and similar grey values of bone and non-bone material. (B) Result from the median and mean of least variance filtered segmentation. The cortex could not be distinguished in the epiphyseal ends of the bone but as the surfaces were going to be cropped, we focused on the cortex of the shaft.

2.2.4. Data collection

This project explored the cortical structure of the phalanges using the R package Morphomap, a novel method of mapping cortical bone distribution along a given length of a long bone (Profico et al., 2021). Prior to analysis within Morphomap, external and internal surfaces were created using Medtool 4.5 (www.dr-pahr.at/medtool), a software package that allows image processing and quantitative analyses of micro-CT scans. Using an in-house script, developed by members of the Kivell/Skinner lab, medtool applies morphological filters that define the cortical and trabecular boundary within the micro-CT scan as well as the non-bone background material within the scan. The methodological workflow and application of Medtool are described in further detail in Gross et al., (2014) and Pahr & Zysset (2009). A brief summary of the application of Medtool within the data collection workflow of this project is given below and depicted in Figure 2.8.

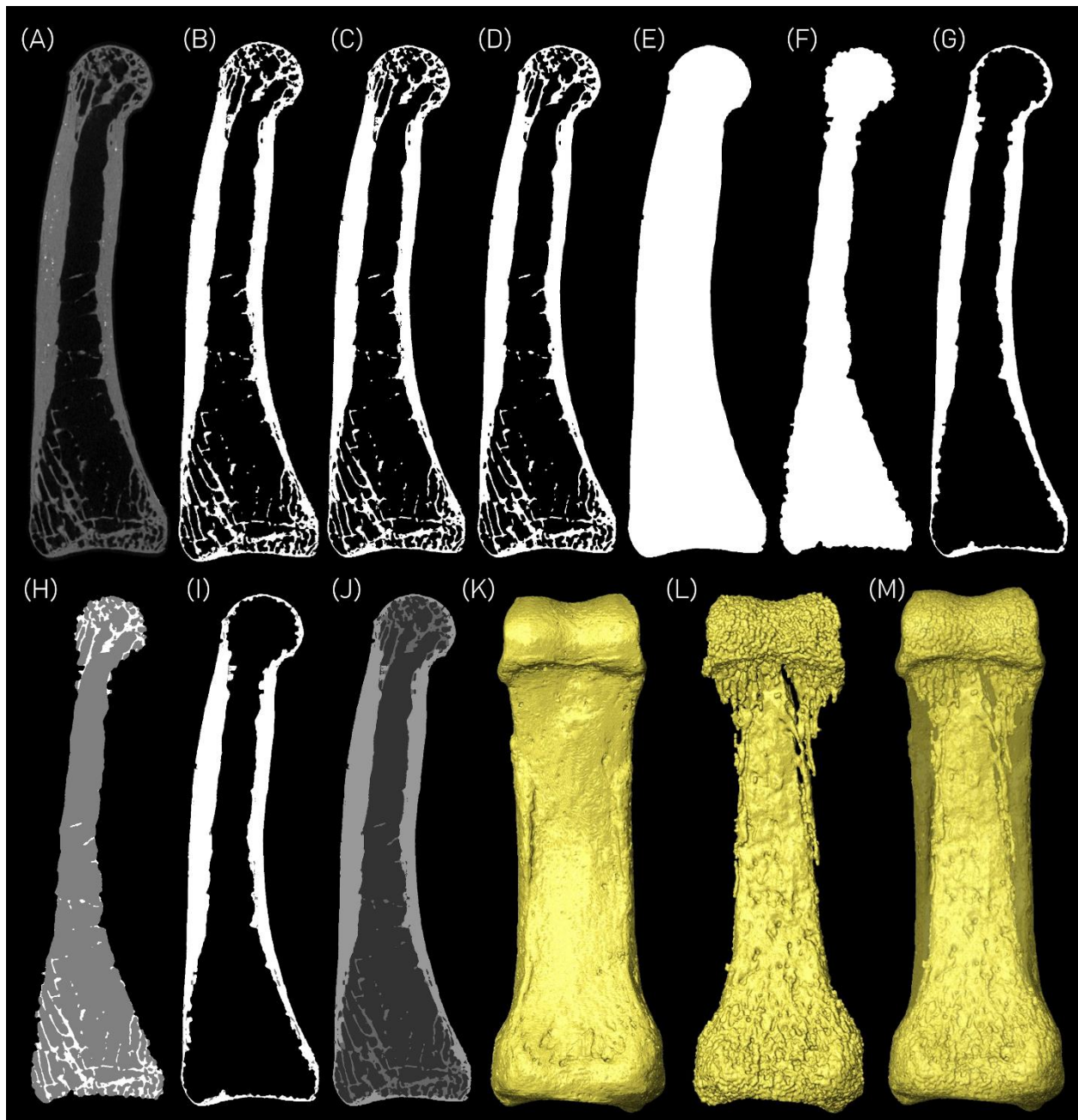


Figure 2.8: Medtool protocol used to create external and internal surfaces for data collection in *Morphomap*. (A) Original micro-CT scan, (B) Binarized MIA segmented scan, (C) 'Clean' scan, (D) 'Close' filter, (E) Outer mask, (F) Inner mask, (G) Thickness mask, (H) Maskseg In, (I) Maskseg Out, (J) Maskseg, (K) External surface, (L) Internal surface, (M) External surface overlaid on internal surface. The specimen depicted here is an *H. sapiens* second proximal phalanx.

As the MIA segmented micro-CT data results in a binary data set (Fig. 2.8B), voxels that represent non-bone material are classified as 0 and bone material is classified as 1. This binarized micro-CT data is used as input into Medtool, which uses a ray-casting algorithm to detect these different materials. Initially, cortical and trabecular bone is detected when rays are sent from the outer edge of the scan inwards, stopping when they reach a bone voxel. However, as

cortical bone is porous, Medtool artificially fills these holes as bone so that the rays do not identify these small holes in the cortex as non-bone material and stop moving inwards, which would result in data that would have thinned out the cortex of the bone. These pores are identified and filled using a kernel, the size of which depends upon the radius of a sphere in voxels using the resolution (voxel size) and trabecular thickness of the scan. This ensures the kernel size is smaller than the trabeculae, which would only result in the closure of pores that are smaller than one trabeculae so that the background space between the trabeculae is not filled and identified as pores. This results in an image stack that identifies cortical and trabecular bone, with a filled cortex (named a CLOSE image stack) (Fig. 2.8D). Using this CLOSE image stack, rays define the outer contour of the whole bone in the stack, creating an 'Outer mask' which represents the overall bone shape (Fig. 2.8E). An 'Inner mask' is also created from this CLOSE image stack, which defines the inner region of the bone (representing the shape of the trabecular bone region and non-bone voxels internal to the cortex) (Fig. 2.8F). The 'Inner mask' is subtracted from the 'Outer mask' to create the 'Thickness mask', which is a mask of the cortex of the bone (Fig. 2.8G). These three image stacks are interpolated into: Mask SegIn (Fig. 2.8H), Mask SegOut (Fig. 2.8I), and Mask Seg (Fig. 2.8J), which are then used for analysis. 'Mask SegIn' represents the trabecular bone and medullary cavity of the bone, 'Mask SegOut' represents the cortical bone, and 'Mask Seg' represents cortical bone, trabecular bone, and the medullary cavity and the cortical pores. It is important to note that as these image stacks are used for data collection, pores in the cortex that were artificially closed in the CLOSE image stack are represented in these final image stacks, which are integral to the strength of the bone. Finally, the 'Outer mask' and 'Inner mask' image stacks were used to create smooth external and internal surfaces (Fig. 2.8K and 2.8L) using an in-house in Paraview v 4.4 and Meshlab v 2020.03.

2.2.4.a. Morphomap input

This study quantifies cortical bone distribution patterns and cross-sectional geometric properties across the phalangeal shaft using the R package Morphomap (Profico et al., 2021). *Morphomap* uses 3D meshes of external and internal surfaces (Fig. 2.9A) of long bones to map cortical bone thickness and quantify cross-sectional geometric (CSG) properties. Firstly, the external and internal surfaces of a long bone are divided into a user-defined number of cross-sections across a certain percentage of the bone length. Then, a user-defined number of paired, equiangular landmarks are placed on the external and internal outline of each cross-section. This landmark data across the cross-sections allows for the mapping and quantification of cortical bone distribution and thickness, while the CSG parameters are calculated separately at each cross-section.

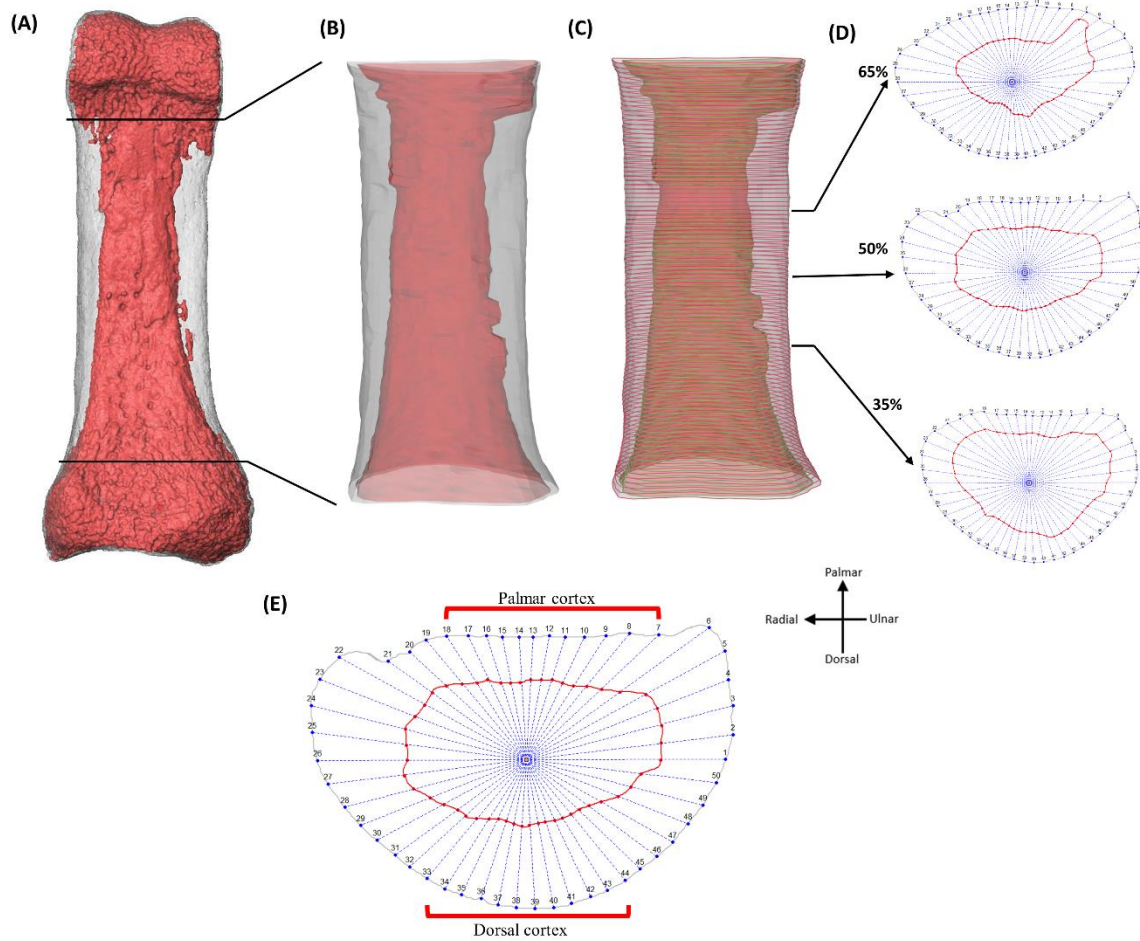


Figure 2.9: Data acquisition in Morphomap. (A) External (grey) and internal (red) 3D surface model of proximal phalanx of digit 4 in an *H. sapiens* individual (B) Cut external and internal 3D surfaces defining the shaft (as defined in text) for cortical thickness quantification (C) Cortical bone parameters are measured in 1% cross-sectional increments along the shaft and arrows indicate cross-section locations (35%, 50%, 65%) where CSG parameters were analysed (D) Cross-sections at 35%, 50% and 65% of the bone length. At each cross-section, 50 semilandmarks were placed on the external and internal surface equiangularly and were used to calculate cortical thickness. (E) Landmarks used to divide the cortex into the palmar and dorsal cortex.

This study focuses on quantifying cortical bone of the phalangeal shaft, but the variable external phalangeal morphology across hominids does not allow for a standardized percentage of phalangeal length that could be defined as the 'shaft' across all taxa. The shape and size of the base and trochlea of the proximal and intermediate phalanges differs across and within taxa, such that these features extend into the phalangeal shaft to varying degrees. Thus, a region of interest (ROI) was defined that represented the shaft in a homologous manner across all taxa. The proximal end of the ROI was defined as the distal most extent of the base and the distal end of the ROI was defined as the proximal most extent of the trochlea (Fig. 2.9B). This ROI was defined individually using these morphological features on the external surface of each phalanx.

Using Avizo Lite 9.0.0 (Visualization Sciences Group, SAS), these external morphological features were identified in the palmar, lateral, and medial views to ensure only the shaft of the bone is included in the ROI. Once these features were identified, the external and internal surfaces were cropped at the same locations within Avizo Lite 9.0.0. Since these surfaces were cropped, *Morphomap* did not recognize them as closed, complete surfaces and thus required a buffer on either end of the cropped surfaces. This buffer resulted in an additional 2% of the bone above and below the defined ROI so that cortical bone thickness could be mapped across the entire shaft. Prior to the cropping of surfaces, the identification of this ROI was independently checked by T. L. Kivell in a sample of three proximal and three intermediate phalanges of each digit in each taxon ($n = 24$ total specimens) to assess the homology of the identified ROI.

Once these cropped external and internal surfaces were created, 97 cross-sections were extracted at increments of 1% between 2% and 98% of the ROI length within *Morphomap* (Fig. 2.9C). Due to the 2% buffer, this ensured the entire length of the phalangeal shaft was being studied. At each cross-section, 50 paired equiangular semilandmarks were placed on the outlines of the external and internal surfaces. These landmarks were centred around the cortical area of each cross-section and ensured that the complex morphology of the phalangeal shaft was accurately captured. A set of lines is then drawn from the centroid of each slice outwards to the semilandmarks placed on the external and internal outline of each cross-section. Cortical thickness is calculated as the length of the line between the external and internal surfaces.

2.2.4.a.1. Cross-sectional geometry

Cross-sectional geometric properties were calculated at each slice across the shaft with the R package *Morphomap*. Different CSG properties quantify different aspects of the diaphysis and the most commonly used properties to understand the dynamic loads incurred by locomotion are: cortical area (CA; measure of axial strength), polar moment of area (J; measure of bending and torsional rigidity), and polar section modulus (Z_{pol} ; measure of maximum bending strength) (Lieberman et al., 2004; Marchi, 2005; Patel et al., 2020; Ruff & Runstead, 1992; Schaffler et al., 1985; Trinkaus & Ruff, 2012). We studied these cross-sectional properties at three positions along the shaft (35%, 50%, and 65% of the shaft length) (Fig. 2.9D) of each phalanx to quantify variation in cortical robusticity within the phalangeal shaft. The specific cross-sections were chosen to account for variation in the proximodistal extension of the base and trochlear morphology across our sample and to ensure each cross-section sampled only the diaphysis.

2.2.4.a.2. Palmar and dorsal cortical thickness

The proximal and intermediate phalanges of our extant taxa have FSRs that are variable in size and shape and as they are bony projections that have thicker cortical bone, we wanted to analyse cortical bone thickness in the palmar and dorsal shaft without the influence of the FSRs. This was achieved using a landmark-defined palmar and dorsal shaft. An equal number of landmarks on the palmar and dorsal surface of the shaft were selected, which excluded the medial and lateral aspects of the bone, to ensure we are analysing aspects of the bone that do not include the FSRs (Fig. 2.9E). Relative palmar and dorsal cortical thickness without the influence of FSRs was assessed as a ratio of palmar/dorsal thickness.

Parts of the methodology applied during the processing of micro-CT scans (segmentation) and data collection (Medtool script) were developed by members of the Kivell/Skinner lab group

and were used as a springboard for this research project. I modified and adapted the methodology to accurately capture the bone structure of phalanges, which are bones this methodology had not been applied on before. Excluding the development of the MIA segmentation method and the Medtool script, all pre-analysis processing of the data, including reorientation and segmentation, creating external and internal surfaces in Medtool, cropping surfaces in Avizo, and analysing phalangeal surfaces within Morphomap were all conducted by myself.

2.2.5. Excluded specimens

Out of the total sample of proximal and intermediate phalanges, phalanges from 7 *Pan* and 12 *Gorilla* individuals were excluded from our study sample due to their thick cortices. Across the 7 individuals of *Pan*, 11 intermediate phalanges and 2 proximal phalanges were excluded and from the 12 *Gorilla* individuals, 28 intermediate phalanges and 9 proximal phalanges were excluded. In each of these specimens, the cortex was extremely thick at the distal end of the phalanx such that the medullary cavity closed completely (Fig. 2.10). Since Medtool creates surfaces by sending rays that detect bone vs. non-bone voxels, in individuals with thick distal cortex, an internal distal surface could not be created because there were no non-bone voxels that could be detected. As Morphomap requires an external and internal surface to map cortical thickness, these individuals were removed from our study sample.

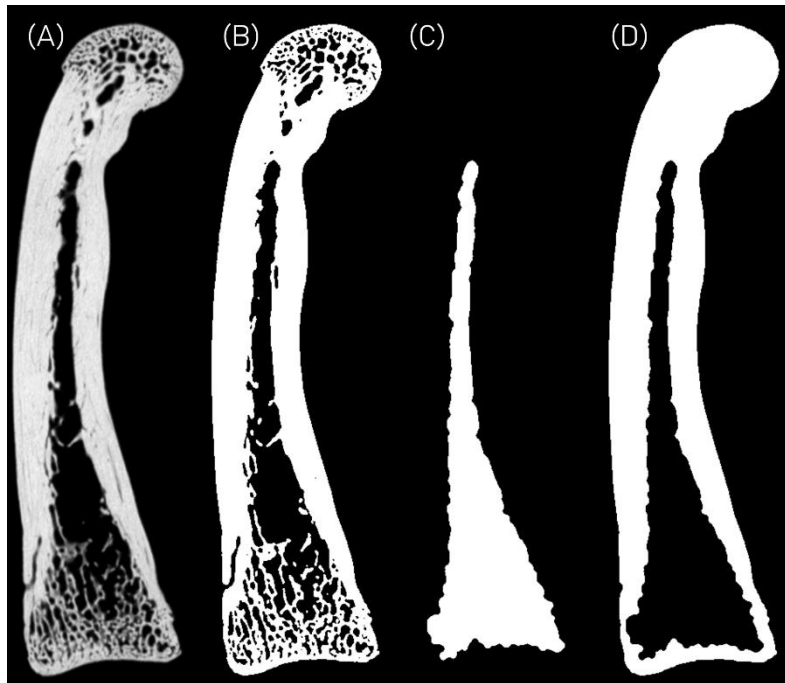


Figure 2.10: Example of a specimen with a closed medullary cavity. (A) Original micro-CT scan, (B) 'Close' scan, (C) Inner mask, (D) Thickness mask. The thickened cortex prevents Medtool from detecting non-bone voxels in the distal region of the phalanx, as such a complete surface of the internal aspect of the bone cannot be created.

2.2.6. Data visualisation

Cortical bone thickness distribution was visualised using 2D and 3D morphometric maps created within *Morphomap* (Fig. 2.11). The cortical bone thickness distribution map of each individual is scaled to itself so that thickness is depicted relative to that individual, with red regions representing the areas of the thickest cortex while dark blue regions representing areas of the thinnest cortical bone. Absolute maps of cortical thickness distribution were also created to visualise absolute differences in cortical thickness across our sample. However, due to the wide range of cortical thickness values in our sample, the absolute maps were not particularly informative and were not incorporated into subsequent analyses.

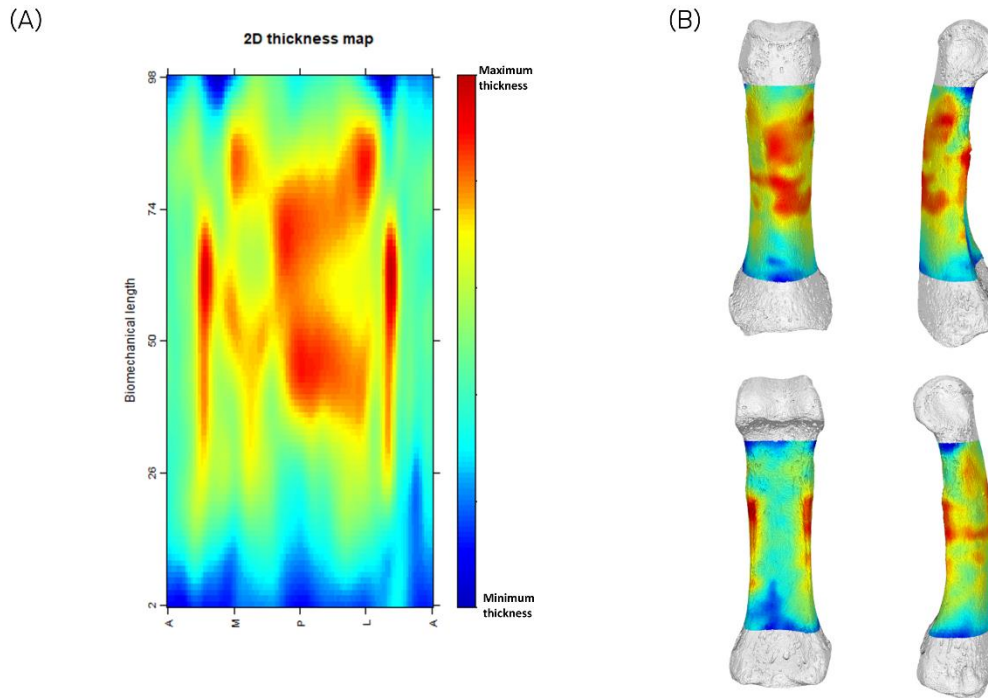


Figure 2.11: *Morphomap* output of (A) 2D and (B) 3D cortical bone distribution maps.

2.2.7. Measurements of external morphological features

Along with analysing the cortical structure of the phalanges, we also evaluated the relationship between cortical bone thickness and external morphological features of the phalanges that previous research has suggested will influence how load is experienced by the phalanx. These external features are phalangeal curvature, flexor sheath ridge (FSR) and median bar morphology of the palmar surface.

2.2.7.a. Phalangeal curvature

The degree of phalangeal curvature was measured using the included angle (IA) method (Fig. 2.12A). The IA (θ) method assumes the curvature of a phalanx in the dorsopalmar direction is represented by an arc length on the perimeter of a circle (Stern et al., 1995). Low values of θ are characteristic of straighter phalanges, commonly associated with quadrupedalism and bipedalism, and higher values of θ are characteristic of increasingly curved phalanges, commonly associated

with arboreality (Jungers et al., 1997; Stern et al., 1995). It is important to note that the IA method is not as accurate as other methods of measuring phalangeal curvature (e.g., Deane et al., 2005; Wenneman et al., 2022 method) as IA assumes a consistent degree of curvature throughout the proximodistal length of the phalanx, which is often not the case (i.e. the distal end is typically more curved than the proximal end). However, the IA method was chosen because it has been the most prevalent approach to calculate phalangeal curvature in comparative morphological studies, does not require specialised software, and has been shown to distinguish broad categories of locomotor behaviours across primate taxa (Jungers et al., 1997; Matarazzo, 2008; Rein, 2011; Stern et al., 1995). Since the IA method is susceptible to measurement error (Deane & Begun, 2008; Patel & Maiolino, 2016), three repeated measurements were taken on a sub-sample of three proximal and intermediate phalanges of each digit of each taxon (n = 96 total specimens) to correct for intra-observer measurement error.

2.2.7.b. Palmar phalangeal morphology

The variation observed in the FSRs and the median bar in the intermediate phalanges has been linked to hand function (Marzke et al., 2007; Nguyen et al., 2014; Patel & Maiolino, 2016; Tocheri et al., 2008). Experimental work has shown that the FSRs reduce strain experienced by the remaining shaft (Nguyen et al., 2014). However, there has been no experimental study of the potential biomechanical role of the median bar, despite its presence in fossil hominins often being linked to specific behaviours and functions (e.g., Begun et al., 2004; Ricklan, 1987; Stern & Susman, 1983; Susman et al., 1984). Therefore, variation in the shape of these features (i.e., primarily how much these features extend anteriorly from the palmar shaft) was quantified to investigate their potential influence on cortical thickness. FSR morphology was quantified by two measurements (**Fig. 2.12B**): (1) FSR length, defined as the maximum length from the proximal to the distal end of the ridge; (2) FSR depth, defined as the highest protruding point of the ridge. The anterior extension of the median bar was measured at the tallest point of the bar from the palmar surface (**Fig. 2.12B**). It is important to note that these morphological features are quite complex and variable within and between taxa, and I acknowledge that these simple measurements do not completely represent their morphology, especially in regard to the median bar. However, as neither feature has been formally quantified in comparative morphological studies, these measurements allow for a general understanding of projection from the palmar surface and the potential influence this might have on internal cortical architecture.



Figure 2.12: Measurements of phalangeal external morphology. (A) Calculating phalangeal curvature using the Included Angle (IA) method. Interarticular length (L), dorsopalmar midshaft diameter (D), and projected height measurement (H) are input into the formulas to get degree of curvature. (B) Images depicting measurements of flexor sheath ridge length, flexor sheath ridge depth, and median bar depth. The specimen depicted is a *Gorilla* third proximal phalanx. All measurements were taken in Avizo 9.0.0.

2.2.8. Statistical analysis

Statistical analyses conducted across the different cortical bone measurements for our sample of proximal and intermediate extant phalanges are described in detail in chapters 3 and 4. Analyses relating to our fossil specimens are described in detail in Chapter 5.

Table 2.1: Detailed information on study sample.

Taxon	Specimen	Sex	Side	Subsistence	IP2	IP3	IP4	IP5	PP2	PP3	PP4	PP5	IPs	PPs
<i>Australopithecus afarensis</i>	AL333-19	UK	UK	Fossil										X
<i>Australopithecus africanus</i>	StW12	UK	UK	Fossil										X
<i>Australopithecus africanus</i>	StW293	UK	UK	Fossil										X
<i>Australopithecus africanus</i>	StW331	UK	UK	Fossil									X	
<i>Australopithecus sediba</i>	MH2	F	R	Fossil		X	X	X	X	X	X	X		
<i>Homo habilis</i>	OH7	UK	R	Fossil	X	X	X	X		X				
<i>Homo naledi</i>	Hand 1	UK	R	Fossil	X	X	X	X	X	X	X	X		
<i>Homo floresiensis</i>	LB1-40	UK	L	Fossil									X	
<i>Homo floresiensis</i>	LB1-42	UK	L	Fossil									X	
<i>Homo floresiensis</i>	LB1-48	UK	L	Fossil									X	
<i>Homo floresiensis</i>	LB6-8	UK	UK	Fossil										X
<i>Homo floresiensis</i>	LB6-9	UK	UK	Fossil									X	
<i>Homo floresiensis</i>	LB-XV-42-2008	UK	UK	Fossil									X	
<i>Homo floresiensis</i>	LB-XXI-44-2010	UK	UK	Fossil										X
Swartkrans hominin	SKX 27431	UK	UK	Fossil										X
Swartkrans hominin	SKX 5018	UK	UK	Fossil										X
Swartkrans hominin	SKX 15468	UK	UK	Fossil										X
Neanderthal	Kebara 2	UK	R/L	Fossil	X	X	X		X	X	X	X		
Neanderthal	Feldhofer 1	UK	R	Fossil	X								X	
Neanderthal	Tabun C1	UK	L	Fossil	X		X							
Neanderthal	El Sidron-21	UK	UK	Fossil			X							
Neanderthal	El Sidron-53	UK	R	Fossil					X					
Neanderthal	El Sidron-54	UK	R	Fossil								X		
Neanderthal	El Sidron-57	UK	R	Fossil						X				
Neanderthal	El Sidron-92	UK	L	Fossil										X
Neanderthal	El Sidron-352a	UK	UK	Fossil									X	
Neanderthal	El Sidron-552	UK	R	Fossil										X
Neanderthal	El Sidron-604	UK	UK	Fossil									X	
Neanderthal	El Sidron-619	UK	UK	Fossil										X
Neanderthal	El Sidron-720	UK	UK	Fossil									X	

<i>Homo sapiens</i>	DCW_AM_3_0_2	UK	R/L	Pre-industrial	X		X		X	X	X	
<i>Homo sapiens</i>	DCW_OC_1_0_141	UK	R/L	Pre-industrial		X	X	X	X	X	X	X
<i>Homo sapiens</i>	DCW_OC_1_0_26	UK	L	Pre-industrial	X		X		X		X	
<i>Homo sapiens</i>	FCS8	M	R/L	Post-industrial					X	X	X	X
<i>Homo sapiens</i>	81-H1035	M	R	Post-industrial					X			
<i>Homo sapiens</i>	81-H1040	M	R	Post-industrial						X	X	
<i>Homo sapiens</i>	81-H1068-DD	M	R	Post-industrial							X	
<i>Homo sapiens</i>	FCS16	M	R/L	Post-industrial					X	X	X	X
<i>Homo sapiens</i>	FCS17	M	R/L	Post-industrial					X	X	X	
<i>Homo sapiens</i>	81-H172-H	M	R/L	Post-industrial	X	X	X	X		X	X	X
<i>Homo sapiens</i>	DV-13	M	L	Pre-industrial			X		X		X	
<i>Homo sapiens</i>	DV-14	M	R	Pre-industrial			X				X	
<i>Homo sapiens</i>	DV-15	M	R/L	Pre-industrial	X	X	X		X	X		
<i>Homo sapiens</i>	DV-16	M	R/L	Pre-industrial	X	X	X			X	X	
<i>Pan paniscus</i>	MRAC_27698	F	L	Wild	X	X	X		X	X	X	X
<i>Pan paniscus</i>	MRAC_29042	F	R	Wild	X	X	X	X	X	X	X	X
<i>Pan paniscus</i>	MRAC_29045	F	L	Wild	X		X	X	X	X	X	X
<i>Pan paniscus</i>	MRAC_29052	M	R	Wild	X	X	X	X	X	X	X	X
<i>Pan paniscus</i>	MRAC_27696	M	L	Wild	X	X	X	X	X	X	X	X
<i>Pan paniscus</i>	MRAC_20881	M	L	Wild					X	X	X	X
<i>Pan paniscus</i>	MRAC_29060	F	R	Wild	X	X	X	X	X	X	X	X
<i>Pan troglodytes</i>	MPITC_11778	F	R	Wild			X		X	X	X	
<i>Pan troglodytes</i>	MPITC_14996	F	L	Wild			X	X	X	X	X	
<i>Pan troglodytes</i>	NH_CAM1_204	F	L	Wild	X	X	X	X	X	X	X	X
<i>Pan troglodytes</i>	NH_CAM2_301	F	R	Wild	X	X	X	X	X	X	X	X
<i>Pan troglodytes</i>	NH_MER_279	F	L	Wild	X	X	X	X	X	X	X	X
<i>Pan troglodytes</i>	NH_MER35_86	F	L	Wild	X	X	X	X	X	X	X	X
<i>Pan troglodytes</i>	NH_MER35_105	F	R	Wild	X	X	X	X	X	X	X	X
<i>Pan troglodytes</i>	MPITC_11903	M	L	Wild					X	X	X	
<i>Pan troglodytes</i>	MPITC_11789	M	L	Wild	X	X	X	X	X	X	X	
<i>Pan troglodytes</i>	MPITC_11781	M	L	Wild			X	X	X	X	X	
<i>Pan troglodytes</i>	ZSM_AP-122	M	R	Wild	X	X	X	X	X	X	X	X
<i>Pan troglodytes</i>	PC_ZVII_24	M	R	Wild						X	X	

<i>Pan troglodytes</i>	NH_MER33_712	M	R	Wild	X		X	X	X	X	X	X
<i>Pan troglodytes</i>	NH_MER33_724	M	L	Wild	X	X	X	X	X	X	X	X
<i>Pan troglodytes</i>	NH_MER32_401	M	L	Wild	X	X	X		X	X	X	X
<i>Pan troglodytes</i>	NH_MER33_440	M	R	Wild	X	X	X	X	X	X	X	X
<i>Pan troglodytes</i>	NH_MER36_254	M	L	Wild		X	X	X	X	X	X	X
<i>Gorilla gorilla</i>	ZMB_11642	UK	R	Wild			X		X	X		X
<i>Gorilla gorilla</i>	ZMB_83545	M	R	Wild	X	X	X	X	X	X	X	X
<i>Gorilla gorilla</i>	PC_MER_95	F	R	Wild		X	X		X	X	X	
<i>Gorilla gorilla</i>	PC_MER_135	M	L	Wild	X		X	X	X	X	X	X
<i>Gorilla gorilla</i>	PC_MER_264	M	L	Wild	X	X	X		X	X	X	X
<i>Gorilla gorilla</i>	PC_MER_300	F	R	Wild				X	X	X	X	X
<i>Gorilla gorilla</i>	PC_MER_372	M	R	Wild	X	X	X		X	X	X	X
<i>Gorilla gorilla</i>	PC_MER_962	M	R	Wild	X	X						
<i>Gorilla gorilla</i>	PC_MER1_29	F	R	Wild		X	X					X
<i>Gorilla gorilla</i>	PC_MER_138	F	L	Wild					X	X	X	X
<i>Gorilla gorilla</i>	PC_MER_174	F	R	Wild					X	X	X	X
<i>Gorilla gorilla</i>	PC_MER_696	F	R	Wild	X	X	X	X	X	X	X	X
<i>Gorilla gorilla</i>	PC_MER_856	F	L	Wild	X	X	X	X	X	X	X	X
<i>Gorilla gorilla</i>	PC_ZII_64	M	R	Wild					X	X		
<i>Gorilla gorilla</i>	PC_ZVI_32	M	R	Wild				X	X	X		X
<i>Gorilla gorilla</i>	NH_MER33_755	F	R	Wild	X	X	X		X	X	X	X
<i>Gorilla gorilla</i>	NH_MER33_461	M	R	Wild		X			X	X	X	X
<i>Gorilla gorilla</i>	NH_CAM1_106	M	R	Wild		X	X	X	X	X	X	X
<i>Gorilla gorilla</i>	NH_CAM1_105	M	R	Wild	X	X	X	X	X	X	X	X
<i>Gorilla gorilla</i>	NH_MER35_150	F	R	Wild	X	X	X	X	X	X	X	X
<i>Gorilla gorilla</i>	NH_CAM1_98	F	L	Wild	X	X	X	X	X	X	X	X
<i>Gorilla gorilla</i>	NH_MER35_136	F	L	Wild	X	X	X	X	X	X	X	
<i>Gorilla gorilla</i>	NH_MER35_139	F	L	Wild	X	X	X	X	X	X	X	X
<i>Gorilla gorilla</i>	NH_FC_130	M	L	Wild	X	X	X	X	X	X	X	X
<i>Gorilla gorilla</i>	NH_FC_123	M	L	Wild	X	X	X	X	X	X	X	X
<i>Pongo abelii</i>	SMF_6785	M	R	Wild						X	X	X
<i>Pongo abelii</i>	SMF_6779	F	L	Wild						X	X	X
<i>Pongo pygmaeus</i>	ZSM_1907_0633b	F	R	Wild	X	X	X	X	X	X	X	X

<i>Pongo pygmaeus</i>	ZSM_1907_0629b	M	R	Wild	X	X	X	X	X	X	X	X
<i>Pongo pygmaeus</i>	ZSM_1907_0660	F	R	Wild	X	X	X	X	X	X	X	X
<i>Pongo pygmaeus</i>	ZSM_AP-120	M	L	Wild	X	X	X	X	X	X	X	X
<i>Pongo pygmaeus</i>	ZSM_1907_0483	F	R	Wild	X	X	X	X	X	X	X	X
<i>Pongo pygmaeus</i>	ZSM_1909_0801	M	R	Wild	X	X	X		X	X	X	X
<i>Pongo pygmaeus</i>	ZMB_87092	F	R	Wild					X	X	X	

Note: M = male; F = female; R = right; L = left; UK = unknown sex/side; R/L = to have all four digits represented, some phalanges were from the right side of the body and some from the left; IPs/PPs = intermediate phalanges (IPs) and proximal phalanges (PPs) with no digit assigned.

3 – Cortical bone distribution of the proximal phalanges in great apes and implications for reconstructing manual behaviours

Published article: Syeda, S. M., Tsegai, Z. J., Cazenave, M., Skinner, M. M., & Kivell, T. L. (2023). Cortical bone distribution of the proximal phalanges in great apes: implications for reconstructing manual behaviours. *Journal of Anatomy*, 243(5), 707–728.

3.1. Abstract

Primate fingers are typically in direct contact with the environment during both locomotion and manipulation, and aspects of external phalangeal morphology are known to reflect differences in hand use. Since bone is a living tissue that can adapt in response to loading through life, the internal bone architecture of the manual phalanges should also reflect differences in manual behaviours. Here, we use the R package Morphomap to analyse high-resolution micro-CT scans of hominid proximal phalanges of digits 2–5 to determine whether cortical bone structure reflects variation in manual behaviours between predominantly bipedal (*Homo*), knuckle-walking (*Gorilla*, *Pan*), and suspensory (*Pongo*) taxa. We test the hypothesis that relative cortical bone distribution patterns and cross-sectional geometric properties will differ both among extant great apes and across the four digits due to locomotor and postural differences. Results indicate that cortical bone structure reflects the varied hand postures employed by each taxon. The phalangeal cortices of *Pongo* are significantly thinner and have weaker cross-sectional properties relative to the African apes, yet thick cortical bone under their flexor sheath ridges corresponds with predicted loading during flexed finger grips. Knuckle-walking African apes have even thicker cortical bone under the flexor sheath ridges, as well as in the region proximal to the trochlea, but *Pan* also has thicker diaphyseal cortices than *Gorilla*. Humans display a distinct pattern of distodorsal thickening, as well as relatively thin cortices, which may reflect the lack of phalangeal curvature combined with frequent use of flexed-fingered hand grips during manipulation. Within each taxon, digits 2–5 have a similar cortical distribution in *Pongo*, *Gorilla* and, unexpectedly, *Homo*, which suggests similar loading of all fingers during habitual locomotion or hand use. In *Pan*, however, cortical thickness differs between the fingers, potentially reflecting differential loading during knuckle-walking. Inter- and intra-generic variation in phalangeal cortical bone structure reflects differences in manual behaviours, offering a comparative framework for reconstructing hand use in fossil hominins.

3.2. Introduction

As the primate hand, and particularly the fingers, interact directly with the external environment, they have the potential to provide functional information about both locomotion and/or manipulation. Studies exploring phalangeal external morphology (Inouye, 1992; Matarazzo, 2008; Patel & Maiolino, 2016; Rein et al., 2011; Rein & McCarty, 2012; Susman, 1979), phalangeal curvature (Jungers et al., 1997; Richmond, 2007; Stern et al., 1995), and internal bone architecture of the wrist (Bird et al., 2021; 2022; Tocheri et al., 2007), metacarpals (Dunmore et al., 2019; Stephens et al., 2018; Tsegai et al., 2013; Zeininger et al., 2011), and phalanges (Matarazzo, 2015; Stephens et al., 2018) have demonstrated a functional signal between the external and/or internal morphology of the hand and manual behaviours (Kivell, 2015). The functional link between internal bone structure and locomotor behaviour has been established in several skeletal elements (Arias-

Martorell et al., 2021; Cotter et al., 2009; Saers et al., 2016; Scherf et al., 2013; Tsegai et al., 2017b); however, the internal architecture of the manual phalanges remains relatively understudied, despite the phalanges of digits 2-5 being involved in grasping during both locomotion and manipulation (Bardo et al., 2017; Byrne & Byrne, 2001; Marzke, 1997; Matarazzo, 2013; Neufuss et al., 2017). Here, we investigate variation in the cortical bone structure of the proximal phalanges of digits 2-5 (PP2-PP5) in humans and other extant hominids.

Much of the work to date exploring fossil and extant primate phalangeal morphology has focused on quantifying variation in shaft curvature, as it is considered to be functionally informative about hand use during locomotion and particularly differences in arboreality (Deane & Begun, 2008; Jungers et al., 1997; Richmond, 1998; Matarazzo, 2008; Rein, 2011; Stern and Susman, 1983; Stern et al., 1995; Susman et al., 1984; but see Wallace et al., 2020). During grasping, longitudinally curved phalanges are thought to be more effective than straight phalanges because the curvature helps to reduce bending moments by aligning the bone more closely with the joint reaction force (Oxnard, 1973; Preuschoft, 1973). Finite element (FE) modelling techniques have validated these functional hypotheses regarding phalangeal curvature by testing differences in strain distribution in curved vs. mathematically straightened phalanges, revealing curved phalanges experience overall lower strain (Nguyen et al., 2014; Richmond, 2007). Furthermore, the degree of phalangeal curvature changes throughout ontogeny depending on mechanical loading (Richmond, 1998; 2007). For example, juvenile chimpanzees and gorillas have a higher degree of phalangeal curvature than adults (Richmond, 1998; Sarringhaus, 2013), reflecting a decrease in arboreality throughout ontogeny (Doran, 1997). This research suggests a strong functional link between locomotor behaviour and the external morphology of phalanges (but see Wallace et al., 2020).

In contrast to research on phalangeal external shape, the functional relationship between the internal bone morphology of phalanges and locomotor behaviour has yet to be thoroughly explored. Internal bone architecture consists of cortical and trabecular bone, both of which are subject to changes that result from loading experienced by the bone during an individual's lifetime; a process known as bone functional adaptation (Currey, 2003; Pearson & Lieberman, 2004; Ruff et al., 2006). Cortical bone adapts to the functional demands placed upon it through adjustments to its mineralisation to adapt its stiffness, changes in overall shape to resist loads, or by increasing its thickness (Currey, 2003; Ruff et al., 2006). Overall, both cortical and trabecular bone adapt in response to their mechanical environment by removing bone in skeletal areas where stress is low and adding bone where stress is high (Pearson & Lieberman, 2004; Ruff et al., 2006).

Cortical bone is usually studied through analysis of cross-sectional geometric (CSG) properties that offer robust estimations of strength and rigidity of a bone (Ruff & Runestad, 1992; Ruff et al., 2006). Understanding how CSG patterns correlate with loading regimes of an individual is complex and drawing functional interpretations can be challenging, but CSG patterns provide an indirect method to understand potential loading patterns when direct biomechanical data are not available or not possible to measure. Recently, studies of cortical thickness distribution of long bones have also revealed that the cortex varies throughout the shaft across different skeletal elements in ways that relate to locomotor behaviour (Cazenave et al., 2019; Jashashvili et al., 2014; Puymeraul, 2013; Tsegai et al., 2017a; Wei et al., 2021). Combining the analysis of CSG with cortical bone distribution and thickness can allow inference of bone adaptation in relation to habitual loading (Jashashvili et al., 2014).

Within the hand, only cortical structure of the metacarpals has been studied in extant hominids (Dunmore et al., 2020b; Marchi, 2005; Patel et al., 2020), which found cross-sectional properties can distinguish habitual locomotor behaviours of extant great apes. Several studies have also explored the functional morphology of trabecular bone in the carpals and metacarpals (Bird et al., 2021, 2022; Dunmore et al., 2019; Schilling et al., 2014; Tsegai et al., 2013). However, to date, there have only been three studies published to our knowledge that have explored the internal bone structure of proximal phalanges of the fingers (Doden, 1993; Matarazzo, 2015; Stephens et al., 2018). Doden (1993) studied the internal cortical structure of the phalanges in gibbons and humans, noting a functional link between the shape and density of cortical bone and manual behaviours. Matarazzo (2015) analysed the trabecular architecture at the proximal and distal epiphysis of the phalanges of digit 3 in extant non-human hominoids and macaques, with patterns of trabecular orientation differing between the locomotor modes of the taxa. However, other variables of trabecular bone (e.g. bone volume fraction, degree of anisotropy, isotropy index) in the phalanges failed to distinguish between locomotor behaviours (Matarazzo, 2015). Stephens and colleagues (2018) documented variation in the structure of trabecular bone in post-Neolithic and foraging human hands, revealing greater trabecular bone volume fraction in foragers that is consistent with higher intensity loading than that experienced by post-Neolithic individuals. Therefore, the analysis of the internal bone structure of manual phalanges of extant great apes holds potential for reconstructing the behaviour of fossil hominin species. However, there has yet to be a detailed analysis of variation in cortical thickness in hominid phalanges, which is important to consider in light of differences in trabecular structure (Matarazzo, 2015; Stephens et al., 2018) and phalangeal curvature (Jungers et al., 1997; Matarazzo, 2008; Rein, 2011; Richmond, 1998; Stern et al., 1995; Wennemann et al., 2022).

Here, we conduct a detailed examination of cortical structure of the proximal phalanges of digits 2-5 in extant hominids. We assume phalangeal cortical bone morphology in non-human hominids will primarily reflect locomotor loading. This is due to the high mechanical loads on the fingers from dynamic loading and body mass that occur during locomotion (Preuschoft, 2019). Although all non-human hominids show enhanced manual dexterity and tool use abilities in the wild (e.g., Byrne & Byrne, 2001; Lesnik et al., 2015; Marzke et al., 2015; van Schaik et al., 1996) and captivity (e.g., Bardo et al., 2016; 2017; Pouydebat et al., 2005), we assume that loading during manipulation will be lower than that of locomotion. In contrast, we assume human phalangeal cortical structure will reflect loading during manipulation given the rarity with which individuals in our sample likely used their hands for locomotion.

3.2.1. Predictions

This study examines the cortical structure of the proximal manual phalanges of digits 2-5 to determine whether variation in manual behaviours associated with locomotion and manipulation correlates with cortical bone properties in *Pongo*, *Gorilla*, *Pan*, and *H. sapiens*, and how potential differences in cortical thickness vary with differences in phalangeal curvature. We quantify both variation in cortical thickness throughout the phalangeal shaft and cross-sectional geometric properties at sections along the shaft (35%, 50% and 65% of bone length). We test three main predictions regarding variation in cortical bone structure based on observations of great ape, including humans, manual behaviour, bone functional adaptation, and studies on phalangeal external morphology and biomechanics.

Our first prediction is that relative cortical bone distribution patterns will significantly differ among extant great apes due to locomotor and postural differences. Secondly, we predict that across the four digits of each species, there will be variation in cortical bone thickness distribution, mean cortical bone thickness, and CSG properties. Finally, we predict that mean cortical bone thickness and cross-sectional properties will significantly differ across the great apes. We discuss these specific predictions for each taxon below.

Pongo is highly arboreal, with torso-orthograde suspension dominating their complex postural and locomotor behaviours (Cant, 1987; Thorpe & Crompton, 2006; Thorpe et al., 2009). During suspension, the hand is positioned like a hook around the substrate, which may mitigate bending stress during suspension, because joint reaction forces load the articular ends of the phalanges dorsally in compression, while the forces from the digital flexor muscles, along with the joint reaction and gravitational forces, pull the phalanges palmarly (Carlson & Patel, 2006; Richmond, 2007; Schmitt et al., 2016). In *Pongo* phalanges, the high degree of longitudinal curvature (**Fig. 3.1**), combined with flexor sheath ridges (FSRs) located opposite the maximum arc of curvature, are thought to be advantageous for frequent flexed-finger grasping (Susman, 1979). Thus, we predict *Pongo* will exhibit a pattern of maximum thickness on the disto-palmar surface of the phalangeal shaft, as the proximal phalanges are most often being loaded in flexed finger grasping during locomotion and are experiencing tensile and compressive forces from the joint reaction forces and substrate reaction forces (Matarazzo, 2015; Nguyen et al., 2014; Preuschoft, 1973; Tsegai et al., 2013). We predict that this cortical distribution pattern, as well as mean cortical bone thickness and CSG properties, will be similar across the four digits, as all four digits are thought to be used in a similar manner during manual behaviours (Rose, 1988 but see McClure et al., 2012). Across the great apes, we expect cortical properties, associated with strength and rigidity against bending and torsional loads, of *Pongo* to be less than that of the African apes as the external phalangeal morphology helps mitigate stress from arboreal locomotion.

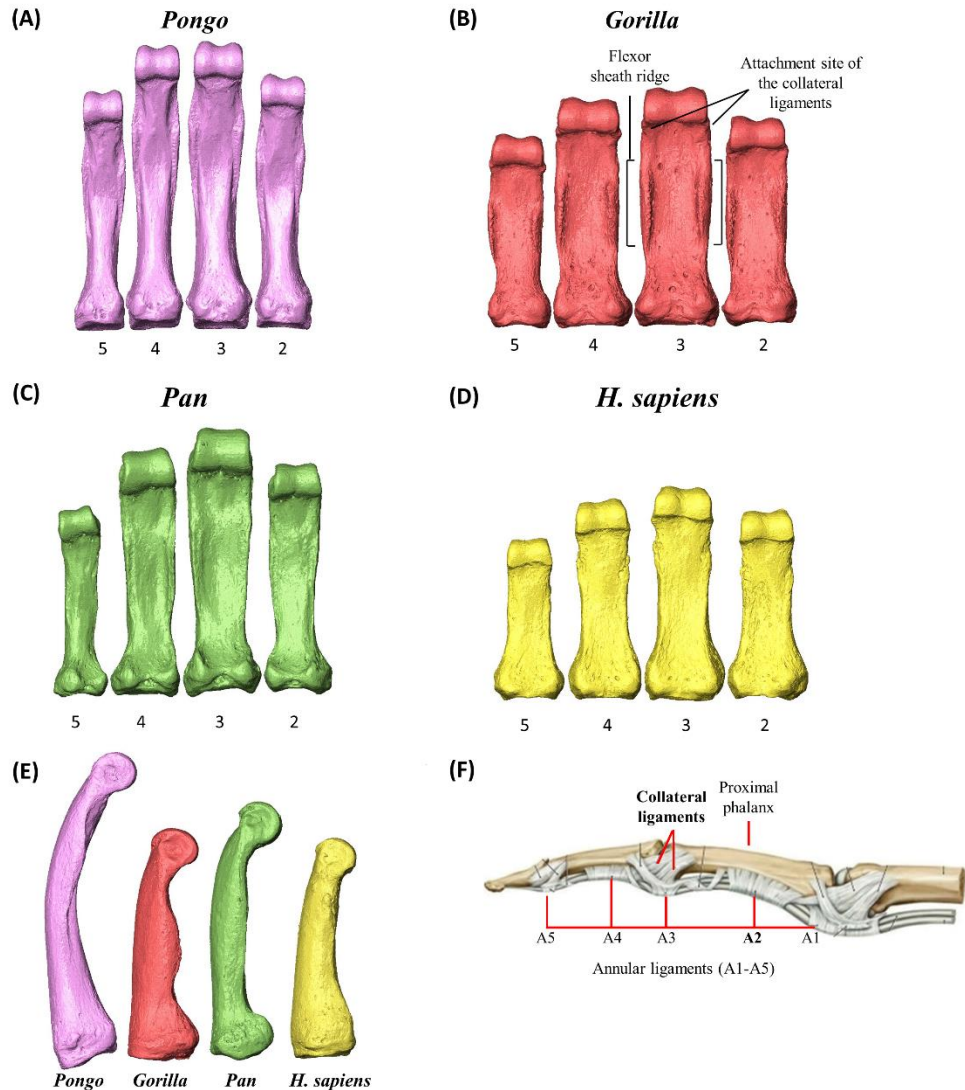


Figure 3.1: Representative 3D surfaces of proximal phalanges of (A) *Pongo pygmaeus*, (B) *Gorilla gorilla*, (C) *Pan troglodytes*, (D) *Homo sapiens*. Digits 2-5 are represented from right to left. The proximal phalanges have been scaled to relative size. (E) Medial surface of the third proximal phalanx of each taxa. Variation in curvature and flexor sheath ridge morphology is evident. (F) Depiction of ligaments of the finger. The second annular pulley (A2) and collateral ligament of the PIP joint are highlighted in subset F (modified from Gilroy et al., 2016) and the flexor sheath ridges and attachment sites of the collateral ligaments are shown in subset B.

Gorilla engage primarily in knuckle-walking (Doran, 1996; 1997; Inouye, 1994; Tuttle & Watts, 1985), during which the dorsal surfaces of the intermediate phalanges are in contact with the substrate and the proximal phalanges, metacarpals, and body mass of the animal are elevated above the hand (Preuschoft, 1973; Tuttle, 1967; Wunderlich & Jungers, 2009). Zoo-housed *Gorilla* most often use a palm-back (pronated) position and experience relatively even pressure across digits 2-5 (Matarazzo, 2013; Tuttle, 1969a), while wild *Gorilla* have been observed to have more variable hand postures (Thompson et al., 2018). The radio-ulnarly wide, stout, and flat phalanges are thought to reflect these frequent knuckle-walking hand postures. The proximal phalanges also

have prominent FSRs, indicating forceful grasping during arboreal locomotion and/or food processing (Neufuss et al., 2019; Remis, 1998; Susman, 1979; Tuttle & Watts, 1985). We predict that the cortical thickness pattern of *Gorilla* will be similar palmarly and dorsally due to loading of a flexed proximal interphalangeal (PIP) and hyper-extended metacarpophalangeal (McP) joint (Tsegai et al., 2013). Across digits 2–5, we expect no differences in cortical thickness and cross-sectional properties, due to the similar pressure experienced by digits 2–5 during knuckle-walking (Matarazzo, 2013). Relative to *Pongo* and *H. sapiens*, the phalanges of *Gorilla* are predicted to have thicker cortices and stronger CSG properties, as the phalanges are incurring ground reaction forces from locomotion and joint reaction forces resulting from the contraction of the finger flexor and extensor musculature, along with the gravitational forces supporting the body mass (Jenkins & Fleagle, 1975; Tsegai et al., 2013). However, it is important to acknowledge that wild mountain gorilla (*Gorilla beringei*) knuckle-walking hand postures in their natural habitat are much more variable than those of zoo-housed gorilla and they commonly use non-knuckle walking hand postures (Thompson et al., 2018). These variable hand postures could result in different degrees of flexion/extension of the finger joints and more variable loading of the proximal phalanges (Thompson et al., 2018).

Pan (*Pan troglodytes* and *Pan paniscus*) also engages primarily in terrestrial knuckle-walking but is more variable in its positional behaviour than *Gorilla*, both within and across populations (Doran, 1996; Doran & Hunt, 1996; Hunt, 2020; Sarringhaus et al., 2014). Zoo studies show that *P. troglodytes* use more more variable hand postures than *Gorilla* (Tuttle, 1969a; Inouye, 1994). In zoo-housed *Pan*, digits 3 and 4 typically experience the highest loads during knuckle-walking, while in some bouts of knuckle-walking digit 5 does not touch down or experiences significantly less loading than the radial three digits (Matarazzo, 2013; Wunderlich & Jungers, 2009). Arboreal behaviours are more common in *Pan*, compared to *Gorilla*, but the frequency can vary substantially among sexes, communities and (sub)species (Doran, 1996; Doran & Hunt, 1996; Hunt, 2020; Ramos, 2014; Remis, 1998; Sarringhaus et al., 2014). *Pan* proximal phalanges show a greater degree of dorsal curvature than *Gorilla* (Fig. 3.1), which may reflect an increased degree of arboreality in their locomotor repertoire (Susman, 1979; but see Wallace et al., 2020). However, the frequency of habitual knuckle-walking is greater than arboreal behaviours (Doran & Hunt, 1996; Hunt 2020) and, as such, knuckle-walking signals will likely be reflected in the internal structure of manual phalanges. Thus, we predict *Pan* and *Gorilla* will share a similar pattern of cortical bone distribution due to their similar locomotor repertoires, along with cortical thickness and CSG properties of strength and rigidity against loads that are greater than those of *Pongo* and *H. sapiens*. Within *Pan*, we expect relative differences in cortical thickness and properties across the digits due to the more variable hand postures employed during their locomotor repertoire (Doran & Hunt, 1996; Matarazzo, 2013; Wunderlich & Jungers, 2009).

Humans are unique among great apes in using their hands mainly for manipulation, rather than in locomotion. Forceful precision grips, power squeeze grips, and precise in-hand manipulation are important in stone tool making and use and are thought to distinguish modern human manipulatory abilities from other hominids (Marzke, 1997; Williams-Hatala, 2016). Across modern human adults, power grips are employed most frequently during daily activities (Dollar, 2014; Feix et al., 2015). Power grips require the fingers to be in flexion, with experimental studies quantifying the biomechanics of power grips revealing that joint forces increase disto-proximally and digit 2

experiences the greatest loads followed by digits 3, 4, and 5 (de Monsabert et al., 2012; Sancho-Bru et al. 2014; Vigouroux et al. 2011). Human proximal phalanges are gracile and lack dorsopalmar curvature and strong muscle markings (Patel & Maiolino, 2016; Susman, 1979), likely reflecting lower loads incurred during manipulation compared with those of locomotion. We predict the pattern in *H. sapiens* will be of maximum thickness in the dorsal aspect of the shaft, as the straight proximal phalanges are typically in a flexed position during manipulation (Marzke, 1997; Rolian et al., 2011) and are experiencing bending stresses (Doden, 1993; Nguyen et al., 2014; Richmond, 2007), which are concentrated on the dorsal surface in straight phalanges. We also predict humans to show greater variability across the digits due to the frequent loading of digits 2 and 3 during daily manipulative activities (de Monsabert et al., 2012; Sancho-Bru et al. 2014). Finally, cortical thickness and CSG properties, associated with strength and rigidity against bending and torsional loads, of *H. sapiens* are predicted to be lower than that of the other great apes as humans most frequently use their hands for manipulation (Marzke, 2013; Tocheri et al., 2008).

3.3. Methods

3.3.1. Study sample

The study sample consists of manual proximal phalanges from digit 2 (n = 80 elements), digit 3 (n = 86 elements), digit 4 (n = 83 elements), and digit 5 (n = 70 elements) of *Homo sapiens* (n = 33 individuals), *Pan* (n = 24 individuals, including *P. troglodytes* and *P. paniscus*), *Gorilla gorilla* (n = 25 individuals), and *Pongo* (n = 9 individuals, including *Pongo abelii* and *Pongo pygmaeus*) (Table 3.1). Details of the study sample are shown in **Supplementary Table 3.1** and representative morphology of each taxon is depicted in **Figure 3.1**. All non-human apes were wild individuals with no obvious signs of pathologies within their hand skeletons or upper limbs. Our human sample originates from diverse post-industrial populations including 20th century Syracuse, Italy (n=2 individuals), 18th-19th century Inden, Germany (n=5), 16th century males of the Mary Rose shipwreck (n=7). It also includes pre-industrial populations including 6th – 11th century Nubian Egyptians (n=4), 19th century Tierra del Fuego (n =3), an indigenous Inuit from Greenland and two Aboriginal Australians. We also included in our *H. sapiens* sample several fossil *H. sapiens* including Qafzeh 8 and 9 (n=2 individuals, 80 – 130 Ka, Qafzeh, Israel; Niewoehner, 2001), Ohalo II H2 (n=1, 19 Ka, Sea of Galilee, Israel; Hershkovitz et al., 1995), Barma Grande (n=1, 15-17 Ka, Ventimiglia, Italy; Churchill & Formicola, 1997), Arene Candide (n=1, 12-11 Ka, Liguria, Italy; Sparacello et al., 2021), and Dolní Věstonice (n=4, 31 Ka, Dolní Věstonice, Czech Republic; Fewlass et al., 2019).

Table 3.1: Summary of study sample included in the study.

Taxon	N	PP2	PP3	PP4	PP5
<i>Homo sapiens</i>	33	22	26	27	21
<i>Pan paniscus</i>	7	7	7	7	6
<i>Pan troglodytes</i>	17	16	17	17	12
<i>Gorilla gorilla</i>	25	23	23	20	21
<i>Pongo abelii</i>	2	2	2	2	2
<i>Pongo pygmaeus</i>	7	7	7	7	6

3.3.2. MicroCT scanning

All phalanges were scanned with high-resolution micro-computed tomography (microCT) using a BIR ACTIS 225/300, Diondo D3 or Skyscan 1172 scanner housed at the Department of Human Evolution, Max Planck Institute for Evolutionary Anthropology (Leipzig, Germany), a Nikon 225/XTH scanner at the Cambridge Biotomography Centre, University of Cambridge (Cambridge, UK), or with a Diondo D1 scanner at the Imaging Centre for Life Sciences University of Kent (Canterbury, UK). The scan parameters included acceleration voltages of 100–160 kV and 100–140 μ A using a 0.2 to 0.5 mm copper or brass filter. Scan resolution ranged between 0.018 mm to 0.044 mm depending on the size of the bone. Images were reconstructed as 16-bit TIFF stacks.

3.3.3. Data processing

Non-bone inclusions or remaining soft tissues were removed from the scans and each phalanx was rotated into a standard orientation using Avizo Lite 9.0.0 (Visualization Sciences Group, SAS). Scans were subsequently segmented using the medical image analysis (MIA) clustering method (Dunmore et al., 2018). Once segmented, the outer and inner layer of the cortex was defined using Medtool v 4.5 (www.dr-pahr.at/medtool), following Tsegai et al. (2013) and Gross et al. (2014). This involves use of a ray-casting method to isolate the external and internal edge of the cortex in 3D and morphological filters to fill the bone, resulting in a mask of the inner and outer region of the cortex. Smooth external and internal surfaces of this voxel data were created using a custom script in Paraview v 4.4 and Meshlab v 2020.03 (**Fig. 3.2**). Six *Pan* and five *Gorilla* phalanges were excluded from the study sample (i.e., not included in sample sizes listed above) because their cortices were so thickened distally (i.e., almost completely filling the medullary cavity) that it did not allow for the creation of a distal internal surfaces because the rays could not detect a non-bone voxel.

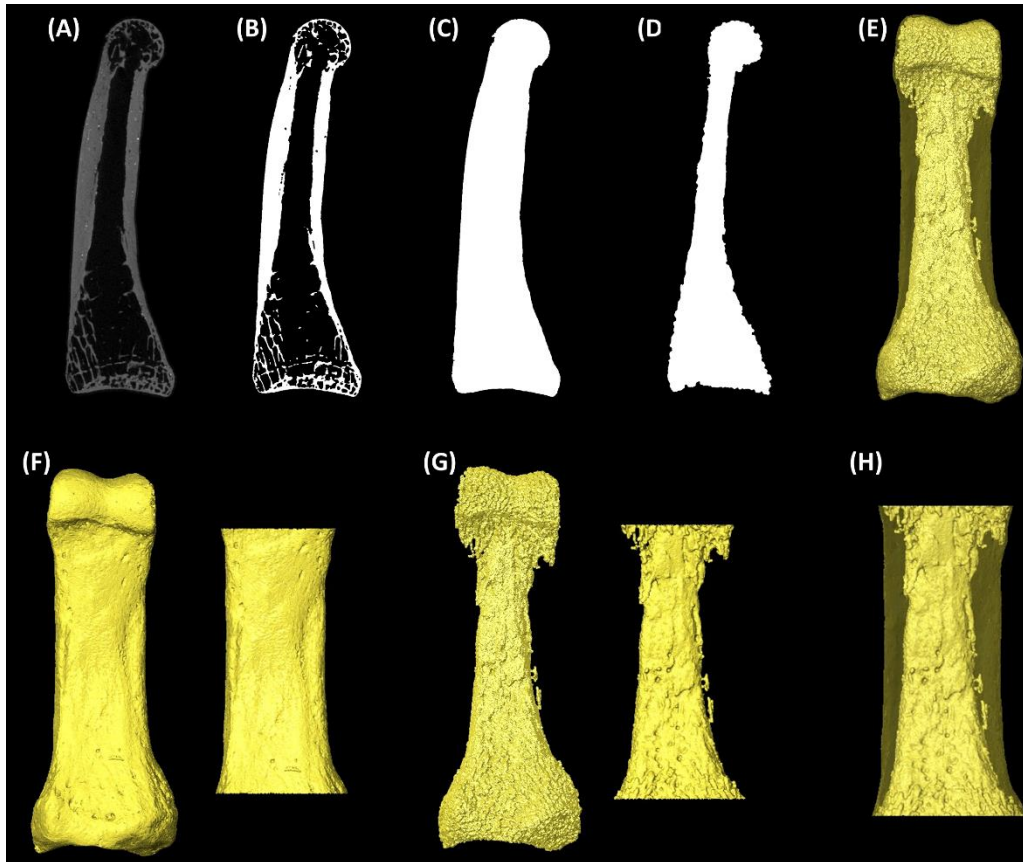


Figure 3.2: Steps taken to create surfaces for cortical thickness analysis. In Medtool 4.5 morphological filters were applied in the following steps: (a) Original microCT data of a Homo sapiens fourth proximal phalanx, (b) microCT data after MIA segmentation, (c) creation of outer layer of the cortex, (d) creation of inner layer of the cortex, (e) creation of an external (cortical) 3D surface from step c and an internal 3D surface from step d. Following surface creation, using Avizo Lite 9.0.0 the external and internal surface were cut (f and g) to define the shaft of the phalanx and (h) create cut surfaces for cortical bone thickness analysis in morphomap.

3.3.4. Cortical bone analysis

This study quantifies cortical bone distribution patterns and CSG parameters using the R package morphomap (Profico et al., 2021). In brief, morphomap allows the user to divide a 3D mesh of a long bone surface into a certain number of cross-sections and place a desired number of landmarks on the periosteal and endosteal outline of the bone. The landmark data allows for the quantification and mapping of cortical bone thickness, while the associated periosteal and endosteal outlines of each slice are used to measure CSG properties.

3.3.4.a. Morphomap parameters

Morphomap is designed to produce cross-sections across a certain percentage of the bone defined by the user (Profico et al., 2021). Since the current study quantifies cortical thickness of the phalangeal shaft across species of varying morphology, there was not a standardized percentage of phalangeal length that we could consistently define as the shaft across all

individuals/taxa. Variation in the shape and size of the proximal phalanx base and the trochlea meant that these features extended onto the diaphysis to differing degrees (**Fig. 3.1**). Thus, to compare homologous structures, we defined a region of interest (ROI) of the shaft as between the distal most extent of the base and the proximal end of the trochlea individually for each specimen.

The ROI was defined based on the external morphological features outlined above, both in palmar and lateral views, to ensure the greatest extent of the trochlea or base was not included in the ROI. The external and internal surfaces were cropped using Avizo Lite 9.0.0 (Visualization Sciences Group, SAS), however, as morphomap required a slight buffer on either end of the cropped ROI, this crop was at 2% above and below the defined shaft, so cortical thickness could be mapped across the entire ROI (**Fig. 3.2F-H & 2.9A-C**). Within morphomap, the cut external and internal ROIs were used to extract 97 sections at increments of 1% between 2% and 98% of the ROI length (i.e. the defined shaft length). At each cross-section, 50 paired equiangular semilandmarks, centred around the cortical area of each cross-section, were placed on the outlines of the external and internal surface to accurately capture the complex morphology of the phalangeal shaft. The combination of cross-sections and the landmarks placed on them allow a set of lines to be drawn from the centroid of each slice outwards to the landmarks placed on the internal and external outline of the 3D surfaces (Profico et al., 2021). Using these lines, cortical thickness is calculated as the length of the line between the internal and external surface outlines.

Along with measuring cortical thickness along the entire shaft, we also measured cortical thickness of landmark-defined palmar and dorsal surfaces of the shaft, which was assessed as a ratio of palmar/dorsal mean thickness. This allowed comparison of cortical thickness across genera without the influence of variation in size or shape of the FSRs, which are not represented by the dorsal and palmar landmarks. This morphology was defined by selecting an equal number of landmarks on the palmar and dorsal surface of the shaft but excluding the medial or lateral aspects of the bone, where the FSRs are located (**Fig. 2.9E**). To visualise the pattern of cortical bone distribution, morphometric maps of cortical thickness for each individual were created using R package morphomap.

3.3.4.b. Cross-sectional geometry

Cross-sectional geometric properties were calculated at each slice across the shaft with the R package morphomap. Different CSG properties quantify different aspects of the diaphysis and the most commonly used properties to understand the dynamic loads incurred by locomotion are: cortical area (CA; measure of axial strength), polar moment of area (J; measure of bending and torsional rigidity), and polar section modulus (Z_{pol} ; measure of maximum bending strength) (Lieberman et al., 2004; Marchi, 2005; Patel et al., 2020; Ruff & Runstead, 1992; Schaffler et al., 1985; Trinkaus & Ruff, 2012). We studied these cross-sectional properties at three positions along the shaft (35%, 50%, and 65% of the shaft length) of each phalanx to quantify variation in cortical robusticity within the phalangeal shaft. The specific cross-sections were chosen to account for variation in the proximodistal extension of the base and trochlear morphology across our sample and to ensure each cross-section sampled only the diaphysis.

3.3.5. Phalangeal curvature

The degree of phalangeal curvature was measured using the included angle (IA) method. The IA (θ) method assumes the curvature of a phalanx in the dorsopalmar direction is represented

by an arc length on the perimeter of a circle (Stern et al., 1995). Low values of θ are characteristic of straighter phalanges, commonly associated with quadrupedalism and bipedalism, and higher values of θ are characteristic of increasingly curved phalanges, commonly associated with arboreality (Jungers et al., 1997; Stern et al., 1995). The IA method was chosen as it has been the most prevalent approach to calculate phalangeal curvature and does well to distinguish the locomotor behaviours of species (Jungers et al., 1997; Matarazzo, 2008; Rein, 2011; Stern et al., 1995). However, it is important to note that the IA method is susceptible to measurement errors (Deane & Begun, 2008; Patel & Maiolino, 2016), therefore three repeated measurements were taken to correct for intra-observer measurement error.

3.3.6. Statistical analyses

As larger bones and individuals will potentially have higher absolute values of cortical bone and larger cross-sections, we scaled the data by the length of the bone. Phalangeal length was measured digitally on surface models in Avizo 9.0., from the most proximal extent of the base to the most distal extent of the trochlea in dorsal view. All statistical analyses were conducted on the scaled data, as well as on raw data for intra-generic comparisons.

3.3.6.a. Cortical thickness distribution pattern

Cortical thickness values were calculated from a measurement between each pair of corresponding landmarks at the inner and outer cortical surface on each slice of the defined shaft, resulting in 4850 measurements per phalanx. To explore differences in the distribution of cortical bone thickness between taxa, each of the 4850 measurements were treated as a variable in a principal component analysis (PCA). To test if cortical thickness distribution patterns of each taxon were significantly different from each other, an omnibus permutational multivariate analysis of variance was run on the first three PC scores using the R package Vegan. If this test was statistically significant ($p < 0.05$), it was followed by a pairwise one-way permutational multivariate analysis of variance with a Bonferroni correction to test which groups were significantly different from one another. Permutational multivariate analysis of variance tests were conducted because Shapiro-Wilk tests revealed that not all data were normally distributed.

3.3.6.b. Mean cortical thickness

Inter- and intra-generic differences in mean cortical thickness were assessed using Kruskal-Wallis tests, as Shapiro-Wilk tests revealed the data was not normally distributed, followed by a post hoc Dunn Test. Inter-generic testing was conducted on each digit separately. Paired sample t-tests were used to analyse differences in palmar and dorsal cortical thickness, as the palmar cortical thickness and the dorsal cortical thickness data sets were normally distributed.

3.3.6.c. Cross-sectional geometric properties

Intra-generic differences in cross-sectional properties (CA, Z_{pol} , and J) at the three diaphyseal positions (35%, 50%, 65%) across the digits of each taxon were compared using a Kruskal-Wallis test, followed by a post hoc Dunn test separately, along with intra-generic differences in diaphysis position within each digit. Inter-generic differences in cross-sectional geometric properties were assessed for each property at each position for each digit using a Kruskal-Wallis test, followed by a post hoc Dunn test.

3.3.6.d. Relationship between curvature and cortical thickness

Regression analyses were used to test the relationship between phalangeal curvature (IA values) and mean cortical thickness for each taxon. For each taxon, all four digits were pooled together to increase the sample size and to produce a more reliable fit of the regression model.

All statistical tests were performed using the R package RVAideMemoire (v 0.9-79 Hervé, 2021), Stats (R Core Team 2021) and FSA (v 0.9.3 Ogle et al., 2022). Statistical tests were carried out in R version 4.1.3 and all tests were considered statistically significant with a $p < 0.05$.

3.4. Results and Discussion

This study explored the relationship between expected loading during various locomotor and hand-use behaviours and the cortical structure of non-pollical proximal phalanges in extant hominids. The distribution of cortical bone, as well as its overall thickness and CSG properties differed among genera, and across the digits within genera, in line with some of our predictions. These results support a relationship between cortical morphology of the manual phalanges and loading of the hand among great apes. **Figure 3.3** depicts cortical thickness distribution morphometric maps of the proximal phalanges (digits 2-5) in a representative individual for each taxon, while morphometric maps for all individuals within our sample are presented in **Supplementary Figure 3.1**. **Figure 3.5** depicts average cortical thickness plotted across the shaft for each taxon and **Table 3.2** shows mean values of cortical thickness. **Supplementary Table 3.2** shows mean values of all cross-sectional properties across the three cross-sections. Variation in cortical bone distribution patterns were assessed via principal component analysis. This is followed by a description of cortical distribution patterns, as well as variation in cortical thickness and cross-sectional properties for each study taxon.

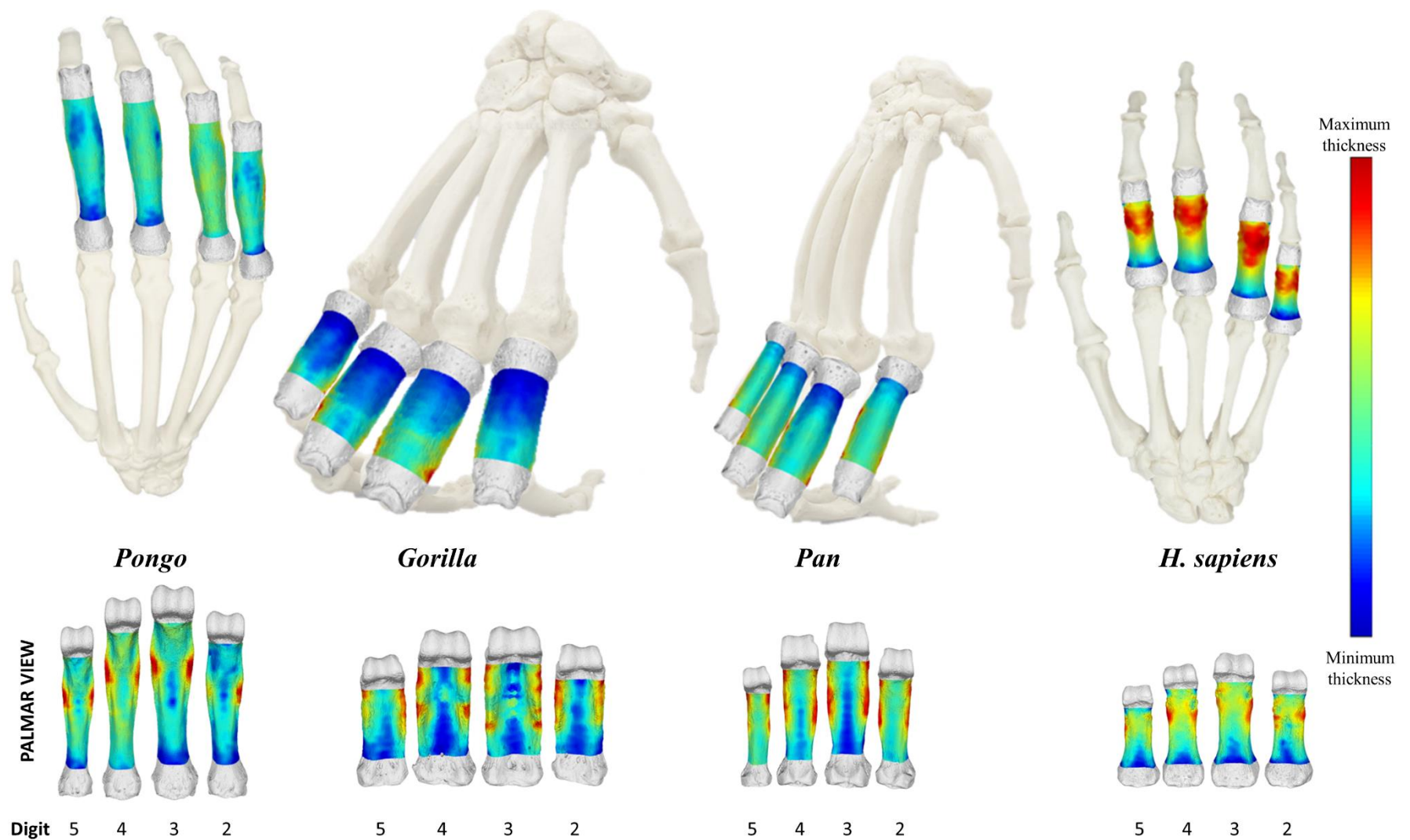


Figure 3.3: Representative 3D maps of cortical bone distribution of proximal phalanges of digits 2-5 of *Pongo pygmaeus*, *Gorilla gorilla*, *Pan troglodytes*, *Homo sapiens* in dorsal (top) and palmar (bottom) view. Thickness maps of each bone are independent of each other. Proximal phalanges are not scaled.

Table 3.2: Summary statistics of raw (mm) and standardised (dimensionless) cortical thickness measurements of the phalangeal shaft.

	<u><i>H. sapiens</i></u> Mean (SD)	<u><i>Pan</i></u> Mean (SD)	<u><i>Gorilla</i></u> Mean (SD)	<u><i>Pongo</i></u> Mean (SD)
<u>Raw</u>				
PP2	1.477 (0.290)	2.520 (0.438)	2.862 (0.550)	2.078 (0.328)
PP3	1.561 (0.261)	2.679 (0.481)	3.220 (0.563)	2.187 (0.341)
PP4	1.507 (0.264)	2.605 (0.452)	2.924 (0.512)	2.212 (0.360)
PP5	1.199 (0.262)	2.257 (0.361)	2.556 (0.504)	1.981 (0.298)
<u>Standardized*</u>				
PP2	0.036 (0.007)	0.051 (0.007)	0.054 (0.006)	0.033 (0.005)
PP3	0.034 (0.006)	0.048 (0.008)	0.055 (0.006)	0.031 (0.004)
PP4	0.035 (0.006)	0.049 (0.007)	0.053 (0.006)	0.032 (0.005)
PP5	0.035 (0.007)	0.053 (0.008)	0.055 (0.008)	0.033 (0.004)

*standardized by bone length

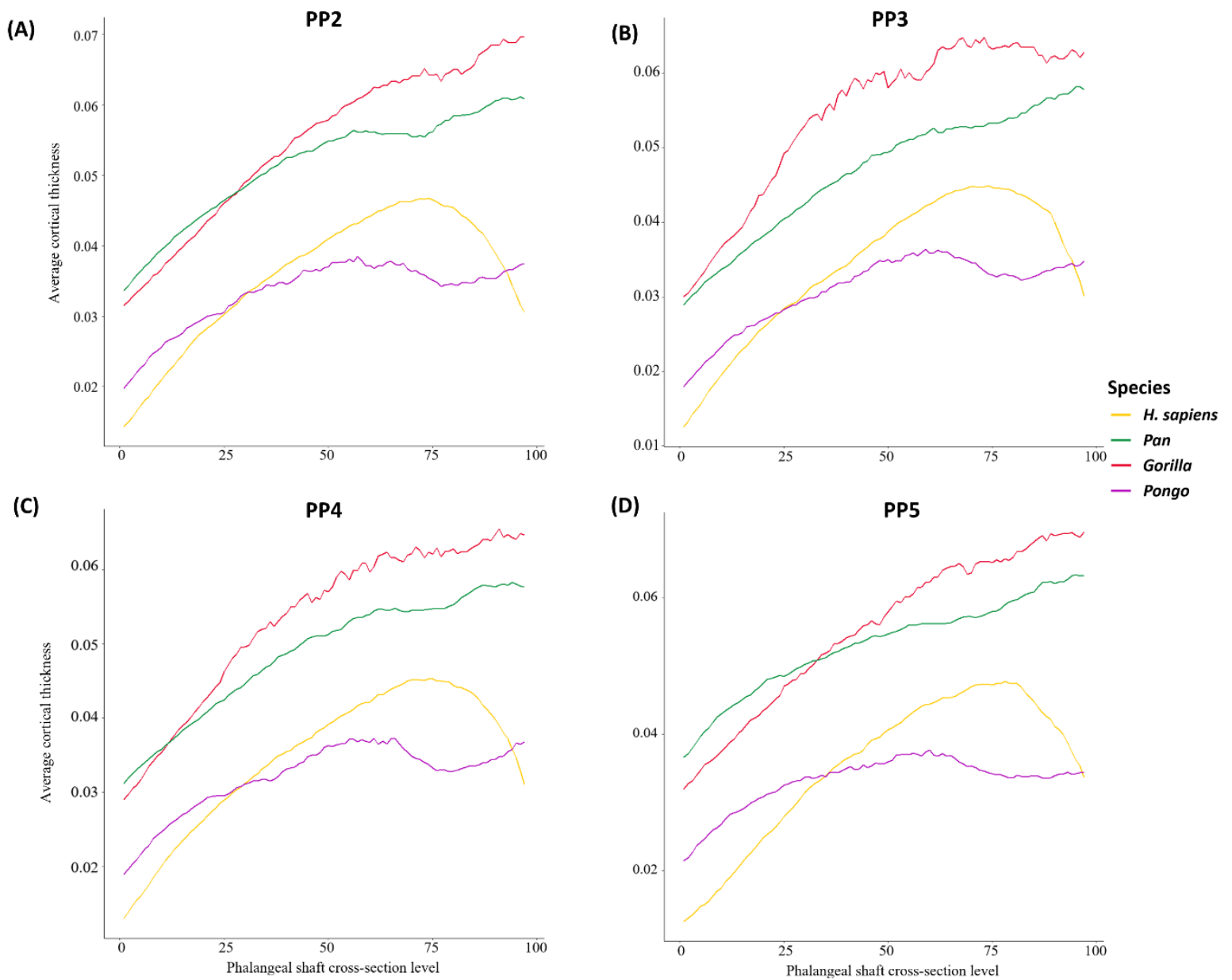


Figure 3.4: Average scaled cortical bone thickness plotted from the proximal end (0) to the distal end (100) of the phalangeal shaft of *H. sapiens*, *Pan*, *Gorilla*, and *Pongo*. (A) PP2; (B) PP3; (C) PP4; (D) PP5.

3.4.1. Cortical bone thickness distribution

Principal component analysis of scaled cortical thickness values from each phalanx (digits 2–5) was used to assess whether cortical thickness distribution patterns differ among taxa and whether this corresponds with their respective differences in hand use (Fig. 3.5; S. Fig. 3.2). PCA was conducted for each digit, but due to comparable separation among the study taxa across all four digits (S. Table 3.2), as well as similar PC1 and PC2 loadings, we describe the general pattern common to the proximal phalanges of each taxa, but highlight instances where particular digits differed from the general pattern.

PC1 explains 56% – 63% of the total variance in each of the four digits. *Gorilla* is separated from the other taxa by having low PC1 scores, representing more developed FSRs, and *H. sapiens* is characterized by high PC1 scores, reflecting a thicker distodorsal cortex in PP2-4. *Pan* and *Pongo* are intermediate and variably overlap with other taxa. The overlap of *Pan* and *Pongo* in PP2-PP4 may be due to the greater frequency of arboreal locomotion in *Pan* relative to *Gorilla* (Tuttle & Watts 1985; Doran 1992; Doran & Hunt 1996; **Fig. 3.5**; **S. Fig. 3.2**).

For PP3, low PC1 values separating *Gorilla* from other taxa are related to thickened FSRs with a low-to-intermediately thick dorsal region of the shaft, compared to high PC1 values in *Pongo* and *H. sapiens* reflecting distodorsal thickness and thick cortices on the FSR. The greater overlap between *Gorilla* and *Pan* in PP3 relative to the other digits is due to a few individuals of *Gorilla* displaying an intermediately thick shaft similar to *Pan*.

For PP5, low values of PC1 characterize *Gorilla* and *Pan* with thick FSRs and high values reflect distodorsal and FSR thickness in *Pongo* and *H. sapiens*. The complete overlap of *Pongo* with *H. sapiens* in PP5 is due to a distal thickening of the region under the trochlea in PP5 of both species.

PC2 explains <8% of the variance in the PCAs of all four digits and represents the region of overall maximum cortical thickness. Low values along PC2 are driven by a proximal to distal cortical bone distribution on the palmar surface and high values represent a cortical bone concentration on either the mid-shaft to distal region of the palmar or dorsal surface of the shaft. *Gorilla* and *Pan* are the only taxa to be separated along PC2, reflecting a palmar proximo-distal concentration of cortical bone in *Gorilla* and a mid-shaft to distal concentration in *Gorilla* and *Pan*.

A 3D plot of PC1, PC2, and PC3 (<6%) provides clear separation among taxa, especially for PP5, with only slight overlap in *Pan* and *Pongo* in PP2 and PP4 and between *Pan*, *Pongo*, and *H. sapiens* in PP3 (**S. Fig. 3.2**).

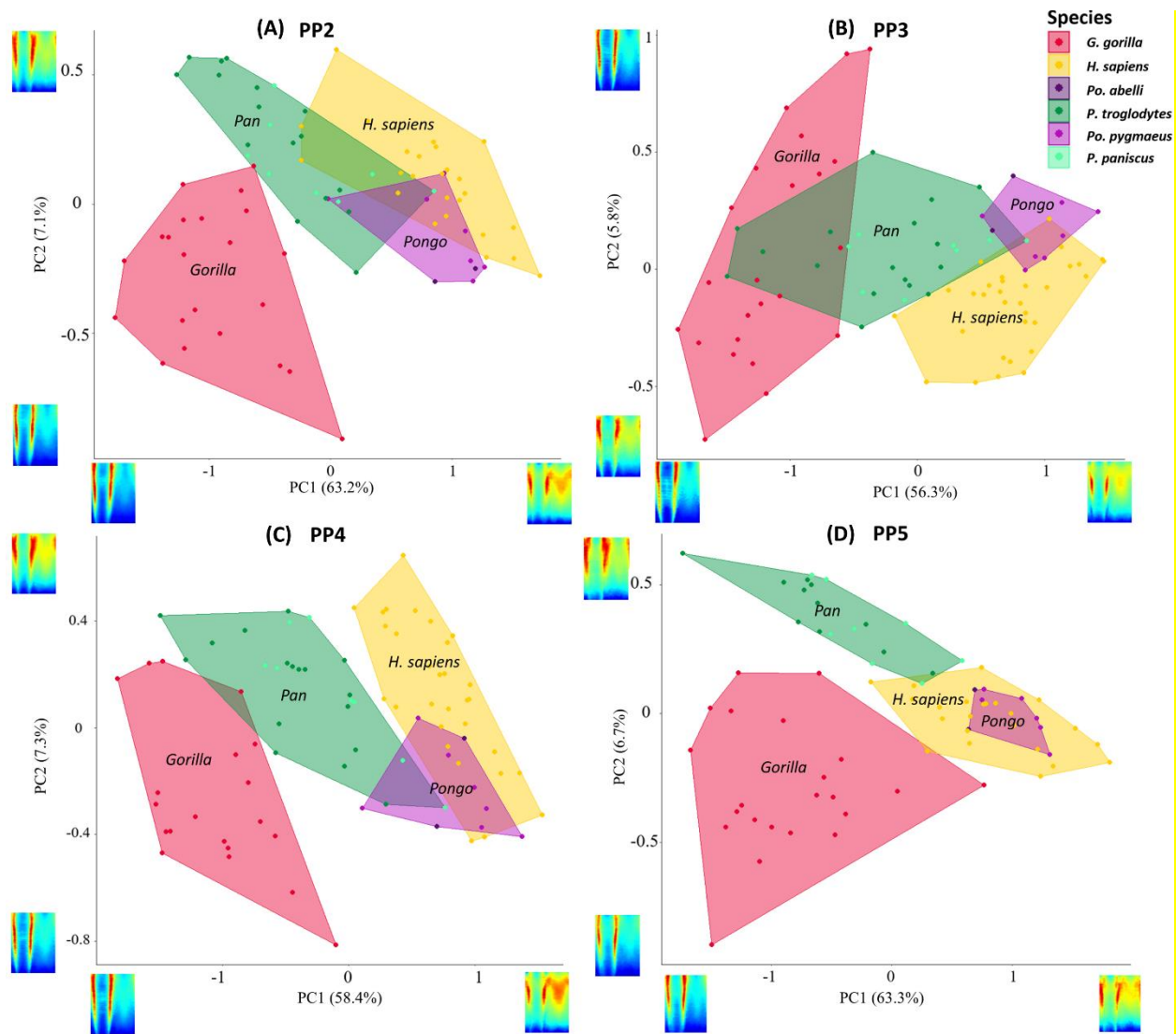


Figure 3.5: PC1 and PC2 for cortical bone distribution of proximal phalanges of PP2, PP3, PP4, and PP5 of *H.sapiens*, *Pan* sp., *Gorilla*, and *Pongo* sp.

3.4.2. Mean cortical thickness

Table 3.2 shows mean values of cortical thickness. Scaled mean cortical thickness values across the shaft reveal the African apes have significantly thicker cortex than *H. sapiens* and *Pongo* (Table 3.2; S. Fig. 3.3).

3.4.3. Cross-sectional geometry

Descriptive statistics of the scaled cross-sectional geometric properties at 35%, 50% and 65% of the shaft are presented in Supplementary Table 3.3 and depicted in Figures 3.7–3.9. Only *Gorilla* has significantly larger values of CA, Z_{pol} and J across all digits and cross-sectional levels compared to the other taxa (S. Table 3.4; 3.5). CSG properties differ across the digits in all taxa except *Pongo* (S. Table 3.6; 3.7).

3.4.4. *Pongo*

As the hand of *Pongo* is used primarily for grasping, we predicted that *Pongo* would have thicker regions of cortical bone distopalmarly on the shaft, especially close to the FSRs, and that this pattern would be consistent across the hand. In support of this prediction, we find cortical bone in *Pongo* to be thickest at the FSRs in all phalanges (**Fig. 3.3; S. Fig. 3.1**), corresponding with expected loading during grips in which the PIP joint is flexed. The point of maximum thickness within the shaft is at the distal end of the FSR, with cortical thickness reducing just distal to the FSRs and then increasing again proximal to the trochlea (**Fig. 3.4**). The ratio of cortical thickness of the dorsal and palmar shaft (i.e., removing the influence of the FSRs) demonstrates that the palmar aspect of the shaft is always thicker than the dorsal (**Table 3.3; Fig. 3.6**). A biomechanical function of FSRs is to reduce strain on the shaft, such that the taller the ridge, the more strain it experiences and consequently the amount of strain distributed to the palmar shaft is reduced (Nguyen et al., 2014). However, the FSRs in *Pongo* are not particularly prominent (i.e., do not extend far above the palmar surface of the shaft) relative to other taxa, such as *Gorilla* (Syeda et al., 2021). This suggests that the strain resulting from grasping arboreal substrates during suspension is dissipated across the FSRs, without requiring modelling of the cortical structure along the remainder of the shaft.

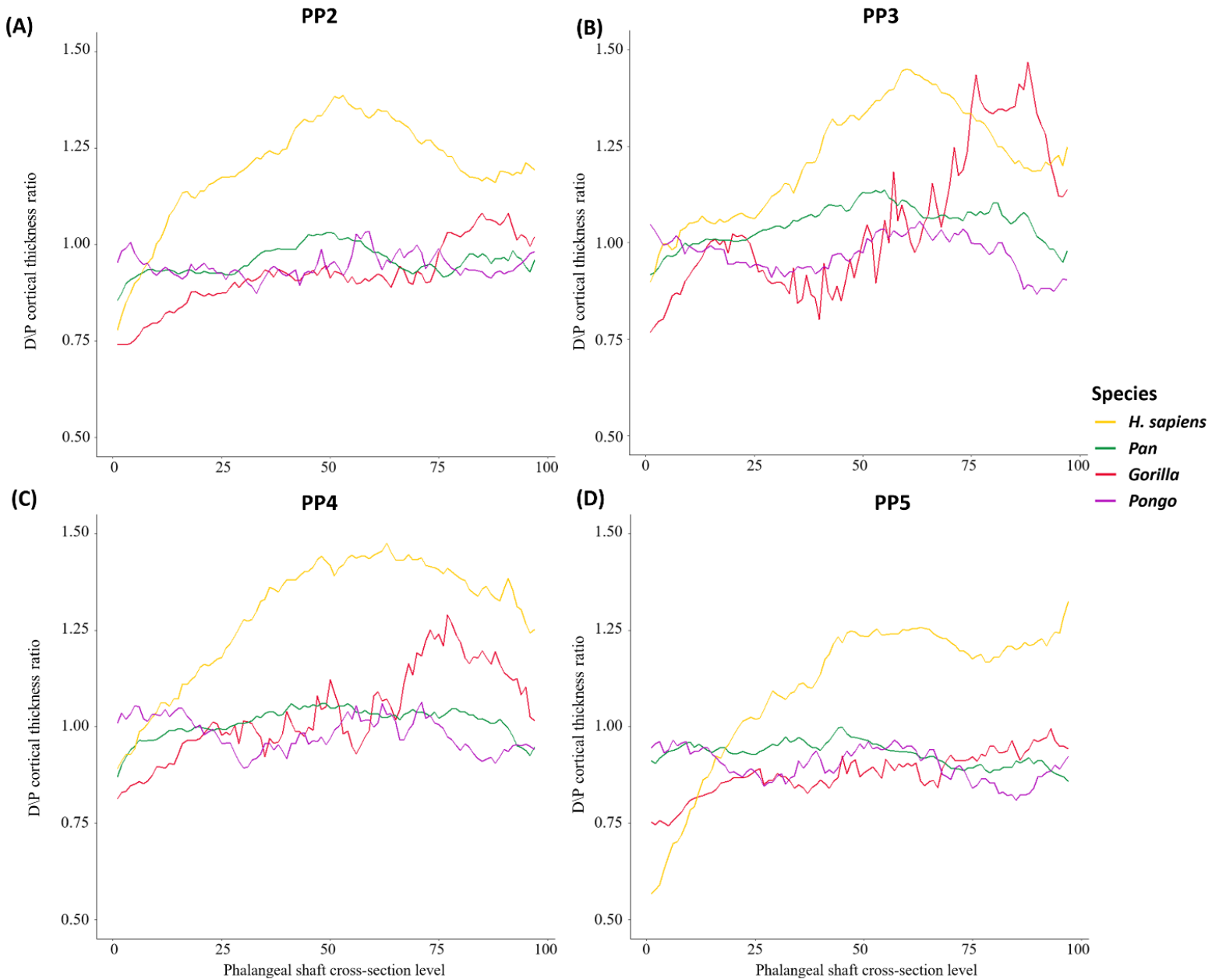


Figure 3.6: Ratio of dorsal/palmar cortical bone thickness plotted from the proximal end to the distal end of the phalangeal shaft of *H. sapiens*, *Pan*, *Gorilla*, and *Pongo*. (A) PP2; (B) PP3; (C) PP4; (D) PP5. Values greater than 1 represent more dorsal cortex relative to the palmar cortex in the shaft.

Table 3.3: Paired samples t-tests on scaled palmar vs. dorsal cortical thickness across species.

		<i>H. sapiens</i>	<i>Pan</i>	<i>Gorilla</i>	<i>Pongo</i>
PP2	Palmar mean	0.031	0.048	0.048	0.033
	Dorsal mean	0.038	0.046	0.044	0.031
	t-ratio	-3.489	1.057	2.363	0.904
	p	0.001	0.296	0.023	0.380
PP3	Palmar mean	0.029	0.042	0.043	0.030
	Dorsal mean	0.037	0.044	0.045	0.029
	t-ratio	-4.447	-1.178	-0.945	0.516
	p	<0.001	0.245	0.350	0.613
PP4	Palmar mean	0.029	0.045	0.043	0.031
	Dorsal mean	0.038	0.045	0.044	0.030
	t-ratio	-5.682	-0.335	-0.926	0.326
	p	<0.001	0.739	0.361	0.749
PP5	Palmar mean	0.031	0.052	0.052	0.033
	Dorsal mean	0.035	0.048	0.046	0.030
	t-ratio	-2.149	1.583	2.940	1.791
	p	0.037	0.123	0.005	0.096

Abbreviations: NS = not significant ($p > 0.05$).

Comparison of these patterns across the hand shows that, as we predicted, cortical bone distribution is similar across the digits in *Pongo*, with the exception of PP2, where cortical bone is thicker on the radial aspect of the palmar shaft (*Pongo* PP2 in **S. Fig. 3.1**). This radial asymmetry could reflect grasping of very thin substrates, during which the second digit is greatly extended relative to the ulnar digits (Napier, 1960). Despite this differing pattern of cortical bone distribution in PP2, there are no significant differences in mean cortical thickness or CSG properties across the *Pongo* digits (**S. Fig. 3.4**). The absence of significant differences in mean cortical thickness or CSG properties between the digits is consistent with relatively equal loading of all fingers during arboreal locomotion in *Pongo* (Rose, 1988; Susman, 1974; Thorpe & Crompton, 2006; Thorpe et al., 2009).

Regarding CSG properties, we predicted that *Pongo* phalanges would have thinner cortices and be less resistant to bending and torsion than those of the African apes. *Pongo* has the thinnest mean relative cortical thickness when scaled by bone length (**Table 3.2**; **S. Fig. 3.3**), which is significantly thinner than that of African apes, partially supporting our third prediction (**S. Fig. 3.3**). Cross-sectional properties of *Pongo* are only significantly lower than those of *Gorilla*. However, while not significantly different from *Pan* and *H. sapiens*, relative mean values of CSG properties are lowest in *Pongo* among our sample. (**Figs. 3.7–3.9**; **S. Table 3.3**). This thin cortical structure and

low cross-sectional properties of the *Pongo* proximal phalanges may relate to aspects of their external morphology. Among the great apes, *Pongo* phalanges have the greatest degree of curvature and their FSRs are located opposite the point of the maximum arc of this curvature, thus preventing the long tendons of the digital flexor muscles from being pulled into an extreme palmar position (Susman, 1979). This acts to reduce joint reaction forces and also aligns the bone more closely with this joint reaction force, ultimately leading to optimised distribution of load across the phalanx (Nguyen et al., 2014; Richmond, 2007; Susman, 1979). Thus, in *Pongo* a thicker cortex may not be needed due to the functional adaptations of the external shape to minimize strain experienced by the phalanx (Pearson & Lieberman, 2004; Ruff et al., 2006).

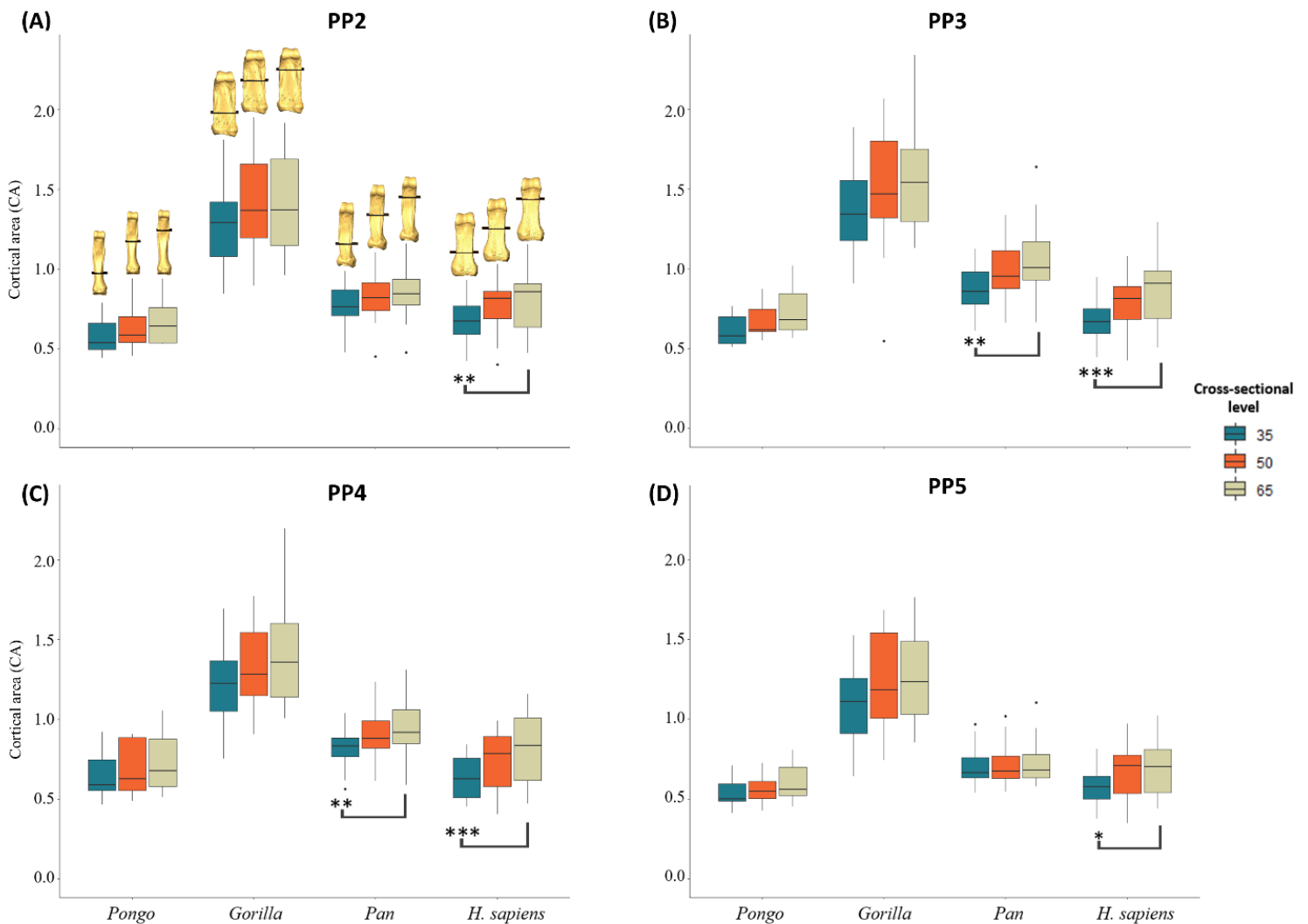


Figure 3.7: Boxplots representing cortical area for digits 2-5 of *H. sapiens*, *Pan* sp., *Gorilla*, and *Pongo* sp. at 35%, 50%, and 65% of the bone length. Section locations are represented on 3D surfaces of PP2 of an individual from each taxon.

3.4.5. Gorilla

In support of our predictions, morphometric maps of cortical bone thickness distribution reveal the regions of thickest cortex in *Gorilla* PP2–PP4 are located in patches along the FSRs, as well as proximal to the trochlea (**Fig. 3.3**; **S. Fig. 3.1**). The shaft shows low to intermediate cortical thickness, with the FSRs being thicker than the remaining aspects of the shaft. Quantitative comparisons of *Gorilla* mean cortical thickness values across the shaft show a distal increase in cortical thickness in all digits (**Fig. 3.4**). The distinctive regions of thicker palmar cortical bone are located at the attachment points of the soft tissues involved in stabilising the fingers in flexed positions during knuckle-walking. On the FSR, these locations of thicker cortical bone correspond with the attachment points of the ligaments and pulleys (**Fig. 3.3**) that provide biomechanical advantage by keeping the flexor tendons close to the bone and in line with the joint axis. This decreases the moment arm and allows for optimal joint function and force transmission during finger flexion (Ayhan & Ayhan, 2020; Doyle, 2001). During knuckle-walking, the stress in the flexor tendon is concentrated distally on the second annular pulley (A2), at the location where the tendon is maximally bent during knuckle-walking (Leijnse et al., 2021). When the phalangeal joints are in flexion during knuckle-walking, the flexor tendons are pulled palmarly and the digital pulleys are then stretched, which leads to increased strain in the phalanx in the same regions as we find thicker cortical bone (Ayhan & Ayhan, 2020; Leijnse et al., 2021; Ruff et al., 2006). The region of thick cortical bone proximal to the trochlea coincides with the attachment site of the collateral ligaments of the PIP joint. The collateral ligaments arise from the radial and ulnar sides of the distal end of the proximal phalanx and run obliquely to the palmar radial and ulnar surfaces of the intermediate phalanx (**Fig. 3.1F**), providing lateral stability to the phalangeal joints during flexion and extension (Ayhan & Ayhan, 2020). This stability is essential for the intermediate phalanx to accommodate high loads during knuckle-walking.

Contrary to our predictions, the pattern of cortical bone thickness distribution in PP5 is distinct from that of the more radial digits, in that the region of maximum thickness is consistently located between the proximal end of the FSR and the region just proximal to the trochlea (**S. Fig. 3.1**). This variation in thickness may be due to lower pressure being placed on the fifth digit during knuckle-walking compared to the other rays (Matarazzo, 2013), such that the pressure is being evenly dissipated from the proximal end of the FSRs to the distal end of the bone. The attachment points of the pulleys and ligaments may not be experiencing enough strain to elicit a biomechanical remodelling response at those regions. There is some asymmetry in the cortical thickness distribution patterns of PP2 and PP5, such that the thickest portion of the shaft in PP2 is on the palmar ulnar surface and in PP5 is on the palmar radial surface (**S. Fig. 3.1**). This may reflect the location of pressures experienced during knuckle-walking, which are highest on the third digit (Matarazzo, 2013; Preuschoft, 1973; Samuel et al., 2018).

Furthermore, there is variation in the patterning of palmar and dorsal cortical thickness in the proximal phalanges of *Gorilla*. There is no significant difference in thickness between the palmar and dorsal cortex of PP3 and PP4, but in PP2 ($p = 0.023$) and PP5 ($p = 0.005$) the cortex is significantly thicker palmarly compared to dorsally (**Table 3.3**). This could be due to the smaller FSRs of PP2 and PP5 compared to PP3 and PP4, in which the strain on the palmar shaft is reduced due to the tall FSRs (Nguyen et al., 2014; Susman, 1979). While there are nuanced differences in each of the digits in regard to cortical bone distribution pattern and relative palmar and dorsal

cortical thickness, we predicted no overall differences in mean cortical thickness and cross-sectional properties across the *Gorilla* digits. However, PP5 has significantly lower CSG than PP3 (S. Table 3.3, 3.7). These results could be due to more neutral position of the *Gorilla* hand during the majority of knuckle-walking hand postures, along with similar lengths of the metacarpus and proximal phalanges, which allows them to consistently touch down with their fifth digit despite placing significantly less pressure on it relative to the other digits (Matarazzo, 2013; Susman, 1979; Susman & Stern, 1979; Thompson et al., 2018). However, it is important to acknowledge the studies that quantified pressure distribution during locomotion in extant non-human great apes (e.g. Matarazzo, 2013; Wunderlich & Jungers, 2009; Samuel et al., 2018) have, for logistical reasons, focused on animals in captivity in an enclosed space and likely do not fully reflect manual behaviours in the wild.

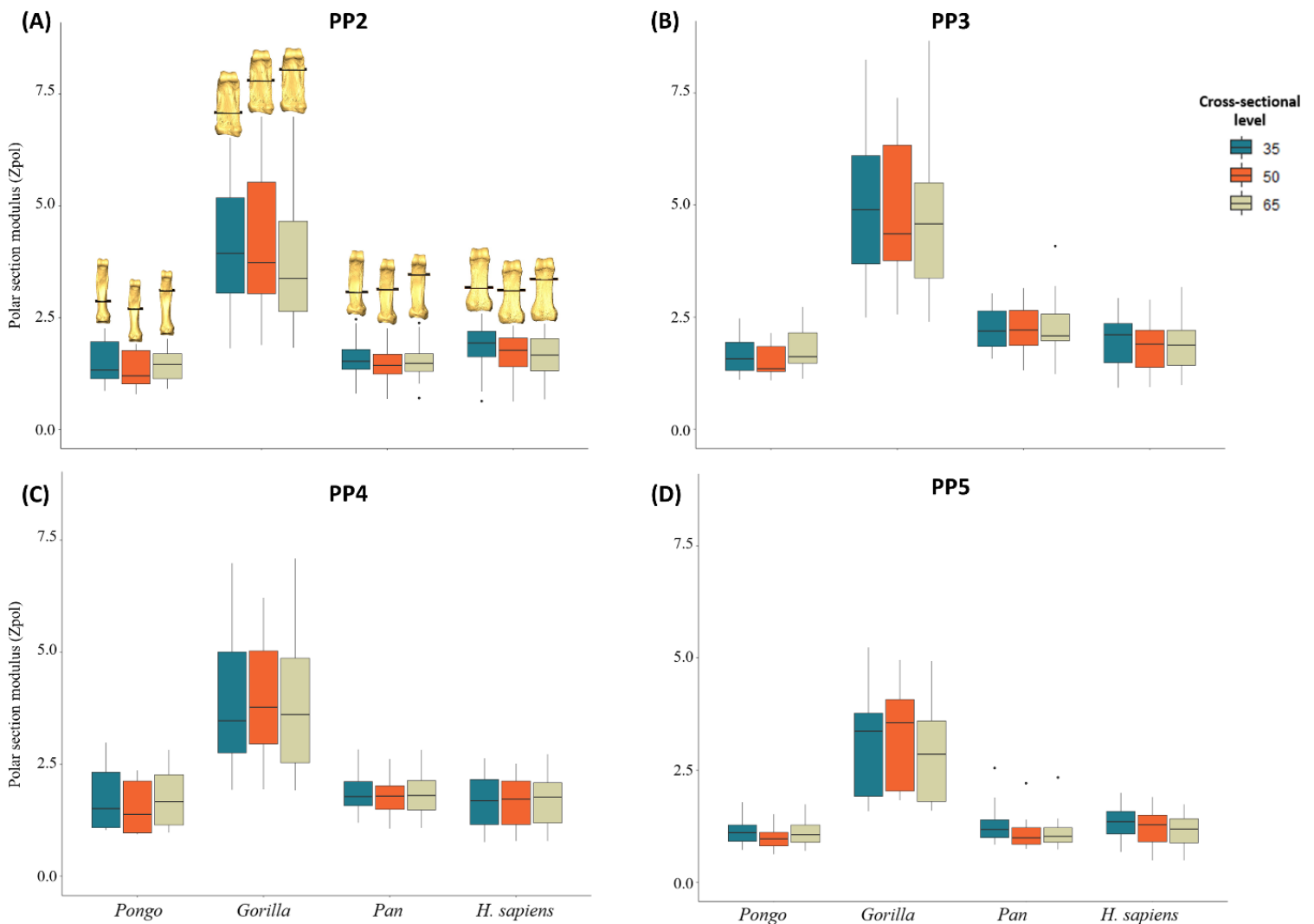


Figure 3.8: Boxplots representing polar section modulus (Z_{pol}) for digits 2-5 of *H. sapiens*, *Pan sp.*, *Gorilla*, and *Pongo sp.* at 35%, 50%, and 65% of the bone length. Section locations are represented on 3D surfaces of PP2 of an individual from each taxon.

3.4.6. *Pan*

Our expectations for *Pan* were generally supported. The pattern of cortical bone distribution in *Pan* is similar to *Gorilla* in having thicker cortical bone at the FSRs and in the region proximal to the trochlea. However, unlike *Gorilla*, the shaft is relatively intermediate in its thickness compared to the thin proximal region of the bone (**Fig. 3.3; S. Fig. 3.1**). This difference in cortical bone thickness patterning among the knuckle-walking apes could be a reflection of *Pan* participating in arboreal behaviours to a greater extent than *Gorilla* (Doran, 1996;1997; Hunt, 2020; MacKinnon, 1976; Sarringhaus et al., 2014; Susman, 1984). While the magnitude of loads during knuckle-walking and arboreal locomotion have been shown to be similar (Synek et al., 2020), loads of knuckle-walking may be reflected in the internal morphology more so than the overall forces of infrequent arboreal behaviours. External morphological features may play a role in these differences in internal bone structure. Within the African apes, the higher degree of curvature of the *Pan* phalanges, relative to that of *Gorilla*, should be an advantage for load distribution during arboreal behaviours (Deane & Begun, 2008; Hunt, 1991b; Oxnard, 1973; Richmond, 2007; Stern et al., 1995) but the less prominent FSRs would not act to reduce strain experienced by the remainder of the shaft to the same extent as in *Gorilla* (Nguyen et al., 2014). As such, CSG properties, mean cortical bone thickness and distribution patterns may reflect the greater degree of arboreal behaviours in *Pan*.

Our prediction that there will be variation in cortical thickness pattern and properties across the *Pan* digits was not fully supported. Unexpectedly, PP5 has significantly thicker cortex ($p = 0.044$; **S. Fig. 3.4**) than PP3, but when compared to PP5, the radial three digits are significantly stronger in resisting axial, bending and torsional loads, along with PP3 being stronger than PP2 (**S. Table 3.3, 3.7**). Overall, these results may reflect low loading of the fifth digit during knuckle-walking, as it is loaded significantly less than the other digits and sometimes does not make contact with the substrate (Matarazzo, 2013; Wunderlich & Jungers, 2009). While surprising, the relatively thinner cortex in PP3 may be reflecting the impact of external morphology (taller FSRs, high degree of curvature), which are most prominent in the third digit within the *Pan* hand, on cortical remodelling. The similarity in cortical properties among the radial digits could be explained by the variability of hand postures used by *Pan* (Inouye, 1994; Matarazzo, 2013; Samuel et al., 2018; Tuttle, 1967; 1969; Wunderlich & Jungers, 2009), such that the varying hand positions during locomotion result in differing sequences of digital placement, affecting which digit receives the greatest pressures (Wunderlich & Jungers, 2009). The variation in knuckle-walking hand postures and greater degree of arboreality in the *Pan* locomotor repertoire, may also explain the intermediate thickness of the shaft with no significant difference in palmar and dorsal cortical thickness (**Fig. 3.3; Table 3.3**). PP5 is also distinct from the other digits in displaying a radial concentration in its thickness pattern (**S. Fig. 3.1**), potentially reflecting peak pressures during locomotion being located around the centre of the hand and lower pressures under the 5th digit (Matarazzo, 2013; Preuschoft, 1973; Samuel et al., 2018).

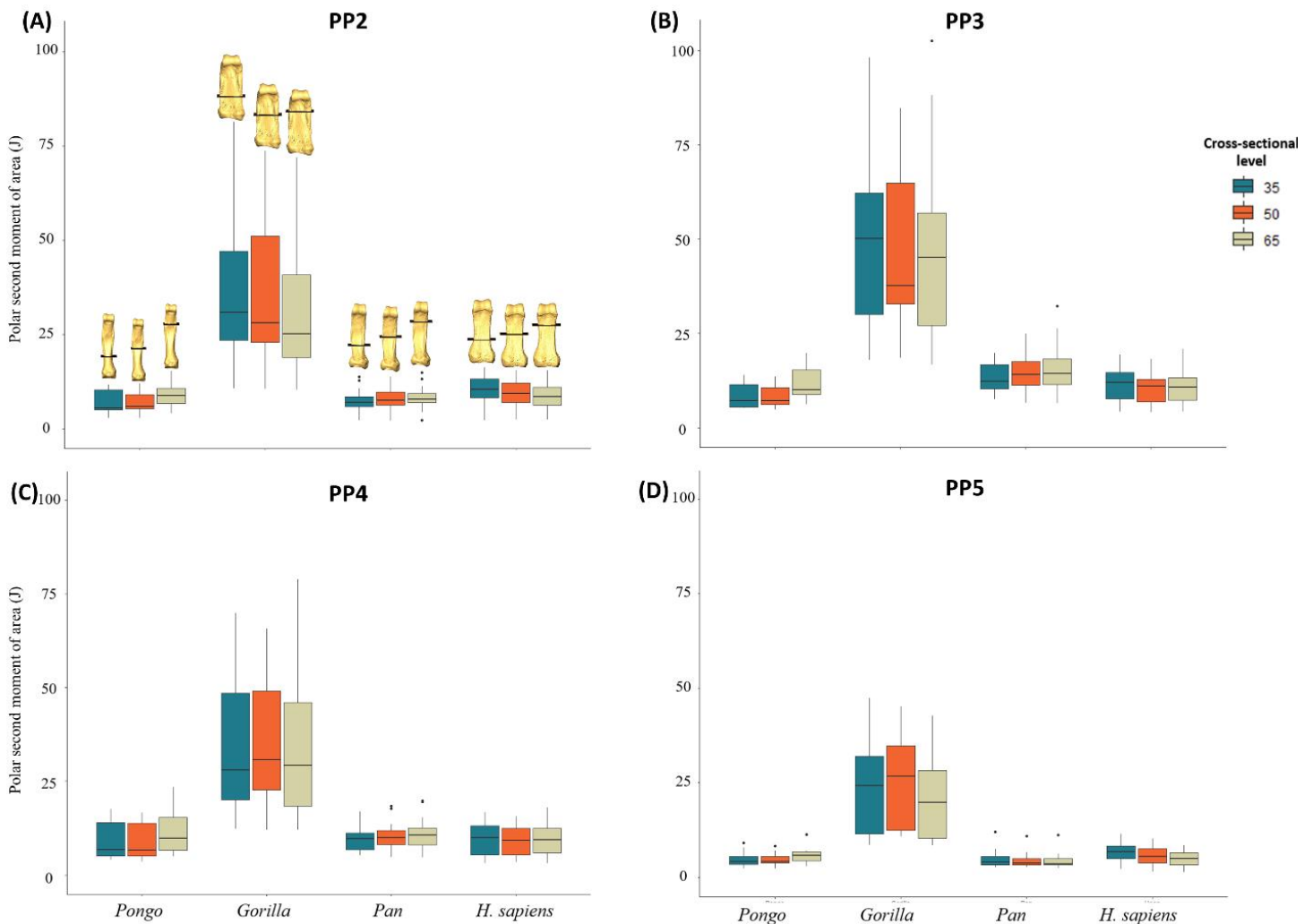


Figure 3.9: Boxplots representing polar second moment of area (J) for digits 2-5 of *H. sapiens*, *Pan sp.*, *Gorilla*, and *Pongo sp.* at 35%, 50%, and 65% of the bone length. Section locations are represented on 3D surfaces of PP2 of an individual from each taxon.

3.4.7. *Homo sapiens*

Our predictions that *H. sapiens* would display the thickest cortex in the distodorsal region of the shaft and that they would be characterised by thick cortical bone where FSRs are present, are generally supported (Fig. 3.3; S. Fig. 3.1). Although the distal dorsal and palmar aspect of the phalangeal shaft is thick as predicted, cortical thickness is concentrated on the midshaft to distodorsal region of the diaphysis. Cortical thickness of the dorsal surface is significantly greater than the palmar surface (Fig. 3.6; Table 3.3) and decreases past the distodorsal region of maximum cortical thickness (Fig. 3.4). This could reflect the lack of phalangeal curvature in *H. sapiens* and the frequent use of flexed hand postures during modern human manipulation. Hand grips used during manipulation result in bending forces being placed on the phalanges, with the dorsal surface on the bone experiencing higher tensile forces and the palmar surface experiencing compression, and the lack of curvature characteristic of *H. sapiens* phalanges results in higher bending forces experienced by the bone overall (Oxnard, 1973; Preuschoft, 1973; Richmond, 2007).

Across the digits, we predicted PP2 and PP3 would display the thickest cortices and greatest cross-sectional strength, as experimental studies have revealed that the thumb and radial digits experience the highest loads during manipulation (Key, 2016; Rolian et al., 2011; Williams-Hatala et al., 2018). Furthermore, experimental studies testing force distribution of power grips used in modern human daily activities have revealed that, within digits 2–5, digit 2 experiences the greatest loads and the three ulnar digits experience relatively equal loads when grasping larger objects (de Monsabert et al., 2012; Sancho-Bru et al., 2014; Vigouroux et al., 2011). In contrast, loading of the digits is variable when grasping objects with a smaller diameter (<6.4 cm), as positioning of the fingers can be adjusted to maximise endurance without losing hold of the object (Sancho-Bru et al., 2014). Mean cortical thickness and cross-sectional properties are greatest in PP3, followed by PP2, PP4, and PP5, but there were no significant differences in cortical thickness across the digits (Table 3.2; S. Fig. 3.4). Only PP5 was significantly lower in its measure of axial strength (CA), bending strength (Z_{pol}) and bending and torsional rigidity (J) (S. Table 3.3, 3.7; Figs. 3.7–3.9). As our sample includes a diverse range of pre- and post-industrial populations, our results could simply reflect the varied hand postures employed during the daily activities of individuals from these populations, and not necessarily correspond with those employed during stone tool production (see Key et al., 2019).

3.4.8. Phalangeal curvature and cortical thickness

The regression analyses showed no relationship between the degree of curvature (IA) and phalangeal cortical thickness in *Pongo*, *Gorilla*, and *H. sapiens* (S. Fig. 3.8). There was a significant ($p = 0.001$) but weak ($R^2 = 0.106$) positive relationship between curvature and cortical thickness in *Pan* proximal phalanges. Our results suggest a weak relationship between phalangeal curvature and cortical thickness, despite a curved phalanx having been shown to dissipate load differently than a straight phalanx (Oxnard, 1973; Preuschoft, 1973). These results may also reflect the lack of precision offered by the IA method, which assumes a consistent degree of curvature throughout the phalanx (see Deane & Begun, 2008; Wennemann et al., 2021).

3.4.9. Behavioural signals in the cortex of the proximal phalanges

Great apes use their hands in distinct ways and adopt variable hand postures to accomplish a wide range of locomotor and/or manipulative tasks. Aspects of their external hand bone morphology aid them in successfully participating in these manual behaviours, with associated modelling of internal cortical and trabecular bone morphology (Bird et al., 2022; Dunmore et al., 2019; Kivell, 2015; Marchi, 2005; Matarazzo, 2008; Nguyen et al., 2014; Tsegai et al., 2013). Here, we demonstrate that cortical bone in the proximal phalanges reflects differences in hand use behaviours and external morphology.

While cortical bone properties and distribution patterns differed across the great apes, the functional role of FSRs is clear across all taxa. Within the non-human great apes, the location of maximum cortical thickness always includes the FSRs and in human individuals, where FSRs are present, they are maximally thick as well (Fig. 3.3; S. Fig. 3.1). These results, coupled with the pattern in *Gorilla* where phalanges with less prominent FSRs (PP2 and PP5) have thicker palmar cortex than dorsal cortex, while phalanges with more prominent FSRs (PP3 and PP4) show no differences, further suggests that prominent FSRs reduce strain experienced by the palmar shaft (Nguyen et al., 2014). This is also apparent in the cortical thickness distribution pattern of *Pongo*

phalanges, where although FSRs are the thickest region of the shaft, the shaft is also intermediately thick because *Pongo* FSRs are not very prominent. While *Pongo* FSRs are small, they are optimally located to resist forces during flexion and are coupled with high phalangeal curvature (Patel & Maiolino, 2016; Susman, 1979; Syeda et al., 2021), such that the external morphology of *Pongo* phalanges and cortical bone distribution pattern may be optimal for the manual loads they experience during flexed finger grasping. We draw this conclusion based on the fact that *Pongo* phalanges have thin cortices and weak cross-sectional properties relative to the other great apes, suggesting that a mechanical modelling response for a thicker cortex might not be needed (Pearson & Lieberman, 2004).

Gorilla and *Pan* have a similar locomotor repertoire (Doran, 1996; Matarazzo, 2013; Samuel et al., 2018; Wunderlich & Jungers, 2009), which is reflected in the cortical bone morphology of their proximal phalanges. Specifically, a shared pattern of thick cortex at the FSRs and in the distal region under the trochlea in *Gorilla* and *Pan* is indicative of the loading pattern incurred during knuckle-walking (Matarazzo, 2013; Samuel et al., 2018; Wunderlich & Jungers, 2009). Even though loads experienced by the metacarpals, and possibly the proximal phalanges, during knuckle-walking and arboreal behaviours are similar (Synek et al., 2020), the frequency of knuckle walking is greater (e.g. Doran, 1996; 1997; Hunt, 1991b). We assume, therefore, that the cortical patterns we found primarily reflect knuckle-walking, and this is supported by variation in external and internal morphology between African apes and *Pongo*. However, it is important to acknowledge that infrequent behaviours can also result in bone (re-) modelling (Barak et al., 2011; Burr, 1990; Pontzer et al., 2006). For example, the digital flexor muscles are minimally active during knuckle-walking but highly active during arboreal climbing and suspension (Leijnse et al., 2021; Susman & Stern 1979; Thompson et al., 2019; Tuttle et al., 1972), and thus arboreal behaviours likely contribute to some of the patterns we observe in *Gorilla* and *Pan* proximal phalanges. As for differences, the variation in hand morphology and postures employed by the two species during locomotion likely leads to differences in the pattern of loading across the non-pollical digits, and this is also reflected in our results (Inouye, 1994; Tuttle, 1969a).

The distinct dorsal thickening of human phalanges is expected for phalanges that are relatively straight and are consistently loaded in a flexed position. We predicted that cortical structure of PP2 and PP3 would reflect their more frequent use during daily manipulative behaviours but instead found a consistent pattern across the digits. This could reflect use of a diverse set of precision and power grips by modern humans (Dollar, 2014; Feix et al., 2015; Sancho-Bru et al., 2014). Furthermore, it is important to acknowledge that studies of recent modern human (often industrialised, Western populations) daily hand use are likely not representative of daily hand use in our geographically and temporally diverse sample. However, PP5 was significantly weaker and had a thinner cortex than the remaining three digits across our sample, which could reflect a general pattern of more limited recruitment of the fifth digit during habitual manual activities (but see Key et al., 2019; Marzke, 1997).

Evaluating bone strength using cross-sectional properties plotted across the shaft showed a distinct pattern in non-human great apes (S. Figs. 3.5-3.7). Specifically, the proximal phalangeal shaft exhibits a CA that is generally greatest on the distal end of the bone while the rigidity and resistance to torsion are greatest on the proximal end (Fig. 3.7; S. Figs. 3.5-3.7; S. Table 3.3). This

pattern may reflect the disto-proximal transfer of load across the digit, such that the proximal aspect of the bone needs to be structurally adapted to resist greater loads (Matarazzo, 2015).

While our results support the conclusion that phalangeal cortical bone structure reflects differences in manual behaviours in extant great apes, these interpretations rely on predictions of loading patterns and force transfer that are dependent upon the function of muscles, ligaments, and other soft tissue structures, about which we know very little. Furthermore, we chose to scale our cortical bone measures by the length of the proximal phalanx but there are fundamental differences in hand proportions across the great apes (Patel & Maiolino, 2016) that do not show a direct relationship to body mass, and thus a different scaling factor might produce different relative patterns. We tested this potential difference by scaling our data by a geometric mean of: phalangeal length, midshaft breadth, breadth of the base, and breadth of the trochlea, which reflect proximal phalanx size, but found a similar pattern to scaling with phalangeal bone length. Detailed behavioural and kinematic studies on various manual behaviours used by great apes, ideally in natural environments, together with musculoskeletal modelling and cadaveric validation are required (e.g., Leijnse et al., 2021; Lu et al., 2018; Synek et al., 2020). In addition, further investigation of ontogenetic changes in both external morphology (e.g., phalangeal curvature, enthesal morphology) and internal bone structure would also provide insight into the functional interplay between bone shape and bone modelling.

3.5. Conclusions

While, among great apes, cortical bone thickness patterns generally reflect the predicted loading regimes of different locomotor and manual behaviours, more nuanced information about loading during varying hand postures is evident from patterns of cortical bone distribution and cross-sectional properties. Cortical bone and its cross-sectional parameters reflected not just hand postural differences, but also the differences within the hand of each great ape species. More research is needed on phalangeal external and internal form, however, this study has demonstrated that cortical bone of proximal phalanges of digits 2-5 holds functional signals of hand use and thus, the cortex of proximal phalanges has the potential to aid in reconstruction of manual behaviours of fossil hominids, including hominins.

4 – Cortical bone architecture of hominid intermediate phalanges reveals functional signals of locomotion and manipulation

Published article: Syeda, S. M., Tsegai, Z. J., Cazenave, M., Skinner, M. M., & Kivell, T. L. (2023). Cortical bone architecture of hominid intermediate phalanges reveals functional signals of locomotion and manipulation. *American Journal of Biological Anthropology*. e24902.

4.1. Abstract

Reconstruction of fossil hominin manual behaviours often relies on comparative analyses of extant hominid hands to understand the relationship between hand use and skeletal morphology. In this context, the intermediate phalanges remain understudied. Thus, here we investigate the cortical bone morphology of the intermediate phalanges of extant hominids and compare it to the cortical structure of the proximal phalanges, to investigate the relationship between cortical bone structure and inferred loading during manual behaviours. Using micro-CT data, we analyse the cortical bone structure of the intermediate phalangeal shaft of digits 2–5 in *Pongo pygmaeus* (n = 6 individuals), *Gorilla gorilla* (n = 22), *Pan* sp. (n = 23), and *Homo sapiens* (n = 23). The R package Morphomap is used to study cortical bone distribution, cortical thickness and cross-sectional properties within and across taxa. Non-human great apes generally have thick cortical bone on the palmar shaft, with *Pongo* only having thick cortex on the peaks of the flexor sheath ridges, while African apes have thick cortex along the entire flexor sheath ridge and proximal to the trochlea. Humans are distinct in having a thicker dorsal shaft cortex as well as thick cortex at the disto-palmar region of the shaft. Variation in cortical bone distribution and properties of the intermediate phalanges is consistent with differences in locomotor and manipulative behaviours in extant great apes. Comparisons between the intermediate and proximal phalanges reveal similar patterns of cortical bone distribution within each taxon but with potentially greater load experienced by the proximal phalanges, even in knuckle-walking African apes. This study provides a comparative context for the reconstruction of habitual hand use in fossil hominins and hominids.

4.2. Introduction

Extant great apes and modern humans use a range of hand postures during positional (locomotor and postural) and manipulative behaviours (e.g., Kivell et al., 2020; Schmitt, et al., 2016), which have been successfully linked to the morphological variation within great ape hands (Bird et al., 2021; 2022; Dunmore et al., 2019; 2020a; 2020b; Marchi, 2005; Matarazzo, 2008; 2015; Tsegai et al., 2013). This form-function link among extant taxa has been used to infer habitual manual activities of fossil taxa, ranging from Miocene apes (Almécija et al., 2009a; 2012; Susman, 2004) to fossil *H. sapiens* (Bardo et al., 2020; Kivell et al., 2022; Stephens et al., 2018). Recent discoveries of hominin hand fossils have revealed mosaic morphologies suggesting hand use during both arboreal locomotion and dextrous manipulation (Dunmore et al., 2020b; Kivell et al., 2015; 2018a). Notably, the intermediate phalanges within the hominin hand fossil record show a mix of primitive and derived morphologies that are unique and morphologically distinct, pointing towards a diverse range of manual behaviours during the evolution of the hominin hand (Alba et al., 2003; Haile-Selassie et al., 2009; Kivell et al., 2015; 2018a; 2020; Larson et al., 2009; Napier,

1962a; Susman & Creel, 1979). Functional inferences regarding the manual behaviours of these fossil specimens have been made using elements of the carpus (Kivell et al., 2013; Marzke et al., 2010; Tocheri et al., 2007), the metacarpus (Dunmore et al., 2020b; Galletta et al., 2019; Skinner et al., 2015) and the phalanges (Almécija et al., 2010; Kivell et al., 2015; 2018a; 2022), but the intermediate phalanges are relatively understudied. Here we build on our previous work presented in Chapter 3 (Syeda et al., 2023) and investigate the relationship between variation in cortical bone structure of the intermediate phalanges of digits 2–5 (IP2–IP5), in the context of inferred hand use in humans and other extant hominids. We also conduct inter-digit comparisons of, both, the proximal and intermediate phalanges and discuss how the combined cortical structure of these two elements can inform us regarding the function of the fingers during manual behaviours.

Phalangeal external morphology, as well as the internal bone structure, have been shown to be functionally informative (Jungers et al., 1997; Karakostis et al., 2018; Matarazzo, 2008; Patel & Maiolino, 2016; Susman, 1979). The structure of both cortical and trabecular bone can adapt in response to mechanical loading by removing bone in skeletal areas where stress is low and adding bone where stress is high (Barak et al., 2011; Currey, 2013; Pearson & Lieberman, 2004; Ruff et al., 2006) and/or changing orientation and alignment of the trabecular struts (Barak et al., 2011; Pontzer et al., 2006). Preserved cortical and trabecular architecture of fossil specimens of different limb elements has been used to infer locomotor behaviour and manipulative activities (e.g., Cazenave et al., 2019; Chirchir, 2019; Dunmore et al., 2020b; Georgiou et al., 2020; Ruff et al., 2016; Skinner et al., 2015; Su & Carlson, 2017; Zeininger et al., 2016; see also the review in Cazenave & Kivell, 2023). These behavioural reconstructions rely on understanding the relationship between bone structure and known behaviours of extant taxa.

4.2.1. External morphology of the intermediate phalanges

Among great apes, external morphology of the intermediate phalanges is variable in the degree of longitudinal curvature, shape of the base, shaft, and trochlea, as well as a suite of morphological features on the palmar surface (Marzke et al., 2007; Patel & Maiolino, 2016; Susman, 1979; Syeda et al., 2021). These morphological features include a palmar median bar, lateral fossae, and flexor sheath ridges (FSRs; **Fig. 4.1**). The palmar median bar typically runs along the length of the palmar shaft and, in most cases, is bounded by the lateral fossae that vary in depth and are bounded by FSRs (Marzke et al., 2007; Susman, 2004). The lateral fossae of the intermediate phalanges are thought to be attachment sites for the flexor digitorum superficialis muscle (FDS) (Marzke et al., 2007), and the size and shape of these are quite variable across great apes (Susman, 1979) and throughout the fossil hominin record (Alba et al., 2003; Bush et al., 1982; Haile-Selassie et al., 2009; Kivell et al., 2015; 2018a; 2020; Larson et al., 2009; Napier, 1962a; Pickering et al., 2018; Susman & Creel, 1979; Ward et al., 2012). The relative size and overall morphology of these fossae have been used to make functional inferences regarding the locomotion of fossil hominins (Bush et al., 1982; Day, 1978; Ricklan, 1987; Stern & Susman, 1983; Susman, 1979; Susman & Creel, 1979; Susman & Stern, 1979; Tuttle, 1981). The deep lateral fossae of *Australopithecus afarensis* and *Australopithecus africanus* intermediate phalanges have been interpreted as evidence of efficient power grasping, which would have allowed them to engage in climbing and suspensory locomotion despite having short fingers, with *A. africanus* also potentially participating in tool-using activities (Ricklan, 1987; Stern & Susman, 1983; Susman et al., 1984). Similar inferences have been made for the intermediate phalanges of the OH

7 *H. habilis* hand (Susman & Creel, 1979). While these previous studies have linked FSR morphology to the size and use of the FDS muscles, there is a lack of evidence linking the morphology of muscle attachment sites and the size of the muscle (Shrewsbury et al., 2003; Williams-Hatala et al., 2016; but see Karakostis et al., 2017). Furthermore, as the morphology of the intermediate phalanges is understudied, the functional implications of the variation observed in FSR morphology and the palmar median bar have remained relatively unexplored.

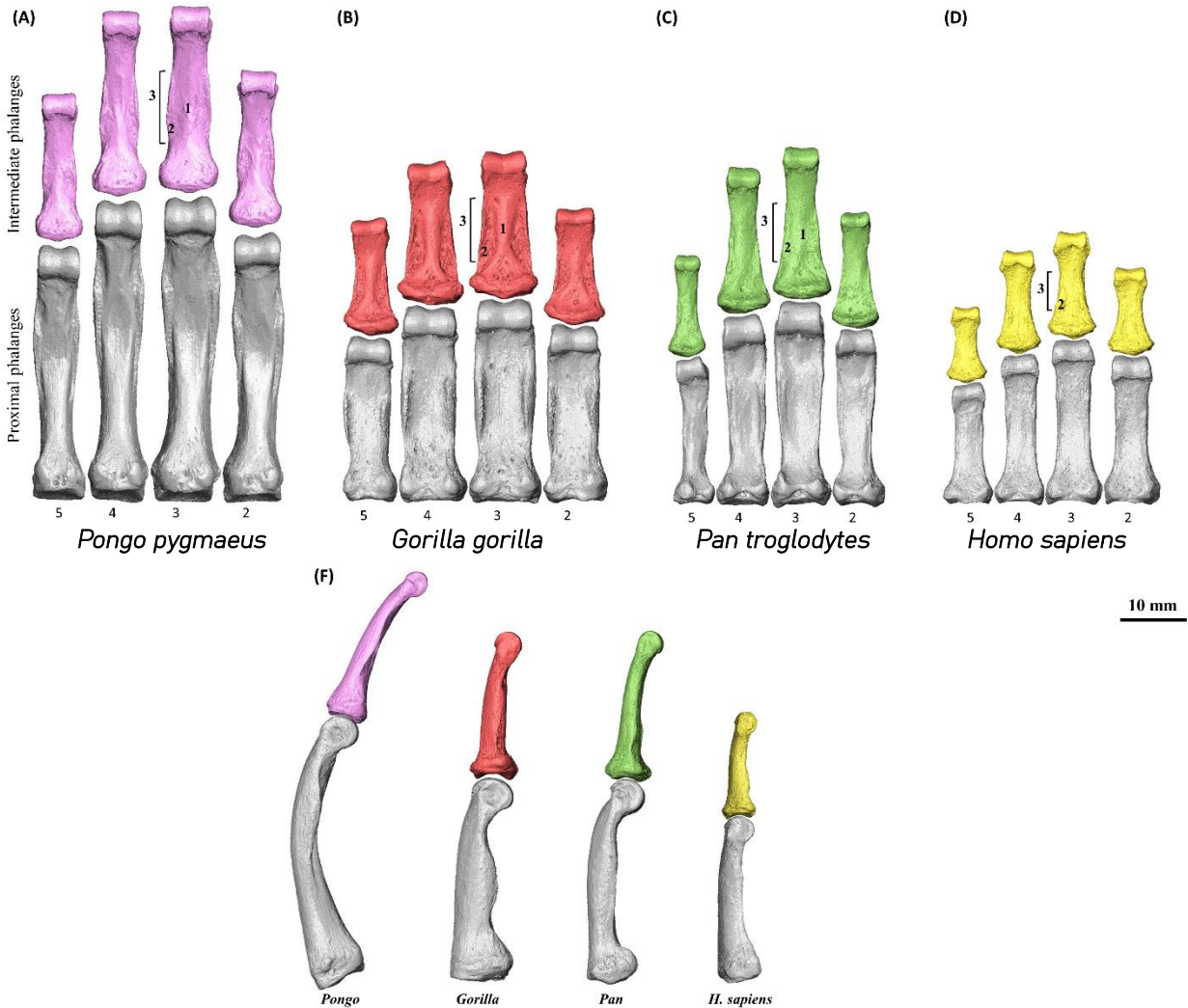


Figure 4.1: Surface models derived from micro-CT scans of proximal and intermediate phalanges of digits 2-5 from (A) *Pongo pygmaeus*, (B) *Gorilla gorilla*, (C) *Pan troglodytes*, (D) *Homo sapiens* showing variation in external morphology. External morphological features are labelled: 1: Palmar median bar, 2: Lateral fossae, 3: flexor sheath ridge. (E) Proximal and intermediate phalanges of the third digit in the ulnar view to demonstrate variation in longitudinal curvature across the sample.

4.2.2. Functional morphology of the intermediate phalanges

To date, only two studies of which we are aware have directly investigated the biomechanical and behavioural implications of palmar phalangeal morphology (Marzke et al., 2007; Nguyen et al.,

2014). In a comparative anatomical study of primate intermediate phalanges, Marzke and colleagues (2007) showed that the FDS tendon does not exclusively insert onto the lateral fossae and, when it does, it does not occupy the whole fossa. Instead, the FDS tendon mainly inserted onto the FSRs at varying distances from the base, with the fibres running towards different aspects of the palmar shaft (Marzke et al., 2007). The length of the lateral fossae also did not predict the cross-sectional area or length of the FDS tendon, concluding that the development of this external morphology cannot be explained by the FDS tendon attachments or the stresses associated with FDS muscle activity (Marzke et al., 2007). An alternative explanation of lateral fossae development proposed by Marzke et al. (2007) is that the lateral fossae could be a by-product of the median bar thickening and developing anteriorly in response to loading. This hypothesis is consistent with Begun and colleagues' (1994) study of the pedal intermediate phalanges of *Proconsul* in which they posited that the palmar median bar reflects dorsopalmarly directed bending stresses that accompany the contraction of the digital flexor muscles and substrate reaction forces. On the other hand, Walker & Leakey (1993) suggested that the palmar median bar could form as a result of the lateral fossae excavations, but this hypothesis requires a functional explanation for the hollowing out of the palmar phalangeal shaft. While Marzke et al. (2007) focused on the shape and size of the lateral fossae, they did not explicitly explain or address the role and morphology of the FSRs. The work of Nguyen and colleagues (2014) sheds light on the biomechanical importance of the FSRs in the proximal phalanx of hylobatids. Using 3D micro finite element modelling, they showed that the larger FSRs experienced higher peak strains and were associated with lower peak strains on the palmar shaft, suggesting that taller FSRs helped to reduce the strain experienced by the palmar shaft (Nguyen et al., 2014). If the same is true for intermediate phalanges, this may help to explain variation in FSR development across hominoid taxa.

Variations in hominoid external intermediate phalangeal shape, especially regarding phalangeal curvature, FSR morphology and soft tissue anatomy, make functional interpretations in extant and fossil phalangeal form challenging. However, exploration of internal bone structure may provide more direct information about finger use. To date, only three studies have investigated the functional relationship between the internal bone morphology of intermediate phalanges and hand use behaviours (Doden, 1993; Matarazzo, 2015; Stephens et al., 2018). Doden (1993) showed that the intermediate phalanges of modern humans have thinner cortical bone towards the distal end, with overall thicker cortical bone on the dorsal surface of the phalanx and the midshaft having the highest density of bone. Matarazzo (2015) and Stephens and colleagues (2018) studied the trabecular structure of anthropoid and modern human phalanges, respectively, and noted a functional link between manual behaviours and the orientation and volume of trabecular bone.

We previously explored cortical bone distribution patterns and properties in the proximal phalanges of digits 2-5 (PP2-PP5) in extant great apes and showed that the pattern of cortical bone within the non-pollical proximal phalanges is capable of distinguishing varied hand postures employed by each taxon and corresponds with predicted loading during these hand postures. Results described in Chapter 3 also indicated that cortical bone patterns and properties reflect the variable digital loading within the hand of each taxon. Here, we build upon this research and provide the first detailed, comparative study of the cortical morphology of extant hominid intermediate phalanges in digits 2-5. We examine cortical bone distribution patterns and cortical

robusticity via cross-sectional geometry (CSG) in the phalangeal shaft to test whether these cortical properties reflect predicted loading differences during manual behaviours. We then discuss the cortical bone morphology of the intermediate phalanges alongside the proximal phalanges to provide a more holistic insight into the relationship between phalangeal morphology and hominid hand use.

4.2.3. Predictions

4.2.3.a. Inter-specific comparisons of cortical bone structure

We expect cortical bone distribution patterns will differ among the extant great apes, reflecting the presumed loading associated with the typical hand postures employed by each taxon. *Pongo* locomotor repertoire is dominated by suspensory, arboreal behaviours (Hunt, 1991b; Thorpe & Crompton, 2006 but see Sarmiento, 1988; Susman, 1974; Tuttle, 1967) in which the hand wraps around the substrate using flexed-finger postures. We predict that the intermediate phalanges of *Pongo* will display a pattern of thick cortical bone on the midshaft-to-distal palmar surface, as the flexed finger posture of the phalanges will result in joint and substrate reaction forces that will load the phalanx in compression dorsally and tension palmarly, with the FSRs and longitudinal curvature of the phalanx helping reduce overall strain experienced by the shaft (Nguyen et al., 2014; Preuschoft, 1973; Richmond, 2007).

The African apes (*Gorilla* and *Pan*) most often engage in knuckle-walking (on average ~ 90 % of time spent locomoting, but this can vary substantially across groups and individuals; Hunt, 2020) and, less often in arboreal behaviours (Doran, 1996; 1997; Hunt, 2020; Remis, 1998; Schaller, 1963; Tuttle & Watts, 1985). During knuckle-walking, the intermediate phalanges contact the substrate with the dorsal surface, the metacarpophalangeal (McP) joint is hyperextended, the PIP joint is hyper-flexed, and the DIP joint is flexed (Inouye, 1994; Matarazzo, 2013; Thompson et al., 2018; Thompson, 2020; Tuttle 1967). We predict *Gorilla* and *Pan* will share a similar pattern of cortical bone distribution compared to *Pongo* and *H. sapiens*, with an overall thick phalangeal shaft due to ground reaction forces being dissipated on the dorsal surface and large compressive forces from supporting the body mass during knuckle-walking on the overall phalanx (Matarazzo, 2015; Wunderlich & Jungers, 2009).

Modern humans primarily use their hands for manipulation, employing power grips frequently, as well as power squeeze grips and precision grips between the finger pads and thumb (Dollar, 2014; Feix et al., 2015; Zheng et al., 2011). These grips most often result in flexion at the fingers, which will result in compressive strain and bending stresses on the dorsal surface of the relatively straight phalanges (Doden, 1993; Marzke, 1997; Preuschoft, 1973; Zheng et al., 2011). As such, we expect humans to have the thickest cortex on the dorsal surface of the phalanx.

Along with differences in cortical distribution patterns, we predict there will be differences in cortical thickness values and cross-sectional geometric (CSG) properties across the taxa. It is predicted the African apes will have thicker mean cortical thickness and stronger cross-sectional properties relative to *Pongo* and *H. sapiens*. *Pongo* will display cortical bone thickness and properties intermediate between the African apes and modern humans, as they are not using their intermediate phalanges to support their body mass (as African apes do during knuckle-walking) but are still using their hands for locomotion. Human intermediate phalanges are predicted to have the thinnest cortices and weakest CSG properties compared to the other taxa,

as the lower loads experienced during manipulation are predominant in humans, and loading during locomotion is likely to be negligible in the human sample used.

4.2.3.b. Intra-specific comparisons of cortical bone structure

Given differences in loading among the digits during habitual hand postures, we also predict that cortical bone distribution, mean thickness and CSG properties will differ across the digits within each taxon. Within the African apes, captive *Gorilla* have been observed to load its digits 2-5 more evenly (but see Thompson et al., 2018) compared to captive *Pan*, which is more variable in its positional behaviour (Doran & Hunt, 1996; Doran, 1996; Hunt, 1992; Inouye, 1994; Matarazzo, 2013; Sarringhaus et al., 1969). Generally, in *Pan* digits 3 and 4 experience the greatest loads and digit 5 sometimes does not even touch down while knuckle-walking (Matarazzo, 2013; Samuel et al., 2018; Wunderlich & Jungers, 2009). Thus, *Gorilla* is predicted to have similar cortical bone distribution and properties across digits 2-5 compared to *Pan*, which is predicted to be more variable with greater cortical bone thickness and properties in the third digit (Wunderlich & Jungers, 2009; Samuel et al., 2018). In *Pongo*, cortical distribution, thickness and properties are expected to be similar across the digits compared to the other non-human great apes, since *Pongo* is thought to typically use all four fingers in a similar manner during arboreal grasping (Rose, 1988; but see McClure et al., 2012). Within modern humans, we expect digits 2 and 3 to have thicker cortices and stronger CSG properties than digits 4 and 5 as experimental studies have shown the greatest loads experienced by the radial digits during modern human grasping (Cepriá-Bernal et al., 2017; de Monsabert, et al., 2012; Sancho-Bru et al., 2014).

4.2.3.c. Comparison of proximal and intermediate phalanges

We expect to observe similar relative patterns and interspecific differences in cortical morphology of the intermediate phalanges that we did in the proximal phalanges (PPs). Specifically, we expect the African apes to show greater differences between the IPs and PPs due to direct loading of the IPs during knuckle-walking.

A summary of all the predictions is listed in Table 4.1

Table 4.1: Summary of the hypotheses and predictions of this study.

Hypothesis	Prediction
1) Cortical bone distribution patterns will differ among extant great apes, which will reflect loading associated with manual behaviours	<i>Pongo</i> : thick cortex on midshaft-to-distal palmar surface <i>Gorilla</i> and <i>Pan</i> : overall thick phalangeal shaft <i>H. sapiens</i> : thick cortex on the dorsal surface
2) Mean cortical bone thickness and cross-sectional properties will significantly differ across taxa	<i>Gorilla</i> and <i>Pan</i> : thickest average cortical thickness and stronger CSG properties <i>Pongo</i> : intermediate cortical thickness and CSG property values <i>H. sapiens</i> : lowest cortical thickness and weakest CSG property values
3) All aspects of cortical bone distribution patterns, thickness and CSG values will differ across the digits within each taxon	<i>Pongo</i> : similar distribution, thickness and CSG values across all four digits <i>Gorilla</i> : similar distribution, thickness, and CSG values across all four digits

	<i>Pan</i> : similar distribution across all four digits; thicker cortex and stronger properties in digit 3 <i>H. sapiens</i> : similar distribution across all four digits; thicker cortex and stronger CSG property values in digits 2 and 3
4) Proximal and intermediate phalanges will significantly differ in their cortical bone properties	Cortical bone properties of proximal and intermediate phalanges will differ in the African apes but not in <i>Pongo</i> and <i>H. sapiens</i>

Table 4.2: Summary of the sample included in the study.

Taxon	N	IP2	IP3	IP4	IP5
<i>Homo sapiens</i>	23	15	19	18	13
<i>Pan paniscus</i>	6	6	5	6	5
<i>Pan troglodytes</i>	17	11	13	15	14
<i>Gorilla gorilla</i>	22	18	19	19	16
<i>Pongo pygmaeus</i>	6	6	6	6	5

4.3. Methods

4.3.1. Sample

This study included high-resolution micro-CT scans of intermediate phalanges of modern *Homo sapiens* (n = 23 individuals, including recent and early modern specimens), *Pan* spp. (n = 23 individuals), *Gorilla* sp. (n = 22 individuals), and *Pongo* sp. (n = 6 individuals) for manual digit 2 (n = 56 elements), digit 3 (n = 62 elements), digit 4 (n = 64 elements), and digit 5 (n = 53 elements) (Table 4.2). Non-human specimens were adult wild-shot individuals with no indication of pathologies and included associated intermediate phalanges (IP) of digits 2–5 from a single hand. The human sample consists of adults from pre-industrial (n = 6) and post-industrial (n = 7) modern human populations, as well as nine fossil *H. sapiens* specimens (further detail on populations and fossil specimens are provided in S. Table 4.1). The majority (74%) of our human sample did not have all four associated digits. Thus, we assigned phalanges to a digit using morphological characteristics described in Susman (1979) and Case & Heilman (2006). For individuals in our sample that had associated PPs (see Chapter 3), we compared cortical distribution and properties with the IPs.

4.3.2. MicroCT data collection

Specimens were scanned using a BIR ACTIS 225/300, Diondo D3 or Skyscan 1172 scanner housed at the Department of Human Evolution, Max Planck Institute for Evolutionary Anthropology (Leipzig, Germany), a Nikon 225/XTH scanner at the Cambridge Biotomography Centre, University of Cambridge (Cambridge, UK), or with the Diondo D1 scanner at the Imaging Centre for Life Sciences University of Kent (Canterbury, UK). The scan parameters included acceleration voltages of 100–160 kV and 100–140 μ A using a 0.2 to 0.5 mm copper or brass filter. Scan resolution ranged between 0.018 mm to 0.044 mm depending on the size of the bone.

Images were reconstructed as 16-bit TIFF stacks. All scans were cleaned (i.e., the removal of soft tissue or other non-bone material) and reoriented into a standard anatomical position using Avizo Lite 9.0.0 (Visualization Sciences Group, SAS). These scans were then segmented using medical image analysis (MIA), a clustering algorithm method (Dunmore, Wollny & Skinner, 2018).

4.3.3. Analysis of cortical bone structure

The R package morphomap (Profico et al., 2021) was used to quantify cortical bone structure distribution and CSG properties. To prepare the data for analysis, we used Medtool v 4.5 (www.dr-pahr.at/medtool; Tsegai et al., 2013; Gross et al., 2014) on the original and MIA segmented scans, to define the inner and outer layer of cortical bone in the segmented scans. The protocol identified the external and internal border by casting rays in 3D and used morphological filters to fill the bone, which resulted in masks of the outer and inner regions of cortical bone. These masks were converted into smooth external and internal surfaces for processing in morphomap using an in-house script for Paraview v 4.4 and Meshlab v 2020.03.

Prior to analysis, we extracted a region of interest (ROI) from the inner and outer surfaces that defined the phalangeal shaft in all taxa. This ensured that the cortical region analysed was homologous across the morphologically variable phalangeal shafts of the hominid sample. The ROI was defined distally by the proximal end of the trochlea and proximally by the distal end of the base. Cortical morphology was quantified using the R package morphomap (Profico et al., 2021) and the methodological steps and parameters applied were the same as described in Chapter 3. Briefly, 97 cross-sections were extracted between 2% and 98% of the length of the ROI at 1% increments and 50 equiangular semi-landmarks were placed on each cross-section to capture the morphologically complex shape of the phalangeal shaft (Fig. 4.2). To define these landmarks, rays were sent from the centroid of each cross-section outward, with cortical thickness calculated as the length of the segment between the landmarks placed on the internal and external outline. Morphometric maps of cortical bone distribution were used to visualise cortical bone distribution patterns for each individual. Mean morphometric maps were also created to visualize the overall pattern of cortical bone distribution of each digit within each taxon. To compare cortical thickness between the dorsal and palmar shaft, equiangular semi-landmarks were defined that excluded those placed on the flexor sheath ridges, which would bias measurements, and a ratio of dorsal to palmar mean cortical thickness was calculated.

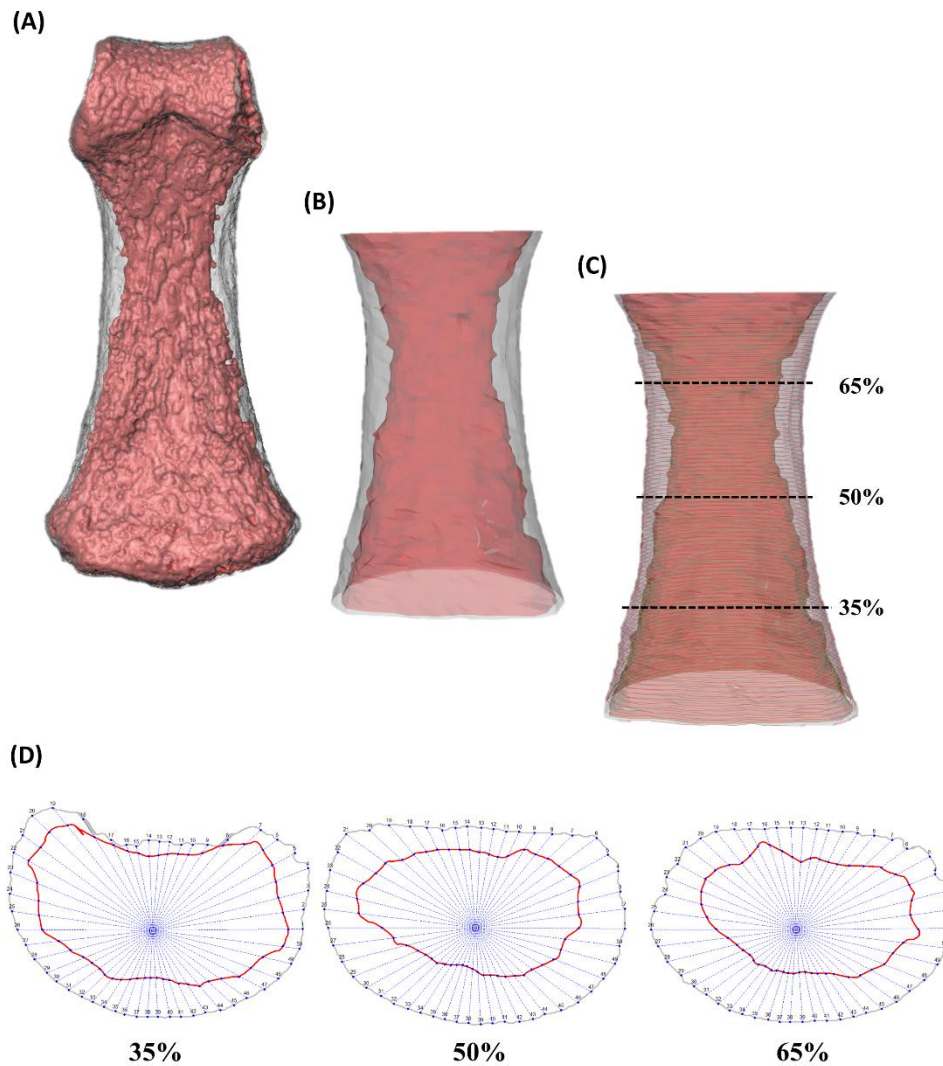


Figure 4.2: Images showing the steps taken in Morphomap for cortical bone analysis in a human third intermediate phalanx. (A) External (grey) and internal (red) 3D surface model of the phalanx, (B) cut external and internal surfaces defining the ROI for input into Morphomap, (C) cross-sections placed in 1% increments along the shaft to calculate cortical thickness with the dotted black lines indicating the cross-sectional levels at which cross-sectional properties were assessed, (D) cross-sections at 35%, 50%, and 65% of the phalanx, depicting the landmarks placed on the external and internal outline.

4.3.4. External morphological features

External morphological features (i.e., FSRs, median bar and phalangeal curvature depicted in Fig. 4.1) of the intermediate phalanx were quantified to explore the potential relationship between external form and internal cortical architecture. We quantified phalangeal curvature using the included angle method (Stern et al., 1995) and size of the median bar and FSRs using 3D linear measurements (Avizo Lite 9.0.0, Visualization Sciences Group, SAS). The size of the median bar was quantified from the palmar most protruding part of the bar to the palmar shaft. The size of the FSRs was quantified by measuring its depth (the tallest point of the ridge to the palmar

shaft) and its proximodistal length (S. Fig. 4.5). The relationship between FSR and median bar morphology was only quantified in the IP3s of our sample..

4.3.5. Cross-sectional geometry

Cross-sectional geometric properties quantifying the strength and rigidity of the phalangeal shaft of great apes were calculated across the shaft using Morphomap (Profico et al., 2021). We analysed cortical area (CA; a measure of compressive and tensile strength), polar section modulus (Z_{pol} ; measure of maximum bending strength), and polar moment of area (J; a measure of bending and torsional rigidity) at 35%, 50%, and 65% of the phalangeal length (Fig. 4.3) to quantify variation in cortical bone strength properties across the phalangeal shaft.

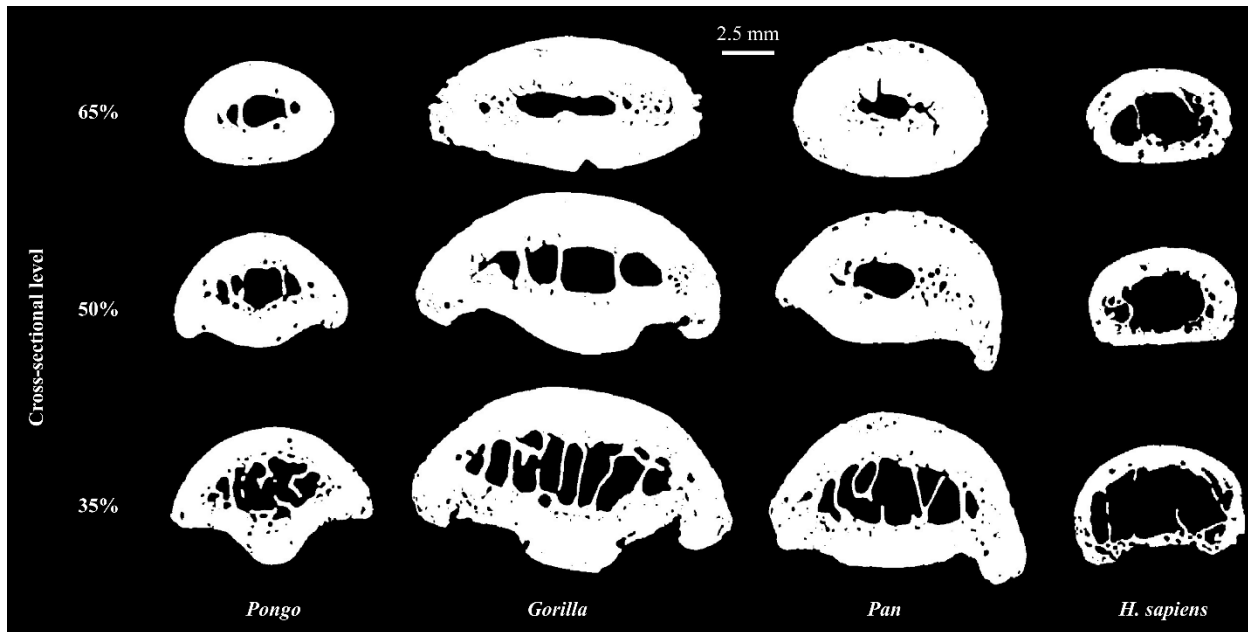


Figure 4.3: Cross-sections at 35%, 50% and 65% of a third intermediate phalanx for each taxon. Cross-sections are scaled to relative size.

4.3.6. Statistical analysis

Cortical bone thickness values, CSG properties, and metric measurements of the palmar shaft morphology were scaled by the inter-articular length of the phalanx. We also scaled our data by a geometric mean of several measurements of phalanx size, which yielded the same overall results. Thus, we chose to use phalangeal length alone to scale our data due to its direct relationship with bending stresses. Firstly, to investigate cortical bone distribution patterns across the taxa, a principal component analysis (PCA) was conducted on the cortical thickness values of the entire shaft. Following the PCA, an omnibus permutational multivariate analysis of variance was conducted on the first three PC scores to test if these cortical bone distribution patterns were significantly different across the taxa. If results were statistically significant ($p < 0.05$), a pairwise one-way permutational multivariate analysis of variance with a Bonferroni correction to determine significant differences between the groups.

Secondly, to test for differences in the cortical bone thickness of the shaft, mean differences were compared inter- and intra-generically using Kruskal-Wallis and post hoc Dunn tests. Paired sample t-tests were conducted on the mean palmar and dorsal cortical thickness values to test whether they statistically differed due to the normality of the palmar and dorsal cortical thickness data sets. Spearman's correlation tests were used to assess whether a statistically significant relationship exists between the cortical thickness of the shaft and the degree of phalangeal curvature, as well as between cortical thickness and median bar height.

Additionally, each cross-sectional property (CA, Z_{pol} , and J) was analysed at each cross-section (35%, 50%, 65%) to test for inter- and intra-generic mean differences using Kruskal-Wallis and post hoc Dunn tests, as the results of Shapiro-Wilks tests revealed the data was not normally distributed.. Further intra-generic testing evaluated mean differences in cross-sectional properties (CA, Z_{pol} , and J) within a phalanx at the different cross-sectional levels (35%, 50%, and 65%) using a Kruskal-Wallis test, followed by a post hoc Dunn test.

Finally, we compared the cortical morphology of the intermediate phalanges with associated proximal phalanges, the analysis of which was reported in Chapter 3 (Syeda et al., 2023). The same data collection protocol was used to quantify cortical thickness in both the intermediate and proximal phalanges. We used Wilcoxon signed-rank tests to evaluate intra-generic mean differences in cortical thickness and cross-sectional properties between proximal and intermediate phalanges. We tested whether the mean cortical thickness of proximal and intermediate phalanges was significantly different across digits 2-5 of each taxon. The same tests were conducted for each cross-sectional property at each cross-section as well.

All statistical analysis was performed in R (v 4.1.3) and packages RVAideMemoire (v 0.9-79 Hervé, 2021), Stats (R Core Team 2021), Vegan (v 2.5-7 Oksanen et al., 2020), and FSA (v 0.9.3 Ogle et al., 2022) were used. Tests were considered statistically significant with a $p < 0.05$.

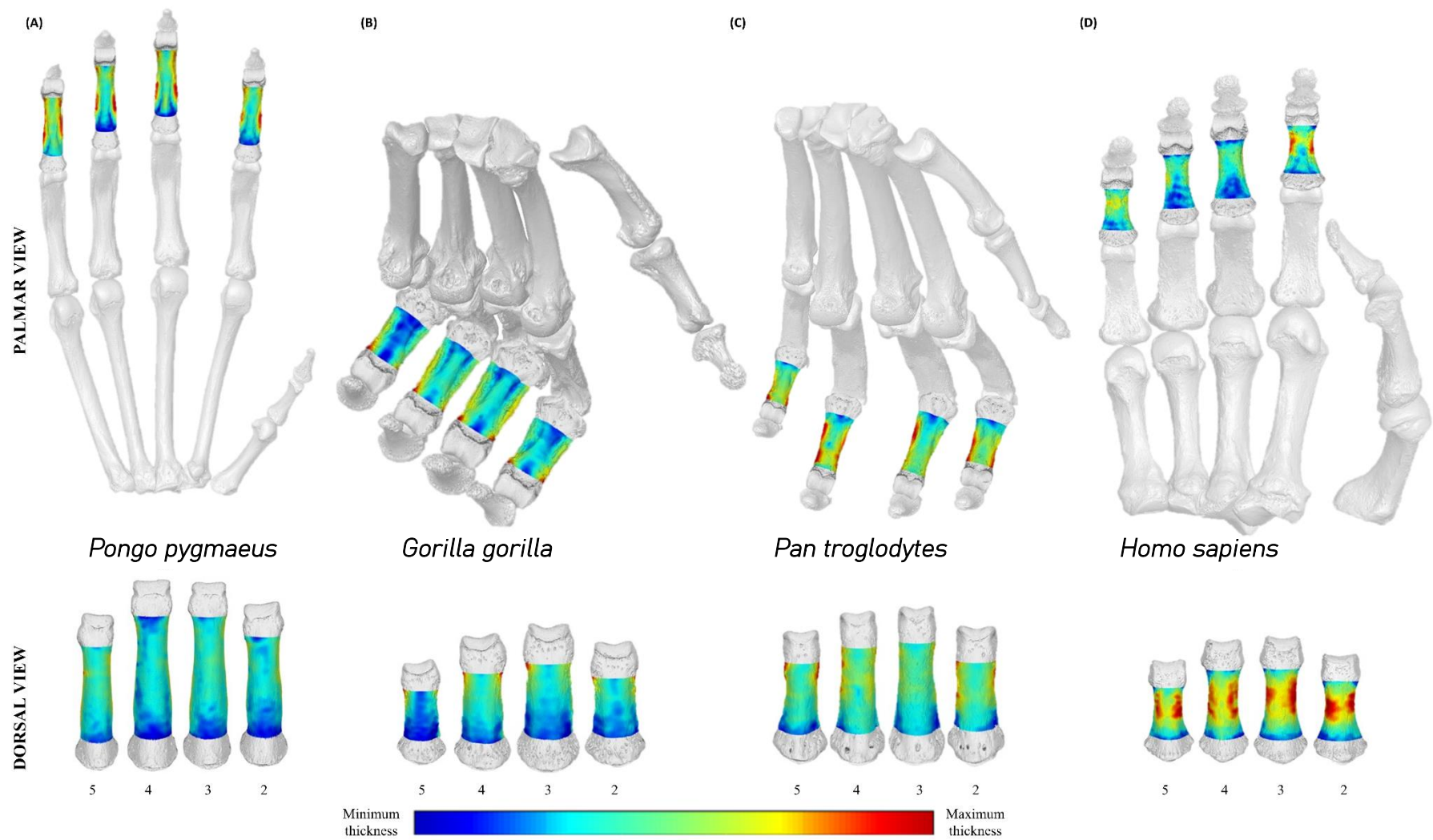


Figure 4.4: 3D maps of cortical bone distribution across the intermediate phalanges in a representative individual of each taxon: (A) *Pongo pygmaeus*, (B) *Gorilla gorilla*, (C) *Pan troglodytes*, and (D) *Homo sapiens*. Thickness maps are independent of each other, and images are not to scale.

4.4. Results

4.4.1. Cortical bone distribution and thickness

Mean morphometric maps of cortical bone distribution patterns in IP2–5 for each taxon are shown in **Figure 4.4** and mean thickness data is presented in **Table 4.3**. Below we describe in detail the cortical bone distribution patterns qualitatively and variation in scaled mean cortical thickness values for each taxon.

4.4.1.a. Cortical bone distribution patterns

Suspensory *Pongo* has thick cortical bone on the peak of the FSRs and the region proximal to the trochlea, with the shaft ranging from low to intermediate thickness relative to the regions of maximum thickness (**Fig. 4.4A**). This pattern is generally similar across the four digits, with the exception of IP2 and IP5, where cortical bone is thicker on the ulnar FSR relative to the radial FSR (**Fig. 4.4A, S. Fig. 4.1**).

In knuckle-walking apes, thickest cortical bone is typically found from the FSRs up to the region proximal to the trochlea, while the cortical thickness of the shaft ranges from relatively low to intermediately thick (**Fig. 4.4B–C**). However, compared to *Pan*, cortex of the *Gorilla* phalangeal shaft is generally low in thickness. Across *Gorilla* IP2–IP4, individuals that possess thick and prominent FSRs have a shaft relatively low in thickness, while individuals with relatively thinner and smaller FSRs have a shaft that is intermediate in thickness (**Fig. 4.4B, S. Fig. 4.1**). In *Pan* individuals that do not possess prominent FSRs, only the region proximal to the trochlea is maximally thick while the remainder of the phalangeal shaft (including the FSRs) is relatively intermediate in its thickness (**Fig. 4.4C, S. Fig. 4.1**). Across the *Pan* hand, some individuals show thicker cortex radially in IP2 and IP3 compared to the ulnar surface.

The human pattern of cortical bone distribution is distinct from the other great apes, with the thickest cortical bone found on the dorsal midshaft-to-distal region as well as the disto-palmar region across the digits (**Fig. 4.4D, S. Fig. 4.1**). The FSRs, when present, are maximally thick as well.

Table 4.3: Summary statistics of raw (mm) and standardised (dimensionless) cortical thickness measurements of the phalangeal shaft.

	<i>H. sapiens</i> Mean (SD)	<i>Pan</i> Mean (SD)	<i>Gorilla</i> Mean (SD)	<i>Pongo</i> Mean (SD)
<u>Raw</u>				
IP2	1.074 (0.300)	2.147 (0.289)	2.430 (0.361)	1.734 (0.240)
IP3	1.393 (0.383)	2.392 (0.342)	2.820 (0.387)	1.837 (0.300)
IP4	1.359 (0.387)	2.291 (0.293)	2.703 (0.457)	1.818 (0.250)
IP5	0.967 (0.264)	1.923 (0.346)	2.265 (0.428)	1.669 (0.300)
<u>Standardized*</u>				
IP2	0.042 (0.011)	0.068 (0.010)	0.070 (0.008)	0.047 (0.004)
IP3	0.047 (0.012)	0.058 (0.008)	0.067 (0.007)	0.042 (0.006)
IP4	0.046 (0.012)	0.061 (0.008)	0.068 (0.009)	0.041 (0.005)
IP5	0.046 (0.012)	0.070 (0.012)	0.073 (0.011)	0.046 (0.003)

*standardized by bone length.

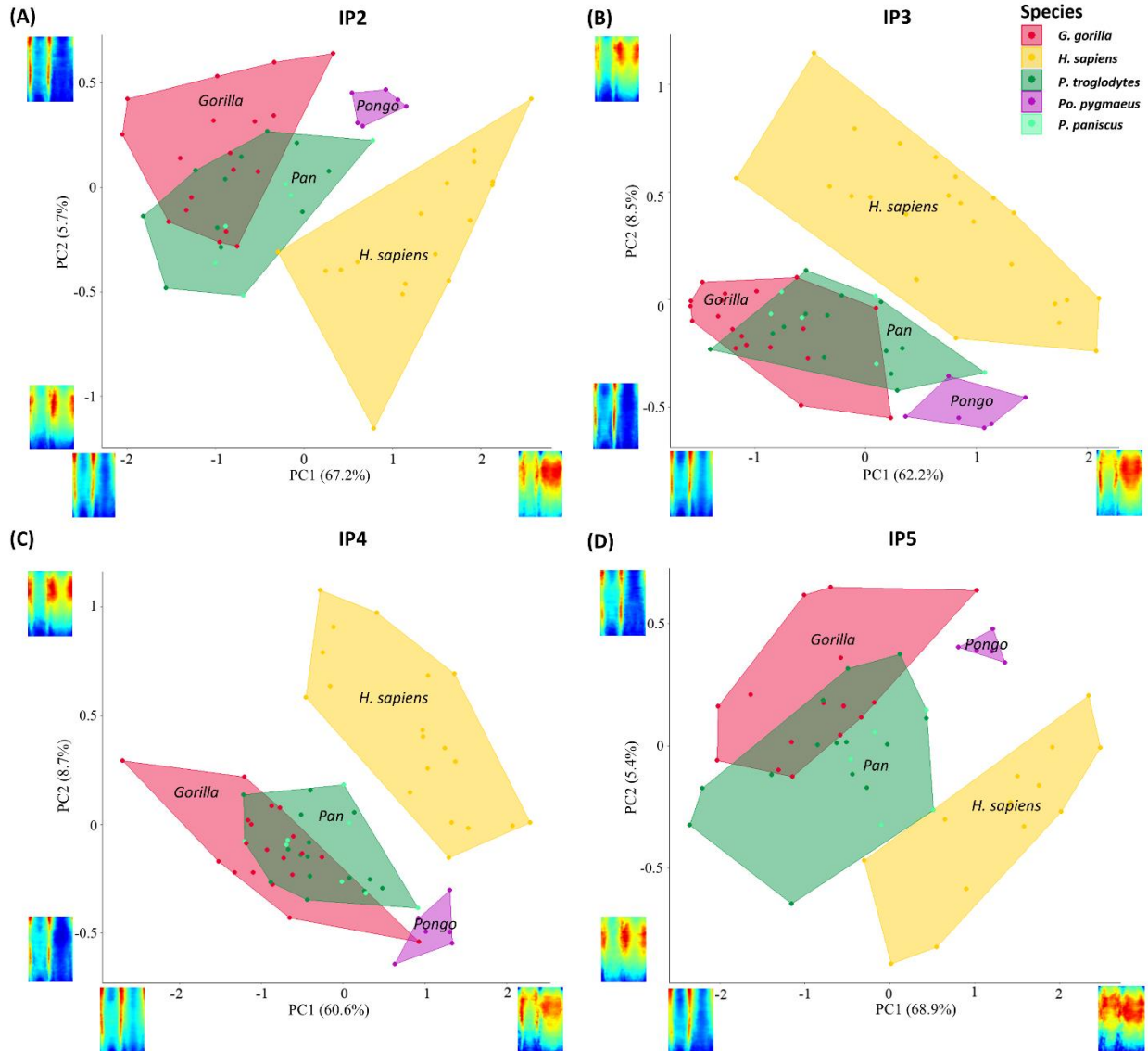


Figure 4.5: PC1 and PC2 for cortical bone distribution of intermediate phalanges of (A) IP2, (B) IP3, (C) IP4, and (D) IP5 of *Pongo sp.*, *Gorilla sp.*, *Pan spp.*, and *H. sapiens*.

4.4.1.b. Cortical bone distribution variation across taxa

The PCA distinguishes taxa based on scaled cortical thickness distribution patterns of each phalanx (S. Table 4.2). The results of the PCAs were similar between digits, with similar loadings and separation among the humans and non-human great apes (Fig. 4.5; 3D PCA in S. Fig. 4.2). PC1 explains between 60% - 69% of the total variance for each of the four digits. Low PC1 scores separate the African apes, with relatively thicker FSRs and high PC1 scores distinguish humans, with thicker cortex on the dorsal shaft along with thick radial and ulnar palmar cortex in IP2-IP4. IP5 distinguishes the species similarly, with the same loadings on low PC1 values, but high PC1 values represent thick midshaft-to-distal dorsal and palmar shaft thickness. African apes variably

overlap with each other, and *Pongo* is intermediate between humans and African apes across all digits (Fig. 4.5).

PC2 explains between 5-9% of the variance in the PCAs for each of the four digits and represents the region of overall maximum cortical thickness. Within IP2 and IP5, humans have generally lower PC2 scores than the other taxa, with maximum cortical thickness located on the radial and ulnar surface of the mid-to-distal shaft, while higher PC2 scores tend to characterise African apes with thicker palmar proximodistal cortex. The PCA of IP3 and IP4 represents the same relative patterns, but the axes are flipped such that lower PC2 scores generally characterise African apes with thicker palmar proximodistal cortex and higher PC2 values generally reflect humans having thicker cortical bone on the radial and ulnar surface of the mid-to-distal shaft. Together, PC1 and PC2 generally separate humans from the other taxa in all rays.

Table 4.4: Significance values for post hoc comparisons of cortical thickness among species.

		<i>Pan</i>	<i>Gorilla</i>	<i>Pongo</i>
IP2	<i>H. sapiens</i>	<0.001	<0.001	1.000
	<i>Pan</i>		1.000	0.021
	<i>Gorilla</i>			0.004
IP3	<i>H. sapiens</i>	0.033	<0.001	1.000
	<i>Pan</i>		0.119	0.035
	<i>Gorilla</i>			<0.001
IP4	<i>H. sapiens</i>	0.007	<0.001	1.000
	<i>Pan</i>		0.172	0.010
	<i>Gorilla</i>			<0.001
IP5	<i>H. sapiens</i>	<0.001	<0.001	1.000
	<i>Pan</i>		1.000	0.034
	<i>Gorilla</i>			0.008

4.4.1.c. Mean cortical thickness

In interspecific comparisons, African apes have significantly thicker cortical bone than *Pongo* and *H. sapiens* across all digits ($p < 0.001$; Table 4.4). No significant differences in cortical thickness were found between *Gorilla* and *Pan* ($p = 1$, $p = 0.119$, $p = 0.172$, $p = 1$ across IP2-IP5 respectively) or between *Pongo* and *Homo* ($p = 1$ across all digits) in any digit. In comparisons of cortical thickness patterns across the hand, the mean cortical thickness between the IPs does not significantly differ ($p > 0.05$) within *Pongo*, *Gorilla*, and *H. sapiens* (S. Fig. 4.3). In contrast, in *Pan* mean cortical thickness of IP5 was significantly greater than that of IP3 ($p = 0.004$) and IP4 ($p = 0.040$), with mean cortical thickness of IP2 being significantly greater than IP3 ($p = 0.023$) as well (S. Fig. 4.3).

4.4.1.d. Mean cortical thickness across the shaft

Mean cortical thickness of the shaft reveals that all non-human great apes have a shared pattern across each of the four IPs (Fig. 4.6). Mean cortical thickness increases up until the midshaft and from there remains consistent with the thickest cortex located at the distal end of the shaft. In contrast, in humans cortical thickness increases proximo-distally, peaking just distal to the midshaft and then decreases at the distal shaft in IP2-5.

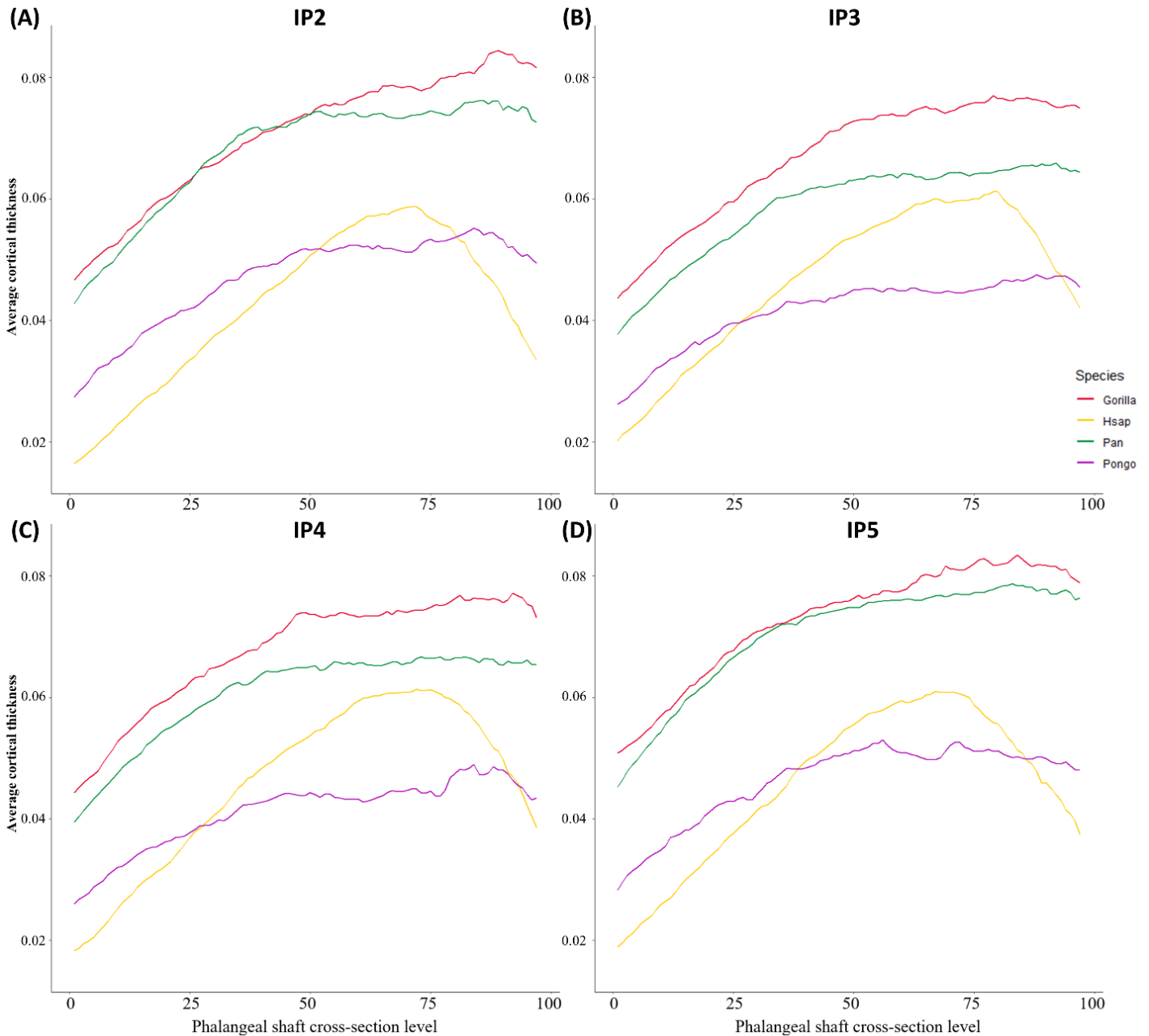


Figure 4.6: Average cortical bone thickness plotted from the proximal end (0) to the distal end (100) of the phalangeal shaft of *Pongo*, *Gorilla*, *Pan*, and *H. sapiens*. (A) IP2; (B) IP3; (C) IP4; (D) IP5.

Table 4.5: Paired samples t-tests palmar vs. dorsal thickness across species

		<i>H. sapiens</i>	<i>Pan</i>	<i>Gorilla</i>	<i>Pongo</i>
IP2	Palmar mean	0.035	0.061	0.062	0.046
	Dorsal mean	0.045	0.058	0.058	0.039
	t-ratio	-3.328	1.522	2.170	4.061
	p	<0.001	0.297	0.033	<0.001
IP3	Palmar mean	0.037	0.053	0.057	0.040
	Dorsal mean	0.050	0.051	0.057	0.036
	t-ratio	-5.634	0.861	-0.222	2.021
	p	<0.001	0.552	0.878	0.203
IP4	Palmar mean	0.036	0.056	0.058	0.041
	Dorsal mean	0.049	0.053	0.058	0.035
	t-ratio	-5.038	-1.531	-0.016	2.757
	p	<0.001	0.291	0.991	0.013
IP5	Palmar mean	0.042	0.066	0.064	0.046
	Dorsal mean	0.047	0.062	0.062	0.038
	t-ratio	-1.689	2.036	1.158	4.992
	p	0.252	0.045	0.427	<0.001

4.4.1.e. Palmar vs. dorsal cortical thickness

A ratio of palmar and dorsal cortical thickness (S. Fig. 4.4) reveals that within the *Pongo* digits, cortex on the palmar surface is significantly thicker than the dorsal surface in all four digits except IP3 (Table 4.5). *Gorilla* and *Pan* have similar thickness values in the palmar and dorsal shaft, except in the *Gorilla* IP2 ($p = 0.033$) and *Pan* IP5 ($p = 0.045$) where the palmar cortex is significantly thicker. Across the human digits, the dorsal surface of the shaft has significantly thicker cortex than the palmar surface, with the exception of IP5 where there are no significant differences ($p > 0.05$).

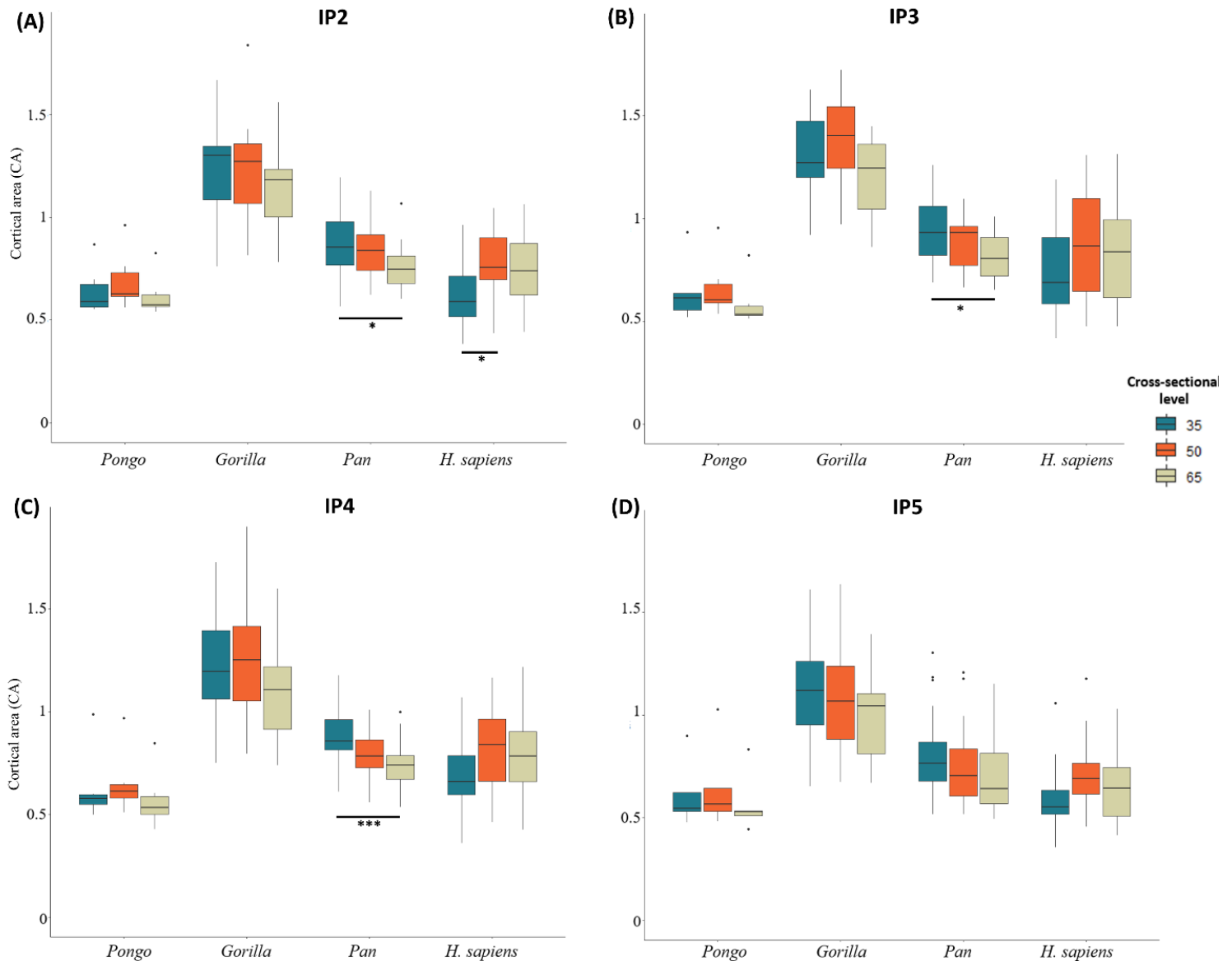


Figure 4.7: Cortical area (CA) for digits 2-5 of *H. sapiens*, *Pan* spp., *Gorilla*, and *Pongo* at 35%, 50%, and 65% of the bone length. * = $p < 0.05$; ** = $p < 0.01$; *** = $p < 0.001$.

4.4.2. Cross-sectional geometry

Descriptive statistics of the scaled cross-sectional geometric properties (CA, Z_{pol} and J) at 35%, 50% and 65% of the shaft are presented in S. Table 4.3 and depicted in Figure 4.7-4.9. There were differences across species in the different cross-sections in CA, Z_{pol} , and J for all four digits ($p < 0.05$), which are presented in S. Table 4.5.

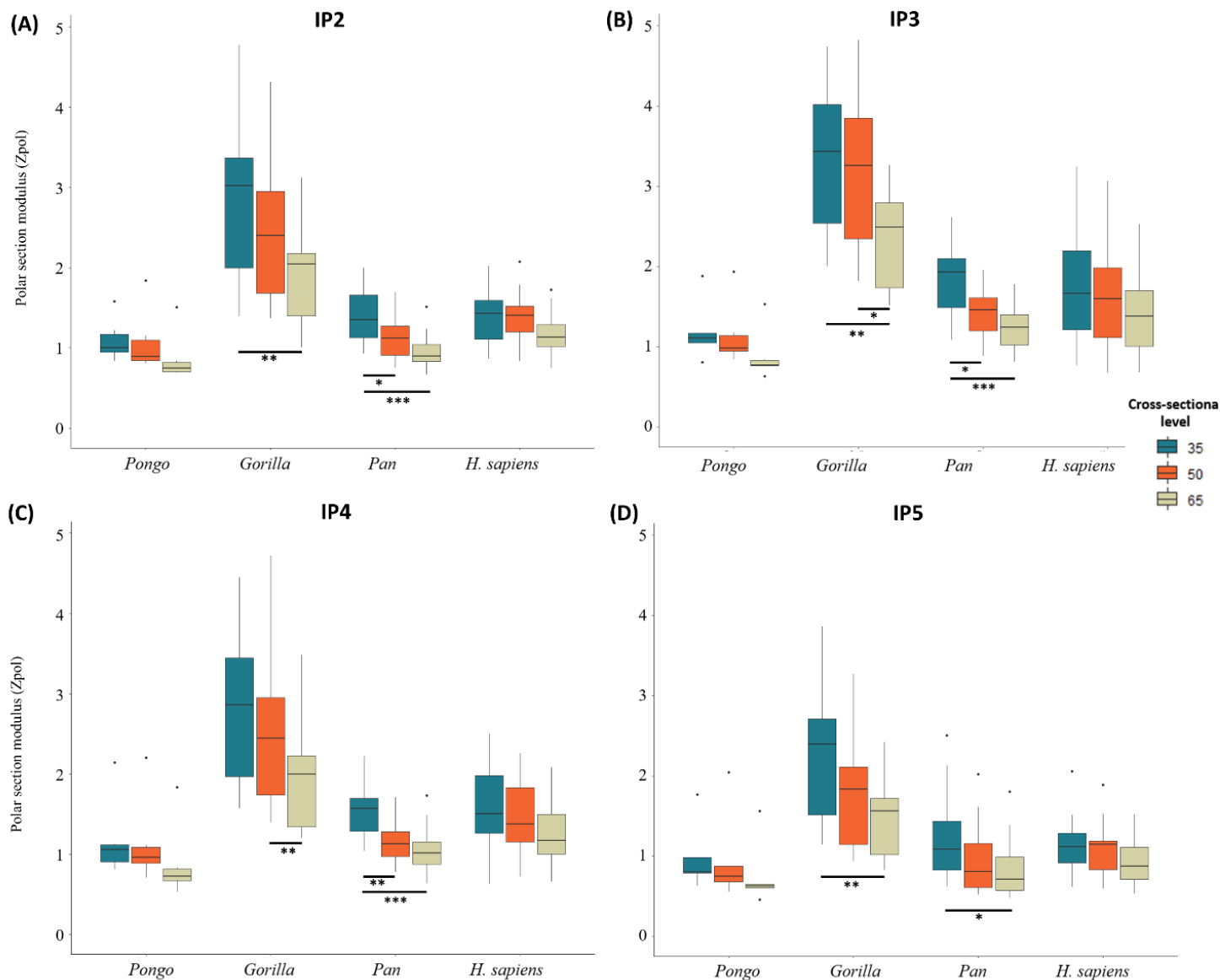


Figure 4.8: Polar section modulus (Z_{pol}) for digits 2-5 of *H. sapiens*, *Pan* sp., *Gorilla*, and *Pongo* at 35%, 50%, and 65% of the bone length. * = $p < 0.05$; ** = $p < 0.01$; *** = $p < 0.001$.

In *Pongo*, CSG properties are similar in all cross-sections (35%, 50%, 65%) (Figs. 4.7-4.9), with no significant differences across IP2-IP5. Within *Gorilla*, IP3 is significantly greater than IP5 in all cross-sectional properties with some variation at the different cross-sectional levels (S. Table 4.7). At the 35% cross-section, there are no significant differences in CA across the *Gorilla* digits and at the 50% level, J of IP4 is also significantly greater than IP5. In *Pan*, the CSG properties across IP2-IP5 follow a similar pattern to that of *Gorilla*, with IP3 being significantly greater than IP5 in all CSG properties across the different cross-sections, with some variation in values of Z_{pol} and J at specific cross-sections (S. Table 4.7). In *H. sapiens* digits, only Z_{pol} of IP3 is significantly greater than IP5 and J of IP3 and IP4 greater than IP5 across all cross-sections (S. Table 4.7).

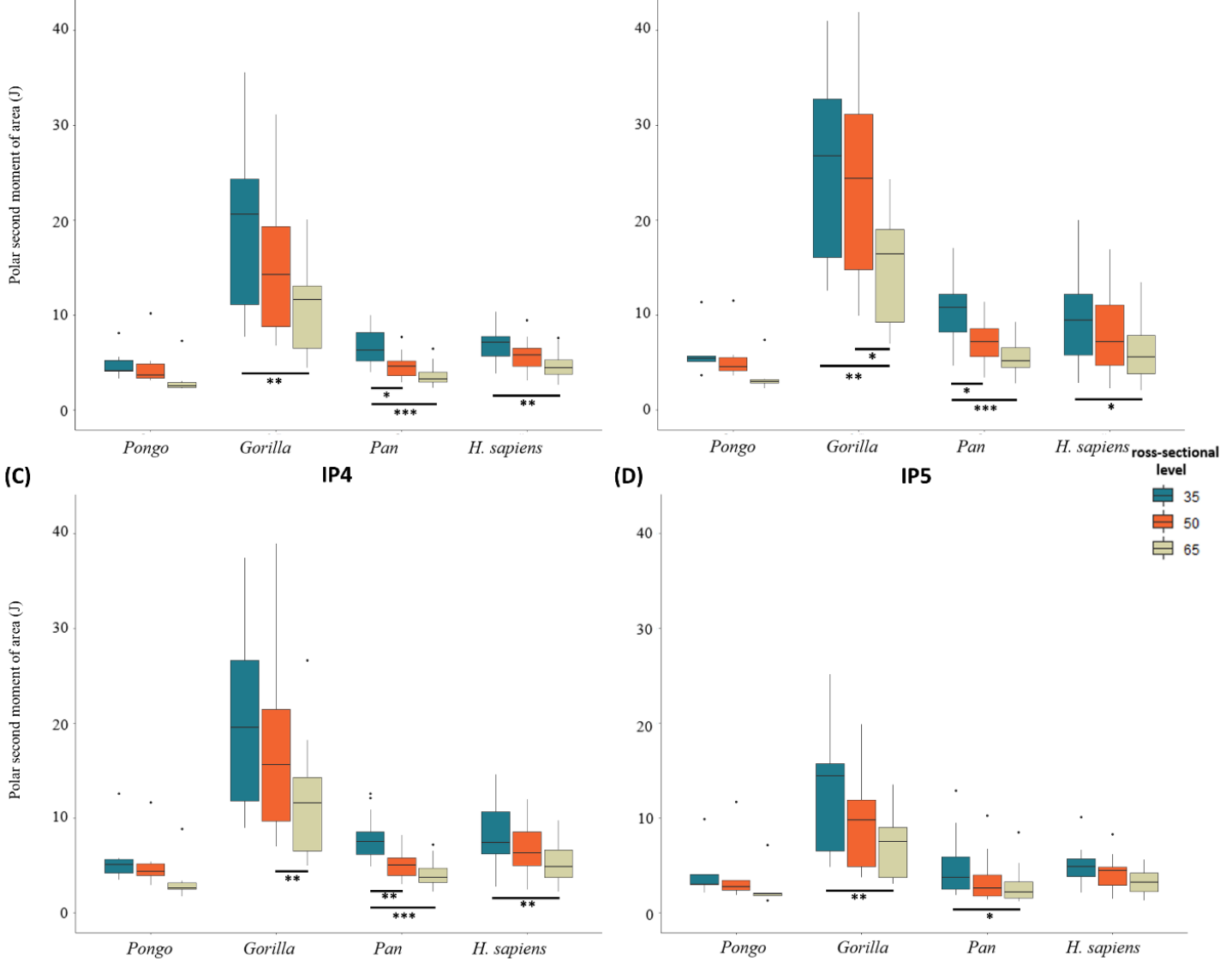


Figure 4.9: Polar second moment of area (J) for digits 2–5 of *H. sapiens*, *Pan* sp., *Gorilla*, and *Pongo* at 35%, 50%, and 65% of the bone length. * = $p < 0.05$; ** = $p < 0.01$; *** = $p < 0.001$.

Analysis of intra-taxic differences in CSG properties at the different cross-sectional levels reveals significant differences in CSG properties within the phalangeal shaft of *Gorilla*, *Pan*, and *H. sapiens* (S. Table 4.8). There are no significant differences across the *Pongo* digits ($p > 0.05$). Within the *Gorilla* digits, CA at the midshaft of IP3 is significantly greater than at 65% of the shaft ($p = 0.019$). Z_{pol} and J increase disto-proximally within the shaft, with values at the proximal end (35% of the shaft) being significantly greater than values at the distal end (65% of the shaft) in IP2–IP5 (S. Table 4.8). Within IP3, the values at the midshaft (50% of the shaft) are also significantly greater than values at the distal end (65% of the shaft). Mean values of all three CSG properties in *Pan* phalanges increase disto-proximally within the shaft (S. Table 4.3). In IP2–IP4, all CSG properties at the proximal end are significantly greater than the distal end of the shaft, with values of Z_{pol} and J at the proximal end also being significantly greater than at the midshaft. Within IP5, only Z_{pol} and J at 35% of the shaft are greater than 65% of the shaft ($p = 0.011$ and $p = 0.014$ respectively; S. Table 4.8). Within *H. sapiens*, CA is greatest at the midshaft and Z_{pol} and J increase disto-proximally, similar to *Pongo* and *Gorilla* (Figs 4.7–4.9; S. Table 4.3). There is little variation within the shaft of each digit such that only J at 35% of the shaft is greater than 65% of

the shaft across IP2-4 ($p = 0.003$, $p = 0.019$, $p = 0.005$ respectively) and CA at 50% is significantly greater than 35% of the shaft only in IP2 ($p = 0.046$; **S. Table 4.8**).

4.4.2.a. Inter-taxic analysis of cross-sectional properties

Values of scaled cross-sectional properties are greatest in *Gorilla*, followed variably by *Pan* and *H. sapiens*, and lowest in *Pongo* at the proximal end (35%) of the shaft. Distally (50% and 65% of the shaft) the pattern of CA is similar, but Z_{pol} and J is greatest in *Gorilla*, followed by *H. sapiens*, *Pan*, and *Pongo* (**S. Table 4.3**). Significance tests reveal *Gorilla* has significantly larger values of CA, Z_{pol} and J across all digits and cross-sectional levels compared to the other taxa, except for Z_{pol} and J in IP5 at 50% cross-section (**S. Table 4.5**). At the 50% level in IP5, *Gorilla* is only greater than *Pan* in Z_{pol} ($p < 0.001$) and greater than *Pan* and *H. sapiens* in J ($p < 0.001$ and $p = 0.026$ respectively). Overall, the remaining taxa, *Pongo*, *Pan*, and *H. sapiens* are not significantly different from each other in any cross-sectional properties across the different levels, except for CA. Values of CA in the IP2 of *Pan* are significantly greater than that of *H. sapiens* at 35% of the shaft ($p = 0.025$).

4.4.3. Cortical thickness and external morphology

4.4.3.a. Phalangeal curvature and cortical thickness

Spearman's correlation analysis testing the relationship between phalangeal cortical thickness and curvature across the extant great apes reveal that there is no relationship between the cortical thickness and degree of curvature of the intermediate phalanges, except in IP3 of *Pongo* and IP5 of *H. sapiens* (**S. Table 4.9**). There is a significant, strong, positive relationship between the curvature and cortical thickness of *Pongo* IP3 ($p = 0.017$ and $\rho = 0.943$) and a significant, positive, weak relationship of *H. sapiens* IP5 ($p = 0.039$ and $\rho = 0.282$) (**S. Table 4.9**).

4.4.3.b. Palmar surface morphology and cortical thickness

Testing the relationship between phalangeal cortical thickness, median bar height, FSR length, and FSR depth in the IP3 of our sample reveals no significant relationships between these variables (**S. Tables 4.10-4.14**).

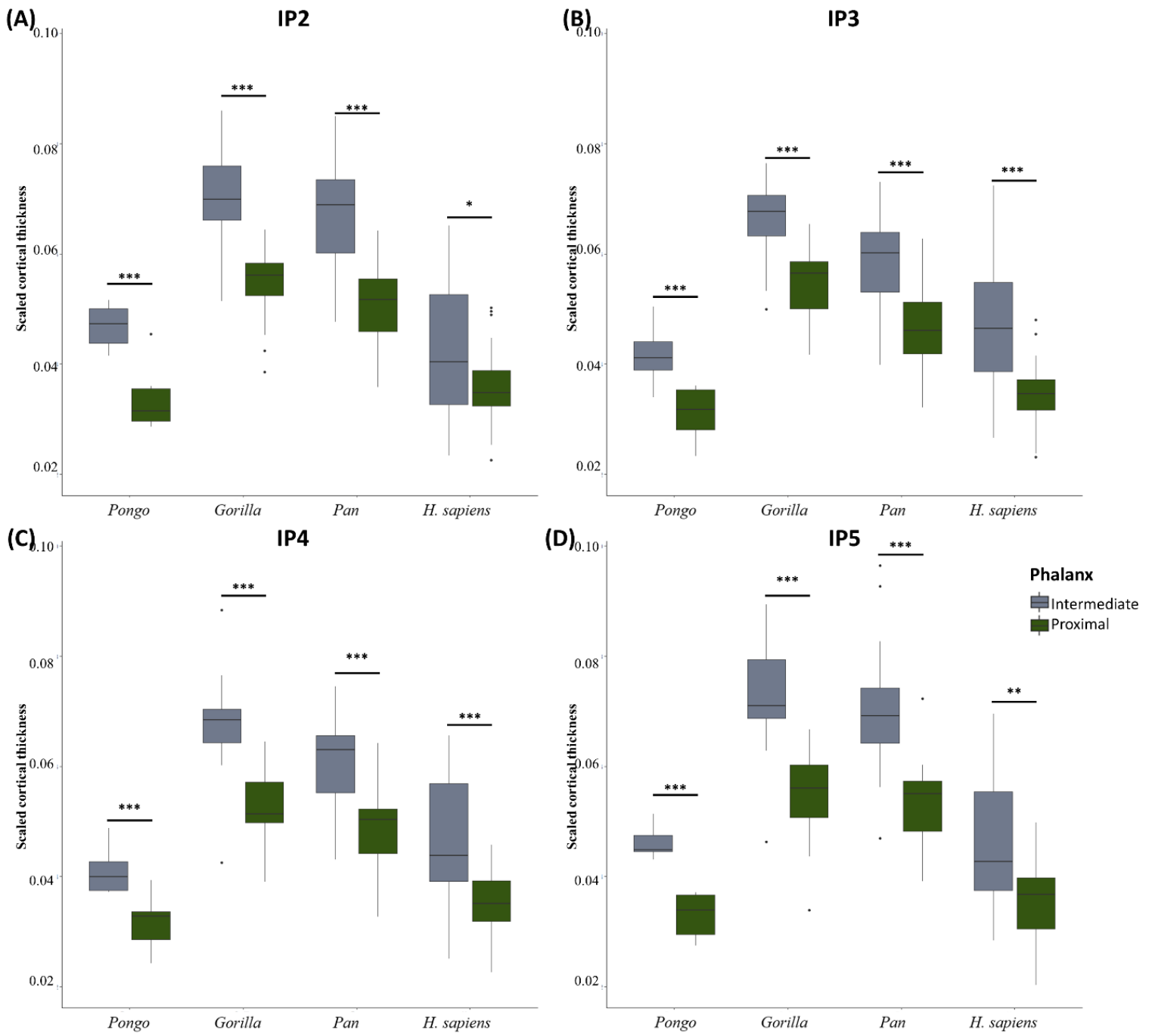


Figure 4.10: Scaled cortical thickness of the proximal and intermediate phalanges across (A) IP2; (B) IP3; (C) IP4; (D) IP5 of *H. sapiens*, *Pan* sp., *Gorilla*, and *Pongo*. * = $p < 0.05$; ** = $p < 0.01$; *** = $p < 0.001$. Intermediate phalanges have significantly thicker cortices in all taxa across the digits.

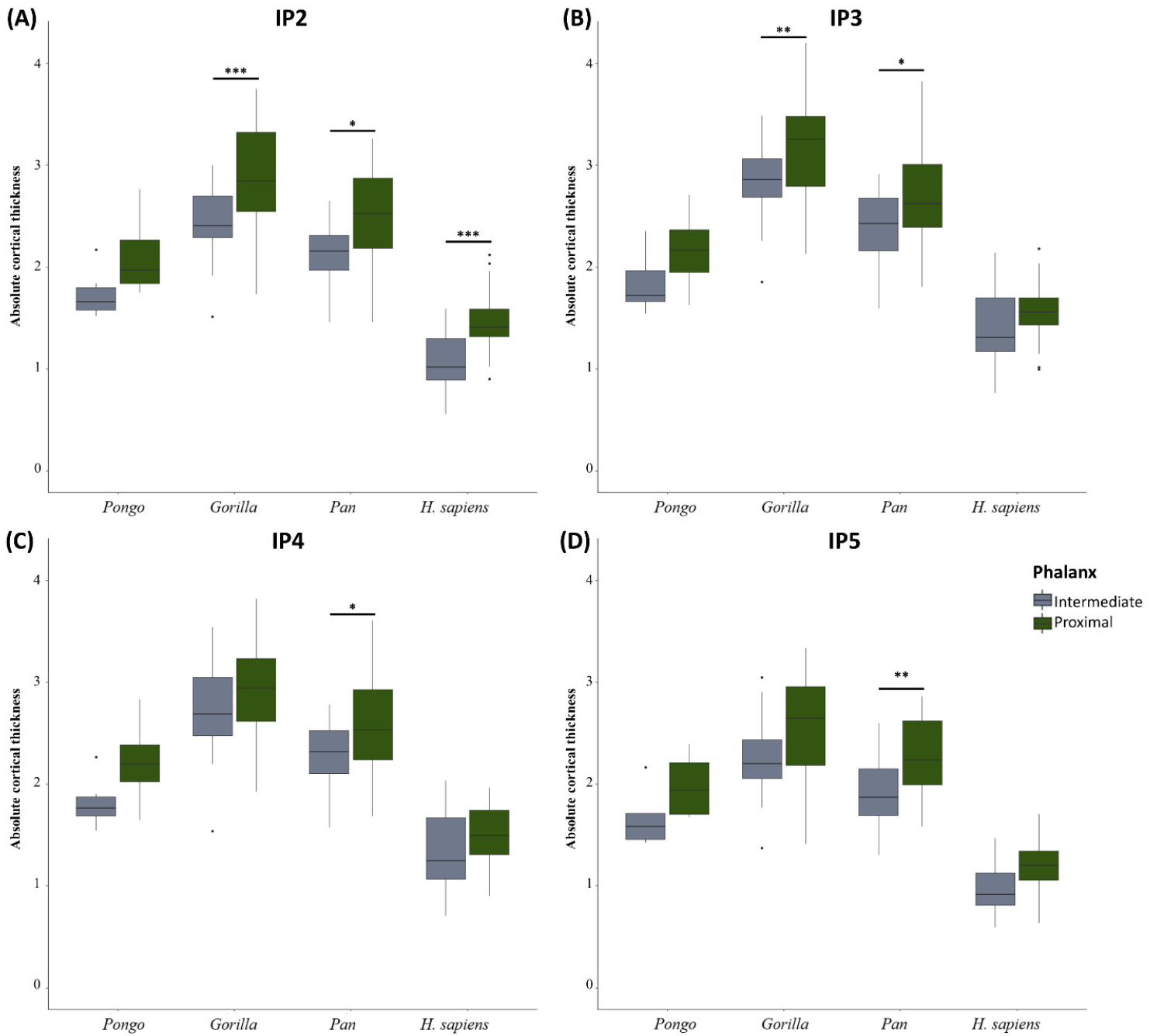


Figure 4.11: Absolute cortical thickness of the proximal and intermediate phalanges across (A) IP2; (B) IP3; (C) IP4; (D) IP5 of *H. sapiens*, *Pan* sp., *Gorilla*, and *Pongo*. * = $p < 0.05$; ** = $p < 0.01$; *** = $p < 0.001$.

4.4.4. Comparisons of proximal and intermediate phalanges

4.4.4.a. Mean cortical thickness

Comparing scaled mean cortical thickness values in the proximal and intermediate phalanges of digits 2–5, cortical thickness values of the intermediate phalanges are significantly greater than the proximal phalanges across all taxa (Fig. 4.10). However, the raw values reveal a

different pattern for each species (Fig. 4.11). In *Pongo*, there are no significant differences between the raw cortical thickness of the proximal and intermediate phalanges. Within the knuckle-walkers, *Gorilla* cortical thickness of the proximal phalanges is greater in digits 2 and 3 ($p < 0.001$ and $p = 0.006$), while *Pan* proximal phalanges have significantly thicker cortex than the intermediate phalanges ($p = 0.024$, $p = 0.044$, $p = 0.012$, $p = 0.006$ across IP2-IP5 respectively). In humans, there are no significant differences across the digits except for digit 2 in which the cortical thickness of the proximal phalanx is significantly greater than the cortical thickness of the intermediate phalanx ($p < 0.001$).

4.4.4.b. Cross-sectional geometry

Analysing relative CSG properties between the proximal and intermediate phalanges of digits 2-5 reveals greater variation in the mean values of Z_{pol} and J compared to CA. Across the digits and three cross-sections, there are no significant differences in the mean values of CA between the proximal and intermediate phalanges of *Pongo*, *Gorilla*, and *H. sapiens* (S. Table 4.15). *Pan* has significantly greater values of CA in the proximal phalanges of digits 2-4 at 35% and 65% of the shaft.

Mean values of Z_{pol} in *Pongo* are significantly greater in the proximal phalanx of digit 2 at 35% and 65% of the shaft ($p = 0.013$ and $p = 0.003$ respectively), and in the proximal phalanx of digit 3 at 50% and 65% of the shaft ($p = 0.123$ and $p = 0.021$ respectively) (S. Table 4.16). Within the proximal and intermediate phalanges of *Gorilla*, Z_{pol} values are significantly greater in the proximal phalanges across all digits and cross-sections. Mean Z_{pol} values of *Pan* are significantly greater in the proximal phalanges of digits 3 and 4 at 35% of the shaft ($p = 0.263$ and $p = 0.049$), digits 2-4 at 50% ($p < 0.001$, $p = 0.247$ and $p = 0.008$) of the shaft, and across all digits at 65% of the shaft (S. Table 4.16). Within the human proximal and intermediate phalanges, the proximal phalanx of digit 2 has significantly greater values than the intermediate phalanx at 35% and 50% of the shaft ($p = 0.003$ and $p = 0.002$) and across digits 2-4 at 65% of the shaft ($p = 0.005$, $p < 0.001$, and $p = 0.041$).

Across the digits of *Pongo*, relative mean values of J are greater in the proximal phalanx of digit 3 at 50% of the shaft ($p = 0.123$) and across digits 2-4 at 65% of the shaft ($p = 0.001$, $p = 0.014$, and $p = 0.003$; S. Table 4.17). Similar to the Z_{pol} values of *Gorilla*, mean values of J are significantly greater in the proximal phalanges of all four digits across all three cross-sections. Within the proximal and intermediate phalanges of *Pan*, the proximal phalanx of digit 4 has significantly greater values of J than the intermediate phalanx at 35% of the shaft ($p = 0.047$). At 50% and 65% of the shaft, the proximal phalanges of all four digits have significantly greater values of J compared to the intermediate phalanges. The human proximal phalanges have significantly greater values of J for digit 2 at 35% of the shaft ($p = 0.003$), digits 2 and 3 at 50% of the shaft ($p < 0.001$ for both), and digits 2-4 at 65% of the shaft ($p = 0.002$, $p < 0.001$, and $p = 0.019$).

4.5. Discussion

Studies of the internal structure of the hand have generally focused on the metacarpus and elements of the carpus, with the phalanges being comparatively understudied. Here, we investigated variation in hominid cortical bone distribution patterns of the intermediate phalanges of digits 2-5 in relation to hand use and postures, building upon our previous study of proximal

phalanges in the same taxa (and specimens). Cortical bone distribution patterns, along with overall cortical bone thickness and CSG properties, were consistent with differences in hand use among suspensory *Pongo*, knuckle-walking *Gorilla* and *Pan*, and humans. Comparisons of cortical bone structure between the proximal and intermediate phalanges provide greater insight into digit loading during manual behaviours.

4.5.1. Extant great ape intermediate phalangeal cortical distribution, thickness and cortical properties

We predicted that cortical bone in *Pongo* would be thickest in the midshaft-to-distal palmar surfaces with no significant differences in cortical structure across the digits, reflecting the flexed-finger, hook grip of all the fingers during suspensory behaviour (Rose, 1988; Sarmiento, 1988). Our predictions are supported, as in *Pongo* regions of thickest cortical bone are located on the FSRs and in the region proximal to the trochlea, with the shaft having low to intermediate thickness across all IPs. This pattern reflects the known biomechanical role of the FSRs, which is to reduce strain on the phalangeal shaft (Nguyen et al., 2014). The lack of significant differences in cortical thickness and CSG properties across the digits is consistent with equal use and similar loading of all four digits during suspensory locomotion in *Pongo* (Rose, 1988; Thorpe & Crompton, 2006; Susman, 1974).

Within the African apes, we predicted that *Gorilla* and *Pan* would have a similar pattern of cortical bone distribution compared to the other extant taxa but would differ in their cortical bone properties across the digits. Our predictions are not fully supported. The general African ape pattern across the rays is characterised by thick cortical bone at the FSRs and proximal to the trochlea, with a low to intermediately thick cortex along the shaft. This pattern is surprising as EMG data on subadult chimpanzees has shown minimal to no activation of flexor muscles during knuckle-walking (Susman & Stern, 1979). However, a recent experimental study has shown stress is concentrated on pulleys, which hold the flexor tendon close to the bone during interphalangeal joint flexion (Leijnse et al., 2021). These pulleys arise from the radial and ulnar edges of the palmar surface, with annular pulleys A2 and A4 being the main pulleys within the fingers (Ayhan & Ayhan, 2020). The A4 pulley is located on the intermediate phalanges and Leijnse et al. (2021) have shown that stress is concentrated proximally on the A4 pulley, which coincides with the location of the FSRs. Although Marzke et al. (2007) found no relationship between the size and attachment point of the FDS tendon and palmar phalangeal morphology, if the regions of thickest cortex reflect stress related to the adjacent A4 pulley insertions, then cortical bone distribution patterns may be reflecting the role of the flexor muscles during different African ape manual behaviours that is not reflected in external morphology alone. These manual behaviours could include, stretching of the flexor tendons during knuckle-walking (Leijnse et al., 2021) or activation of flexor muscles during arboreal grasping (Susman & Stern, 1979). While the overall pattern is generally similar, the majority (82%) of *Pan* individuals had an intermediately thick shaft while the majority (69%) of *Gorilla* individuals have relatively thin shaft cortex. This difference may reflect the greater frequency of arboreal behaviours in *Pan* and thus flexor muscle activation, as well as differences in the external morphology (Hunt, 2020; Susman, 1979; Susman & Stern, 1979). *Gorilla* have a significantly lower degree of phalangeal curvature than *Pan*, which have significantly smaller FSRs than *Gorilla* (Doran, 1996; Hunt, 1992; Sarringhaus et al., 2014; Susman, 1979; Syeda et al., 2021).

Along with differences in cortical bone distribution patterns between the African apes, cortical properties of the intermediate phalanges across the digits differ between *Gorilla* and *Pan*, which is consistent with data from captive individuals showing differences in digit use and loading between these two taxa (Matarazzo, 2013; Samuel et al., 2018; Thompson, 2020; Wunderlich & Jungers, 2009). While recent observations of mountain gorillas in the wild show much greater variation in manual postures than in captivity (Thompson et al., 2018), zoo-housed *Gorilla* load digits 2–5 more evenly than *Pan* (Matarazzo, 2013; Tuttle, 1969a). This is reflected in the variation in cortical properties across the digits of the respective taxa. *Gorilla* mean cortical thickness does not significantly differ across the digits but CSG properties show that IP3 is significantly stronger than IP5, which is consistent with pressure studies that have shown greater loads occurring around the middle of the hand during knuckle-walking (Samuel et al., 2018; Tuttle, 1972). Contrary to our prediction, IP5 of *Pan* has significantly thicker cortical bone than IP3 and IP4, which are the digits that experience the highest loading (Matarazzo, 2013; Samuel et al., 2018; Wunderlich & Jungers, 2009). However, IP3 did have CSG properties reflecting greater strength relative to IP5. The thicker cortex and weaker CSG properties of IP5 relative to IP3 may reflect the role of external morphological features in the remodelling of internal bone structure. IP5 has smaller FSRs and a lower degree of phalangeal curvature (Susman 1979; Syeda et al., 2021) and as such might not be able to effectively resist the loads placed upon it, resulting in cortical remodelling but also may not be experiencing much loading during locomotion (Wunderlich & Jungers, 2009).

As predicted, human cortical bone is thickest on the distodorsal region, including in individuals that possess well-developed FSRs. This cortical bone distribution pattern may reflect the role of phalangeal curvature in dissipating forces across the phalanx (Preuschoft, 1973; Richmond, 2007). Typically, *H. sapiens* manual behaviours involve flexed finger postures in which the dorsal surfaces of the phalanges experience high tensile forces and the palmar surfaces experience compressive forces. These bending forces dissipated across a relatively straight phalanx result in greater stress experienced by the dorsal surface (Preuschoft, 1973). Along with thick distodorsal cortex in humans, cortical bone on the distal palmo-radial and palmo-ulnar surfaces is thick irrespective of the presence of FSRs (**S. Fig. 4.1**). In contrast, human proximal phalanges did not show consistently thick cortex at the radial and ulnar edges of the palmar surface, suggesting that the pattern found in human IPs reflects the point of insertion of the FDS tendon. Across the hand, we predicted that digits 2 and 3 would have thicker cortices and stronger cortical properties than digits 4 and 5 as experimental studies have shown that the greatest loads are experienced by the radial digits and the thumb (Cepriá-Bernal et al., 2017; de Monsabert et al., 2012; Sancho-Bru et al. 2014). However, our prediction is not supported; only IP3 was higher than IP5 in measures of bending strength (Z_{pol}) and only IP3 and IP4 were higher than IP5 in measures of bending and torsional rigidity (J). The lack of distinct differences across the digits may reflect the presumed varied manual behaviours employed by our *H. sapiens* sample, which ranges from fossil specimens to a diverse range of pre- and post-industrial populations.

4.5.2. Intermediate phalangeal pattern of cortical bone distribution compared to proximal phalanges

4.5.2.a. *Pongo*

This cortical bone distribution pattern of *Pongo* IPs is similar to that of their PPs, further reflecting similar loading across the digits during flexed-fingered grips of the hand. It is an oversimplification to classify *Pongo* hand postural behaviours as just hook-like grips, as variation in *Pongo* locomotion has been increasingly observed (McClure et al., 2012). However, we expected phalangeal cortical structure to reflect the repetitive hand postural behaviours of *Pongo*, which have generally been observed to be flexed fingered grips (Napier, 1960; Rose, 1988). While the proximal and intermediate phalanges share a general pattern of thickness localised at the FSRs with an intermediately thick shaft, there is a slightly different pattern observed in PP2. The PP2 of some individuals showed thicker palmar radial cortex, which was hypothesised to reflect the greater extension of the second digit when grasping thin substrates (Napier, 1960). However, if this hypothesis is correct, we would expect a similar cortical distribution on the IP2, which we did not find. Instead, our sample of IP2s has relatively thicker cortex on the ulnar, rather than the radial, edge of the palmar surface. However, our sample of intermediate phalanges is constrained to six individuals, as such these patterns may reflect general variation within the taxa and deducing more subtle differences in hand postures may require larger sample sizes.

Comparing cortical thickness values and cross-sectional properties of *Pongo* intermediate and proximal phalanges reveal mixed signals. Scaled average cortical thickness of the IPs is significantly greater than the PPs across all digits. However, bending strength of PP2 and PP3 is significantly higher than their IPs and the bending and torsional rigidity of digit 2-4 PPs is significantly greater than the IPs in the distal region of the shaft (65% cross-section). While the IPs have thicker cortices than the PPs on average, higher CSG values of the PPs relative to the IPs could reflect the disto-proximal direction of load, such that the PPs are experiencing greater forces and are better structurally adapted to resist greater loads (Matarazzo 2015).

4.5.2.b. *Gorilla*

Similar to the pattern previously identified in the *Gorilla* PPs, the regions of thickest cortical bone in the IPs coincide with attachment points of soft tissues that stabilize the interphalangeal joints. Cortical bone of the PPs was thickest in patches along the FSRs, while in the IPs thick cortical bone is found across the length of the FSRs. The FSRs of the IPs are located on the proximal half of the phalangeal shaft, and as stress is concentrated proximally at the A4 annular pulley (Leijnse et al., 2021), this thickness of the FSRs in the proximal region of the bone may reflect the stress that occurs when the flexor tendons are bent during knuckle-walking. Similarly, the cortical bone distribution pattern of the PPs reflects FDS tendon bending that occurs distally at the A2 annular pulley. These similar patterns of thick cortical bone in regions that are thought to be stressed by flexor tendon stretching and phalangeal soft tissue attachment points may provide support for experimental evidence that suggests that, during knuckle-walking, stress is concentrated at the maximum bending point of the tendons and at the pulleys which hold these tendons (Leijnse et al., 2021). On the other hand, these patterns might be a signal of less frequent (relative to knuckle-walking) arboreal behaviours (Hunt, 2020) in which the flexor muscles are highly active (Susman & Stern, 1979).

Across the PPs and IPs of *Gorilla* digits 2–5, the average scaled IP cortical thickness is significantly thicker than the PPs. Along with their thick cortices, there is also greater variation within the CSG properties across the phalangeal shaft in the IPs compared to that of the PPs, such that the CSG properties at the proximal end of the bone are significantly greater than at the distal end. However, bending strength and resistance to bending and torsional rigidity is significantly greater in the PPs relative to the IPs. These results could indicate that despite the IPs making the initial contact with the substrate and directly incurring the ground reaction forces during knuckle-walking, the proximal end of the IPs and the PPs, as a whole, are better able to resist the forces generated during manual behaviours. Across the PPs and IPs, digit 2 shows thicker palmar cortex, which may reflect the relatively small FSRs of digit 2 compared to digits 3 and 4 (Susman, 1979), although it does not explain why PP5 has relatively thicker palmar cortex but IP5 does not.

4.5.2.c. *Pan*

The pattern of cortical bone distribution of *Pan* IPs is similar to that reported for the PPs, in that the region of thickest cortical bone is located proximodistally along the FSRs. Across our sample, *Pan* is the only taxa that showed differences in mean cortical thickness across the digits in the PPs and the IPs. The proximal and intermediate phalanx of digit 5 has significantly thicker cortical bone than the proximal and intermediate phalanx of digit 3. However, the CSG properties of digit 3 are significantly greater than digit 5. This may be because the external morphological features of digit 5 (i.e. prominent FSRs, phalangeal curvature) are not as prominent as they are in the other radial digits, as such loads may not be dissipated as effectively in digit five and leading to higher strains, increased cortical bone remodelling and thus thicker cortical bone than digit 3, in which external morphological features that lower strain are most pronounced (Nguyen et al., 2014; Susman, 1979). Comparing the average cortical thickness and CSG properties of the PPs and IPs, average cortical thickness is greater in the IPs while the PPs have significantly stronger CSG properties than the IPs, a pattern similar to that found in *Gorilla*. As the primary mode of locomotion of *Gorilla* and *Pan* is knuckle-walking, these similarities in cortical bone structure of the PPs and IPs are expected.

4.5.2.d. *Homo sapiens*

The pattern of *H. sapiens* IPs is similar to that found in their PPs in that the thickest region of cortical bone is concentrated at the distodorsal surface of the phalanges, but the IPs are distinct in also having thick cortical bone along the distodorsal region of the palmar surface (regardless of the development of the FSRs). There are no significant differences in cortical thickness across the digits in either the PPs or the IPs and the dorsal cortex is consistently thicker than the palmar cortex, except for IP5. In IP5, similar dorsal and palmar cortical thickness may indicate that IP5 is not being loaded in the same manner as the other phalanges. This has been noted in an experimental study of load distribution during power grips, in which the fifth digit does not remain active throughout the length of a gripping task, in contrast to the remaining digits (Sancho-Bru et al., 2014). This is also reflected in the CSG properties of the PPs and IPs, with CSG properties in the PPs of digits 2–4 significantly stronger than the IPs, but the absence of differences in the CSG properties of the phalanges of digit 5 suggest overall lower levels of loading.

4.5.3. Relationship between proximal and intermediate cortical bone thickness

While the pattern of cortical bone distribution is similar in the proximal and intermediate phalanges within our study taxa, the scaled values of mean cortical thickness are not. Intermediate phalanges on average have thicker cortical bone in the phalangeal shaft when scaled to the length of the bone. This could be due to many factors. Firstly, external morphological features that are thought to help resist forces are generally less developed in the IPs compared to the PPs (i.e. degree of curvature; FSRs). Therefore, the relative cortical thickness in the intermediate phalanges may need to be greater to withstand loading. Secondly, the FDS tendons insertion site is located on the intermediate phalanges, whereas they only pass across the proximal phalanx (with pulleys inhibiting the buckling of the tendon). Therefore, the majority of the internal forces exerted by these muscular tendons are likely incurred by the intermediate phalanges. Finally, it could be that the relationship between bone length and required cortical thickness is not linear, perhaps there is a minimum amount of cortical bone needed when scaled for length that is larger than cortical bone in proximal phalanges.

Comparing absolute values of PP and IP cortical thickness reveals a unique relationship between the two in each taxon (Figs. 4.10–4.11). Similar values of absolute average cortical thickness across the PPs and IPs of *Pongo*, coupled with their thin cortex and low cross-sectional properties, may further reflect that due to their external morphology minimising strain on the phalanges, cortical remodelling and thicker cortex might not be needed (Ruff et al., 2006). Within the African apes, *Gorilla* has significantly thicker cortical bone in the PP of digits 2 and 3 while *Pan* has significantly thicker PP cortical structure across all digits. These results provide additional support for our inference that the PPs of African apes might be better adapted to the loads resulting from their manual behaviours. Across *H. sapiens* digits, only digit 2 has significantly thicker PP cortical bone while the remaining digits show no differences. The significantly thicker cortices of the PPs can be attributed to the absolutely larger size of the PPs compared to the IPs, but the lack of significant differences in PP and IP cortical thickness of *Pongo*, *Gorilla*, and *H. sapiens* digits indicates phalangeal size is not the only factor impacting phalangeal cortical thickness.

4.5.4. Phalangeal curvature

We found no strong correlation between cortical thickness and the degree of curvature in either the IPs or PPs in our sample. These results might therefore call into question the functional significance or plasticity of phalangeal curvature (see also Wallace et al., 2020). Phalangeal curvature has been shown to change throughout ontogeny based on the frequency of arboreality (Richmond, 1998) and has been experimentally demonstrated to reduce strain experienced by the (proximal) phalanx during suspensory loading (Nguyen et al., 2014; Richmond, 2007). If cortical thickness reflects loads incurred during life (Ruff et al., 2006), one might expect taxa with more curved phalanges to have thinner cortex or for humans to have more curved phalanges if they are habitually using flexed-finger postures. However, our results suggest that the relationship between cortical bone thickness and curvature is more complex. Overall length of the phalanx and the shape and size of the flexor sheath ridges will also influence how loads are incurred by the phalanx, and the frequency and magnitude of external and internal loads are critical. For example, musculoskeletal modelling of the third digit shows that the ratio of (internal) tendon load relative to (external) fingertip force and bone load magnitude to fingertip force was 42% and 55%

higher, respectively, in a bonobo than a human (Synek et al., 2019). Thus, we propose that loads incurred during flexed-finger postures in human manipulative activities are not of sufficient magnitude to stimulate plasticity in curvature, but are sufficient to cause cortical modelling of the dorsum (in comparatively straight phalanges).

4.5.5. Flexor sheath ridges

The development of the FSRs has been linked to arboreal behaviours (Nakatsukasa et al., 2003) and our study supports the hypothesised biomechanical role of the FSR in reducing the strain on the phalangeal shaft (Nguyen et al., 2014). It can be called into question that FSRs will always be the thickest region of cortical bone within a phalanx, as it is a bony projection. However, individuals with small FSRs, or with no FSRs, have a shaft that is relatively thicker compared with the phalangeal shaft thickness of individuals with larger FSRs.

While an experimental study has explained the biomechanical function of the FSRs (Nguyen et al., 2014), the ontogenetic development of the FSRs has yet to be studied. Currently, there is a lack of evidence explaining the variability of the FSRs and the functional implications of this variability. For example, it is not clear as to why *Gorilla* have the most prominent FSRs among the extant great apes, when at least mountain gorillas spend considerably less time arboreally than *Pan* and *Pongo* (Doran, 1997). We also observed variation in FSR morphology within *Pan*, with some individuals displaying FSRs that project minimally from the palmar shaft while others are quite prominent. This variation is present within male and female individuals of *Pan paniscus* and *Pan troglodytes*, as such sexual dimorphism and systemic differences in the skeleton of these two species cannot explain the differences in FSR morphology. These differences in morphology could be explained by other aspects of external morphology, such that the large FSRs of *Gorilla* can be explained by their relatively straight phalanges, so these large FSRs might help them participate in arboreal behaviours. Larger FSRs in *Gorilla* might also be related to the large forces the *Gorilla* hand must withstand during knuckle-walking, as the prominent FSRs provide a greater bone surface to dissipate forces. Similarly, *Pan* does not have large FSRs because of their curved phalanges, which allow optimal load distribution. However, these explanations require experimental and developmental validation to confirm the functional implications of this bony morphology.

4.5.6. Palmar median bar

Along with the FSRs, the functional morphology and the development of the palmar median bar and its (generally) accompanying lateral fossae are not well understood or studied. The palmar median bar is an anterior extension of cortical bone on the palmar surface, thought to have a biomechanical function (Tocheri et al., 2008). As such, we expected that the palmar cortical thickness of the phalangeal shaft would have been significantly thicker in taxa which possess strong palmar median bars (i.e., *Pongo* and *Gorilla*). However, the preliminary analyses on a subset of our sample shows no evidence of a functional signal in the palmar median bar (S. Table 4.10, 4.13, 4.14). An alternate explanation for the presence of palmar median bar is that it is simply a by-product of the hollowing out of the lateral fossae. However, this hypothesis would imply a thin cortical bone at the lateral fossae, which was not observed here. Cortical thickness of the lateral fossae is similar to the thickness of the palmar shaft (except for FSRs) across our sample. Nonetheless, despite that the palmar median bar does not affect the overall palmar

phalangeal cortical thickness, this morphology will affect the shape and distribution of mass, and therefore the CSG and bending rigidity and strength are likely to be different. Ontogenetic and biomechanical data testing the functional role of these palmar features is needed to improve our understanding of the form-function relationships and interactions between these morphological features.

4.5.7. Limitations

Biomechanical remodelling occurs throughout life in response to loading, with force transfer of these loads dependent upon external shape and internal anatomy, the relationship of which has not yet been thoroughly explored. Furthermore, functional interpretations resulting from cross-sectional properties of bones that are less cylindrical (such as the IPs) may not be as robust or straightforward to interpret. However, there is evidence that (e.g., Gosman et al., 2013; Rodriguez et al., 2018) CSG properties of non-cylindrical regions of bone can be successfully linked to function. Ultimately, a thorough investigation into the relationship between external morphology and internal morphology, alongside kinematic and musculoskeletal modelling is needed to provide a holistic understanding of great ape manual behaviours

4.6. Conclusions

Our results provide, for the first time, a detailed analysis of the internal structure of the great ape intermediate phalanges. Cortical bone structure of the intermediate phalanges across the extant great apes reflected differences in hand postures during manual behaviours across the taxa and within the hand of each taxon. Results of this study coupled with the known cortical structure of the proximal phalanges, revealed a similar pattern of cortical bone distribution across the proximal and intermediate phalanges but greater load resistance by proximal phalanges. This demonstrates the functional signals that can be gleaned from the cortex of the proximal and intermediate phalanges of digits 2-5, which can be applied to the reconstruction hand use in fossil hominins. It also highlights the importance of considering variation in external morphological features for the interpretation of the biomechanical environment that leads to variation in internal bone structure.

5 – Hand use in fossil hominins: reconstruction of manual behaviours via phalangeal cortical bone morphology

5.1. Abstract

Chapters 3 and 4 explored the cortical bone structure of the proximal and intermediate phalanges of digits 2-5 in extant great apes. These chapters successfully linked the patterns of cortical bone distribution, thickness, and cross-sectional geometric properties with the distinct habitual manual postures employed by each of the extant taxa. Testing and demonstrating this form-function link between cortical bone morphology and hand use provides a comparative context in which to infer manual behaviours in fossil hominins. Below I discuss what is known about the manual function of the fossils hominins reviewed in Chapter 1, ranging from *Australopithecus* to Neanderthals, and apply the same methodological protocol described in Chapter 2 to map the cortical bone thickness and measure cortical bone properties of their proximal and intermediate phalanges. Following that, I use the cortical bone distribution pattern and relative thickness to infer the potential locomotory and manipulative behaviours in each fossil individual, within the context of extant ape phalangeal cortical morphology and previous studies that have explored the internal structure of the hand. Results reveal manual behaviours and postures of fossil hominins likely varied across taxa, representing both, a hand being used for locomotion but also for manipulation, making it clear that the trajectory of hominin hand evolution was not linear.

5.2. Introduction

Fossil hominin hand morphology demonstrates a functional shift in hand use, from a hand used for locomotion to a hand used primarily for manipulation. When and how this functional shift occurred is difficult to reconstruct, as the morphological correlates of modern human-like dexterity are present alongside features that indicate the locomotory use of the hand (Alba et al., 2003; Bush et al., 1982; Haile-Selassie et al., 2009; Kivell et al., 2015; 2018a; 2020; Larson et al., 2009; Napier, 1962a; Pickering et al., 2018; Susman & Creel, 1979; Ward et al., 2012). Furthermore, majority of the fossil hominin hand remains are usually found in isolation, making the task even more challenging. In order to overcome this challenge and to better understand the functional morphology of fossil hominin hands, many studies exploring the external and internal morphology of fossil hominin hand remains have occurred alongside a comparative sample of extant hominids (e.g., Bird et al., 2023; Dunmore et al., 2020; Kivell et al., 2018; Skinner et al., 2015). These comparative studies have revealed hand remains of Plio-Pleistocene hominins, such as *Australopithecus*, *Paranthropus*, and *Homo*, demonstrate a striking amount of external morphological variation, which coupled with their internal bone structure, suggests diversity of manual behaviours throughout the Plio-Pleistocene. This diversity of manual function evidenced in earlier fossil hominins has also been observed in *Homo neanderthalensis* remains (Kivell et al., 2018b; Niewoehner, 2006; Rosas et al., 2006; Stephens, 2018). Neanderthal dexterity has been shown to be comparable to modern humans, with differing degrees of different grips and postures employed compared to modern humans (Bardo et al., 2020; Karakostis et al., 2018; Stephens, 2018). Within the fossil taxa, various number of skeletal remains represent each fossil hominin taxa. Within the Plio-pleistocene fossils, earlier fossil hominin taxa, such as *A. afarensis* and *A. africanus*, hand morphology is well-represented through several skeletal elements of the hand (see Kivell et al., 2022), while some species are only represented by a hand full of elements, such

as the OH 7 hand of *Homo habilis*. Despite the large number of fossil evidence of the *A. afarensis* and *A. africanus* hand, there is not yet a complete associated hand of either of these species. Associated fossils provide a great deal of information regarding the overall function of the skeleton, making associated fossil remains highly valuable in behavioural reconstruction of fossil hominins. Recent discoveries of South African hominins *A. sediba* and *H. naledi* have yielded nearly complete associated hand remains of each species. A complete right hand of *A. sediba* specimen MH2 and *H. naledi* Hand1 demonstrate morphology that is unique within the extant great apes but also within the fossil hominin record. The same can be said of the multiple isolated remains of *H. floresiensis*. Hand remains of these Plio-pleistocene fossils are scarce compared to the extensive fossil record of hand remains of Later *Homo*, particularly the Neanderthals (e.g., Kivell et al., 2018b; Musgrave, 1973; Niewoehner, 2006; Niewoehner et al., 2003; Trinkaus, 2016; Trinkaus and Villedieu, 1991). Previous work that has aimed to reconstruct the manual behaviours of these fossil hominins has focused on the internal structure of the wrist and metacarpals. Here, we expand on this previous research and study the internal structure of the non-pollical proximal and intermediate phalanges of *A. afarensis*, *A. africanus*, *A. sediba*, *H. habilis*, Swartkrans fossil hominins (*P. robustus*/Early *Homo*), *H. naledi*, *H. floresiensis* and *H. neanderthalensis*. We focus on the phalanges, as they are the first point of contact with the substrate or object during manipulation and locomotion and are consistently loaded during those behaviours as well.

Each of the fossil hominin taxa studied here displayed a distinct mosaic of morphologies within the hand and the phalanges as well, potentially pointing towards their variable manual behaviours. As such, I describe the manual remains of each fossil separately and discuss their behavioural repertoire in the context of previous studies on their hand remains, starting from the earliest fossil hominin taxa in my sample, *A. afarensis*, to later *Homo*, with the discussion of Neanderthals. The descriptions of the fossil hominin hand remains are followed by predictions regarding the potential manual behaviours of each fossil taxa, on and a brief discussion of the importance of studying internal structure in reconstructing behaviours.

5.2.1. *Australopithecus afarensis*

The hand of *A. afarensis* (4.2 – 2.9 mya; Alemseged, 2023) is represented by numerous isolated elements, including carpals, metacarpals and phalanges from multiple individuals and localities. Preservation of complete metacarpals and phalanges allow estimates of the intrinsic hand proportions in this species, but these estimates range from gorilla-like to modern human-like (Alba et al., 2003; Almécija & Alba, 2014; Rolian & Gordon, 2013). Parts of the carpus indicate mosaic morphology, in that the orientation of the trapezium suggests a modern human-like ability to pronate the second metacarpal, while the capitate shape suggests greater mobility at the capitate-Mc3 joint (Tocheri et al., 2003; Rein & Harvati, 2013). The carpus is coupled with metacarpals that suggest the *A. afarensis* hand was capable of manipulation but with a limited range of motion and grips compared to humans (Marzke, 1971; Ward et al., 2012). Evidence of the *A. afarensis* manipulation capabilities is evident in the radioulnarly broad distal pollical phalanx and asymmetrical metacarpal heads, but the proximal and intermediate phalanges have prominent FSRs and an intermediate degree of curvature, which are features generally associated with flexed-finger grasping during arboreal locomotion (Alba et al., 2003; Marzke, 1997; Ward et al., 2012). Curvature and prominent FSRs of the phalanges, along with features of the upper limb,

support the interpretation that *A. afarensis* locomotor repertoire included habitual arboreal behaviours (Stern, 2000; Stern & Susman, 1983; Ruff et al., 2016; Green & Alemseged, 2012). Coupling these morphologies together, there have been several functional interpretations of the manual capabilities of *A. afarensis*. It has been suggested that *A. afarensis* could perform precision pad-to-side grips and would have been capable of performing precision handling and power squeeze grips as well (Marzke 1997; Tocheri et al., 2003). However, others argue against the ability of *A. afarensis* to produce modern human-like precision grips (Rolian & Gordon, 2013).

This analysis aims to build on the current evidence of *A. afarensis* manual behaviours through the cortical bone analysis of the AL 333-19 phalanx. While I had access to scans of at least four other *A. afarensis* phalanges, I only analysed the AL 333-19 phalanx as it was the only phalanx in which the cortex could successfully be separated from the matrix. The internal structure of the remaining phalanges was not sufficiently preserved to conduct cortical bone analyses. The external morphology of the AL 333-19 phalanx suggests it is from ray(s) two or four, due to its slight asymmetry of the base and trochlea. I hypothesize, based on the overall bauplan of the *A. afarensis* skeleton and external phalanx morphology, that *A. afarensis* phalanx will display a pattern of cortical bone distribution and thickness most similar to the non-human great apes (hereafter referred to as 'great apes'), reflecting habitual use of flexed-finger postures employed during locomotion.

5.2.2. *Australopithecus africanus*

Similar to *A. afarensis*, fossil evidence of *A. africanus* (3.3 – 2.1 mya) hand morphology consists of several isolated specimens (see Kivell et al., 2022 for an updated review). *A. africanus* hand bones display a mixture of features that are either similar to modern humans, great apes or intermediate between the two. Within the carpus, the capitate displays morphology that is intermediate between African apes and modern humans, the scaphoid indicates a deep, ape-like carpal arch, and the junction of the trapezium and Mc1 suggest limited joint mobility (Kibii et al., 2011a; McHenry, 1983; Tocheri et al., 2007). The metacarpals of *A. africanus* are generally gracile in their morphology, with the relative breadth of the first metacarpal resembling great apes and the relative length resembling humans (Green & Gordon, 2008; Kivell et al., 2020). Features of the wrist and the gracility of the metacarpals, including the thumb, suggest that *A. africanus* hands were not adapted to stress associated with manipulation to the same degree as seen in modern humans (Kivell et al., 2020). However, analysis of the internal trabecular structure of the pollical metacarpal reveals a pattern typically associated with forceful opposition of the thumb during manipulation (Skinner et al., 2015). These trabecular results are consistent with the estimated modern human-like hand proportions of *A. africanus* (Green & Gordon, 2008; Kivell et al., 2020; Ostrofsky & Richmond, 2015). The relatively longer thumb-to-finger ratio would have allowed *A. africanus* to perform precision grips similar to that of modern humans, which is reinforced by the trabecular structure (Skinner et al., 2015). The external morphology of the *A. africanus* phalanges further adds to its mosaic morphology. Both the proximal and intermediate phalanges are intermediately curved and robust, suggesting that *A. africanus* was using their hands for locomotory behaviours as well (Kivell et al., 2020). *A. africanus* manual remains suggest a species that was participating in arboreal locomotion but was capable of performing manipulative tasks, unique to *Australopithecus* and different from what we observe in *Homo* (Dunmore et al., 2020b; Green & Gordon, 2008; Kivell et al., 2020; Skinner et al., 2015).

Two proximal phalanges (StW 122 and StW 293) and an intermediate phalanx (StW 331) are included in the study sample, all of which display a moderate degree of curvature and strong FSRs. Their external morphology suggests that StW 293 and StW 331 are from ray three due to their overall symmetric appearance, and StW 122 from ray four or two because of its asymmetrical trochlea and FSRs. It is predicted that the *A. africanus* phalanges will be more similar to the great apes than to humans because despite being able to perform precision grips *A. africanus* is thought to be habitually taking part in arboreal behaviours as well. As such the higher loads associated with locomotion will be apparent in the cortex compared to the loads associated with manipulation.

5.2.3. *Australopithecus sediba*

Hand remains of *A. sediba* are represented by two individuals, Malapa Hominin 1 (MH1) and 2 (MH2), from Malapa, South Africa (1.977 mya) (Berger et al. 2010; Kivell et al., 2011, 2018; Pickering et al., 2011). The hand of MH1, a juvenile individual, only preserves a third metacarpal (missing its distal epiphysis), while MH2, a female adult, preserves a nearly complete right hand and a partial left hand (Churchill et al., 2013; Kivell et al., 2018a). The multiple hand bones of MH2 are associated with its complete right upper limb and provide us with a rare and holistic insight into the manual behaviours of this species (Churchill et al., 2018).

Along with a nearly complete hand skeleton, MH2 upper and lower limb bones are well preserved as well and give us insight into the locomotory capabilities of this Pleistocene hominin. The lower limb indicates *A. sediba* could walk bipedally, potentially with a hyper-pronated foot (DeSilva et al., 2013; Holliday et al., 2018; Kibii et al., 2011b; Prang, 2016; Zipfel et al., 2011), while the upper limb morphology is interpreted as being advantageous for arboreal behaviours (Churchill et al., 2013; 2018). Within the hand, the MH2 carpus displays a mix of ape-like and human-like features, with a unique lunate morphology that suggests a greater range of abduction when compared to other fossil hominins and modern humans (Kivell et al., 2018a). The internal structure of the capitate also indicates a distinct wrist movement and loading; the distribution and orientation of trabecular bone suggests modern human-like loading but through the employment of postures that are distinct from modern humans (Bird et al., 2023). The metacarpals of MH2 are gracile in external morphology and indicate poor force production by the thumb (Kivell et al., 2018a). However, internal structure of the pollex suggests human-like postures (Dunmore et al., 2020b). The MH2 intrinsic hand proportions are also distinct, with a remarkably long thumb that would have facilitated human-like precision grips and thumb opposition (Kivell et al., 2011; 2018). This gracile but modern human-like first metacarpal, however, is coupled with gracile ulnar metacarpals (MC2–5s) that exhibit internal bone structure that is most similar to *Pongo*, suggesting habitual use of flexed-finger power grasping (Dunmore et al., 2020b).

Evidence of strong grasping within the metacarpals is consistent with the external morphology of the phalanges. Both the proximal and intermediate phalanges are curved and have prominent FSRs. In particular, the intermediate phalanges are unique within the known hominin fossil record in having notably prominent FSRs while lacking a median bar and accompanying lateral fossae (Kivell et al., 2018a). While the external morphological features of the phalanges are consistent with the internal structure of the metacarpals (Dunmore et al., 2020b), aspects of the wrist (Bird et al., 2023) and upper limb external morphology (Kivell et al., 2018a) show

evidence for arboreal behaviours, with the internal structure of the morphologically-distinct phalanges yet to be studied.

Here, I analyse the cortical structure of the MH2 proximal phalanges of digits 2-5 and intermediate phalanges of digits 3-5. The intermediate phalanx of digit 2 was not studied because the shaft is fractured and it is encased in breccia. I hypothesize that the *A. sediba* phalanges will have cortical bone morphology that will reflect a locomotory use of the hand, similar to the great apes, due to their prominent external features that suggest the use of forceful finger flexion associated with arboreal behaviours.

5.2.4. *Homo habilis*

The hand of *H. habilis* is represented by a few elements of a juvenile individual, OH 7 (1.8 mya; Leakey et al., 1964). The hand skeletal remains include four intermediate phalanges missing their proximal epiphyses, interpreted as belonging to digits 2-5 of a right hand, along with two fragmentary proximal phalanges, three distal phalanges (including from the pollex), the proximal end of the second metacarpal, and three incomplete carpal bones (Leakey et al., 1964; Napier, 1962a; Susman and Creel, 1979). All these bones are considered to represent a single individual, together with the mandibular and cranial remains of OH 7 (Spoor et al., 2015). However, the specimens identified as the intermediate phalanges of digit 3 and digit 4 may be contralateral intermediate phalanges of the same digit of the same individual due to their extreme morphological similarities (Kivell, pers. comm.). There is also debate regarding the attribution of the OH 7 remain to the genus *Homo*. Moyà-Solà and colleagues (2008) highlighted similarities in the overall robust external morphology between the OH 7 phalanges and *Paranthropus* phalanges, which was further supported by Almécija and colleagues (2009) morphometric analysis on the distal phalanges (Almécija et al., 2009b). Regardless of their taxonomic attribution, morphology of the OH 7 hand has been discussed in detail in regard to its potential manipulative abilities due to the geographical and temporal association with Oldowan tools. Similar to other early hominin fossils, the OH 7 remains also show a mosaic of morphology. The distal phalanges have radioulnarly broad apical tufts and the trapezium has an extremely broad and flat articulation for the first metacarpal, suggesting manual dexterity for tool production and use (Susman & Creel, 1979; Trinkaus, 1989). However, this morphology is associated with robust, curved, African ape-like phalangeal morphology that is thought to reflect arboreal behaviours (Susman & Creel, 1979). Along with being curved and robust, the intermediate phalanges are unusually radioulnarly broad and have a well-developed median bar and lateral fosse, which are features that suggest powerful grasping abilities associated with climbing and arboreality (Susman, 1979; Susman & Stern, 1979; 1982). The fragmentary, curved proximal phalanges also have thick cortices (Susman & Stern, 1982). Although Susman and Creel (1979) radiographed the phalanges, a detailed study of internal morphology has not yet been conducted.

Due to poor preservation of the proximal phalanges, here I focus on the cortical structure of the intermediate phalanges and the distal half of proximal phalanx FLK-NN-I. The IPs lack their proximal epiphyses, but that did not affect the cortical bone analyses as I focused on the phalangeal shaft, which is well preserved in all the IPs. Due to the overall robusticity and curvature of the OH 7 phalanges, and previous reconstructions of a relatively long upper limb to lower limb ratio of *H. habilis* (Haeusler & McHenry, 2004; Ruff, 2009), I predict that OH 7 cortical bone morphology will reflect manual postures employed during locomotion. The lack of directly

associated stone tools with the OH 7 hand remains (Leakey, 1971) further supports this prediction, although a detailed examination is needed to determine the function of these hand bones and test the manual capabilities of the OH 7 hand.

5.2.5. Swartkrans (*Paranthropus robustus*/early *Homo*) phalanges

Paranthropus robustus is well represented by its craniodental remains (Wood & Constantino, 2007; Wood & Schroer, 2013) but there are limited postcranial remains confidently attributed to this taxon. Therefore, our current understanding of *P. robustus* manipulative abilities is limited. Excavations at Swartkrans, South Africa have yielded postcranial material, including several hand fossils. However, both *P. robustus* and early *Homo* are found throughout the geological layers at Swartkrans, and thus taxonomic attribution of these fossils is not known (Susman, 1988a; 1991; Susman et al., 2001; Trinkaus & Long, 1991). The external morphology of the manual remains is well described (Susman, 1988a; 1989; Susman et al., 2001), but only a triquetrum and two first metacarpals have been analysed in relation to a comparative sample. SKX 3948 is a triquetrum that was initially described as human-like in its shape and facet morphology, but Kivell (2011) emphasized its general similarities to African apes and humans, being closest to Neanderthals (Susman, 1988a; 1989; Kivell, 2011). Specimens SK 84 and SKX 5020 differ in their size but are robust and have well-developed entheses, with SK84 having internal structure similar to that of great apes despite its robust external morphology (Dunmore et al., 2020b; Susman, 1988a; 1991; Trinkaus & Long, 1991).

Here, I study three proximal phalanges from Swartkrans: SKX 27431, SKX 5018, and SKX 15468. SKX 27431 is a proximal phalanx from Member 3 with ape-like curvature and external morphology that is more similar to humans than great apes, as such it has been argued to be a *Homo* specimen rather than *P. robustus* (Susman, 1988a). SKX 5018 and SKX 15468 are proximal phalanges from the lower bank of Member 1. Both SKX 15468 and SKX 5018 display robust external morphology (e.g. well-developed FSRs) but with human-like curvature (Susman et al., 2001). This combination of morphology has been used to argue for its inclusion in *P. robustus* (Susman, 1988a; Susman et al., 1991) and to infer precision grasping and manipulative abilities of *P. robustus* (Susman, 1988b). However, these specimens also show thick cortex, which has been recognised as unusual in combination with human-like features (Susman, 1988a; Susman & Creel, 1979). Along with the uncertainty around the taxonomic attribution of the Swartkrans manual remains, there is debate regarding the manual abilities of the Swartkrans hominins (Marzke, 1997; Marzke et al., 1992; Susman, 1988b). Thus, I study the cortical structure of all three phalanges, with the SKX 27431 phalanx showing a different external morphology from that of the SKX 5018 and SKX 15468 phalanges. I predict the cortical structure of the SKX 5018 and SKX 15468 will resemble a more human-like pattern in relation to the great apes. due to the lower degree of phalangeal curvature, while the SKX 27431 phalanx will display a pattern distinct from the other phalanges.

5.2.6. *Homo naledi*

Skeletal remains of *H. naledi* come from the fossiliferous Rising Star cave system in South Africa (~300 thousand years ago (kya) (Dirks et al., 2017)). A minimum of 15 individuals have been discovered so far within the Dinaledi Chamber, including numerous hand bones from juvenile and adult individuals (Berger et al., 2015; Kivell et al., 2015). Within these skeletal hand

remains, Hand 1 is a right, nearly complete hand from an adult individual, missing only its pisiform (Berger et al., 2015; Kivell et al., 2015). Similar to the few other relatively complete fossil hominin hand skeletons, particularly *A. sediba* (Kivell et al., 2018a) but also StW 573 (Clarke, 1999), Hand 1 depicts a unique mix of primitive and derived traits within the carpus, metacarpus, and phalanges (Kivell et al., 2015).

External morphology of the radial wrist exhibits features found only in *H. sapiens* and Neandertals that are typically associated with the habitual production and use of tools (Kivell et al., 2015). However, the internal structure of the Hand 1 scaphoid and capitate suggest that *H. naledi* would not be able to resist the high loads on the radial carpus that are associated with human-like manipulation (Bird et al., 2023). If *H. naledi* was using and producing tools, it likely was doing so in a manner different from that of modern humans (Bird et al., 2023). Furthermore, the internal structure of the wrist and the trapeziometacarpal joint morphology are at odds with the external morphology of the thumb and palm. The morphology of the first metacarpal, pollical phalanges, and overall hand proportions suggests *H. naledi* would have been capable of using forceful human-like grips, but that would result in high forces at the relatively small trapeziometacarpal joint (Kivell et al., 2015). The *H. naledi* first metacarpals exhibit a unique medial longitudinal crest, narrow base and a broad flange, which has been interpreted as a transitional state between the gracility associated with early hominins participating in arboreal behaviours and later hominins that are considered advantageous for manipulation (Bowland et al., 2021; Kivell et al., 2015).

Hand 1 phalangeal morphology further adds to this puzzling mix of *H. naledi* manual features. The proximal and intermediate phalanges of Hand 1 are highly curved, with the intermediate phalanges displaying the greatest degree of curvature across all known fossil hominin IPs (Kivell et al., 2015). Strong curvature and prominent FSRs of the intermediate phalanges coupled with the morphology of the upper limb suggests that *H. naledi* may have been using its hands in a flexed-finger grasping posture during locomotion (Feuerriegel et al., 2017; Kivell et al., 2015). However, the locomotory grasping of *H. naledi* most likely was unique from other hominins, fossil and extant, as evidenced by the mix of carpal and metacarpal morphology, and lack of prominent FSRs on the proximal phalanges. Furthermore, if the curvature of *H. naledi* phalanges suggests its ability to engage in arboreal behaviours due to its biomechanical function of reducing strain experienced by the phalanx, FSRs should be considered as well since they hold the same biomechanical function (Richmond, 2007; Nguyen et al., 2014). As such, it is unusual that the intermediate phalanges display prominent FSRs, while the proximal phalanges do not. Typically, in locomotory grasping among apes, all joints of the fingers are flexed, which would cause strain on the phalanx which the FSRs help reduce, so it is peculiar that only the intermediate phalanges show the development of FSRs. This unusual morphology may be an indication that *H. naledi* is employing unique postures that are loading the intermediate phalanges more or in a different manner than that of the proximal phalanges. However, the internal structure of the phalanges has yet to be explored, as such I analyse the cortical bone morphology of Hand 1 phalanges and predict that the cortical bone morphology of *H. naledi* phalanges will be intermediate between the cortical bone patterns and properties observed in extant humans versus great apes.

5.2.7. *Homo floresiensis*

H. floresiensis was first primarily represented by LB1 (100 – 60 kya; Sutikna et al., 2016), a nearly complete skeleton with well-preserved upper and lower limb remains. The upper limb displays shoulder morphology that is unique compared to humans, lacking adaptations for stone tool production, which is considered to represent a transitional stage in hominin shoulder evolution (Larson et al., 2007; 2009), while the mosaic morphology of the lower limbs suggest *H. floresiensis* bipedalism would have differed from that of humans (Holliday & Franciscus, 2009; Jungers et al., 2009a; b). Within the upper limb, the carpals and phalanges are well represented while only a few fragmentary metacarpals have been recovered (Larson et al., 2009; Tocheri et al., 2007). Morphology of the wrist bones suggest an ape-like carpus that does not possess derived features associated with the modern human wrist (Orr et al. 2013; Tocheri et al., 2007). However, the remains of *H. floresiensis* are found alongside Oldowan stone tools (Brumm et al., 2006; Moore & Brumm, 2007) which provides evidence for some capacity of tool-using behaviours (Kivell et al., 2022). Analysis of the internal structure of the *H. floresiensis* carpus provides evidence for this behavioural interpretation (Bird et al., 2023). The internal structure of the capitate suggests loading of the ulnar side of the wrist, indicating the use of transverse grips that are commonly used when making Oldowan tools (Bird et al., 2023; Key et al., 2018; 2019; Orr et al., 2013; Williams-Hatala et al., 2018; 2021). The ulnar loading of the midcarpal joint is also consistent with climbing. Therefore, Bird and colleagues (2023) suggested that the production of tools using transverse grips may reflect a balance or trade-off in using hands for locomotion and manipulation. These functional interpretations of the manual behaviours of *H. floresiensis* are consistent with the phalangeal morphology, which is described as having a moderate, *A. afarensis*-like degree of curvature, with some specimens possessing strong flexor sheath ridges, and a modern human-like distal pollical phalanx (Larson et al., 2009).

To confirm these functional interpretations, I analyse the cortical structure of *H. floresiensis* proximal and intermediate phalanges from multiple individuals: LB1, LB6, LB-XXI-44-2010, and LB-XV-42-2008. LB1 is represented by three intermediate phalanges, the morphology of which suggests LB1-40 and LB1-42 are from the second or fourth ray, while LB1-48 comes from the third ray. LB6 is represented by two intermediate phalanges and one proximal phalanx, all of which potentially come from rays two or four. LB-XXI-44-2010 and LB-XV-42-2008 are two juvenile phalanges, proximal and intermediate, respectively. While *H. floresiensis* phalanges have been described as having prominent palmar features (Larson et al., 2009), the proximal (and intermediate) phalanges included in the current study do not possess well-developed FSRs but instead are unusually circular cross-section that creates a convex palmar surface. Thus, I hypothesize cortical bone properties and patterns will be more similar to humans than the great apes, but, as observed in the carpus, cortical bone morphology will be distinct from modern humans.

5.2.8. *Homo neanderthalensis*

H. neanderthalensis remains are well represented in the fossil hominin record, which has caused continued debate regarding the distinctiveness of their morphology and behaviour compared to *H. sapiens* (Benazzi et al., 2011; Froehle et al., 2013; Hublin, 2009; Klein, 2000; McBrearty & Brooks, 2000; Pearson et al., 2006; Trinkaus et al., 1991; Weaver, 2009). Many of

these debates centre around the cognitive and manipulative capabilities in relation to varying tool industries, novel tool production, and the production of cave art (Bardo et al., 2020; Churchill, 2001; Delpiano et al., 2019; Dunmore et al., 2023; Leder et al., 2021; Milks et al., 2019; Niewoehner, 2001; 2006; Patino et al., 2017; Schmitt et al., 2003; Williams-Hatala, 2016). The Neanderthal hand has been hypothesized to be capable of modern human-like dextrous manipulation due to the overall similarity with the modern human hand, but Neanderthal hands are also characterised by several distinctive features (Churchill, 2001; Marzke & Shackey, 1986; Musgrave, 1971; 1973; Niewoehner, 2001; 2006). These features include: large projecting tubercles on carpal bones, a dorsopalmarly flat first trapeziometacarpal joint, a parasagittally-oriented capitate-second metacarpal facet, reduced styloid process of the third metacarpal, radioulnarly flat fifth metacarpal base, shorter proximal phalanges when compared to humans that result in differing hand ratios, expanded tuberosities on the distal phalanges, and overall rugose and expanded muscle and tendon attachment sites (Kivell et al., 2018b; Marzke, 1992; Marzke & Marzke, 2000; Niewoehner, 2001; 2005; 2006; Tocheri et al., 2008; Trinkaus 2016; Trinkaus & Villedieu, 1991). These differences in hand morphology have been interpreted as adaptations for greater force production and the transmission of larger loads across the fingertips, indicating the effective use and production of power grips (Niewoehner, 2006; Niewoehner et al., 2003; Trinkaus & Villedieu, 1991).

Within the phalanges, the dorsopalmar and radioulnar expansion of the trochlea and base along with well-developed FSRs of the proximal and intermediate phalanges provide increased flexion and load displacement at the PIP and DIP joints. Furthermore, within the pollex, the proximal phalanx is proportionally shorter than the distal phalanx, which provides enhanced mechanical advantage at the thumb (Stephens, 2018). The hypertrophied muscles coupled with increased mechanical advantage may indicate habitual transmission of higher forces through the manual joints and greater grip strength in Neanderthals (Niewoehner, 2006). It has been suggested that Neanderthals may have been habitually employing transverse power grip postures, in which the ulnar side of the hand is engaged in force production and the thumb is used to support and control the object (Niewoehner, 2006). Stephens (2018) tested this hypothesis through an exploration of trabecular bone parameters across the human and Neanderthal hand. Results suggested differences in habitual grip types used between humans and Neanderthals, with the Neanderthal hand showing evidence of tool use using a transverse power grip (Stephens, 2018). Furthermore, Stephens (2018) also suggested that the flat Neanderthal trapeziometacarpal joint would be less stable than the modern human thumb. This flat morphology of the trapeziometacarpal joint complex was studied through a morphometric analysis by Bardo and colleagues (2020), which revealed the morphology of the trapezium-carpometacarpal joint orientation favours a thumb that is extended and adducted during opposition. This thumb posture is most consistent with the use of transverse power squeeze grips, which imply the use of hafted tools (Bardo et al., 2020; Niewoehner, 2006). The use of habitual transverse power grips by Neanderthals was contested by Karakostis and colleagues (2018), who suggested that muscle attachment sites within the Neanderthal hand are most similar to recent humans, indicating the habitual use of precision grips rather than power grips.

The potential habitual hand grips employed by Neanderthals have been further explored through the internal structure of the metacarpals and wrist bones. Dunmore and colleagues (2020) studied the internal structure of Neanderthal metacarpals, suggesting Neanderthals

habitually used less flexed-finger postures and a more adducted thumb than *H. sapiens*. These hand postures are consistent with power squeeze grips, used to grasp hafted tools, and/or precision grips used to secure non-hafted tools (such as scrapers) (Niewoehner, 2006). Investigation into midcarpal joint loading provides further support for the potential ability of Neanderthals to employ transverse power grips, power squeeze grips, and precision grips (Bird et al., 2023). These studies have established the dexterous ability of Neanderthals, but debates regarding the difference in manipulative abilities of Neanderthals in relation to their technological complexes continues. This debate is furthered by morphological differences between the northern and southern Neanderthals (Rosas et al., 2006), which are evident within the internal structure of the hand (Kivell et al., 2018b; Dunmore et al., 2020b).

While the palm and wrist internal morphology of Neanderthals has been studied, the phalanges remain relatively understudied, with only Stephens (2018) studying the trabecular structure in some Neanderthal individuals. As such, here I study the proximal and intermediate phalanges of different populations of Neanderthals to gain a broad perspective on Neanderthal manual behaviours. The populations/individuals studied here represent Neanderthals from the Near East (Tabun C1 and Kebara 2), southern Europe (El Sidron and La Ferrassie 2), and a Northern European Neanderthal (Feldhofer 1). It is predicted that the cortical bone morphology of the Neanderthals will be similar to modern humans, but due to the morphological variability of the sample studied we predict high variation across the Neanderthal individuals.

5.2.9. Aims and predictions

As bone (re-)models throughout life, internal bone structure can help us resolve the debate regarding whether the external morphological features observed are actually functionally relevant, reflecting the habitual behaviours of fossil individuals. As reviewed earlier, internal bone structure studies have been conducted on the wrist and metacarpals of the fossils discussed, but studies on the phalanges are lacking. Recent work on the internal structure of extant hominid non-pollical proximal and intermediate phalanges has shown a thick concentration of cortical bone on the palmar phalangeal surface in non-human great apes that is associated with flexed-finger postures during the locomotory use of the hand, and a dorsal concentration of cortical bone in humans is associated with their manipulatory abilities (Chapters 3 and 4; Syeda et al., 2023; 2024). Using this comparative context, we aim to infer habitual manual behaviours in phalangeal remains of the fossils hominins discussed throughout the introduction. Overall, I predict all fossil hominins will display a unique pattern that will not be similar to each other. Predictions based on our knowledge of the external hand morphology of these fossil hominins, previous work addressing the functional morphology of the wrist and metacarpals of these hominins, and our knowledge on the cortical structure of extant great ape phalanges are laid out within each previous section and summarised in Table 5.1.

Table 5.1: Predictions of phalangeal cortical bone morphology of the fossil hominins studied in this chapter.

Species	Predictions
<i>A. afarensis</i>	Will display a primarily locomotor use of the hand, resembling a great ape-like pattern
<i>A. africanus</i>	Will display a primarily locomotor use of the hand, resembling a great ape-like pattern
<i>A. sediba</i>	Will display a primarily locomotor use of the hand, resembling a great ape-like pattern
<i>H. habilis</i>	Will display a primarily locomotor use of the hand, resembling a great ape-like pattern
Swartkrans hominins	SKX5018 and SKX15468 = will resemble modern humans SKX 27431 = will be distinct from the other two Swartkrans phalanges and extant taxa
<i>H. naledi</i>	Will display a pattern intermediate between modern humans and great apes, suggesting a hand uniquely used for locomotion and manipulation
<i>H. floresiensis</i>	Will display a pattern that is more modern human-like than great ape-like, but still distinct from modern humans, suggesting unique manual behaviours not observed in extant taxa
<i>H. neanderthalensis</i>	Will display a modern human-like pattern suggesting a primarily manipulatory use of the hand. Greater variation across the Neanderthal populations, compared to humans, is also predicted.

5.3. Methods

5.3.1. Materials

The fossil sample studied in this chapter comprised of phalangeal specimens attributed to *A. afarensis*, *A. africanus*, *A. sediba*, *H. habilis*, *P. robustus*/Early *Homo*, *H. naledi*, *H. floresiensis* and *H. neanderthalensis*. The *A. afarensis* sample consisted of one proximal phalanx and the *A. africanus* sample consisted of two proximal phalanges and an intermediate phalanx, likely belonging to different individuals. *A. sediba* is represented by all eight non-pollical proximal and intermediate phalanges, except the second intermediate phalanx of the right MH2 hand. The *H. habilis* OH 7 hand is represented by one fragmentary proximal phalanx and all four intermediate phalanges. Phalanges from Swartkrans attributed to *P. robustus*/Early *Homo* consist of three proximal phalanges. The *H. naledi* sample consists of all eight non-pollical proximal and intermediate phalanges of Hand1. *H. floresiensis* phalanges include six adult, one proximal and five intermediate, and two juvenile phalanges, one proximal and one intermediate, from several individuals. The Neanderthal sample consists of several different Neanderthal populations from variable geographic locations. Within the Neanderthal populations, all phalanges belong to the

right/left hand of the same individual, with the exception of the El Sidron Neanderthals, which are represented by multiple individuals. The lack of associated remains of *A. afarensis*, *A. africanus*, the Swartkrans specimens and the El Sidron Neanderthals makes it challenging to accurately assign digit number to the individual phalanges. The fossil sample is detailed in **Table 5.2**. The extant comparative sample used in this study consists of non-pollical proximal and intermediate phalanges from 92 great ape and human individuals (*Pongo* = 9, *Gorilla* = 25, *Pan* = 24, and *Homo* = 33). This extant sample is the same data set as in Chapters 3 and 4 (Syeda et al., 2023; 2024).

Table 5.2: Fossil specimens included in the study.

Species	Specimen	Side	Elements	Age
<i>Australopithecus afarensis</i>	AL 333-19	?	PP	Adult
<i>Australopithecus africanus</i>	StW 122	?	PP	Adult
	StW 293	?	PP	Adult
	StW 331	?	IP	Adult
<i>Australopithecus sediba</i>	MH2	R	PP2-5; IP3-5	Adult
<i>Homo habilis</i>	OH 7	R	PP fragment; IP2-5	Juvenile
<i>Homo naledi</i>	Hand 1	R	PP2-5 and IP2-5	Adult
Swartkrans	SKX 5018	?	PP	Adult
	SKX 15468	?	PP	Adult
	SKX 27431	?	PP	Adult
<i>Homo floresiensis</i>	LB1	?	3 IPs	Adult
	LB6	?	PP; 2 IPs	Adult
	LB-XV-42-2008	?	IP	Juvenile
	LB-XXI-44-2010	?	PP	Juvenile
Neanderthals	Tabun C1	L	IP2; IP4	Adult
	Kebara 2	R	PP2;PP5; IP2-IP4	Adult
		L	PP2-3; IP2; IP4	Adult
	El Sidron	R&L	12 PPs; 10 IPs	Adult
	La Ferrassie 2	L	PP3; PP5; IP5	Adult
		R	PP2-3;PP5; IP2-5	Adult
	Feldhofer 1	R	PP5; IP2	Adult

Abbreviations: PP = proximal phalanges; IP = intermediate phalanges; R = right; L = left.

5.3.2. Micro-computed tomography and image segmentation

The cortical bone structure of the phalanges was explored using high-resolution micro-computed tomography (micro-CT) scans. Extant and fossil specimens were scanned using a BIR

ACTIS 225/300, Diondo D3 or Skyscan 1172 scanner housed at the Department of Human Evolution, Max Planck Institute for Evolutionary Anthropology (Leipzig, Germany), a Nikon 225/XTH scanner at the Cambridge Biotomography Centre, University of Cambridge (Cambridge, UK), or with the Diondo D1 scanner at the Imaging Centre for Life Sciences University of Kent (Canterbury, UK). The scan parameters included acceleration voltages of 100–160 kV and 100–140 μ A using a 0.2 to 0.5 mm copper or brass filter. Scan resolution ranged between 0.018 mm to 0.044 mm depending on the size of the bone. Images were reconstructed as 16-bit TIFF stacks. All scans were cleaned (i.e., the removal of soft tissue or other non-bone material) and reoriented into a standard anatomical position using Avizo Lite 9.0.0 (Visualization Sciences Group, SAS). These scans were then segmented using medical image analysis (MIA) (Dunmore et al., 2018).

Segmentation of the micro-CT scans depends on the greyscale values of materials within the scans, segmentation is a challenging task when scans have multiple materials with differing density/voxel values, which was the case for the fossil specimens studied here. Preservation in each fossil specimen was different due to differing taphonomic conditions. As such, unlike the extant sample that was only segmented through the MIA method, the fossil specimens were initially segmented within MIA and then followed by image filters and manual cleaning within Avizo 6.3 (see Chapter 2 for details and an example segmentation).

5.3.3. Cortical bone analysis

The methods for cortical bone analysis applied in this study are the same as detailed in Chapters 3 and 4 (Syeda et al., 2023; 2024), as such we briefly outline the methods below. The cortical bone structure and cross-sectional properties were studied using 3D digital external and internal surfaces of the phalanges in R package Morphomap (Profico et al., 2021). Medtool v 4.5 (www.drpahr.at/medtool/; Tsegai et al., 2013; Gross et al., 2014) was used on the segmented micro-CT data to outline the outer and inner layer of cortex. Within Medtool, the outer and inner border of the cortex is identified through the 3D casting of rays and use of morphological filters, which create masks of the outer and internal area of cortical bone. These masks are then input into Paraview v 4.4 and Meshlab v 2020.03 to create smooth external and internal surfaces. As I am only interested in analysing cortical bone of the phalangeal shaft, we extracted the defined phalangeal shaft (Syeda et al., 2023; 2024) from the external and internal surfaces. These defined surfaces were then input into R package Morphomap for cortical bone analysis. Within Morphomap, 97 cross-sections, in 1% increments, were extracted between 2% and 98% of the phalangeal shaft and 50 equiangular semi-landmarks were placed on each cross-section to capture the shape of the shaft. The number of cross-sections and semi-landmarks placed on the specimens in this study is the same as previously published data to ensure the fossil data is comparable to our extant sample. At each cross-section, rays are sent outward from the centroid towards the pair of equiangular semi-landmarks and cortical thickness is calculated as the length of the ray between the landmark on the external and internal surface. The cortical bone thickness data was used to create morphometric maps representing the cortical bone distribution patterns of each individual phalanx. Morphomap also quantified the strength and rigidity of the fossil phalangeal shafts through cross-sectional geometric properties. We analysed the cortical area, which is a measure of compressive and tensile strength, and the polar section modulus, which is a measure of maximum bending strength, and a measure of bending and torsional rigidity at three different cross-sections (35%, 50% and 65%) across the phalanx.

5.3.4. Statistical analysis

In order to reduce our large data set for statistical analysis, we performed principal components analysis (PCA) on the cortical bone thickness values of the phalangeal shaft using the 'prcomp' function in the Stats (R Core Team 2021) package in R. As analyses on the extant sample have been conducted (see Chapters 3 and 4 for details), we only conducted tests on fossil specimens to determine if they were significantly different from the extant comparative sample. Permutational Hotelling one sample T-squared tests were conducted on the fossil sampled to provide statistical power to the results visualized in the PCA. The permutational hotelling one sample T-squared tests were conducted using R package ICSNP (Nordhausen et al., 2023).

5.4. Results

5.4.1. *Australopithecus afarensis*

The AL 333-19 *A. afarensis* proximal phalanx cortical bone distribution pattern reveals a generally low to intermediately thick cortex (Fig. 5.1A). The flexor sheath ridges and dorsal surface of the shaft show increased thickness relative to the palmar shaft, with the thickest region of the shaft being on the right (when viewed palmarly) FSR. Maximum thickness on the right FSR is just proximal to the trochlea and on the peak of the FSR. This pattern of cortical bone distribution is most similar to the pattern observed in *Pan* proximal phalanges, although the FSRs in AL 333-19 are not as thick as the typical FSRs in *Pan*. This observation is further supported by the *A. afarensis* AL 333-19 phalanx plotting close to the *Pan* distribution in the PCA (Fig. 5.2).

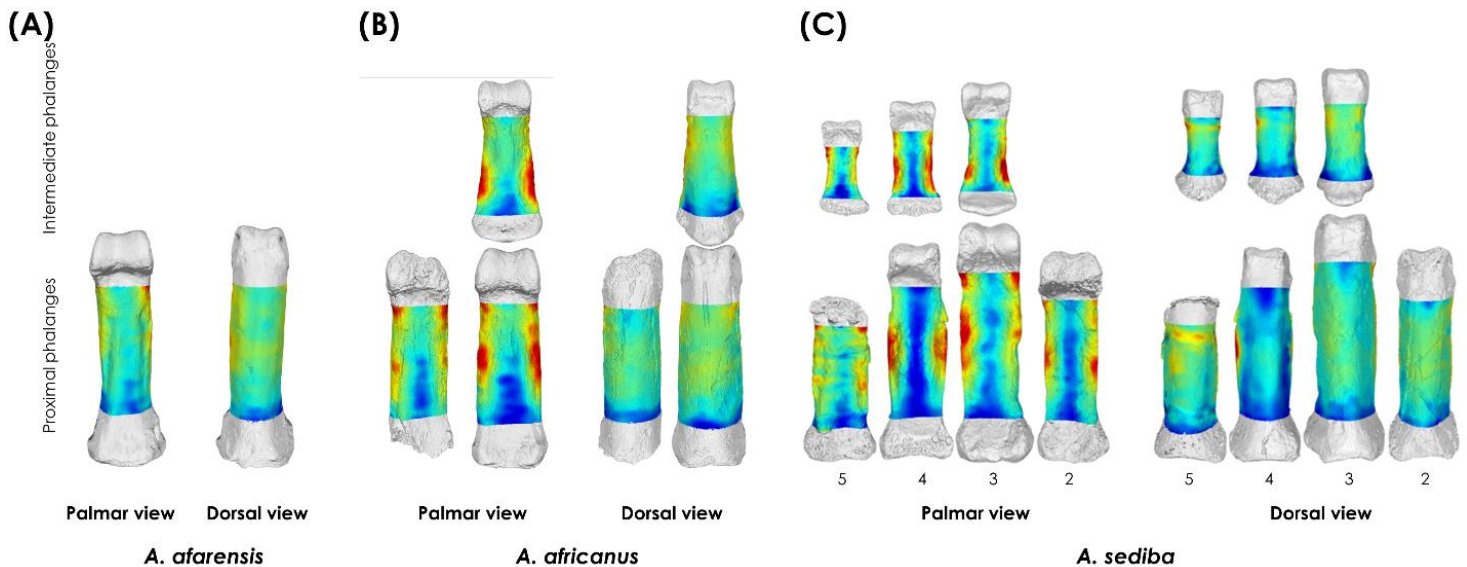


Figure 5.1: Cortical bone distribution maps of (A) *Australopithecus afarensis* (AL 333-19), (B) *Australopithecus africanus* (Proximal phalanges from left to right: StW 122, StW 293; Intermediate phalanx: StW 331), (C) *Australopithecus sediba* (MH2). The maps display the palmar and dorsal surface of the phalanges, with the digits listed under the phalanx.

Cortical thickness values across the shaft are also most similar to great apes. Cortical thickness increases proximodistally, peaking around the midshaft, slightly decreasing distal to

that, and then increasing again. This pattern is most similar to *Pongo* (Fig. 5.3A). Scaled mean cortical thickness of the *A. afarensis* proximal phalanx falls within the upper end of the African ape range (Fig. 5.4A).

Cross-sectional properties of the AL 333-19 phalanx show a proximodistal increase in cortical area (CA), while values of Z_{pol} and J are greatest proximally, showing similarities with the cross-sectional property patterns observed in great apes (Figs. 5.5A–5.7A). This falls in line with the measured dorsopalmar curvature of the phalanx as well, which falls in the upper end of *Pan* (Fig. 5.8A).

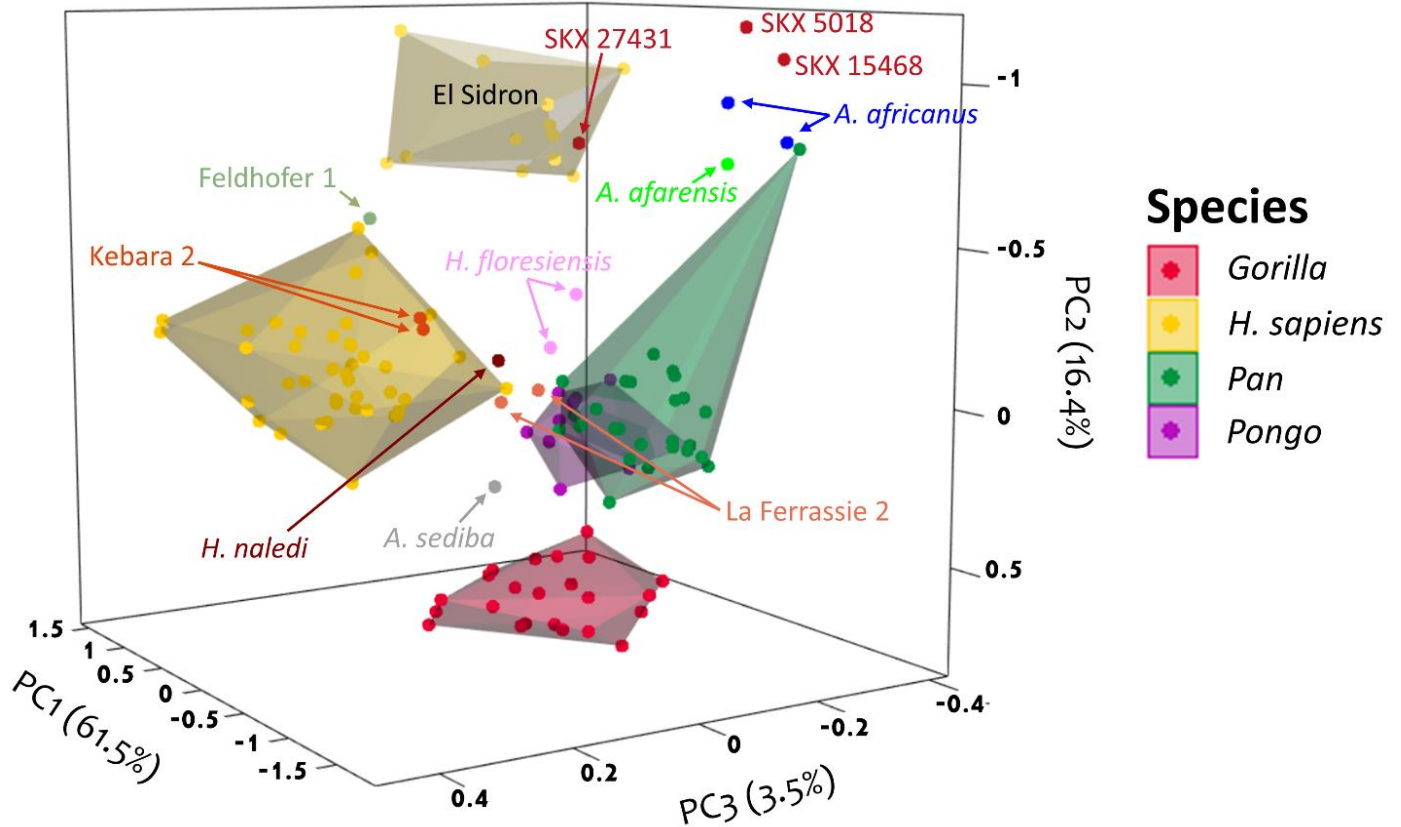
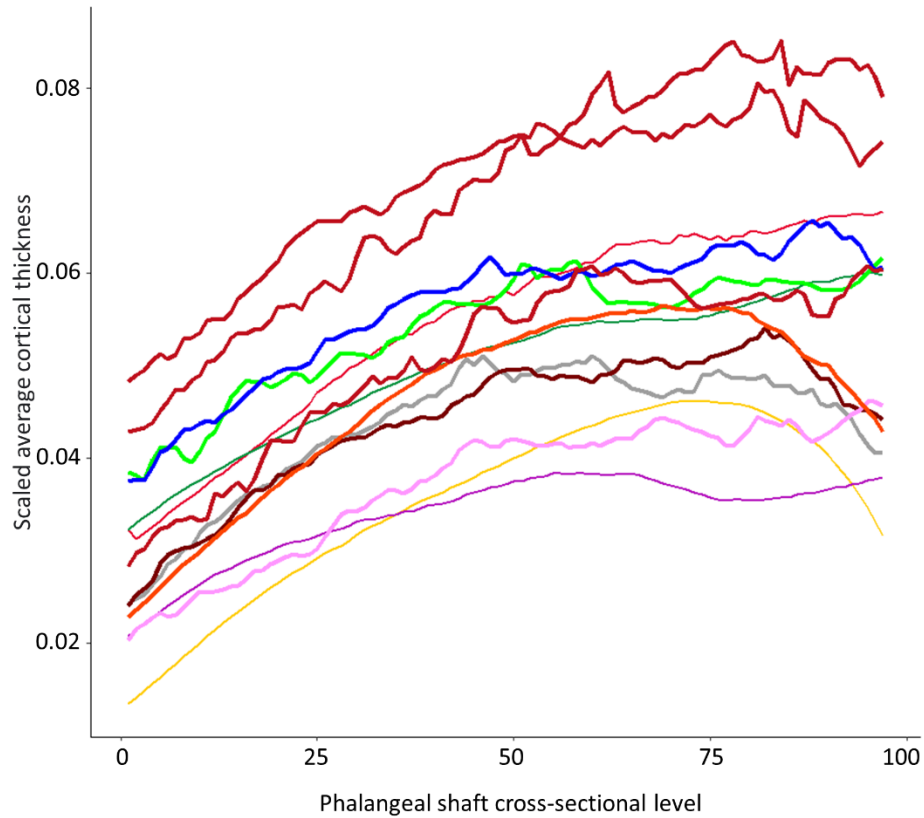


Figure 5.2: Results of the principal component analysis (PCA) of the proximal phalanges in 3D, showing separation among the extant taxa and fossil hominins. Associated phalanges are pooled together. Labels of the extant taxa are depicted in the legend. Fossil hominins are labelled individually.

(A) Proximal phalangeal cortical thickness across shaft



(B) Intermediate phalangeal cortical thickness across shaft

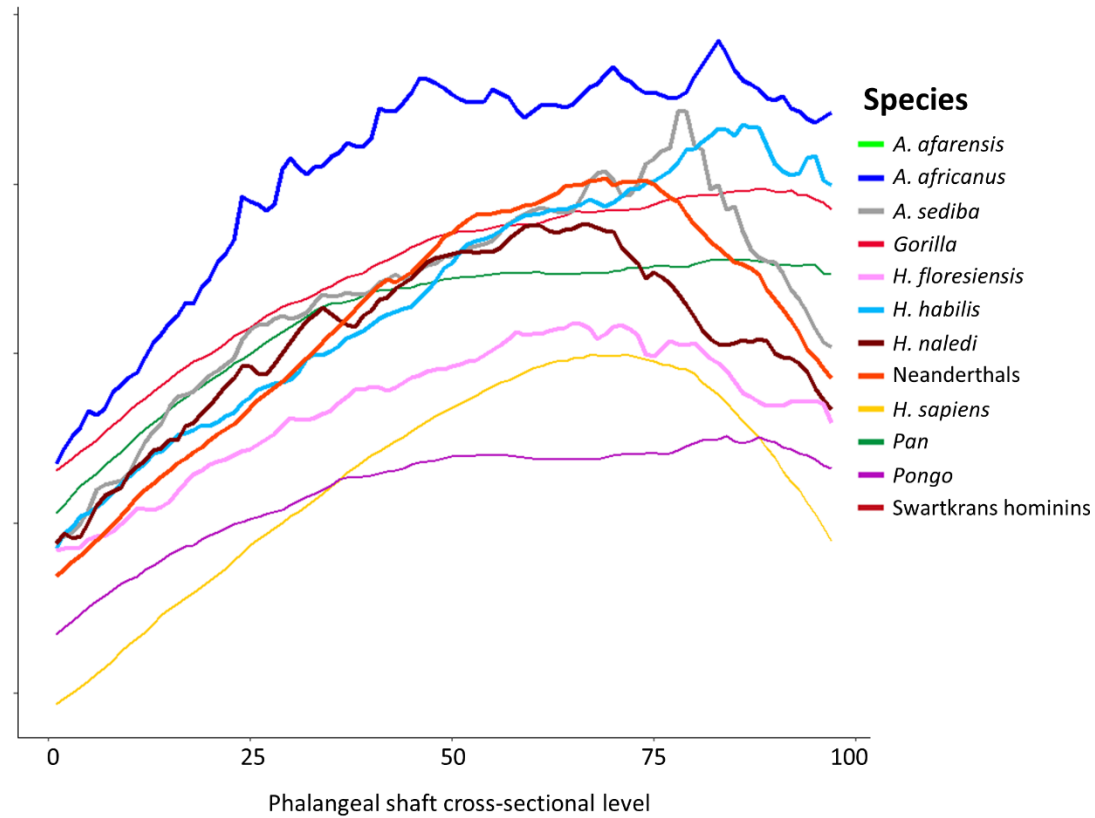


Figure 5.3: Cortical thickness plotted across the phalanges shaft of the (A) proximal phalanges and (B) intermediate phalanges in extant great apes and fossil hominins.

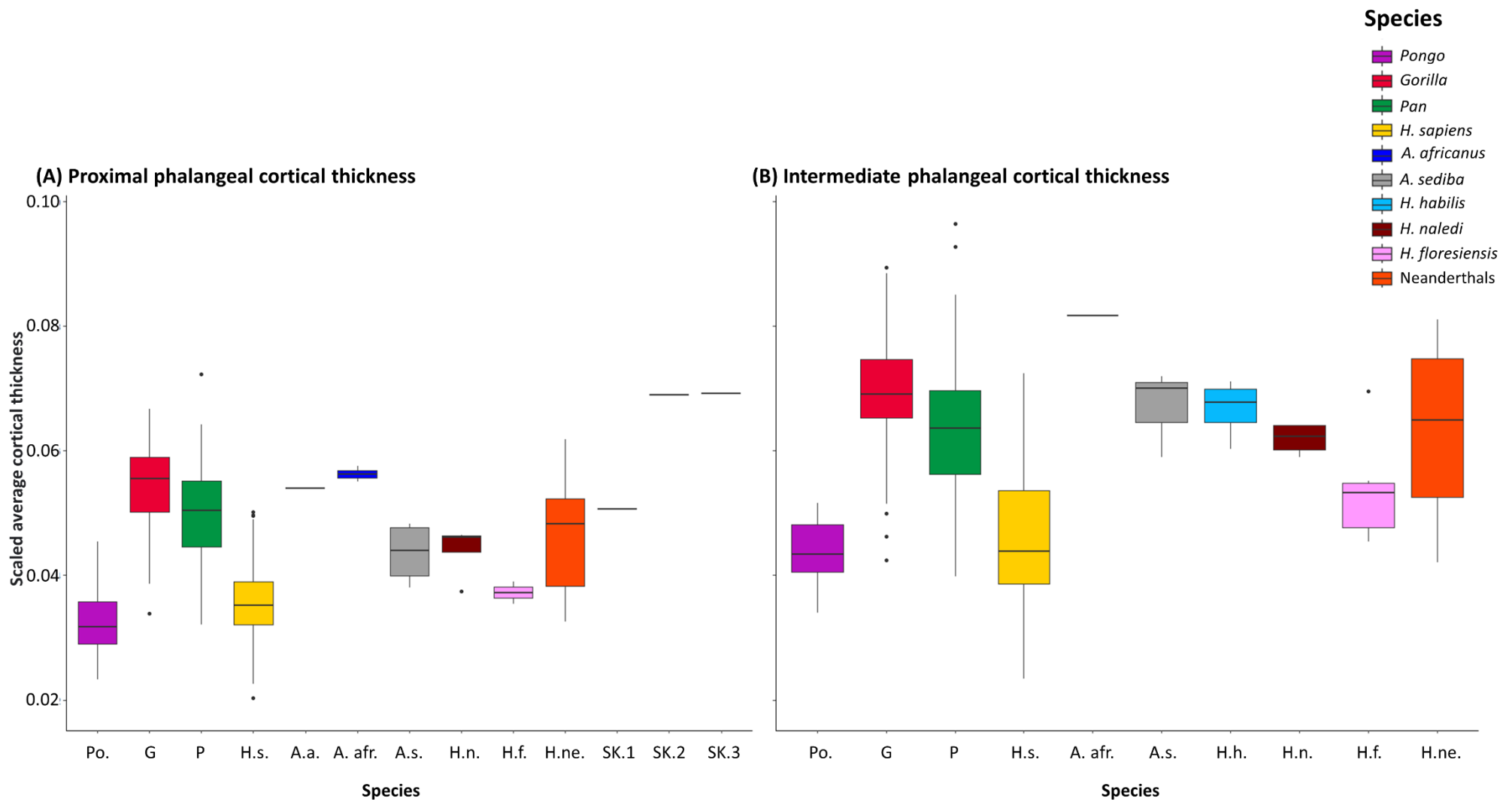


Figure 5.4: Boxplots representing the scaled average cortical thickness of the (A) proximal phalanges and (B) intermediate phalanges in extant great apes and fossil hominins. Species names are abbreviated: Po. = *Pongo*; G = *Gorilla*; P = *Pan*; H.s. = *H. sapiens*; A.a. = *A. afarensis*; A.afr. = *A. africanus*; A.s. = *A. sediba*; H.h. = *H. habilis*; H.n. = *H. naledi*; H.f. = *H. floresiensis*; H.ne. = Neanderthals; SK.1 = SKX 27431; SK.2 = SKX 15468; SK.3 = SKX 5018.

5.4.2. *Australopithecus africanus*

The cortical bone distribution pattern of the *A. africanus* phalanges reveals that cortical bone is thickest on the FSRs, with the dorsal shaft of the PPs and the distal half of the IP shaft intermediately thick (**Fig. 5.1B**). Furthermore, the PPs differ from the IPs in that the thickest cortex of the PPs is on the peaks of the FSRs and proximal to the trochlea, while in the IP maximum thickness is along the entirety of the FSRs. The pattern observed in the PPs and the IP is most similar to what has been observed in great apes. In the PCAs, the proximal phalanx StW 122 plots close to the *Pan* distribution, with StW 293 plotting slightly further away, while the intermediate phalanx StW 331 occupies its own morphospace (**Fig. 5.2, Fig. 5.9**).

Similarity to the great apes is also reflected in the pattern of cortical thickness values across the shaft and mean cortical thickness of the phalanges. Cortical thickness values of the PPs and the IP increase proximodistally and plateau proximal to the midshaft, which is most similar to the pattern observed in the African apes (**Fig. 5.3**). Average cortical thickness of the PPs and the IP fall within the upper end of the African ape range of variation (**Fig. 5.4**).

Calculating cross-sectional properties at three sections along the shaft of the PPs and the IP reveals that CA is greatest distally and lowest at 50% of the shaft in the PPs, but increases proximodistally in the IPs. Both, Z_{pol} and J, increase proximodistally in the PPs and the IP (**Figs. 5.5-5.5.7**). Comparing the values of CSG properties of the PPs and the IP reveals a pattern unique from what has been observed in the extant sample. Relative values of all CSG properties of the IP are greater than the CSG values of the PPs across all cross-sections, except for at 50% of the shaft. At 50% of the shaft, values of Z_{pol} and J are greater in the PPs relative to the IP.

Evaluating the phalangeal curvature of the phalanges reveals curvature of the PPs is within the range of *Pan* and the upper end of the *Gorilla* range of variation, while IP curvature is in the range of *Gorilla* and upper end of the human range (**Fig. 5.8**).

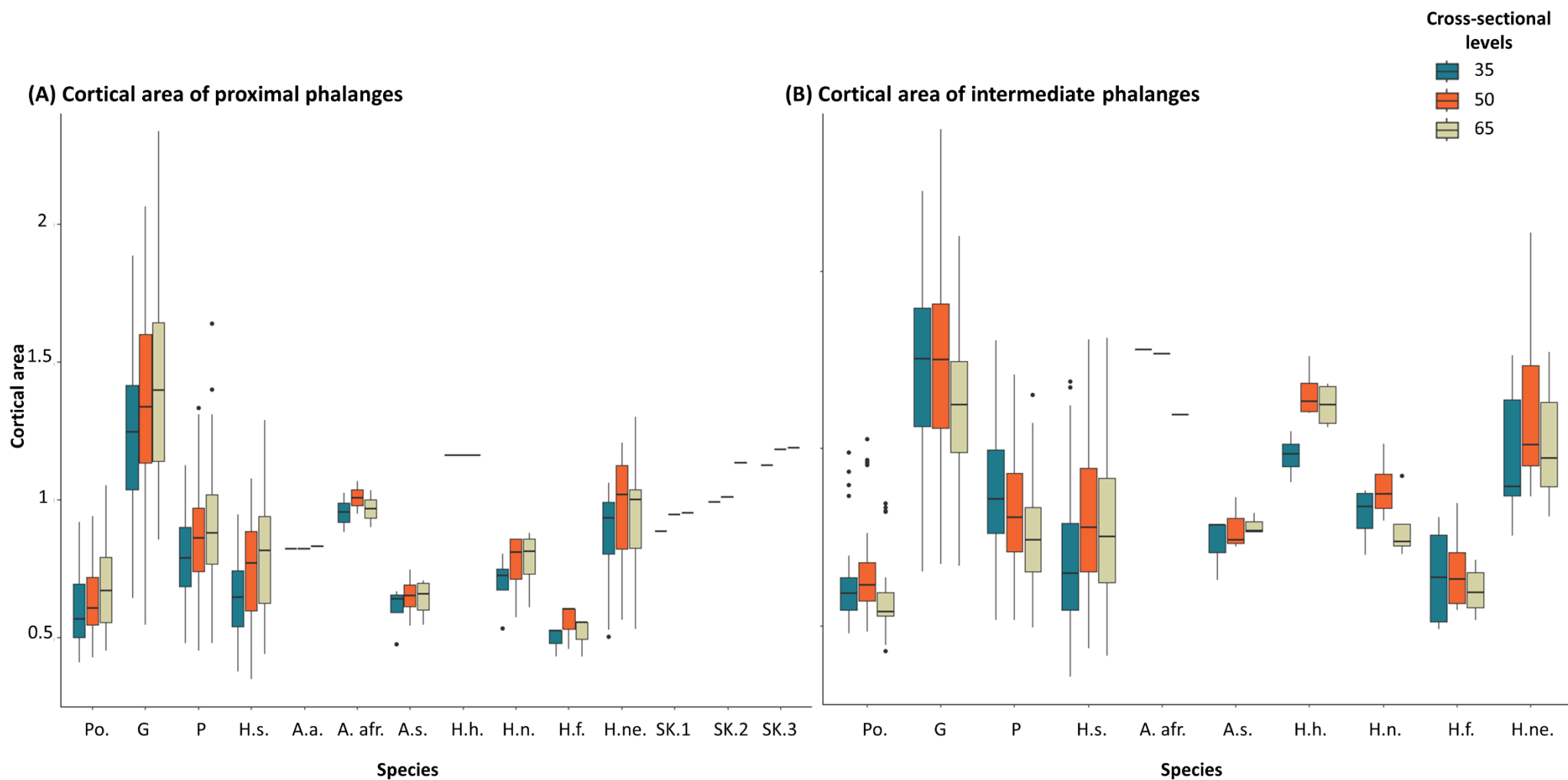


Figure 5.5: Boxplots representing scaled values of cortical area of the (A) proximal phalanges and (B) intermediate phalanges in extant great apes and fossil hominins. Species names are abbreviated: Po. = *Pongo*; G = *Gorilla*; P = *Pan*; H.s. = *H. sapiens*; A.a. = *A. afarensis*; A.afr. = *A. africanus*; A.s. = *A. sediba*; H.h. = *H. habilis*; H.n. = *H. naledi*; H.f. = *H. floresiensis*; H.ne. = Neanderthals; SK.1 = SKX 27431; SK.2 = SKX 15468; SK.3 = SKX 5018.

Cross-sectional levels

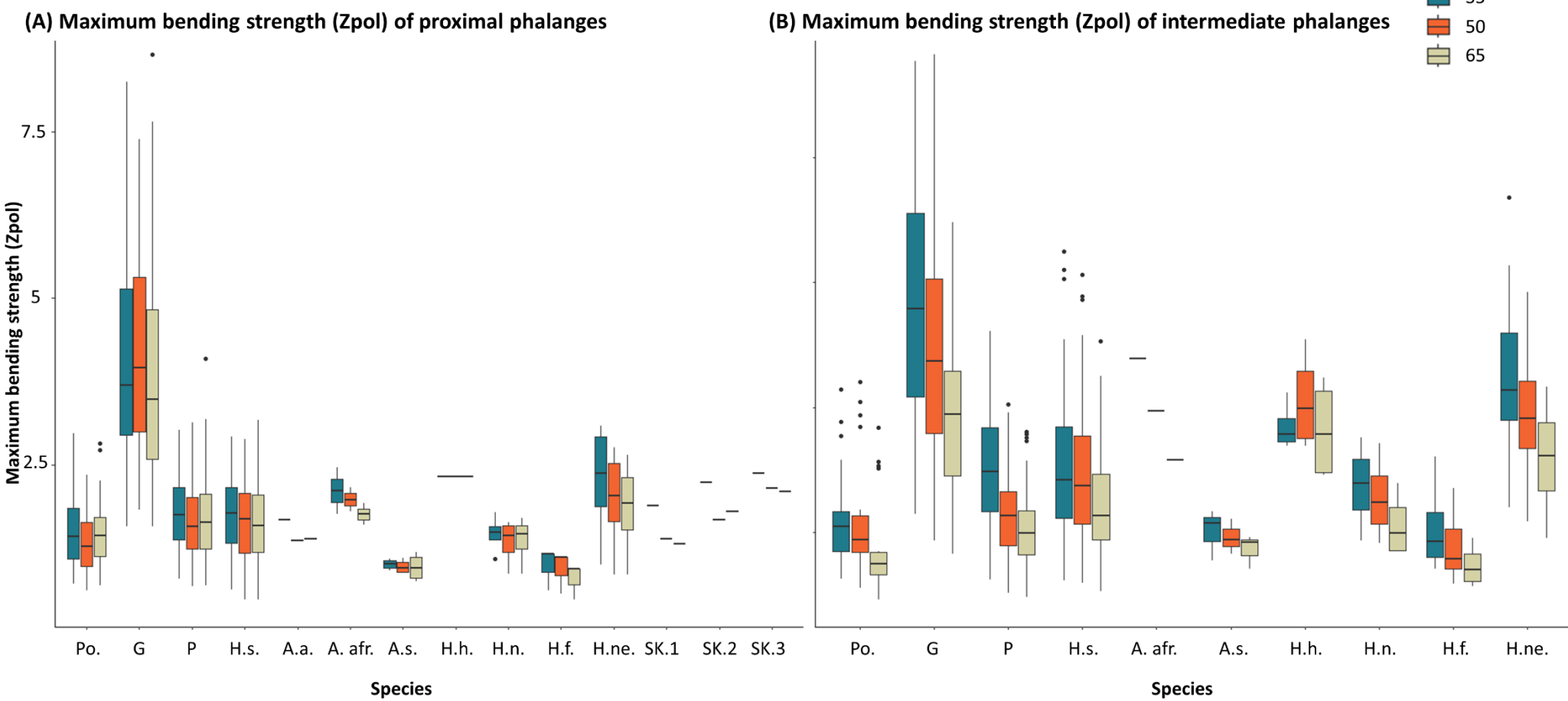
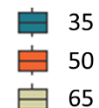


Figure 5.6: Boxplots representing scaled values of maximum bending strength (Z_{pol}) of the (A) proximal phalanges and (B) intermediate phalanges in extant great apes and fossil hominins. Species names are abbreviated: Po. = *Pongo*; G = *Gorilla*; P = *Pan*; H.s. = *H. sapiens*; A.a. = *A. afarensis*; A.afr. = *A. africanus*; A.s. = *A. sediba*; H.h. = *H. habilis*; H.n. = *H. naledi*; H.f. = *H. floresiensis*; H.ne. = Neanderthals; SK.1 = SKX 27431; SK.2 = SKX 15468; SK.3 = SKX 5018.

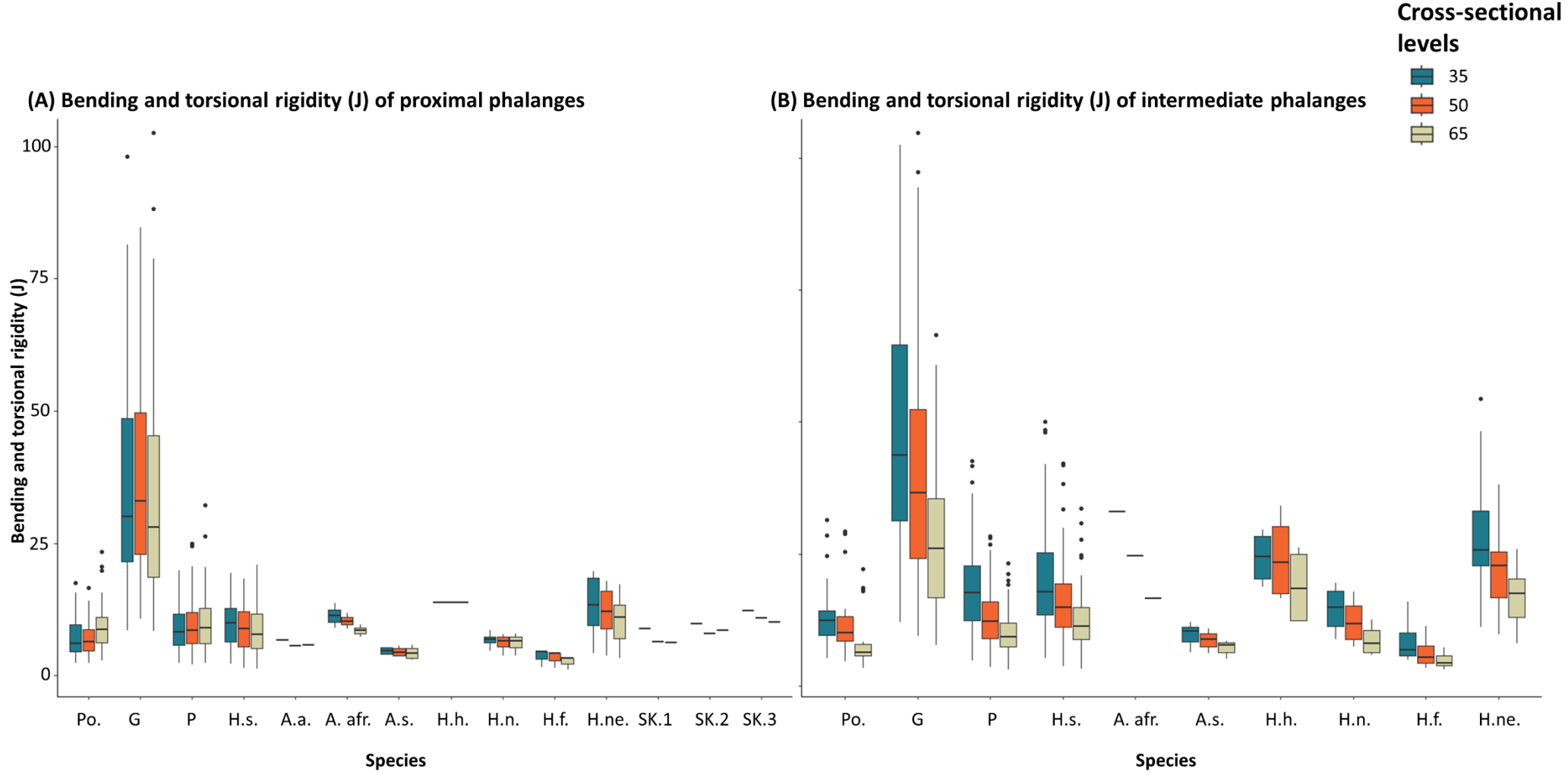


Figure 5.7: Boxplots representing scaled values of bending and torsional rigidity (J) of the (A) proximal phalanges and (B) intermediate phalanges in extant great apes and fossil hominins. Species names are abbreviated: Po. = *Pongo*; G = *Gorilla*; P = *Pan*; H.s. = *H. sapiens*; A.a. = *A. afarensis*; A.afr. = *A. africanus*; A.s. = *A. sediba*; H.h. = *H. habilis*; H.n. = *H. naledi*; H.f. = *H. floresiensis*; H.ne. = Neanderthals; SK.1 = SKX 27431; SK.2 = SKX 15468; SK.3 = SKX 5018.

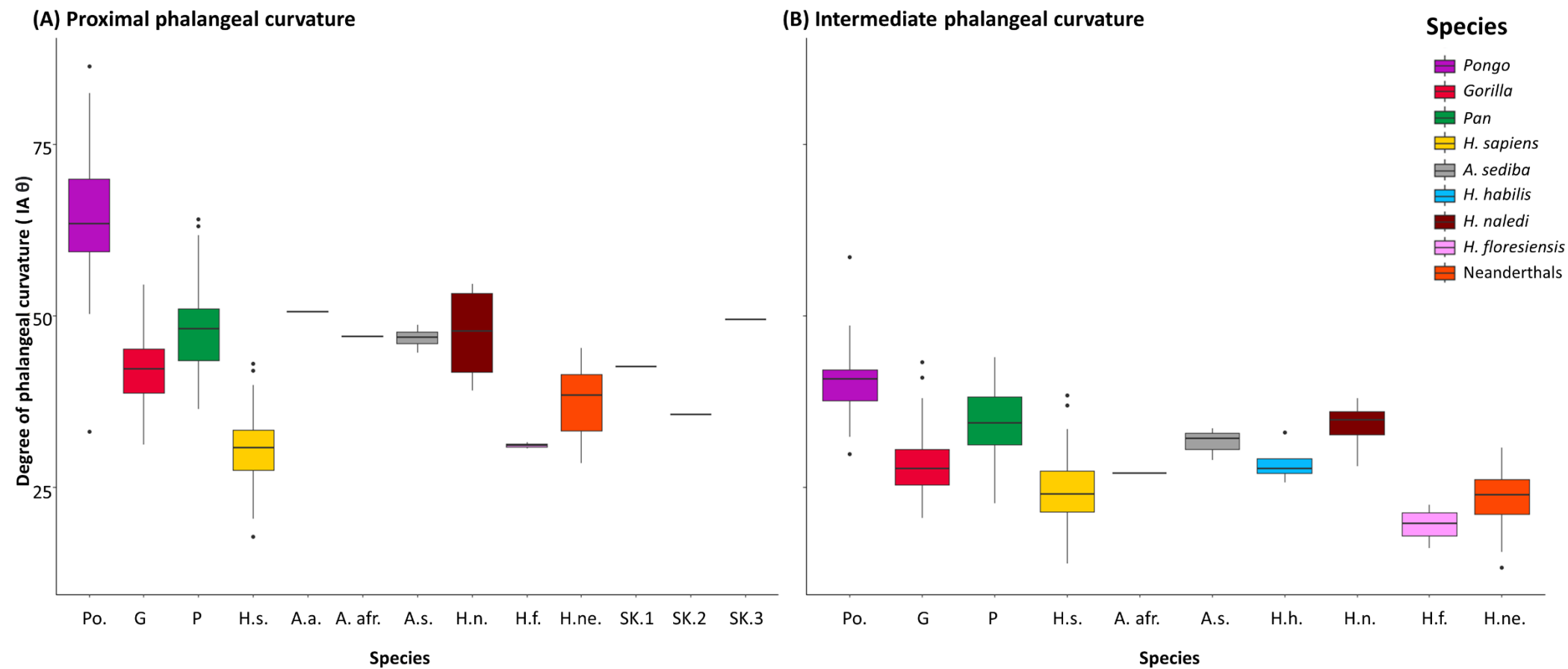


Figure 5.8: Boxplots representing the phalangeal curvature (measured via Included Angle) of the (A) proximal phalanges and (B) intermediate phalanges in extant great apes and fossil hominins. Species names are abbreviated: Po. = *Pongo*; G = *Gorilla*; P = *Pan*; H.s. = *H. sapiens*; A.a. = *A. afarensis*; A.afr. = *A. africanus*; A.s. = *A. sediba*; H.h. = *H. habilis*; H.n. = *H. naledi*; H.f. = *H. floresiensis*; H.ne. = Neanderthals; SK.1 = SKX 27431; SK.2 = SKX 15468; SK.3 = SKX 5018.

5.4.3. *Australopithecus sediba*

The cortical bone thickness distribution pattern of the *A. sediba* proximal and intermediate phalanges is unique among the comparative sample (Fig. 5.1C). The region of thickest cortical bone in PP2-PP4 is on the peaks of the FSRs and proximal to the trochlea, with a thin palmar shaft and an intermediately thick dorsal shaft. Within PP5, patches of thick cortical bone are along the FSRs and on the distodorsal region of the shaft. Across the IPs, cortical bone is thickest across the entire FSRs and proximal to the trochlea, with similar palmar and dorsal cortical thickness in IP3-IP4 and IP5 showing slight distodorsal thickness. The pattern across digits 2-4 resembles the great ape-like pattern, while digit 5 is distinct in showing a mixture of non-human and human-like cortical bone distribution. In both the proximal and intermediate phalangeal cortical bone distribution PC analyses, *A. sediba* falls out in between the great ape distributions and human distribution (Fig. 5.2, Fig. 5.9).

While the cortical bone distribution largely resembles great apes, changes in mean cortical thickness along the shaft is most similar to humans (Fig. 5.3). However, there is some variation across the PPs and IPs. Generally, cortical thickness in PP2, PP4 and PP5 increases proximodistally and decreases distal to the point of greatest cortical thickness, which varies across the three phalanges. PP3 cortical thickness increases proximodistally and plateaus around the midshaft. Across the IPs, there is a general proximodistal increase in cortical thickness, which decreases just proximal to the trochlea. Apart from PP3, the pattern of cortical thickness across the shaft of PPs resembles a human-like pattern while the pattern in the IPs is most similar to the great apes.

This mixed pattern is observed in the mean cortical thickness of the phalanges as well. Mean cortical thickness of the PPs overlaps with the lower end of the African ape range of variation and upper end of the human range, while mean cortical thickness of the IPs is only within the African ape range (Fig. 5.4). Dorsopalmar curvature of the *A. sediba* PPs and IPs is African ape-like, falling within the range of *Pan* and upper end of *Gorilla* variation, and outside human variation (Fig. 5.8).

Cross-sectional geometric properties of the *A. sediba* phalanges show a similar pattern across the different cross-sections as that of extant great apes. The CA values are greatest at 50% of the shaft in the IPs and increase proximodistally in the PPs, while Z_{pol} and J increase distoproximally in the IPs and PPs (Figs. 5.5-5.7). Within *A. sediba*, CA is greater in the IPs than PPs across all cross-sections, which deviates from the extant ape pattern, in which PP CA is greater than IP CA across all cross-sections. Values of Z_{pol} and J decrease proximodistally across the shaft, similar to the extant pattern and are generally higher in the PPs than in the IPs. The only exception to this is Z_{pol} at 35% of the shaft where the IPs have greater values than the PPs. Overall, the *A. sediba* phalangeal CSG values are within the range of *H. sapiens* and the lower range of *Pan*.

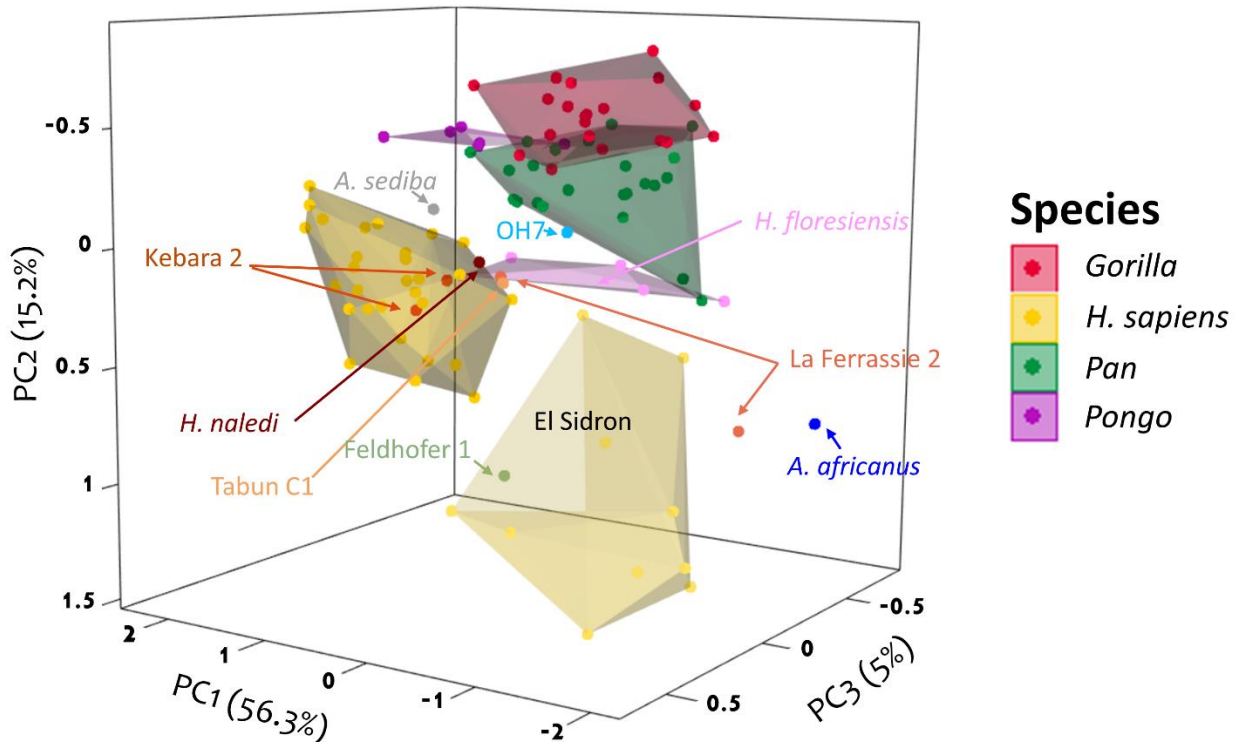


Figure 5.9: Results of the principal component analysis (PCA) of the intermediate phalanges in 3D, showing separation among the extant taxa and fossil hominins. Associated phalanges are pooled together. Labels of the extant taxa are depicted in the legend. Fossil hominins are labelled individually.

5.4.4. *Homo habilis*

The overall cortical bone distribution pattern of the OH 7 IPs is characterised as having an intermediately thick phalangeal shaft and thick cortex along the palmar radial and ulnar surface of the phalanges (Fig. 5.10). Across the IPs, this thick palmar cortical bone is localised to the region proximal to the trochlea, but there is variation within the IPs. IP2 displays thick cortex on the left (when viewed dorsally) distodorsal surface, while IP3 and IP4 palmar cortical thickness extends proximally to the distal end of the FSRs as well. The pattern observed in the IPs is most similar to what has been observed in the great apes. In the PCA, the OH 7 intermediate phalanges plot on the edge of the *Pan* range (Fig. 5.9).

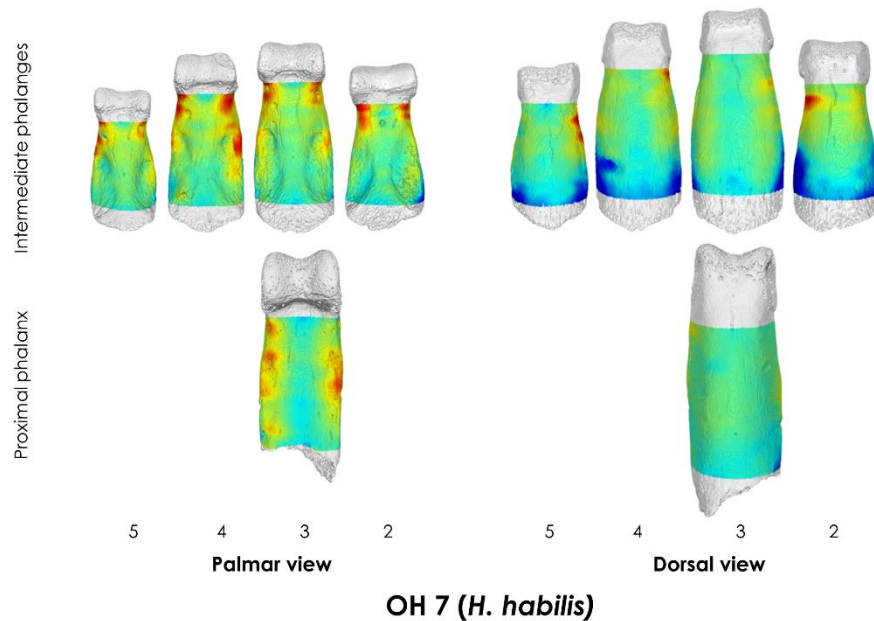


Figure 5.10: Cortical bone distribution maps of *Homo habilis* specimen OH 7. The maps display the palmar and dorsal surface of the phalanges, with the digits listed under the phalanx.

Just as the cortical bone distribution pattern of the OH 7 phalanges is similar to great apes, the pattern of cortical thickness values across the shaft and average cortical thickness is also similar to the great apes. Cortical thickness in all the IPs increases proximodistally and falls within the range of the African apes and the upper end of humans (Fig. 5.3B, Fig. 5.4B). The estimated phalangeal curvature of the OH 7 IPs is in the upper end of the human range and within the *Gorilla* range (Fig. 5.8B).

Cross-sectional properties were analysed at 35%, 50%, and 65% of the shaft in the IPs, with values of CA and Z_{poi} greatest at the midshaft and values of J decreasing proximodistally. Values of CA in the IPs are within the upper range of *Pan* and *H. sapiens* and within the range of *Gorilla*. Values of Z_{poi} and J in the IPs are within the range of African apes and humans, (Figs. 5.5B–5.7B).

The cortical bone distribution pattern of the PP fragment was of thick cortical bone along the FSRs and proximal to the trochlea, bearing close resemblance to the great apes. Average cortical thickness, the pattern of cortical thickness values across the shaft, and the curvature of the PP could not be analysed as it was a fragment. All CSG properties were calculated at 50% of the shaft and were within the upper range of *Pan* and *H. sapiens* variation and within the range of *Gorilla* variation (Figs. 5.5B–5.7B).

5.4.5. Swartkrans hominins

The three proximal phalanges from Swartkrans have differing morphologies and differing cortical bone distribution patterns (Fig. 5.11). The cortical bone distribution pattern of specimen SKX 27431 is of an intermediately thick shaft, with the dorsal shaft displaying a slightly thicker shaft relative to the palmar shaft (Fig. 5.11A). The thickest region of cortical bone of specimen SKX 27431 is on the distal end of the FSR and proximal to the trochlea. Specimen SKX 5018 cortical bone distribution pattern reveals thickest bone on the dorsal surface of the phalanx and

on the distopalmar region of the shaft (Fig. 5.11B). The cortical bone distribution pattern of specimen SKX 15468 is distinct from that of the other two Swartkrans specimens such that the cortex is thickest on the distal half of the palmar radial and ulnar surfaces. (Fig. 5.11C). In the PCA, SKX 5018 and SKX 15468 plot close to each other, occupying their own morphospace, while SKX 27431 plots separately on the edge of the El Sidron Neanderthal morphospace due to its smaller size and lack of prominent external morphology (Fig. 5.2).

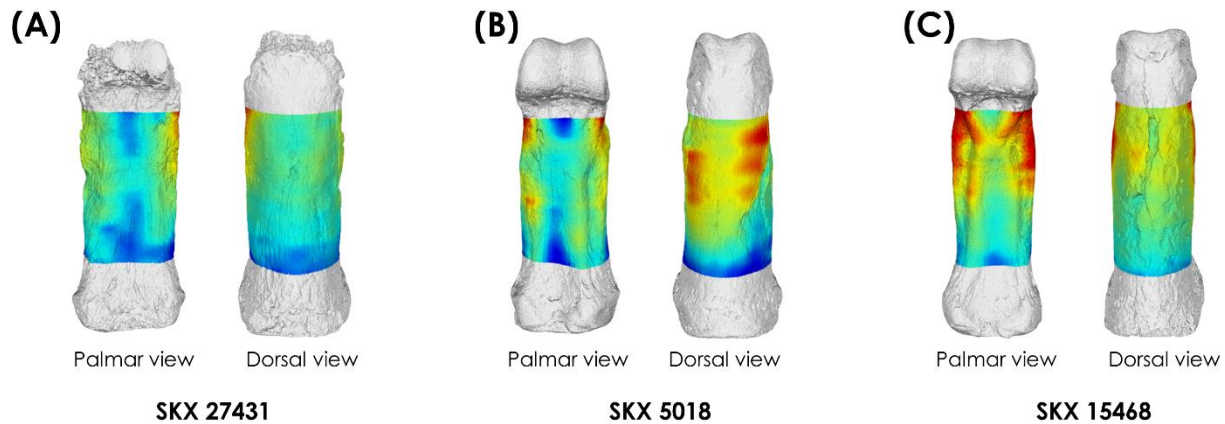


Figure 5.11: Cortical bone distribution maps of (A) SKX 27431, (B) SKX 5018, (C) SKX 15468. The maps display the palmar and dorsal surface of the phalanges,

While the three Swartkrans phalanges have differing cortical bone distribution patterns, the pattern of cortical bone thickness values across the shaft of the three phalanges is similar, resembling closely to the great ape pattern (Fig. 5.3A). Cortical thickness values across the shaft of specimen SKX 27431 and SKX 5018 increase proximodistally, decrease slightly distal to the midshaft, and increase distal to that, while the pattern of cortical thickness values of specimen SKX 15468 increases proximodistally.

The cortical bone distribution pattern and cortical bone thickness values across the shaft are concomitant with the average cortical thickness of the three phalanges (Fig. 5.4A). SKX 27431 cortical thickness falls within the range of African ape phalangeal cortical thickness, similar to its cortical bone distribution pattern and cortical thickness values across the shaft. SKX 5018 and SKX 15468 have the thickest cortex within the study sample, with cortical thickness of SKX5018 being slightly thicker than SKX 15468. The thick cortex of SKX 5018 is contradictory to the thick dorsal cortical bone distribution pattern of this phalanx but is in line with the general proximodistal increase in cortical thickness values across the shaft.

Measuring the phalangeal curvature of the Swartkrans phalanges reveals specimen SKX 27431 falls within the range of *Pan* proximal phalangeal curvature and the upper end of the *Gorilla* proximal phalangeal curvature (Fig. 5.8A). Specimen SKX 5018 falls within the upper end of the African ape phalangeal curvature and lower end of *Pongo* proximal phalangeal curvature, while specimen SKX 15468 has the lowest degree of phalangeal curvature, falling within the upper range of human curvature and lower end of *Gorilla* curvature.

In the cross-sectional properties of the three Swartkrans phalanges, all three phalanges display a proximodistal increase in CA. Overall the CA values of SKX 27431 are the lowest, followed by SKX 15468, and SKX 5018 has the greatest values of CA. SKX 15468 has the greatest difference between the midshaft and distal end of the bone. Values of Z_{pol} and J decrease proximodistally in SKX 27431 and SKX 5018, while in SKX 15468 values are greatest proximally and lowest at the midshaft (Fig. 5.5A-5.7A).

5.4.6. *Homo naledi*

H. naledi phalanges show a distinct pattern across and within the proximal and intermediate phalanges (Fig. 5.12). The proximal phalanges display thick cortical bone on the FSRs and the dorsal surface of the bone. The thickness on the palmar surface is localised to the midshaft-to-distal region of the bone and not the entire length of the FSRs. Furthermore, the palmar ulnar region of PP2 is thicker than the radial region and PP5 is variably thick across the FSRs. Across the IPs, cortical bone is thickest across the FSRs, with an intermediately thick dorsal shaft. IP2 also displays thick cortex under the trochlea. Despite the proximal and intermediate phalanges displaying distinct cortical bone distribution patterns, in their respective PCAs the *H. naledi* phalanges plot on the edge of the *H. sapiens* morphospace (Fig. 5.2, Fig. 5.9). The PPs plot close to the *H. sapiens* due to their thick dorsal cortices, and because the IPs are pooled together, the intermediately thick dorsal cortex of IP2 may explain the IPs plotting close to the humans as well.

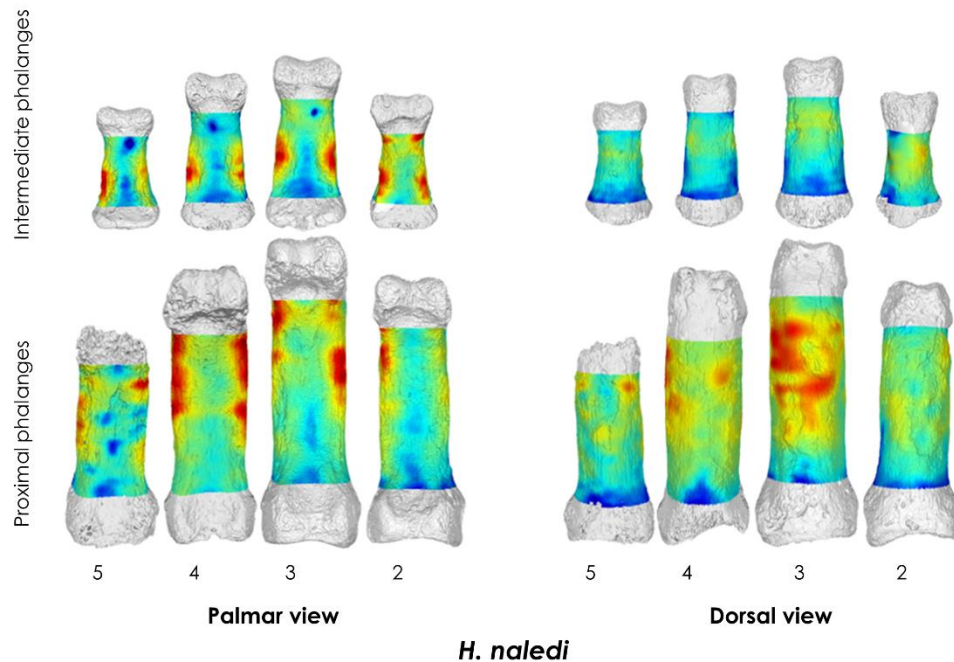


Figure 5.12: Cortical bone distribution maps of *Homo naledi* (Hand 1). The maps display the palmar and dorsal surface of the phalanges, with the digits listed under the phalanx.

The pattern of average cortical thickness across the PP and IP shafts is most similar to humans, with the exception of PP5. Within the IPs, cortical thickness increases proximodistally, peaks around the midshaft and decreases distally, while in PP2-PP4 cortical thickness peaks

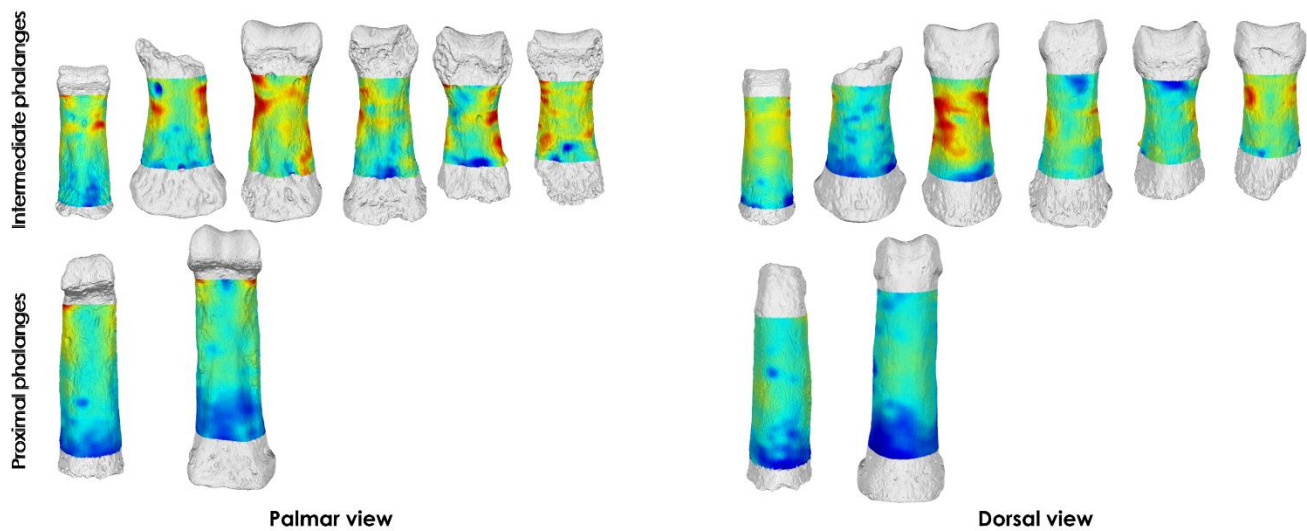
distal to the midshaft and decreases distally (Fig. 5.3). PP5 cortical thickness increases proximodistally; a pattern most similar to great apes.

This mixed signal from the cortical bone distribution pattern and cortical bone thickness pattern across the shaft is coincident with the thick cortices of the *H. naledi* phalanges. Average cortical thickness values of the PPs and IPs are within the African ape range of variation and upper end of the human range (Fig. 5.4). The curvature of the PPs and IPs is more similar to Pan but also falls within the upper range of *Gorilla* (Fig. 5.8).

Cross-sectional properties of the *H. naledi* phalanges have a differing pattern in the PPs and IPs, except for values of J, which decrease proximodistally across the IPs and the PPs. Values of CA increase proximodistally in the PPs and are highest distally (65% of the shaft) in the IPs and values of Z_{pol} decrease proximodistally in the IPs and are highest proximally (35% of the shaft) in the PPs. Within the proximal and intermediate phalanges, values of Z_{pol} and J are higher in the PPs than the IPs across all cross-sections, while CA in the IPs is greater than the PPs at 35% and 50% of the shaft (Figs. 5.5–5.7).

5.4.7. Homo floresiensis

Within the *H. floresiensis* hand remains, my sample includes IPs from at least three individuals and PPs from two, with one of the individuals being a juvenile. Results show a similar cortical bone distribution pattern across the intermediate phalanges and between adult and juvenile proximal phalanx, but the proximal and intermediate phalanges each show distinct patterns (Fig. 5.13). Cortical bone of the PPs is thickest proximal to the trochlea, with a relatively low to intermediately thick shaft. The IPs display thick cortical bone on the palmar surface in patches, with some individuals displaying thick cortex wrapping around the radial and ulnar dorsal surface as well. Within the IPs, LB6–9 has a thick dorsal cortex that was not visible in any other specimen. The pattern of both the proximal and the intermediate phalanges is unique to *H. floresiensis* and not observed in any other extant taxa. The unique nature of the *H. floresiensis* phalanges is further reinforced in the PCAs, where the *H. floresiensis* phalanges occupy their own morphospace between the *Pan* and *H. sapiens* distribution (Fig. 5.2, Fig. 5.9).



H. floresiensis

Figure 5.13: Cortical bone distribution maps of *Homo floresiensis* phalanges. Proximal phalanges, from left to right: LB-XXI-44-2010, LB6-8; Intermediate phalanges, from left to right: LB-XV-42-2008, LB6-10, LB6-9, LB1-48, LB1-42, LB1-40. The maps display the palmar and dorsal surface of the phalanges.

While the pattern of cortical bone distribution within the *H. floresiensis* phalanges is distinct, the pattern of cortical thickness across the shaft shares similarities with the extant sample. The *H. floresiensis* intermediate phalanges resemble the human pattern but deviate slightly from it, as the decrease in cortical thickness distal to the midshaft is not as stark, but there is a visible decrease that is not observed in great apes (Fig. 5.3B). However, the pattern of the proximal phalanges increases proximodistally, resembling the pattern of great apes (Fig. 5.3A).

The differences observed in the cortical bone distribution pattern and cortical thickness across the shaft between the proximal and intermediate phalanges are not observed in the average cortical thickness results. The average cortical thickness of both the proximal and intermediate phalanges falls within the human range of variation and the lower range of African apes (Fig. 5.4). Similarly, the phalangeal curvature of both the proximal and intermediate phalanges is also within the human range of variation.

Cross-sectional geometric properties of the *H. floresiensis* phalanges show a similar pattern across the different cross-sections as the extant sample. Values of CA are greatest at 50% of the shaft in the PPs and decrease proximodistally in the IPs, while Z_{pol} and J decrease proximodistally in the IPs and PPs. Values of all CSG properties are within the lower range of variation in humans.

5.4.8. *Homo neanderthalensis*

Across the different Neanderthal populations included, the general pattern of cortical bone distribution is of palmar thickness on the FSRs along with varying degrees of thick dorsal cortex (Fig. 5.14). The oldest sample of Neanderthal phalanges comes from the two IPs of Tabun C1 (~ 122 kya; Grun & Stringer, 2000). The Tabun C1 phalanges have thick cortex on the FSRs, with thick cortex on the radial and ulnar dorsal surface as well (Fig. 5.14A). All preserved phalanges from the Kebara 2 individual (~ 59-64 kya; Rebollo et al., 2011), have thick dorsal cortices throughout

majority of the shaft (Fig. 5.14B). The Kebara 2 PPs also have thick cortex on the midshaft to distal region of the FSRs, as well as across the distal palmar shaft. The Kebara IPs, have thick dorsal cortex while thick cortex on the palmar surface is localised to the distal region. Phalanges from the El Sidron Neanderthals (~49 kya; Wood et al., 2013) have differing patterns in the PPs and IPs (Fig. 5.14E). In the PPs, cortex is thickest on the FSRs with an intermediately thick dorsal shaft. In the IPs, the palmar surface is intermediately thick while the thickest areas of the dorsal cortex occur in patches on the radial and ulnar regions on the distal dorsal shaft. All phalanges from the hand of La Ferrassie 2 (~43–45 kya; Guerin et al., 2015) have similar patterns of cortical bone distribution (Fig. 5.14D). Generally, the shaft is intermediately thick with the distal palmar radial and ulnar regions having the thickest cortex. Within the PPs, the thickest region is not necessarily on the FSRs, but within the IPs, maximum thickness is on the FSRs as well as the distopalmar surface. The final set of Neanderthal phalanges comes from Feldhofer 1 (~40 kya; Roebroeks, 2014), with one PP and one IP. The PP has thick dorsal cortex along with thick cortex on the distal end of the FSRs and proximal to the trochlea. The IP has thin palmar cortex and an intermediately thick dorsal cortex (Fig. 5.14C).

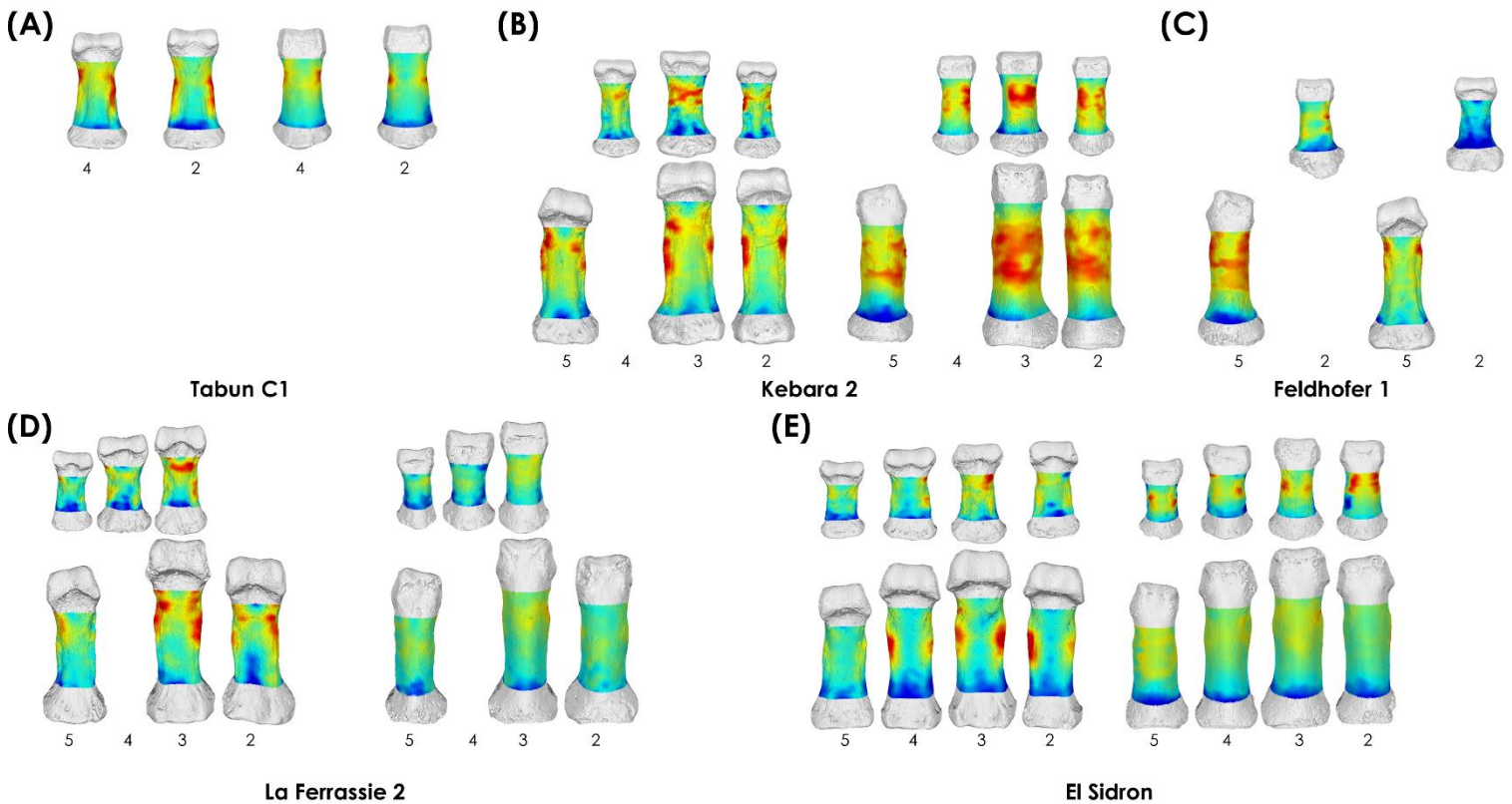


Figure 5.14: Cortical bone distribution maps of (A) Tabun C1, (B) Kebara 2, (C) Feldhofer 1, (D) La Ferrassie 2, (E) El Sidron composite hand. The maps display the palmar and dorsal surface of the phalanges, with the digits listed under the phalanx.

This variation in cortical bone distribution patterns is reflected in the PCA as well (Fig. 5.2, Fig. 5.9). The near eastern Neanderthals, Kebara 2 and Tabun C1, plot within the *H. sapiens*

morphospace. Tabun C1 plots on the edge of the *H. sapiens* distribution while the PPs and IPs of Kebara 2 sit within the *H. sapiens* distribution. The El Sidron Neanderthals occupy their own morphospace, with a large distribution. Feldhofer 1 plots close to this El Sidron distribution, sitting between the humans and El Sidron morphospace. The La Ferrassie 2 proximal phalanges plot close to the *H. sapiens* distribution, plotting between the great apes and human morphospace. The La Ferrassie 2 intermediate phalanges of the right and left hand do not plot together; the right IPs plot on the edge of the *H. sapiens* distribution while the left IPs fall out close to the El Sidron distribution.

While the pattern of cortical bone distribution within the different Neanderthal populations differs, the pattern of cortical thickness values across the shaft is similar across the proximal and intermediate phalanges of all individuals (**Fig. 5.3**). Cortical thickness increases proximodistally, peaks at various points around the midshaft, and decreases distal from that point, similar to the modern human pattern.

Analysing all the Neanderthal populations together reveals the average cortical thickness of the PPs and the IPs has a large range of variation, spanning from the upper end of the human range of variation to falling within the African ape range (**Fig. 5.4**). However, analysing the average cortical thickness within the different Neanderthal populations, some significantly differ from each other. These differences in cortical thickness are only present within the El Sidron population but are not consistent across the proximal and intermediate phalanges. Within the PPs, the El Sidron phalanges are significantly thicker than the La Ferrassie 2 phalanges ($p < 0.01$) and within the IPs, the El Sidron phalanges are significantly thicker than the intermediate phalanges of Kebara 2 ($p < 0.001$) (**Fig. 5.15**). The El Sidron phalanges are also the only Neanderthal population that significantly differs from *H. sapiens*. Furthermore, the La Ferrassie 2, Kebara 2, and El Sidron Neanderthals displayed significantly thicker intermediate phalangeal cortex relative to their respective proximal phalangeal cortex.

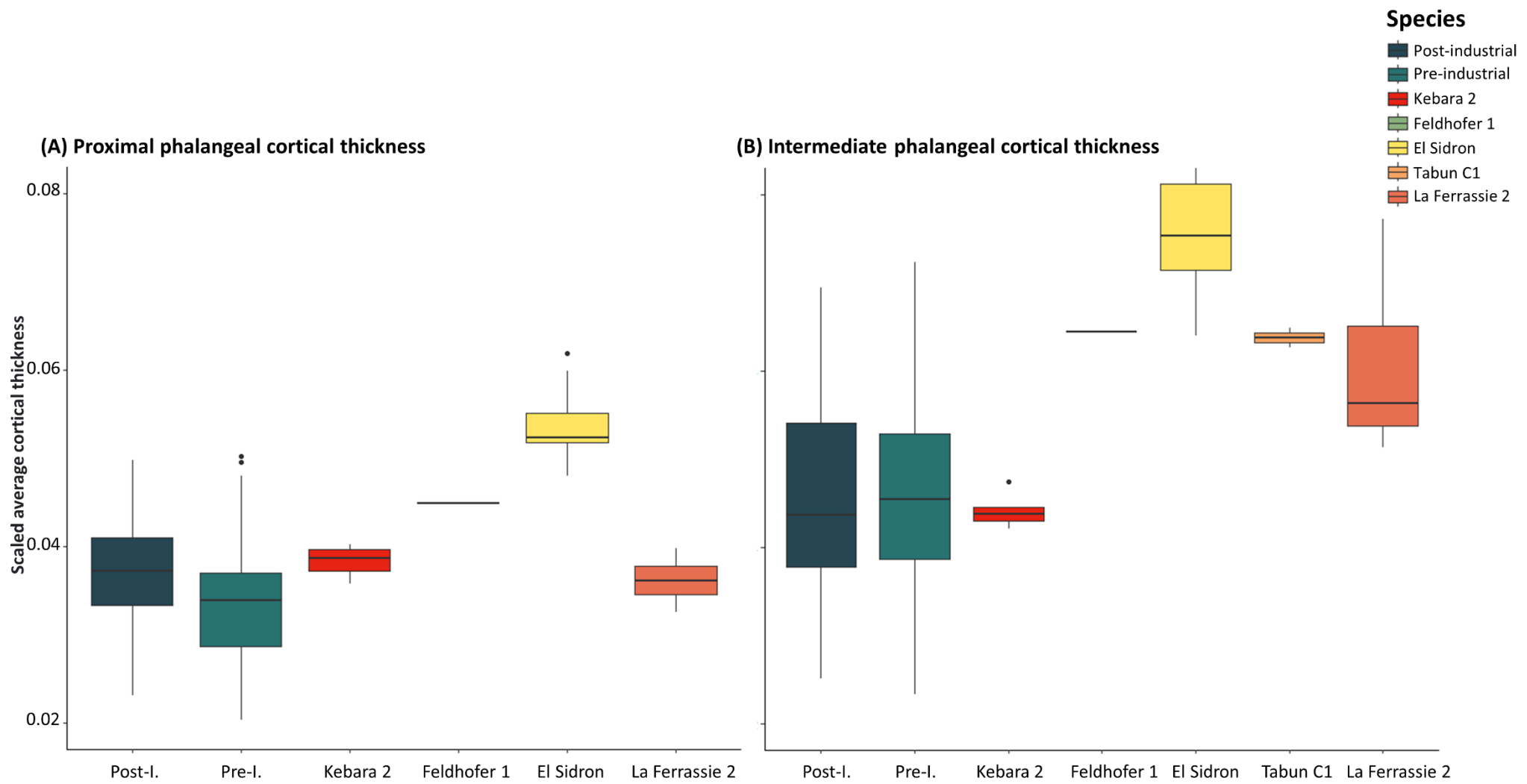


Figure 5.15: Boxplots representing the scaled average cortical thickness of the (A) proximal phalanges and (B) intermediate phalanges in Post-industrial and pre-industrial humans and Neanderthals.

The variation in the average cortical thickness of the different Neanderthal populations, is not as present in the degree of phalangeal curvature of Neanderthals (Fig. 5.8). Overall, Neanderthal proximal phalangeal curvature is in the upper range of the human sample and intermediate phalangeal curvature is in the range of humans, with only El Sidron proximal phalanges being significantly more curved than those of *H. sapiens*. There are no significant differences in the degree of phalangeal curvature of the intermediate phalanges of the different populations. Within the populations that had both proximal and intermediate phalanges preserved (i.e., Kebara 2, El Sidron, and Le Ferrassie), the proximal phalanges were significantly more curved than the intermediate phalanges.

The CSG patterns across the three cross-sections in the proximal and intermediate phalanges reveal values of CA are greatest at the proximal end of the shaft and values of Z_{pol} and J decrease proximodistally (Figs 5.5–5.7). Values of these cross-sectional properties are also greater in the PPs compared to the IPs across all the cross-sections. Evaluating differences in CSG properties across the Neanderthal populations at the different cross-sections reveals differing patterns. The El Sidron Neanderthals have significantly greater CSG properties than pre-industrial *H. sapiens* across all cross-sections in the proximal and intermediate phalanges. The El Sidron Neanderthals also have significantly greater values of CA across all cross-sections in the intermediate and proximal phalanges than post-industrial *H. sapiens*, with the exception of the 65% cross-section in the PPs. Kebara 2 also has significantly greater values of CA at 35% and 50% of the shaft, Z_{pol} at 35% and 65% of the shaft, and J at 35% of the shaft compared to pre-industrial *H. sapiens*. Furthermore, there is variation in the CSG properties within the shaft of the El Sidron phalanges and Kebara 2 IPs. Within the Kebara 2 IPs, values of CA at 50% of the shaft are significantly greater than 35% of the shaft and values of Z_{pol} and J are significantly greater at 35% than 65% of the shaft. In the El Sidron IPs, values of Z_{pol} are significantly greater at 35% than 65% of the shaft, along with values of J being significantly greater at 35% of the shaft than at 65% of the shaft in the IPs. Overall, there are not many significant differences in CSG values within the shafts of Neanderthal phalanges.

5.5. Discussion

Phalangeal cortical bone distribution patterns and properties (e.g. thickness, cross-sectional properties) distinguish manual behaviours of humans and great apes, as described in Chapters 3 and 4. Thick cortical bone along the palmo-radial and palmo-ulnar surfaces reflect the knuckle-walking postures, along with infrequent arboreal behaviours, of the African apes and thick cortical bone on the peak of the FSRs of the highly curved *Pongo* phalanges reflect their habitual flexed finger postures during arboreal grasping. The relatively straight phalanges of *H. sapiens* have thick dorsal cortex, which is consistent with flexed-finger postures during manipulation. Furthermore, cortical thickness of the great apes increases proximodistally along the phalangeal shaft, which is distinguished from the *H. sapiens* pattern of cortical thickness decreasing distal to the midshaft. Coupling these behavioural inferences of extant great apes with kinematic, anatomical, and experimental data, provides support for the functional signals gleaned from phalangeal cortical bone morphology, allowing us to infer fossil hominin hand use.

5.5.1. Australopiths

Within the fossil hominin sample studied, *Australopithecus* demonstrated a pattern of cortical bone distribution most similar to great apes rather than humans, as predicted, but with some important differences across fossil taxa. *A. afarensis* and *A. africanus* cortical bone is thickest along the radial and ulnar sides of the palmar region and increases proximodistally across the phalangeal shaft, while *A. sediba* demonstrates a distinct pattern. While I only analysed one phalanx of *A. afarensis*, the pattern observed was different from what we observed in *A. africanus*, making it likely that the hand use of the two species differed.

However, my prediction that *A. sediba* would be most similar to the great apes, signalling a hand used primarily for locomotion, is not fully supported. The cortical bone distribution of *A. sediba* MH2 phalanges is similar to the other australopiths, with the exception of the fifth digit in which the palmar cortical thickness is coupled with distodorsal thickness. Furthermore, cortical thickness values across the shaft follow a human-like pattern across the PPs and the IPs, except in PP3 and PP5 which display a great ape-like proximodistal increase in cortical thickness. These mosaic signals within the cortex of the MH2 phalanges, which are also present in the internal structure of the wrist (Bird et al., 2023) and metacarpals (Dunmore et al., 2020b), posit a myriad of behavioural scenarios. Based on the MH2 phalanges, the palmar cortical bone distribution, thick African ape-like cortical thickness, curvature of the phalanges, and prominent FSRs suggest fingers that are functionally adapted to strong loads associated with arboreal climbing (Kivell et al., 2011; 2018). This is coupled with trabecular bone distribution of the wrist suggesting Pan-like postures and the metacarpals signalling the habitual use of arboreal grasping in the palm (Bird et al., 2023; Dunmore et al., 2020b).

Alongside phalangeal morphology suggesting a locomotor use of the hand, decreasing cortical thickness distal to the midshaft and the distodorsal thickening of the fifth digit is characteristic of human-like manipulation. Many aspects of the hand suggest manipulation was within the behavioural repertoire of *A. sediba* (Bird et al., 2023; Dunmore et al., 2020b; Kivell et al., 2011; 2018). For example, hand proportions of the MH2 hand reveal a long thumb relative to the fingers, which would have facilitated pad-to-pad precision grip, and the trabecular structure of the thumb suggests it was used in abducted and opposed position, which is characteristic of forceful precision grips (Dunmore et al., 2020b; Kivell et al., 2011; 2018; Marzke, 1997; Napier, 1962b; Patel & Maiolino, 2016; Tocheri et al., 2008). The asymmetry in metacarpal heads of *A. sediba* also suggests the ability of adduction of the fifth digit and thumb, which would have also allowed for precision grip and greater force production (Kivell et al., 2018a; Marzke 1997; Tocheri et al., 2008). While the fingers are in flexion during human manipulation as well, loads are lower and distributed differently when compared to flexed-finger postures during locomotion, as is demonstrated by the strong dorsal cortical reinforcement in humans. As such, the distodorsal thickening of the fifth digit may be indicative of the adduction of the fifth digit during manipulation using precision grips, which has been shown to be forcefully and frequently loaded during stone tool production (Key et al., 2019).

The combination of human-like and great ape-like cortical bone morphology suggests a hand that was capable of effective manipulation but was regularly used during locomotion with flexed-finger postures. These results are consistent with previous interpretations of MH2 hand morphology (Kivell et al., 2018a; Dunmore et al., 2020b), although here I also provide evidence of

a manipulation signal within the fingers of *A. sediba* that has only been observed in the thumb thus far. Phalangeal cortical bone further reinforced the mosaic nature of the *A. sediba* hand, and while *A. sediba* may have had the ability to locomote arboreally and manipulate objects, it is likely these behaviours and the loading resulting from these behaviours was distinct from what we have observed within the comparative extant taxa.

All the australopiths demonstrated a pattern of palmar cortical thickness, with the exception of the *A. sediba* fifth digit, suggesting the habitual use of flexed-finger postures for the locomotor use of the hand. The palmar pattern of cortical thickness in *A. africanus* and *A. sediba* is similar, with cortical thickness generally on the peak of the FSRs and distal to the trochlea, differing from *A. afarensis*. However, the cortical bone morphology of the australopith specimens included in this study makes it difficult to infer behavioural patterns of the genera or the species within the genera, with the exception of *A. sediba*. The nearly complete MH2 hand provides us with a great deal of functional data from which we can reconstruct a more accurate picture of *A. sediba* hand use compared to the isolated remains of *A. afarensis* and *A. africanus*. The isolated phalanges of *A. afarensis* and *A. africanus* shed light on their potential manual postures, but more specimens are needed to test if the cortical bone morphology observed here is representative of hand use of these species.

5.5.2. Early *Homo* and *Paranthropus*

Variation in manual behaviours of Plio-pleistocene fossil hominins is evident as the *Homo habilis* specimen OH 7 displays external morphology that is distinct from the australopiths but cortical bone structure that is not. The juvenile OH 7 phalanges have a palmar cortical bone distribution pattern and cortical thickness across the shaft that largely resembles that of the great apes. Thick cortical bone concentrated on the distal half of the palmo-radial and palmo-ulnar surfaces of these developmentally immature phalanges is most similar to the cortical bone distribution of adult *Pan* and *Gorilla*. These results are consistent with the external morphology of the OH 7 phalanges (i.e., radioulnarly broad, ape-like phalangeal curvature, and prominent FSRs) that have been interpreted as primarily reflecting arboreal grasping rather than manipulation (Napier, 1962b; Susman & Creel, 1979). There is no evidence of a manipulative signal within the OH 7 phalangeal cortical bone, which is consistent with the overall limb proportions and upper limb morphology of OH 62. Coupling the arboreal signal in the OH 7 and OH 62 remains with the OH 8 foot and OH 35 lower limb indicates *H. habilis* was capable of bipedal locomotion as well as arboreal behaviours (DeSilva et al., 2019; Patel et al., 2018; Ruff, 2009; Susman & Stern, 1982; Susman, 2008). However, the OH 7 hand was also found in close proximity to Oldowan tools suggesting some manipulative ability (Leakey et al., 1964 but see Napier, 1962a), but to uncover the manipulative abilities, if any, of *H. habilis*, further work on the distal phalanges and the trapezium of the OH 7 hand needs to be conducted.

Skeletal remains at Swartkrans include specimens attributed to *P. robustus* and early *Homo*, two species that traditionally are thought to have used distinct manual postures and had distinct manipulation abilities (Susman, 1988a; b). The cortical bone morphology of the Swartkrans phalanges provides evidence of variable manual activities occurring at Swartkrans, but not in a manner that was predicted. SKX 5018 and SKX 15468 have been argued to belong to *P. robustus*, yet they display different cortical bone distribution patterns, with SKX 5018 having a human-like pattern of dorsal thickness and SKX 15468 having thick palmar cortex. These differing patterns

are coupled with a great ape-like proximodistal increase in cortical thickness and thick African ape-like cortices. Furthermore, SKX 5018 has a high degree of phalangeal curvature, in contrast to previous measurements (Susman, 1988a; Susman et al., 2001). The discrepancy in IA values may be due to the interobserver measurement error associated with the IA method (Deane & Begun, 2008; Wennemann et al., 2022). Despite the differing patterns of cortical bone distribution and phalangeal curvature of SKX 15468 and SKX 5018, they have similar cortical thickness values and cluster closely together in the PCA. SKX 27431 on the other hand is thought to belong to *Homo* and displays palmar thickness, however not as strongly as SKX 15468, and resembles the African apes in its cortical morphology. The differing pattern of cortical bone distribution, curvature, and relatively lower cortical thickness (compared to SKX 15468 and SKX 5018) of SKX 27431 separates it from the other two phalanges in the PCA.

Due to their exceptionally thick cortices, SKX 5018 and SKX 15468 may belong to the same species. Susman (1988a, 1989; Susman et al., 2001) attributed both specimens to *P. robustus*. However, the cortical bone distribution pattern differs greatly within these two phalanges, and also from that of SKX 27431. The difference found between SKX 5018 and SKX 15468 could not be explained as reflecting variation between digits or left/right hands or sex within a single taxon because this variation has not been observed between the digits, hands, or sex of any of the extant taxa. Furthermore, we potentially have phalanges from multiple individuals of *A. africanus* and *H. floresiensis* and they do not display such a stark difference in cortical bone distribution. Only Neanderthals have differing patterns of cortical bone distribution, but these differences are related to populations that are geographically and temporally widespread with proven differences in the skeleton of Northern and Southern Neanderthals (Dunmore et al., 2020b; Kivell et al., 2018b; Rosas et al., 2006). SKX 5018 and SKX 15468 both were recovered from the same geological layer of Swartkrans (Susman 1988a) and if they belong to the same species, their phalangeal cortical bone suggests that each individual varies considerably in their manual behaviours (Susman et al., 2001).

As SKX 27431 plots further away from the two phalanges and has lower cortical thickness, it could belong to a separate species than SKX 5018 and SKX 15468. These three phalanges from Swartkrans are different from each other, each with a unique mix of cortical bone properties. With no clear indication of a *P. robustus* or early *Homo* pattern, the attribution of these phalanges to their respective taxa requires questioning. The 'primitive' external morphology of SKX 5018 and SKX 15468 that clusters them within *P. robustus* is concomitant with different patterns of cortical bone distribution in both. The dorsal cortical reinforcement of SKX 5018 is unique in a robust, thick, and highly curved phalanx and challenges the knowledge on *P. robustus* hand use as well as the current knowledge on taxonomic attribution within the layers of Swartkrans (Susman, 1988a). However, regardless of their taxonomic attribution, all three phalanges display cortical bone properties that are closer to great apes than to humans.

The variability observed in the phalanges from Swartkrans sheds light on the potential behavioural diversity present in early *Homo*. *H. habilis* specimen OH 7 and *P. robustus* /early *Homo* specimens SKX 27431 and SKX 15468 all indicate the habitual locomotor use of the hand, but the dorsal cortical thickness of specimen SKX 5018 and the stone tools found in close association with these species (Kuman et al., 2021; Leakey et al., 1964), suggest manipulative abilities as well. However, if OH 7 and Swartkrans specimens SKX 27431 and SKX 15468 were

using their hands for locomotion, their behaviour was likely distinct due to the strong palmar features on the Swarktrans phalanges that would have helped dissipate loads across the phalanx in a distinctive manner (Susman, 1988a; Susman et al., 2001). These differences in external and internal phalangeal morphology would have likely affected the manual postures of these species during manipulation as well, despite both species being geographically and temporally associated with Oldowan tools (Kuman et al., 2021; Leakey et al., 1964). While a specific, early *Homo* or *P. robustus* pattern of cortical bone morphology cannot be identified using this study sample, the results here suggest it is probably the hand use in these two species contrasted with each other.

5.5.3. Later Homo

H. naledi Hand 1 phalanges exhibit distinct patterns of cortical bone distribution from both the extant sample and other fossil hominins. In particular, *H. naledi* is distinct in having cortical morphology that suggests the proximal phalanges were loaded differently from the intermediate phalanges. The proximal phalanges have a dorsal, human-like pattern combined with palmo-radial and palmo-ulnar thickness, while the intermediate phalanges have thick cortex along the FSRs with an intermediately thick dorsal shaft. The palmar thickness of the proximal phalanges may be interpreted as evidence of flexed-finger postures during locomotion, as observed in great apes, however, *H. sapiens* individuals that possess prominent FSRs had a similar pattern of palmar cortical thickness as observed in the *H. naledi* proximal phalanges. Therefore, overall the Hand 1 PPs are best described as showing a human-like cortical bone distribution. In contrast, the intermediate phalanges closely resemble the cortical pattern of great apes. This is an interesting pattern from a biomechanical perspective; the phalanges primarily move in the extension/flexion plane and if flexion at the DIP joint occurs, flexion at the PIP joint occurs as well. Therefore, if the intermediate phalanges are resisting loads associated with powerful grasping during locomotion (as indicated by the cortical bone properties) it would be expected the proximal phalanges are being loaded in a similar manner. These varying cortical bone distribution patterns across the proximal and intermediate phalanges may reflect the role of external morphological features in mitigating forces across the hand. The intermediate phalanges of *H. naledi* Hand 1 have the greatest degree of curvature within the current fossil hominin record and have prominent FSRs, while the proximal phalanges are moderately curved and lack protruding FSRs. Therefore, if *H. naledi* is participating in arboreal locomotion, in which the greater degree of curvature and FSRs help reduce strain experienced by the phalanx (Richmond, 2007; Nguyen et al., 2014), the proximal phalanges that are intermediately curved and do not possess prominent FSRs, may be responding to that stress by increasing overall cortical thickness in the dorsal and palmar surface. However, this functional explanation would call into question the adaptive role of the FSRs, i.e., if *H. naledi* proximal phalanges were experiencing such high loads why do they not possess prominent FSRs as observed in the intermediate phalanges?

An alternative behavioural explanation posited regarding the locomotor repertoire of *H. naledi* has been the possibility that they may have been climbing vertical rock surfaces (Voisin et al., 2020). Rock climbing results in high forces across the flexor system of the hand, especially at the annular pulleys that hold the tendon close to the bone and provide mechanical advantage during flexion at the phalangeal joints (Ayhan & Ayhan, 2020; Schweizer, 2001; Schweizer & Hudek, 2011; Schweizer et al., 2008). Such loading could result in thick cortex on the palmar surface relative to the dorsal side. Two common grips employed during modern human rock climbing are the crimp grip and the slope grip (Bollen, 1990; Schweizer, 2001; Schweizer et al., 2008). During the crimp grip, the PIP joint is flexed around 90–110° while the DIP joint is extended or hyperextended, while in the slope grip, the PIP joint only flexes around 40–60° and the DIP joint is also flexed (Schweizer et al., 2008) (**Fig. 5.16**). The crimp grip is thought to be the most effective and powerful grip during rock climbing (Schweizer, 2001). However, despite the effectiveness of the crimp grip, the slope grip is employed quite frequently on less contoured and curved rocks (Schweizer et al., 2008). The differing patterns of cortical bone distribution found in the intermediate and proximal phalanges may support the hypothesis that *H. naledi* was climbing rocks, specifically through the utilisation of the slope grip. The high degree of flexion of the DIP joint and the minimal flexion of the PIP joint during the use of the slope grip may explain the strong palm-radial and palmo-ulnar thickness, prominent FSRs, and high degree of curvature in the intermediate phalanges, along with the mixture of palmar and dorsal cortical thickness and the lack of prominent external morphological features of the proximal phalanges. Furthermore, humans who rock climb regularly have been shown to have thicker metacarpal and phalangeal cortex than those who do not (Sylvester et al., 2006), which may explain the thick cortex of the proximal and intermediate phalanges.

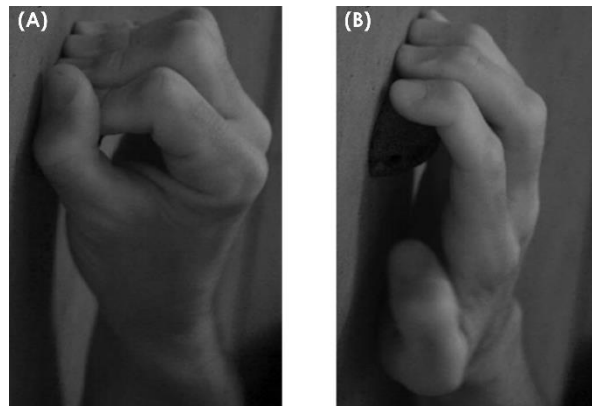


Figure 5.16: Illustration adapted from Amca et al., 2012 depicting flexion at the phalangeal joints in the (A) crimp grip and (B) slope grip.

The Hand 1 proximal phalanges also show a human-like thick dorsal cortex that may represent a manipulation signal; a pattern not seen in *H. naledi* intermediate phalanges (in which the cortical bone is (re-)modelling in response to greater stress associated with rock climbing that 'overrides' loading from manipulation). These differing patterns and morphology between the proximal and intermediate phalanges are coupled with a human-like pattern of cortical thickness across the shaft in both the proximal and intermediate phalanges, as such it would be parsimonious, to suggest that *H. naledi* was participating in human-like manipulation. During

flexion of the fingers, higher forces are experienced distally in the fingers due to the reduced size of flexor tendons (Qiu & Kamper, 2014), which may explain the increased curvature in the intermediate phalanges and higher phalangeal curvature distally as a compromise morphology between manipulation and locomotion. *H. naledi* manipulation was likely distinct within the fossil record, as they were also using their hands to locomote. This locomotor behaviour may have been rock climbing, or another behaviour not yet described that loads the phalanges in flexion but does so uniquely in the intermediate and proximal phalanges.

The hand of *H. floresiensis* is represented primarily by carpal and phalangeal remains, with a limited preservation of the metacarpals. An initial study of the external morphology of the carpus revealed the remarkably great ape-like morphology (Orr et al., 2013). However, *H. floresiensis* remains are also associated with Oldowan tools, which points towards the manipulative abilities of this taxon. Cortical bone distribution patterns in the intermediate phalanges reveal cortical bone is thickest in patches across the palmar phalangeal shaft, with some intermediate phalanges displaying thick dorsal cortex as well. This palmar cortical thickness is concentrated on the radial and ulnar surfaces, indicating power flexion of the fingers, as well as across the palmar shaft in a few individuals, which may be indicative of the lack of prominent FSRs that function to reduce strain on the palmar shaft (Nguyen et al., 2014). However, the patched nature of the cortical bone distribution makes *H. floresiensis* phalanges unique from what is observed in the extant taxa. This may be due to the internal morphology of the *H. floresiensis* phalanges. The *H. floresiensis* phalanges, along with long bones of the lower limb (personal observations), display a uniquely porous cortex which the patched distribution of cortical bone may be reflecting. The cause of this porosity is not yet understood, however, it is known that increased porosity in cortical bone reduces its performance under mechanical load (Augat & Schorlemmer, 2006; Yeni et al., 1997), which would have had an effect on the locomotor/manipulative behaviours of *H. floresiensis*.

Recent work on the internal structure of the *H. floresiensis* wrist bones revealed that *H. floresiensis* may frequently be adapting transverse grips as a compromise posture between climbing efficiency and effective tool use and making (Bird et al., 2023). Thus, suggesting the manual behaviours used by *H. floresiensis* are unique when compared to our extant analogues, which these results provide further support for. However, it is difficult to confirm the hypothesis of ulnar loading of the digits associated with transverse grips within the digits because we cannot reliably assign digits to the phalanges due to minor variations in phalangeal morphology (Susman, 1979; Patel & Maiolino, 2016). However, it is curious that one specimen (LB6-9) shows a strong dorsal thickness pattern. It is possible that this specimen may belong to the fourth digit, as such is experiencing higher loading and has thicker cortical bone around more of its surface compared to the other specimens. Regardless, the dorsal thickening, whether maximally thick or intermediately thick, coupled with a modern human-like pattern across the shaft may be interpreted as evidence of the manipulatory abilities of *H. floresiensis*. While the proximal phalanges may have a functional signal associated with locomotion, with strong flexion at the PIP joint, the *H. floresiensis* phalanges studied in the sample are of a juvenile and an adult, both of which do not show strong FSRs or phalangeal curvature that is associated with flexed finger postures during locomotion. However, other proximal phalanges that have been found display intermediate curvature and FSRs with a midline keel (Larson et al., 2009). With a mixture of human-like and great ape-like pattern of cortical bone distribution and all other aspects of

cortical bone properties being most similar to humans, the internal structure of the phalanges suggests that the *H. floresiensis* hand was adapted for manipulation but would have been able to use its hand for locomotion as well. The specific hand grips hypothesized to have been employed by *H. floresiensis* during these behaviours (Bird et al., 2023; Orr et al., 2013; Tocheri et al., 2007) cannot be reconstructed from these results due to the lack of associated phalanges.

5.5.4. Neanderthals

The Neanderthal phalanges analysed in this study span a wide temporal and geographic range, as such the variation observed in the cortical bone properties of the sample was expected. The broad pattern of cortical bone distribution within the Neanderthal phalanges was of palmar thickness coupled with intermediate dorsal thickness. Kebara 2 deviated from this pattern and displayed thick cortex on the palmar and dorsal surface. The proximal phalanx of Feldhofer 1 also displayed palmar and dorsal cortical thickness. Within the Near Eastern Neanderthals, further behavioural variation is identified through the cortical bone distribution patterns. The phalanges of Tabun C1 and Kebara 2 are strikingly different, with the Tabun C1 phalanges showing no indication of dorsal cortical reinforcement while the Kebara 2 phalanges have a strong dorsal signal. However, as Tabun C1 is only represented by two intermediate phalanges, it is possible this pattern is not representative of the proximal phalanges of this individual. Within the European Neanderthals, the two populations of southern Neanderthals also show varying patterns. La Ferrassie 2 has thick palmar cortex in the proximal and intermediate phalanges, while the El Sidron phalanges display differing patterns in the proximal and intermediate phalanges.

The proximal phalanges of El Sidron Neanderthals have thick cortical bone on the peak of the FSRs with an intermediately thick dorsal shaft, while the intermediate phalanges have thick dorsal cortex and intermediately thick palmar cortex. The dorsal thickness of the intermediate phalanges is unique to what is observed in Kebara 2, Feldhofer1 and modern humans, as the cortex is maximally thick in patches on the dorso-radial and dorso-ulnar surfaces. Within the proximal phalanges, two individuals do display thick dorsal cortex and they do so in the same patched manner as in intermediate phalanges. Furthermore, the El Sidron phalanges are the only Neanderthal population that has significantly thicker cortex than *H. sapiens*. Despite the El Sidron Neanderthals and La Ferrassie 2 sharing a similar pattern of palmar cortical thickness in the proximal phalanges, the cortical thickness of the El Sidron phalanges is significantly thicker than La Ferrassie 2 proximal phalanges. Similarly, within the Neanderthal sample, only the El Sidron Neanderthals and the Kebara 2 intermediate phalanges display thick dorsal cortical bone, and the El Sidron intermediate phalanges have significantly thicker cortex than the Kebara 2 phalanges. The cortical robusticity of the El Sidron phalanges is also reflected in the degree of their phalangeal curvature, El Sidron are the only Neanderthal population that had a significantly higher degree of curvature than *H. sapiens*. These differences in cortical bone properties may be reflective of slight variations in manual behaviours that may result from the use of different tool technologies across the different populations.

Regardless of the variation present within the Neanderthals, the broad pattern of thick cortical bone distributed in the palmar surface coupled with varying degrees of dorsal thickness is reflective of the opposition of the finger towards the thumb during manipulation (Drapeau, 2015; Key et al., 2018; Marzke, 1997). Coupling this pattern with the thicker cortex of the Neanderthal phalanges relative to *H. sapiens* provides evidence for the forceful loading of the phalanges during

manipulation. While investigation into the trabecular structure of the Neanderthal phalanges has provided support for the use of transverse power grips, precision pinching, and greater loading of digits 2–3 (Stephens, 2018), we do not find evidence of specific grips employed within the cortical structure of the phalanges. There are no significant differences in cortical thickness or properties across the digits that would suggest greater loading of the ulnar digits as is observed in transverse power grips or higher loading in digits 2–3 that would be characteristic of precision grips (Marzke, 1997; Tocheri et al., 2005; Marzke, 2013; An et al., 1985; Bjornerm et al., 2011; Wu et al., 2015; Niewoehner et al., 1997; Niewoehner, 2011; 2006; Shaw et al., 2012; Borel et al., 2016; Marzke et al., 1998). The overall robustness of the Neanderthal phalanges does, however, provide evidence for active palm force generation during manipulation of large objects (Ergen & Oksuz, 2016; Key et al., 2017), in which the hand is highly and forcefully loaded and the digits experience compressive forces as they hold on to the large object (Stephens, 2018; Marzke et al., 1992; Marzke & Wullstein, 1996; de Monsabert et al., 2014; Muhldorfer-Fodor et al., 2017; Ergen & Oksuz, 2016).

While we were not able to detect functional signals relating to specific grips during manipulation, the different grip types were identified in the trabecular structure which was also highly variable within the Neanderthals (Stephens, 2018). As such, it is possible that if the trabecular structure of the Neanderthal populations included in Stephens' (2018) work was studied separately for each population, we may be able to detect differences in trabecular morphology which coupled with the cortical bone morphology results could provide more information on the grasp and grip types employed by the variable Neanderthals. Furthermore, the varying external morphology across the different populations may be distributing the loads of similar grips across the phalanx differently. For example, The El Sidron phalanges are radioulnarly broad and have dorsopalmarly prominent FSRs while the Kebara 2 phalanges are narrower and have FSRs that are prominent in radioulnar width, which would have an impact on load transmission (Nguyen et al., 2014). Overall, my results suggest that loads associated with Neanderthal manipulation are distinct from those of modern *H. sapiens* but are highly variable within the Neanderthals. This distinction and variation provide some support for the morphological divide in the northern and southern Neanderthals but make it challenging to infer how this variation relates to specific manual postures and behaviours.

5.5.5. Conclusions

The external morphology of the proximal and intermediate phalanges in fossil hominins represent a transition in manual behaviours, from using the hand during locomotion to increasing dexterity and manipulation. This transition is also apparent in the cortical bone morphology of the phalangeal shafts. The shift from a pattern of palmar cortical thickness that is closely related to flexed-finger postures employed during locomotion, to a mix of palmar and dorsal cortical thickness, and finally thick dorsal cortices related to loading during human manipulation allows us to map the evolution of hand use across the fossil record. This transition is not linear and displays a wide and unique mix of morphologies, which could have allowed for a diversity of manual postures and behaviours leading to the evolution of modern human dexterity. However, the manual diversity observed in the fossil hominin record does not have extant analogues, as such it limits our ability to reconstruct hand use because, for example, we do not know the biomechanics of how a hominin with a relatively small hand, human-like manual proportions, and

robust and curved fingers was climbing or using tools. The hand postures employed by fossil hominins may be completely different to what paleoanthropologists reconstruct, and while studying the internal structure helps us reconstruct these behaviours more accurately, more research is warranted to understand how loads related to locomotion and manipulation are dissipated across morphologically variable phalanges.

Chapter 6 – Discussion and conclusions

Within the hand, the phalanges of digits 2–5 can be used to reconstruct manual behaviours, as they are the first point of contact between the substrate/object and the hand during majority of primate manual postures and behaviours. Phalanges remain relatively understudied when compared to the carpus and the metacarpus (Bird et al., 2022; Dunmore et al., 2019; Orr, 2016; Tocheri et al., 2007; Tsegai et al., 2013), but form–function links have been observed in the cortical and trabecular morphology of the phalanges (Doden, 1993; Matarazzo, 2015; Stephens et al., 2018). A detailed analysis of the functional morphology of the internal structure of the phalanges has yet to be explored but is needed as recent discoveries of fossil hominin phalanges have come to light (Kivell et al., 2011; 2015; Tocheri et al., 2007). As such, the cortical bone structure of the proximal and intermediate phalanges of digits 2–5 was studied in detail in this thesis, with the goal of reconstructing fossil hominin manual behaviours. The first aim of this thesis was to explore if and how the cortical bone structure of the proximal and intermediate phalanges of digits 2–5 differs in extant great apes in relation to their habitual manual postures and behaviours (Chapters 3–4). Within this extant comparative context, I investigated fossil hominin phalangeal cortical bone structure to infer their behavioural repertoires (Chapter 5). A brief summary of the results related to these aims is provided below, along with a broader discussion of the functional and evolutionary implications.

6.1. Functional morphology of phalangeal cortical bone in extant hominids

Exploration of proximal and intermediate cortical bone morphology across extant hominids (including humans) clearly demonstrated cortical differences that correspond with the presumed loading associated with differences in habitual manual postures and hand use behaviours. I discuss the results of each extant taxa below.

6.1.1. *Pongo* phalangeal cortical bone and behavioural variability

Pongo is the most arboreal great ape and although its locomotor repertoire is typically summarized simply as suspensory, but orangutan locomotor repertoire is more diverse (Thorpe & Crompton, 2006). Orangutan arboreal hand postures are poorly (and not easily) studied but are likely more variable than typically reported (McClure et al., 2012; Rose, 1988). Within this diversity, presumed forceful power grips are used by orangutans as they try to navigate their arboreal environment. The fingers are flexed and wrapped around the superstrate with the body below it, in which joint reaction forces along with muscular and gravitational forces are loading the phalanges. My results are consistent with the employment of flexed–finger postures during arboreal behaviours (e.g., suspension, climbing, clambering) and confirm previous interpretations of the biomechanical efficiency of orangutan phalangeal shape (Susman, 1979). Cortical bone in the proximal and intermediate phalanges of orangutans is thickest at the FSRs and the region proximal to the trochlea, with low cross–sectional properties and thin phalangeal cortex when compared to the other extant hominids included in this study. Thick cortical bone proximal to the trochlea is associated with attachment sites of collateral ligaments that stabilise the phalangeal joints. This cortical bone morphology is coupled with highly curved phalanges and FSRs that are located opposite the maximum arc, which is an optimal location to help keep the flexor tendon in line with joint reaction forces and to prevent bowstringing of the flexor tendons (Susman, 1979). This external morphology allows load associated with locomotory flexed–finger postures in

suspension to be dissipated across the phalanx efficiently (Nguyen et al., 2014; Richmond, 2007; Susman, 1979). As such, the external morphology and cortical bone of orangutan phalanges may already be well-adapted to the loads associated with their habitual arboreal behaviours that thick cortex might not be needed (Ruff et al., 2006; Susman, 1979). Across the proximal and intermediate phalanges of digits 2-5, cortical bone distribution and thickness does not differ, which is consistent with the equal loading of digits 2-5 during arboreal behaviours using hook, power, and double-locked grips. However, the PP2 of some individuals demonstrates a radial concentration of thick cortex, which may potentially reflect the relatively greater extension of the second digit during the grasping of thin branches (Napier, 1960). In a zoo-based study, the long fingers of orangutans have been observed to grasp thin branches and substrates using a diagonal double-locked grip, in which the second metacarpal and proximal phalanx are relatively more extended compared to the ulnar digits that are highly flexed (Napier, 1960). However, as the radial concentration of thick cortical bone associated with the greater extension of the second digit is only observed in the proximal phalanx, this pattern could simply be reflecting normal variation in extant orangutans.

A larger sample of orangutan phalanges will help elucidate whether this is a functional pattern reflecting variable hand postures and manual behaviours of orangutans or not. The complexity of the orangutan arboreal habitat should lend itself to a variety of hand postures required to effectively grasp substrates of varying sizes, and if the hyperextended second digit pattern proves to reflect this variation, we would have a functional skeletal signal supporting the observational studies of diverse orangutan behavioural repertoires.

6.1.2. Gorilla

Gorilla primarily uses its hand to locomote terrestrially using knuckle-walking, touching down with the dorsum of their intermediate phalanges with their body mass atop it (Inouye, 1994; Remis, 1994; Schaller, 1963; Thompson et al., 2018; Tuttle, 1967). The ground reaction forces, gravitational forces, and the support of the body mass above the hand results in high forces and stress experienced by the phalanges (Inouye, 1994; Matarazzo, 2013; 2015; Tsegai et al., 2013; Wunderlich & Jungers, 2009). In order to effectively deal with these high forces, the phalanges must be stable throughout bouts of locomotion, stability that is provided by the soft tissue anatomy. The current understanding of the biomechanics of gorilla knuckle-walking is consistent with my results. I found that the pattern of cortical bone distribution across the proximal and intermediate phalanges of digits 2-5 is of thick cortical bone occurring in patches across the FSRs and proximal to the trochlea, with thick cortex in the intermediate phalanges often across the entire length of the FSRs. Gorilla phalanges also have the thickest cortex and strongest CSG properties within the hominids and demonstrate no differences in cortical bone morphology across the digits, with the exception of the significantly lower CSG properties of the fifth digit compared to the third. Some individuals have an asymmetrical pattern of thick cortical bone in the second and fifth digit, with the former showing an ulnar concentration and the latter showing a radial concentration. The pattern of cortical bone distribution is consistent with the recruitment of soft tissue structures that provide a stable platform for knuckle-walking. Lack of activity of the flexor muscles during knuckle-walking has been noted (Tuttle et al., 1972; Susman & Stern, 1979), although the flexor tendons do get pulled palmarly when the hand is in a knuckle-walking position (Leijnse et al., 2021; Preuschoft, 1973; Susman, 1979; Susman & Stern, 1979; Tuttle, 1969a). In a knuckle-walking position, the DIP and PIP joints are highly flexed, which pulls the

flexor tendons away from the palmar surface of the bone, reducing biomechanical advantage (Doyle, 2001). To counteract this palmar pulling of the tendons and to maintain biomechanical advantage, the pulleys and ligaments that hold the tendon in place and attach to the phalanges are being stretched and loaded (Leijnse et al., 2021). Particularly, the second and fourth annular pulleys and the collateral ligaments of the interphalangeal joints are loaded. The annular pulleys work to keep the flexor tendon in line with the joint axis, which decreases the moment arm, allowing for optimal force transmission during finger flexion (Leijnse et al., 2021) while the collateral ligaments provide lateral stability to the phalangeal joints, that is essential for the intermediate phalanx to accommodate high loads during knuckle-walking (Ayhan & Ayhan, 2020). Furthermore, the *Gorilla* palm-back knuckle-walking posture has been shown, in zoo-housed individuals, to load the fingers more equally (compared to *Pan*), with the highest pressure/force experienced in the midline of the hand (Inouye, 1994; Matarazzo, 2013; Preuschoft, 1973; Thompson et al., 2018). However, the more equal loading of the gorilla hand is relative to the variable patterns of *Pan*, but differences in loading across the gorilla digits has been noted, with the fifth digit shown to experience relatively lower pressures compared to digits 2-4 (Matarazzo, 2013; Susman & Stern, 1979; Thompson et al., 2018). My results are in line with these biomechanical studies, as only the cross-sectional properties of the fifth digit were significantly lower when compared to the third digit, but not when compared to digits 2 or 4. The midline loading of the hand during knuckle-walking is further confirmed by the asymmetry in cortical bone distribution pattern of digits 2 and 5, which has also been observed in the heads of the second and fifth metacarpals (Dunmore et al., 2019).

Given this evidence in the gorilla phalanges, it can be suggested that the phalangeal cortical bone morphology of gorillas is primarily associated with knuckle-walking hand posture and loading, rather than less frequent arboreal locomotion. *Gorilla* phalangeal cortex is thickest at the attachment sites of ligaments and pulleys loaded during knuckle-walking while the rest of the shaft is relatively thinner. In contrast, *Pan* cortical bone is thickest across the entire length of the FSRs and the shaft is intermediately thick, potentially reflecting both knuckle-walking and arboreal behaviours (MacKinnon, 1976; Badrian & Badrian, 1977; Susman, 1984; Doran, 1992; Hunt, 1992). As discussed earlier, a recent experimental study demonstrated the loading of the annular pulleys during knuckle-walking (Leijnse et al., 2021), which the *Gorilla* cortical pattern reflects but the *Pan* pattern does not. These differences may reflect the impact of external morphology in the distribution of loads during similar behaviours, with *Gorilla* proximal and intermediate phalanges being relatively straighter and with significantly more prominent FSRs compared to *Pan*. For example, the relatively flat phalanges of *Gorilla* are used to argue their lack of arboreal behaviours, but *Gorilla* phalanges have the most prominent FSRs within the hominids (Susman, 1979; Syeda et al., 2021). If *Gorilla* FSRs were not as prominent, it is likely that the *Gorilla* phalangeal shaft would be intermediately thick rather than low in thickness, resembling the *Pan* pattern, which would then impact our interpretation of African ape phalangeal functional morphology.

It is important to note, however, that the same soft tissue anatomy that is shown to be loaded during knuckle-walking is loaded during arboreal behaviours as well (Leijnse et al., 2021; Susman & Stern, 1979), making it difficult to determine whether the palmar thickness of *Gorilla* is associated with knuckle-walking or a reflection of loads associated with arboreal grasping with relatively straight phalanges. The prominence of the FSRs is generally associated with a greater

degree of arboreality (Susman, 1979; Patel & Maiolino, 2016; Nakatsukasa et al., 2003; Nguyen et al., 2014). On the one hand, the morphology of *Gorilla* FSRs can be used to support the interpretation that the palmar signal of cortical bone thickness reflects their arboreal behaviours rather than knuckle-walking, particularly due to the fact that the flexor muscles have been shown to be minimally activated during knuckle-walking (Susman & Stern, 1979). On the other hand, the more prominent FSRs may be providing a larger surface on which to dissipate the high loads associated with knuckle-walking, and thus this palmar pattern coupled with the stretching and loading of the annular pulleys during knuckle-walking may be reflecting both terrestrial and arboreal hand use. Furthermore, if the cortical bone morphology was reflecting a knuckle-walking signal, then cortical bone morphology of the proximal and intermediate phalanges should have differed as they are positioned and experiencing loads differently. Thus, based on the results presented in this thesis, I cannot confidently attribute the cortical bone morphology of *Gorilla* phalanges as primarily reflecting knuckle-walking since *Pan* also habitually knuckle-walks but with different external and internal phalangeal morphology (see below). My results indicate that caution needs to be applied when reconstructing specific manual behaviours from phalangeal shaft cortical bone alone and that it is important to consider phalangeal shape as well. Specific manual behaviours have been reconstructed from trabecular bone variables across different elements of the hand (Matarazzo, 2015; Dunmore et al., 2019; Bird et al., 2022; Tsegai et al., 2013; Chrichir et al., 2017), and thus combining phalangeal shaft cortex with its trabecular structure may provide more information and nuance regarding the hand use behaviours and, particularly, the differences between the African apes. The addition of a larger sample of gorillas to conduct comparisons across different subspecies and between females and males may allow us to tease apart the knuckle-walking from the arboreal signal within the gorilla hand.

6.1.3. *Pan*

The locomotor repertoire of *Pan* is characterised primarily by knuckle-walking and typically a higher degree of arboreal behaviour compared to gorillas (Badrian & Badrian, 1977; Doran, 1992; 1996; Hunt, 1992; MacKinnon, 1976; Sarringhaus et al., 2014). Due to the higher frequency of knuckle-walking relative to their arboreal behaviours, I expected similar patterns of cortical bone morphology in the *Pan* phalanges as observed in the gorilla phalanges. This was not the case. My results indicate differing patterns of cortical bone distribution within the African apes, but also across the digits within each genus. I found that *Pan* cortical bone is thick throughout the entire length of the FSR, proximal to the trochlea, and is the only extant taxa that displayed differences in cortical bone thickness across the hand. Cortical bone thickness of the fifth digit was significantly thicker than the third digit, potentially reflecting the differing loading of digits during knuckle-walking and the role of external morphological features in dissipating those loads. *Pan* knuckle-walking differs from *Gorilla* knuckle-walking in that they tend to employ both palm-in and palm-back postures (Doran & Hunt, 1996; Doran, 1996; Hunt, 1992; Inouye, 1994; Matarazzo, 2013; Sarringhaus et al., 2014). During palm-in knuckle-walking, zoo-housed *Pan* employs a 'rolling' method in which the digits touchdown ulnoradially, while during palm-back knuckle-walking, *Pan* places its third digit in front of the rest. However, during both forms of knuckle-walking, the fifth digit is not frequently used (Inouye, 1994; Matarazzo, 2013; Wunderlich & Jungers, 2009). Within *Pan*, knuckle-walking is not as well studied in bonobos, but zoo-housed bonobos have been observed to use the 'rolling' method during knuckle-walking and recruit the fifth digit more frequently than chimpanzees (Samuel et al., 2018). Regardless of the hand postures

employed during knuckle-walking (palm-in vs. palm-back) and substrate used (terrestrial vs. arboreal), peak pressures are lowest in the fifth digit which is associated with the early touchdown and loading of the fifth digit during a gait cycle (Wunderlich & Jungers, 2009). The inconsistent use of the fifth digit during *Pan* knuckle-walking may explain why the relative cross-sectional properties of the fifth digit are lower than the third digit, despite having thicker relative cortex than the third digit. The phalanges of the fifth digit possess a lower degree of phalangeal curvature and less prominent FSRs compared to the radial digits, which may lead to thicker cortex.

Differences in phalangeal cortical bone morphology between the African apes may potentially reflect differences in the frequency of arboreal behaviours of the two genera, rather than a knuckle-walking signal in morphologically variable phalanges. Thickness across the FSRs coupled with an intermediately thick shaft of the *Pan* phalanges compared to the patched palmar thickness and relatively thinner shaft of the *Gorilla* phalanges can be considered as evidence of greater recruitment of the flexor muscles during arboreal grasping. During climbing behaviours, wild chimpanzees have been observed to employ power grips and diagonal power grips, and during suspensory behaviours, zoo-housed bonobos contact the substrate with all digits (Neufuss et al., 2017; Samuel et al., 2018). I interpret differences in phalangeal cortical bone morphology between the African apes as evidence of arboreal behaviours rather than knuckle-walking with differing phalangeal external morphology for two reasons. Firstly, phalangeal structure has been experimentally and developmentally shown to be a plastic feature capable of reflecting function (Richmond, 2007; Nguyen et al., 2014). Therefore, the greater curvature of *Pan* compared to *Gorilla* is best interpreted as evidence of the greater arboreality of *Pan* (but see Wallace et al. 2020). Secondly, experimental work has shown that the flexor muscles are not as active during knuckle-walking as they are during arboreal climbing/suspensory behaviours (Susman & Stern, 1979), and while there are soft tissue structures that are loaded/activated during knuckle-walking, they are restricted to certain regions across the phalanx (i.e., annular pulleys and ligaments) and likely do not induce as much stress on the phalanx as compared to activation of flexor tendons arboreal locomotion. The biomechanics and functional role of soft tissue structures, such as ligaments and pulleys, during different manual behaviours (locomotion and manipulation), needs to be studied in detail to show their impact on skeletal morphology (e.g., Tatara et al., 2014). In summary, *Pan* proximal and intermediate phalanges suggest phalangeal cortical bone and morphology is adapted and more consistent with both loading of the phalanges in knuckle-walking and arboreal behaviours with differences across the digits associated with variable loading during knuckle-walking.

6.1.4. *Homo sapiens* – identification of specific grips

The human hands analysed in this thesis demonstrate the most distinct cortical bone morphology within the sample of extant hominids, reflecting the primary use of the hand for manipulation and not locomotion. My results found a distodorsal pattern of cortical thickness in the proximal and intermediate phalanges, and more surprisingly, no differences within the digits. The concentration of cortical thickness at the distodorsal region is consistent with the habitual use of flexed-finger postures during manipulation in a relatively straight phalanx (Preuschoft, 1973). The lack of curvature results in high bending forces experienced by the phalanx, with the large bending forces on the dorsal surface resulting in thicker cortex in the region (Oxnard, 1973; Preuschoft, 1973; Richmond, 2007). Human manipulation has been studied extensively in regard

to the hand grips used during daily modern human life as well as stone tool use and production (de Monsabert et al., 2012; Key, 2016; Key et al., 2020; Rolian et al., 2011; Sancho-Bru et al., 2014; Vigouroux et al., 2011; Williams et al., 2012; Williams-Hatala et al., 2018). These studies have revealed employment of various grips which variably employ and load the digits across the hand, with the thumb and digits 2 and 3 experiencing the greatest loads (de Monsabert et al., 2012; Dollar, 2014; Feix et al., 2015; Key et al., 2018; Rolian et al., 2011; Sancho-Bru et al., 2014; Williams et al., 2012; Williams-Hatala et al., 2018). However, the results of this thesis do not reflect variable digital loading during manipulation as there are no significant differences in cortical bone distribution, thickness or cross-sectional properties across the digits. The only exception is the fifth digit, with significantly lower cross-sectional properties compared to the third digit, which is not unexpected as the more ulnar digits, and particularly digit 5, has been shown to not be active throughout the length of a manual task (De Monsabert et al., 2012; Rossi et al., 2012; Sancho-Bru et al., 2014). Furthermore, the lack of differences across the human digits could potentially reflect the variable employment of different power and precision grips by our human sample, which includes pre-industrial, post-industrial, and fossil *H. sapiens*. The fifth digit has been experimentally shown to be recruited frequently during manipulation (Marzke, 1997; Key et al., 2019).

An aim of this thesis was to establish an extant comparative context of phalangeal cortical bone for the reconstruction of fossil hominin manual behaviours, this homogenous cortical bone morphology across the human 2-5 digits needs to be acknowledged. Stephens and colleagues (2018) studied the trabecular structure of different human populations, similar to the sample studied in this thesis, and revealed intense and variable loading in their pre-industrial sample. Dunmore and colleagues (2019) analysed the trabecular structure of human metacarpals, observing signals associated with specific grip types during manipulation. These studies suggest it is possible to detect differences across the digits related to different manual postures during human manipulation, which were not detected in the cortical bone of the phalanges. My results have demonstrated that there is a distinct manipulation signal within hominid phalangeal cortex, but morphology of this cortex cannot identify specific hand grips or variable manual postures associated with manipulation. The fossil and pre-industrial human populations of our sample range from around 80 kya to the 18th century and span geographically from the Czech Republic in the West to Israel in the East, and are presumed to load their hands with greater intensity and differently from the post-industrial populations, which include modern humans primarily from western Europe. Despite the hypothesized differences in hand use and loading, no differences in cortical bone distribution or thickness were observed. Experimental studies of a variety of different manual tasks, such as stone tool use, production, and daily day-to-day tasks involving precision or power grips, have all demonstrated that loads are greatest on the thumb and digits 2 and 3 (de Monsabert et al., 2012; Rolian et al., 2011; Sancho-Bru et al., 2014; Williams et al., 2012; Williams-Hatala et al., 2018). Therefore, despite the temporal and geographic variability of the human sample, I expected a functional signal of differential loading of the digits to be found in the cortical bone morphology.

My results differentiate flexion associated with manipulation in humans compared with flexion associated with locomotion in the great apes, which results in high loads across the palmar phalangeal shaft. The locomotor use of the hand signalled by the cortical bone morphology of the great apes further reflects variation in hand use associated with their behaviours, even within the

African apes that primarily use their hands for knuckle-walking (Doran, 1996; Remis, 1994; Schaller, 1963; Tuttle & Watts, 1985). The current results on the human sample support the identification of broad manual postures in phalangeal cortical bone morphology rather than specific manual behaviours or specific grip types. Specific grip types have been identified in the internal structure of hominid metacarpals (Dunmore et al., 2019; 2020a), as such the study of phalangeal trabecular bone alongside cortical bone may be needed to identify specific grips within the internal structure of the phalanges.

6.2. Insights into phalangeal external form and internal structure

The proximal and intermediate phalanges of non-human primates have external morphological features that have been interpreted as advantageous for dissipating the loads associated with arboreal behaviours. These external morphological features are: (1) phalangeal curvature, (2) FSRs, and, (3) for the intermediate phalanges only, the median bar with its accompanying lateral fossae (Jungers et al., 1997; Nguyen et al., 2004; Patel & Maiolino, 2016; Richmond, 2007; Susman, 1979). As such, the presence, prominence, or lack of these features on fossil hominin phalanges has led to inferences about the locomotor repertoire and manipulative abilities of fossil hominins (e.g., Begun et al., 1994; Kivell et al., 2015; 2018a; Leakey et al., 1964). However, how these features individually, and in combination, function to dissipate loads associated with different manual behaviours is not well understood. The biomechanics and functional role of these features have been discussed in detail in Chapters 1, 3 and 4, so here I will focus on how the results presented throughout this thesis have provided new insight into the role of these features. Starting with phalangeal curvature, I expected a relationship between the degree of phalangeal curvature and cortical thickness, which was not found. As phalangeal curvature functions to reduce overall bending stress experienced by the phalanx during flexed-finger postures, I expected individuals with a greater degree of curvature to have thinner cortex compared to individuals with less phalangeal curvature. In both the proximal and intermediate phalanges, the relationship between phalangeal curvature and cortical thickness was not significant across most taxa. The limited correlation between cortical thickness and curvature should not necessarily be construed as a lack of a functional role of phalangeal curvature, which has been previously suggested (Wallace et al., 2020). Instead, this lack of statistical significance may be affected by the fact that the analyses pooled phalanges from digits 2-5 together. A larger sample size is needed to conduct digit-specific analyses with appropriate statistical power to interpret the results in a functionally meaningful manner.

Based on the biomechanical function of the FSRs (Nguyen et al., 2014), I also predicted that, within taxa, individuals with prominent FSRs will have a relatively thinner shaft compared to individuals with smaller FSRs. Qualitatively assessing the phalangeal cortical bone distribution maps within each taxon does suggest the size of the FSRs impacts phalangeal shaft thickness, particularly within *Pan* and *Gorilla* individuals. Within *Gorilla* there is also statistical evidence that the size of the FSRs may impact cortical thickness. Comparisons of palmar and dorsal cortical thickness, reveal digits 2 and 5 of *Gorilla* display thicker palmar cortex relative to dorsal cortex, which may be reflecting the functional role of the FSR in reducing strains on the palmar shaft, as the FSRs of digit 2 and 5 are not as prominent as digits 3 and 4 (Syeda et al., 2021). Furthermore, a preliminary analysis of the palmar features of the intermediate phalanges suggest no significant relationships between the prominence of these features and cortical thickness. An increased

sample size may help us determine whether there is a strong relationship between these phalangeal features, that are regarded as functionally informative, and cortical thickness.

The prominence of these external morphological features differs between the proximal and intermediate phalanges within each taxon. For example, *Gorilla* intermediate phalanges are straight in comparison to their proximal phalanges but have strong palmar external morphological features, while *Pongo* has highly curved proximal and intermediate phalanges but lack prominent palmar phalangeal features. The differences in proximal and intermediate phalangeal morphology within taxa should then be reflected in their phalangeal cortex as these external morphological features are thought to reduce strain experienced by the phalanx and are generally less developed in intermediate phalanges. However, differences in cortical bone morphology of the proximal and intermediate phalanges are only reflected in average cortical thickness and not other aspects of phalangeal cortex (distribution pattern, cortical thickness pattern across the shaft, and CSG properties). Across the extant and fossil sample included in this thesis, scaled average cortical thickness of the intermediate phalanges is always higher compared to the associated proximal phalanx, which may be due to the less developed palmar external morphology of the intermediate phalanges. Furthermore, as discussed in Chapter 4, the variation in FSR, median bar, and lateral fossae morphology across our extant sample merits further experimental study of these features to truly understand how loads are dissipated across these features, if/what is the biomechanical significance of these features, and how they are developed throughout ontogeny.

Previous studies have demonstrated that phalangeal curvature responds to loads throughout ontogeny (Richmond, 1998). Therefore, future studies that focus on the timing and development of these external features throughout ontogeny in relation to hand use and locomotion would offer a test of the 'functional' role and plasticity of the features. My preliminary observations of *Gorilla* and *Pan* external phalangeal morphology at different developmental stages (i.e., neonates, infants, juveniles, and adults) revealed that there is substantial variation in the development and timing of these features in both species. For example, for both *Pan* and *Gorilla*, some juvenile individuals displayed a median bar with lateral fossae, some with just a median bar, and other times the shape of the lateral fossae was etched into the palmar surface but there was no median bar. As such, using the presence and/or prominence of these features in fossil hominin phalanges as definite indicators of arboreal behaviour may be a premature assessment of the locomotor repertoire of fossil hominins. Using these features in conjunction with other aspects of morphology will allow for a more holistic reconstruction of fossil hominin behaviours.

6.3. Phalangeal curvature of *Homo sapiens*

The cortical bone distribution patterns of human phalanges are distinguished from the non-human great apes due to their strong dorsal thickness. I interpret this dorsal thickness as reflecting the dissipation of loads associated with flexed-finger postures of manipulation across a relatively straight phalanx. Flexed-finger postures result in bending forces on the phalanges, where the dorsal surface experiences tension and the palmar surface experiences **compression**, and as curvature works to reduce these forces, relatively straighter phalanx experience higher bending forces (Preuschoft, 1973; Richmond, 2007). This raises the question: if human phalanges habitually employ flexed-finger postures, in which the phalanges experience bending, then why are the phalanges not more curved? An ontogenetic study of phalangeal curvature has shown that

species whose locomotor strategies differ significantly during development have significant differences in phalangeal curvature through growth, while species with consistent locomotor repertoires throughout ontogeny do not have differing values of phalangeal curvature (Richmond, 1998). This suggests a developmentally early impact of locomotor/manual behaviours on phalangeal form (but see Wallace et al., 2020). Studies of Western, industrial societies reveal juvenile modern humans do not participate in forceful manual activities as juveniles (Connolly & Elliot, 1972; Häger-Ross & Rösblad, 2002), which may be why they do not possess curved phalanges. There may be genetic factors at play regarding phalangeal curvature (see Wallace et al., 2020), but an alternative explanation for the low degree of phalangeal curvature in humans could be the frequency and magnitude of loads incurred on the phalanx. Synek and colleagues (2019) used musculoskeletal modelling to show internal load of the tendon relative to external fingertip force was consistently higher in a bonobo than in a human. Using this data, it can be proposed that loads associated with flexed-finger manipulation in humans are not of a high enough magnitude to stimulate plasticity in curvature but may be sufficient enough to simulate cortical remodelling in the distodorsal region of the proximal and intermediate phalanges. Future studies on humans that highly load their hands would help us understand the biomechanics and plasticity of *H. sapiens* phalanges (e.g., Sylvester et al., 2006).

6.4. African ape phalangeal cortical thickness in relation to cross-sectional properties

This thesis investigated how mean cortical bone thickness and CSG varied along the phalangeal shaft (proximal to distal) across the extant sample and found patterns that were consistent with differences in manual behaviours. Within these patterns, African apes displayed a proximodistal increase in cortical thickness in both the proximal and intermediate phalanges, which slightly differs from the *Pongo* pattern in which there is a decrease in cortical thickness past the midshaft before increasing proximal to the trochlea. The great ape pattern differed from humans, as human cortical thickness across the shaft increases proximodistally up until the midshaft and decreases distally from there. This thick cortex at the distal end of the phalanges is coupled with strong cross-sectional properties at the proximal end of the bone. Strong rigidity and resistance against torsion on the proximal end of the bone may be reflecting the dorsoproximal transfer of loads, with the proximal end structurally adapted against greater loads (Matarazzo, 2013; 2015). The lower cross-sectional properties at the distal end of the bone coupled with thick cortices reflect the opposite phenomenon as the proximal end, suggesting that the distal end of the bone is not structurally adapted to resist the considerably high compressive loads associated with knuckle-walking, as such cortical bone increases its thickness in the distal region of the bone (Matarazzo, 2013; Ruff et al., 2006). Using CSG properties to make the inferences that the distal end of the bone is not structurally adapted as well as the proximal end, could potentially be supported by the reduced size of the medullary cavity distally. Reduction of the medullary cavity reduces the structural integrity of the bone and makes the bone less resistant to bending forces, thus affecting the efficient distribution of loads across the bone, which could then lead to a thicker cortex to effectively deal with the high loads associated with African ape locomotion (Lieberman et al., 2004; Ruff et al., 2006). An alternative explanation for the thick distal cortex could be the role of soft tissue structure in dissipating loads. Experimental work has shown that during extreme flexion, like that observed during knuckle-walking, greater joint contact forces occur at the phalangeal joints and that these forces are highest in the distal end as there is a reduction in tendon mass (Qiu & Kamper, 2014). As such, the thick cortex at the distal

end of the phalanges may be a compensatory mechanism for the relatively smaller soft tissue structures at the distal end of the bone.

6.5. Extant non-human great ape sample

The non-human great ape sample studied throughout this thesis consisted of wild-shot individuals. Despite having access to micro-CT scans of zoo-housed individuals, only wild-shot individuals were included as they are likely to accurately represent manual behaviours in the wild compared to zoo-housed individuals. Zoo-housed individuals adapt to their local environment, which is restricted in zoo-settings, likely underscoring the natural environment and the variety of behaviours that result from an animal being in its natural habitat. In studies of internal bone structure, wild individuals are preferred and more commonly used (e.g., ADD REFS) because they give us a chance to capture the full range of variation of natural primate behaviours. Within palaeoanthropology, a comparative extant sample is helpful in reconstructing fossil behaviours, with an ideal comparative sample consisting of wild individuals, as the fossil hominins being studied lived in their natural environments, like wild specimens. While wild-shot specimens are ideal for these studies, access to a complete, associated set of bones of a wild, individual is not entirely possible, particularly with small bone such as phalanges, due to preservation and collection of skeletal material in a natural, wild setting.. In this scenario, there is a higher chance of zoo-housed individuals having all their skeletal material preserved. The study of zoo-housed individuals also has other benefits. Firstly, behaviour of zoo-housed individuals could be monitored and studied consistently and closely, as there is a greater, comprehensive understanding of their environment and behaviour that can be well documented, which is rare in wild environments. Secondly, much of the experimental and kinematic work is done on zoo-housed individuals (ADD REFS), Furthermore, comparison amongst zoo-housed and wild individuals within each taxon could also be helpful. While here we decided to only include wild-shot specimen because we believed they better addressed our questions and long term goal of establishing a comparative context for fossil hominin behavioural reconstruction. There are circumstances and instances where the inclusion of captive individuals would be beneficial as well.

6.6. Implications for fossil hominin behaviours

Fossil hominin hand use has been traditionally simplified as either a primitive, ape-like hand used for locomotion or a modern human-like, dexterous hand capable of forceful manipulation. This dichotomous view ignores the variation present in fossil hominin hands and limits our interpretations to a hominin hand that was either effective for locomotion or manipulation but not both. Increasing discoveries of hominin hand fossils, and particularly relatively complete, associated hand skeletons, coupled with the results presented in this thesis suggest a more nuanced view of hominin hand use and evolution is needed. Recent discoveries of fossil hominin hands of *Australopithecus sediba* (Kivell et al., 2011; 2018a), *Homo naledi* (Kivell et al., 2015), and *Homo floresiensis* (Tocheri et al., 2007; Larson et al., 2009) evidence mosaic morphology that is unique within the fossil hominin record (for a review see Kivell et al., 2022). Phalangeal cortical bone morphology of these fossil hominins suggest multiple transitions in manual behaviours, instead of a linear trajectory towards increasingly dexterous manipulation across time. This

evidence is consistent with a diversity of manual behaviours across the fossil hominin record (summarised in **Table 6.1**), in which hominins were likely using their hands for locomotion as well as frequently recruiting them for manipulation.

This variation is present within every fossil hominin species analysed in this thesis. As stated above, we may not be able to equate cortical bone morphology to specific grip types, but instead to general, habitual hand postures. In my analyses, certain fossil hominins can be grouped with regard to their general cortical bone distribution pattern and thickness. Based on the results, I suggest that *A. afarensis*, *A. africanus*, and *H. habilis* phalangeal cortical bone reflects a hand used habitually for arboreal locomotion (although it is important to note that a holistic review of all preserved hand morphology in these fossil hominins suggests that this locomotory hand use was likely distinct in each taxon as well; Alba et al., 2003; Marzke, 1997; Ward et al., 2012; Green & Gordon, 2008; Kivell et al., 2020; Ostrofsky & Richmond, 2015; Leakey et al., 1964; Napier, 1962a; Susman & Creel, 1979). The inference that these species were habitually using their hands for locomotion is based on the great-ape like palmar cortical distribution pattern, cortical thickness pattern across the shaft, and cortical thickness values, as well as intermediately curved phalanges. However, these locomotor signals do not detract from their potential manipulative abilities. *A. sediba* and possibly *A. afarensis* have intrinsic hand proportions that would facilitate opposition of the thumb to the fingers during manipulation, while the OH 7 *H. habilis* hand was found in close proximity to stone tools (Leakey et al., 1964; Almécija & Alba, 2014; Rolian & Gordon, 2013). Within the australopiths, *A. sediba* phalanges also suggest a hand used for arboreal locomotion but are distinguished from the other australopiths due to the fifth digit demonstrating a human-like manipulation signal in its cortical bone distribution pattern and the overall human-like cortical thickness patterns across the shaft in all the digits...

Furthermore, australopith and early *Homo* hand use and behaviours should also be reconstructed within the context of the archaeological record. There is an extensive record of stone, and in some cases, bone, tool technologies that span large temporal and geographic ranges. Early tool industries associated with the fossil hominin record have been thought to play a key role in shaping the function and morphology of the hominin hand. The earliest artefacts are dated to around 3.3 mya with the Lomekwian stone tool industry, which is defined by having large cores and flakes, as well as the presence of percussive tools (Harmand et al., 2015). Due to the large size of the Lomekwian tools, passive hammer and bipolar techniques are thought to be used to produce these tools (Harmand et al., 2015). The Oldowan industry is also well-represented from 2.6 mya (Braun et al., 2019; Semaw, 2000; Semaw et al., 1997), which includes a wide diversity of flakes, retouched flakes, flaked stones, and hammerstones (Schick & Toth, 2006; Shea, 2013). This diversity of Oldowan tools is represented in the techniques associated with the production of these tools, which have been classified as hard hammer percussion, striking core against the anvil and bipolar reduction (e.g., Braun et al., 2019; de la Torre & Mora, 2018; Stout et al., 2010). However, both these tool industries also share the bipolar reduction technique, in which a core is positioned on an anvil and then struck by a hammer stone, producing flakes (Braun et al., 2019; Harmand et al., 2015) and the passive hammer technique (Schick & Toth, 2006; Stout et al., 2010). The temporal range of the Lomekwian and Oldowan stone tool industries places them in the same temporal range as australopiths and early *Homo*. As such, the similarities in stone tool-making techniques could potentially indicate that australopiths and early *Homo* may have been using similar techniques to produce tools, suggesting there may be shared characteristics

within the phalanges of these species. It is probable that loading associated with locomotion will override signals of manipulation, but results presented in Chapter 5 demonstrate that it is possible to detect a great-ape like signal of locomotion and a human-like signal of manipulation in some fossil hominin phalanges. For example, within the cortical bone distribution patterns of *A. sediba* phalanges, only the fifth digit has a human-like signal, but the pattern of human-like cortical thickness across the phalanx along with relatively low CSG properties indicates a non-locomotory use of the hand. In comparison, *A. afarensis*, *A. africanus*, and *H. habilis* not only demonstrate a pattern of cortical bone distribution similar to the great apes, but all other aspects of their cortical bone morphology also aligns them closer to the great apes than humans, providing no indication of a manipulatory use of the hand. These differences in cortical bone morphology across the australopiths and early *Homo* may be reflecting differences in time spent using the hand for locomotion compared to manipulation across these species.

Further mosaic signals are found in *H. naledi*, which possessed differing patterns in the proximal and intermediate phalanges, suggesting a unique loading pattern not yet observed within the fossil hominin record. *H. naledi* phalangeal cortical bone suggested manual postures in which the distal end of the digit was highly flexed while the proximal end was neutral or slightly flexed, this hand posture is employed consistently during rock-climbing, which has been suggested as a potential locomotor behaviour of *H. naledi* (Voisin et al., 2020). *H. floresiensis* also signals a unique loading pattern of its hand, which has also been demonstrated in the midcarpal joint of the wrist (Bird et al., 2023). It is parsimonious to infer that *H. floresiensis* possessed some level of manual dexterity due to its young age, proximity to stone tools, and cortical bone morphology of the intermediate phalanges (Brumm et al., 2006; Moore & Brumm, 2007). This dexterity would have been quite distinct within the extant hominids and fossil hominins due to the uniquely circular shape of the proximal phalanges and its cortical bone morphology that closely resembles great apes.

I grouped *A. afarensis*, *A. africanus* and *H. habilis* because their phalangeal cortical bone morphology suggested an overarching similarity, while *H. naledi* and *H. floresiensis* have both cortical bone and external morphology that is distinct from each other and all other fossil hominins in my sample. It is possible that the unique external morphology in *H. naledi* and *H. floresiensis* could be a result of founder effects on the predecessor of both species, respectively. Founder effects are thought to cause speciation through geographic isolation of a small population, which shifts selection pressures and increases genetic drift, resulting in a shift of genes that can create novel adaptations (Mayr, 1942; for a detailed review of founder effect speciation see Barton & Charlesworth, 1984 and Gavrillets & Hastings, 1996). Furthermore, the remaining skeletal elements of the hand of both species preserve a distinct mix of morphologies not yet observed in any other taxa, extant or fossil (Kivell et al., 2015; Larson et al., 2009; Tocheri et al., 2007). As reviewed in Chapter 1, distinct combinations of morphologies are also present throughout the skeleton of both species (Berger et al., 2015; Feuerriegel et al., 2017; Jungers et al., 2009a; b; Larson et al., 2009; Marchi et al., 2017). Morphological variability of the *H. naledi* and *H. floresiensis* skeletons makes reconstructing their behavioural repertoires challenging and without a clear phylogenetic context (however see Davies et al., 2020 for *H. naledi* and Aiello, 2010 for *H. floresiensis*), our understanding and ability to reconstruct their complete behavioural repertoire is limited. Although we may be currently limited in the inferences we can draw from these fossil hominin remains, comparative functional studies demonstrate that this mosaic

morphology results in behaviours that do not have extant analogues and likely differed in their performance of similar behaviours (e.g., Bird et al., 2023; Kivell et al., 2015; Tocheri et al., 2007).

Surprisingly, the cortical bone morphology of the Neanderthals was highly variable across the different populations. Morphological variation across different Neanderthal populations has been demonstrated (Dunmore et al., 2020b; Kivell et al., 2018b; Rosas et al., 2006), but as my results were broadly differentiating manual postures among extant hominids, the extent of Neanderthal variation observed was not expected. The Southern European Neanderthals, La Ferrassie 2 and the El Sidron sample, primarily displayed a palmar pattern of cortical bone distribution in the proximal and intermediate phalanges, while the intermediate phalanges of the El Sidron sample displayed a distinct dorsal thickening as well. Feldhofer 1 and the Near Eastern Neanderthals, Kebara 2 and Tabun C1, had strong dorsal cortical thickness throughout the entire shaft along with slight palmar thickness in the proximal and intermediate phalanges. The palmar patterns observed in the Southern European Neanderthals resemble those observed in extant great apes and may challenge our interpretation of palmar distribution of thick cortical bone representing a locomotor signal. However, since Neanderthals were likely not regularly using their hands for locomotion, this pattern may be reflecting the use of power squeeze grips that are thought to be employed frequently by this species (Marzke et al., 1992; Niewoehner, 2006). It could be possible that, in terms of gripping substrates, the hand is in a similar posture while grabbing a branch or a spherical object (e.g., *Pan* grabbing a branch using a (transverse) power grip and a Neanderthal grabbing a hafted spear using a forceful, power squeeze grip). The magnitude of loading between these two behaviours will differ but the manual postures are similar, leading to the palmar pattern of cortical bone distribution in La Ferrassie 2 and the El Sidron Neanderthals. As our Neanderthal samples comprise a large temporal and geographic range, this variation in cortical bone morphology may also be reflecting the variable behaviours of these differing populations. It is difficult to equate the patterns observed in each of the Neanderthal populations to specific manual behaviours as discussed earlier, but the current results demonstrate previously unknown manual diversity within Neanderthals.

Viewing these results through the lens of evolutionary time sheds light on the high degree of variability in fossil hominin manual behaviours. The present evidence not only argues for diversity of manual postures across different fossil hominin genera, but within them as well. Each of the fossil hominin species studied in this thesis likely had distinct manual postures and behaviours, despite having the ability to use their hands for locomotion and manipulation. This probable diversity of manual behaviours would have resulted from the variation and mosaic morphologies of the hand and the upper limb of each species (e.g., Churchill et al., 2018; Larson et al., 2007; 2009). Here, I demonstrate diversity in hand use and the persistence of the locomotor use of the hand within the fossil record, suggesting that the abandonment of arboreal behaviours was not needed for the advent of hominin dexterity.

6.7. Developmental plasticity of the hand in relation to variation of phalangeal shape

All mammals share a general genetic architecture in regard to limb development, and despite the morphological variation observed across mammals, the general pattern of limb development has been genetically conserved throughout mammalian evolution (Shubin et al., 2009). Within the hand, there have been regions that are thought to have a degree of independent development. Hamrick (2012) proposed that the thumb, the distal phalanges, and the digits 2-5 (including their

metacarpals, proximal phalanges, and intermediate phalanges) are independent of each other, allowing for morphological changes in these regions that result in variation of the primate hand. Within the discussion of limb development, serial homology suggests that the genetic regulation of the hindlimb and forelimb are duplicated, resulting in strong covariation between homologous elements across the limbs (Hall, 1995; Young & Hallgrímsson, 2005). For example, covariation/integration between the humerus and femur should be relatively strong, which should be reflected between the radius/ulna and tibia/fibula, along with the hand and foot as well (Young & Hallgrímsson, 2005). Furthermore, the serial homology hypothesis also states distal segments within limbs are thought to be less developmentally constrained with the more proximal elements (e.g., the humerus vs. the hand) (Young et al., 2010). This suggests two things. Firstly, strong covariation between the hand and foot may be reflecting functionally significant and highly selective pressures imposed on one region leading to changes in the other, rather than independent evolution. Secondly, the reduction of developmental constraints on the distal segments of the limbs can provide support for the variation observed across the fossil hominin record. As such, within the hand, the distal most segments (the phalanges) also show variation that may be explained by the processes underlying overall limb development.

A study of limb development in anthropoids has shown that extant hominids and fossil hominins have diverged from the general limb development pattern and have reduced limb integration compared to old- and new- world monkeys, demonstrating a high degree of variability in limb proportions and suggesting that limb segments do not always conform to serial homology (Young et al., 2010). Variations in homologous limb elements are observed across fossil hominins with preserved hands and feet (as reviewed in Chapter 1), the majority of which demonstrate variable morphology in both. I want to emphasize that this discussion on phalangeal shape and fossil hominin phalangeal variation in relation to genetically-regulated developmental processes, is only discussing phalangeal form not the cortical bone morphology of the phalanges. While this deviates from serial homology, fossil hominin phalanges do demonstrate a considerable amount of variation that would support the notion that distal segments are less constrained developmentally. Throughout this thesis, the morphological variability of fossil hominin phalanges has been established, with no one fossil demonstrating external morphology that resembles another, and even within the Neanderthals, this external morphological variation is present. This morphological variation relates to whole phalangeal form, but also to specific features that are thought to have functional relevance (i.e., FSRs, phalangeal curvature, median bar, lateral fossae). While the development of these features is not well understood (as discussed earlier), this variation may have come about as a result of the developmental plasticity of the distal segments. The inference regarding the developmental plasticity of the phalanges due to their distal position in the upper limb is supported by a recent study that highlighted the variation in different segments of the finger (i.e., proximal phalanges and distal phalanges; Dickinson et al., 2023). Differences in shape will result in the dissipation of loads across the phalanx differently, leading to differences in internal bone structure (assumed to result, at least in part, from bone functional adaptation), as such differences in internal morphology should always be analysed in relation to and in context with external morphology. Furthermore, this discussion also does not undermine the functional relevance of plastic external morphological features of the phalanges as there have been multiple comparative studies demonstrating the functional and biomechanical role of these features (Nguyen et al., 2014; Patel & Maiolino, 2016; Richmond, 2007; Susman, 1979). A recent

study suggested phalangeal curvature may be primarily genetically regulated (Wallace et al., 2020), but these inferences were made based on a single individual. As it is stated throughout this thesis, there is a lack of knowledge on the developmental processes that underlie the striking degree of variation present within the fossil hominin record, and working towards understanding the developmental aspects of morphological variability will allow us to reconstruct fossil hominin behaviours with a greater degree of confidence.

6.8. Conclusions

The research projects conducted throughout this thesis were undertaken in recognition of the fact that there was a lack of studies on phalangeal internal structure and morphology. My initial goal with this thesis was to explore the relationship, if any, between the habitual manual behaviours of extant great apes and humans and the cortical bone morphology of the proximal and intermediate phalanges of digits 2-5. The results of the first two chapters demonstrated phalangeal cortical bone is capable of differentiating modern humans from extant great apes, suggesting that the modern human manipulation signal is statistically distinct from the locomotory use of the hand. Furthermore, cortical bone morphology of the extant great apes also differentiated their habitual manual postures.

The second aim was to use this comparative context to reconstruct manual behaviours of fossil hominins. The results suggested that there were multiple transitions in fossil hominin manual behaviours that did not occur linearly, instead, it was likely that fossil hominins were using their hands for locomotion and manipulation but just with varying frequencies. Variation across the fossil hominin phalanges highlighted the diversity of fossil hominin behaviours, diversity that should not be underscored as it provides functional proof of morphology that can be considered a primitive retention. Here, I hope to have emphasized that the relationship between phalangeal morphology and manual postures and behaviours is not as straightforward as perhaps previously thought. Schmitt and colleagues (2016) reviewed the patterns and variability present in the primate hand during locomotion and suggested the variability observed in primate hand postures reflects the flexible use of the hand as an adaptive strategy. This suggests that habitual manual postures may be predicted from hand anatomy, but the habitual postures do not reflect the extent of mechanical flexibility the hand is capable of (Schmitt et al., 2016). The mechanical flexibility of the hand is evident in our fossil sample, the majority of which demonstrate the potential ability to manipulate and use their hands for locomotion, but all of them are also morphologically variable. This project has implications for the inferences of manual behaviours based on external morphology, the evolution of modern human dexterity, the retention of arboreality, and their relationship to the development and adaptation of obligate bipedalism.

6.9. Limitations and future directions

Bone functional adaptation of phalangeal cortex reflects the mechanical environment and loading of hominid fingers (Ruff et al., 2006), but relating signals found within the cortical bone morphology of the phalanges to specific grips and manual behaviours is challenging. The majority of hominid manual behaviours result in similar postures but differing loading of the phalangeal joints and related soft tissue structures. For example, African apes terrestrially knuckle-walk and participate in arboreal behaviours (e.g., climbing, suspension) in which the fingers are in a flexed postures and are experiencing substantial compressive and tensile forces, but loads associated with these differing locomotor behaviours are distinct from each other (Matarazzo, 2015;

Preuschoft, 1973; Tuttle, 1967). *Pan* and *Gorilla* cortical bone is differentiated from each other, but it is not clear whether the functional signals observed represent knuckle-walking postures, infrequent arboreal behaviours, or a combination of both. This problem is further complicated by a lack of detailed knowledge of great ape hand use (Kivell et al., 2022; Marzke, 2013), with much of our data referencing studies conducted on captive, zoo-housed individuals (Leijnse et al., 2021; Matarazzo, 2013; Samuel et al., 2018; Wunderlich & Jungers, 2009). Studies on wild great ape hand use are rare due to the challenging nature of observing manual postures and behaviours but have reported a greater diversity of manual behaviours in the wild than was traditionally described in the literature (McClure et al., 2012; Neufuss et al., 2017; 2018; 2019; Thompson et al., 2018). The inferences made throughout this thesis are generally based on the broad manual behaviours observed and described in behavioural studies and that are likely underrepresenting the true variation of manual behaviours of the studied taxa, but detailed studies on the kinetics of these variable hand postures and behaviours is needed before the data is used to infer specific grips.

A larger sample size may also aid in the identification of specific grips within our sample. Although the sample of associated hominid proximal and intermediate phalanges analysed here are the largest known to me for the analysis of phalangeal internal bone structure, it still likely underrepresents the variable manual behaviours of the great apes. Particularly, additional *Pongo* individuals would be valuable to identify variation in orangutans (McClure et al., 2012), such as the extension of the second digit (Napier, 1960). The inclusion of mountain gorilla individuals would also prove to be useful, as there are detailed studies on mountain gorilla hand use (Byrne & Byrne, 1991; Kinnai & Zimmerman, 2015; Neufuss et al., 2017; 2018; 2019; Thompson et al., 2018). Within our sample, consideration was given to equalise the number of right to left hands and sex of the sample but a larger sample would allow us to analyse potential differences in loading within these intraspecific factors.

An additional limitation of this project is related to the methodology applied. As detailed in Chapter 2, Morphomap analyses cortical bone by placing orthogonal cross-sections across the entire bone. Within our sample these axial cross-sections were placed orthogonally to the long axis of the phalanges which were all anatomically orientated (Profico et al., 2020). This raises an issue regarding phalangeal curvature, many of the phalanges included in our sample are curved (e.g. *Pongo*) and that results in these orthogonal cross-sections in a curved phalanx not being homologous to individuals with straighter phalanges (e.g. *Homo*, *Gorilla*). Furthermore, curvature in the phalanges means the cross-sections being placed are not accurately capturing homologous structure of the phalanx, similar to how a non-orthogonal cross-section placed on a straight phalanx will not be capturing accurate morphology.

The manner in which the data in this thesis was scaled may be considered as another limitation, which has been addressed briefly in Chapters 3 and 4 (Syeda et al., 2023; 2024). In comparative studies of internal bone structure, body mass of each individual is considered an ideal scaling factor, but as that is difficult to obtain many studies have used a geometric mean in place of body mass (e.g., Kivell et al. 2018a; Schilling et al. 2014; Tsegai et al. 2013; 2017b). For this thesis, the data was ultimately scaled by the interarticular length of the phalanx. Interarticular length of the phalanx has not yet been shown to relate to estimations of body mass as there are differences in hand proportions across the great apes (see Patel & Maiolino, 2016

for a review). With the lack of a direct relationship between hand size and body mass in mind, the data was also scaled by a geometric mean of interarticular phalangeal length, trochlear breadth, mid-shaft breadth, and the breadth of the base. Using a geometric mean compared to single linear measurement may be a more accurate way of scaling, however using a geometric mean required the complete preservation of a phalanx, which many of the fossil specimens were not. As stated earlier, one of the main aims of this project was to create a comparative data set for fossil hominin phalanges, so the same scaling factor was needed for the extant sample and the fossil sample. Scaling the data using the geometric mean revealed similar patterns within the data as scaling with interarticular length did, as such the data in this thesis was scaled by interarticular length. The comparison between the data scaled by geometric mean and the data scaled by interarticular length allowed me to move forward with this scaling factor, however it is important to acknowledge that performing correlations of cortical bone thickness and interarticular phalangeal length revealed varying levels of relationships depending on the taxa, digit, and phalanx (**S. Table 6.1**). Thus, it is possible a different scaling factor might produce differing patterns and a scaling factor that closely estimates accurate body mass may be helpful.

Furthermore, it is necessary to address that while experimental research and studies on internal bone structure have demonstrated the functional significance of bone functional adaptation, they have also highlighted the limitations on the functional interpretations that can be inferred from these studies. One such limitation was discussed during the *viva voce* of this dissertation, which was the importance of phylogeny. The link between behaviour of great apes and their internal bone structure can be questioned due to their phylogenetic closeness, but previous research has demonstrated that internal bone structure may not be constrained by phylogeny (O'Neill & Dobson, 2008; Ryan and Shaw, 2012; 2013; Tsegai et al., 2013). Studying trabecular bone structure in differing bones across primates, Tsegai and colleague's (2013) and Ryan & Shaw (2012; 2013), separately, failed to find a phylogenetic signal in trabecular bone parameters across different primates. The work of O'Neill and Dobson (2008) on the long bones of several primate species also did not identify a strong phylogenetic signal in the cross-sectional geometric properties of those long bones. Ruff and colleagues' (2018) study on the phylogenetic effects on the long bones of three closely-related species of *Gorilla* found significant differences in the cross-sectional geometric properties across the three species; demonstrating a lack of phylogenetic constraints on internal bone structure. Despite the large sample of hominid phalanges studied here, much work still needs to be conducted to investigate and understand the functional morphology of primate phalanges and fossil hominin hand use. Firstly, as the results presented here established a relationship between hominid manual behaviours and cortical bone morphology, this analysis can be extended to other non-hominid primate species. Primate hands are incredibly diverse in form and function, but majority of the studies have focused on the great apes, with other primate species remaining understudied, particularly in regards to internal bone structure. Primates that employ specific manual behaviours, such as palmigrady and digitigrady, may be of particular interest as these hand postures are commonly employed across multiple anthropoids and would allow us to gain a deeper understanding of primate hand evolution. Secondly, this project has identified the need for holistic analyses that include internal and external bone morphology for the reconstruction of fossil behaviours. A first step towards the holistic analyses of bone morphology should quantification of cortical bone and trabecular together, as both internal bony structures work together to efficiently dissipate loads placed upon

bone. This data coupled with external shape variation would allow us to more accurately reconstruct fossil hominin behaviours as we would be aware of the interplay between different aspects of internal bone structure and external shape. The external shape of a bone, its trabecular and cortical structure and the soft tissue anatomy all function together and impact how bone behaves under mechanical loading, as such an integrated study combining the external and internal structure of bone would allow us to gain a deeper understanding of the functional morphology of any skeletal element. Integrated studies is a way to truly understand the variation and functional anatomy of extant and fossil primates.

Our understanding of extant and fossil primate functional anatomy can then be furthered by 3D musculoskeletal models, which can combine aspects of musculoskeletal anatomy to understand how anatomy affects the biomechanics of specific movements. 3D musculoskeletal models are helpful for reconstructing locomotion in fossil hominins. Recent methodological developments have led to the creation of accurate 3D musculoskeletal models of extant great apes (Goh et al., 2017; 2019; Johnson et al., 2022; MacLean et al., 2020; O'Neill et al., 2013) , which have then been used as a useful reference point for fossil musculoskeletal reconstructions as well (O'Neill et al., 2024; Wiseman et al., 2024). Many of these studies have focused on the lower limb and hip mechanics, so expanding these studies to include models of other limbs and joints would expand our knowledge of extant primate anatomy, which could then be applied to fossil hominins for a more accurate reconstruction of their locomotion and behaviour. An additional area of study that can provide us with greater insight into musculoskeletal anatomy is X-ray analysis of moving morphology (XROMM). X-ROMM allows the study of muscle function *in vivo* , helping us understand how soft and hard tissues interact with one another to generate movement (Brainerd et al., 2010), allowing us to visualise which soft tissue structures are used and how they are used during specific movements. XROMM can help us link how and which musculoskeletal morphology relates to the manual behaviours and functional patterns we observe in primate hands.

Knowledge from XROMM studies could also be combined with diffusible iodine-based contrast enhanced computed tomography (diceCT), to understand the actual soft tissue structure and morphology that allows for muscular movements (e.g., Orsbon et al., 2020). DiceCT allows for high-resolution imaging of the soft tissue and bony structure within cadavers, allowing for virtual dissections and detailed anatomical studies on muscular structure, fibres, and ligaments (Gignac et al., 2016), which could, on its own, help us link these soft tissues structures to actual skeletal material. Within the hand, the prominence of rugosities, that are considered muscle attachment sites, are used as indicators of specific manual behaviours and mechanical loading (e.g., Karakostis et al., 2017; 2018), but there is little evidence in support of that (see Williams-Hatala et al., 2016). DiceCT can allow us to visualise where muscles and other soft tissues actually attach and then we can actually test whether muscle attachment sites are actually reflecting muscle architecture and being (re-)modelled. This would allow us to better understand hand function, hand musculoskeletal anatomy, and ultimately, make more robust behavioural inferences regarding fossil hominins.

Reconstruction of fossil hominin behaviours relies on extant analogues, which has been proven to be effective, but we do not know how loads of these similar behaviours are dissipated across morphology that does not resemble any of extant analogues. For example, we do not know how

the loads associated with manipulation or arboreal behaviours were experienced by a small, gracile hand that has modern human-like proportions, but highly curved fingers. It may be possible that certain fossil hominins were participating in similar behavioural repertoires, but the mixture of derived and primitive features across all hands of fossil hominins would have resulted in distinct load distribution patterns. Finite element modelling can take into account variation in external and internal morphology and shed light on the pressures experienced by the hand, but prior to the application of this method, as mentioned above, a more nuanced understanding of phalangeal biomechanics, including soft tissue anatomy, in extant taxa is needed. There is still significant opportunity to further explore and understand phalangeal morphology and biomechanics, allowing for an increased understanding of primate hand evolution and the revision of the traditional views of the hominin hand.

Table 6.1: Summary of cortical bone morphology patterns of fossil hominins.

Species/Specimens	Cortical bone distribution pattern	Cortical bone thickness pattern across the shaft	Average cortical bone thickness	CA Pattern	Z _{pol} Pattern	J Pattern	Curvature
<i>A. afarensis</i>	Great ape-like	Great ape-like	Upper range of African ape variation	Resembles extant sample (35<50<65)	Pan-like (50<65<35)	50<65<35	Within African ape range of variation
<i>A. africanus</i>	Great ape-like	Great ape-like	Upper range of African ape variation	PPs: 35<65<50 IP: African ape-like (65<50<35)	PPs (Human-like) and IP (resembles extant sample) (65<50<35)	PPs (Human-like) and IP (resembles extant sample) (65<50<35)	PPs: Within African ape range of variation IP: Within human range of variation
<i>A. sediba</i>	Great ape-like; fifth digit also displays a human-like pattern	Human-like	Upper range of human variation and within the African ape range of variation	Resembles extant sample (35<50<65)	PPs (Human-like) and IPs (resembles extant sample) (65<50<35)	PPs (Human-like) and IPs (resembles extant sample) (65<50<35)	PPs: Within African ape range of variation IPs: Within upper end of human range of variation and lower end of African ape range of variation
<i>H. habilis</i>	Great ape-like	Great ape-like	Upper range of human variation and within the African ape range of variation	Human-like (35<65<50)	65<35<50	Resembles extant sample (65<50<35)	Within upper end of human range of variation and lower end of African ape range of variation
<i>H. naledi</i>	PPs: Great ape-like and human-like IPs: Great ape-like	Human-like	Upper range of human variation and within the African ape range of variation	PPs: 35<65<50 IPs: African ape-like (65<50<35)	PPs: Pan-like (50<65<35) IPs: Resembles extant sample (65<50<35)	PPs (Human-like) and IPs (resembles extant sample) (65<50<35)	Within African ape range of variation
<i>H. floresiensis</i>	PPs: Great ape-like IPs: unique mix of Great ape-like and human-like	PPs: Great ape-like IPs: Human-like	Within the human range of variation	PPs: Resembles extant sample (35<50<65) IPs: Pongo-like (65<35<50)	PPs (Human-like) and IPs (resembles extant sample) (65<50<35)	PPs (Human-like) and IPs (resembles extant sample) (65<50<35)	Within human range of variation
Neanderthals	Variable patterns of palmar and dorsal thickness	Human-like	Large range spanning from upper end of the human range to African ape range of variation	PPs: 35<65<50 IPs: Human-like (35<65<50)	PPs (Human-like) and IPs (resembles extant sample) (65<50<35)	PPs (Human-like) and IPs (resembles extant sample) (65<50<35)	PPs: Within upper end of human range of variation and lower end of African ape variation IPs: Within human range of variation
SKX 27431	Great ape-like	Great ape-like	Upper range of human variation and within the African ape range of variation	Resembles extant sample (35<50<65)	Human-like (65<50<35)	Human-like (65<50<35)	Within African ape range of variation
SKX 15468	Human-like	Great ape-like	Upper range of African ape variation	Resembles extant sample (35<50<65)	Pan-like (50<65<35)	50<65<35	Within upper end of human range of variation and lower end of African ape variation
SKX 5018	Great ape-like	Great ape-like	Upper range of African ape variation	Resembles extant sample (35<50<65)	Human-like (65<50<35)	Human-like (65<50<35)	Within African ape range of variation

7 – References

- Aiello, L. C. (2010). Five years of *Homo floresiensis*. *American Journal of Physical Anthropology*, 142, 167-179.
- Aiello, L. C., Wood, B., Key, C., & Wood, C. (1998). Laser scanning and paleoanthropology. In: Strasser, E., Fleagle, J. G., Rosenberger, A. L., McHenry, H. M. (Eds.) *Primate locomotion: recent advances*, pp. 223-236. Boston, MA: Springer,
- Alba, D. M., Moyà-Solà, S., & Köhler, M. (2003). Morphological affinities of the *Australopithecus afarensis* hand on the basis of manual proportions and relative thumb length. *Journal of Human Evolution*, 44, 225-254.
- Alemseged, Z. (2023). Reappraising the palaeobiology of *Australopithecus*. *Nature*, 617, 45-54.
- Alexander, C. J. (1994). Utilisation of joint movement range in arboreal primates compared with human subjects: an evolutionary frame for primary osteoarthritis. *Annals of the Rheumatic Diseases*, 53, 720-725.
- Almécija, S., Alba, D. M., & Moyà-Solà, S. (2009a). *Pierolapithecus* and the functional morphology of Miocene ape hand phalanges: paleobiological and evolutionary implications. *Journal of Human Evolution*, 57, 284-297.
- Almécija, S., Alba, D. M., & Moyà-Solà, S. (2009b). OH 7, the curious case of the original handy man?. *Paleolusitana*, 1, 85-92.
- Almécija, S., Moyà-Solà, S., & Alba, D. M. (2010). Early Origin for Human-Like Precision Grasping: A Comparative Study of Pollical Distal Phalanges in Fossil Hominins. *PLoS One*, 5, e11727.
- Almécija, S., Alba, D. M., & Moyà-Solà, S. (2012). The thumb of Miocene apes: new insights from Castell de Barberà (Catalonia, Spain). *American Journal of Physical Anthropology*, 148, 436-450.
- Almécija, S., & Alba, D. M. (2014). On manual proportions and pad-to-pad precision grasping in *Australopithecus afarensis*. *Journal of Human Evolution*, 73, 88-92.
- Almécija, S., Smaers, J. B., & Jungers, W. L. (2015). The evolution of human and ape hand proportions. *Nature Communications*, 6, 7717.
- An, K. N., Ueba, Y., Chao, E. Y., Cooney, W. P., & Linscheid, R. L. (1983). Tendon excursion and moment arm of index finger muscles. *Journal of Biomechanics*, 16, 419-425.
- An, K. N., Chao, E. Y., Cooney, W. P., & Linscheid, R. L. (1985). Forces in the normal and abnormal hand. *Journal of Orthopaedic Research*, 3, 202-211.
- Arias-Martorell, J., Zeininger, A., & Kivell, T. L. (2021). Trabecular structure of the elbow reveals divergence in knuckle-walking biomechanical strategies of African apes. *Evolution*, 75, 2959-2971.
- Augat, P., & Schorlemmer, S. (2006). The role of cortical bone and its microstructure in bone strength. *Age and Ageing*, 35, ii27-ii31.
- Ayhan, Ç., & Ayhan, E. (2020). Kinesiology of the Wrist and the Hand. In *Comparative Kinesiology of the Human Body*, pp. 211-282. Cambridge, MA: Academic Press.
- Badrian, A., and Badrian, N. (1977). Pygmy chimpanzees, *Oryx* 13, 463-468.

- Bandini, E., Harrison, R. A., & Motes-Rodrigo, A. (2022). Examining the suitability of extant primates as models of hominin stone tool culture. *Humanities and Social Sciences Communications*, *9*, 1-18.
- Barak, M. M. (2019). Bone modeling or bone remodeling: That is the question. *American Journal of Physical Anthropology*, *172*, 153-155
- Barak, M. M., Lieberman, D. E., & Hublin, J. J. (2011). A Wolff in sheep's clothing: trabecular bone adaptation in response to changes in joint loading orientation. *Bone*, *49*, 1141-1151.
- Barak, M. M., Lieberman, D. E., & Hublin, J. J. (2013a). Of mice, rats and men: Trabecular bone architecture in mammals scales to body mass with negative allometry. *Journal of Structural Biology*, *183*, 123-131.
- Barak, M. M., Lieberman, D. E., Raichlen, D., Pontzer, H., Warrener, A. G., & Hublin, J. J. (2013b). Trabecular evidence for a human-like gait in *Australopithecus africanus*. *PLoS One*, *8*, e77687.
- Barak, M. M., Sherratt, E., & Lieberman, D. E. (2017). Using principal trabecular orientation to differentiate joint loading orientation in the 3rd metacarpal heads of humans and chimpanzees. *Journal of Human Evolution*, *113*, 173-182.
- Bardo, A., Borel, A., Meunier, H., Guéry, J. P., & Pouydebat, E. (2016). Behavioral and functional strategies during tool use tasks in bonobos. *American Journal of Physical Anthropology*, *161*, 125-140.
- Bardo, A., Cornette, R., Borel, A., & Pouydebat, E. (2017). Manual function and performance in humans, gorillas, and orangutans during the same tool use task. *American Journal of Physical Anthropology*, *164*, 821-836.
- Bardo, A., Vigouroux, L., Kivell, T. L., & Pouydebat, E. (2018). The impact of hand proportions on tool grip abilities in humans, great apes and fossil hominins: A biomechanical analysis using musculoskeletal simulation. *Journal of Human Evolution*, *125*, 106-121.
- Bardo, A., Moncel, M. H., Dunmore, C. J., Kivell, T. L., Pouydebat, E., & Cornette, R. (2020). The implications of thumb movements for Neanderthal and modern human manipulation. *Scientific Reports*, *10*, 19323.
- Barton, N. H., & Charlesworth, B. (1984). Genetic revolutions, founder effects, and speciation. *Annual Review of Ecology and Systematics*, *15*, 133-164.
- Begun, D. R. (1993). New catarrhine phalanges from Rudabánya (Northeastern Hungary) and the problem of parallelism and convergence in hominoid postcranial morphology. *Journal of Human Evolution*, *24*, 373-402.
- Begun, D. R., Teaford, M. F., & Walker, A. (1994). Comparative and functional anatomy of *Proconsul* phalanges from the Kaswanga primate site, Rusinga Island, Kenya. *Journal of Human Evolution*, *26*, 89-165.
- Benazzi, S., Douka, K., Fornai, C., Bauer, C. C., Kullmer, O., Svoboda, J., Pap, I., Mallegni, F., Bayle, P., Coquerelle, M., Condemi, S., Ronchitelli, A., Harvati, K., & Weber, G. W. (2011). Early dispersal of modern humans in Europe and implications for Neanderthal behaviour. *Nature*, *479*, 525-528.

Berger, L. R., De Ruiter, D. J., Churchill, S. E., Schmid, P., Carlson, K. J., Dirks, P. H., & Kibii, J. M. (2010). *Australopithecus sediba*: a new species of *Homo*-like australopith from South Africa. *Science*, *328*, 195-204.

Berger, L. R., Hawks, J., de Ruiter, D. J., Churchill, S. E., Schmid, P., Deleuzene, L. K., Kivell, T. L., Garvin, H. M., Williams, S. A., DeSilva, J. M., Skinner, M. M., Musiba, C. M., Cameron, N., Holliday, T. W., Harcourt-Smith, W., Ackermann, R. R., Bastir, M., Bogin, B., Bolter, D., Brophy, J., Cofran, Z. D., Congdon, K. A., Deane, A. S., Dembo, M., Drapeau, M., Elliott, M. C., Feuerriegel, E. M., Garcia-Martinez, D., Green, D. J., Gurto, A., Irish, J. D., Kruger, A., Laird, M. F., Marchi, D., Meyer, M. R., Nalla, S., Negash, E. W., Orr, C. M., Radovicic, D., Schroeder, L., Scott, J. E., Throckmorton, Z., Tocheri, M. W., VanSickle, C., Walker, C. S., Wei, P., & Zipfel, B. (2015). *Homo naledi*, a new species of the genus *Homo* from the Dinaledi Chamber, South Africa. *elife*, *4*, e09560.

Biewener, A. A., Fazzalari, N. L., Konieczynski, D. D., & Baudinette, R. V. (1996). Adaptive changes in trabecular architecture in relation to functional strain patterns and disuse. *Bone*, *19*, 1-8.

Bird, E. E., Kivell, T. L., & Skinner, M. M. (2021). Cortical and trabecular bone structure of the hominoid capitate. *Journal of Anatomy*, *239*, 351-373.

Bird, E. E., Kivell, T. L., & Skinner, M. M. (2022). Patterns of internal bone structure and functional adaptation in the hominoid scaphoid, lunate, and triquetrum. *American Journal of Biological Anthropology*, *177*(2), 266-285.

Bird, E. E., Kivell, T. L., Dunmore, C. J., Tocheri, M. W., & Skinner, M. M. (In press.). Trabecular bone structure of the proximal capitate in extant hominids and fossil hominins with implications for midcarpal joint loading and the 'dart-thrower's motion. *American Journal of Biological Anthropology*.

Boesch, C. (1993). Aspects of transmission of tool-use in wild chimpanzees. In: K. R. Gibson & T. Ingold (Eds.) *Tools, Language and Cognition in Human Evolution*, pp. 171-183. New York, NY: Cambridge University Press.

Boesch, C. (1995). Innovation in wild chimpanzees (*Pan troglodytes*). *International Journal of Primatology*, *16*, 1-16.

Boesch, C., & Boesch, H. (1990). Tool use and tool making in wild chimpanzees. *Folia Primatologica*, *54*, 86-99.

Boesch, C., & Boesch, H. (1993). Different hand postures for pounding nuts with natural hammers by wild chimpanzees. In: H. Preuschoft & D. J. Chivers (Eds.) *Hands of Primates*, pp. 31-43. Vienna: Springer.

Bowland, L. A., Scott, J. E., Kivell, T. L., Patel, B. A., Tocheri, M. W., & Orr, C. M. (2021). *Homo naledi* pollical metacarpal shaft morphology is distinctive and intermediate between that of australopiths and other members of the genus *Homo*. *Journal of Human Evolution*, *158*, 103048.

Brainerd, E. L., Baier, D. B., Gatesy, S. M., Hedrick, T. L., Metzger, K. A., Gilbert, S. L., & Crisco, J. J. (2010). X-ray reconstruction of moving morphology (XROMM): precision, accuracy and applications in comparative biomechanics research. *Journal of Experimental Zoology Part A: Ecological Genetics and Physiology*, *313*, 262-279.

Braun, D. R., Aldeias, V., Archer, W., Arrowsmith, J. R., Baraki, N., Campisano, C. J., Deino, A. L., DiMaggio, E. N., Dupont-Nivet, G., Engda, B., Feary, D. A., Garello, D. I., Kerfelew, Z., McPherron, S.

P., Patterson, D. B., Reeves, J. S., Thompson, J. C., & Reed, K. E. (2019). Earliest known Oldowan artifacts at > 2.58 Ma from Ledi-Geraru, Ethiopia, highlight early technological diversity. *Proceedings of the National Academy of Sciences*, *116*, 11712–11717.

Breuer, T., Ndoundou-Hockemba, M., & Fishlock, V. (2005). First observation of tool use in wild gorillas. *PLoS Biology*, *3*, e380.

Brown, P., Sutikna, T., Morwood, M. J., Soejono, R. P., Jatmiko, Wayhu Saptomo, E., & Awe Due, R. (2004). A new small-bodied hominin from the Late Pleistocene of Flores, Indonesia. *Nature*, *431*, 1055–1061.

Brumm, A., Aziz, F., Van Den Bergh, G. D., Morwood, M. J., Moore, M. W., Kurniawan, I., Hobbs, D. R., & Fullagar, R. (2006). Early stone technology on Flores and its implications for *Homo floresiensis*. *Nature*, *441*, 624–628.

Burr, D. B. (1980). The relationships among physical, geometrical and mechanical properties of bone, with a note on the properties of nonhuman primate bone. *American Journal of Physical Anthropology*, *23*, 109–146.

Burr, D. B. (1990). Experimental overload and bone adaptation. In H. E. Takahashi (Ed.) *Bone Morphometry*, pp. 140–148. Japan, Nishimura: Nishimura Co Ltd.

Bush, M. E., Lovejoy, C. O., Johanson, D. C., & Coppens, Y. (1982). Hominid carpal, metacarpal, and phalangeal bones recovered from the Hadar Formation: 1974–1977 collections. *American Journal of Physical Anthropology*, *57*, 651–677.

Byrne, R. W. (2004). The manual skills and cognition that lie behind hominid tool use. In: A. E., Russon & D. R. Begun (Eds.). *The Evolution of Thought: Evolutionary Origins of Great Ape Intelligence*, pp. 31 – 44. Cambridge, UK: Cambridge University Press.

Byrne, R. W., & Byrne, J. M. (1991). Hand preferences in the skilled gathering tasks of mountain gorillas (*Gorilla g. berengei*). *Cortex*, *27*, 521–546.

Byrne, R. W., Corp, N., & Byrne, J. M. (2001). Manual dexterity in the gorilla: bimanual and digit role differentiation in a natural task. *Animal Cognition*, *4*, 347–361.

Cant, J. G. (1987). Positional behavior of female Bornean orangutans (*Pongo pygmaeus*). *American Journal of Primatology*, *12*, 71–90.

Carlson, K. J. (2005). Investigating the form-function interface in African apes: Relationships between principal moments of area and positional behaviors in femoral and humeral diaphyses. *American Journal of Physical Anthropology*, *127*, 312–334.

Carlson, K. J., Doran-Sheehy, D. M., Hunt, K. D., Nishida, T., Yamanaka, A., & Boesch, C. (2006). Locomotor behavior and long bone morphology in individual free-ranging chimpanzees. *Journal of Human Evolution*, *50*, 394–404.

Carlson, K. J., & Patel, B. A. (2006). Habitual use of the primate forelimb is reflected in the material properties of subchondral bone in the distal radius. *Journal of Anatomy*, *208*, 659–670.

Carlson, K. J., Jashashvili, T., Houghton, K., Westaway, M. C., & Patel, B. A. (2013). Joint loads in marsupial ankles reflect habitual bipedalism versus quadrupedalism. *PLoS One*, *8*, e58811.

- Case, D. T., & Heilman, J. (2006). New siding techniques for the manual phalanges: a blind test. *International Journal of Osteoarchaeology*, *16*, 338–346.
- Cazenave, M., Braga, J., Oettlé, A., Thackeray, J. F., De Beer, F., Hoffman, J., Endalamaw, M., Redae, B.E., Puymérail, L. & Macchiarelli, R. (2017). Inner structural organization of the distal humerus in *Paranthropus* and *Homo*. *Comptes Rendus Palevol*, *16*, 521–532.
- Cazenave, M., Braga, J., Oettlé, A., Pickering, T. R., Heaton, J. L., Nakatsukasa, M., Thackeray, J. F., de Beer, F., Hoffman, J., Dumoncel, J., & Macchiarelli, R. (2019). Cortical bone distribution in the femoral neck of *Paranthropus robustus*. *Journal of Human Evolution*, *135*, 102666.
- Cazenave, M., & Kivell, T. L. (2023). Challenges and perspectives on functional interpretations of australopith postcrania and the reconstruction of hominin locomotion. *Journal of Human Evolution*, *175*, 103304.
- Cebeiro, A., & Key, A. (In press.). Captive bonobos (*Pan paniscus*) apply precision grips when using flaked stone tools. *American Journal of Biological Anthropology*.
- Cepriá-Bernal, J., Pérez-González, A., Mora, M. C., & Sancho-Bru, J. L. (2017). Grip force and force sharing in two different manipulation tasks with bottles. *Ergonomics*, *60*, 957–966.
- Chao, E. Y., Opgrande, J. D., & Axmear, F. E. (1976). Three-dimensional force analysis of finger joints in selected isometric hand functions. *Journal of Biomechanics*, *9*, 387–IN2.
- Chapple, S. A., & Skinner, M. M. (2023). Primate tooth crown nomenclature revisited. *PeerJ*, *11*, e14523.
- Chirchir, H., Zeininger, A., Nakatsukasa, M., Ketcham, R. A., & Richmond, B. G. (2017). Does trabecular bone structure within the metacarpal heads of primates vary with hand posture?. *Comptes Rendus Palevol*, *16*, 533–544.
- Chirchir, H. (2019). Trabecular bone fraction variation in modern humans, fossil hominins and other primates. *The Anatomical Record*, *302*, 288–305.
- Churchill, S. E., & Formicola, V. (1997). A case of marked bilateral asymmetry in the upper limbs of an Upper Palaeolithic male from Barma Grande (Liguria), Italy. *International Journal of Osteoarchaeology*, *7*, 18–38.
- Churchill, S. E. (2001). Hand morphology, manipulation, and tool use in Neandertals and early modern humans of the Near East. *Proceedings of the National Academy of Sciences*, *98*, 2953–2955.
- Churchill, S. E., Holliday, T. W., Carlson, K. J., Jashashvili, T., Macias, M. E., Mathews, S., Sparling, T. L., Schmid, P., de Ruiter, D. J., & Berger, L. R. (2013). The upper limb of *Australopithecus sediba*. *Science*, *340*, 1233477.
- Churchill, S. E., Green, D. J., Feuerriegel, E. M., Macias, M. E., Matthews, S., Carlson, K. J., Schmid, P., & Berger, L. R. (2018). *Australopithecus sediba*—The Shoulder, Arm, and Forearm of *Australopithecus sediba*. *PaleoAnthropology*, *2018*, 234–281.
- Clarke, R. J. (1999). Discovery of complete arm and hand of the 3.3 million-year-old *Australopithecus* skeleton from Sterkfontein. *South African Journal of Science*, *95*, 477–480.

- Clarke, B. (2008). Normal bone anatomy and physiology. *Clinical Journal of the American Society of Nephrology*, 3, S131-S139.
- Congdon, K. A. (2012). Interspecific and ontogenetic variation in proximal pedal phalangeal curvature of great apes (*Gorilla gorilla*, *Pan troglodytes*, and *Pongo pygmaeus*). *International Journal of Primatology*, 33, 418-427.
- Connolly, K., & Elliott, J. (1972). The evolution and ontogeny of hand function. In: N. B., Jones (Eds.). *Ethological Studies of Child Behavior*, pp. 329-383. London, UK: Cambridge University Press.
- Cotter, M. M., Simpson, S. W., Latimer, B. M., & Hernandez, C. J. (2009). Trabecular microarchitecture of hominoid thoracic vertebrae. *The Anatomical Record: Advances in Integrative Anatomy and Evolutionary Biology*, 292, 1098-1106.
- Cowin, S. C., Hart, R. T., Balsler, J. R., & Kohn, D. H. (1985). Functional adaptation in long bones: establishing in vivo values for surface remodeling rate coefficients. *Journal of Biomechanics*, 18, 665-684.
- Cowin, S. C. (2001). *Bone Mechanics Handbook*. Boca Raton: CRC press.
- Crast, J., Fragaszy, D., Hayashi, M., & Matsuzawa, T. (2009). Dynamic in-hand movements in adult and young juvenile chimpanzees (*Pan troglodytes*). *American Journal of Physical Anthropology*, 138, 274-285.
- Crompton, R. H., Sellers, W. I., & Thorpe, S. K. (2010). Arboreality, terrestriality and bipedalism. *Philosophical Transactions of the Royal Society: Biological Sciences*, 365, 3301-3314.
- Currey, J. D. (2003). The many adaptations of bone. *Journal of Biomechanics*, 36, 1487-1495.
- Currey, J. D. (2006). *Bones: Structure and Mechanics*. Princeton, NJ: Princeton University Press.
- Currey, J. D. (2012). The structure and mechanics of bone. *Journal of Materials Science*, 47, 41-54.
- d'Août, K., Vereecke, E., Schoonaert, K., De Clercq, D., Van Elsacker, L., & Aerts, P. (2004). Locomotion in bonobos (*Pan paniscus*): differences and similarities between bipedal and quadrupedal terrestrial walking, and a comparison with other locomotor modes. *Journal of Anatomy*, 204, 353-361.
- Davies, T. W., Delezene, L. K., Gunz, P., Hublin, J. J., Berger, L. R., Gidna, A., & Skinner, M. M. (2020). Distinct mandibular premolar crown morphology in *Homo naledi* and its implications for the evolution of *Homo* species in southern Africa. *Scientific Reports*, 10, 13196.
- Davies, T.W., Alemseged, Z., Gidna, A., Hublin, J.J., Kimbel, W.H., Kullmer, O., Spoor, F., Zanolli, C. and Skinner, M.M. (2021). Accessory cusp expression at the enamel-dentine junction of hominin mandibular molars. *PeerJ*, 9, e11415.
- Day, M. H. (1976). Hominid postcranial material from Bed I, Olduvai Gorge. In: G. L. Isaac & E. R. McKown (Eds.) *Human origins: Louis Leakey and the East African Evidence*, pp. 363-374. Menlo Park, CA: W.A. Benjamin Inc.
- Day, M. H. (1978). Functional interpretations of the morphology of postcranial remains of early African hominids. In: C. J. Jolly (Ed.), *Early Hominids of Africa*, pp. 311- 345. New York, NY: St. Martin's Press.

- De La Torre, I., & Mora, R. (2018). Oldowan technological behaviour at HWK EE (Olduvai Gorge, Tanzania). *Journal of Human Evolution*, *120*, 236-273.
- De Monsabert, B. G., Rossi, J., Berton, E., & Vigouroux, L. (2012). Quantification of hand and forearm muscle forces during a maximal power grip task. *Medicine and Science in Sports and Exercise*, *44*, 1906-1916.
- Deane, A. S., Kremer, E. P., & Begun, D. R. (2005). New approach to quantifying anatomical curvatures using high-resolution polynomial curve fitting (HR-PCF). *American Journal of Physical Anthropology*, *128*, 630-638.
- Deane, A. S., & Begun, D. R. (2008). Broken fingers: retesting locomotor hypotheses for fossil hominoids using fragmentary proximal phalanges and high-resolution polynomial curve fitting (HR-PCF). *Journal of Human Evolution*, *55*, 691-701.
- Delpiano, D., Zupancich, A., & Peresani, M. (2019). Innovative Neanderthals: Results from an integrated analytical approach applied to backed stone tools. *Journal of Archaeological Science*, *110*, 105011.
- Demes, B. (2007). In vivo bone strain and bone functional adaptation. *American Journal of Physical Anthropology*, *133*, 717-722.
- DeSilva, J. M., Holt, K. G., Churchill, S. E., Carlson, K. J., Walker, C. S., Zipfel, B., & Berger, L. R. (2013). The lower limb and mechanics of walking in *Australopithecus sediba*. *Science*, *340*, 1232999.
- DeSilva, J. M., Churchill, S. E., Zipfel, B., Walker, C. S., Sylvester, A. D., McNutt, E. J., Sylvester, A. D., Walker, C. S., Zipfel, B., Churchill, S. E., & Berger, L. R. (2018). *Australopithecus sediba* -The Anatomy of the Lower Limb Skeleton of *Australopithecus sediba*. *PaleoAnthropology*, *2018*, 357-405.
- DeSilva, J., McNutt, E., Benoit, J., & Zipfel, B. (2019). One small step: A review of Plio-Pleistocene hominin foot evolution. *American Journal of Physical Anthropology*, *168*, 63-140.
- Dickinson, E., Young, M. W., Flaim, N. D., Sawiec, A., & Granatosky, M. C. (2023). A functional framework for interpreting phalangeal form. *Journal of the Royal Society Interface*, *20*, 20230251.
- Diogo, R., Richmond, B. G., & Wood, B. (2012). Evolution and homologies of primate and modern human hand and forearm muscles, with notes on thumb movements and tool use. *Journal of Human Evolution*, *63*, 64-78.
- Dirks, P. H., Kibii, J. M., Kuhn, B. F., Steininger, C., Churchill, S. E., Kramers, J. D., Pickering, R., Farber, D. L., Meriaux, A.-S., Herries, A. I. R., King, G. C. P., & Berger, L. R. (2010). Geological setting and age of *Australopithecus sediba* from southern Africa. *Science*, *328*, 205-208.
- Dirks, P. H., Roberts, E. M., Hilbert-Wolf, H., Kramers, J. D., Hawks, J., Dosseto, A., Duval, M., Elliot, M., Evans, M., Grun, R., Hellstron, J., Herries, A. I. R., Joannes-Boyau, R., Makhubela, T. V., Placzek, C. J., Robbins, J., Spandler, C., Wiersma, J., Woodhead, J., & Berger, L. R. (2017). The age of *Homo naledi* and associated sediments in the Rising Star Cave, South Africa. *Elife*, *6*, e24231.
- Doden, E. (1993). The relationship between the function and the inner cortical structure of metacarpal and phalangeal bones. In: H. Preuschoft & D. J. Chivers (Eds.) *Hands of Primates*, pp. 271-284. Vienna: Springer.

- Dollar, A. M. (2014). Classifying human hand use and the activities of daily living. In: R. Balasubramaian & V. J. Santos (Eds.) *The Human Hand as an Inspiration for Robot Hand Development*, pp. 201–216. Cham: Springer.
- Domalain, M., Bertin, A., & Daver, G. (2017). Was *Australopithecus afarensis* able to make the Lomekwian stone tools? Towards a realistic biomechanical simulation of hand force capability in fossil hominins and new insights on the role of the fifth digit. *Comptes Rendus Palevol*, 16, 572–584.
- Doran, D. M. (1992). The ontogeny of chimpanzee and pygmy chimpanzee locomotor behavior: a case study of paedomorphism and its behavioral correlates. *Journal of Human Evolution*, 23, 139–157.
- Doran, D. M. (1993a). Comparative locomotor behavior of chimpanzees and bonobos: the influence of morphology on locomotion. *American Journal of Physical Anthropology*, 91, 83–98.
- Doran, D. M. (1993b). Sex differences in adult chimpanzee positional behavior: the influence of body size on locomotion and posture. *American Journal of Physical Anthropology*, 91, 99–115.
- Doran, D. M. (1996). Comparative positional behavior of the African apes. In W. McGrew & T. Nishida (Eds.) *Great Ape Societies*, pp. 213–224. Cambridge, UK.: Cambridge University Press.
- Doran, D. M. (1997). Ontogeny of locomotion in mountain gorillas and chimpanzees. *Journal of Human Evolution*, 32, 323–344.
- Doran, D. M. & Hunt, K. D. (1996). Comparative locomotor behavior of Chimpanzees and Bonobos: Species and habitat differences. In: R.W. Wrangham, W.C. McGrew, F.B.M. de Waal & P.G. Heltne (Eds.) *Chimpanzee Cultures*, pp. 93–108. Cambridge, MA: Harvard University Press.
- Doyle, J. R. (2001). Palmar and digital flexor tendon pulleys. *Clinical Orthopaedics and Related Research*, 383, 84–96.
- Drapeau, M. S. (2015). Metacarpal torsion in apes, humans, and early *Australopithecus*: implications for manipulatory abilities. *PeerJ*, 3, e1311.
- Drummond-Clarke, R. C., Kivell, T. L., Sarringhaus, L., Stewart, F. A., Humle, T., & Piel, A. K. (2022). Wild chimpanzee behavior suggests that a savanna-mosaic habitat did not support the emergence of hominin terrestrial bipedalism. *Science Advances*, 8, eadd9752.
- Dunmore, C. J., Wollny, G., & Skinner, M. M. (2018). MIA-Clustering: a novel method for segmentation of paleontological material. *PeerJ*, 6, e4374.
- Dunmore, C. J., Kivell, T. L., Bardo, A., & Skinner, M. M. (2019). Metacarpal trabecular bone varies with distinct hand-positions used in hominid locomotion. *Journal of Anatomy*, 235, 45–66.
- Dunmore, C. J., Bardo, A., Skinner, M. M., & Kivell, T. L. (2020a). Trabecular variation in the first metacarpal and manipulation in hominids. *American Journal of Physical Anthropology*, 171, 219–241.
- Dunmore, C. J., Skinner, M. M., Bardo, A., Berger, L. R., Hublin, J. J., Pahr, D. H., Rosas, A., Stephens, N. B., & Kivell, T. L. (2020b). The position of *Australopithecus sediba* within fossil hominin hand use diversity. *Nature Ecology & Evolution*, 4, 911–918.

- Dunmore, C. J., Karakostis, F. A., van Leeuwen, T., Lu, S. C., & Proffitt, T. (2023). Tool use and the hand. In: C. S. Hirst, R. J. Gilmour, F. A. Cardoso & K. A. Plomp (Eds.) *Behaviour in our Bones: How Human Behaviour Influences Skeletal Morphology*, pp. 135-171. Amsterdam: Elsevier.
- Eriksen, E. F. (1986). Normal and pathological remodeling of human trabecular bone: three dimensional reconstruction of the remodeling sequence in normals and in metabolic bone disease. *Endocrine Reviews*, 7, 379-408.
- Eriksen, E. F. (2010). Cellular mechanisms of bone remodeling. *Reviews in Endocrine and Metabolic Disorders*, 11, 219-227.
- Fajardo, R. J., Ryan, T. M., & Kappelman, J. (2002). Assessing the accuracy of high-resolution X-ray computed tomography of primate trabecular bone by comparisons with histological sections. *American Journal of Physical Anthropology*, 118, 1-10.
- Fajardo, R. J., Müller, R., Ketcham, R. A., & Colbert, M. (2007). Nonhuman anthropoid primate femoral neck trabecular architecture and its relationship to locomotor mode. *The Anatomical Record: Advances in Integrative Anatomy and Evolutionary Biology*, 290, 422-436.
- Falótico, T., Proffitt, T., Ottoni, E. B., Staff, R. A., & Haslam, M. (2019). Three thousand years of wild capuchin stone tool use. *Nature Ecology & Evolution*, 3, 1034-1038.
- Feix, T., Romero, J., Schmiedmayer, H. B., Dollar, A. M., & Kragic, D. (2015). The grasp taxonomy of human grasp types. *IEEE Transactions on human-machine systems*, 46, 66-77.
- Feuerriegel, E. M., Green, D. J., Walker, C. S., Schmid, P., Hawks, J., Berger, L. R., & Churchill, S. E. (2017). The upper limb of *Homo naledi*. *Journal of Human Evolution*, 104, 155-173.
- Feuerriegel, E. M., Voisin, J. L., Churchill, S. E., Haeusler, M., Mathews, S., Schmid, P., Hawks, J., & Berger, L. R. (2019). Upper limb fossils of *Homo naledi* from the lesedi chamber, rising Star System, South Africa. *PaleoAnthropology*, 2019, 311-349.
- Fewlass, H., Talamo, S., Kromer, B., Bard, E., Tuna, T., Fagault, Y., Sponheimer, A., Ryder, C., Hublin, J.-J., Perri, A., Sazelova, S., & Svoboda, J. (2019). Direct radiocarbon dates of mid Upper Palaeolithic human remains from Dolní Věstonice II and Pavlov I, Czech Republic. *Journal of Archaeological Science: Reports*, 27, 102000.
- Fontaine, B., Moisson, P. Y., & Wickings, E. J. (1995). Observations of spontaneous tool making and tool use in a captive group of western lowland gorillas (*Gorilla gorilla gorilla*). *Folia Primatologica*, 65, 219-223.
- Fox, E. A., Sitompul, A. F., & Van Schaik, C. P. (1999). Intelligent tool use in wild Sumatran orangutans. In: S. T. Parker, R. W. Mitchell & H. L. Miles (Eds.) *The Mentalities of Gorillas and Orangutans: Comparative Perspectives*, pp. 99-116. Cambridge, UK: Cambridge University Press.
- Fox, E. A., & Bin'Muhammad, I. (2002). New tool use by wild Sumatran orangutans (*Pongo pygmaeus abelii*). *American Journal of Physical Anthropology*, 119, 186-188.
- Fox, E. A., van Schaik, C. P., Sitompul, A., & Wright, D. N. (2004). Intra-and interpopulational differences in orangutan (*Pongo pygmaeus*) activity and diet: implications for the invention of tool use. *American Journal of Physical Anthropology*, 125, 162-174.

- Froehle, A. W., Yokley, T. R., & Churchill, S. E. (2013). Energetics and the origin of modern humans. In: F. H. Smith & J. C. M. Ahern (Eds.) *The origins of modern humans: biology reconsidered*, pp. 285-320. Hoboken, NJ: John Wiley & Sons, Inc.
- Frost, H. M. (1987). Bone "mass" and the "mechanostat": a proposal. *The Anatomical Record*, 219, 1-9.
- Galletta, L., Stephens, N. B., Bardo, A., Kivell, T. L. and Marchi, D. (2019). Three-dimensional geometric morphometric analysis of the first metacarpal distal articular surface in humans, great apes and fossil hominins. *Journal of Human Evolution*, 132, 119-136.
- Gavrilets, S., & Hastings, A. (1996). Founder effect speciation: a theoretical reassessment. *The American Naturalist*, 147, 466-491.
- Gebo, D. L. (1996). Climbing, brachiation, and terrestrial quadrupedalism: historical precursors of hominid bipedalism. *American Journal of Physical Anthropology*, 101, 55-92.
- Georgiou, L., Dunmore, C. J., Bardo, A., Buck, L. T., Hublin, J. J., Pahr, D. H., Stratford, D., Synek, A., Kivell, T. L., & Skinner, M. M. (2020). Evidence for habitual climbing in a Pleistocene hominin in South Africa. *Proceedings of the National Academy of Sciences*, 117, 8416-8423.
- Gibbon, R. J., Pickering, T. R., Sutton, M. B., Heaton, J. L., Kuman, K., Clarke, R. J., Brain, C. K., & Granger, D. E. (2014). Cosmogenic nuclide burial dating of hominin-bearing Pleistocene cave deposits at Swartkrans, South Africa. *Quaternary Geochronology*, 24, 10-15.
- Gignac, P. M., Kley, N. J., Clarke, J. A., Colbert, M. W., Morhardt, A. C., Cerio, D., Cost, I. N., Cox, P. G., Daza, J. D., Early, C. M., Echols, S., Henkelman R. M., Herdine, A. N., Holliday, C. M., Li, Z., Mahlow, K., Merchant, S., Muller, J., Orsbon, C. P., Paluh, D. J., Thies, M. L., Tsai, H. P., & Witmer, L. M. (2016). Diffusible iodine-based contrast-enhanced computed tomography (diceCT): an emerging tool for rapid, high-resolution, 3-D imaging of metazoan soft tissues. *Journal of Anatomy*, 228, 889-909.
- Gilroy, A. M., MacPherson, B. R., Ross, L. M., Broman, J., & Josephson, A. (2008). *Atlas of Anatomy*. New York, NY: Thieme.
- Goh, C., Blanchard, M. L., Crompton, R. H., Gunther, M. M., Macaulay, S., & Bates, K. T. (2017). A 3D musculoskeletal model of the western lowland gorilla hind limb: moment arms and torque of the hip, knee and ankle. *Journal of Anatomy*, 231, 568-584.
- Goh, C., Blanchard, M. L., Crompton, R. H., Gunther, M. M., Macaulay, S., & Bates, K. T. (2019). A three-dimensional musculoskeletal model of the western lowland gorilla foot: Examining muscle torques and function. *Folia Primatologica*, 90, 470-493.
- Goodship, A. E., Lanyon, L. E., & McFie, H. (1979). Functional adaptation of bone to increased stress. An experimental study. *The Journal of Bone and Joint Surgery*, 61, 539-546.
- Gosman, J. H., Hubbell, Z. R., Shaw, C. N., & Ryan, T. M. (2013). Development of cortical bone geometry in the human femoral and tibial diaphysis. *The Anatomical Record*, 296, 774-787.
- Green, D. J., Gordon, A. D., & Richmond, B. G. (2007). Limb-size proportions in *Australopithecus afarensis* and *Australopithecus africanus*. *Journal of Human Evolution*, 52, 187-200.
- Green, D. J., & Gordon, A. D. (2008). Metacarpal proportions in *Australopithecus africanus*. *Journal of Human Evolution*, 54, 705-719.

- Green, D. J., & Alemseged, Z. (2012). *Australopithecus afarensis* scapular ontogeny, function, and the role of climbing in human evolution. *Science*, *338*, 514–517.
- Gross, T., Kivell, T. L., Skinner, M. M., Nguyen, N. H., & Pahr, D. H. (2014). A CT-image-based framework for the holistic analysis of cortical and trabecular bone morphology. *Palaeontologia Electronica*, *17*, 1–13.
- Grün, R., & Stringer, C. (2000). Tabun revisited: revised ESR chronology and new ESR and U-series analyses of dental material from Tabun C1. *Journal of Human Evolution*, *39*, 601–612.
- Guérin, G., Frouin, M., Talamo, S., Aldeias, V., Bruxelles, L., Chiotti, L., Dibble, H. L., Goldberg, P., Hublin, J.-J., Jain, M., Lahaye, C., Madelaine, S., Maureille, B., McPherron, S. J. P., Mercier, N., Murray, A. S., Sandgathe, D., Steele, T. E., Thomsen, K. J. & Turq, A. (2015). A multi-method luminescence dating of the Palaeolithic sequence of La Ferrassie based on new excavations adjacent to the La Ferrassie 1 and 2 skeletons. *Journal of Archaeological Science*, *58*, 147–166.
- Haeusler, M., & McHenry, H. M. (2004). Body proportions of *Homo habilis* reviewed. *Journal of Human Evolution*, *46*, 433–465.
- Häger-Ross, C., & Rösblad, B. (2002). Norms for grip strength in children aged 4–16 years. *Acta Paediatrica*, *91*, 617–625.
- Haile-Selassie, Y., Suwa, G., & White, T. (2009). Hominidae. In: Y. Haile-Selassie & G. WoldeGabriel, (Eds.) *Ardipithecus kadabba: Late Miocene Evidence from the Middle Awash, Ethiopia*, pp. 159–236. Los Angeles, CA: University of California Press.
- Hall, B. K. (1995). Homology and embryonic development. In: M. K. Hecht, R. J. Macintyre & M. T. Clegg (Eds.) *Evolutionary Biology*, pp. 1–37. New York, NY: Springer.
- Hamrick, M. W. (2012). The developmental origins of mosaic evolution in the primate limb skeleton. *Evolutionary Biology*, *39*, 447–455.
- Hamrick, M. W., Meldrum, D. J., & Simons, E. L. (1995). Anthropoid phalanges from the Oligocene of Egypt. *Journal of Human Evolution*, *28*, 121–145.
- Harcourt-Smith, W. E., Throckmorton, Z., Congdon, K. A., Zipfel, B., Deane, A. S., Drapeau, M. S., Churchill, S. E., Berger, L. R., & DeSilva, J. M. (2015). The foot of *Homo naledi*. *Nature Communications*, *6*, 8432.
- Harmand, S., Lewis, J. E., Feibel, C. S., Lepre, C. J., Prat, S., Lenoble, A., Boes, X., Quinn, R. L., Brenet, M., Arroyo, A., Taylor, N., Clement, S., Daver, G., Brugal, J.-P., Leakey, L., Mortlock, R. A., Wright, J. D., Lokorodi, S., Kirwa, C., Kent, D. V., & Roche, H. (2015). 3.3-million-year-old stone tools from Lomekwi 3, West Turkana, Kenya. *Nature*, *521*, 310–315.
- Haslam, M., Hernandez-Aguilar, R. A., Proffitt, T., Arroyo, A., Falótico, T., Fragaszy, D., Gumert, M., Harris, J. W. K., Huffman, M. A., Kalan, A. K., Malaivijitnond, S., Matsuzawa, T., McGrew, W., Ottoni, E. B., Pascual-Garrido, A., Piel, A., Pruett, J., Schuppli, C., Stewart, F., Tan, A., Visalberghi, E., & Luncz, L. V. (2017). Primate archaeology evolves. *Nature Ecology & Evolution*, *1*, 1431–1437.
- Hershkovitz, I., Edelson, G., Spiers, M., Arensburg, B., Nadel, D., & Levi, B. (1993). Ohalo II man—unusual findings in the anterior rib cage and shoulder girdle of a 19000-year-old specimen. *International Journal of Osteoarchaeology*, *3*, 177–188.

- Hervé, M. (2022). RVAideMemoire: Testing and plotting procedures for biostatistics. R package version 0.9-81-2.
- Holliday, T. W., & Franciscus, R. G. (2009). Body size and its consequences: allometry and the lower limb length of Liang Bua 1 (*Homo floresiensis*). *Journal of Human Evolution*, 57, 223-228.
- Holliday, T. W., Churchill, S. E., Carlson, K. J., DeSilva, J. M., Schmid, P., Walker, C. S., & Berger, L. R. (2018). *Australopithecus sediba*--Body Size and Proportions of *Australopithecus sediba*. *PaleoAnthropology*, 2018, 406-422.
- Hublin, J. J. (2009). The origin of Neandertals. *Proceedings of the National Academy of Sciences*, 106, 16022-16027.
- Hublin, J. J. (2017). The last neanderthal. *Proceedings of the National Academy of Sciences*, 114, 10520-10522.
- Hunt, K. D. (1991a). Positional behavior in the Hominoidea. *International Journal of Primatology*, 12, 95-118.
- Hunt, K. D. (1991b). Mechanical implications of chimpanzee positional behavior. *American Journal of Physical Anthropology*, 86, 521-536.
- Hunt, K. D. (1992). Positional behavior of *Pan troglodytes* in the Mahale mountains and Gombe stream national parks, Tanzania. *American Journal of Physical Anthropology*, 87, 83-105.
- Hunt, K. D. (2020). *Chimpanzee: Lessons from our sister species*. Cambridge, UK: Cambridge University Press.
- Inoue-Nakamura, N., & Matsuzawa, T. (1997). Development of stone tool use by wild chimpanzees (*Pan troglodytes*). *Journal of Comparative Psychology*, 111, 159.
- Inouye, S. E. (1992). Ontogeny and allometry of African ape manual rays. *Journal of Human Evolution*, 23, 107-138.
- Inouye, S. E. (1994). Ontogeny of knuckle-walking hand postures in African apes. *Journal of Human Evolution*, 26, 459-485.
- Jacobs, C. R. (2000). The mechanobiology of cancellous bone structural adaptation. *Journal of Rehabilitation Research and Development*, 37, 209-216.
- Jashashvili, T., Dowdeswell, M. R., Lebrun, R., Carlson, K. J. (2015) Cortical Structure of Hallucal Metatarsals and Locomotor Adaptations in Hominoids. *PLoS One* 10, e0117905.
- Jenkins, F. A., & Fleagle, J. G. (1975). Knuckle-walking and the functional anatomy of the wrists in living apes. In: R.H. Tuttle (Ed.) *Primate Functional Morphology and Evolution*, pp. 213-227. Berlin: De Gruyter Mouton.
- Johanson, D. C., Masao, F. T., Eck, G. G., White, T. D., Walter, R. C., Kimbel, W. H., Asfaw, B., Manega, P., Ndeessokia, P., & Suwa, G. (1987). New partial skeleton of *Homo habilis* from Olduvai Gorge, Tanzania. *Nature*, 327, 205-209.
- Johnson, R. T., O'Neill, M. C., & Umberger, B. R. (2022). The effects of posture on the three-dimensional gait mechanics of human walking in comparison with walking in bipedal chimpanzees. *Journal of Experimental Biology*, 225, jeb243272.

- Jones-Engel, L. E., & Bard, K. A. (1996). Precision grips in young chimpanzees. *American Journal of Primatology*, 39, 1-15.
- Jungers, W. L., Godfrey, L. R., Simons, E. L., & Chatrath, P. S. (1997). Phalangeal curvature and positional behavior in extinct sloth lemurs (Primates, *Palaeopropithecidae*). *Proceedings of the National Academy of Sciences*, 94, 11998-12001.
- Jungers, W. L., Godfrey, L. R., Simons, E. L., Wunderlich, R. E., Richmond, B. G., & Chatrath, P. S. (2002). Ecomorphology and behavior of giant extinct lemurs from Madagascar. In: J. M. Plavcan, R. F. Kay, W. L. Jungers, C. P. van Schaik (Eds.) *Reconstructing Behavior in the Primate Fossil Record*, pp. 371-411. Boston, MA: Springer.
- Jungers, W. L., Harcourt-Smith, W. E., Wunderlich, R. E., Tocheri, M. W., Larson, S. G., Sutikna, T., Awe, R. D., & Morwood, M. J. (2009a). The foot of *Homo floresiensis*. *Nature*, 459, 81-84.
- Jungers, W. L., Larson, S. G., Harcourt-Smith, W., Morwood, M. J., Sutikna, T., Awe, R. D., & Djubiantono, T. (2009b). Descriptions of the lower limb skeleton of *Homo floresiensis*. *Journal of Human Evolution*, 57, 538-554.
- Karakostis, F.A., Hotz, G., Scherf, H., Wahl, J., & Harvati, K. (2017). Occupational manual activity is reflected on the patterns among hand entheses. *American Journal of Physical Anthropology*, 164, 30-40.
- Karakostis, F. A., Hotz, G., Turloukis, V., & Harvati, K. (2018). Evidence for precision grasping in Neandertal daily activities. *Science Advances*, 4, p.eaat2369.
- Kargov, A., Pylatiuk, C., Martin, J., Schulz, S., & Döderlein, L. (2004). A comparison of the grip force distribution in natural hands and in prosthetic hands. *Disability and Rehabilitation*, 26, 705-711.
- Keaveny, T. M., Morgan, E. F., Niebur, G. L., & Yeh, O. C. (2001). Biomechanics of trabecular bone. *Annual Review of Biomedical Engineering*, 3, 307-333.
- Keir, P. J., & Wells, R. P. (2002). The effect of typing posture on wrist extensor muscle loading. *Human Factors*, 44, 392-403.
- Key, A. J. (2016). Manual loading distribution during carrying behaviors: implications for the evolution of the hominin hand. *PLoS One*, 11, e0163801.
- Key, A., Merritt, S. R., & Kivell, T. L. (2018). Hand grip diversity and frequency during the use of Lower Palaeolithic stone cutting-tools. *Journal of Human Evolution*, 125, 137-158.
- Key, A. J., Dunmore, C. J., & Marzke, M. W. (2019). The unexpected importance of the fifth digit during stone tool production. *Scientific Reports*, 9, 1-8.
- Key, A. J., Farr, I., Hunter, R., & Winter, S. L. (2020). Muscle recruitment and stone tool use ergonomics across three million years of Palaeolithic technological transitions. *Journal of Human Evolution*, 144, 102796.
- Kibii, J. M., Clarke, R. J., & Tocheri, M. W. (2011a). A hominin scaphoid from Sterkfontein, Member 4: Morphological description and first comparative phenetic 3D analyses. *Journal of Human Evolution*, 61, 510-517.
- Kibii, J. M., Churchill, S. E., Schmid, P., Carlson, K. J., Reed, N. D., De Ruiter, D. J., & Berger, L. R. (2011b). A partial pelvis of *Australopithecus sediba*. *Science*, 333, 1407-1411.

- Kinani, J. F., & Zimmerman, D. (2015). Tool use for food acquisition in a wild mountain gorilla (*Gorilla beringei beringei*). *American Journal of Primatology*, *77*, 353–357.
- Kivell, T. L. (2011). A comparative analysis of the hominin triquetrum (SKX 3498) from Swartkrans, South Africa. *South African Journal of Science*, *107*, 1–10.
- Kivell, T. L. (2015). Evidence in hand: recent discoveries and the early evolution of human manual manipulation. *Philosophical Transactions of the Royal Society: Biological Sciences*, *370*, 20150105.
- Kivell, T. L. (2016). A review of trabecular bone functional adaptation: what have we learned from trabecular analyses in extant hominoids and what can we apply to fossils?. *Journal of Anatomy*, *228*, 569–594.
- Kivell, T. L., Kibii, J. M., Churchill, S. E., Schmid, P., & Berger, L. R. (2011). *Australopithecus sediba* hand demonstrates mosaic evolution of locomotor and manipulative abilities. *Science*, *333*, 1411–1417.
- Kivell, T. L., Barros, A. P. and Smaers, J. B. (2013). Different evolutionary pathways underlie the morphology of wrist bones in hominoids. *BMC Evolutionary Biology*, *13*, 1–12.
- Kivell, T. L., Deane, A. S., Tocheri, M. W., Orr, C. M., Schmid, P., Hawks, J., Berger, L. R., & Churchill, S. E. (2015). The hand of *Homo naledi*. *Nature Communications*, *6*, 1–9.
- Kivell, T. L., Churchill, S. E., Kibii, J. M., Schmid, P., & Berger, L. R. (2018a). The hand of *Australopithecus sediba*. *PaleoAnthropology 2018*, 282–333.
- Kivell, T. L., Rosas, A., Estalrich, A., Huguet, R., García-Tabernero, A., Ríos, L., & de la Rasilla, M. (2018b). New Neandertal wrist bones from El Sidrón, Spain (1994–2009). *Journal of Human Evolution*, *114*, 45–75.
- Kivell, T. L., Davenport, R., Hublin, J. J., Thackeray, J. F., & Skinner, M. M. (2018a). Trabecular architecture and joint loading of the proximal humerus in extant hominoids, Ateles, and *Australopithecus africanus*. *American Journal of Physical Anthropology*, *167*, 348–365.
- Kivell, T. L., Ostrofsky, K. R., Richmond, B. G., & Drapeau, M. S. (2020). Metacarpals and manual phalanges. In: B. Zipfel, B.G. Richmond & C. V. Ward (Eds.) *Hominin Postcranial Remains from Sterkfontein, South Africa, 1936–1995*, 106. Oxford, UK: Oxford University Press
- Kivell, T. L., Baraki, N., Lockwood, V., Williams-Hatala, E. M., & Wood, B. A. (2022). Form, function and evolution of the human hand. *American Journal of Biological Anthropology*, *181*, 6–57.
- Klein, R. G. (2003). Whither the Neanderthals?. *Science*, *299*, 1525–1527.
- Koops, K., Visalberghi, E., & van Schaik, C. P. (2014). The ecology of primate material culture. *Biology Letters*, *10*(11), 20140508.
- Kraft, T. S., Venkataraman, V. V., & Dominy, N. J. (2014). A natural history of human tree climbing. *Journal of Human Evolution*, *71*, 105–118.
- Krause, J., Orlando, L., Serre, D., Viola, B., Prüfer, K., Richards, M. P., Hublin, J.-J., Hänni, C., Derevianko, A. P., & Pääbo, S. (2007). Neanderthals in central Asia and Siberia. *Nature*, *449*, 902–904.
- Kuman, K., Granger, D. E., Gibbon, R. J., Pickering, T. R., Caruana, M. V., Bruxelles, L., Clarke, R. J., Heaton, J. L., Stratford, D., & Brain, C. K. (2021). A new absolute date from Swartkrans Cave for

the oldest occurrences of *Paranthropus robustus* and Oldowan stone tools in South Africa. *Journal of Human Evolution*, 156, 103000.

Larson, S. G., Jungers, W. L., Morwood, M. J., Sutikna, T., Saptomo, E. W., Awe, R. D., & Djubiantono, T. (2007). *Homo floresiensis* and the evolution of the hominin shoulder. *Journal of Human Evolution*, 53, 718-731.

Larson, S. G., Jungers, W. L., Tocheri, M. W., Orr, C. M., Morwood, M. J., Sutikna, T., Awe, R. D., & Djubiantono, T. (2009). Descriptions of the upper limb skeleton of *Homo floresiensis*. *Journal of Human Evolution*, 57, 555-570.

Lazenby, R. A., Angus, S., Cooper, D. M., & Hallgrímsson, B. (2008). A three-dimensional microcomputed tomographic study of site-specific variation in trabecular microarchitecture in the human second metacarpal. *Journal of Anatomy*, 213, 698-705.

Lazenby, R. L., Skinner, M. M., Hublin, J. J., & Boesch, C. (2010). Tool use and inter-population variation in metacarpal trabecular microarchitecture in *Pan troglodytes*. *American Journal of Physical Anthropology*, 141, 152-152.

Lazenby, R. A., Skinner, M. M., Hublin, J. J., & Boesch, C. (2011). Metacarpal trabecular architecture variation in the chimpanzee (*Pan troglodytes*): Evidence for locomotion and tool-use?. *American Journal of Physical Anthropology*, 144, 215-225.

Leakey, L. S., Tobias, P. V., & Napier, J. R. (1964). A new species of the genus *Homo* from Olduvai Gorge. *Nature*, 202,7-9.

Leakey, M. D. (1971). *Olduvai Gorge: Volume 3, excavations in beds I and II, 1960-1963* (Vol. 3). Cambridge, UK: Cambridge University Press.

Leder, D., Hermann, R., Hüls, M., Russo, G., Hoelzmann, P., Nielbock, R., Böhner, U., Lehmann, J., Meier, M., Schwalb, A., Tröller-Reimer, A., Koddenberg, T., & Terberger, T. (2021). A 51,000-year-old engraved bone reveals Neanderthals' capacity for symbolic behaviour. *Nature Ecology & Evolution*, 5, 1273-1282.

Leijnse, J. N., Spoor, C. W., Pullens, P., & Vereecke, E. E. (2021). Kinematic and dynamic aspects of chimpanzee knuckle walking: finger flexors likely do not buffer ground impact forces. *Journal of Experimental Biology*, 224, jeb236604.

Lemelin, P., & Schmitt, D. (1998). The relation between hand morphology and quadrupedalism in primates. *American Journal of Physical Anthropology*, 105, 185-197.

Lesnik, J. J., Sanz, C. M., & Morgan, D. B. (2015). The Interdigital Brace and Other Grips for Termite Nest Perforation by Chimpanzees of the Goulougo Triangle, Republic of Congo. *American Journal of Physical Anthropology*, 157, 252-259.

Levenston, M. E., Beaupré, G. S., & Carter, D. R. (1998). Loading mode interactions in simulations of long bone cross-sectional adaptation. *Computer Methods in Biomechanics and Biomedical Engineering*, 1, 303-319.

Lewis, J. E., & Harmand, S. (2016). An earlier origin for stone tool making: implications for cognitive evolution and the transition to *Homo*. *Philosophical Transactions of the Royal Society: Biological Sciences*, 371, 20150233.

- Lieberman, D. E. (1997). Making behavioral and phylogenetic inferences from hominid fossils: considering the developmental influence of mechanical forces. *Annual Review of Anthropology*, 26, 185-210.
- Lieberman, D. E., Polk, J. D., & Demes, B. (2004). Predicting long bone loading from cross-sectional geometry. *American Journal of Physical Anthropology*, 123, 156-171.
- Lu, S. C., Vereecke, E.E., Synek, A., Pahr, D.H., & Kivell, T.L. (2018). A novel experimental design for the measurement of metacarpal bone loading and deformation and fingertip force. *PeerJ*, 6, e5480.
- Lutsky, K., Matzon, J., Walinchus, L., Ross, D. A., & Beredjiklian, P. (2014). Collateral ligament laxity of the finger metacarpophalangeal joints: an in vivo study. *The Journal of Hand Surgery*, 39, 1088-1093.
- MacKinnon, J. (1976). Mountain gorillas and bonobos. *Oryx*, 13, 372-382.
- MacLean, K. F., & Dickerson, C. R. (2020). Development of a comparative chimpanzee musculoskeletal glenohumeral model: implications for human function. *Journal of Experimental Biology*, 223, jeb225987.
- Malaivijitnond, S., Lekprayoon, C., Tandavanittj, N., Panha, S., Cheewatham, C., & Hamada, Y. (2007). Stone-tool usage by Thai long-tailed macaques (*Macaca fascicularis*). *American Journal of Primatology*, 69, 227-233.
- Manduell, K. L., Morrogh-Bernard, H. C., & Thorpe, S. K. (2011). Locomotor behavior of wild orangutans (*Pongo pygmaeus wurmbii*) in disturbed peat swamp forest, Sabangau, Central Kalimantan, Indonesia. *American Journal of Physical Anthropology*, 145, 348-359.
- Manduell, K. L., Harrison, M. E., & Thorpe, S. K. (2012). Forest structure and support availability influence orangutan locomotion in Sumatra and Borneo. *American Journal of Primatology*, 74, 1128-1142.
- Marangoni, A., Belli, M. L., Caramelli, D., Moggi Cecchi, J., Zavattaro, M., & Manzi, G. (2011). Tierra del Fuego, its ancient inhabitants, and the collections of skeletal remains in the Museums of Anthropology of Florence and Rome. *Museologia Scientifica*, 5, 88-96.
- Marchi, D. (2005). The cross-sectional geometry of the hand and foot bones of the Hominoidea and its relationship to locomotor behavior. *Journal of Human Evolution*, 49, 743-761.
- Marchi, D., Walker, C. S., Wei, P., Holliday, T. W., Churchill, S. E., Berger, L. R., & DeSilva, J. M. (2017). The thigh and leg of *Homo naledi*. *Journal of Human Evolution*, 104, 174-204.
- Marzke, M. W. (1992). Evolutionary development of the human thumb. *Hand Clinics*, 8, 1-8.
- Marzke, M. W. (1997). Precision grips, hand morphology, and tools. *American Journal of Physical Anthropology*, 102, 91-110.
- Marzke, M. W. (2013). Tool making, hand morphology and fossil hominins. *Philosophical Transactions of the Royal Society: Biological Sciences*, 368, 20120414.
- Marzke, M. W., & Shackley, M. S. (1986). Hominid hand use in the Pliocene and Pleistocene: evidence from experimental archaeology and comparative morphology. *Journal of Human Evolution*, 15, 439-460.
- Marzke, M. W., Wullstein, K. L., & Viegas, S. F. (1992). Evolution of the power ("squeeze") grip and its morphological correlates in hominids. *American Journal of Physical Anthropology*, 89, 283-298.

- Marzke, M. W., & Wullstein, K. L. (1996). Chimpanzee and human grips: a new classification with a focus on evolutionary morphology. *International Journal of Primatology*, *17*, 117-139.
- Marzke, M. W., & Marzke, R. F. (2000). Evolution of the human hand: approaches to acquiring, analysing and interpreting the anatomical evidence. *Journal of Anatomy*, *197*, 121-140.
- Marzke, M. W., Shrewsbury, M. M. and Horner, K. E. (2007). Middle phalanx skeletal morphology in the hand: can it predict flexor tendon size and attachments? *American Journal of Physical Anthropology*, *134*, 141-151.
- Marzke, M. W., Tocheri, M. W., Steinberg, B., Femiani, J. D., Reece, S. P., Linscheid, R. L., Orr, C. M. and Marzke, R. F. (2010). Comparative 3D quantitative analyses of trapeziometacarpal joint surface curvatures among living catarrhines and fossil hominins. *American Journal of Physical Anthropology*, *141*, 38-51.
- Marzke, M. W., Marchant, L. F., McGrew, W. C., & Reece, S. P. (2015). Grips and hand movements of chimpanzees during feeding in Mahale Mountains National Park, Tanzania. *American Journal of Physical Anthropology*, *156*, 317-326.
- Masi, S., Pouydebat, E., San-Galli, A., Meulman, E., Breuer, T., Reeves, J., & Tennie, C. (2022). Free hand hitting of stone-like objects in wild gorillas. *Scientific Reports*, *12*, 11981.
- Matarazzo, S. (2008). Knuckle walking signal in the manual digits of *Pan* and *Gorilla*. *American Journal of Physical Anthropology*, *135*, 27-33.
- Matarazzo, S. A. (2013). Knuckle-walking signal in the manual phalanges and metacarpals of the great apes (*Pan* and *Gorilla*). PhD dissertation, University of Massachusetts Amherst.
- Matarazzo, S. A. (2015). Trabecular architecture of the manual elements reflects locomotor patterns in primates. *PloS One*, *10*, e0120436.
- Matsuzawa, T. (2001). Primate foundations of human intelligence: a view of tool use in nonhuman primates and fossil hominids. In: T. Matsuzawa (Ed.) *Primate Origins of Human Cognition and Behavior*, pp. 3-25. Tokyo: Springer.
- Mayr, E. (1942). *Systematics and the Origin of Species*. New York, NY: Columbia University Press
- McBrearty, S., & Brooks, A. S. (2000). The revolution that wasn't: a new interpretation of the origin of modern human behavior. *Journal of Human Evolution*, *39*, 453-563.
- McClure, N. K., Phillips, A. C., Vogel, E. R., & Tocheri, M. W. (2012). Unexpected pollex and hallux use in wild *Pongo pygmaeus wurmbii*. *American Journal of Physical Anthropology*, *147*, S208.
- McHenry, H. M. (1983). The capitate of *Australopithecus afarensis* and *A. africanus*. *American Journal of Physical Anthropology*, *62*, 187-198.
- McPherron, S. P., Alemseged, Z., Marean, C. W., Wynn, J. G., Reed, D., Geraads, D., Bobe, R., & Béarat, H. A. (2010). Evidence for stone-tool-assisted consumption of animal tissues before 3.39 million years ago at Dikika, Ethiopia. *Nature*, *466*, 857-860.
- Meulman, E. J., & van Schaik, C. P. (2013). Orangutan tool use and the evolution of technology. In: C. M. Sanz, J. Call & C. Boesch (Eds.) *Tool Use in Animals: Cognition and Ecology*, pp. 176-202. New York, NY: Cambridge University Press.

- Milks, A., Parker, D., & Pope, M. (2019). External ballistics of Pleistocene hand-thrown spears: experimental performance data and implications for human evolution. *Scientific Reports*, 9, 820.
- Moore, M. W., & Brumm, A. (2007). Stone artifacts and hominins in island Southeast Asia: new insights from Flores, eastern Indonesia. *Journal of Human Evolution*, 52, 85-102.
- Morwood, M. J., Brown, P., Jatmiko, Sutikna, T., Wahyu Saptomo, E., Westaway, K. E., Due, R. A., Roberts, R. G., Maeda, T., Wasisto S., & Djubiantono, T. (2005). Further evidence for small-bodied hominins from the Late Pleistocene of Flores, Indonesia. *Nature*, 437, 1012-1017.
- Moyà-Solà, S., Köhler, M., Alba, D. M., & Almécija, S. (2008). Taxonomic attribution of the Olduvai hominid 7 manual remains and the functional interpretation of hand morphology in robust australopithecines. *Folia Primatologica*, 79, 215-250
- Musgrave, J. H. (1971). How dextrous was Neanderthal man?. *Nature*, 233, 538-541.
- Musgrave, J. H. (1973). The phalanges of Neanderthal and Upper Palaeolithic hands. *Human Evolution*, 11, 59-85.
- Nakatsukasa, M., Kunimatsu, Y., Nakano, Y., Takano, T., & Ishida, H. (2003). Comparative and functional anatomy of phalanges in *Nacholapithecus kerioi*, a Middle Miocene hominoid from northern Kenya. *Primates*, 44, 371-412.
- Napier, J. R. (1956). The prehensile movements of the human hand. *Journal of Bone and Joint Surgery*, 38, 902-913.
- Napier, J. R. (1960). Studies of the hands of living primates. *Proceedings of the Zoological Society of London*, 134, 647-657.
- Napier, J. R. (1962a). Fossil hand bones from Olduvai Gorge. *Nature*, 196, 409-411.
- Napier, J. R. (1962b). The evolution of the hand. *Scientific American*, 207, 56-65.
- Napier, J. R. (1993). *Hands* (Vol. 9). Princeton, NJ: Princeton University Press.
- Neufuss, J., Robbins, M. M., Baeumer, J., Humle, T., & Kivell, T. L. (2017). Comparison of hand use and forelimb posture during vertical climbing in mountain gorillas (*Gorilla beringei beringei*) and chimpanzees (*Pan troglodytes*). *American Journal of Physical Anthropology*, 164, 651-664.
- Neufuss, J., Robbins, M. M., Baeumer, J., Humle, T., & Kivell, T. L. (2018). Gait characteristics of vertical climbing in mountain gorillas and chimpanzees. *Journal of Zoology*, 306, 129-138.
- Neufuss, J., Robbins, M. M., Baeumer, J., Humle, T., & Kivell, T. L. (2019). Manual skills for food processing by mountain gorillas (*Gorilla beringei beringei*) in Bwindi Impenetrable National Park, Uganda. *Biological Journal of the Linnean Society*, 127, 543-562.
- Nguyen, N. H., Pahr, D. H., Gross, T., Skinner, M. M., & Kivell, T. L. (2014). Micro-finite element (μ FE) modeling of the siamang (*Symphalangus syndactylus*) third proximal phalanx: The functional role of curvature and the flexor sheath ridge. *Journal of Human Evolution*, 67, 60-75.
- Niewoehner, W. A. (2001). Behavioral inferences from the Skhul/Qafzeh early modern human hand remains. *Proceedings of the National Academy of Sciences*, 98, 2979-2984.

- Niewoehner, W. A. (2005). A Geometric Morphometric Analysis of Late Pleistocene Human Metacarpal 1 Base Shape. In: D. E. Slice (Ed.) *Modern Morphometrics in Physical Anthropology*, pp. 285-298. Boston, MA: Springer US.
- Niewoehner, W. A. (2006). Neanderthal hands in their proper perspective. In: J.-J., Hublin, K. Harvati & T. Harrison (Eds.) *Neanderthals Revisited: New Approaches and Perspectives*, pp. 157-190. Dordrecht: Springer.
- Niewoehner, W. A., Bergstrom, A., Eichele, D., Zuroff, M., & Clark, J. T. (2003). Manual dexterity in Neanderthals. *Nature*, 422, 395-395.
- Nordhausen, K., Sirkia, S., Oja, H., & Tyler, D. E. (2023). Tools for Multivariate Nonparametrics. R package version 1.1-2.0.
- Ocobock, C., Lacy, S., & Niclou, A. (2021). Between a rock and a cold place: Neanderthal biocultural cold adaptations. *Evolutionary Anthropology: Issues, News, and Reviews*, 30, 262-279.
- Ogle, D. H., Doll, J. C., Wheeler, A. P., & Dinno, A. (2022). FSA: Simple fisheries stock assessment methods. R package version 0.9.4.
- Oksanen, J., Blanchet, F. G., Friendly, M., Kindt, R., Legendre, P., McGlinn, D., Minchin, P. R., O'Hara, R. B., Simpson, G. L., Solymos, P., Stevens, M. H. H., Szoecs, E., & Wagner, H. (2020). vegan: Community Ecology Package. R package version 2.5-7.
- O'Neill, M. C., & Dobson, S. D. (2008). The degree and pattern of phylogenetic signal in primate long-bone structure. *Journal of Human Evolution*, 54, 309-322.
- O'Neill, M. C., Lee, L. F., Larson, S. G., Demes, B., Stern Jr, J. T., & Umberger, B. R. (2013). A three-dimensional musculoskeletal model of the chimpanzee (*Pan troglodytes*) pelvis and hind limb. *Journal of Experimental Biology*, 216, 3709-3723.
- O'Neill, M. C., Nagano, A., & Umberger, B. R. (2024). A three-dimensional musculoskeletal model of the pelvis and lower limb of *Australopithecus afarensis*. *American Journal of Biological Anthropology*, 183, e24845.
- Orr, C. M. (2016). Functional morphology of the primate hand: Recent approaches using biomedical imaging, computer modeling, and engineering methods. In: T. L. Kivell, P. Lemelin, B. G. Richmond & D. Schmitt (Eds.) *The Evolution of the Primate Hand*, pp. 227-257. New York, NY: Springer.
- Orr, C. M., Tocheri, M. W., Burnett, S. E., Awe, R. D., Saptomo, E. W., Sutikna, T., Jatmiko, Wasisto, S., Morwood, M. J., & Jungers, W. L. (2013). New wrist bones of *Homo floresiensis* from Liang Bua (Flores, Indonesia). *Journal of Human Evolution*, 64, 109-129.
- Orsbon, C. P., Gidmark, N. J., Gao, T., & Ross, C. F. (2020). XROMM and diceCT reveal a hydraulic mechanism of tongue base retraction in swallowing. *Scientific Reports*, 10(1), 8215.
- Ostrowsky, K. R., & Richmond, B. G. (2015). Manual proportions in *Australopithecus*: A comparative analysis including new material from Sterkfontein. *American Journal of Physical Anthropology*, 156, 243.
- Ottoni, E. B. (2015). Tool use traditions in nonhuman primates: The case of tufted capuchin monkeys. *Human Ethology Bulletin*, 30, 22-40.
- Oxnard, C.E., (1973). *Form and Pattern in Human Evolution: Some Mathematical, Physical, And Engineering Approaches*. Chicago: Chicago, IL: University of Chicago Press.

- Pahr, D. H., & Zysset, P. K. (2009). From high-resolution CT data to finite element models: development of an integrated modular framework. *Computer Methods in Biomechanics and Biomedical Engineering*, *12*, 45-57.
- Pal, A., & Sinha, A. (2022). Beyond food for thought: tool use and manufacture by wild nonhuman primates in nonforaging contexts. *Current Opinion in Behavioral Sciences*, *47*, 101201.
- Pang, E. Q., & Yao, J. (2018). Anatomy and biomechanics of the finger proximal interphalangeal joint. *Hand Clinics*, *34*, 121-126.
- Paoli, G., Tartì, S. M. B., Klír, P., Strouhal, E., Tofanelli, S., Del Santo Valli, M. T., & Pavelcová, B. (1993). Paleoerology of the Christian population at Sayala (Lower Nubia): an evaluation of the reliability of the results. *American Journal of Physical Anthropology*, *92*, 263-272.
- Patel, B. A. (2010). Functional morphology of cercopithecoid primate metacarpals. *Journal of Human Evolution*, *58*, 320-337.
- Patel, B. A., & Carlson, K. J. (2007). Bone density spatial patterns in the distal radius reflect habitual hand postures adopted by quadrupedal primates. *Journal of Human Evolution*, *52*, 130-141.
- Patel, B. A., & Maiolino, S. A. (2016). Morphological diversity in the digital rays of primate hands. In: T. L. Kivell, P. Lemelin, B. G. Richmond & D. Schmitt (Eds.) *The Evolution of the Primate Hand*, pp. 55-100. New York, NY: Springer.
- Patel, B. A., Jashashvili, T., Bui, S. H., Carlson, K. J., Griffin, N. L., Wallace, I. J., Orr, C. M., & Susman, R. L. (2018). Inter-ray variation in metatarsal strength properties in humans and African apes: Implications for inferring bipedal biomechanics in the Olduvai Hominid 8 foot. *Journal of Human Evolution*, *121*, 147-165.
- Patel, B. A., Orr, C. M., & Jashashvili, T. (2020). Strength properties of extant hominoid hallucal and pollical metapodials. *Journal of Human Evolution*, *143*, 102774.
- Patiño, F., Luque, M., Terradillos-Bernal, M., & Martín-Loeches, M. (2017). Biomechanics of microliths manufacture: a preliminary approach to Neanderthal's motor constraints in the frame of embodied cognition. *Journal of Anthropological Sciences*, *95*, 203-217.
- Pearson, O. M., & Lieberman, D. E. (2004). The aging of Wolff's "law": ontogeny and responses to mechanical loading in cortical bone. *American Journal of Physical Anthropology*, *125*, 63-99.
- Pearson, O. M., Cordero, R. M., & Busby, A. M. (2006). How different were Neanderthals' habitual activities? A comparative analysis with diverse groups of recent humans. In: J.-J., Hublin, K. Harvati & T. Harrison (Eds.) *Neanderthals Revisited: New Approaches and Perspectives*, pp. 135-156. Dordrecht: Springer.
- Pickering, R., Dirks, P. H., Jinnah, Z., De Ruiter, D. J., Churchill, S. E., Herries, A. I., Woodhead, J. D., Hellstrom, J. C., & Berger, L. R. (2011). *Australopithecus sediba* at 1.977 Ma and implications for the origins of the genus *Homo*. *Science*, *333*, 1421-1423.
- Pickering, T. R., Heaton, J. L., Clarke, R. J. and Stratford, D. (2018). Hominin hand bone fossils from Sterkfontein Caves, South Africa (1998-2003 excavations). *Journal of Human Evolution*, *118*, 89-102.

- Polk, J. D., Blumenfeld, J., & Ahluwalia, D. (2008). Knee posture predicted from subchondral apparent density in the distal femur: an experimental validation. *The Anatomical Record: Advances in Integrative Anatomy and Evolutionary Biology*, 291, 293-302.
- Pontzer, H., Lieberman, D. E., Momin, E., Devlin, M. J., Polk, J. D., Hallgrímsson, B., & Cooper, D. M. L. (2006). Trabecular bone in the bird knee responds with high sensitivity to changes in load orientation. *Journal of Experimental Biology*, 209, 57-65.
- Pouydebat, E., Berge, C., Gorce, P., & Coppens, Y. (2005). Use and manufacture of tools to extract food by captive *Gorilla gorilla gorilla*: experimental approach. *Folia Primatologica*, 76, 180.
- Pouydebat, E., Reghem, E., Borel, A., & Gorce, P. (2011). Diversity of grip in adults and young humans and chimpanzees (*Pan troglodytes*). *Behavioural Brain Research*, 218, 21-28.
- Prang, T. C. (2016). The subtalar joint complex of *Australopithecus sediba*. *Journal of Human Evolution*, 90, 105-119.
- Preuschoft, H. (1970). Functional anatomy of the lower extremity. *The chimpanzee*, pp. 221-294. Atlanta: Krager.
- Preuschoft, H. (1973). Functional anatomy of the upper extremity. In *The chimpanzee*, pp. 34-120. Atlanta: Krager.
- Preuschoft, H. (2019). Power grip or precision handling? What determines hand morphology in primates, including Hominidae?. *Biological Journal of the Linnean Society*, 127, 694-706.
- Profico, A., Bondioli, L., Raia, P., O'Higgins, P., & Marchi, D. (2021). morphomap: An R package for long bone landmarking, cortical thickness, and cross-sectional geometry mapping. *American Journal of Physical Anthropology*, 174, 129-139.
- Puymerail, L. (2013). The functionally-related signatures characterizing the endostructural organisation of the femoral shaft in modern humans and chimpanzee. *Comptes Rendus Palevol*, 12, 223-231.
- Qiu, D., & Kamper, D. G. (2014). Orthopaedic applications of a validated force-based biomechanical model of the index finger. In *2014 36th Annual International Conference of the IEEE Engineering in Medicine and Biology Society*, 4013-4016.
- R Core Team (2021). R: A language and environment for statistical computing. R Foundation for Statistical Computing, Vienna, Austria.
- Rafferty, K. L., & Ruff, C. B. (1994). Articular structure and function in *Hylobates*, *Colobus*, and *Papio*. *American Journal of Physical Anthropology*, 94, 395-408.
- Ramos III, G. L. (2014). *Positional behavior of Pan paniscus at Lui Kotale, Democratic Republic of Congo*. PhD dissertation, Indiana University.
- Rebollo, N. R., Weiner, S., Brock, F., Meignen, L., Goldberg, P., Belfer-Cohen, A., Bar-Yosef, O., & Boaretto, E. (2011). New radiocarbon dating of the transition from the Middle to the Upper Paleolithic in Kebara Cave, Israel. *Journal of Archaeological Science*, 38, 2424-2433.
- Rein, T. R. (2011). The correspondence between proximal phalanx morphology and locomotion: implications for inferring the locomotor behavior of fossil catarrhines. *American Journal of Physical Anthropology*, 146, 435-445.

- Rein, T. R., & McCarty, L. A. (2012). Metacarpophalangeal joint orientation in anthropoid manual phalanges. *The Anatomical Record: Advances in Integrative Anatomy and Evolutionary Biology*, 295, 2057-2068.
- Rein, T. R., & Harvati, K. (2013). Exploring third metacarpal capitate facet shape in early hominins. *The Anatomical Record*, 296, 240-249.
- Remis, M. J. (1994). *Feeding ecology and positional behavior of western lowland gorillas (Gorilla gorilla gorilla) in the Central African Republic*. PhD dissertation, Yale University.
- Remis, M. (1995). Effects of body size and social context on the arboreal activities of lowland gorillas in the Central African Republic. *American Journal of Physical Anthropology*, 97, 413-433.
- Remis, M. J. (1998). The gorilla paradox: the effects of body size and habitat on the positional behavior of lowland and mountain gorillas. In: E. Strasser, J. G. Fleagle, A. L. Rosenberger & H. M. McHenry (Eds.) *Primate Locomotion: Recent Advances*, pp. 95-106. Boston, MA: Springer.
- Remis, M. J. (1999). Tree structure and sex differences in arboreality among western lowland gorillas (*Gorilla gorilla gorilla*) at Bai Hokou, Central African Republic. *Primates*, 40, 383-396.
- Richmond, B. G. (1998). *Ontogeny and biomechanics of phalangeal form in primates*. PhD dissertation, State University of New York at Stony Brook.
- Richmond, B. G. (2007). Biomechanics of phalangeal curvature. *Journal of Human Evolution*, 53, 678-690.
- Richmond, B. G., Begun, D. R., & Strait, D. S. (2001). Origin of human bipedalism: the knuckle-walking hypothesis revisited. *American Journal of Physical Anthropology*, 116, 70-105.
- Richmond, B. G., & Jungers, W. L. (2008). *Orrorin tugenensis* femoral morphology and the evolution of hominin bipedalism. *Science*, 319, 1662-1665.
- Richmond, B. G., Roach, N. T., & Ostrofsky, K. R. (2016). Evolution of the early hominin hand. In: T. L. Kivell, P. Lemelin, B. G. Richmond & D. Schmitt (Eds.) *The Evolution of the Primate Hand*, pp. 515-543. New York, NY: Springer.
- Ricklan, D. E. (1987). Functional anatomy of the hand of *Australopithecus africanus*. *Journal of Human Evolution*, 16, 643-664.
- Rodríguez, L., Carretero, J. M., García-González, R., & Arsuaga, J. L. (2018). Cross-sectional properties of the lower limb long bones in the Middle Pleistocene Sima de los Huesos sample (Sierra de Atapuerca, Spain). *Journal of Human Evolution*, 117, 1-12.
- Roebroeks, W. (2014). Terra incognita: The Palaeolithic record of northwest Europe and the information potential of the southern North Sea. *Netherlands Journal of Geosciences*, 93, 43-53.
- Rolian, C., Lieberman, D. E., & Zermeno, J. P. (2011). Hand biomechanics during simulated stone tool use. *Journal of Human Evolution*, 61, 26-41.
- Rolian, C., & Gordon, A. D. (2013). Reassessing manual proportions in *Australopithecus afarensis*. *American Journal of Physical Anthropology*, 152, 393-406.
- Rolian, C. (2016). The role of genes and development in the evolution of the primate hand. In: T. L. Kivell, P. Lemelin, B. G. Richmond & D. Schmitt (Eds.) *The Evolution of the Primate Hand*, pp. 101-130. New York, NY: Springer.

- Rosas, A., Martínez-Maza, C., Bastir, M., García-Tabernero, A., Lalueza-Fox, C., Hugué, R., Ortiz, J., E., Julia, R., Soler, V., de Torres, T., Martínez, E., Canaveras, J. C., Sánchez-Moral, S., Cuezva, S., Lario, J., Santamaría, D., de la Rasilla, M., & Fortea, J. (2006). Paleobiology and comparative morphology of a late Neandertal sample from El Sidrón, Asturias, Spain. *Proceedings of the National Academy of Sciences*, *103*, 19266–19271.
- Rose, M. D. (1988). Functional anatomy of the cheiridia. In: J. H. Schwartz (Ed.) *Orangutan Biology*, pp. 299–310. New York, NY: Oxford University Press.
- Rossi, J., Berton, E., Grélot, L., Barla, C., & Vigouroux, L. (2012). Characterisation of forces exerted by the entire hand during the power grip: effect of the handle diameter. *Ergonomics*, *55*, 682–692.
- Rubin, C. T., & Lanyon, L. E. (1985). Regulation of bone mass by mechanical strain magnitude. *Calcified Tissue International*, *37*, 411–417.
- Rubin, C., Turner, A. S., Mallinckrodt, C., Jerome, C., McLeod, K., & Bain, S. (2002). Mechanical strain, induced noninvasively in the high-frequency domain, is anabolic to cancellous bone, but not cortical bone. *Bone*, *30*, 445–452.
- Ruff, C. B. (2000). Body size, body shape, and long bone strength in modern humans. *Journal of Human Evolution*, *38*, 269–290.
- Ruff, C. B. (2002). Long bone articular and diaphyseal structure in Old World monkeys and apes. I: locomotor effects. *American Journal of Physical Anthropology*, *119*, 305–342.
- Ruff, C. B. (2003). Long bone articular and diaphyseal structure in Old World monkeys and apes. II: Estimation of body mass. *American Journal of Physical Anthropology*, *120*, 16–37.
- Ruff, C. B. (2009). Relative limb strength and locomotion in *Homo habilis*. *American Journal of Physical Anthropology*, *138*, 90–100.
- Ruff, C. B., & Runestad, J. A. (1992). Primate limb bone structural adaptations. *Annual Review of Anthropology*, *21*, 407–433.
- Ruff, C., Holt, B., & Trinkaus, E. (2006). Who's afraid of the big bad Wolff? "Wolff's law" and bone functional adaptation. *American Journal of Physical Anthropology*, *129*, 484–498.
- Ruff, C. B., & Higgins, R. (2013). Femoral neck structure and function in early hominins. *American Journal of Physical Anthropology*, *150*, 512–525.
- Ruff, C. B., Burgess, M. L., Ketcham, R. A., & Kappelman, J. (2016). Limb bone structural proportions and locomotor behavior in AL 288-1 ("Lucy"). *PloS One*, *11*, e0166095.
- Ruff, C. B., Burgess, M. L., Junno, J. A., Mudakikwa, A., Zollikofer, C. P., Ponce de León, M. S., & McFarlin, S. C. (2018). Phylogenetic and environmental effects on limb bone structure in gorillas. *American Journal of Physical Anthropology*, *166*, 353–372.
- Ryan, T. M., & Ketcham, R. A. (2002a). The three-dimensional structure of trabecular bone in the femoral head of strepsirrhine primates. *Journal of Human Evolution*, *43*, 1–26.
- Ryan, T. M., & Ketcham, R. A. (2002b). Femoral head trabecular bone structure in two omomyid primates. *Journal of Human Evolution*, *43*, 241–263.

- Ryan, T. M., & Ketcham, R. A. (2005). Angular orientation of trabecular bone in the femoral head and its relationship to hip joint loads in leaping primates. *Journal of Morphology*, 265, 249–263.
- Ryan, T. M., & Walker, A. (2010). Trabecular bone structure in the humeral and femoral heads of anthropoid primates. *The Anatomical Record: Advances in Integrative Anatomy and Evolutionary Biology*, 293, 719–729.
- Ryan, T. M., & Shaw, C. N. (2012). Unique suites of trabecular bone features characterize locomotor behavior in human and non-human anthropoid primates. *PloS One*, 7, e41037.
- Ryan, T. M., & Shaw, C. N. (2013). Trabecular bone microstructure scales allometrically in the primate humerus and femur. *Proceedings of the Royal Society: Biological Sciences*, 280, 20130172.
- Ryan, T. M., Carlson, K. J., Gordon, A. D., Jablonski, N., Shaw, C. N., & Stock, J. T. (2018). Human-like hip joint loading in *Australopithecus africanus* and *Paranthropus robustus*. *Journal of Human Evolution*, 121, 12–24.
- Saers, J. P., Cazorla-Bak, Y., Shaw, C. N., Stock, J. T., & Ryan, T. M. (2016). Trabecular bone structural variation throughout the human lower limb. *Journal of Human Evolution*, 97, 97–108.
- Samuel, D. S., Nauwelaerts, S., Stevens, J. M., & Kivell, T. L. (2018). Hand pressures during arboreal locomotion in captive bonobos (*Pan paniscus*). *Journal of Experimental Biology*, 221, jeb170910.
- Samuni, L., Lemieux, D., Lamb, A., Galdino, D., & Surbeck, M. (2022). Tool use behavior in three wild bonobo communities at Kokolopori. *American Journal of Primatology*, 84, e23342.
- Sancho-Bru, J. L., Mora, M. C., León, B. E., Pérez-González, A., Iserte, J. L., & Morales, A. (2014). Grasp modelling with a biomechanical model of the hand. *Computer Methods in Biomechanics and Biomedical Engineering*, 17, 297–310.
- Sanz, C. M., & Morgan, D. B. (2007). Chimpanzee tool technology in the Goualougo Triangle, Republic of Congo. *Journal of Human Evolution*, 52, 420–433.
- Sarmiento, E. E. (1988). Anatomy of the hominoid wrist joint: its evolutionary and functional implications. *International Journal of Primatology*, 9, 281–345.
- Sarmiento, E. E. (1994). Terrestrial traits in the hands and feet of gorillas. *American Museum novitates*; no. 3091. American Museum of Natural History, New York.
- Sarringhaus, L. A., Stock, J. T., Marchant, L. F., & McGrew, W. C. (2005). Bilateral asymmetry in the limb bones of the chimpanzee (*Pan troglodytes*). *American Journal of Physical Anthropology*, 128, 840–845.
- Sarringhaus, L. A. (2013). *Positional and Morphological Development of Wild Chimpanzees, Pan Troglodytes*. PhD dissertation, The University of Michigan.
- Sarringhaus, L. A., MacLatchy, L. M., & Mitani, J. C. (2014). Locomotor and postural development of wild chimpanzees. *Journal of Human Evolution*, 66, 29–38.
- Sarringhaus, L. A., MacLatchy, L. M., & Mitani, J. C. (2016). Long bone cross-sectional properties reflect changes in locomotor behavior in developing chimpanzees. *American Journal of Physical Anthropology*, 160, 16–29.

- Schaffler, M. B., & Burr, D. B. (1984). Primate cortical bone microstructure: relationship to locomotion. *American Journal of Physical Anthropology*, *65*, 191-197.
- Schaffler, M. B., Burr, D. B., Jungers, W. L., & Ruff, C. B. (1985). Structural and mechanical indicators of limb specialization in primates. *Folia Primatologica*, *45*, 61-75.
- Schaller, G. E. (1963). *The Mountain Gorilla: Ecology and Behavior*. Chicago, IL: University of Chicago Press.
- Scherf, H., Harvati, K., & Hublin, J. J. (2013). A comparison of proximal humeral cancellous bone of great apes and humans. *Journal of Human Evolution*, *65*, 29-38.
- Scherf, H., Wahl, J., Hublin, J. J., & Harvati, K. (2016). Patterns of activity adaptation in humeral trabecular bone in Neolithic humans and present-day people. *American Journal of Physical Anthropology*, *159*, 106-115.
- Schick, K., & Toth, N. (2006). An overview of the Oldowan industrial complex: the sites and the nature of their evidence. In: K. Schick & N. Toth (Eds.) *The Oldowan*, pp. 3-42. Bloomington, IN: Stone Age Institute.
- Schilling, A. M., Tofanelli, S., Hublin, J. J., & Kivell, T. L. (2014). Trabecular bone structure in the primate wrist. *Journal of Morphology*, *275*, 572-585.
- Schmitt, D., Churchill, S. E., & Hylander, W. L. (2003). Experimental evidence concerning spear use in Neandertals and early modern humans. *Journal of Archaeological Science*, *30*, 103-114.
- Schmitt, D., Zeininger, A., & Granatosky, M. C. (2016). Patterns, variability, and flexibility of hand posture during locomotion in primates. In: T. L. Kivell, P. Lemelin, B. G. Richmond & D. Schmitt (Eds.) *The Evolution of the Primate Hand*, pp. 345-369. New York, NY: Springer.
- Schweizer, A. (2001). Biomechanical properties of the crimp grip position in rock climbers. *Journal of Biomechanics*, *34*, 217-223.
- Schweizer, A. (2008). Biomechanics of the interaction of finger flexor tendons and pulleys in rock climbing. *Sports Technology*, *1*, 249-256.
- Schweizer, A., & Hudek, R. (2011). Kinetics of crimp and slope grip in rock climbing. *Journal of Applied Biomechanics*, *27*, 116-121.
- Semaw, S. (2000). The world's oldest stone artefacts from Gona, Ethiopia: their implications for understanding stone technology and patterns of human evolution between 2.6-1.5 million years ago. *Journal of Archaeological Science*, *27*, 1197-1214.
- Semaw, S., Renne, P., Harris, J. W., Feibel, C. S., Bernor, R. L., Fesseha, N., & Mowbray, K. (1997). 2.5-million-year-old stone tools from Gona, Ethiopia. *Nature*, *385*, 333-336.
- Shaw, C. N., & Stock, J. T. (2013). Extreme mobility in the Late Pleistocene? Comparing limb biomechanics among fossil *Homo*, varsity athletes and Holocene foragers. *Journal of Human Evolution*, *64*, 242-249.
- Shea, J. J. (2013). *Stone tools in the Paleolithic and Neolithic Near East: A Guide*. New York, NY: Cambridge University Press

- Shea, J. J. (2016). *Stone tools in human evolution: behavioral differences among technological primates*. New York, NY: Cambridge University Press.
- Shrewsbury, M. M., & Johnson, R. K. (1980). Ligaments of the distal interphalangeal joint and the mallet position. *The Journal of Hand Surgery*, *5*, 214-216.
- Shrewsbury, M. M., Marzke, M. W., Linscheid, R. L., & Reece, S. P. (2003). Comparative morphology of the pollical distal phalanx. *American Journal of Physical Anthropology*, *121*, 30-47.
- Skinner, M. M., Stephens, N. B., Tsegai, Z. J., Foote, A. C., Nguyen, N. H., Gross, T., Pahr, D. H., Hublin, J. J., & Kivell, T. L. (2015). Human-like hand use in *Australopithecus africanus*. *Science*, *347*, 395-399.
- Snijders, C. J., Volkers, A. C., Mechelse, K., & Vleeming, A. (1987). Provocation of epicondylalgia lateralis (tennis elbow) by power grip or pinching. *Medicine and Science in Sports and Exercise*, *19*, 518-523.
- Sparacello, V. S., Dori, I., Rossi, S., Varalli, A., Riel-Salvatore, J., Gravel-Miguel, C., Riga, A., Seghi F., Goude, G., Palstra, S. W. L., Starnini, E., Formicola, V., & Moggi-Cecchi, J. (2021). New human remains from the Late Epigravettian necropolis of Arene Candide (Liguria, northwestern Italy): Direct radiocarbon evidence and inferences on the funerary use of the cave during the Younger Dryas. *Quaternary Science Reviews*, *268*, 107131.
- Spoor, F., Gunz, P., Neubauer, S., Stelzer, S., Scott, N., Kwekason, A., & Dean, M. C. (2015). Reconstructed *Homo habilis* type OH 7 suggests deep-rooted species diversity in early Homo. *Nature*, *519*, 83-86.
- Stephens, N. B. (2018). Functional morphology of the hand: Detecting behaviour during life through variation in internal trabecular architecture. PhD dissertation, University of Leipzig.
- Stephens, N. B., Kivell, T. L., Gross, T., Pahr, D. H., Lazenby, R. A., Hublin, J. J., Hershkovitz, I., & Skinner, M. M. (2016). Trabecular architecture in the thumb of *Pan* and *Homo*: implications for investigating hand use, loading, and hand preference in the fossil record. *American Journal of Physical Anthropology*, *161*, 603-619.
- Stephens, N. B., Kivell, T. L., Pahr, D. H., Hublin, J. J., & Skinner, M. M. (2018). Trabecular bone patterning across the human hand. *Journal of Human Evolution*, *123*, 1-23.
- Stern Jr, J. T. (2000). Climbing to the top: a personal memoir of *Australopithecus afarensis*. *Evolutionary Anthropology: Issues, News, and Reviews: Issues, News, and Reviews*, *9*, 113-133.
- Stern Jr, J. T., & Susman, R. L. (1983). The locomotor anatomy of *Australopithecus afarensis*. *American Journal of Physical Anthropology*, *60*, 279-317.
- Stern Jr, J. T., Jungers, W. L., & Susman, R. L. (1995). Quantifying phalangeal curvature: an empirical comparison of alternative methods. *American Journal of Physical Anthropology*, *97*, 1-10.
- Stout, D., Semaw, S., Rogers, M. J., & Cauche, D. (2010). Technological variation in the earliest Oldowan from Gona, Afar, Ethiopia. *Journal of Human Evolution*, *58*, 474-491.
- Su, A., & Carlson, K. J. (2017). Comparative analysis of trabecular bone structure and orientation in South African hominin tali. *Journal of Human Evolution*, *106*, 1-18.

- Sugiyama, T., Price, J. S., & Lanyon, L. E. (2010). Functional adaptation to mechanical loading in both cortical and cancellous bone is controlled locally and is confined to the loaded bones. *Bone*, *46*, 314-321.
- Susman, R. L. (1974). Facultative terrestrial hand postures in an orangutan (*Pongo pygmaeus*) and pongid evolution. *American Journal of Physical Anthropology*, *40*, 27-37.
- Susman, R. L. (1979). Comparative and functional morphology of hominoid fingers. *American Journal of Physical Anthropology*, *50*, 215-236.
- Susman, R. L. (1984). The locomotor behavior of *Pan paniscus* in the Lomako Forest. In: R. L. Susman (Ed.) *The Pygmy Chimpanzee*, pp. 369-393. Boston, MA: Springer.
- Susman, R. L. (1988a). New postcranial remains from Swartkrans and their bearing on the functional morphology and behavior of *Paranthropus robustus*. In F. E. Grine (Ed.) *Evolutionary History of the "Robust" Australopithecines*, pp. 149-172. New Brunswick, NJ: Transaction Publishers.
- Susman, R. L. (1988b). Hand of *Paranthropus robustus* from Member 1, Swartkrans: fossil evidence for tool behavior. *Science*, *240*, 781-784.
- Susman, R. L. (1989). New hominid fossils from the Swartkrans Formation (1979-1986 excavations): postcranial specimens. *American Journal of Physical Anthropology*, *79*, 451-474.
- Susman, R. L. (1994). Fossil evidence for early hominid tool use. *Science*, *265*, 1570-1573.
- Susman, R. L. (2004). *Oreopithecus bambolii*: an unlikely case of hominid like grip capability in a Miocene ape. *Journal of Human Evolution*, *46*, 105-117.
- Susman, R. L. (2008). Brief communication: evidence bearing on the status of *Homo habilis* at Olduvai Gorge. *American Journal of Physical Anthropology*, *137*, 356-361.
- Susman, R. L., & Creel, N. (1979). Functional and morphological affinities of the subadult hand (OH 7) from Olduvai Gorge. *American Journal of Physical Anthropology*, *51*, 311-331.
- Susman, R. L., & Stern Jr, J. T. (1979). Telemetered electromyography of flexor digitorum profundus and flexor digitorum superficialis in *Pan troglodytes* and implications for interpretation of the OH 7 hand. *American Journal of Physical Anthropology*, *50*, 565-574.
- Susman, R. L., Badrian, N. L., & Badrian, A. J. (1980). Locomotor behavior of *Pan paniscus* in Zaire. *American Journal of Physical Anthropology*, *53*, 69-80.
- Susman, R. L., & Stern, J. T. (1982). Functional morphology of *Homo habilis*. *Science*, *217*, 931-934.
- Susman, R. L., Stern, J. T., & Jungers, W. L. (1984). Arboreality and bipedality in the Hadar hominids. *Folia Primatologica*, *43*, 113-156.
- Susman, R. L., de Ruiter, D., & Brain, C. K. (2001). Recently identified postcranial remains of *Paranthropus* and early *Homo* from Swartkrans Cave, South Africa. *Journal of Human Evolution*, *41*, 607-629.
- Susman, R. L., Patel, B. A., Francis, M. J., & Cardoso, H. F. (2011). Metatarsal fusion pattern and developmental morphology of the Olduvai Hominid 8 foot: Evidence of adolescence. *Journal of Human Evolution*, *60*, 58-69.

- Sutikna, T., Tocheri, M. W., Morwood, M. J., Saptomo, E. W., Jatmiko, Awe, R. D., Wasisto, S., Westaway, K. E., Aubert, M., Li, B., Zhao, J-X., Storey, M., Alloway, B. V., Morley, M. W., Meijer, H. J. M., van den Bergh, G. D., Grün, R., Dosseto, A., Brumm, A., Jungers, W. L., & Roberts, R. G. (2016). Revised stratigraphy and chronology for *Homo floresiensis* at Liang Bua in Indonesia. *Nature*, *532*, 366–369.
- Syeda, S. M., Tsegai, Z. J., Dunmore, C. J., Cazenave, M., Skinner, M. M., & Kivell, T. L. (2021). Inferring hand use in *Australopithecus sediba*: Analysis of the external and internal morphology of hominin proximal and intermediate phalanges. *PaleoAnthropology* *2021*, 258.
- Syeda, S. M., Tsegai, Z. J., Cazenave, M., Skinner, M. M., & Kivell, T. L. (2023). Cortical bone distribution of the proximal phalanges in great apes: implications for reconstructing manual behaviours. *Journal of Anatomy*, *243*, 707–728.
- Syeda, S. M., Tsegai, Z. J., Cazenave, M., Skinner, M. M., & Kivell, T. L. (2024). Cortical bone architecture of hominid intermediate phalanges reveals functional signals of locomotion and manipulation. *American Journal of Biological Anthropology*, e24902.
- Sylvester, A. D., Christensen, A. M., & Kramer, P. A. (2006). Factors influencing osteological changes in the hands and fingers of rock climbers. *Journal of Anatomy*, *209*, 597–609.
- Synek, A., Lu, S. C., Vereecke, E. E., Nauwelaerts, S., Kivell, T. L., & Pahr, D. H. (2019). Musculoskeletal models of a human and bonobo finger: parameter identification and comparison to in vitro experiments. *PeerJ*, *7*, e7470.
- Synek, A., Lu, S. C., Nauwelaerts, S., Pahr, D. H., & Kivell, T. L. (2020). Metacarpophalangeal joint loads during bonobo locomotion: model predictions versus proxies. *Journal of the Royal Society Interface*, *17*, 20200032.
- Tatara, A. M., Lipner, J. H., Das, R., Kim, H. M., Patel, N., Ntouvali, E., Silva, M. J., & Thomopoulos, S. (2014). The role of muscle loading on bone (re) modeling at the developing enthesis. *PLoS One*, *9*(5), e97375.
- Thompson, N. E. (2020). The biomechanics of knuckle-walking: 3-D kinematics of the chimpanzee and macaque wrist, hand and fingers. *Journal of Experimental Biology*, *223*, p.jeb224360.
- Thompson, N. E., Ostrofsky, K. R., Mcfarlin, S. C., Robbins, M. M., Rubinstein, D., & Almecija, S. (2018). Preliminary 3-D kinematic data of wild mountain gorilla terrestrial locomotion: using lab-based methods in ape environments. *American Journal of Physical Anthropology*, *165*, 274.
- Thompson, N. E., Patel, B. A., Stern Jr, J. T., & Larson, S. G. (2019). 3-D kinematics, kinetics, and EMG of knuckle-walking in chimpanzees. *American Journal of Physical Anthropology*, *168*, 246–247.
- Thorpe, S. K., & Crompton, R. H. (2006). Orangutan positional behavior and the nature of arboreal locomotion in Hominoidea. *American Journal of Physical Anthropology*, *131*, 384–401.
- Thorpe, S. K. S., Crompton, R. H., & Alexander, R. M. (2007). Orangutans use compliant branches to lower the energetic cost of locomotion. *Biology Letters*, *3*, 253–256.
- Thorpe, S. K., Holder, R., & Crompton, R. H. (2009). Orangutans employ unique strategies to control branch flexibility. *Proceedings of the National Academy of Sciences*, *106*, 12646–12651.

- Tocheri, M. W. (2007). *Three-dimensional riddles of the radial wrist: derived carpal and carpometacarpal joint morphology in the genus Homo and the implications for understanding the evolution of stone tool-related behaviors in hominins*. PhD Dissertation. Arizona State University.
- Tocheri, M. W., Marzke, M. W., Liu, D., Bae, M., Jones, G. P., Williams, R. C., & Razdan, A. (2003). Functional capabilities of modern and fossil hominid hands: Three-dimensional analysis of trapezia. *American Journal of Physical Anthropology*, *122*, 101–112.
- Tocheri, M. W., Razdan, A., Williams, R. C., & Marzke, M. W. (2005). A 3D quantitative comparison of trapezium and trapezoid relative articular and nonarticular surface areas in modern humans and great apes. *Journal of Human Evolution*, *49*, 570–586.
- Tocheri, M. W., Orr, C. M., Larson, S. G., Sutikna, T., Jatmiko, Saptomo, E. W., Due, R. A., Djubiantono, T., Morwood, M. J., & Jungers, W. L. (2007). The primitive wrist of *Homo floresiensis* and its implications for hominin evolution. *Science*, *317*, 1743–1745.
- Tocheri, M. W., Orr, C. M., Jacofsky, M. C., & Marzke, M. W. (2008). The evolutionary history of the hominin hand since the last common ancestor of *Pan* and *Homo*. *Journal of Anatomy*, *212*, 544–562.
- Traynor, S., Green, D. J., & Hawks, J. (2022). The relative limb size of *Homo naledi*. *Journal of Human Evolution*, *170*, 103235.
- Trinkaus, E. (1989). Olduvai hominid 7 trapezium metacarpal 1 articular morphology: Contrasts with recent humans. *American Journal of Physical Anthropology*, *80*, 411–416.
- Trinkaus, E., & Ruff, C. B. (2012). Femoral and tibial diaphyseal cross-sectional geometry in Pleistocene *Homo*. *PaleoAnthropology*, *2012*, 13–62.
- Trinkaus, E. (2016). The evolution of the hand in Pleistocene *Homo*. In: T. L. Kivell, P. Lemelin, B. G. Richmond & D. Schmitt (Eds.) *The Evolution of the Primate Hand*, pp. 545–571. New York, NY: Springer.
- Trinkaus, E., & Villemeur, I. (1991). Mechanical advantages of the Neandertal thumb in flexion: a test of an hypothesis. *American Journal of Physical Anthropology*, *84*, 249–260.
- Trinkaus, E., Churchill, S. E., Villemeur, I., Riley, K. G., Heller, J. A., & Ruff, C. B. (1991). Robusticity versus shape: the functional interpretation of Neandertal appendicular morphology. *Journal of the Anthropological Society of Nippon*, *99*, 257–278.
- Tsegai, Z. J., Kivell, T. L., Gross, T., Nguyen, N. H., Pahr, D. H., Smaers, J. B., & Skinner, M. M. (2013). Trabecular bone structure correlates with hand posture and use in hominoids. *PLoS One*, *8*, e78781.
- Tsegai, Z. J., Stephens, N. B., Treece, G. M., Skinner, M. M., Kivell, T. L., & Gee, A. H. (2017a). Cortical bone mapping: an application to hand and foot bones in hominoids. *Comptes Rendus Palevol*, *16*, 690–701.
- Tsegai, Z. J., Skinner, M. M., Gee, A. H., Pahr, D. H., Treece, G. M., Hublin, J. J., & Kivell, T. L. (2017b). Trabecular and cortical bone structure of the talus and distal tibia in *Pan* and *Homo*. *American Journal of Physical Anthropology*, *163*, 784–805.
- Tuttle, R. H. (1967). Knuckle-walking and the evolution of hominoid hands. *American Journal of Physical Anthropology*, *26*, 171–206.

- Tuttle, R. H. (1969a). Quantitative and functional studies on the hands of the Anthroidea. I. The Hominoidea. *Journal of Morphology*, 128, 309-363.
- Tuttle, R. H. (1969b). Knuckle-Walking and the Problem of Human Origins: Studies on the hands of great apes and man lead to reevaluation of theories on hominoid evolution. *Science*, 166, 953-961.
- Tuttle, R. H. (1981). Evolution of hominid bipedalism and prehensile capabilities. *Philosophical Transactions of the Royal Society of London: Biological Sciences*, 292, 89-94.
- Tuttle, R., & Beck, B. B. (1972). Knuckle walking hand postures in an orangutan (*Pongo pygmaeus*). *Nature*, 236, 33-34.
- Tuttle, R., Basmajian, J. V., Regenos, E., & Shine, G. (1972). Electromyography of knuckle-walking: Results of four experiments on the forearm of *Pan gorilla*. *American Journal of Physical Anthropology*, 37, 255-265.
- Tuttle, R. H. & Watts, D. P. (1985). The positional behavior and adaptive complexes of *Pan gorilla*. In: S. Kondo (Ed.) *Primate Morphophysiology, Locomotor Analyses and Human Bipedalism*, pp. 261-288. Tokyo: University of Tokyo Press.
- van Lawick-Goodall, J. (1968). The behaviour of free-living chimpanzees in the Gombe Stream Reserve. *Animal Behaviour Monographs*, 1, 161-IN12.
- Van Schaik, C. P., Fox, E. A., & Sitompul, A. F. (1996). Manufacture and use of tools in wild Sumatran orangutans. *Naturwissenschaften*, 83, 186-188.
- van Schaik, C. P., Fox, E. A., & Fechtman, L. T. (2003). Individual variation in the rate of use of tree-hole tools among wild orangutans: implications for hominin evolution. *Journal of Human Evolution*, 44, 11-23.
- Vereecke, E. E., & Wunderlich, R. E. (2016). Experimental research on hand use and function in primates. In: T. L. Kivell, P. Lemelin, B. G. Richmond & D. Schmitt (Eds.) *The Evolution of the Primate Hand*, pp. 259-284. New York, NY: Springer.
- Vigouroux, L., Rossi, J., Foissac, M., Grélot, L., & Berton, E. (2011). Finger force sharing during an adapted power grip task. *Neuroscience Letters*, 504, 290-294.
- Voisin, J. L., Feuerriegel, E. M., Churchill, S. E., & Berger, L. R. (2020). The *Homo naledi* shoulder girdle: An adaptation to boulder climbing adaptation. *L'Anthropologie*, 124, 102783.
- Walker, A., Leakey, R. E., & Leakey, R. (1993). *The Nariokotome Homo erectus skeleton*. Cambridge, MA: Harvard University Press.
- Wallace, I. J., Burgess, M. L., & Patel, B. A. (2020). Phalangeal curvature in a chimpanzee raised like a human: Implications for inferring arboreality in fossil hominins. *Proceedings of the National Academy of Sciences*, 117, 11223-11225.
- Ward, C. V. (2002). Interpreting the posture and locomotion of *Australopithecus afarensis*: where do we stand?. *American Journal of Physical Anthropology*, 119, 185-215.
- Ward, C. V., Kimbel, W. H., Harmon, E. H., & Johanson, D. C. (2012). New postcranial fossils of *Australopithecus afarensis* from Hadar, Ethiopia (1990-2007). *Journal of Human Evolution*, 63, 1-51.

- Washburn, S. L. (1959). Speculations on the interrelations of the history of tools and biological evolution. *Human Biology*, 31, 21-31.
- Washburn, S. L. (1960). Tools and human evolution. *Scientific American*, 203, 62-75.
- Weatherholt, A. M., Fuchs, R. K., & Warden, S. J. (2013). Cortical and trabecular bone adaptation to incremental load magnitudes using the mouse tibial axial compression loading model. *Bone*, 52, 372-379.
- Weaver, T. D. (2009). The meaning of Neandertal skeletal morphology. *Proceedings of the National Academy of Sciences*, 106, 16028-16033.
- Webster, D., Wirth, A., van Lenthe, G. H., & Müller, R. (2012). Experimental and finite element analysis of the mouse caudal vertebrae loading model: prediction of cortical and trabecular bone adaptation. *Biomechanics and Modeling in Mechanobiology*, 11, 221-230.
- Wennemann, S. E., Lewton, K. L., Orr, C. M., Almécija, S., Tocheri, M. W., Jungers, W. L., & Patel, B. A. (2022). A geometric morphometric approach to investigate primate proximal phalanx diaphysis shape. *American Journal of Biological Anthropology*, 177, 581-602.
- Wei, P., Zhao, Y., Walker, C. S., He, J., Lu, X., Hui, J., Shui, W., Jin, L., & Liu, W. (2021). Internal structural properties of the humeral diaphyses in an early modern human from Tianyuan Cave, China. *Quaternary International*, 591, 107-118.
- Werner, D., Kozin, S. H., Brozovich, M., Porter, S. T., Junkin, D., & Seigler, S. (2003). The biomechanical properties of the finger metacarpophalangeal joints to varus and valgus stress. *The Journal of Hand Surgery*, 28, 1044-1051.
- Wiseman, A. L., Charles, J. P., & Hutchinson, J. R. (2024). Static versus dynamic muscle modelling in extinct species: a biomechanical case study of the Australopithecus afarensis pelvis and lower extremity. *PeerJ*, 12, e16821.
- Williams-Hatala, E. M. (2016). Biomechanics of the human hand: From stone tools to computer keyboards. In: T. L. Kivell, P. Lemelin, B. G. Richmond & D. Schmitt (Eds.) *The Evolution of the Primate Hand*, pp. 285-312. New York, NY: Springer.
- Williams, E. M., Gordon, A. D., & Richmond, B. G. (2012). Hand pressure distribution during Oldowan stone tool production. *Journal of Human Evolution*, 62, 520-532.
- Williams-Hatala, E. M., Hatala, K. G., Hiles, S., & Rabey, K. N. (2016). Morphology of muscle attachment sites in the modern human hand does not reflect muscle architecture. *Scientific Reports*, 6, p.28353.
- Williams-Hatala, E. M., Hatala, K. G., Gordon, M., Key, A., Kasper, M., & Kivell, T. L. (2018). The manual pressures of stone tool behaviors and their implications for the evolution of the human hand. *Journal of Human Evolution*, 119, 14-26.
- Williams-Hatala, E. M., Hatala, K. G., Key, A., Dunmore, C. J., Kasper, M., Gordon, M., & Kivell, T. L. (2021). Kinetics of stone tool production among novice and expert tool makers. *American Journal of Physical Anthropology*, 174, 714-727.
- Wolff, J. (2012). *The law of bone remodelling*. Springer Science & Business Media.

- Wood, B., Aiello, L., Wood, C., & Key, C. (1998). A technique for establishing the identity of 'isolated' fossil hominin limb bones. *Journal of Anatomy*, 193, 61-72.
- Wood, B., & Constantino, P. (2007). *Paranthropus boisei*: fifty years of evidence and analysis. *American Journal of Physical Anthropology*, 134, 106-132.
- Wood, B., & Schroer, K. (2013). *Paranthropus*. In: D. R. Begin (Ed.) *A companion to Paleoanthropology*, pp. 457-478. Hoboken, NJ: Wiley Blackwell Publishing.
- Wood, R. E., Higham, T. F., De Torres, T., Tisnerat-Laborde, N., Valladas, H., Ortiz, J. E., Lalueza-Fox, C., Sanchez-Moral, S., Canaveras, J. C., Rosas, A., Santamaria, D., & De la Rasilla, M. (2013). A new date for the Neanderthals from El Sidrón Cave (Asturias, northern Spain). *Archaeometry*, 55, 148-158.
- Wroe, S., Parr, W. C., Ledogar, J. A., Bourke, J., Evans, S. P., Fiorenza, L., Benazzi, S., Hublin, J.-J., Strigner, C., Kullmer, O., Curry, M., Rae, T. C., & Yokley, T. R. (2018). Computer simulations show that Neanderthal facial morphology represents adaptation to cold and high energy demands, but not heavy biting. *Proceedings of the Royal Society: Biological Sciences*, 285, 20180085.
- Wu, J. Z., An, K. N., Cutlip, R. G., Krajinak, K., Welcome, D., & Dong, R. G. (2008). Analysis of musculoskeletal loading in an index finger during tapping. *Journal of Biomechanics*, 41, 668-676.
- Wunderlich R. E., & Jungers, W. L. (2009). Manual digital pressures during knuckle-walking in chimpanzees (*Pan troglodytes*). *American Journal of Physical Anthropology*, 139, 394-403.
- Yeni, Y. N., Brown, C. U., Wang, Z., & Norman, T. L. (1997). The influence of bone morphology on fracture toughness of the human femur and tibia. *Bone*, 21, 453-459.
- Young, N. M., & Hallgrímsson, B. (2005). Serial homology and the evolution of mammalian limb covariation structure. *Evolution*, 59, 2691-2704.
- Young, N. M., Wagner, G. P., & Hallgrímsson, B. (2010). Development and the evolvability of human limbs. *Proceedings of the National Academy of Sciences*, 107, 3400-3405.
- Zeininger, A., Richmond, B. G., & Hartman, G. (2011). Metacarpal head biomechanics: a comparative backscattered electron image analysis of trabecular bone mineral density in *Pan troglodytes*, *Pongo pygmaeus*, and *Homo sapiens*. *Journal of Human Evolution*, 60, 703-710.
- Zeininger, A., Patel, B. A., Zipfel, B., & Carlson, K. J. (2016). Trabecular architecture in the StW 352 fossil hominin calcaneus. *Journal of Human Evolution*, 97, 145-158.
- Zheng, J. Z., De La Rosa, S., & Dollar, A. M. (2011). An investigation of grasp type and frequency in daily household and machine shop tasks. *2011 IEEE international conference on robotics and automation*, 4169-4175.
- Zipfel, B., DeSilva, J. M., Kidd, R. S., Carlson, K. J., Churchill, S. E., & Berger, L. R. (2011). The foot and ankle of *Australopithecus sediba*. *Science*, 333, 1417-1420.

8 – Appendix

8.1. Curatorial institutions of the study sample

Table 8.1 details institutions that have curated and provided access to the all specimens studied in this project.

Table 8.1: Curatorial institutions of the extant sample

Taxon	Specimen	Curatorial Institution
<i>Homo sapiens</i>	NHMW-Nubian_J2	Natural History Museum, Vienna
<i>Homo sapiens</i>	NHMW-Nubian_K63	Natural History Museum, Vienna
<i>Homo sapiens</i>	NHMW-Nubian_K5.2	Natural History Museum, Vienna
<i>Homo sapiens</i>	NHMW-Nubian_J7	Natural History Museum, Vienna
<i>Homo sapiens</i>	Qafzeh_9	The Sackler School of Medicine at Tel Aviv University
<i>Homo sapiens</i>	Qafzeh_8	The Sackler School of Medicine at Tel Aviv University
<i>Homo sapiens</i>	OHALO_II_H2	The Sackler School of Medicine at Tel Aviv University
<i>Homo sapiens</i>	UNIFL_4865	University of Florence
<i>Homo sapiens</i>	UNIFL_4887	University of Florence
<i>Homo sapiens</i>	UNIFL_3124	University of Florence
<i>Homo sapiens</i>	UNIFL_3125	University of Florence
<i>Homo sapiens</i>	UNIFL_3127	University of Florence
<i>Homo sapiens</i>	GAUG-Inden_91	Georg-August-University Goettingen, Anthropology Collection
<i>Homo sapiens</i>	GAUG-Inden_113	Georg-August-University Goettingen, Anthropology Collection
<i>Homo sapiens</i>	GAUG-Inden_117	Georg-August-University Goettingen, Anthropology Collection
<i>Homo sapiens</i>	GAUG-Inden_119	Georg-August-University Goettingen, Anthropology Collection
<i>Homo sapiens</i>	GAUG-Inden_243	Georg-August-University Goettingen, Anthropology Collection
<i>Homo sapiens</i>	Barma_Grande_2	Museo Nazionale Preistorico dei Balzi Rossi
<i>Homo sapiens</i>	ARENE_CANDIDE_2	the Museo Archeologico del Finale
<i>Homo sapiens</i>	DCW_AM_3_0_2	The Duckworth Collection, University of Cambridge
<i>Homo sapiens</i>	DCW_OC_1_0_141	The Duckworth Collection, University of Cambridge
<i>Homo sapiens</i>	DCW_OC_1_0_26	The Duckworth Collection, University of Cambridge
<i>Homo sapiens</i>	FCS8	Mary Rose Trust
<i>Homo sapiens</i>	81-H1035	Mary Rose Trust
<i>Homo sapiens</i>	81-H1040	Mary Rose Trust
<i>Homo sapiens</i>	81-H1068-DD	Mary Rose Trust
<i>Homo sapiens</i>	FCS16	Mary Rose Trust
<i>Homo sapiens</i>	FCS17	Mary Rose Trust
<i>Homo sapiens</i>	81-H172-H	Mary Rose Trust
<i>Homo sapiens</i>	DV-13	Institute of Archaeology, Czech Republic

<i>Homo sapiens</i>	DV-14	Institute of Archaeology, Czech Republic
<i>Homo sapiens</i>	DV-15	Institute of Archaeology, Czech Republic
<i>Homo sapiens</i>	DV-16	Institute of Archaeology, Czech Republic
<i>Pan paniscus</i>	MRAC_27698	Royal Museum for Central Africa, Tervuren
<i>Pan paniscus</i>	MRAC_29042	Royal Museum for Central Africa, Tervuren
<i>Pan paniscus</i>	MRAC_29045	Royal Museum for Central Africa, Tervuren
<i>Pan paniscus</i>	MRAC_29052	Royal Museum for Central Africa, Tervuren
<i>Pan paniscus</i>	MRAC_27696	Royal Museum for Central Africa, Tervuren
<i>Pan paniscus</i>	MRAC_20881	Royal Museum for Central Africa, Tervuren
<i>Pan paniscus</i>	MRAC_29060	Royal Museum for Central Africa, Tervuren
<i>Pan troglodytes</i>	MPITC_11778	Max Planck Institute for Evolutionary Anthropology, Taï Chimp Collection
<i>Pan troglodytes</i>	MPITC_14996	Max Planck Institute for Evolutionary Anthropology, Taï Chimp Collection
<i>Pan troglodytes</i>	NH_CAM1_204	Powell-Cotton Museum
<i>Pan troglodytes</i>	NH_CAM2_301	Powell-Cotton Museum
<i>Pan troglodytes</i>	NH_MER_279	Powell-Cotton Museum
<i>Pan troglodytes</i>	NH_MER35_86	Powell-Cotton Museum
<i>Pan troglodytes</i>	NH_MER35_105	Powell-Cotton Museum
<i>Pan troglodytes</i>	MPITC_11903	Max Planck Institute for Evolutionary Anthropology, Taï Chimp Collection
<i>Pan troglodytes</i>	MPITC_11789	Max Planck Institute for Evolutionary Anthropology, Taï Chimp Collection
<i>Pan troglodytes</i>	MPITC_11781	Max Planck Institute for Evolutionary Anthropology, Taï Chimp Collection
<i>Pan troglodytes</i>	ZSM_AP-122	Bavarian State Collection of Zoology
<i>Pan troglodytes</i>	PC_ZVII_24	Powell-Cotton Museum
<i>Pan troglodytes</i>	NH_MER33_712	Powell-Cotton Museum
<i>Pan troglodytes</i>	NH_MER33_724	Powell-Cotton Museum
<i>Pan troglodytes</i>	NH_MER32_401	Powell-Cotton Museum
<i>Pan troglodytes</i>	NH_MER33_440	Powell-Cotton Museum
<i>Pan troglodytes</i>	NH_MER36_254	Powell-Cotton Museum
<i>Gorilla gorilla</i>	ZMB_11642	Natural History Museum, Berlin
<i>Gorilla gorilla</i>	ZMB_83545	Natural History Museum, Berlin
<i>Gorilla gorilla</i>	PC_MER_95	Powell-Cotton Museum
<i>Gorilla gorilla</i>	PC_MER_135	Powell-Cotton Museum
<i>Gorilla gorilla</i>	PC_MER_264	Powell-Cotton Museum
<i>Gorilla gorilla</i>	PC_MER_300	Powell-Cotton Museum

<i>Gorilla gorilla</i>	PC_MER_372	Powell-Cotton Museum
<i>Gorilla gorilla</i>	PC_MER_962	Powell-Cotton Museum
<i>Gorilla gorilla</i>	PC_MER1_29	Powell-Cotton Museum
<i>Gorilla gorilla</i>	PC_MER_138	Powell-Cotton Museum
<i>Gorilla gorilla</i>	PC_MER_174	Powell-Cotton Museum
<i>Gorilla gorilla</i>	PC_MER_696	Powell-Cotton Museum
<i>Gorilla gorilla</i>	PC_MER_856	Powell-Cotton Museum
<i>Gorilla gorilla</i>	PC_ZII_64	Powell-Cotton Museum
<i>Gorilla gorilla</i>	PC_ZVI_32	Powell-Cotton Museum
<i>Gorilla gorilla</i>	NH_MER33_755	Powell-Cotton Museum
<i>Gorilla gorilla</i>	NH_MER33_461	Powell-Cotton Museum
<i>Gorilla gorilla</i>	NH_CAM1_106	Powell-Cotton Museum
<i>Gorilla gorilla</i>	NH_CAM1_105	Powell-Cotton Museum
<i>Gorilla gorilla</i>	NH_MER35_150	Powell-Cotton Museum
<i>Gorilla gorilla</i>	NH_CAM1_98	Powell-Cotton Museum
<i>Gorilla gorilla</i>	NH_MER35_136	Powell-Cotton Museum
<i>Gorilla gorilla</i>	NH_MER35_139	Powell-Cotton Museum
<i>Gorilla gorilla</i>	NH_FC_130	Powell-Cotton Museum
<i>Gorilla gorilla</i>	NH_FC_123	Powell-Cotton Museum
<i>Pongo abelii</i>	SMF_6785	Senckenberg Natural History Museum, Frankfurt
<i>Pongo abelii</i>	SMF_6779	Senckenberg Natural History Museum, Frankfurt
<i>Pongo pygmaeus</i>	ZSM_1907_0633b	Bavarian State Collection of Zoology
<i>Pongo pygmaeus</i>	ZSM_1907_0629b	Bavarian State Collection of Zoology
<i>Pongo pygmaeus</i>	ZSM_1907_0660	Bavarian State Collection of Zoology
<i>Pongo pygmaeus</i>	ZSM_AP-120	Bavarian State Collection of Zoology
<i>Pongo pygmaeus</i>	ZSM_1907_0483	Bavarian State Collection of Zoology
<i>Pongo pygmaeus</i>	ZSM_1909_0801	Bavarian State Collection of Zoology
<i>Pongo pygmaeus</i>	ZMB_87092	Bavarian State Collection of Zoology

8.2. SUPPLEMENTARY MATERIALS: Cortical bone distribution of the proximal phalanges in great apes and implications for reconstructing manual behaviours

8.2.1. Supplementary Information 1: Siding phalanges

For the majority of our sample (65%), we include associated PP2–PP5 from a single hand (right or left, depending on which was most complete) of one individual. However, in instances when this was not possible due to preservation or methodological issues, proximal phalanges from the other hand in the same individual or individuals with an incomplete set of proximal phalanges were also included in the sample. For incomplete sets of phalanges, we assigned phalanges to a digit for the non-human great apes following Susman (1979) and Patel & Maiolino (2016). For humans, whose PP2 and PP4 are not as morphologically distinct as those of non-human great apes, we used minor variations in basal morphology to identify them: PP2 has an enlarged radial tubercle to accommodate the first dorsal interossei muscle, while the PP4 base is more symmetrical with a palmarly projecting radial tubercle (Susman, 1979; Case & Heilman, 2006).

8.2.2. Supplementary tables and figures

Below are supplementary tables and figures that expand on the results presented in the manuscript.

Supplementary Table 3.1: Detailed specimen information.

Taxon	Specimen	Sex	Side	Subsistence	Collection
<i>Homo sapiens</i>	NHMW-Nubian_J2	M	R	Pre-industrial	Natural History Museum, Vienna
<i>Homo sapiens</i>	NHMW-Nubian_K63	M	L	Pre-industrial	Natural History Museum, Vienna
<i>Homo sapiens</i>	NHMW-Nubian_K5.2	M	R	Pre-industrial	Natural History Museum, Vienna
<i>Homo sapiens</i>	NHMW-Nubian_J7	F	R	Pre-industrial	Natural History Museum, Vienna
<i>Homo sapiens</i>	Qafzeh_9	M	R	Pre-industrial	The Sackler School of Medicine at Tel Aviv University
<i>Homo sapiens</i>	Qafzeh_8	UK	R/L	Pre-industrial	The Sackler School of Medicine at Tel Aviv University
<i>Homo sapiens</i>	OHALO_II_H2	M	R/L	Pre-industrial	The Sackler School of Medicine at Tel Aviv University
<i>Homo sapiens</i>	UNIFL_4865	M	R	Post-industrial	University of Florence
<i>Homo sapiens</i>	UNIFL_4887	F	R	Post-industrial	University of Florence
<i>Homo sapiens</i>	UNIFL_3124	UK	UK	Pre-industrial	University of Florence
<i>Homo sapiens</i>	UNIFL_3125	UK	UK	Pre-industrial	University of Florence
<i>Homo sapiens</i>	UNIFL_3127	M	L	Pre-industrial	University of Florence
<i>Homo sapiens</i>	GAUG-Inden_91	M	R	Post-industrial	Georg-August-University Goettingen, Anthropology Collection
<i>Homo sapiens</i>	GAUG-Inden_113	M	L	Post-industrial	Georg-August-University Goettingen, Anthropology Collection
<i>Homo sapiens</i>	GAUG-Inden_117	UK	L	Post-industrial	Georg-August-University Goettingen, Anthropology Collection
<i>Homo sapiens</i>	GAUG-Inden_119	M	R	Post-industrial	Georg-August-University Goettingen, Anthropology Collection
<i>Homo sapiens</i>	GAUG-Inden_243	M	L	Post-industrial	Georg-August-University Goettingen, Anthropology Collection
<i>Homo sapiens</i>	Barma_Grande_2	M	R	Pre-industrial	Museo Nazionale Preistorico dei Balzi Rossi
<i>Homo sapiens</i>	ARENE_CANDIDE_2	M	R/L	Pre-industrial	the Museo Archeologico del Finale
<i>Homo sapiens</i>	DCW_AM_3_0_2	UK	R/L	Pre-industrial	The Duckworth Collection, University of Cambridge
<i>Homo sapiens</i>	DCW_OC_1_0_141	UK	R/L	Pre-industrial	The Duckworth Collection, University of Cambridge
<i>Homo sapiens</i>	DCW_OC_1_0_26	UK	L	Pre-industrial	The Duckworth Collection, University of Cambridge
<i>Homo sapiens</i>	FCS8	M	R/L	Post-industrial	Mary Rose Trust
<i>Homo sapiens</i>	81-H1035	M	R	Post-industrial	Mary Rose Trust
<i>Homo sapiens</i>	81-H1040	M	R	Post-industrial	Mary Rose Trust
<i>Homo sapiens</i>	81-H1068-DD	M	R	Post-industrial	Mary Rose Trust
<i>Homo sapiens</i>	FCS16	M	R/L	Post-industrial	Mary Rose Trust
<i>Homo sapiens</i>	FCS17	M	R/L	Post-industrial	Mary Rose Trust
<i>Homo sapiens</i>	81-H172-H	M	R/L	Post-industrial	Mary Rose Trust
<i>Homo sapiens</i>	DV-13	M	L	Pre-industrial	Institute of Archaeology, Czech Republic

<i>Homo sapiens</i>	DV-14	M	R	Pre-industrial	Institute of Archaeology, Czech Republic
<i>Homo sapiens</i>	DV-15	M	R/L	Pre-industrial	Institute of Archaeology, Czech Republic
<i>Homo sapiens</i>	DV-16	M	R/L	Pre-industrial	Institute of Archaeology, Czech Republic
<i>Pan paniscus</i>	MRAC_27698	F	L	Wild	Royal Museum for Central Africa, Tervuren
<i>Pan paniscus</i>	MRAC_29042	F	R	Wild	Royal Museum for Central Africa, Tervuren
<i>Pan paniscus</i>	MRAC_29045	F	L	Wild	Royal Museum for Central Africa, Tervuren
<i>Pan paniscus</i>	MRAC_29052	M	R	Wild	Royal Museum for Central Africa, Tervuren
<i>Pan paniscus</i>	MRAC_27696	M	L	Wild	Royal Museum for Central Africa, Tervuren
<i>Pan paniscus</i>	MRAC_20881	M	L	Wild	Royal Museum for Central Africa, Tervuren
<i>Pan paniscus</i>	MRAC_29060	F	R	Wild	Royal Museum for Central Africa, Tervuren
<i>Pan troglodytes</i>	MPITC_11778	F	R	Wild	Max Planck Institute for Evolutionary Anthropology, Taï Chimp Collection
<i>Pan troglodytes</i>	MPITC_14996	F	L	Wild	Max Planck Institute for Evolutionary Anthropology, Taï Chimp Collection
<i>Pan troglodytes</i>	NH_CAM1_204	F	L	Wild	Powell-Cotton Museum
<i>Pan troglodytes</i>	NH_CAM2_301	F	R	Wild	Powell-Cotton Museum
<i>Pan troglodytes</i>	NH_MER_279	F	L	Wild	Powell-Cotton Museum
<i>Pan troglodytes</i>	NH_MER35_86	F	L	Wild	Powell-Cotton Museum
<i>Pan troglodytes</i>	NH_MER35_105	F	R	Wild	Powell-Cotton Museum
<i>Pan troglodytes</i>	MPITC_11903	M	L	Wild	Max Planck Institute for Evolutionary Anthropology, Taï Chimp Collection
<i>Pan troglodytes</i>	MPITC_11789	M	L	Wild	Max Planck Institute for Evolutionary Anthropology, Taï Chimp Collection
<i>Pan troglodytes</i>	MPITC_11781	M	L	Wild	Max Planck Institute for Evolutionary Anthropology, Taï Chimp Collection
<i>Pan troglodytes</i>	ZSM_AP-122	M	R	Wild	Bavarian State Collection of Zoology
<i>Pan troglodytes</i>	PC_ZVII_24	M	R	Wild	Powell-Cotton Museum
<i>Pan troglodytes</i>	NH_MER33_712	M	R	Wild	Powell-Cotton Museum
<i>Pan troglodytes</i>	NH_MER33_724	M	L	Wild	Powell-Cotton Museum
<i>Pan troglodytes</i>	NH_MER32_401	M	L	Wild	Powell-Cotton Museum
<i>Pan troglodytes</i>	NH_MER33_440	M	R	Wild	Powell-Cotton Museum
<i>Pan troglodytes</i>	NH_MER36_254	M	L	Wild	Powell-Cotton Museum
<i>Gorilla gorilla</i>	ZMB_11642	UK	R	Wild	Natural History Museum, Berlin
<i>Gorilla gorilla</i>	ZMB_83545	M	R	Wild	Natural History Museum, Berlin
<i>Gorilla gorilla</i>	PC_MER_95	F	R	Wild	Powell-Cotton Museum
<i>Gorilla gorilla</i>	PC_MER_135	M	L	Wild	Powell-Cotton Museum
<i>Gorilla gorilla</i>	PC_MER_264	M	L	Wild	Powell-Cotton Museum
<i>Gorilla gorilla</i>	PC_MER_300	F	R	Wild	Powell-Cotton Museum

<i>Gorilla gorilla</i>	PC_MER_372	M	R	Wild	Powell-Cotton Museum
<i>Gorilla gorilla</i>	PC_MER_962	M	R	Wild	Powell-Cotton Museum
<i>Gorilla gorilla</i>	PC_MER1_29	F	R	Wild	Powell-Cotton Museum
<i>Gorilla gorilla</i>	PC_MER_138	F	L	Wild	Powell-Cotton Museum
<i>Gorilla gorilla</i>	PC_MER_174	F	R	Wild	Powell-Cotton Museum
<i>Gorilla gorilla</i>	PC_MER_696	F	R	Wild	Powell-Cotton Museum
<i>Gorilla gorilla</i>	PC_MER_856	F	L	Wild	Powell-Cotton Museum
<i>Gorilla gorilla</i>	PC_ZII_64	M	R	Wild	Powell-Cotton Museum
<i>Gorilla gorilla</i>	PC_ZVI_32	M	R	Wild	Powell-Cotton Museum
<i>Gorilla gorilla</i>	NH_MER33_755	F	R	Wild	Powell-Cotton Museum
<i>Gorilla gorilla</i>	NH_MER33_461	M	R	Wild	Powell-Cotton Museum
<i>Gorilla gorilla</i>	NH_CAM1_106	M	R	Wild	Powell-Cotton Museum
<i>Gorilla gorilla</i>	NH_CAM1_105	M	R	Wild	Powell-Cotton Museum
<i>Gorilla gorilla</i>	NH_MER35_150	F	R	Wild	Powell-Cotton Museum
<i>Gorilla gorilla</i>	NH_CAM1_98	F	L	Wild	Powell-Cotton Museum
<i>Gorilla gorilla</i>	NH_MER35_136	F	L	Wild	Powell-Cotton Museum
<i>Gorilla gorilla</i>	NH_MER35_139	F	L	Wild	Powell-Cotton Museum
<i>Gorilla gorilla</i>	NH_FC_130	M	L	Wild	Powell-Cotton Museum
<i>Gorilla gorilla</i>	NH_FC_123	M	L	Wild	Powell-Cotton Museum
<i>Pongo abelii</i>	SMF_6785	M	R	Wild	Senckenberg Natural History Museum, Frankfurt
<i>Pongo abelii</i>	SMF_6779	F	L	Wild	Senckenberg Natural History Museum, Frankfurt
<i>Pongo pygmaeus</i>	ZSM_1907_0633b	F	R	Wild	Bavarian State Collection of Zoology
<i>Pongo pygmaeus</i>	ZSM_1907_0629b	M	R	Wild	Bavarian State Collection of Zoology
<i>Pongo pygmaeus</i>	ZSM_1907_0660	F	R	Wild	Bavarian State Collection of Zoology
<i>Pongo pygmaeus</i>	ZSM_AP-120	M	L	Wild	Bavarian State Collection of Zoology
<i>Pongo pygmaeus</i>	ZSM_1907_0483	F	R	Wild	Bavarian State Collection of Zoology
<i>Pongo pygmaeus</i>	ZSM_1909_0801	M	R	Wild	Bavarian State Collection of Zoology
<i>Pongo pygmaeus</i>	ZMB_87092	F	R	Wild	Natural History Museum, Berlin

Note: M = male; F = female; R = right; L = left; UK = unknown sex/side; R/L = to have all four digits represented, some phalanges were from the right side of the body and some from the left.

Supplementary Table 3.2: Test statistics for omnibus permutational multivariate analysis of variance (PERMANOVA) and subsequent pairwise one-way permutational multivariate analysis of variance on the first 3 PC scores of the cortical bone thickness distribution pattern PCAs. The extant taxa all significantly differ from each other in the PCAs across all four digits.

PERMANOVA			Pairwise one-way MANOVA			
			<i>Pan</i>	<i>Gorilla</i>	<i>Pongo</i>	
PP2	R²	0.707	<i>H.sapiens</i>	0.006	0.005	0.006
	p-value	<0.001	<i>Pan</i>		0.021	0.038
			<i>Gorilla</i>			0.016
PP3	R²	0.696	<i>H.sapiens</i>	0.006	0.009	0.006
	p-value	<0.001	<i>Pan</i>		0.010	0.012
			<i>Gorilla</i>			0.001
PP4	R²	0.719	<i>H.sapiens</i>	<0.001	<0.001	<0.001
	p-value	<0.001	<i>Pan</i>		<0.001	<0.001
			<i>Gorilla</i>			<0.001
PP5	R²	0.683	<i>H.sapiens</i>	<0.001	<0.001	<0.001
	p-value	<0.001	<i>Pan</i>		<0.001	<0.001
			<i>Gorilla</i>			<0.001

Supplementary Table 3.3: Mean values of standardised cross-sectional properties across species at 35%, 50%, and 65% of the phalanx

		<i>H. sapiens</i>	<i>Pan</i>	<i>Gorilla</i>	<i>Pongo</i>
35% cross-section					
PP2	CA (mm ²)	0.677	0.780	1.285	0.592
	Z _{pol} (mm ³)	1.815	1.559	4.214	1.462
	J (mm ⁴)	10.380	7.459	37.262	6.864
PP3	CA (mm ²)	0.679	0.876	1.366	0.612
	Z _{pol} (mm ³)	1.975	2.257	4.950	1.669
	J (mm ⁴)	11.606	13.102	48.787	8.446
PP4	CA (mm ²)	0.639	0.819	1.227	0.629
	Z _{pol} (mm ³)	1.672	1.857	4.003	1.742
	J (mm ⁴)	9.549	9.564	36.234	9.119
PP5	CSA (mm ²)	0.566	0.695	1.105	0.541
	Z _{pol} (mm ³)	1.314	1.265	2.986	1.152
	J (mm ⁴)	6.613	4.751	22.827	4.888
50% cross-section					
PP2	CA (mm ²)	0.767	0.832	1.412	0.636
	Z _{pol} (mm ³)	1.678	1.456	4.317	1.302
	J (mm ⁴)	9.092	7.894	37.632	6.901
PP3	CA (mm ²)	0.779	0.978	1.507	0.663
	Z _{pol} (mm ³)	1.838	2.196	5.018	1.496
	J (mm ⁴)	10.479	14.420	49.767	8.330
PP4	CA (mm ²)	0.750	0.893	1.315	0.672
	Z _{pol} (mm ³)	1.637	1.740	4.020	1.529
	J (mm ⁴)	9.076	10.237	36.357	8.800
PP5	CA (mm ²)	0.664	0.711	1.246	0.567
	Z _{pol} (mm ³)	1.207	1.067	3.178	1.000
	J (mm ⁴)	5.683	4.509	24.766	4.805
65% cross-section					
PP2	CA (mm ²)	0.817	0.860	1.417	0.677
	Z _{pol} (mm ³)	1.626	1.514	3.724	1.424
	J (mm ⁴)	8.625	8.158	31.730	8.846
PP3	CA (mm ²)	0.854	1.031	1.563	0.732
	Z _{pol} (mm ³)	1.826	2.277	4.635	1.732
	J (mm ⁴)	10.507	15.152	45.513	11.540
PP4	CA (mm ²)	0.823	0.940	1.389	0.736

	Z_{pol} (mm ³)	1.675	1.847	3.733	1.740
	J (mm ⁴)	9.373	10.891	32.763	11.794
PP5	CA (mm ²)	0.688	0.719	1.263	0.602
	Z_{pol} (mm ³)	1.121	1.096	2.821	1.106
	J (mm ⁴)	4.882	4.355	20.961	6.031

Abbreviations: CA = cortical area; Z_{pol} = polar section modulus; J = polar second moment of area.

Supplementary Table 3.4: Test statistics for the Kruskal-Wallis tests of cross-sectional properties across species at 35%, 50%, and 65% of the phalanx.

			35%	50%	65%
PP2	CA	KW Chi-squared	48.974	47.772	44.482
		df	3	3	3
		p-value	<0.001	<0.001	<0.001
	Z _{pol}	KW Chi-squared	44.875	48.974	42.641
		df	3	3	3
		p-value	<0.001	<0.001	<0.001
	J	KW Chi-squared	48.988	46.298	42.886
		df	3	3	3
		p-value	<0.001	<0.001	<0.001
PP3	CA	KW Chi-squared	62.862	53.026	53.842
		df	3	3	3
		p-value	<0.001	<0.001	<0.001
	Z _{pol}	KW Chi-squared	53.398	56.122	50.671
		df	3	3	3
		p-value	<0.001	<0.001	<0.001
	J	KW Chi-squared	54.122	56.903	53.523
		df	3	3	3
		p-value	<0.001	<0.001	<0.001
PP4	CA	KW Chi-squared	53.725	44.895	40.742
		df	3	3	3
		p-value	<0.001	<0.001	<0.001
	Z _{pol}	KW Chi-squared	37.890	42.415	36.775
		df	3	3	3
		p-value	<0.001	<0.001	<0.001
	J	KW Chi-squared	42.308	43.382	39.561
		df	3	3	3
		p-value	<0.001	<0.001	<0.001
PP5	CA	KW Chi-squared	46.387	44.453	43.900
		df	3	3	3
		p-value	<0.001	<0.001	<0.001
	Z _{pol}	KW Chi-squared	39.899	44.491	42.419
		df	3	3	3
		p-value	<0.001	<0.001	<0.001
	J	KW Chi-squared	45.116	46.606	45.044
		df	3	3	3
		p-value	<0.001	<0.001	<0.001

Abbreviations: CA = cortical area; Z_{pol} = polar section modulus; J = polar second moment of area

Supplementary Table 3.5: Significance values for post hoc comparisons of cross-sectional properties across species at 35%, 50%, and 65% of the phalanx.

			35%			50%			65%		
			<i>Pan</i>	<i>Gorilla</i>	<i>Pongo</i>	<i>Pan</i>	<i>Gorilla</i>	<i>Pongo</i>	<i>Pan</i>	<i>Gorilla</i>	<i>Pongo</i>
PP2	CA	<i>H.sapiens</i>	0.433	<0.001	0.094	1.000	<0.001	0.613	1.000	<0.001	0.682
		<i>Pan</i>		<0.001	0.133		<0.001	0.148		<0.001	0.342
		<i>Gorilla</i>			<0.001			<0.001			<0.001
	Z _{pol}	<i>H.sapiens</i>	0.710	<0.001	0.917	0.938	<0.001	0.552	1.000	<0.001	1.000
		<i>Pan</i>		<0.001	1.000		<0.001	1.000		<0.001	1.000
		<i>Gorilla</i>			<0.001			<0.001			<0.001
	J	<i>H.sapiens</i>	0.263	<0.001	0.379	1.000	<0.001	0.795	1.000	<0.001	1.000
		<i>Pan</i>		<0.001	1.000		<0.001	1.000		<0.001	1.000
		<i>Gorilla</i>			<0.001			<0.001			<0.001
PP3	CA	<i>H.sapiens</i>	0.004	<0.001	1.000	0.029	<0.001	1.000	0.987	<0.001	1.000
		<i>Pan</i>		0.001	0.007		0.003	0.006		<0.001	0.032
		<i>Gorilla</i>			<0.001			<0.001			<0.001
	Z _{pol}	<i>H.sapiens</i>	0.890	<0.001	1.000	0.485	<0.001	1.000	0.259	<0.001	1.000
		<i>Pan</i>		<0.001	0.182		<0.001	0.077		<0.001	0.509
		<i>Gorilla</i>			<0.001			<0.001			<0.001
	J	<i>H.sapiens</i>	1.000	<0.001	0.680	0.224	<0.001	1.000	0.091	<0.001	1.000
		<i>Pan</i>		<0.001	0.185		<0.001	0.101		<0.001	1.000
		<i>Gorilla</i>			<0.001			<0.001			<0.001
PP4	CA	<i>H.sapiens</i>	0.003	<0.001	1.000	0.159	<0.001	1.000	0.624	<0.001	1.000
		<i>Pan</i>		0.004	0.048		<0.001	0.096		<0.001	0.293
		<i>Gorilla</i>			<0.001			<0.001			<0.001
	Z _{pol}	<i>H.sapiens</i>	1.000	<0.001	1.000	1.000	<0.001	1.000	1.000	<0.001	1.000
		<i>Pan</i>		<0.001	1.000		<0.001	1.000		<0.001	1.000
		<i>Gorilla</i>			<0.001			<0.001			<0.001
	J	<i>H.sapiens</i>	1.000	<0.001	1.000	1.000	<0.001	1.000	1.000	<0.001	1.000
		<i>Pan</i>		<0.001	1.000		<0.001	1.000		<0.001	1.000
		<i>Gorilla</i>			<0.001			<0.001			<0.001
PP5	CA	<i>H.sapiens</i>	0.161	<0.001	1.000	1.000	<0.001	1.000	1.000	<0.001	1.000
		<i>Pan</i>		<0.001	0.256		<0.001	0.472		<0.001	1.000
		<i>Gorilla</i>			<0.001			<0.001			<0.001
	Z _{pol}	<i>H.sapiens</i>	1.000	<0.001	1.000	1.000	<0.001	1.000	1.000	<0.001	1.000
		<i>Pan</i>		<0.001	1.000		<0.001	1.000		<0.001	1.000
		<i>Gorilla</i>			<0.001			<0.001			<0.001
	J	<i>H.sapiens</i>	0.447	<0.001	1.000	1.000	<0.001	1.000	1.000	<0.001	1.000
		<i>Pan</i>		<0.001	1.000		<0.001	1.000		<0.001	0.913
		<i>Gorilla</i>			<0.001			<0.001			<0.001

Abbreviations: CA = cortical area; Z_{pol} = polar section modulus; J = polar second moment of area; NS = not significant (p>0.05).

Supplementary Table 3.6: Test statistics for the Kruskal-Wallis tests of cross-sectional properties within species, across the digits at 35%, 50% and 65% of the phalanx.

			35%	50%	65%
<i>H. sapiens</i>	CA	KW Chi-squared	11.361	6.917	10.609
		df	3	3	3
		p-value	0.009	0.075	0.014
	Z _{pol}	KW Chi-squared	19.540	18.003	23.193
		df	3	3	3
		p-value	<0.001	<0.001	<0.001
	J	KW Chi-squared	18.827	20.963	28.576
		df	3	3	3
		p-value	<0.001	<0.001	<0.001
<i>Pan</i>	CA	KW Chi-squared	18.865	27.350	29.112
		df	3	3	3
		p-value	<0.001	<0.001	<0.001
	Z _{pol}	KW Chi-squared	42.073	48.157	45.401
		df	3	3	3
		p-value	<0.001	<0.001	<0.001
	J	KW Chi-squared	50.125	52.442	51.949
		df	3	3	3
		p-value	<0.001	<0.001	<0.001
<i>Gorilla</i>	CA	KW Chi-squared	10.035	9.143	9.754
		df	3	3	3
		p-value	0.018	0.028	0.021
	Z _{pol}	KW Chi-squared	15.951	14.913	16.274
		df	3	3	3
		p-value	0.001	0.001	<0.001
	J	KW Chi-squared	17.825	16.470	19.310
		df	3	3	3
		p-value	<0.001	<0.001	<0.001
<i>Pongo</i>	CA	KW Chi-squared	3.245	3.600	3.952
		df	3	3	3
		p-value	0.355	0.308	0.267
	Z _{pol}	KW Chi-squared	5.556	7.211	6.739
		df	3	3	3
		p-value	0.135	0.065	0.081
	J	KW Chi-squared	7.419	6.911	7.967
		df	3	3	3
		p-value	0.060	0.075	0.051

Abbreviations: CA = cortical area; Z_{pol} = polar section modulus; J = polar second moment of area

Supplementary Table 3.7: Significance values for post hoc comparisons of cross-sectional properties within species, across the digits at 35%, 50% and 65% of the phalanx.

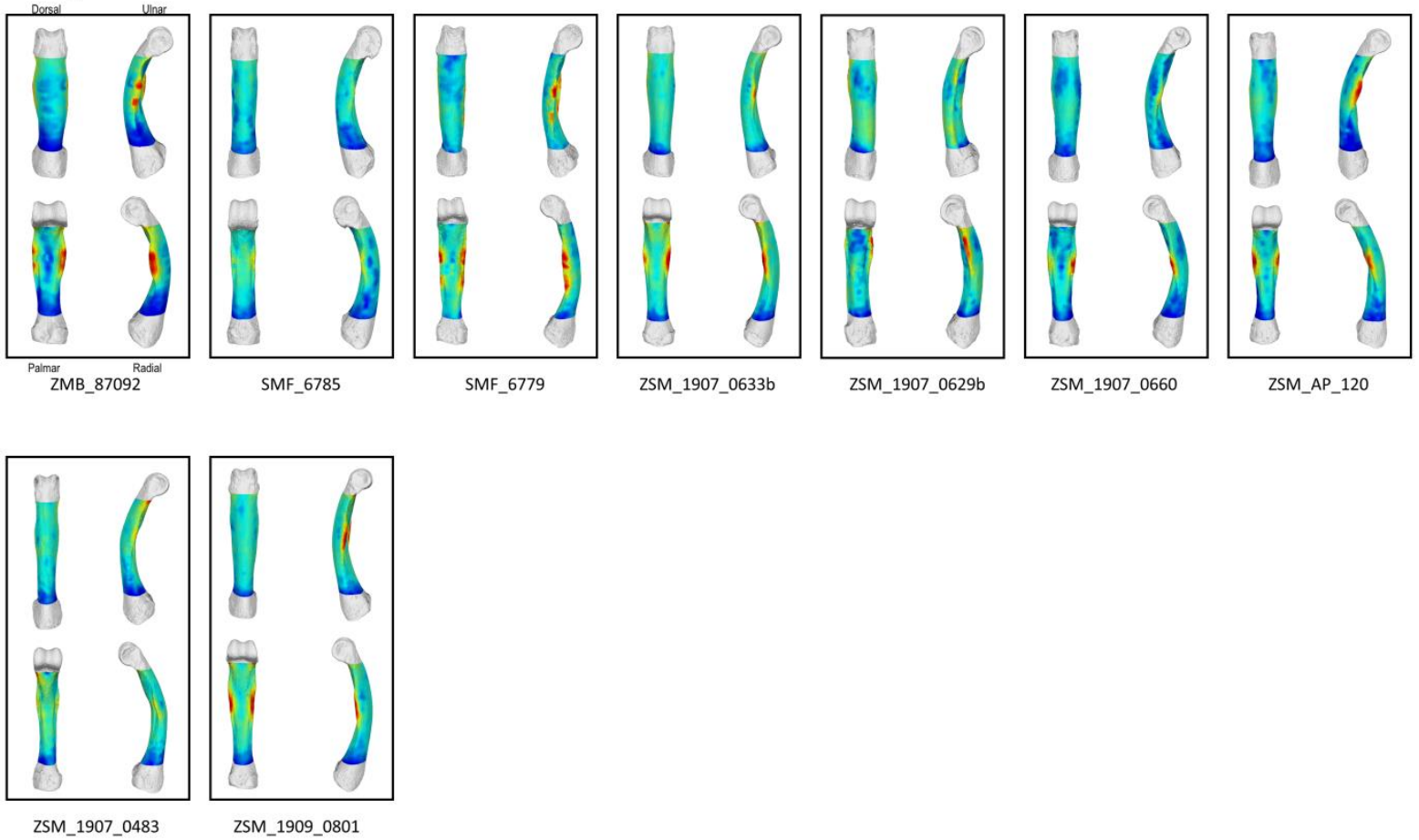
			35%			50%			65%		
			PP3	PP4	PP5	PP3	PP4	PP5	PP3	PP4	PP5
<i>H. sapiens</i>	CA	PP2	1.000	1.000	0.017	-	-	-	1.000	1.000	0.124
		PP3		1.000	0.008		-	-		1.000	0.012
		PP4			0.284			-			0.076
	<i>Z_{pol}</i>	PP2	1.000	1.000	0.007	1.000	1.000	0.014	1.000	1.000	0.003
		PP3		0.275	<0.001		1.000	<0.001		1.000	<0.001
		PP4			0.101			0.027			<0.001
	J	PP2	1.000	1.000	0.006	1.000	1.000	0.011	0.601	1.000	0.004
		PP3		0.544	<0.001		1.000	<0.001		1.000	<0.001
		PP4			0.057			0.006			0.002
<i>Pan</i>	CA	PP2	0.160	1.000	0.221	0.006	1.000	0.048	0.005	0.922	0.049
		PP3		1.000	<0.001		0.863	<0.001		1.000	<0.001
		PP4			0.010			<0.001			<0.001
	<i>Z_{pol}</i>	PP2	<0.001	0.257	0.315	<0.001	0.293	0.064	<0.001	0.290	0.049
		PP3		0.092	<0.001		0.101	<0.001		0.252	<0.001
		PP4			<0.001			<0.001			<0.001
	J	PP2	<0.001	0.256	0.057	<0.001	0.300	0.202	<0.001	0.330	0.011
		PP3		0.092	<0.001		0.117	<0.001		0.185	<0.001
		PP4			<0.001			<0.001			<0.001
<i>Gorilla</i>	CA	PP2	1.000	1.000	0.211	1.000	1.000	0.636	1.000	1.000	0.482
		PP3		0.719	0.005		0.205	0.027		0.499	0.012
		PP4			0.904			1.000			1.000
	<i>Z_{pol}</i>	PP2	0.897	1.000	0.088	0.668	1.000	0.183	0.320	1.000	0.253
		PP3		0.394	<0.001		0.204	<0.001		0.337	<0.001
		PP4			0.275			0.665			0.271
	J	PP2	0.400	1.000	0.126	0.284	1.000	0.272	0.165	1.000	0.208
		PP3		0.297	<0.001		0.241	<0.001		0.256	<0.001
		PP4			0.201			0.358			0.153

Abbreviations: CA = cortical area; *Z_{pol}* = polar section modulus; J = polar second moment of area.

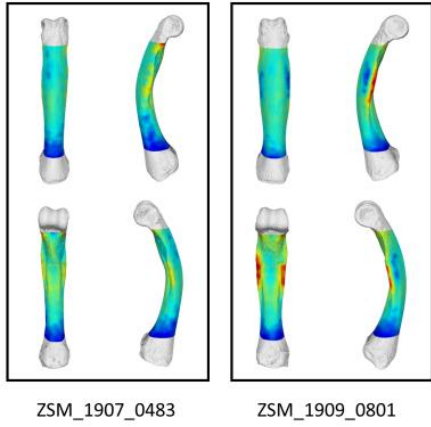
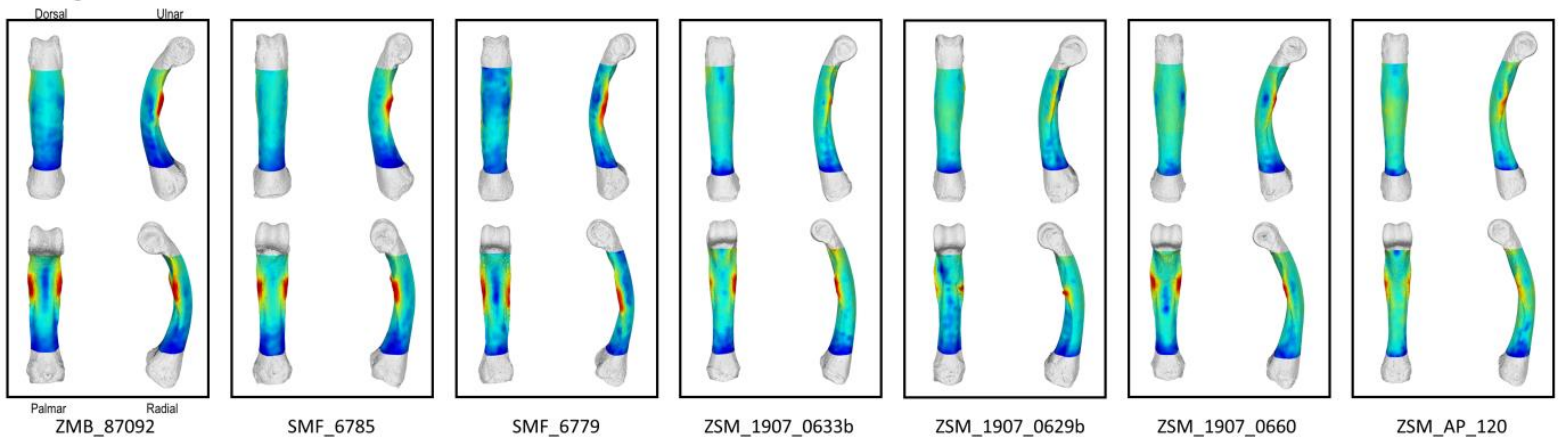
Note: The proximal phalanges of *Pongo* are not represented because they did not show significant differences. CA at 50% of the *H. sapiens* phalanges also did not show significant differences.

Supplementary Figure 3.1: Cortical thickness distribution maps of each individual used in the study. Specimen IDs of individuals are under each map.

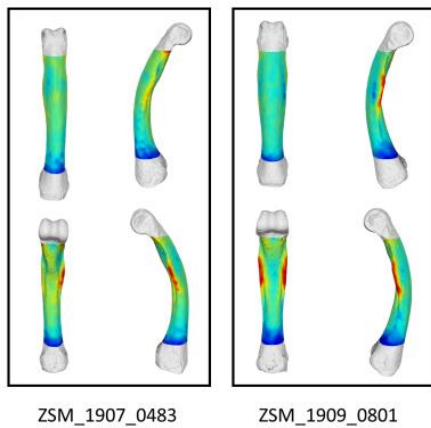
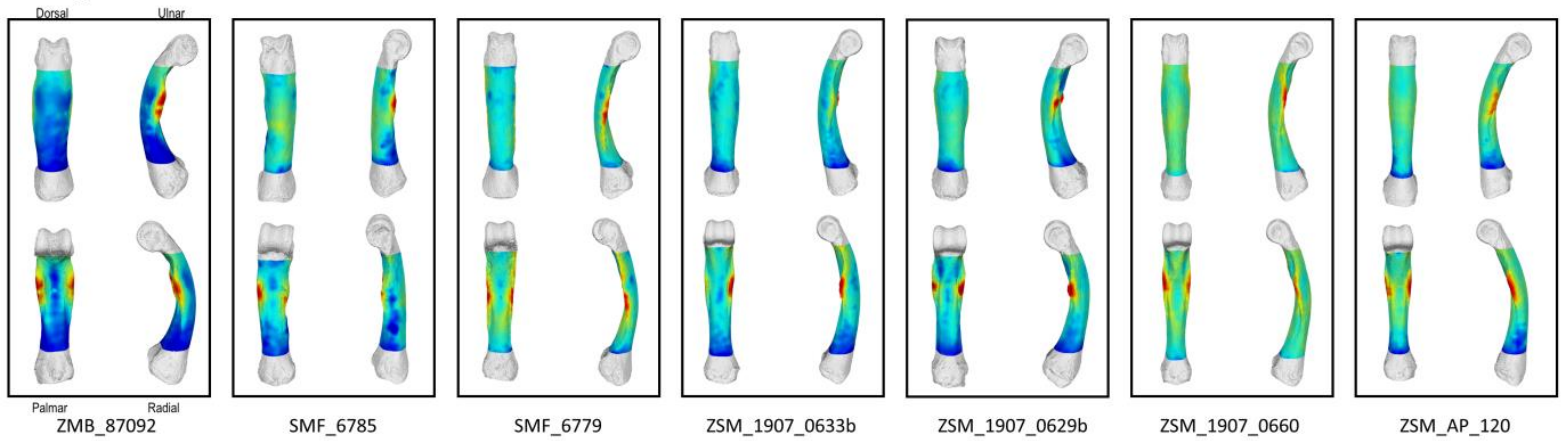
Pongo PP2



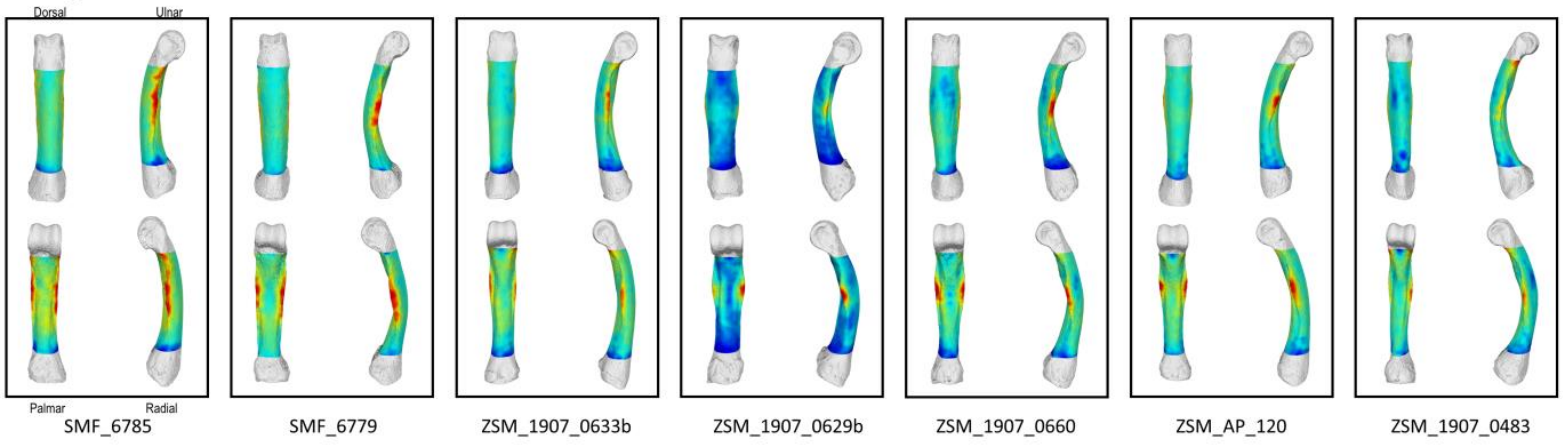
Pongo PP3



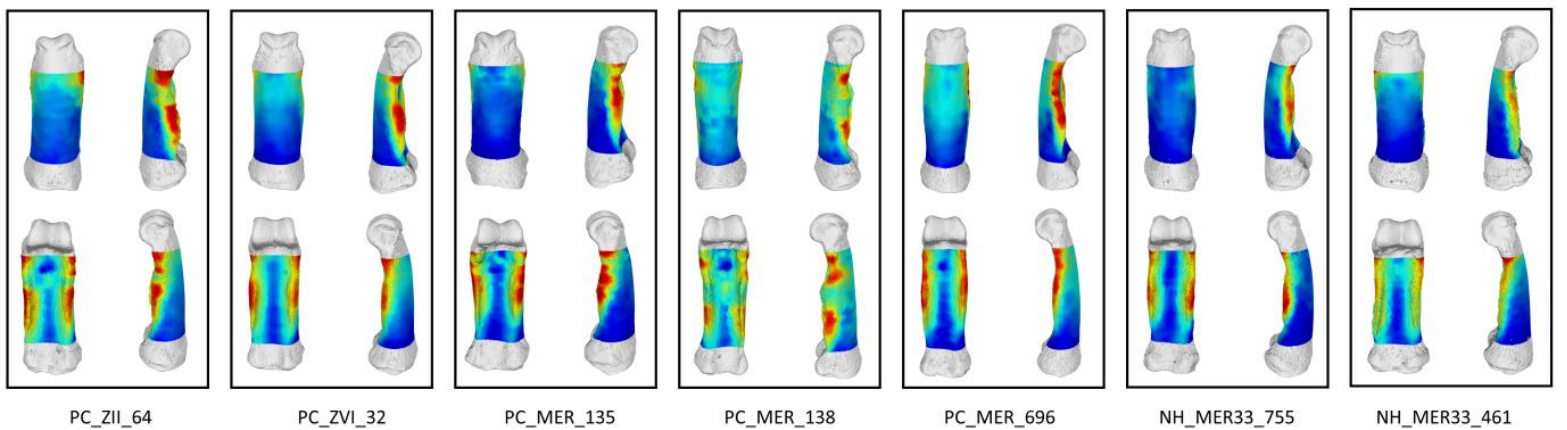
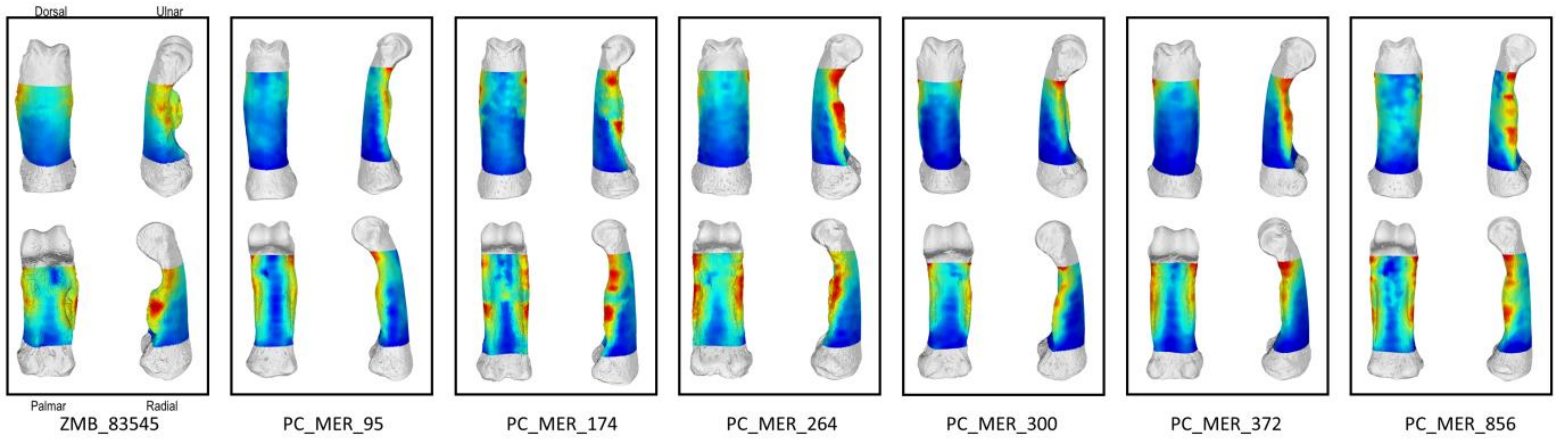
Pongo PP4



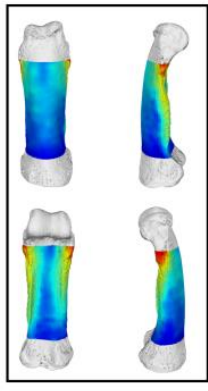
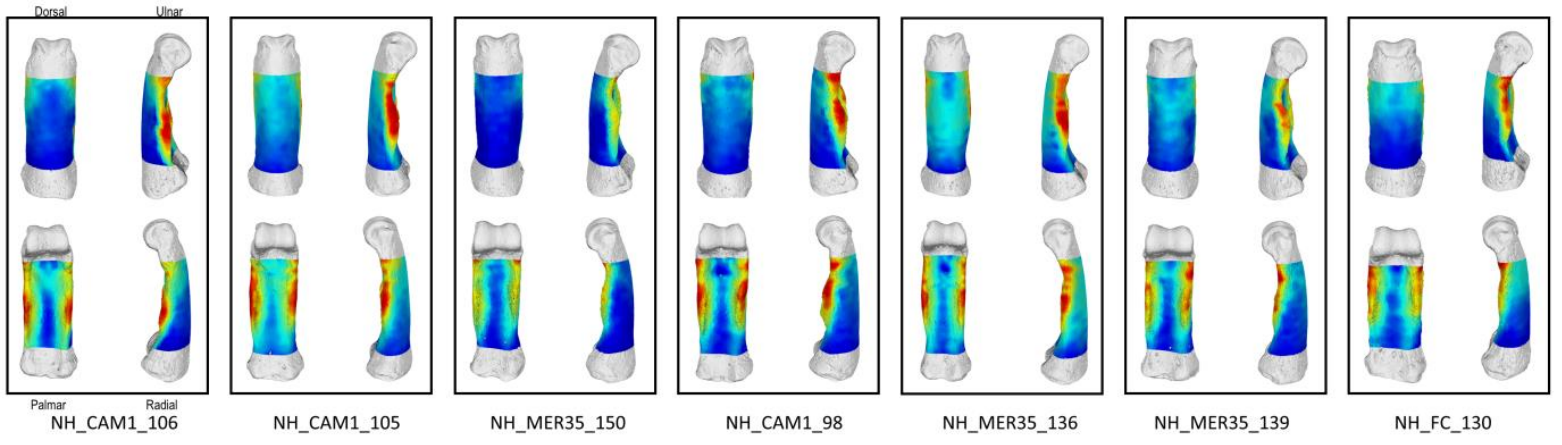
Pongo PP5



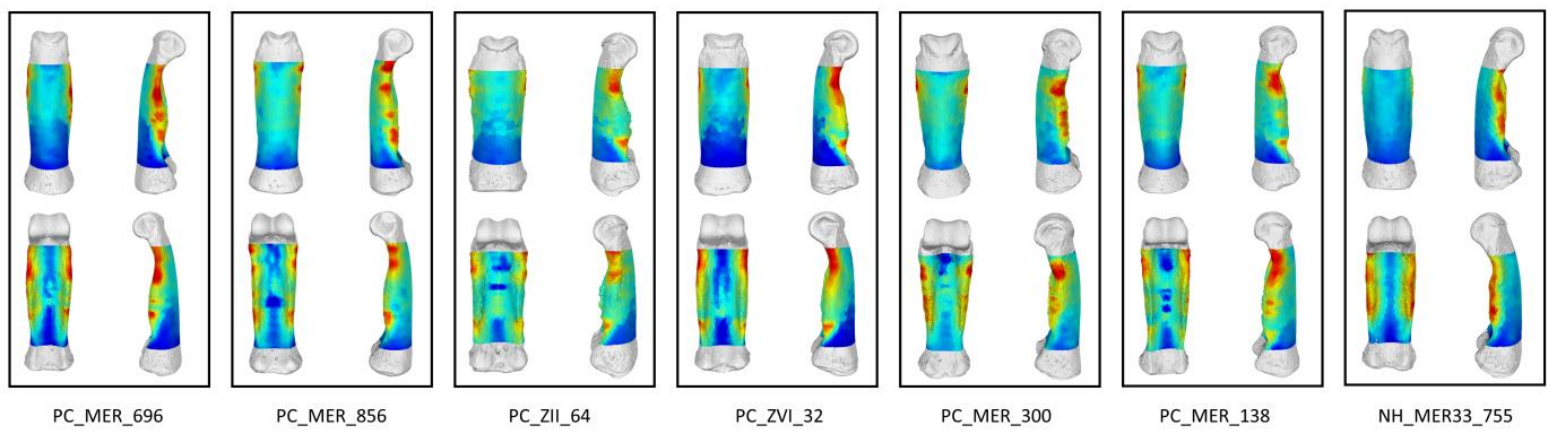
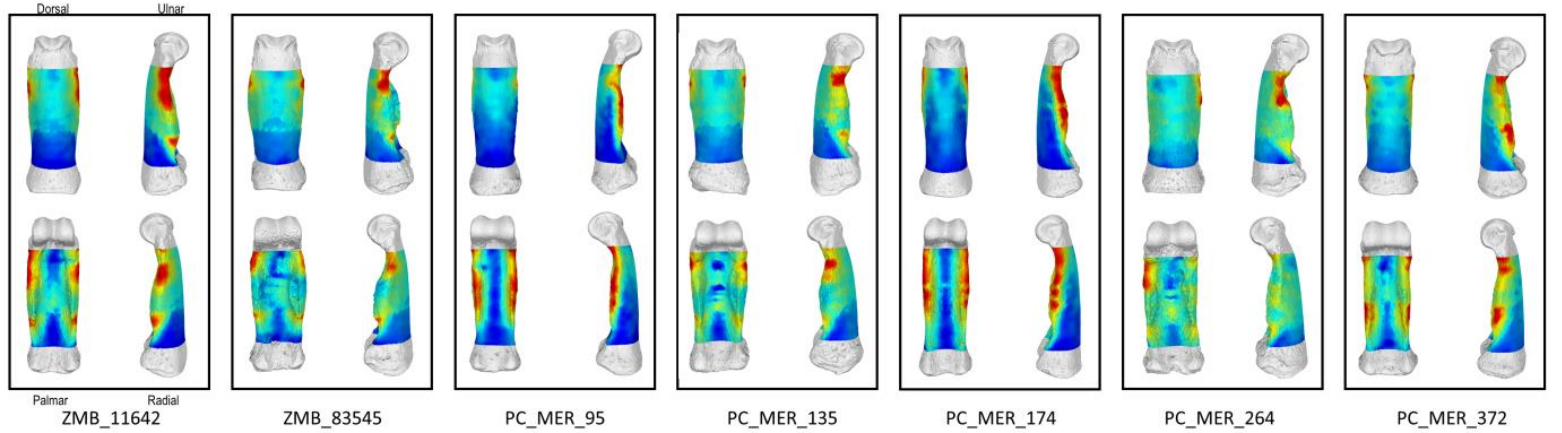
Gorilla PP2



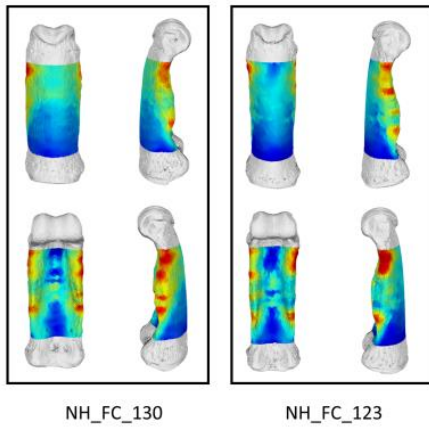
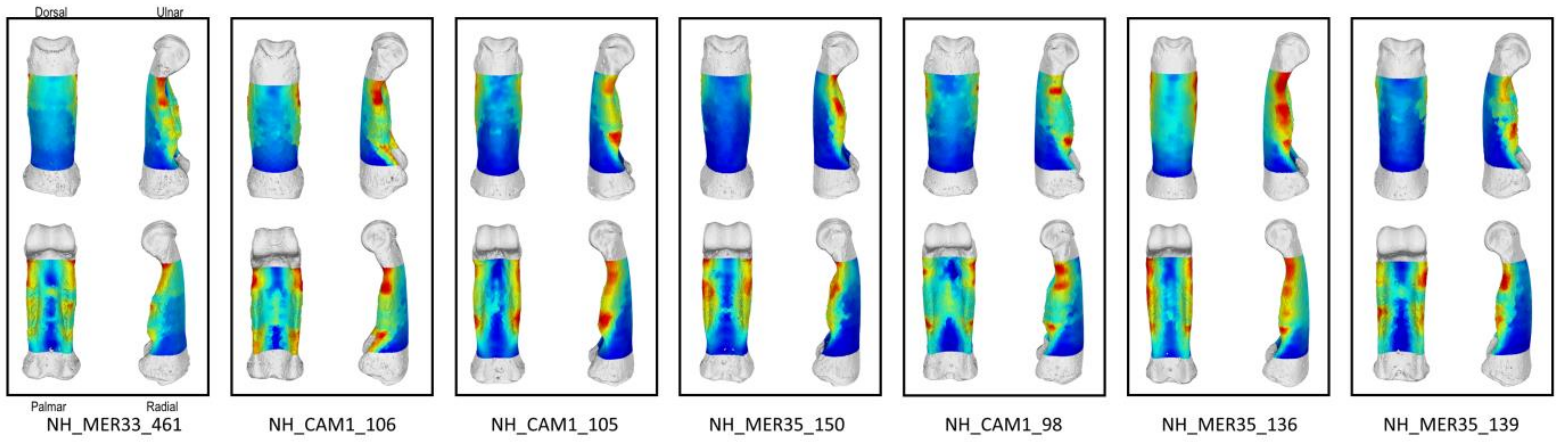
Gorilla PP2



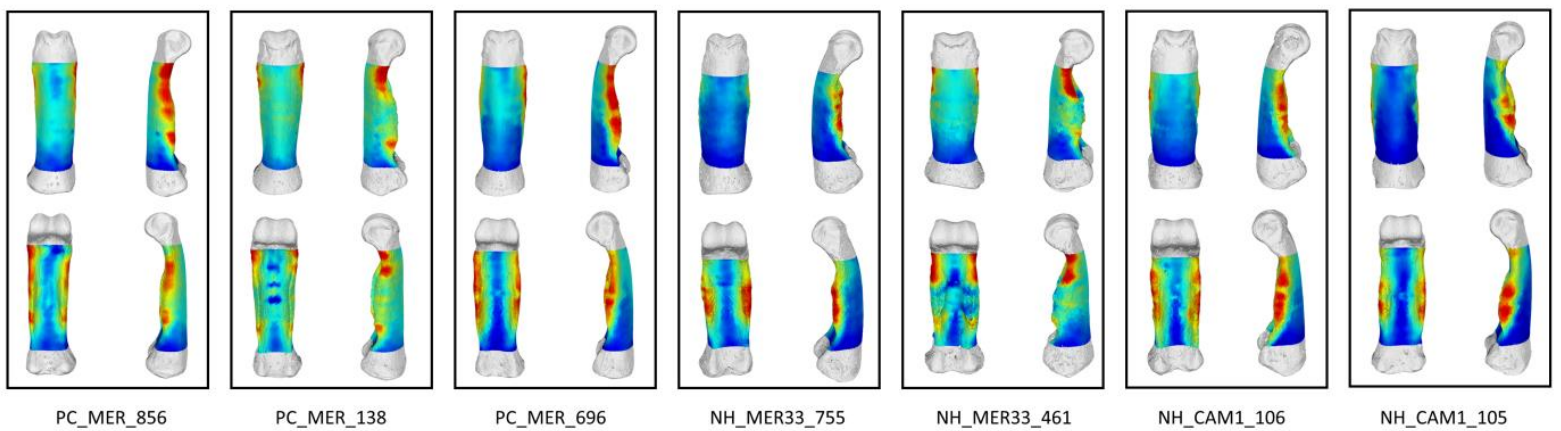
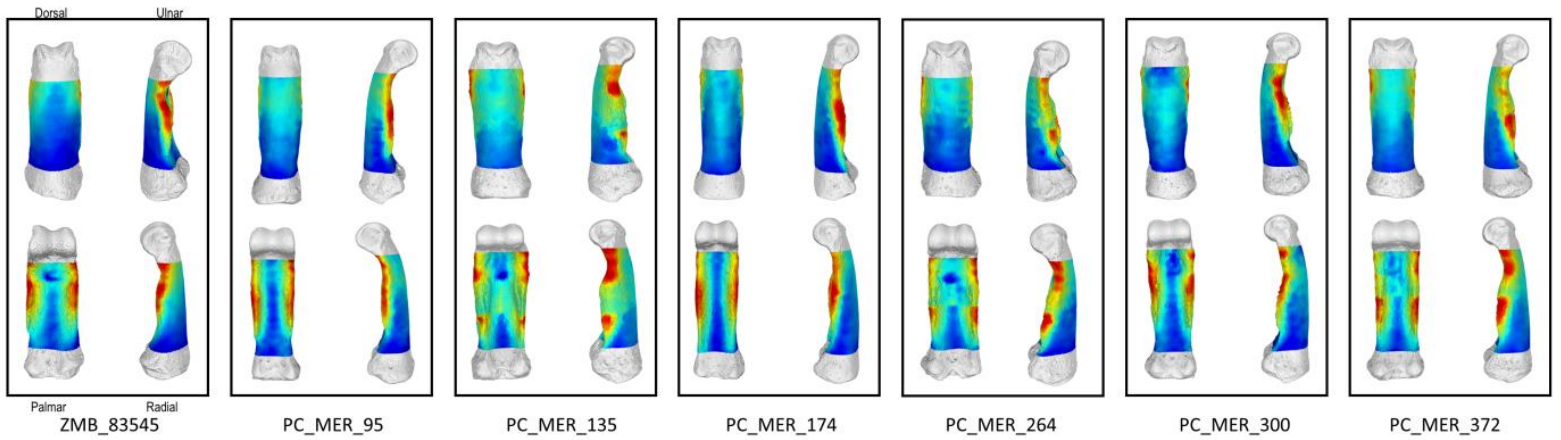
Gorilla PP3



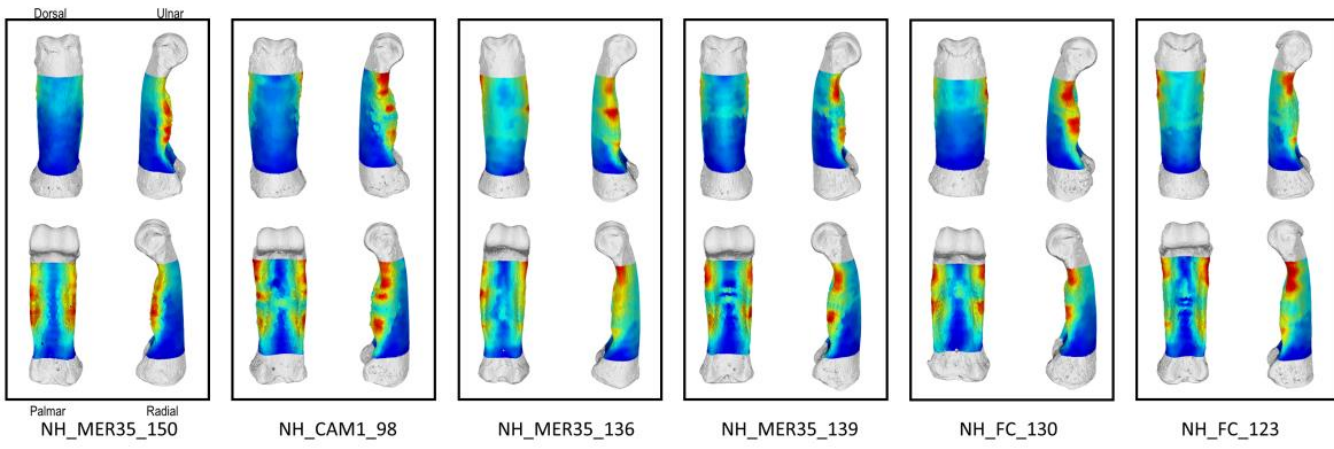
Gorilla PP3



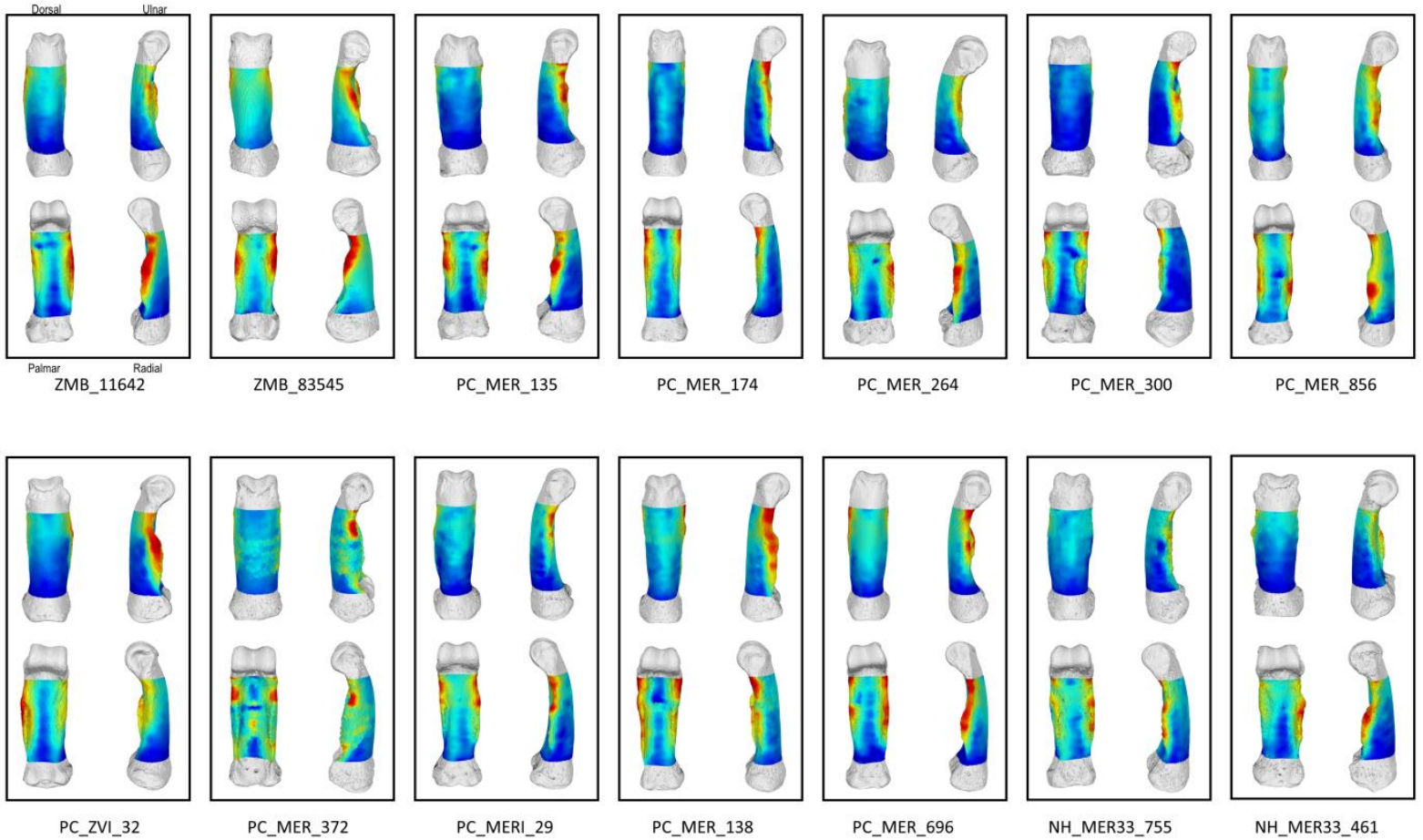
Gorilla PP4



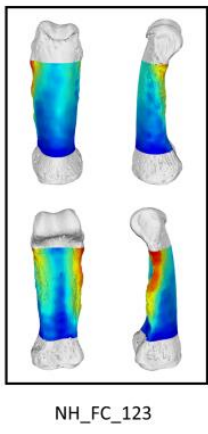
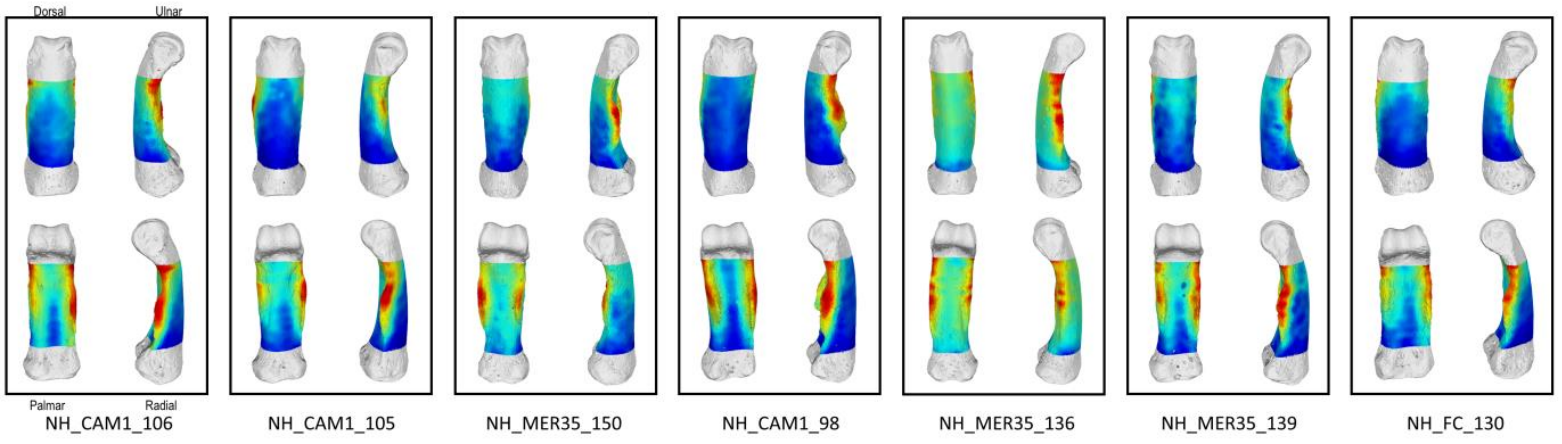
Gorilla PP4



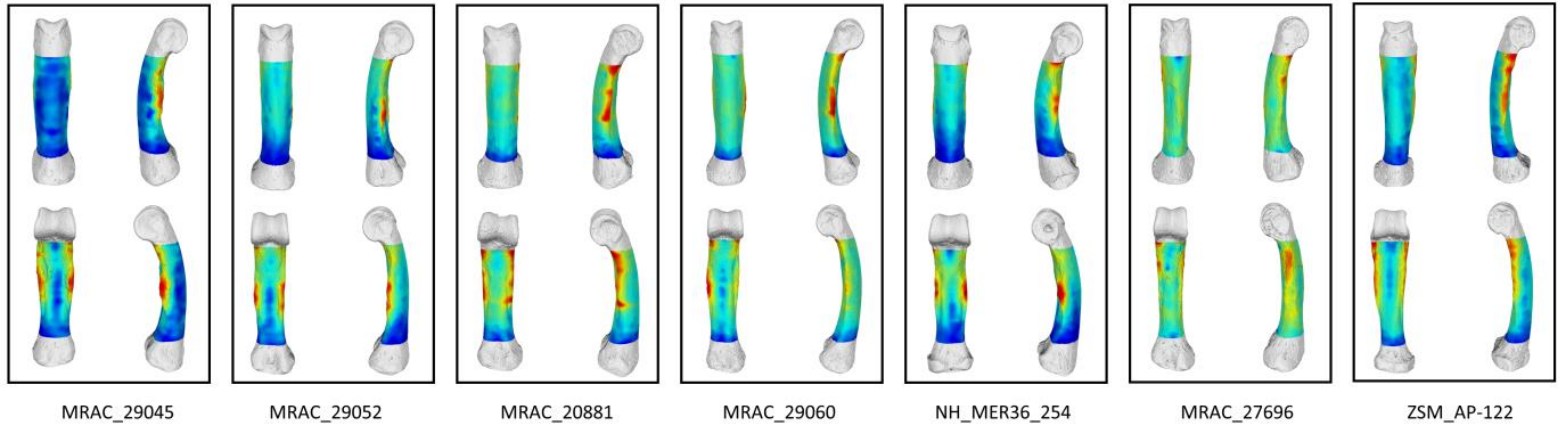
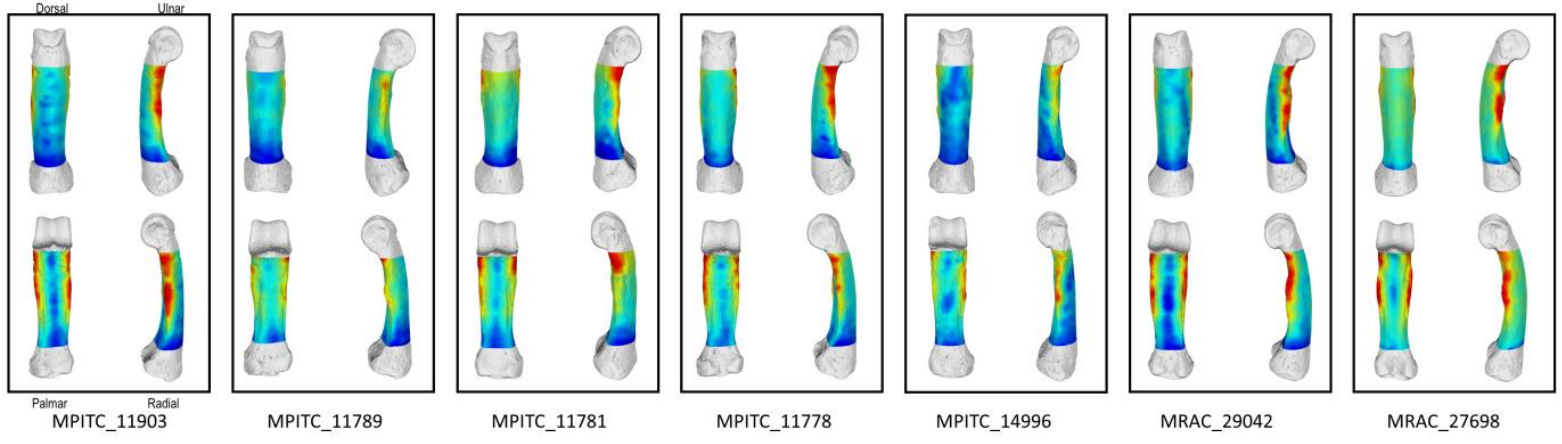
Gorilla PP5



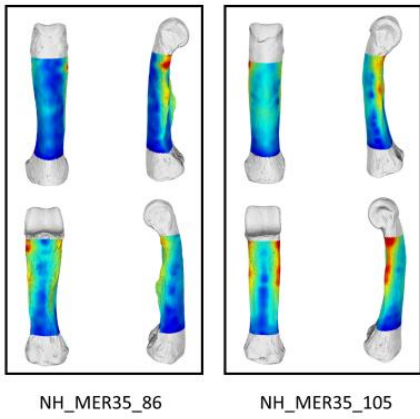
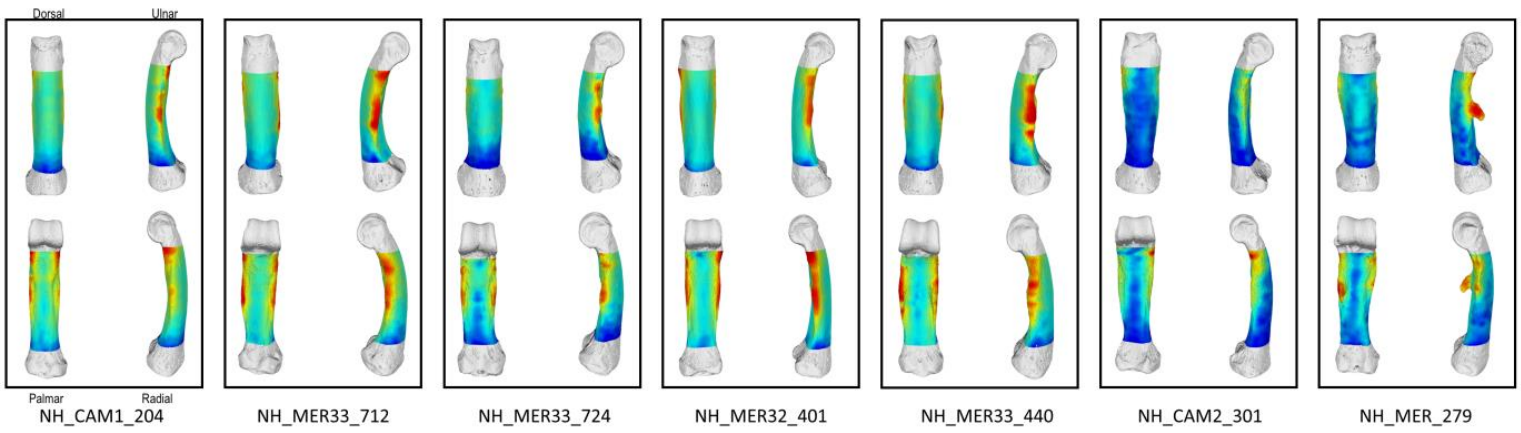
Gorilla PP5



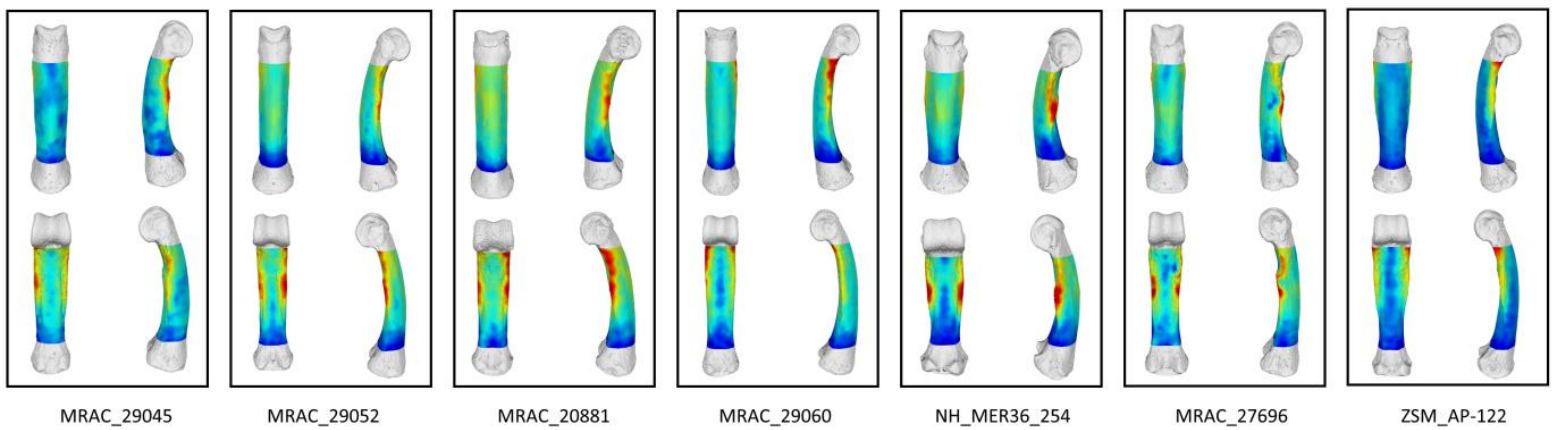
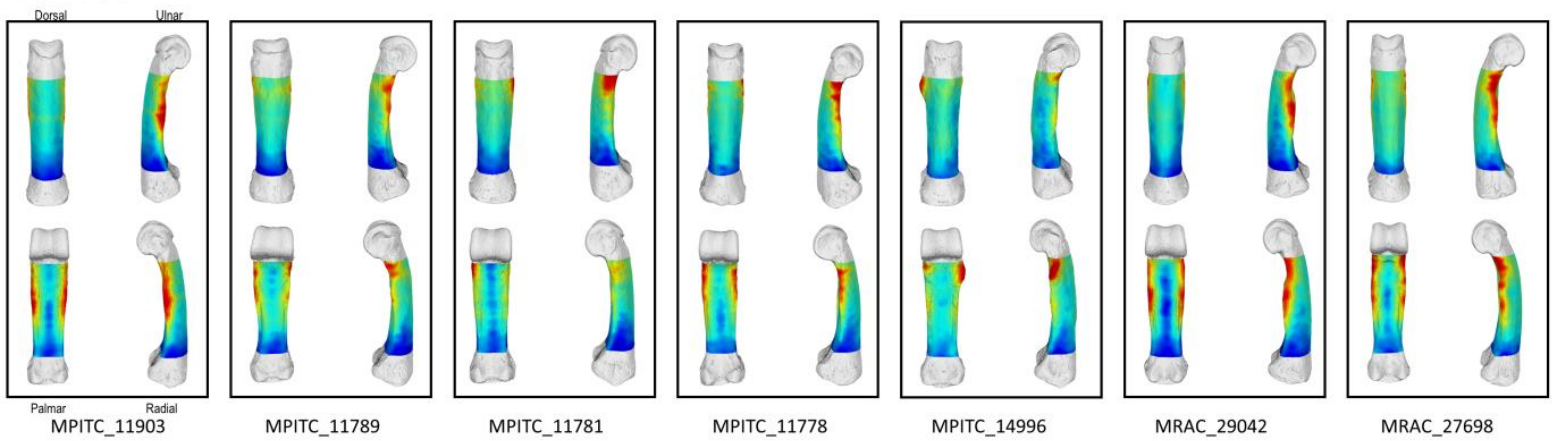
Pan PP2



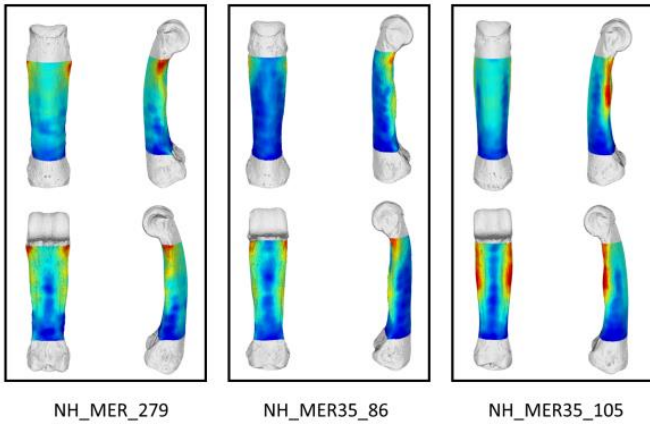
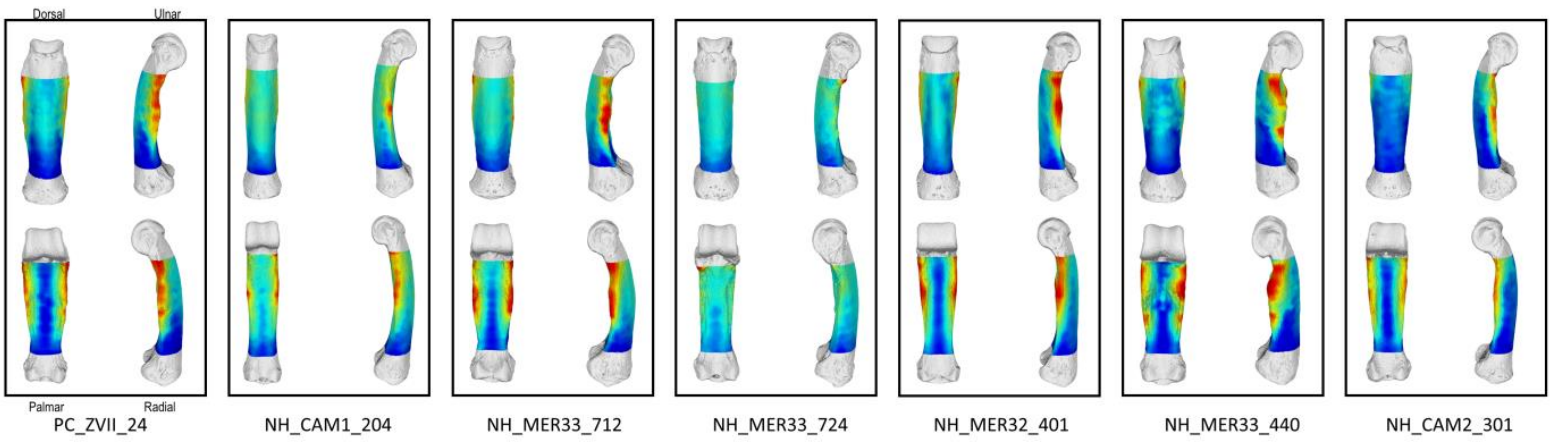
Pan PP2



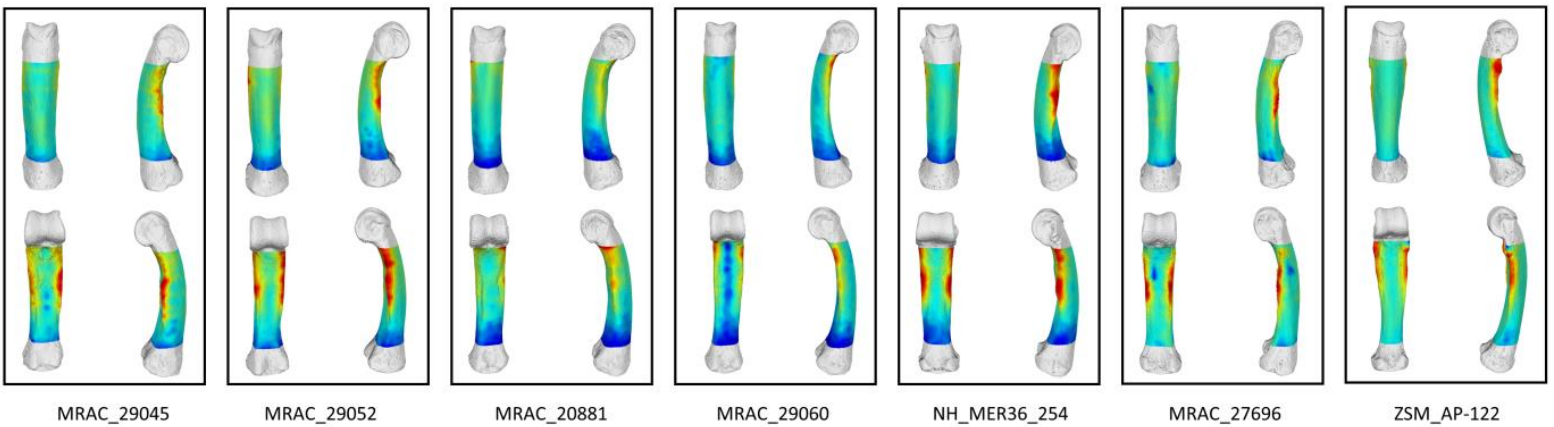
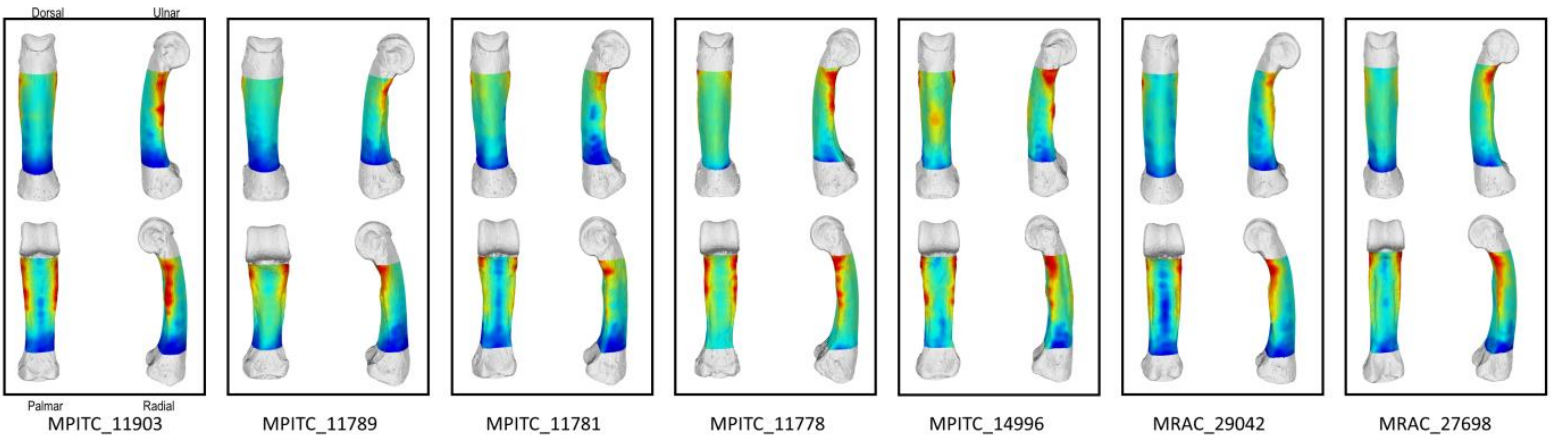
Pan PP3



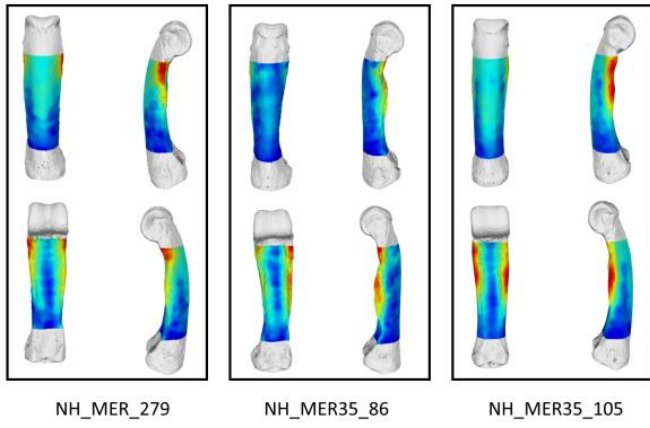
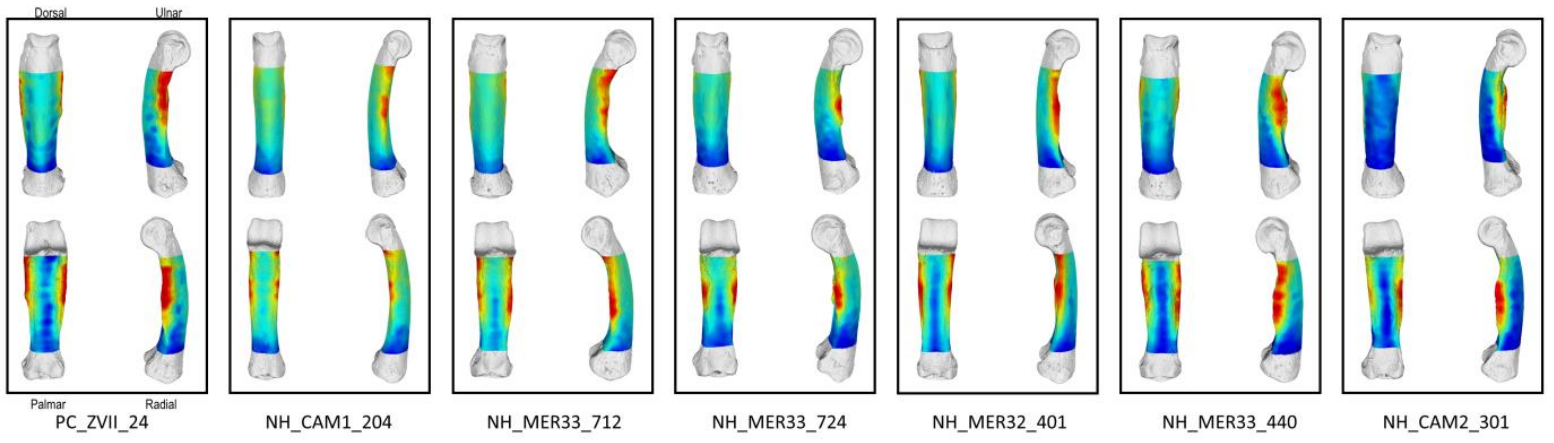
Pan PP3



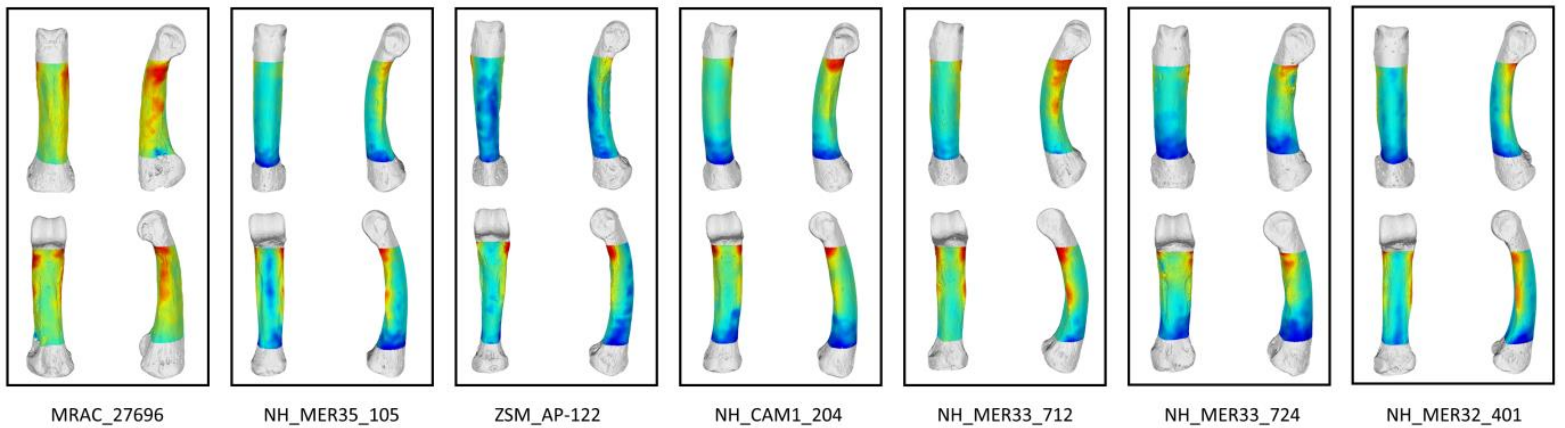
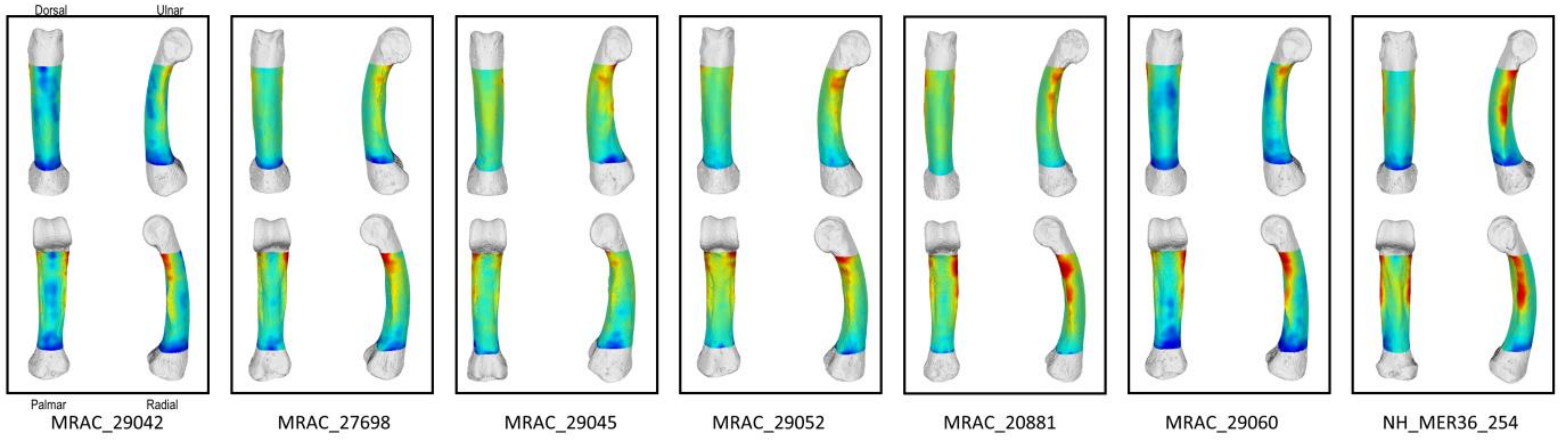
Pan PP4



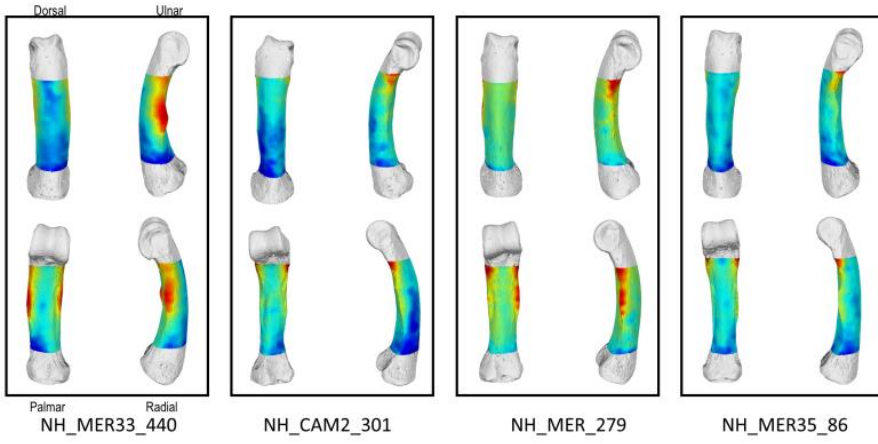
Pan PP4



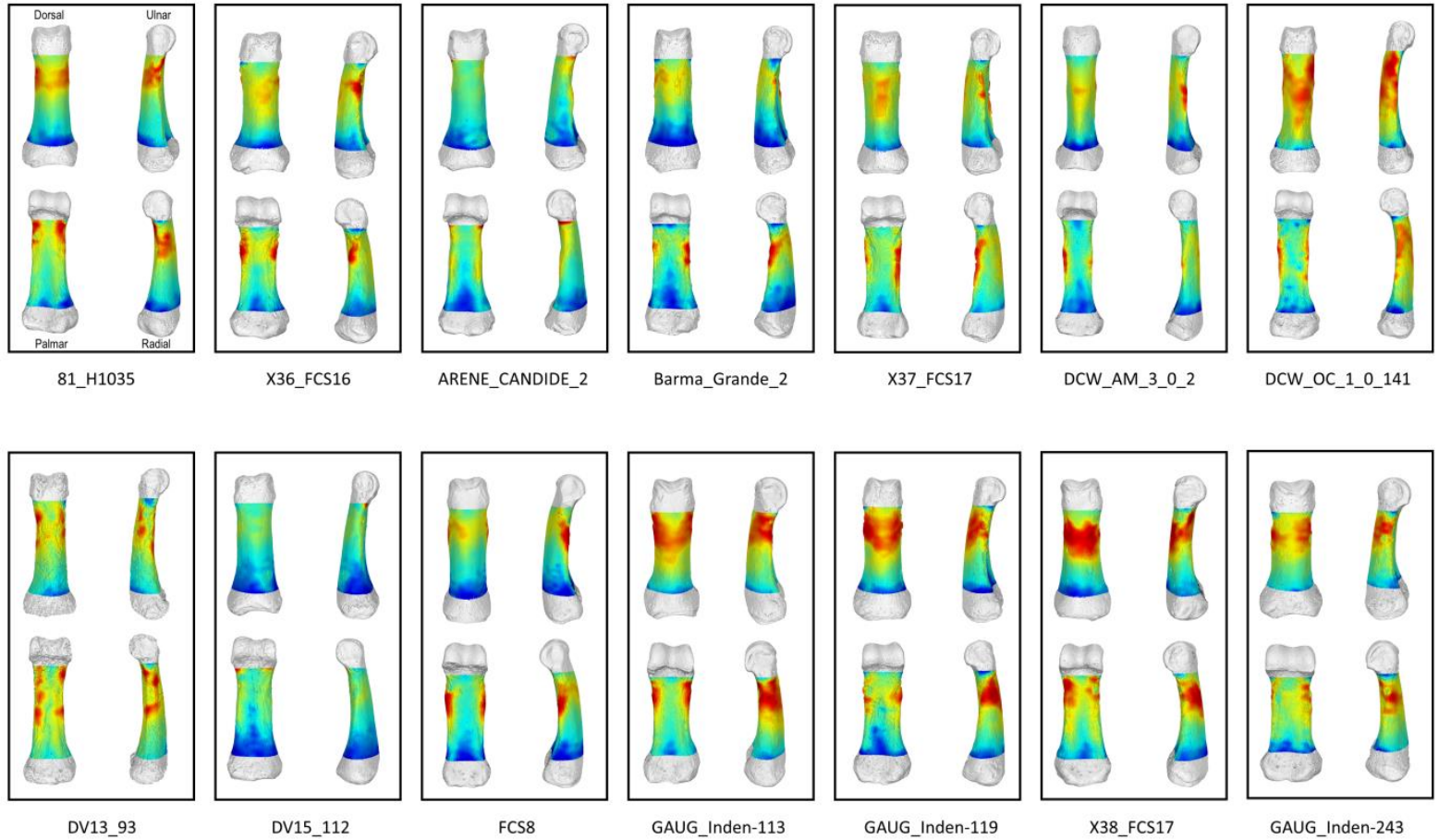
Pan PP5



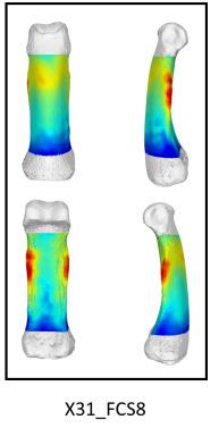
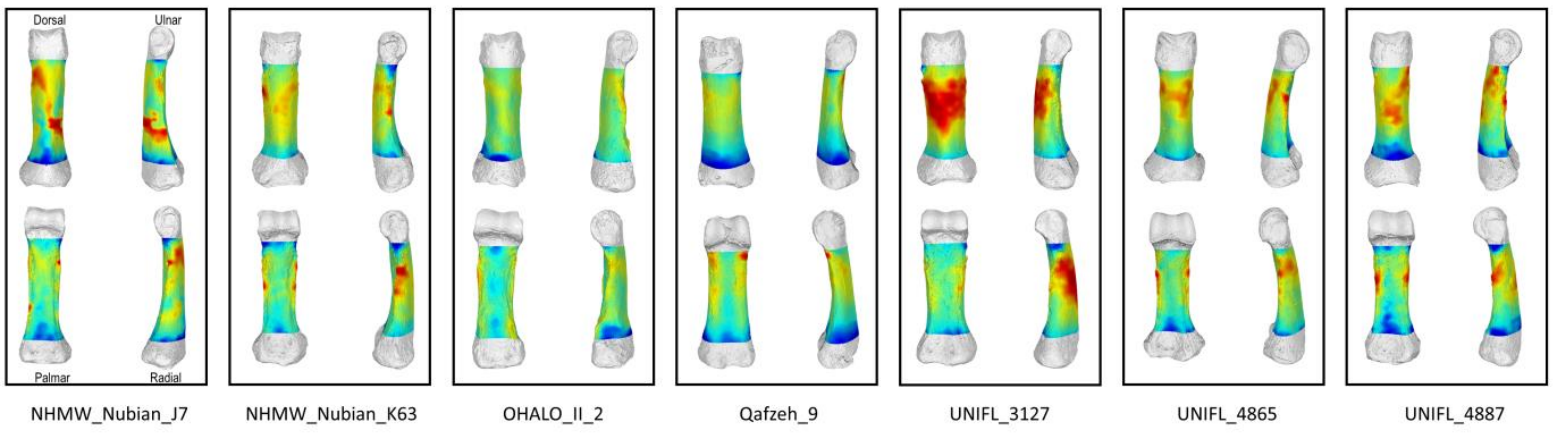
Pan PP5



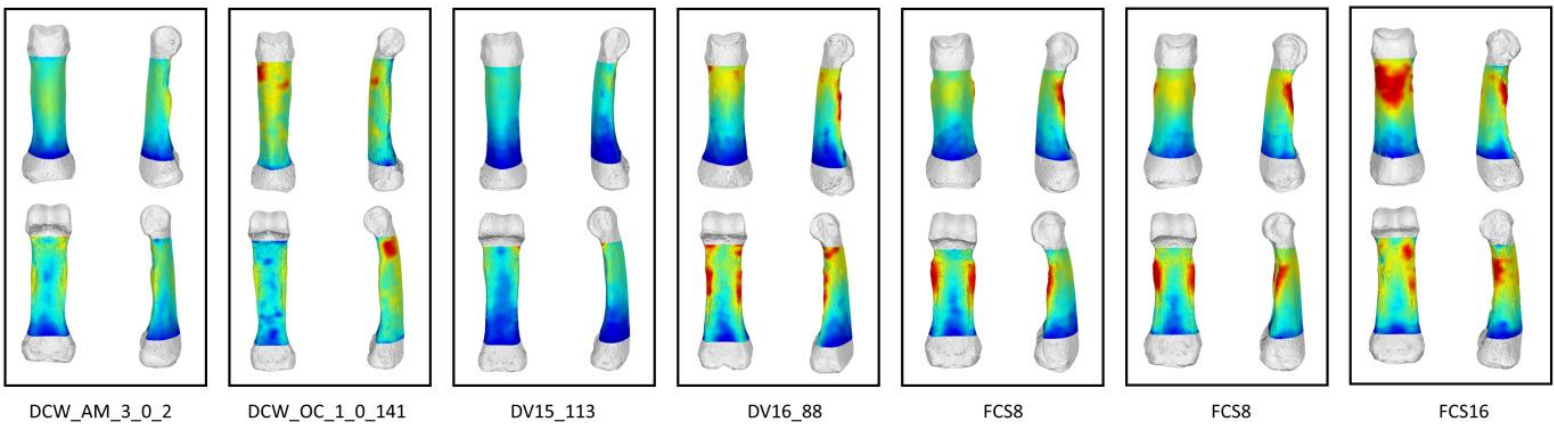
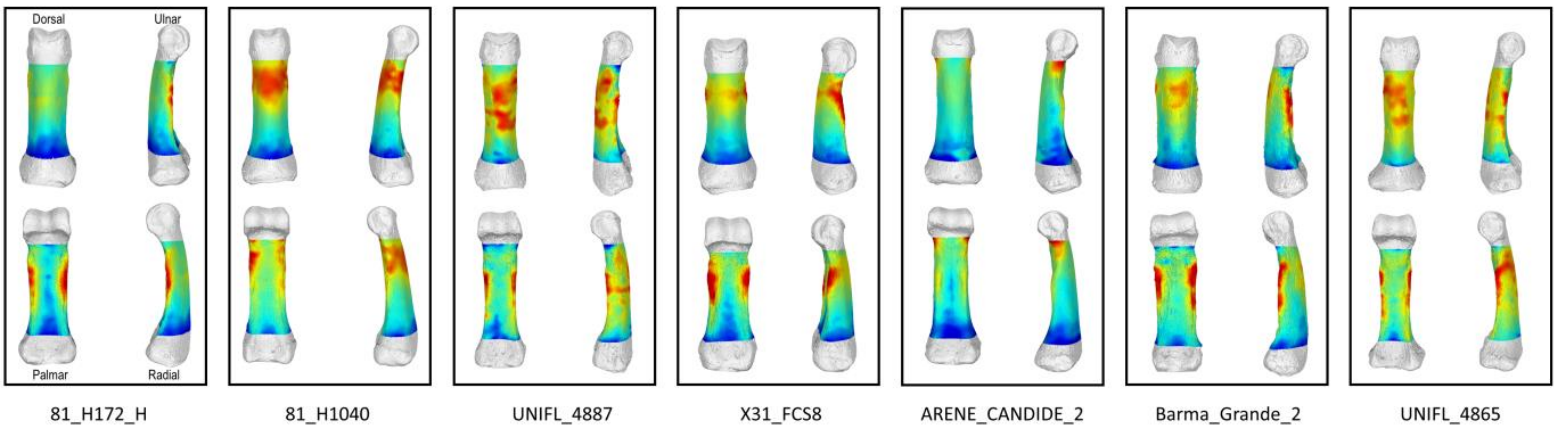
H. sapiens PP2



H. sapiens PP2



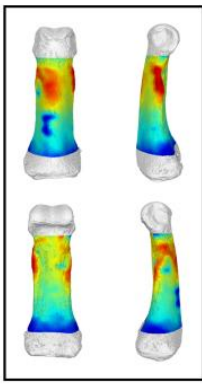
H. sapiens PP3



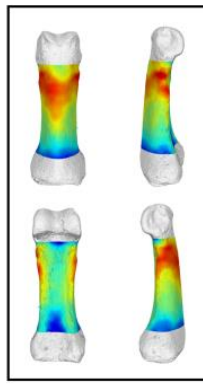
H. sapiens PP3



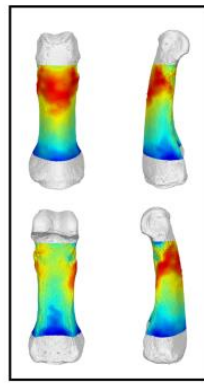
FCS17



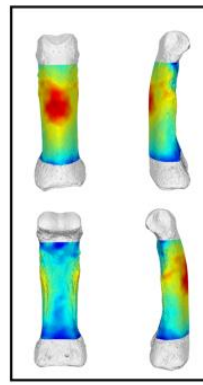
GAUG_Inden-91



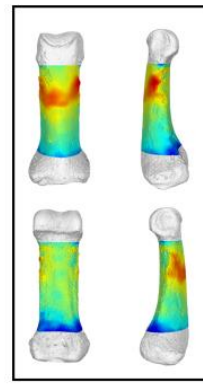
GAUG_Inden-113



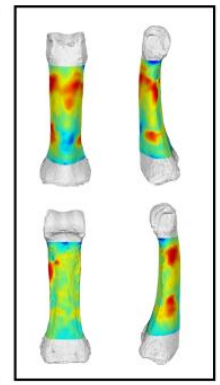
GAUG_Inden-119



UNIFL_3127



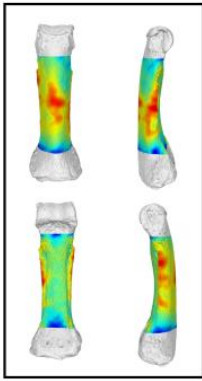
GAUG_Inden-243



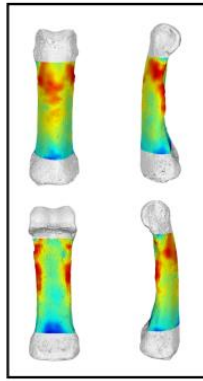
NHMW_Nubian_J7



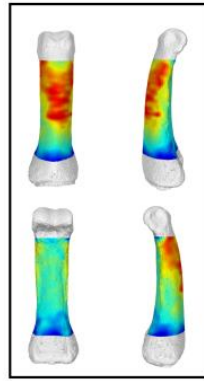
NHMW_Nubian_K5.2



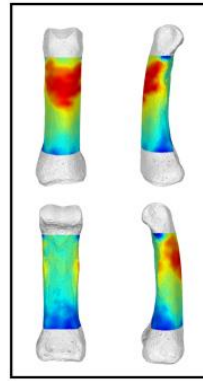
NHMW_Nubian_K63



OHALO_II_H2

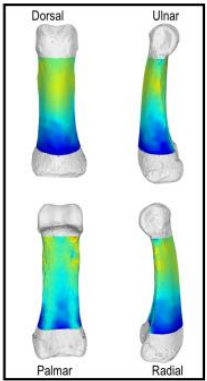


UNIFL_3124

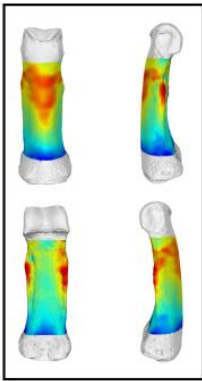


UNIFL_3125

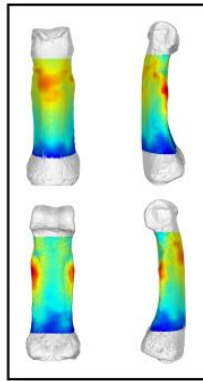
H. sapiens PP4



81_H172_H



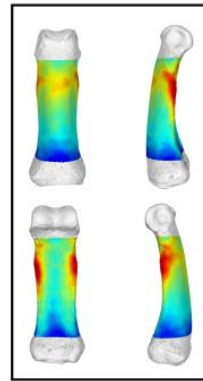
81_H1040



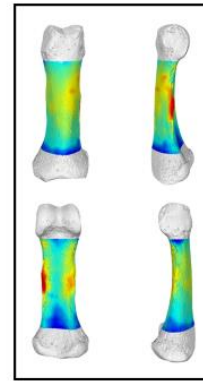
81_H1068_DD



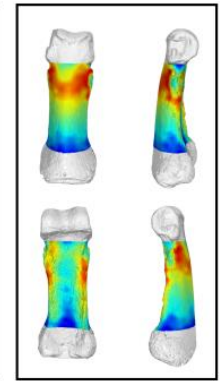
Barma_Grande_2



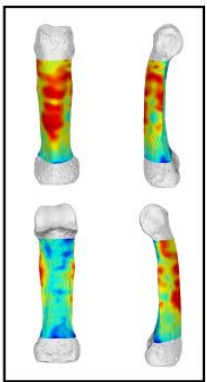
X31_FCS8



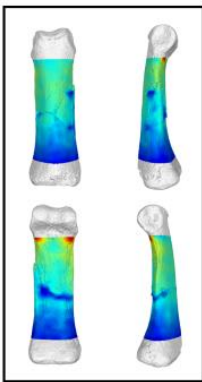
DCW_AM_3_0_2



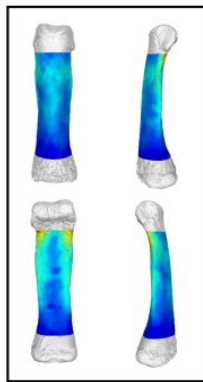
X36_FCS16



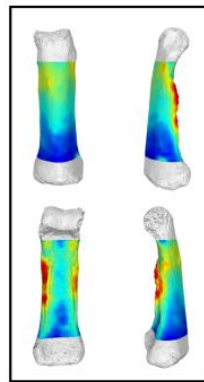
DCW_OC_1_0_141



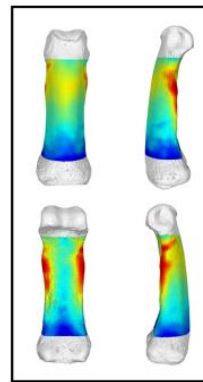
DV13_95



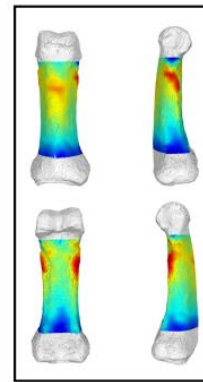
DV14_120



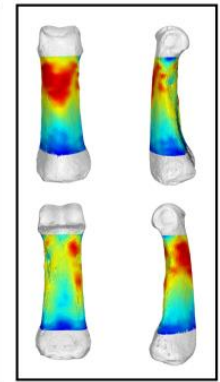
DV16_91



FCS8

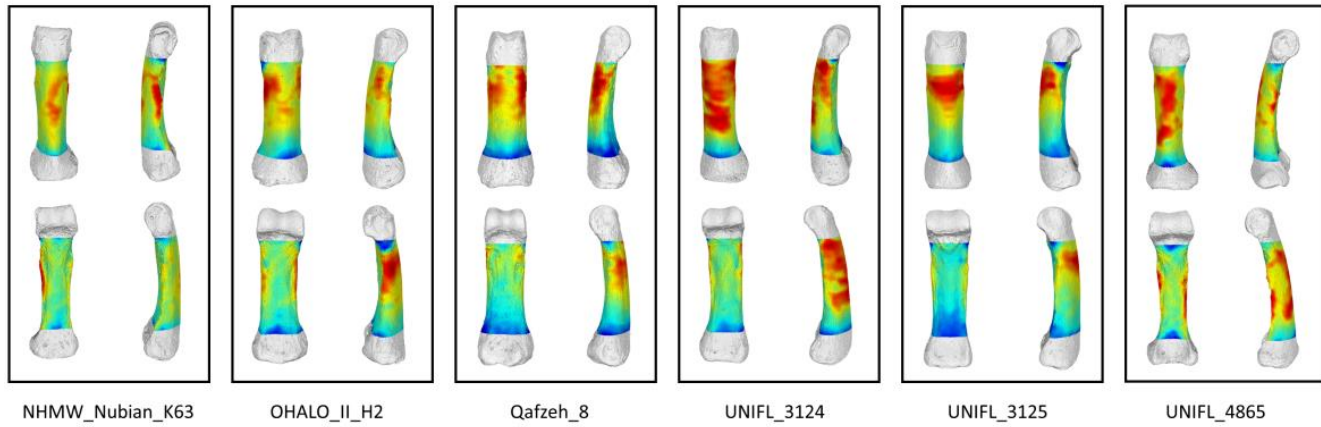
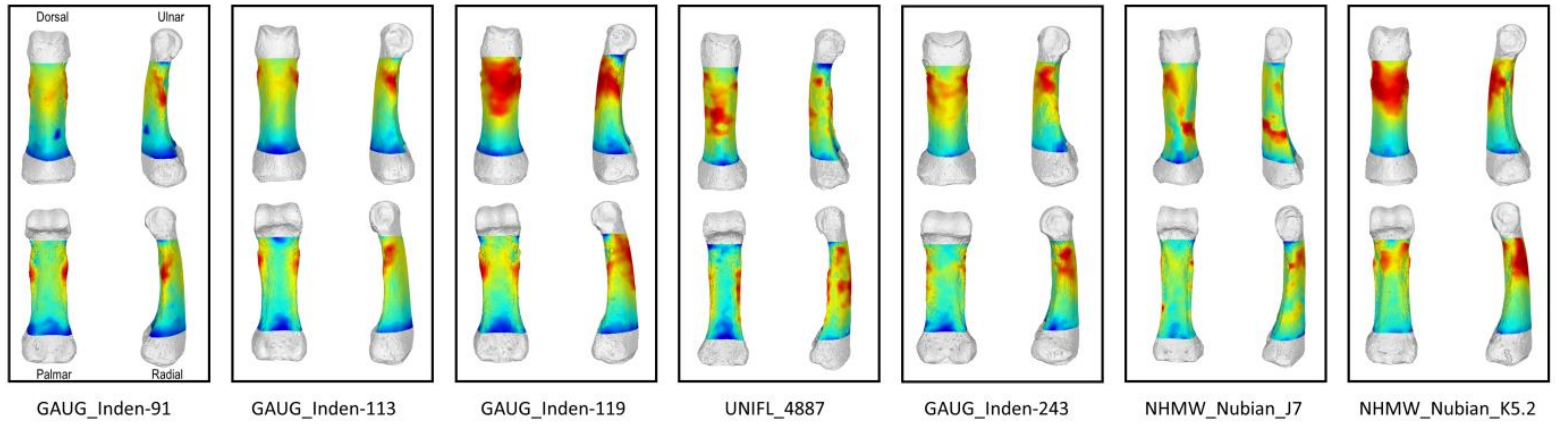


FCS16

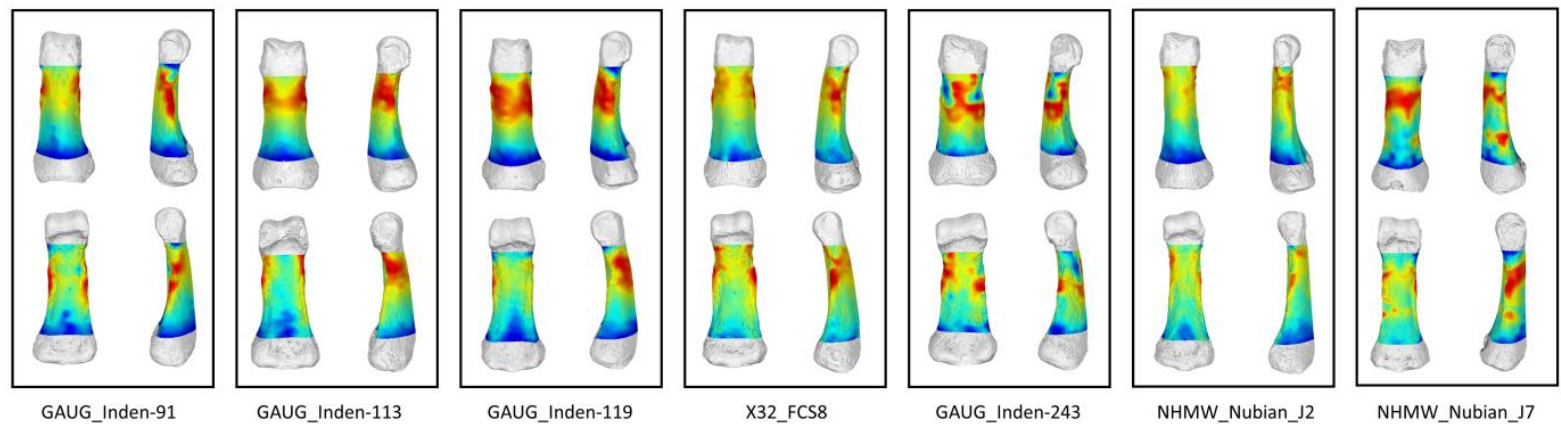
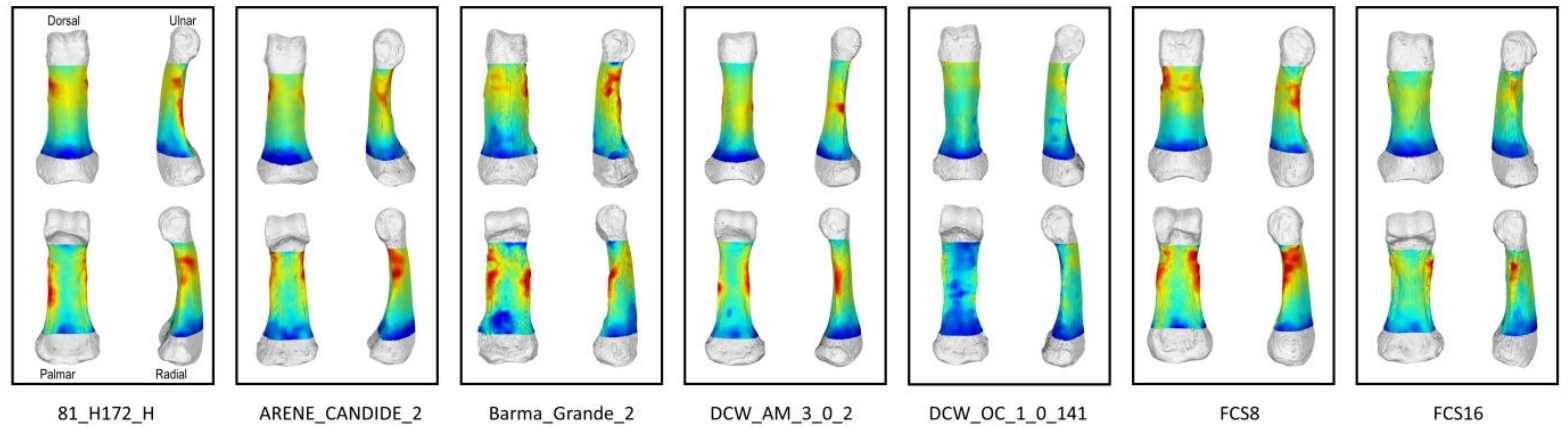


FCS17

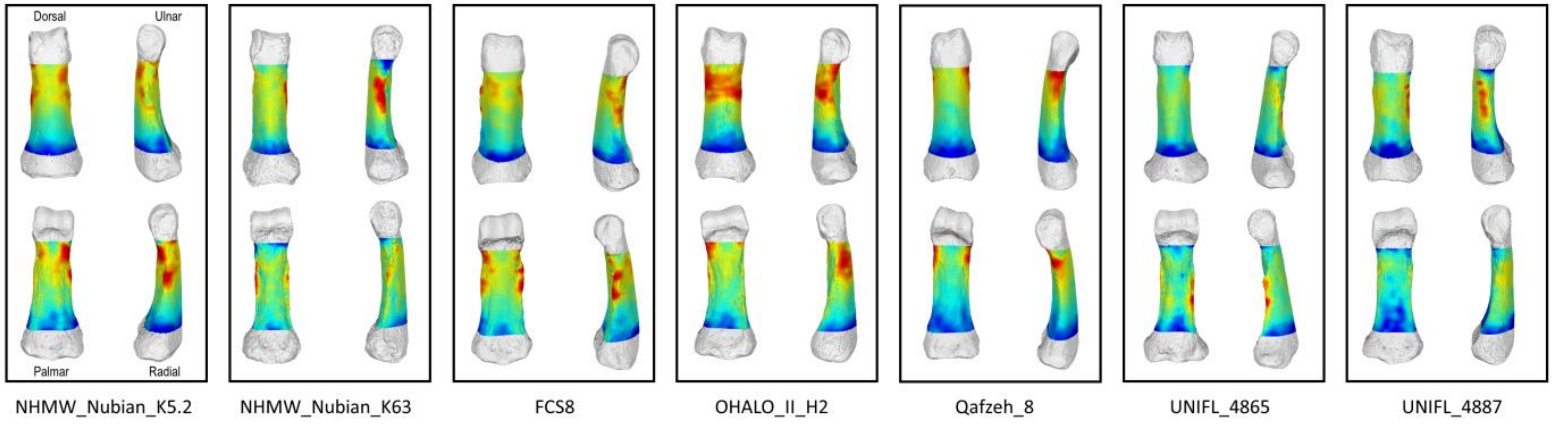
H. sapiens PP4



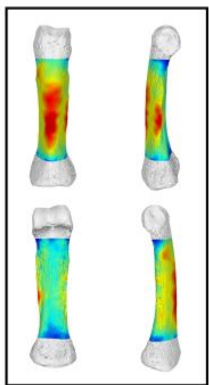
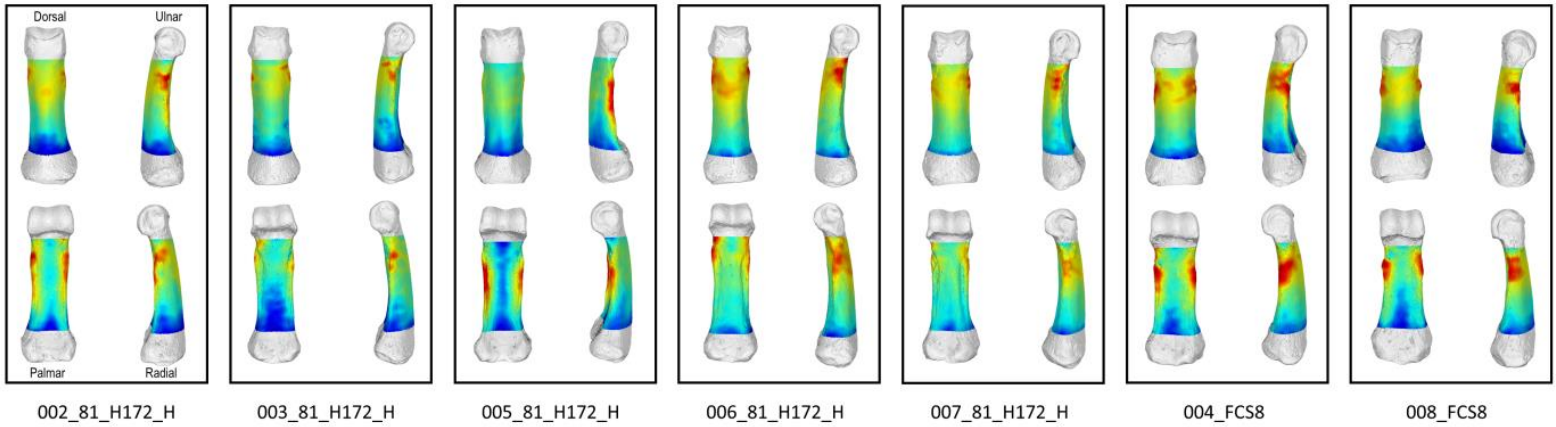
H. sapiens PP5



H. sapiens PP5

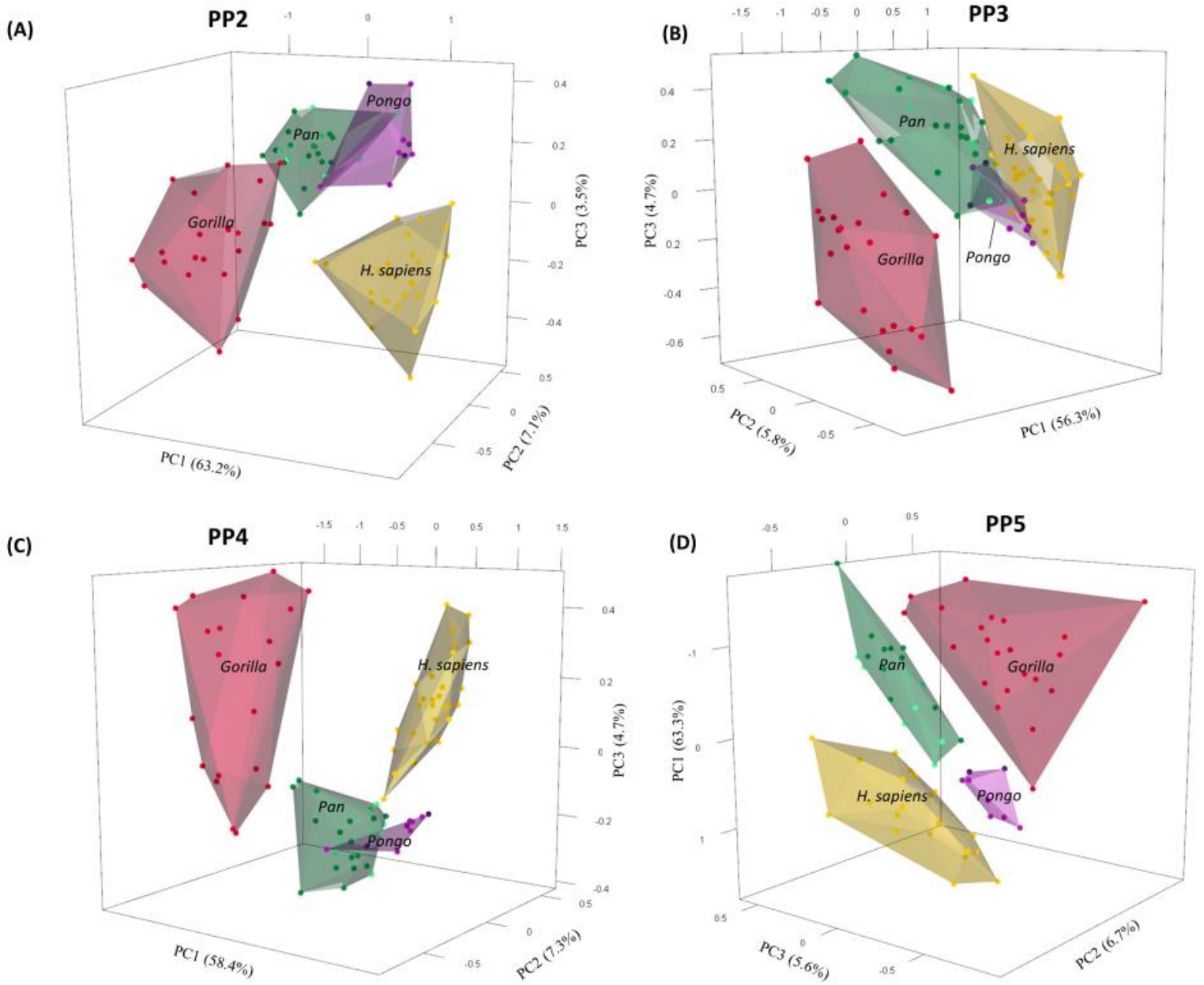


H. sapiens PP2 or PP4

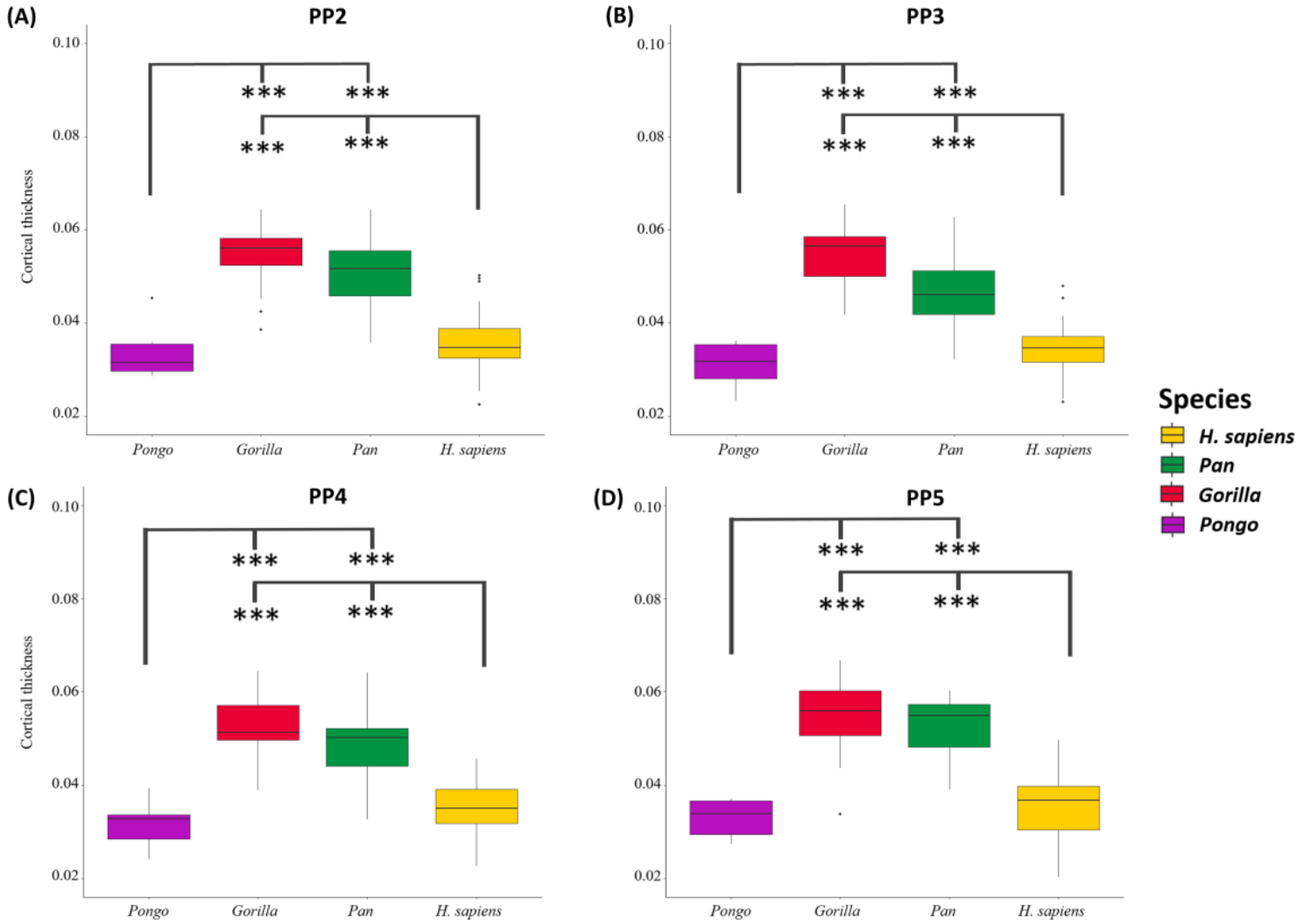


DCW_OC_1_0_26

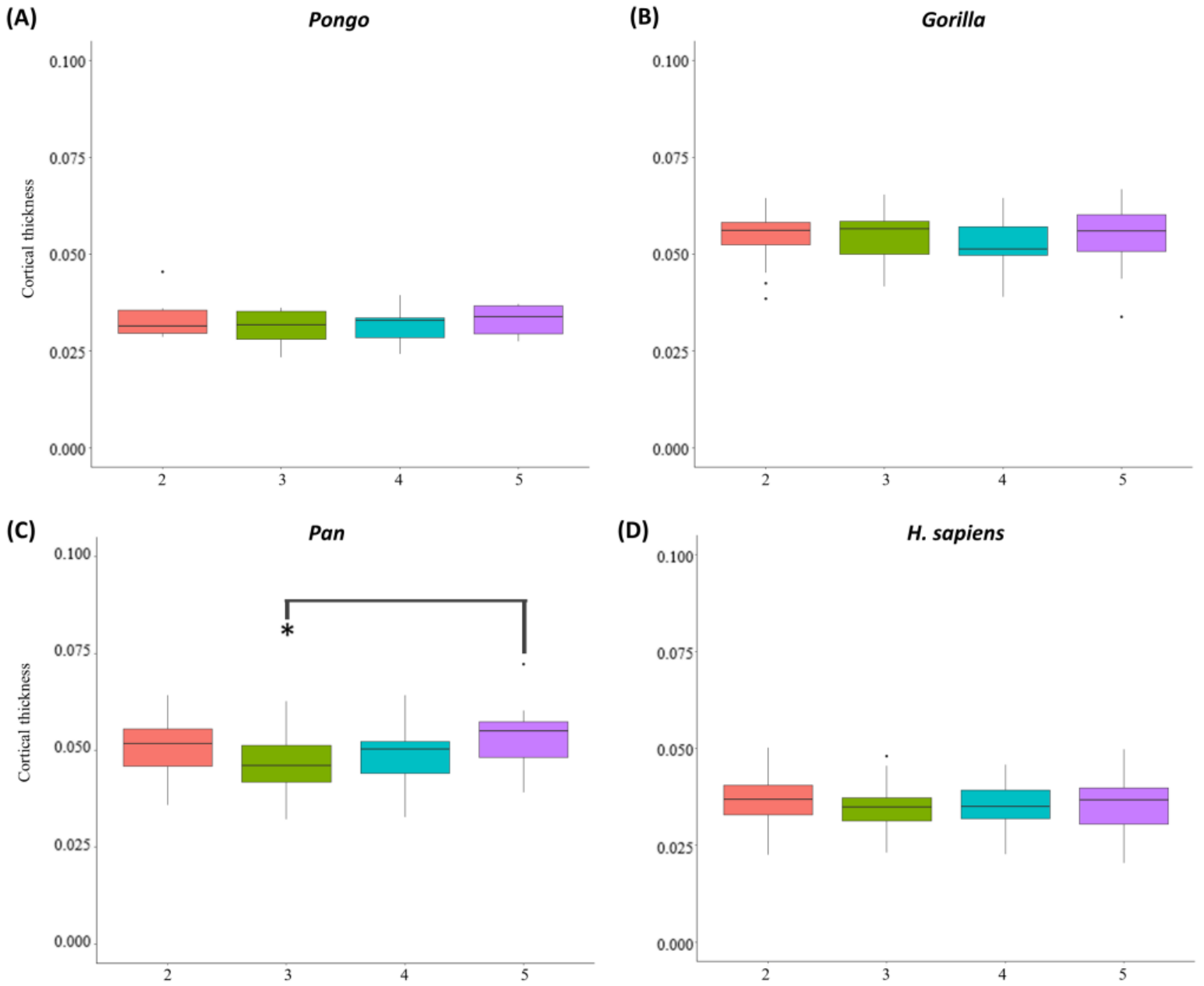
Supplementary Figure 3.2: 3D PCAs for cortical bone distribution of proximal phalanges of PP2, PP3, PP4, and PP5 of *H.sapiens*, *Pan* sp., *Gorilla*, and *Pongo* sp.



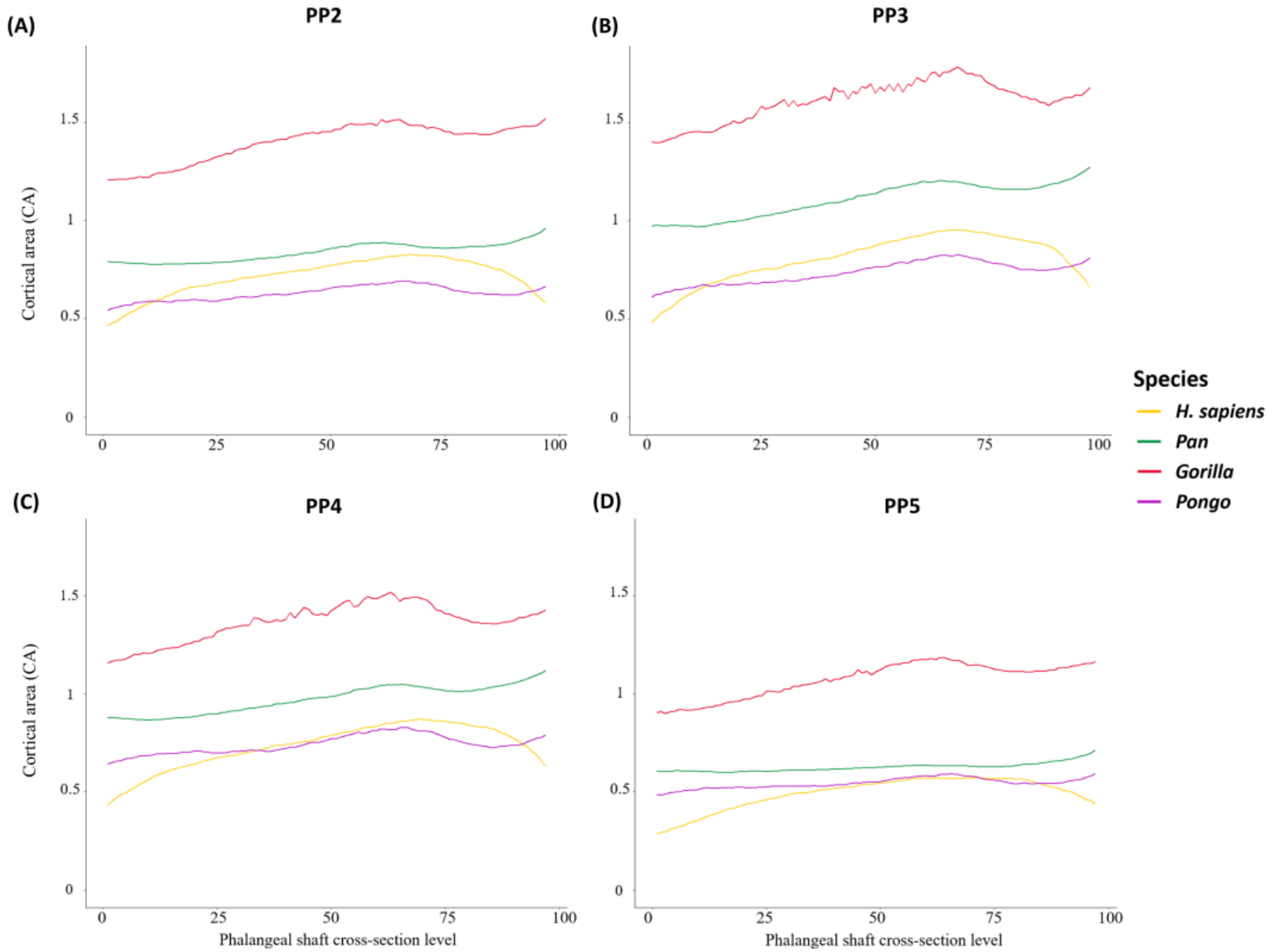
Supplementary Figure 3.3: Boxplots representing the mean cortical thickness across the shaft for (A) PP2, (B) PP3, (C) PP4, and (D) PP5 of *H. sapiens*, *Pan* sp., *Gorilla*, and *Pongo* sp. *** = $p < 0.001$. The African apes are significantly thicker than *H. sapiens* and *Pongo*.



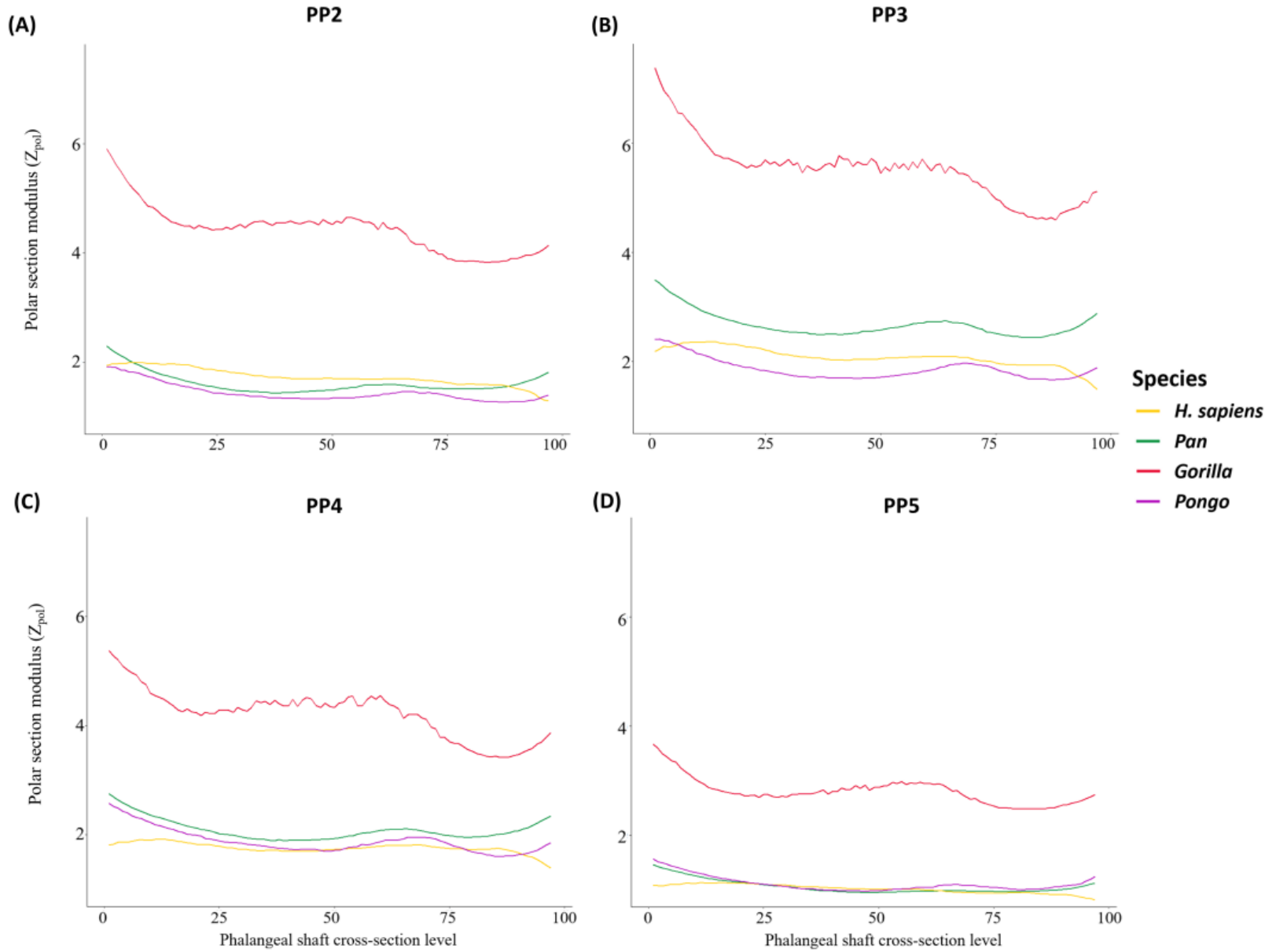
Supplementary Figure 3.4: Boxplots representing the mean cortical thickness across the shaft for (A) *H. sapiens*, (B) *Pan*, (C) *Gorilla*, and (D) *Pongo* of digits 2-5. * = $p < 0.05$. *Pan* PP3 is significantly thicker than *Pan* PP5.



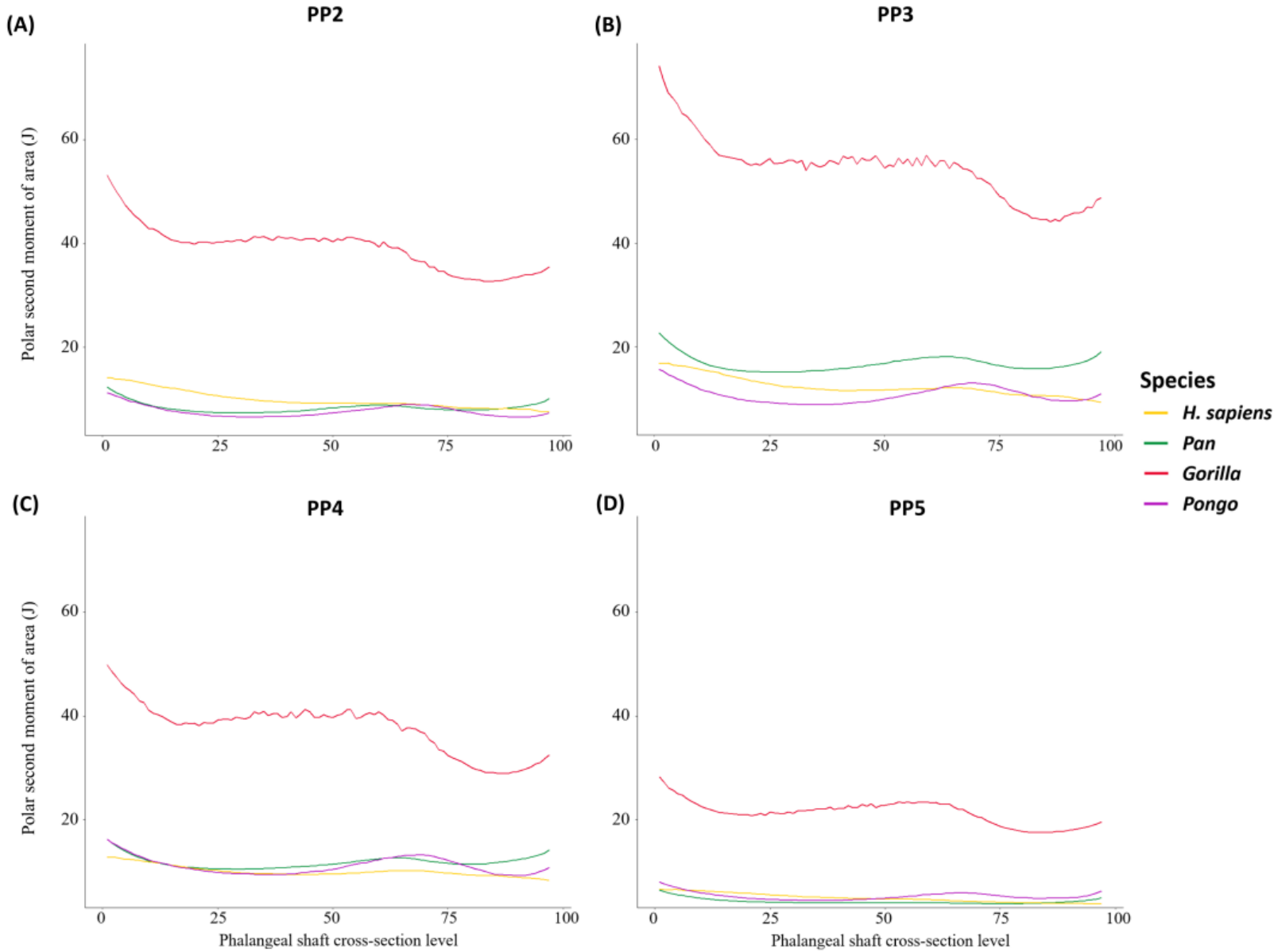
Supplementary Figure 3.5: Average CA plotted from the proximal end to the distal end of the phalangeal shaft of *H. sapiens*, *Pan*, *Gorilla*, and *Pongo*. (A) PP2; (B) PP3; (C) PP4; (D) PP5.



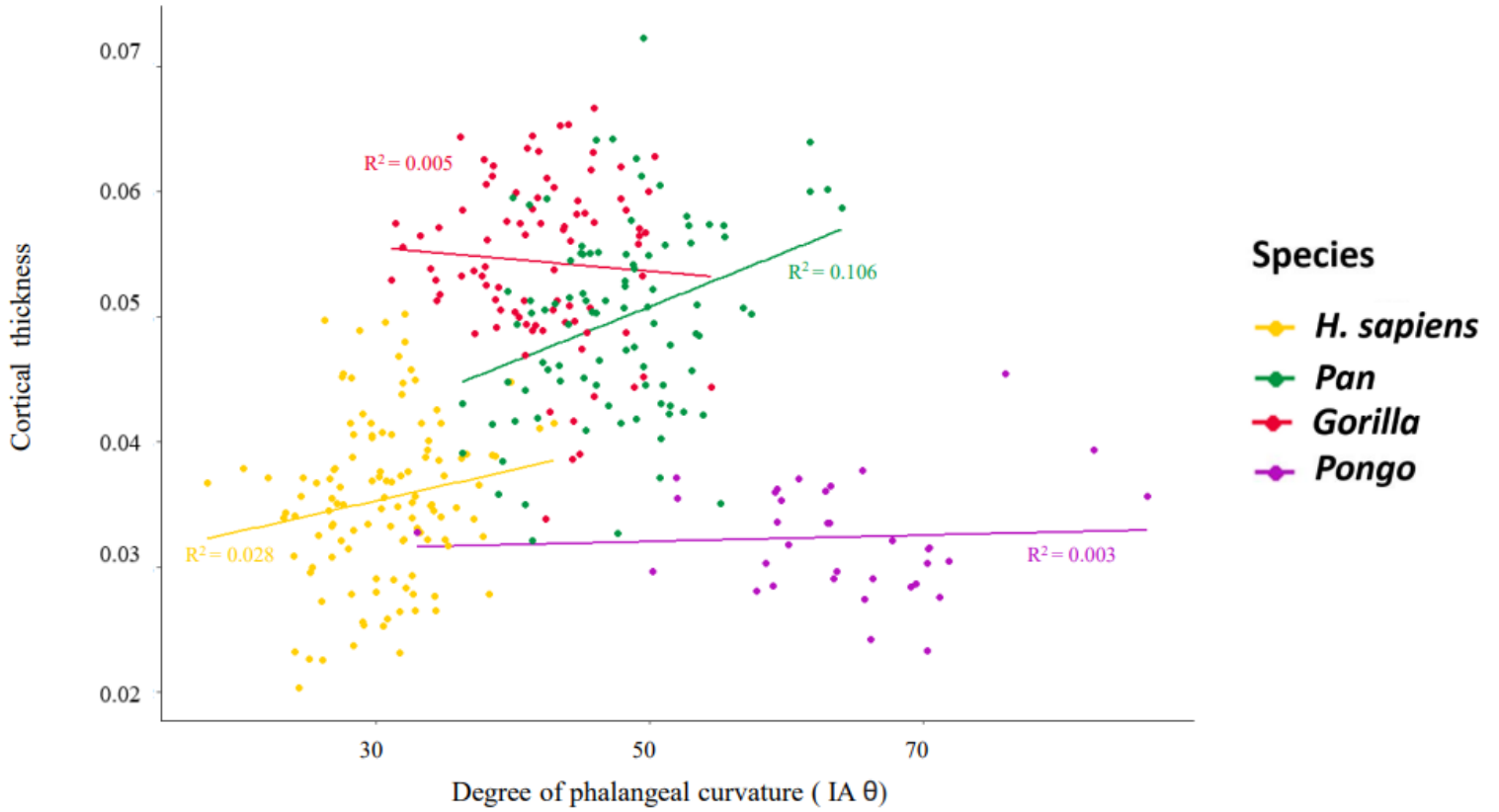
Supplementary Figure 3.6: Average Z_{pol} plotted from the proximal end to the distal end of the phalangeal shaft of *H. sapiens*, *Pan*, *Gorilla*, and *Pongo*. (A) PP2; (B) PP3; (C) PP4; (D) PP5.



Supplementary Figure 3.7: Average J plotted from the proximal end to the distal end of the phalangeal shaft of *H. sapiens*, *Pan*, *Gorilla*, and *Pongo*. (A) PP2; (B) PP3; (C) PP4; (D) PP5.



Supplementary Figure 3.8: Scatterplot of phalangeal curvature against phalangeal shaft cortical thickness of digits 2-5 in *H. sapiens*, *Pan* sp., *Gorilla*, and *Pongo* sp.



8.3. SUPPLEMENTARY MATERIALS: Cortical bone architecture of hominid intermediate phalanges reveals functional signals of locomotion and manipulation.

Detailed below are supplementary tables and figures that expand on the results presented in Chapter 4.

Supplementary Table 4.1: Detailed specimen information.

Taxon	Specimen	Sex	Side	Subsistence	Collection
<i>Homo sapiens</i>	NHMW-Nubian_K63	M	L	Pre-industrial	Natural History Museum, Vienna
<i>Homo sapiens</i>	NHMW-Nubian_K5.2	M	R	Pre-industrial	Natural History Museum, Vienna
<i>Homo sapiens</i>	NHMW-Nubian_J7	F	R	Pre-industrial	Natural History Museum, Vienna
<i>Homo sapiens</i>	Qafzeh_9	M	R	Pre-industrial	The Sackler School of Medicine at Tel Aviv University
<i>Homo sapiens</i>	Qafzeh_8	UK	R/L	Pre-industrial	The Sackler School of Medicine at Tel Aviv University
<i>Homo sapiens</i>	OHALO_II_H2	M	R/L	Pre-industrial	The Sackler School of Medicine at Tel Aviv University
<i>Homo sapiens</i>	UNIFL_4865	M	R	Post-industrial	University of Florence
<i>Homo sapiens</i>	UNIFL_4887	F	R	Post-industrial	University of Florence
<i>Homo sapiens</i>	GAUG-Inden_113	M	L	Post-industrial	Georg-August-University Goettingen, Anthropology Collection
<i>Homo sapiens</i>	GAUG-Inden_117	UK	L	Post-industrial	Georg-August-University Goettingen, Anthropology Collection
<i>Homo sapiens</i>	GAUG-Inden_119	M	R	Post-industrial	Georg-August-University Goettingen, Anthropology Collection
<i>Homo sapiens</i>	GAUG-Inden_243	M	L	Post-industrial	Georg-August-University Goettingen, Anthropology Collection
<i>Homo sapiens</i>	Barma_Grande_2	M	R	Pre-industrial	Museo Nazionale Preistorico dei Balzi Rossi
<i>Homo sapiens</i>	ARENE_CANDIDE_2	M	R/L	Pre-industrial	the Museo Archeologico del Finale
<i>Homo sapiens</i>	DCW_AM_3_0_2	UK	R/L	Pre-industrial	The Duckworth Collection, University of Cambridge
<i>Homo sapiens</i>	DCW_OC_1_0_141	UK	R/L	Pre-industrial	The Duckworth Collection, University of Cambridge
<i>Homo sapiens</i>	DCW_OC_1_0_26	UK	L	Pre-industrial	The Duckworth Collection, University of Cambridge
<i>Homo sapiens</i>	81-H172-H	M	R/L	Post-industrial	Mary Rose Trust
<i>Homo sapiens</i>	DV-13	M	L	Pre-industrial	Institute of Archaeology, Czech Republic
<i>Homo sapiens</i>	DV-14	M	R	Pre-industrial	Institute of Archaeology, Czech Republic
<i>Homo sapiens</i>	DV-15	M	R/L	Pre-industrial	Institute of Archaeology, Czech Republic
<i>Homo sapiens</i>	DV-16	M	R/L	Pre-industrial	Institute of Archaeology, Czech Republic
<i>Pan paniscus</i>	MRAC_27698	F	L	Wild	Royal Museum for Central Africa, Tervuren
<i>Pan paniscus</i>	MRAC_29042	F	R	Wild	Royal Museum for Central Africa, Tervuren
<i>Pan paniscus</i>	MRAC_29045	F	L	Wild	Royal Museum for Central Africa, Tervuren
<i>Pan paniscus</i>	MRAC_29052	M	R	Wild	Royal Museum for Central Africa, Tervuren
<i>Pan paniscus</i>	MRAC_27696	M	L	Wild	Royal Museum for Central Africa, Tervuren
<i>Pan paniscus</i>	MRAC_29060	F	R	Wild	Royal Museum for Central Africa, Tervuren
<i>Pan troglodytes</i>	MPITC_11778	F	R	Wild	Max Planck Institute for Evolutionary Anthropology, Taï Chimp Collection
<i>Pan troglodytes</i>	MPITC_14996	F	L	Wild	Max Planck Institute for Evolutionary Anthropology, Taï Chimp Collection

<i>Pan troglodytes</i>	NH_CAM1_204	F	L	Wild	Powell-Cotton Museum
<i>Pan troglodytes</i>	NH_CAM2_301	F	R	Wild	Powell-Cotton Museum
<i>Pan troglodytes</i>	NH_MER_279	F	L	Wild	Powell-Cotton Museum
<i>Pan troglodytes</i>	NH_MER35_86	F	L	Wild	Powell-Cotton Museum
<i>Pan troglodytes</i>	NH_MER35_105	F	R	Wild	Powell-Cotton Museum
<i>Pan troglodytes</i>	MPITC_11789	M	L	Wild	Max Planck Institute for Evolutionary Anthropology, Taï Chimp Collection
<i>Pan troglodytes</i>	MPITC_11781	M	L	Wild	Max Planck Institute for Evolutionary Anthropology, Taï Chimp Collection
<i>Pan troglodytes</i>	ZSM_AP-122	M	R	Wild	Bavarian State Collection of Zoology
<i>Pan troglodytes</i>	NH_MER33_712	M	R	Wild	Powell-Cotton Museum
<i>Pan troglodytes</i>	NH_MER33_724	M	L	Wild	Powell-Cotton Museum
<i>Pan troglodytes</i>	NH_MER32_401	M	L	Wild	Powell-Cotton Museum
<i>Pan troglodytes</i>	NH_MER33_440	M	R	Wild	Powell-Cotton Museum
<i>Pan troglodytes</i>	NH_MER36_254	M	L	Wild	Powell-Cotton Museum
<i>Gorilla gorilla</i>	ZMB_11642	UK	R	Wild	Natural History Museum, Berlin
<i>Gorilla gorilla</i>	ZMB_83545	M	R	Wild	Natural History Museum, Berlin
<i>Gorilla gorilla</i>	PC_MER_95	F	R	Wild	Powell-Cotton Museum
<i>Gorilla gorilla</i>	PC_MER_135	M	L	Wild	Powell-Cotton Museum
<i>Gorilla gorilla</i>	PC_MER_264	M	L	Wild	Powell-Cotton Museum
<i>Gorilla gorilla</i>	PC_MER_300	F	R	Wild	Powell-Cotton Museum
<i>Gorilla gorilla</i>	PC_MER_372	M	R	Wild	Powell-Cotton Museum
<i>Gorilla gorilla</i>	PC_MER_962	M	R	Wild	Powell-Cotton Museum
<i>Gorilla gorilla</i>	PC_MER1_29	F	R	Wild	Powell-Cotton Museum
<i>Gorilla gorilla</i>	PC_MER_696	F	R	Wild	Powell-Cotton Museum
<i>Gorilla gorilla</i>	PC_MER_856	F	L	Wild	Powell-Cotton Museum
<i>Gorilla gorilla</i>	PC_ZVI_32	M	R	Wild	Powell-Cotton Museum
<i>Gorilla gorilla</i>	NH_MER33_755	F	R	Wild	Powell-Cotton Museum
<i>Gorilla gorilla</i>	NH_MER33_461	M	R	Wild	Powell-Cotton Museum
<i>Gorilla gorilla</i>	NH_CAM1_106	M	R	Wild	Powell-Cotton Museum
<i>Gorilla gorilla</i>	NH_CAM1_105	M	R	Wild	Powell-Cotton Museum
<i>Gorilla gorilla</i>	NH_MER35_150	F	R	Wild	Powell-Cotton Museum
<i>Gorilla gorilla</i>	NH_CAM1_98	F	L	Wild	Powell-Cotton Museum
<i>Gorilla gorilla</i>	NH_MER35_136	F	L	Wild	Powell-Cotton Museum
<i>Gorilla gorilla</i>	NH_MER35_139	F	L	Wild	Powell-Cotton Museum

<i>Gorilla gorilla</i>	NH_FC_130	M	L	Wild	Powell-Cotton Museum
<i>Gorilla gorilla</i>	NH_FC_123	M	L	Wild	Powell-Cotton Museum
<i>Pongo pygmaeus</i>	ZSM_1907_0633b	F	R	Wild	Bavarian State Collection of Zoology
<i>Pongo pygmaeus</i>	ZSM_1907_0629b	M	R	Wild	Bavarian State Collection of Zoology
<i>Pongo pygmaeus</i>	ZSM_1907_0660	F	R	Wild	Bavarian State Collection of Zoology
<i>Pongo pygmaeus</i>	ZSM_AP-120	M	L	Wild	Bavarian State Collection of Zoology
<i>Pongo pygmaeus</i>	ZSM_1907_0483	F	R	Wild	Bavarian State Collection of Zoology
<i>Pongo pygmaeus</i>	ZSM_1909_0801	M	R	Wild	Bavarian State Collection of Zoology

Note: M = male; F = female; R = right; L = left; UK = unknown sex/side; R/L = to have all four digits represented, some phalanges were from the right side of the body and some from the left.

Supplementary Table 4.2: Test statistics for omnibus permutational multivariate analysis of variance (PERMANOVA) and subsequent pairwise one-way permutational multivariate analysis of variance on the first 3 PC scores of the cortical bone thickness distribution pattern PCAs. The extant taxa all significantly differ from each other in the PCAs across all four digits.

PERMANOVA			Pairwise one-way MANOVA			
				<i>Pan</i>	<i>Gorilla</i>	<i>Pongo</i>
<u>IP2</u>	R²	0.662	<i>H.sapiens</i>	<0.001	<0.001	<0.001
	p-value	<0.001	<i>Pan</i>		<0.001	<0.001
			<i>Gorilla</i>			<0.001
<u>IP3</u>	R²	0.557	<i>H.sapiens</i>	<0.001	<0.001	<0.001
	p-value	<0.001	<i>Pan</i>		<0.001	<0.001
			<i>Gorilla</i>			<0.001
<u>IP4</u>	R²	0.579	<i>H.sapiens</i>	<0.001	<0.001	<0.001
	p-value	<0.001	<i>Pan</i>		<0.001	<0.001
			<i>Gorilla</i>			<0.001
<u>IP5</u>	R²	0.615	<i>H.sapiens</i>	0.010	0.010	0.011
	p-value	<0.001	<i>Pan</i>		0.020	0.020
			<i>Gorilla</i>			0.010

Supplementary Table 4.3: Mean values of standardised cross-sectional properties across species at 35%, 50%, and 65% of the phalanx

		<i>H. sapiens</i>	<i>Pan</i>	<i>Gorilla</i>	<i>Pongo</i>
35% cross-section					
IP2	CSA (mm ²)	0.625	0.868	1.234	0.643
	Z _{pol} (mm ³)	1.410	1.430	2.834	1.097
	J (mm ⁴)	6.973	6.628	19.082	4.905
IP3	CSA (mm ²)	0.755	0.943	1.317	0.643
	Z _{pol} (mm ³)	1.780	1.858	3.301	1.189
	J (mm ⁴)	10.000	10.617	25.297	6.123
IP4	CSA (mm ²)	0.704	0.880	1.231	0.631
	Z _{pol} (mm ³)	1.576	1.539	2.745	1.178
	J (mm ⁴)	8.380	7.644	19.775	5.984
IP5	CSA (mm ²)	0.593	0.807	1.115	0.615
	Z _{pol} (mm ³)	1.123	1.226	2.216	0.996
	J (mm ⁴)	4.867	4.742	12.668	4.398
50% cross-section					
IP2	CSA (mm ²)	0.781	0.832	1.237	0.692
	Z _{pol} (mm ³)	1.386	1.114	2.393	1.072
	J (mm ⁴)	5.809	4.700	14.901	4.876
IP3	CSA (mm ²)	0.872	0.881	1.394	0.665
	Z _{pol} (mm ³)	1.657	1.437	3.146	1.146
	J (mm ⁴)	8.087	7.363	23.597	5.708
IP4	CSA (mm ²)	0.827	0.802	1.238	0.655
	Z _{pol} (mm ³)	1.465	1.153	2.464	1.137
	J (mm ⁴)	6.797	5.120	16.924	5.421
IP5	CSA (mm ²)	0.721	0.753	1.082	0.650
	Z _{pol} (mm ³)	1.088	0.922	1.775	0.982
	J (mm ⁴)	4.107	3.294	9.312	4.428
65% cross-section					
IP2	CSA (mm ²)	0.754	0.756	1.135	0.619
	Z _{pol} (mm ³)	1.179	0.950	1.905	0.875
	J (mm ⁴)	4.660	3.619	10.917	3.344
IP3	CSA (mm ²)	0.843	0.811	1.205	0.586
	Z _{pol} (mm ³)	1.394	1.243	2.325	0.887
	J (mm ⁴)	6.186	5.616	14.890	3.639
IP4	CSA (mm ²)	0.801	0.745	1.088	0.573

	Z_{pol} (mm ³)	1.247	1.032	1.924	0.886
	J (mm ⁴)	5.237	4.079	11.320	3.615
IP5	CSA (mm ²)	0.666	0.712	1.002	0.570
	Z_{pol} (mm ³)	0.939	0.834	1.446	0.782
	J (mm ⁴)	3.304	2.790	6.956	2.871

Abbreviations: CA = cortical area; Z_{pol} = polar section modulus; J = polar second moment of area.

Supplementary Table 4.4: Test statistics for the Kruskal-Wallis tests of cross-sectional properties across species at 35%, 50%, and 65% of the phalanx.

			35%	50%	65%
IP2	CA	KW Chi-squared	38.437	32.235	32.487
		df	3	3	3
		p-value	<0.001	<0.001	<0.001
	Z _{pol}	KW Chi-squared	30.764	33.172	31.485
		df	3	3	3
		p-value	<0.001	<0.001	<0.001
	J	KW Chi-squared	33.922	34.537	33.928
		df	3	3	3
		p-value	<0.001	<0.001	<0.001
IP3	CA	KW Chi-squared	41.141	38.152	36.324
		df	3	3	3
		p-value	<0.001	<0.001	<0.001
	Z _{pol}	KW Chi-squared	34.409	35.720	33.890
		df	3	3	3
		p-value	<0.001	<0.001	<0.001
	J	KW Chi-squared	35.564	37.038	36.073
		df	3	3	3
		p-value	<0.001	<0.001	<0.001
IP4	CA	KW Chi-squared	38.894	34.526	32.588
		df	3	3	3
		p-value	<0.001	<0.001	<0.001
	Z _{pol}	KW Chi-squared	30.072	34.596	32.653
		df	3	3	3
		p-value	<0.001	<0.001	<0.001
	J	KW Chi-squared	33.273	35.769	34.200
		df	3	3	3
		p-value	<0.001	<0.001	<0.001
IP5	CA	KW Chi-squared	28.149	20.780	20.982
		df	3	3	3
		p-value	<0.001	<0.001	<0.001
	Z _{pol}	KW Chi-squared	21.030	17.436	18.127
		df	3	3	3
		p-value	<0.001	<0.001	<0.001
	J	KW Chi-squared	22.088	21.113	20.741
		df	3	3	3
		p-value	<0.001	<0.001	<0.001

Abbreviations: CA = cortical area; Z_{pol} = polar section modulus; J = polar second moment of area

Supplementary Table 4.5: Significance values for post hoc comparisons of cross sectional properties across species at 35%, 50%, and 65% of the phalanx.

			35%			50%			65%		
			<i>Pan</i>	<i>Gorilla</i>	<i>Pongo</i>	<i>Pan</i>	<i>Gorilla</i>	<i>Pongo</i>	<i>Pan</i>	<i>Gorilla</i>	<i>Pongo</i>
IP2	CA	<i>H.sapiens</i>	0.025	< 0.001	1.000	1.000	< 0.001	1.000	1.000	< 0.001	0.631
		<i>Pan</i>		0.018	0.383		< 0.001	0.916		< 0.001	0.613
		<i>Gorilla</i>			< 0.001			< 0.001			< 0.001
	<i>Z_{pol}</i>	<i>H.sapiens</i>	1.000	< 0.001	0.747	0.318	0.009	0.453	0.213	0.004	0.151
		<i>Pan</i>		< 0.001	0.685		< 0.001	1.000		< 0.001	1.000
		<i>Gorilla</i>			< 0.001			< 0.001			< 0.001
	J	<i>H.sapiens</i>	1.000	< 0.001	0.861	1.000	< 0.001	1.000	0.526	0.007	0.240
		<i>Pan</i>		< 0.001	1.000		< 0.001	1.000		< 0.001	1.000
		<i>Gorilla</i>			< 0.001			< 0.001			< 0.001
IP3	CA	<i>H.sapiens</i>	0.192	< 0.001	1.000	1.000	< 0.001	0.637	1.000	< 0.001	0.131
		<i>Pan</i>		0.004	0.108		< 0.001	0.565		< 0.001	0.333
		<i>Gorilla</i>			< 0.001			< 0.001			< 0.001
	<i>Z_{pol}</i>	<i>H.sapiens</i>	1.000	< 0.001	0.527	1.000	< 0.001	0.752	1.000	< 0.001	0.219
		<i>Pan</i>		< 0.001	0.232		< 0.001	1.000		< 0.001	0.634
		<i>Gorilla</i>			< 0.001			< 0.001			< 0.001
	J	<i>H.sapiens</i>	1.000	< 0.001	0.853	1.000	< 0.001	1.000	1.000	< 0.001	0.515
		<i>Pan</i>		< 0.001	0.414		< 0.001	1.000		< 0.001	0.756
		<i>Gorilla</i>			< 0.001			< 0.001			< 0.001
IP4	CA	<i>H.sapiens</i>	0.149	< 0.001	1.000	1.000	< 0.001	0.437	1.000	0.002	0.157
		<i>Pan</i>		0.002	0.126		< 0.001	0.628		< 0.001	0.495
		<i>Gorilla</i>			< 0.001			< 0.001			< 0.001
	<i>Z_{pol}</i>	<i>H.sapiens</i>	1.000	< 0.001	0.589	0.412	0.004	0.536	0.632	0.007	0.209
		<i>Pan</i>		< 0.001	0.641		< 0.001	1.000		< 0.001	1.000
		<i>Gorilla</i>			< 0.001			< 0.001			< 0.001
	J	<i>H.sapiens</i>	1.000	< 0.001	0.574	0.613	< 0.001	1.000	0.717	0.003	0.311
		<i>Pan</i>		< 0.001	1.000		< 0.001	1.000		< 0.001	1.000
		<i>Gorilla</i>			< 0.001			< 0.001			< 0.001
IP5	CA	<i>H.sapiens</i>	0.070	< 0.001	1.000	1.000	0.002	1.000	1.000	0.001	1.000
		<i>Pan</i>		0.039	0.562		0.002	1.000		0.006	1.000
		<i>Gorilla</i>			0.003			0.004			0.002
	<i>Z_{pol}</i>	<i>H.sapiens</i>	1.000	0.001	1.000	1.000	0.074	1.000	1.000	0.041	1.000
		<i>Pan</i>		0.001	1.000		< 0.001	1.000		< 0.001	1.000
		<i>Gorilla</i>			0.007			0.546			0.016
	J	<i>H.sapiens</i>	1.000	0.003	1.000	1.000	0.026	1.000	1.000	0.027	1.000
		<i>Pan</i>		< 0.001	1.000		< 0.001	1.000		< 0.001	1.000
		<i>Gorilla</i>			0.009			0.079			0.015

Abbreviations: CA = cortical area; *Z_{pol}* = polar section modulus; J = polar second moment of area.

Supplementary Table 4.6: Test statistics for the Kruskal-Wallis tests of cross-sectional properties across species at 35%, 50%, and 65% of the phalanx.

			35%	50%	65%
<i>H. sapiens</i>	CA	KW Chi-squared	7.568	3.477	5.648
		df	3	3	3
		p-value	0.056	0.323	0.130
	Z _{pol}	KW Chi-squared	10.859	8.622	9.431
		df	3	3	3
		p-value	0.013	0.035	0.025
	J	KW Chi-squared	16.424	13.030	11.763
		df	3	3	3
		p-value	<0.001	0.005	0.008
<i>Pan</i>	CA	KW Chi-squared	7.637	8.899	6.925
		df	3	3	3
		p-value	0.050	0.031	0.074
	Z _{pol}	KW Chi-squared	16.838	20.348	20.406
		df	3	3	3
		p-value	<0.001	<0.001	<0.001
	J	KW Chi-squared	29.174	32.898	29.907
		df	3	3	3
		p-value	<0.001	<0.001	<0.001
<i>Gorilla</i>	CA	KW Chi-squared	6.265	13.300	8.936
		df	3	3	3
		p-value	0.099	0.004	0.030
	Z _{pol}	KW Chi-squared	11.857	19.009	15.485
		df	3	3	3
		p-value	0.008	<0.001	0.001
	J	KW Chi-squared	15.715	22.401	17.903
		df	3	3	3
		p-value	0.001	<0.001	<0.001
<i>Pongo</i>	CA	KW Chi-squared	1.111	1.153	3.536
		df	3	3	3
		p-value	0.774	0.764	0.316
	Z _{pol}	KW Chi-squared	3.577	3.416	3.809
		df	3	3	3
		p-value	0.311	0.332	0.283
	J	KW Chi-squared	4.199	4.338	4.840
		df	3	3	3
		p-value	0.241	0.227	0.184

Abbreviations: CA = cortical area; Z_{pol} = polar section modulus; J = polar second moment of area.

Supplementary Table 4.7: Significance values for post hoc comparisons of cross-sectional properties within species, across the digits at 35%, 50% and 65% of the phalanx.

			35%			50%			65%		
			IP3	IP4	IP5	IP3	IP4	IP5	IP3	IP4	IP5
<i>H. sapiens</i>	Z _{pol}	IP2	1.000	1.000	0.487	1.000	1.000	0.342	1.000	1.000	0.371
		IP3		1.000	0.009		1.000	0.023		1.000	0.015
		IP4			0.068			0.183			0.179
	J	IP2	0.588	1.000	0.195	1.000	1.000	0.270	1.000	1.000	0.331
		IP3		1.000	<0.001		1.000	0.003		1.000	0.005
		IP4			0.012			0.035			0.058
<i>Pan</i>	CA	IP2	1.000	1.000	0.487	1.000	1.000	0.400	-	-	-
		IP3		1.000	0.035		0.543	0.021		-	-
		IP4			0.464			1.000			-
	Z _{pol}	IP2	0.079	1.000	0.487	0.057	1.000	0.470	0.013	1.000	1.000
		IP3		0.424	<0.001		0.119	<0.001		0.143	<0.001
		IP4			0.100			0.110			0.125
	J	IP2	0.010	1.000	0.265	0.007	1.000	0.140	0.004	1.000	0.413
		IP3		0.148	<0.001		0.039	<0.001		0.078	<0.001
		IP4			0.006			0.008			0.011
<i>Gorilla</i>	CA	IP2	-	-	-	0.300	1.000	0.524	1.000	1.000	0.410
		IP3		-	-		0.283	0.002		0.425	0.022
		IP4			-			0.498			1.000
	Z _{pol}	IP2	0.762	1.000	0.364	0.124	1.000	0.225	0.398	1.000	0.200
		IP3		0.327	0.004		0.173	<0.001		0.327	<0.001
		IP4			0.615			0.143			0.216
	J	IP2	0.416	1.000	0.487	0.055	1.000	0.196	0.283	1.000	0.136
		IP3		0.179	<0.001		0.263	<0.001		0.299	<0.001
		IP4			0.131			0.034			0.111

Abbreviations: CA = cortical area; Z_{pol} = polar section modulus; J = polar second moment of area.

Note: The intermediate phalanges *Pongo* are not represented because they did not show significant differences. CA values of *Pan* at 65% of the shaft did not show significant differences.

Supplementary Table 4.8: Significance values for post-hoc comparisons of cross-sectional properties within a phalanx..

				50%	65%	
IP2	<i>H. sapiens</i>	CA	35%	0.046	NS	
			50%		NS	
	<i>Pan</i>	J	35%	NS	0.003	
			50%		NS	
		CA	35%	NS	0.049	
			50%		NS	
		Z _{pol}	35%	0.043	<0.001	
			50%		NS	
	<i>Gorilla</i>	J	35%	0.035	<0.001	
			50%		NS	
		Z _{pol}	35%	NS	0.003	
			50%		NS	
IP3	<i>H. sapiens</i>	J	35%	NS	0.019	
			50%		NS	
	<i>Pan</i>	CA	35%	NS	0.026	
			50%		NS	
		Z _{pol}	35%	0.029	<0.001	
			50%		NS	
		J	35%	0.036	<0.001	
			50%		NS	
	<i>Gorilla</i>	CA	35%	NS	NS	
			50%		0.019	
		Z _{pol}	35%	NS	0.003	
			50%		0.018	
		J	35%	NS	0.003	
			50%		0.017	
	IP4	<i>H. sapiens</i>	J	35%	NS	0.005
				50%		NS
<i>Pan</i>		CA	35%	NS	<0.001	
			50%		NS	
		Z _{pol}	35%	0.001	<0.001	
			50%		NS	

		J	35%	0.001	<0.001
			50%		NS
	<i>Gorilla</i>	Z _{pol}	35%	NS	NS
			50%		0.008
		J	35%	NS	NS
			50%		0.003
IP5	<i>Pan</i>	Z _{pol}	35%	NS	0.011
			50%		NS
		J	35%	NS	0.014
			50%		NS
	<i>Gorilla</i>	Z _{pol}	35%	NS	0.009
			50%		NS
		J	35%	NS	0.006
			50%		NS

Abbreviations: NS = not significant (p>0.05).

Supplementary Table 4.9: Results of spearman's correlation test between phalangeal curvature and cortical thickness of the phalangeal shaft for the total sample and within species.

	ρ	p
IP2		
<i>H. sapiens</i>	0.294	0.251
<i>Pan</i>	-0.162	0.534
<i>Gorilla</i>	0.228	0.361
<i>Pongo</i>	0.543	0.297
IP3		
<i>H. sapiens</i>	0.160	0.453
<i>Pan</i>	0.051	0.837
<i>Gorilla</i>	0.211	0.385
<i>Pongo</i>	0.943	0.017
IP4		
<i>H. sapiens</i>	0.021	0.867
<i>Pan</i>	0.771	0.103
<i>Gorilla</i>	0.044	0.841
<i>Pongo</i>	0.256	0.289
IP5		
<i>H. sapiens</i>	0.282	0.039
<i>Pan</i>	0.400	0.517
<i>Gorilla</i>	-0.191	0.431
<i>Pongo</i>	0.486	0.081

Supplementary Table 4.10: Results of spearman's correlation test between median bar and cortical thickness of the phalangeal shaft for IP3.

	ρ	p
Total sample	0.289	0.022
<i>H. sapiens</i>	-0.114	0.646
<i>Pan</i>	-0.267	0.284
<i>Gorilla</i>	-0.218	0.369
<i>Pongo</i>	0.600	0.242

Supplementary Table 4.11: Results of spearman's correlation test between FSR depth and cortical thickness of the phalangeal shaft for IP3

	ρ	p
Total sample	0.142	0.271
<i>H. sapiens</i>	-0.133	0.585
<i>Pan</i>	0.055	0.831
<i>Gorilla</i>	0.054	0.826
<i>Pongo</i>	0.314	0.564

Supplementary Table 4.12: Results of spearman's correlation test between FSR length and cortical thickness of the phalangeal shaft for IP3.

	ρ	p
Total sample	-0.244	0.056
<i>H. sapiens</i>	-0.048	0.256
<i>Pan</i>	-0.247	0.322
<i>Gorilla</i>	-0.379	0.110
<i>Pongo</i>	-0.429	0.419

Supplementary Table 4.13: Results of spearman's correlation test between median bar and FSR length of the phalangeal shaft for IP3.

	ρ	p
Total sample	0.165	0.200
<i>H. sapiens</i>	0.299	0.214
<i>Pan</i>	0.495	0.037
<i>Gorilla</i>	-0.035	0.888
<i>Pongo</i>	-0.314	0.564

Supplementary Table 4.14: Results of spearman's correlation test between median bar and FSR depth of the phalangeal shaft for IP3.

	ρ	p
Total sample	0.149	0.249
<i>H. sapiens</i>	0.052	0.834
<i>Pan</i>	0.105	0.678
<i>Gorilla</i>	-0.221	0.362
<i>Pongo</i>	0.086	0.919

Supplementary Table 4.15: Wilcoxon signed rank tests of scaled proximal phalanx vs. intermediate phalanx CA across species

		<i>H. sapiens</i>	<i>Pan</i>	<i>Gorilla</i>	<i>Pongo</i>
35%					
Digit 2	Proximal mean	0.692	0.759	1.205	0.625
	Intermediate mean	0.643	0.868	1.212	0.643
	W	191	222	20	61
	p-value	0.017	0.820	<0.001	0.018
Digit 3	Proximal mean	0.702	0.851	1.296	0.598
	Intermediate mean	0.769	0.952	1.319	0.642
	W	254	152	153	65
	p-value	0.090	0.002	0.046	0.771
Digit 4	Proximal mean	0.611	0.806	1.278	0.550
	Intermediate mean	0.664	0.880	1.241	0.631
	W	108	228	205	57
	p-value	0.468	0.104	0.452	0.606
Digit 5	Proximal mean	0.517	0.702	1.108	0.503
	Intermediate mean	0.538	0.787	1.115	0.615
	W	9	166	102	40
	p-value	0.287	0.375	0.067	0.750
50%					
Digit 2	Proximal mean	0.767	0.832	1.412	0.636
	Intermediate mean	0.781	0.832	1.237	0.692
	W	178	270	28	61
	p	0.061	0.146	<0.001	0.018
Digit 3	Proximal mean	0.779	0.978	1.507	0.663
	Intermediate mean	0.872	0.881	1.394	0.665
	W	256	186	181	75
	p	0.139	0.014	0.187	0.346
Digit 4	Proximal mean	0.750	0.893	1.315	0.672
	Intermediate mean	0.827	0.802	1.238	0.655
	W	130	270	198	99
	p	0.956	0.419	0.359	0.044

Digit 5	Proximal mean	0.664	0.711	1.246	0.567
	Intermediate mean	0.721	0.753	1.082	0.650
	W	75	220	146	37
	p	0.047	0.606	0.671	0.964
65%					
Digit 2	Proximal mean	0.817	0.860	1.417	0.677
	Intermediate mean	0.754	0.756	1.135	0.619
	W	178	345	72	68
	p	0.061	<0.001	<0.001	0.001
Digit 3	Proximal mean	0.854	1.031	1.563	0.732
	Intermediate mean	0.843	0.811	1.205	0.586
	W	272	379	182	87
	p	0.027	0.202	0.195	0.080
Digit 4	Proximal mean	0.823	0.940	1.389	0.736
	Intermediate mean	0.801	0.745	1.088	0.573
	W	132	432	265	99
	p	0.897	0.020	0.526	0.044
Digit 5	Proximal mean	0.688	0.719	1.263	0.602
	Intermediate mean	0.666	0.712	1.002	0.570
	W	123	247	154	47
	p	0.867	0.127	0.863	0.336

Supplementary Table 4.16: Wilcoxon signed rank tests of scaled proximal phalanx vs. intermediate phalanx Z_{POL} across species.

		<i>H. sapiens</i>	<i>Pan</i>	<i>Gorilla</i>	<i>Pongo</i>
35%					
Digit 2	Proximal mean	1.815	1.559	4.214	1.462
	Intermediate mean	1.410	1.430	2.834	1.097
	W	205	345	96	62
	p	0.003	<0.001	0.001	0.013
Digit 3	Proximal mean	1.975	2.257	4.950	1.669
	Intermediate mean	1.780	1.858	3.301	1.189
	W	288	371	204	81
	p	0.007	0.263	0.438	0.180
Digit 4	Proximal mean	1.672	1.857	4.003	1.742
	Intermediate mean	1.576	1.539	2.745	1.178
	W	130	414	280	95
	p	0.956	0.049	0.323	0.079
Digit 5	Proximal mean	1.314	1.265	2.986	1.152
	Intermediate mean	1.123	1.226	2.216	0.996
	W	166	257	179	49
	p	0.160	0.132	0.560	0.250
50%					
Digit 2	Proximal mean	1.678	1.456	4.317	1.302
	Intermediate mean	1.386	1.114	2.393	1.072
	W	207	353	104	61
	p	0.002	< 0.001	0.002	0.018
Digit 3	Proximal mean	1.838	2.196	5.018	1.496
	Intermediate mean	1.657	1.437	3.146	1.146
	W	322	373	210	84
	p	<0.001	0.247	0.526	0.123
Digit 4	Proximal mean	1.637	1.740	4.020	1.529
	Intermediate mean	1.465	1.153	2.464	1.137
	W	188	447	250	107
	p	0.023	0.008	0.778	0.011

Digit 5	Proximal mean	1.207	1.067	3.178	1.000
	Intermediate mean	1.088	0.922	1.775	0.982
	W	126	304	221	41
	p	0.956	0.005	0.053	0.682
65%					
Digit 2	Proximal mean	1.626	1.514	3.724	1.424
	Intermediate mean	1.179	0.950	1.905	0.875
	W	201	411	177	66
	p	0.005	<0.001	0.245	0.003
Digit 3	Proximal mean	1.826	2.277	4.635	1.732
	Intermediate mean	1.394	1.243	2.325	0.887
	W	334	492	273	95
	p	<0.001	<0.001	0.411	0.021
Digit 4	Proximal mean	1.675	1.847	3.733	1.740
	Intermediate mean	1.247	1.032	1.924	0.886
	W	178	527	350	110
	p	0.061	<0.001	0.007	0.006
Digit 5	Proximal mean	1.121	1.096	2.821	1.106
	Intermediate mean	0.939	0.834	1.446	0.782
	W	166	309	226	52
	p	0.160	0.002	0.036	0.151

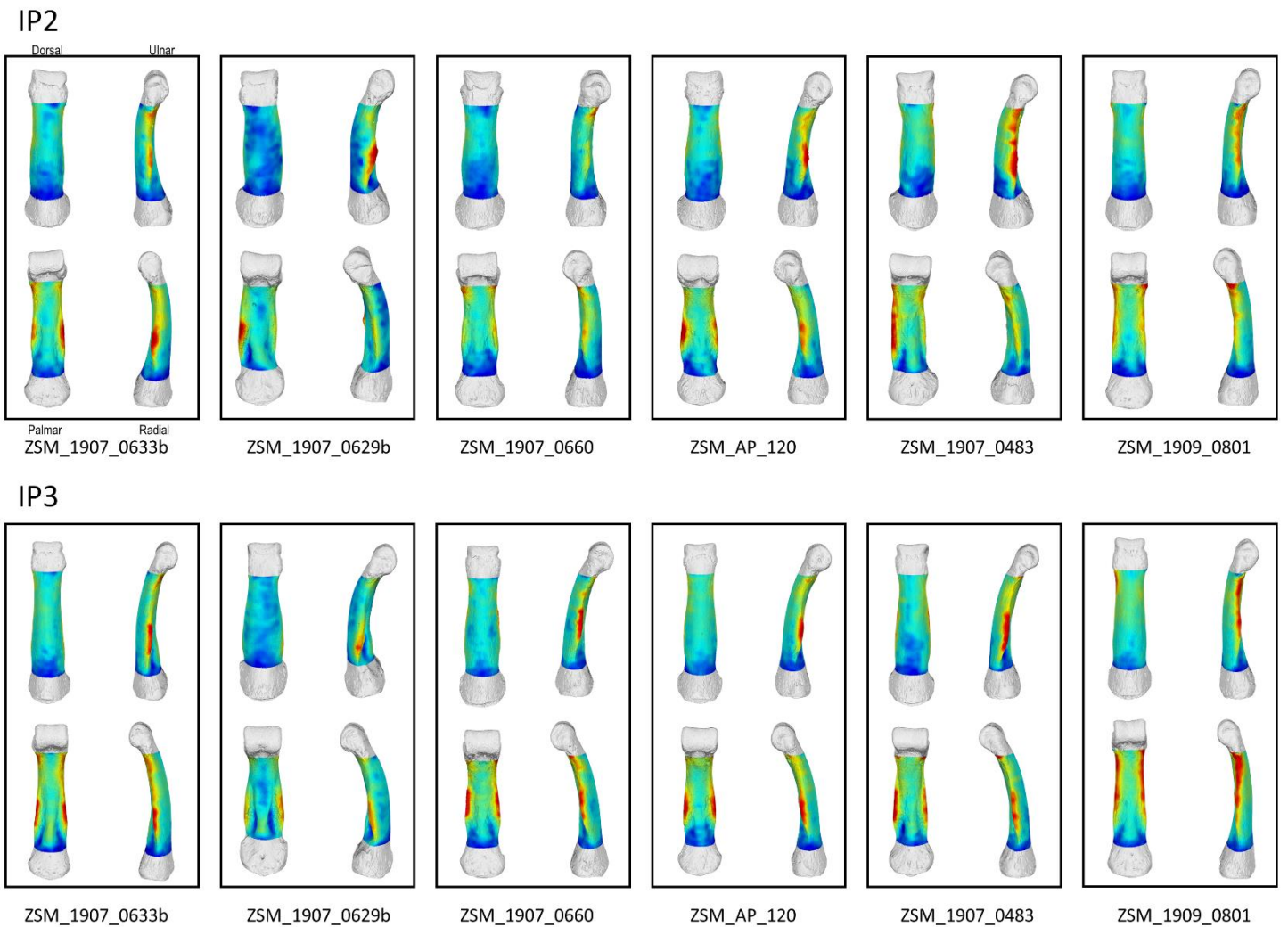
Supplementary Table 4.17: Wilcoxon signed rank tests of Scaled proximal phalanx vs. intermediate phalanx J across species.

		<i>H. sapiens</i>	<i>Pan</i>	<i>Gorilla</i>	<i>Pongo</i>
35%					
Digit 2	Proximal mean	10.380	7.459	37.262	6.864
	Intermediate mean	6.973	6.628	19.082	4.905
	W	205	351	99	61
	p	0.003	<0.001	0.001	0.018
Digit 3	Proximal mean	11.606	13.102	48.787	8.446
	Intermediate mean	10.000	10.617	25.297	6.123
	W	299	354	198	75
	p	0.003	0.429	0.359	0.346
Digit 4	Proximal mean	9.549	9.564	36.234	9.119
	Intermediate mean	8.380	7.644	19.775	5.984
	W	148	415	270	93
	p	0.468	0.047	0.452	0.104
Digit 5	Proximal mean	6.613	4.751	22.827	4.888
	Intermediate mean	4.867	4.742	12.668	4.398
	W	179	265	200	45
	p	0.057	0.085	0.211	0.437
50%					
Digit 2	Proximal mean	9.092	7.894	37.632	6.901
	Intermediate mean	5.809	4.700	14.901	4.876
	W	225	372	108	62
	p	<0.001	<0.001	0.003	0.013
Digit 3	Proximal mean	10.479	14.420	49.767	8.330
	Intermediate mean	8.087	7.363	23.597	5.708
	W	351	392	232	84
	p	<0.001	0.126	0.907	0.123
Digit 4	Proximal mean	9.076	10.237	36.357	8.800
	Intermediate mean	6.797	5.120	16.924	5.421
	W	201	480	276	106
	p	0.005	<0.001	0.371	0.013

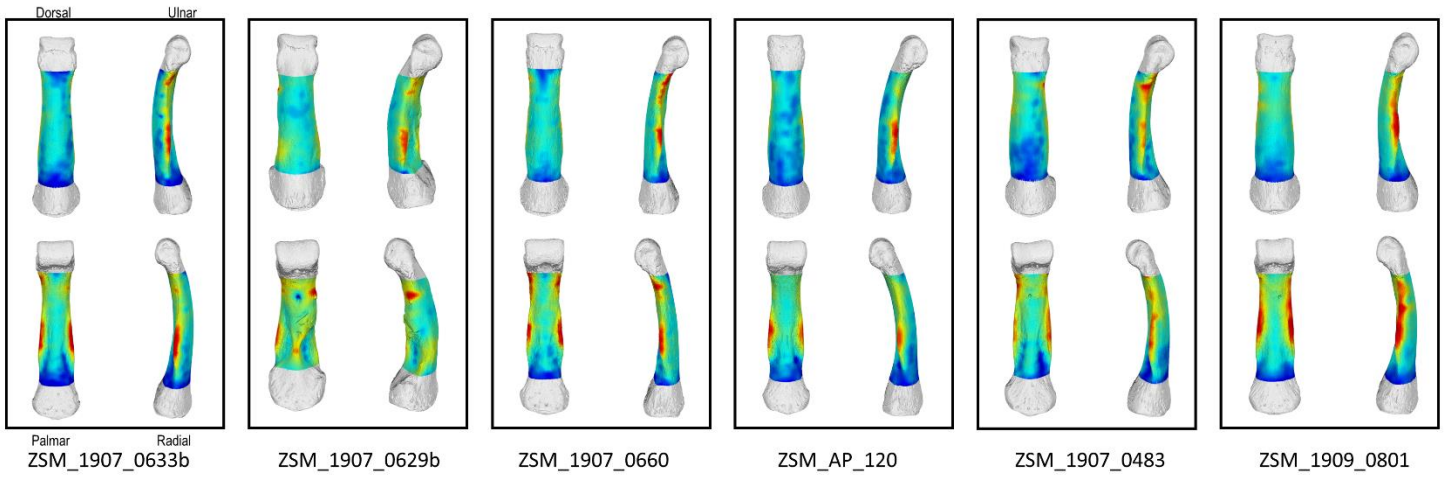
Digit 5	Proximal mean	5.683	4.509	24.766	4.805
	Intermediate mean	4.107	3.294	9.312	4.428
	W	152	318	237	44
	p	0.381	0.001	0.014	0.494
65%					
Digit 2	Proximal mean	8.625	8.158	31.730	8.846
	Intermediate mean	4.660	3.619	10.917	3.344
	W	207	421	193	68
	p	0.002	<0.001	0.442	0.001
Digit 3	Proximal mean	10.507	15.152	45.513	11.540
	Intermediate mean	6.186	5.616	14.890	3.639
	W	349	517	309	97
	p	<0.001	<0.001	0.092	0.014
Digit 4	Proximal mean	9.373	10.891	32.763	11.794
	Intermediate mean	5.237	4.079	11.320	3.615
	W	190	554	380	113
	p	0.019	<0.001	<0.001	0.003
Digit 5	Proximal mean	4.882	4.355	20.961	6.031
	Intermediate mean	3.304	2.790	6.956	2.871
	W	181	328	247	57
	p	0.047	<0.001	0.005	0.053

Supplementary Figure 4.1: Cortical thickness distribution maps of each individual used in the study. Specimen IDs of individuals are under each map.

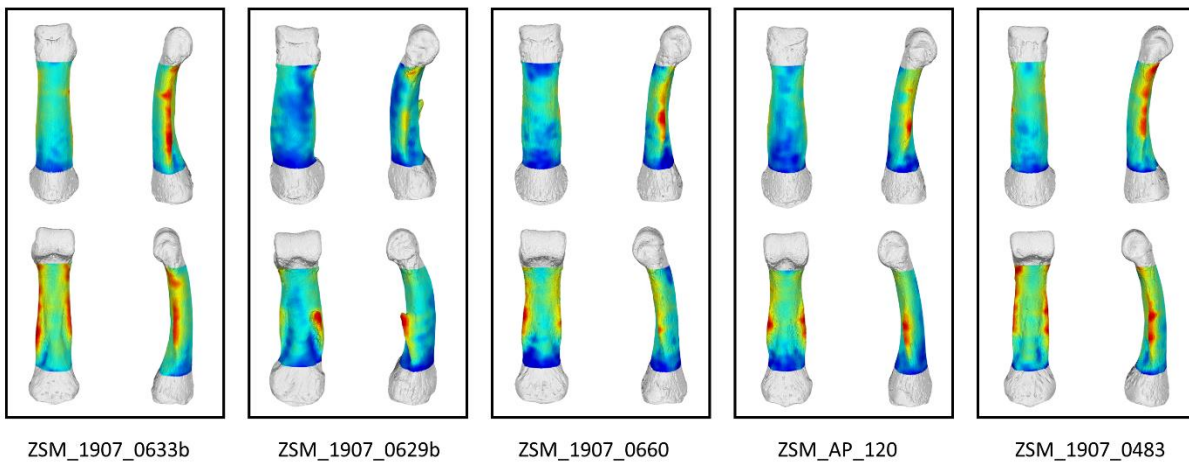
Pongo



IP4

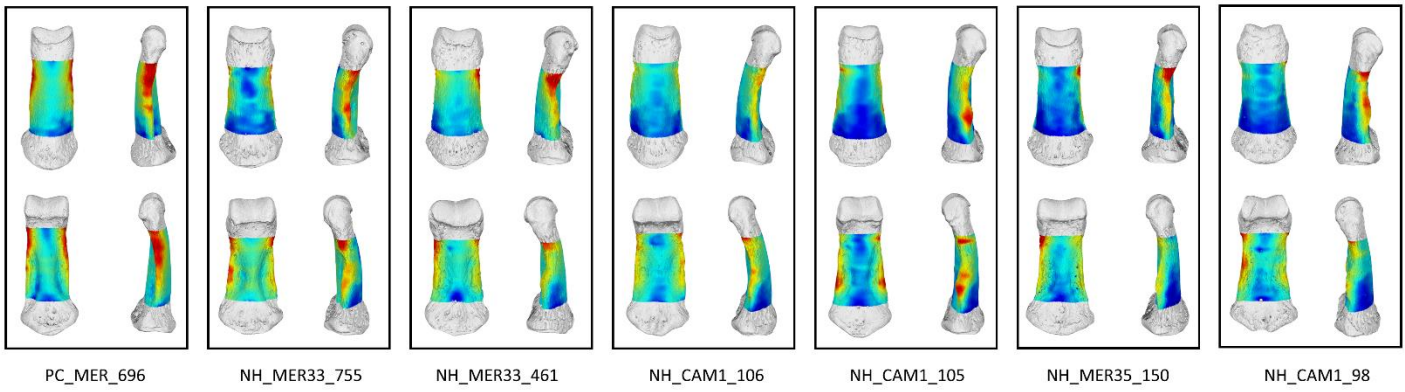
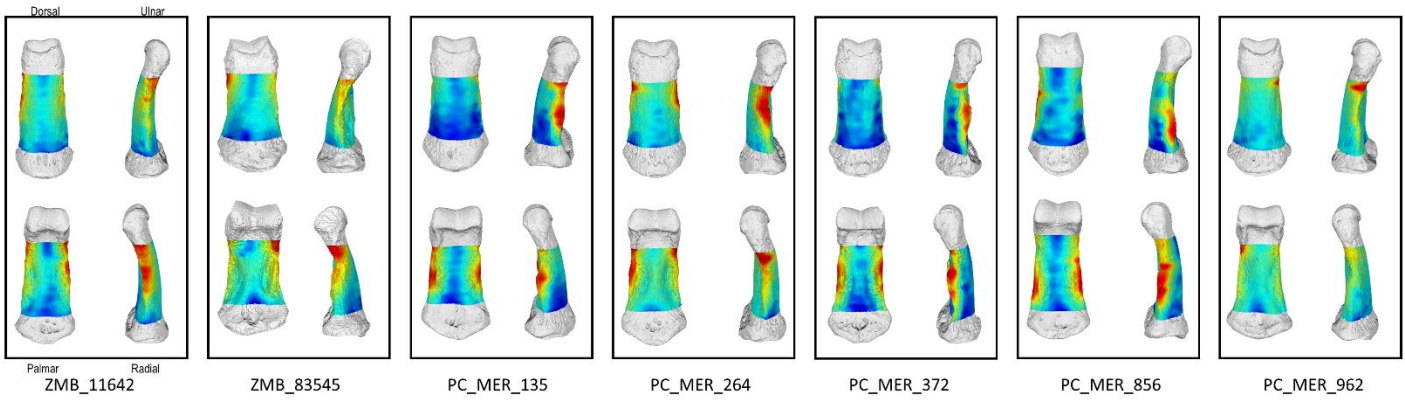


IP5

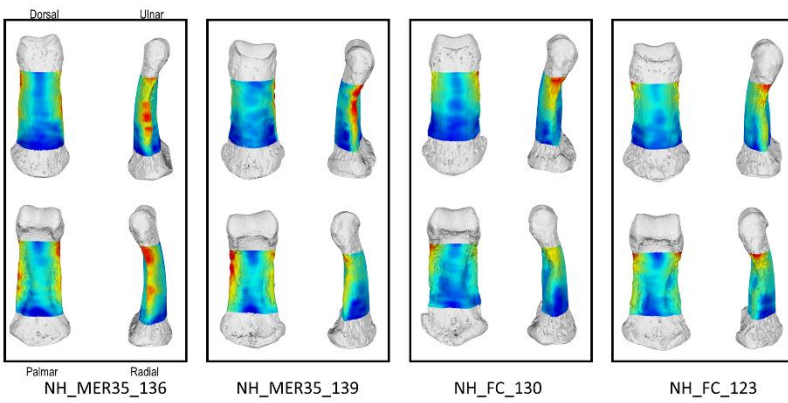


Gorilla

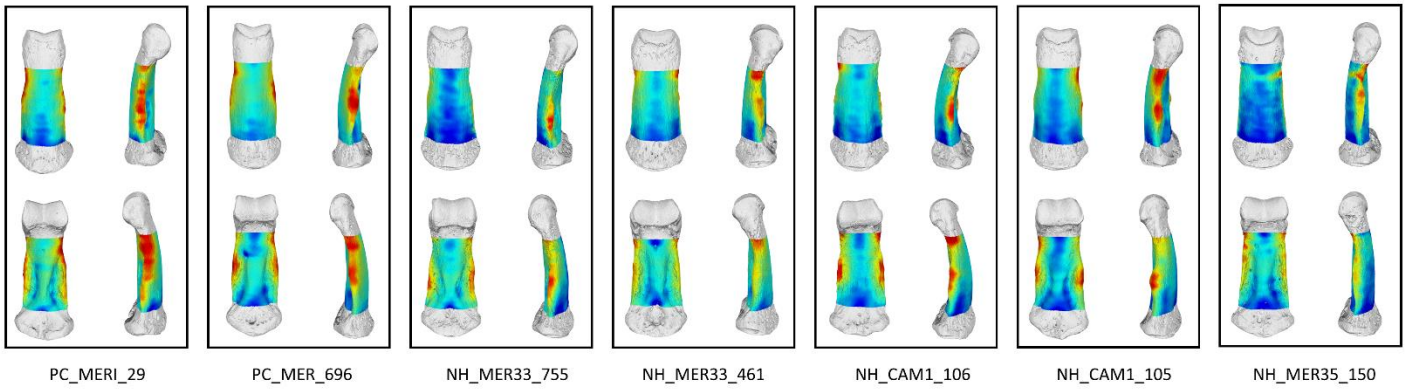
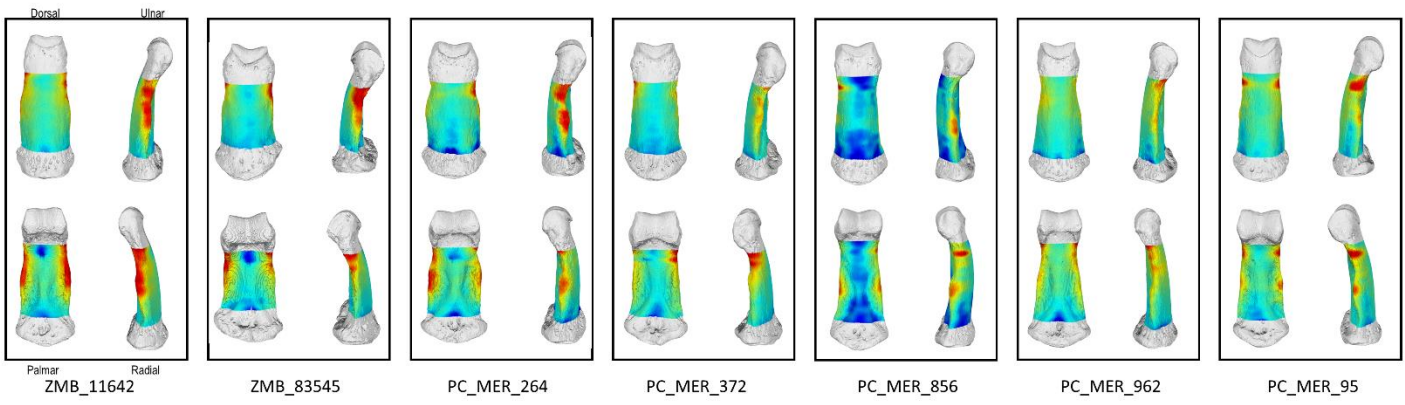
IP2



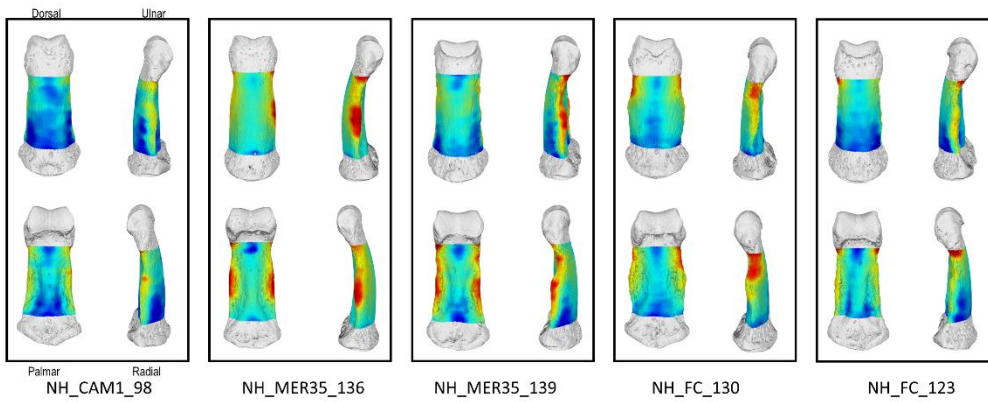
IP2



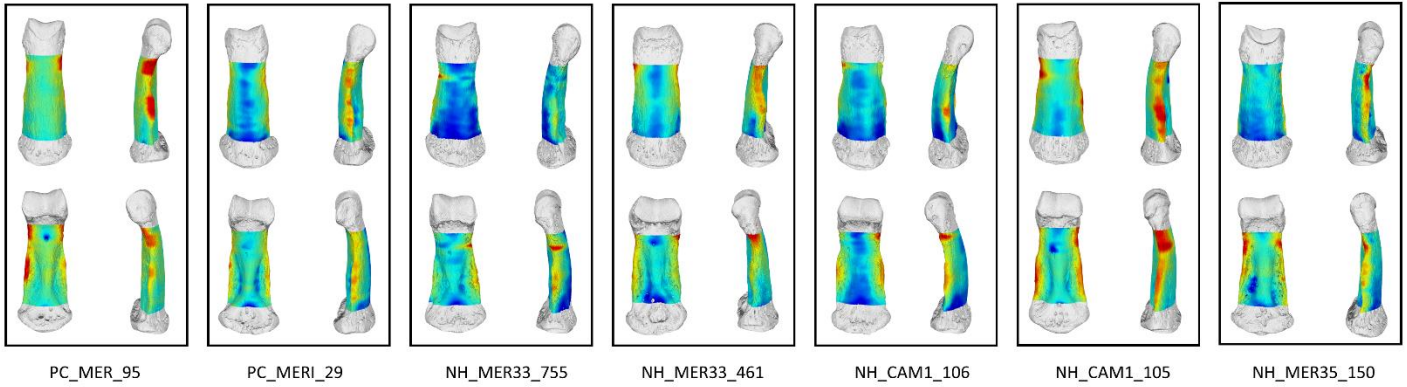
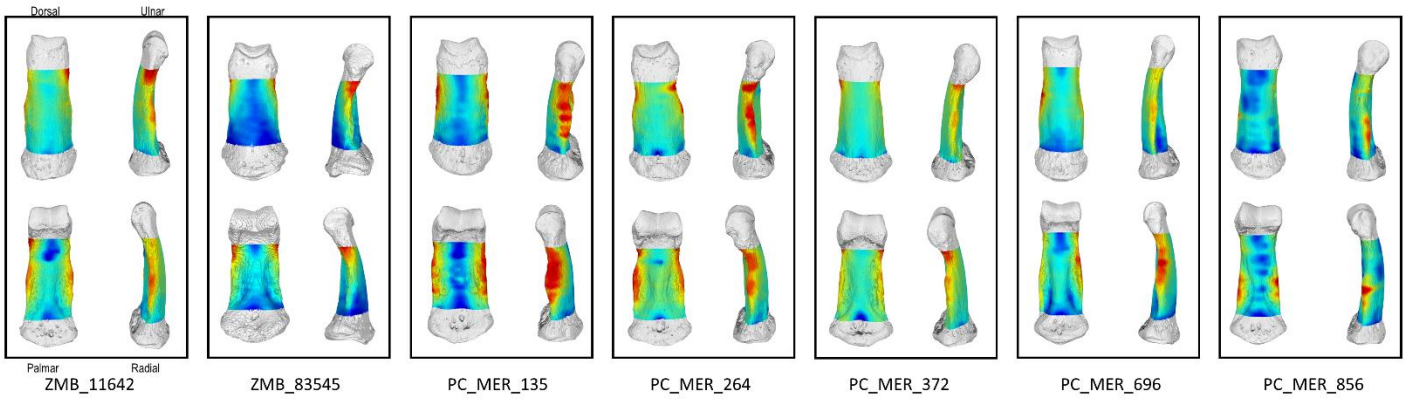
IP3



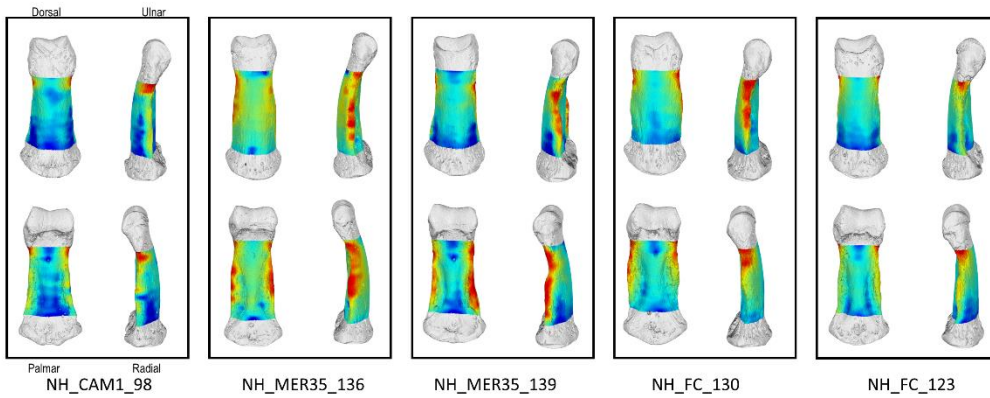
IP3



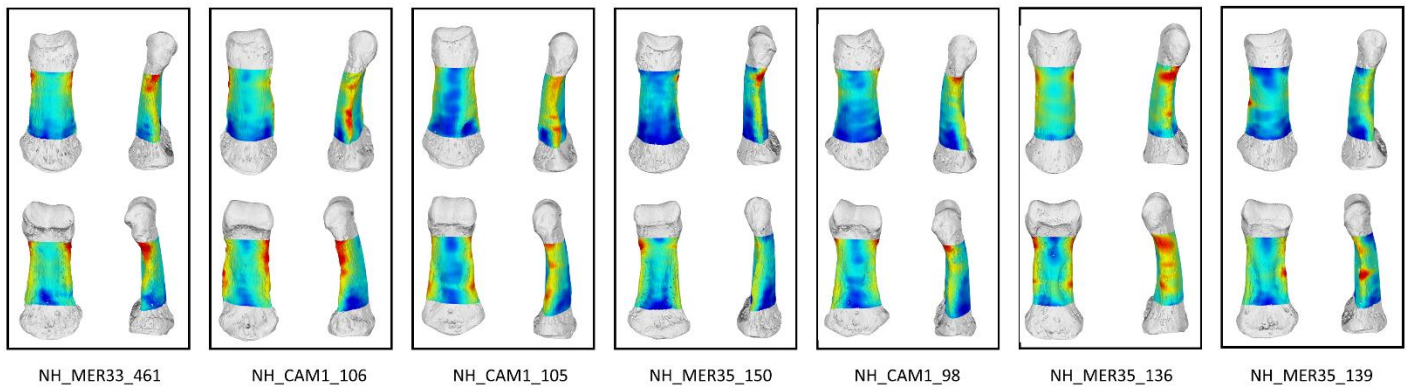
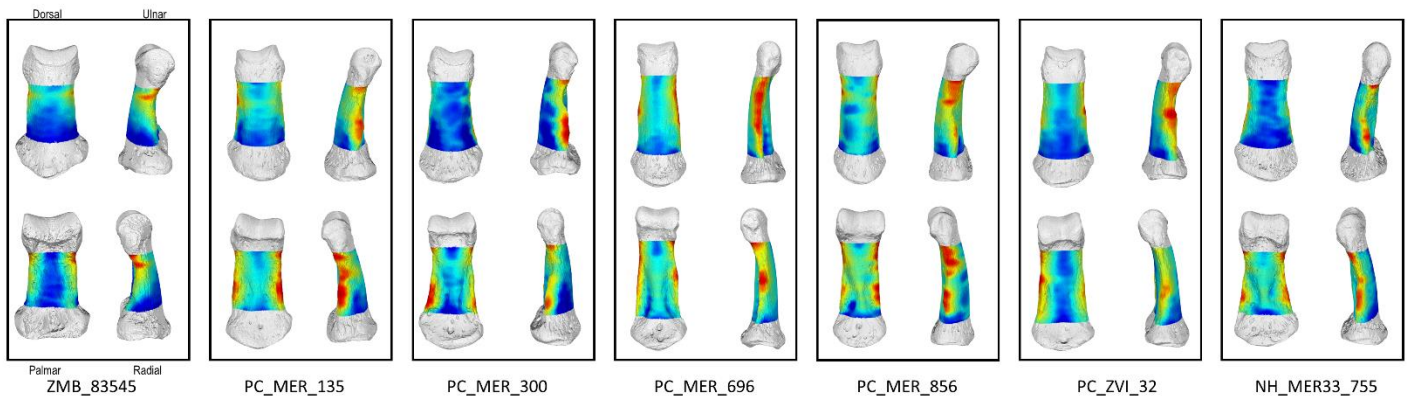
IP4



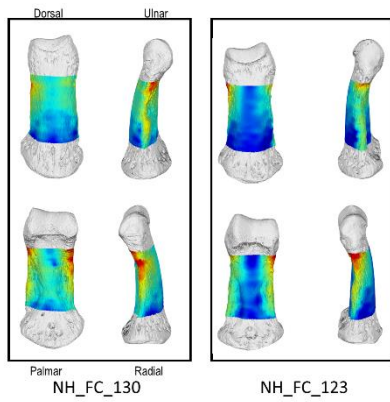
IP4



IP5

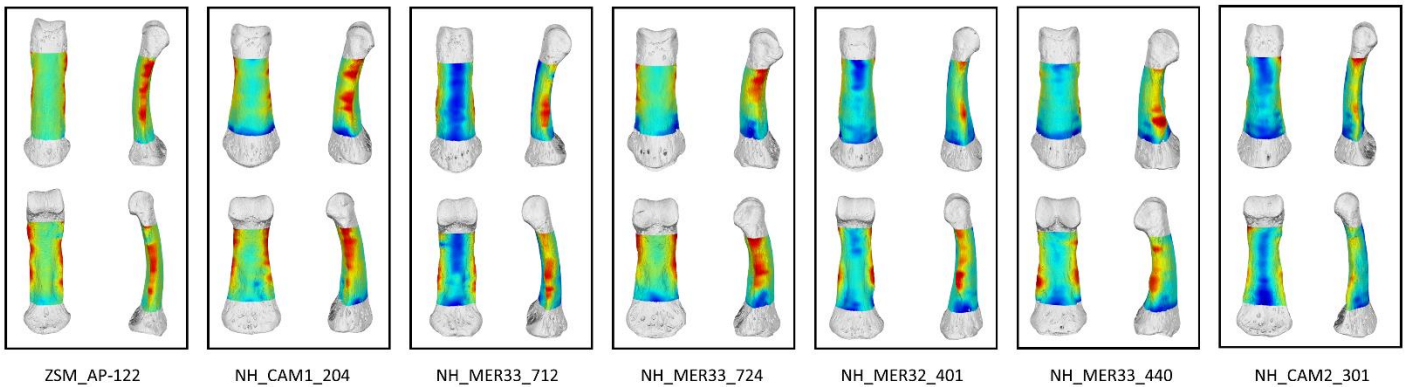
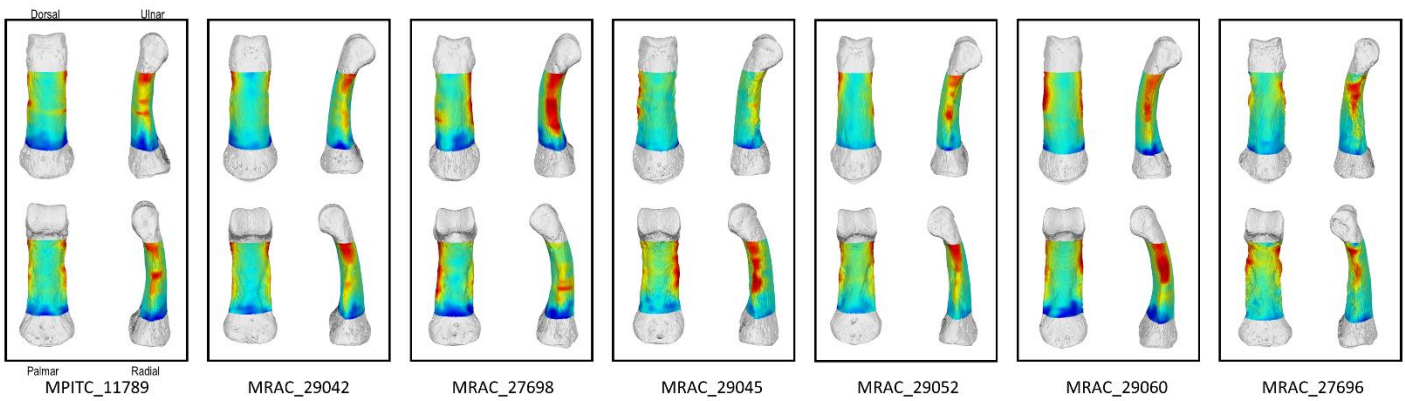


IP5

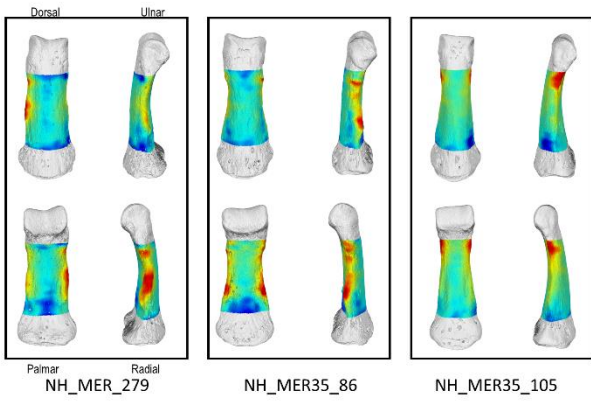


Pan

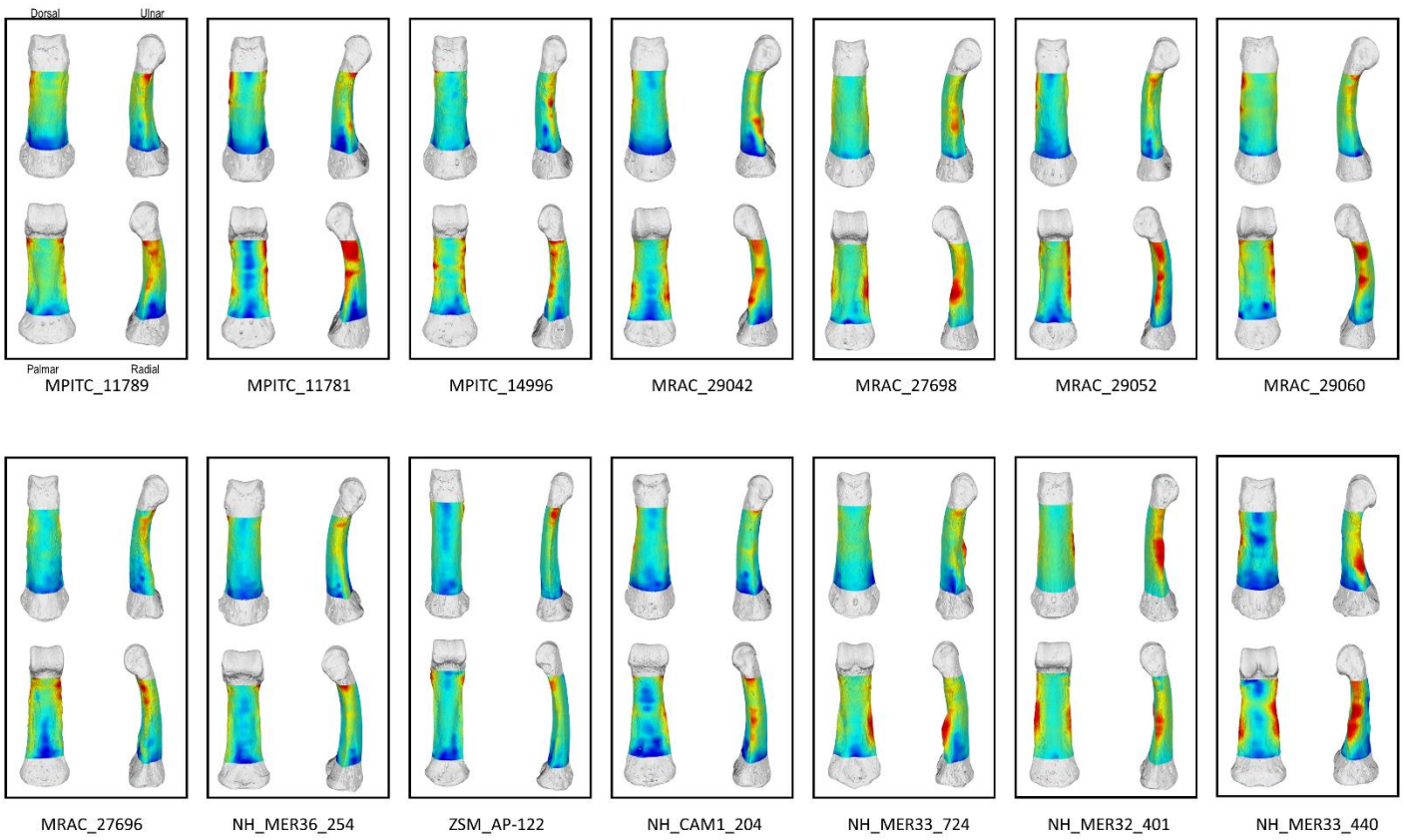
IP2



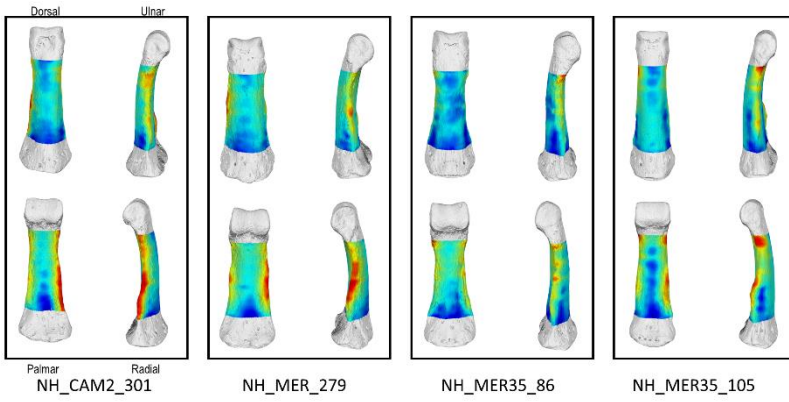
IP2



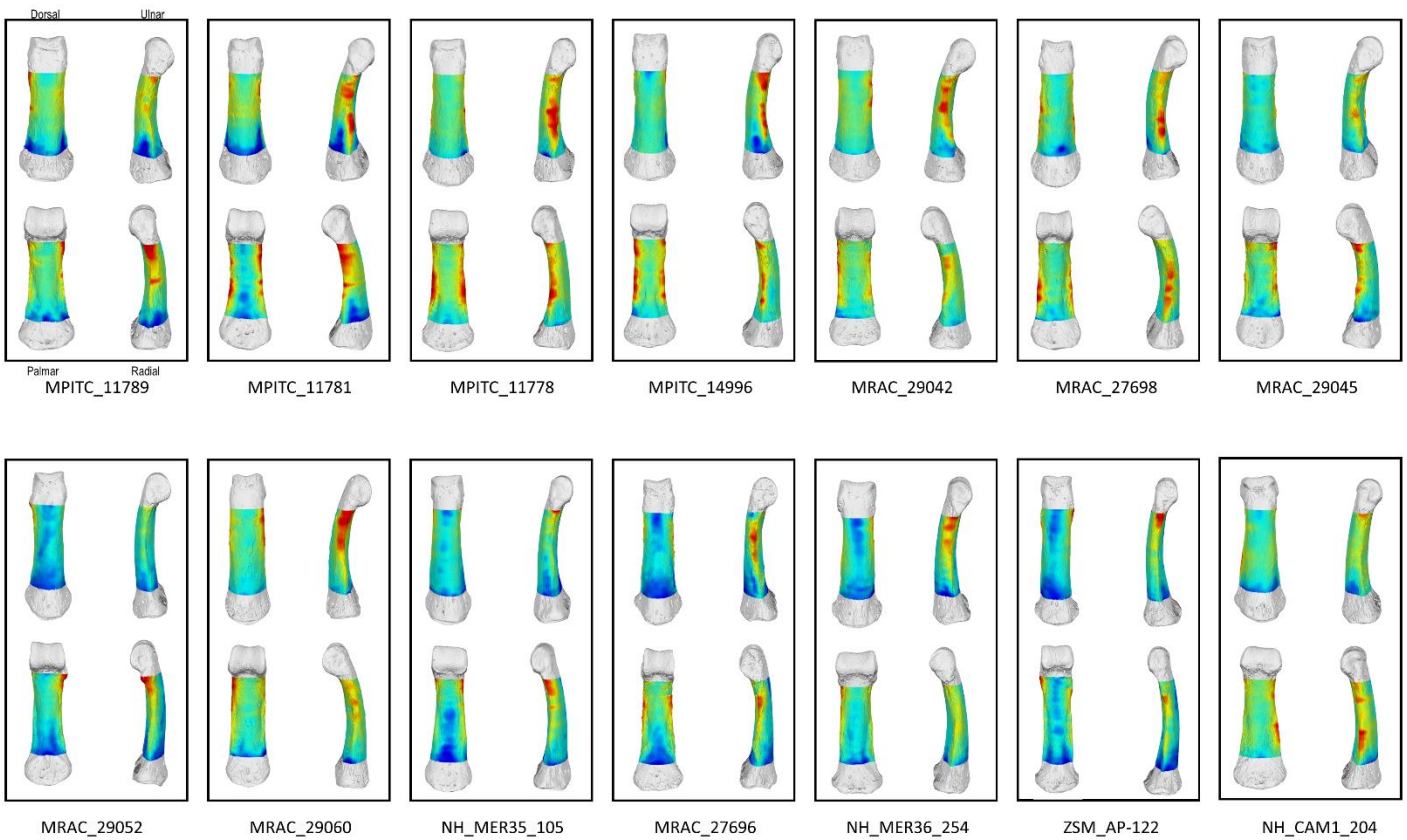
IP3



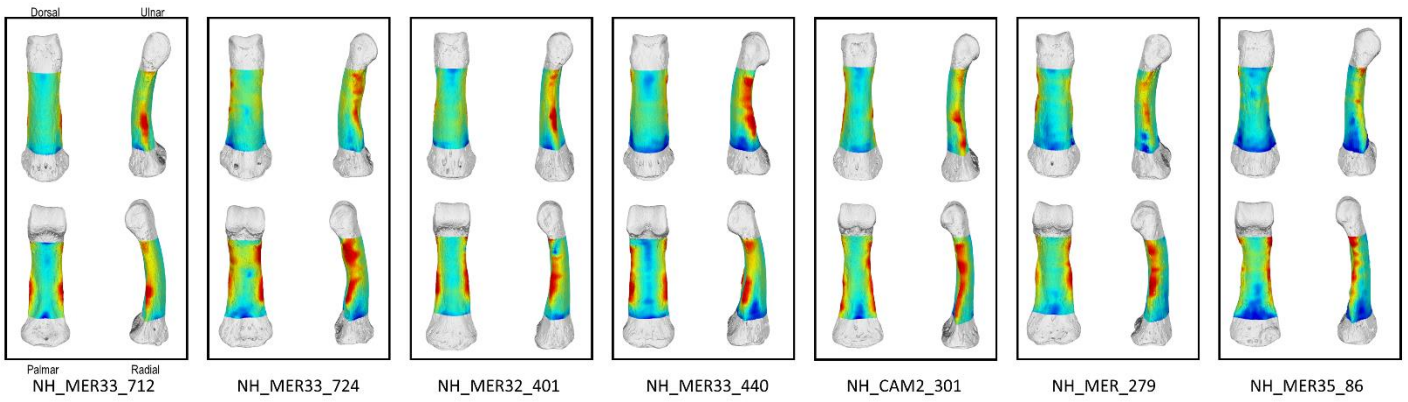
IP3



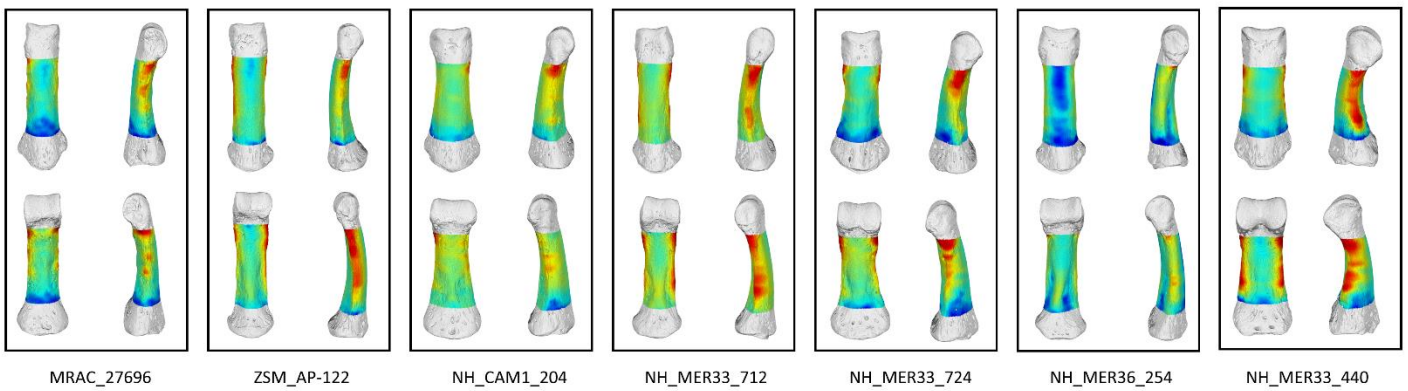
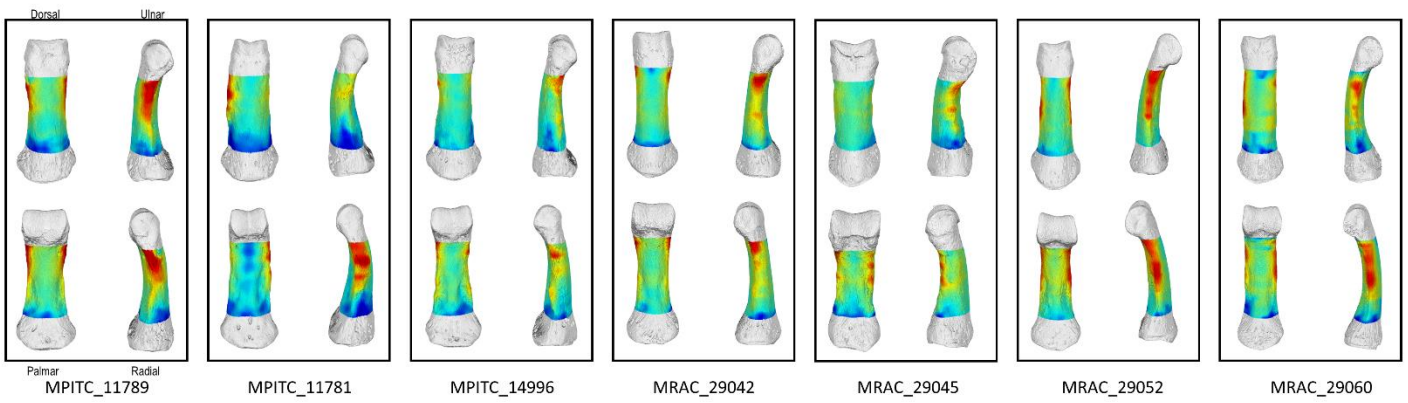
IP4



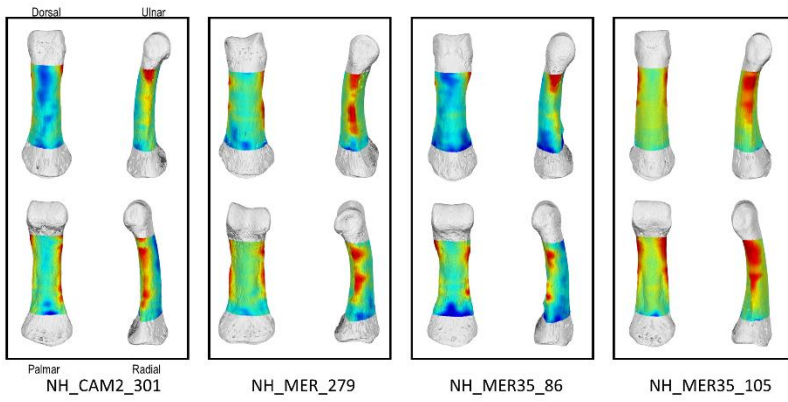
IP4



IP5

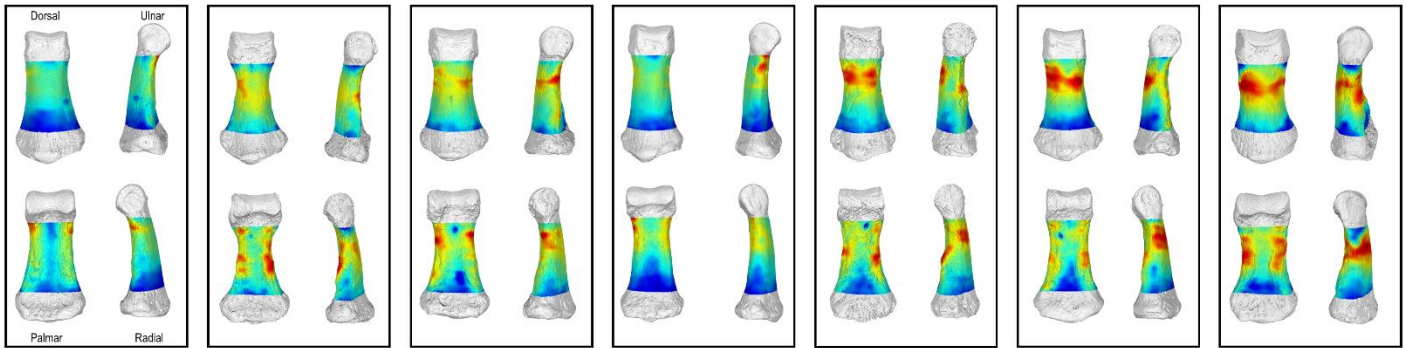


IP5

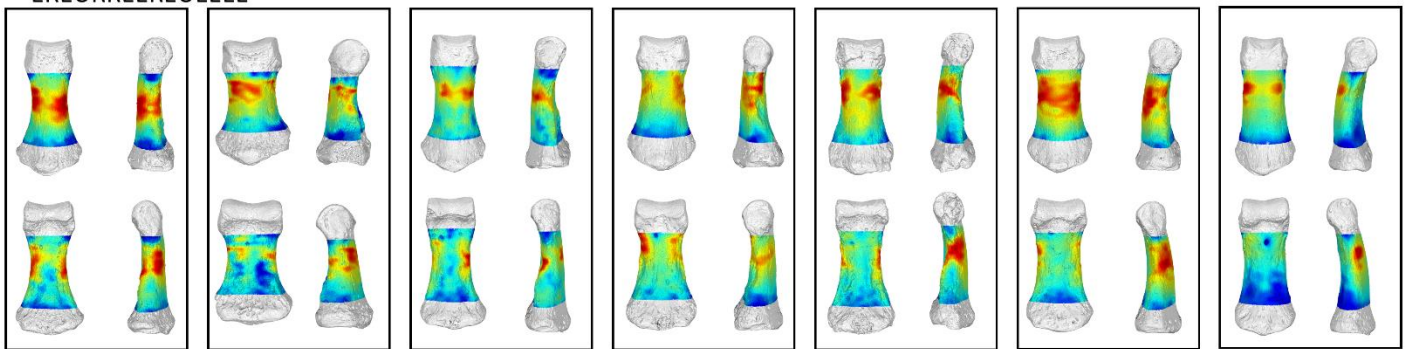


H. sapiens

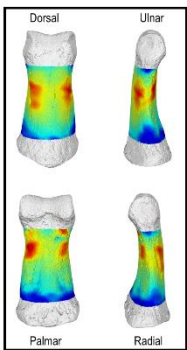
IP2



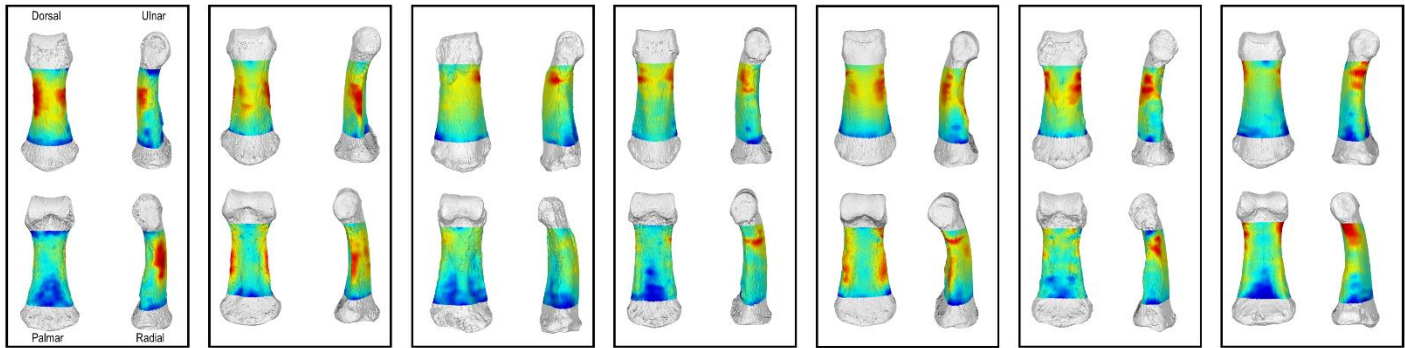
EREURREEREUEEEE



IP2



IP3



UNIFL_4887

DCW_AM_3_0_2

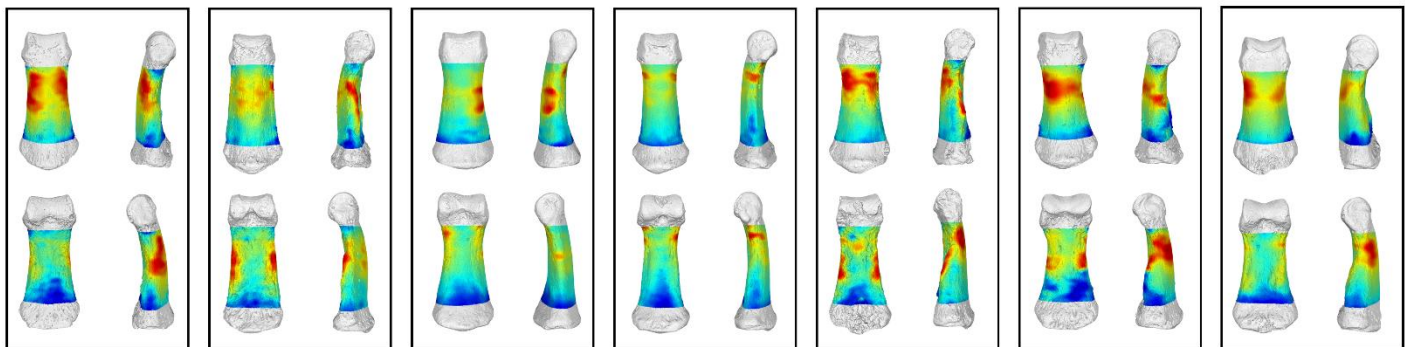
Qafzeh_8

DCW_OC_1_0_141

81_H172_H

NHMW_Nubian_K5.2

ARENE_CANDIDE_2



OHALO_II_H2

Barma_Grande_2

DV13_96

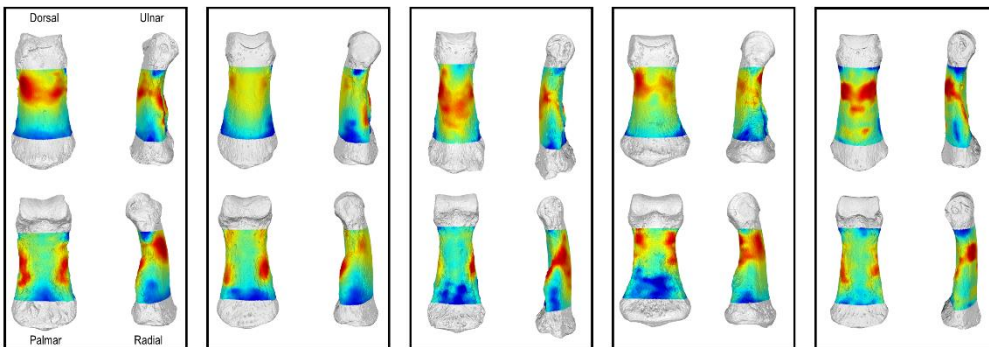
DV15_116

DV16_96

GAUG_Inden_91

GAUG_Inden_113

IP3



GAUG_Inden_117

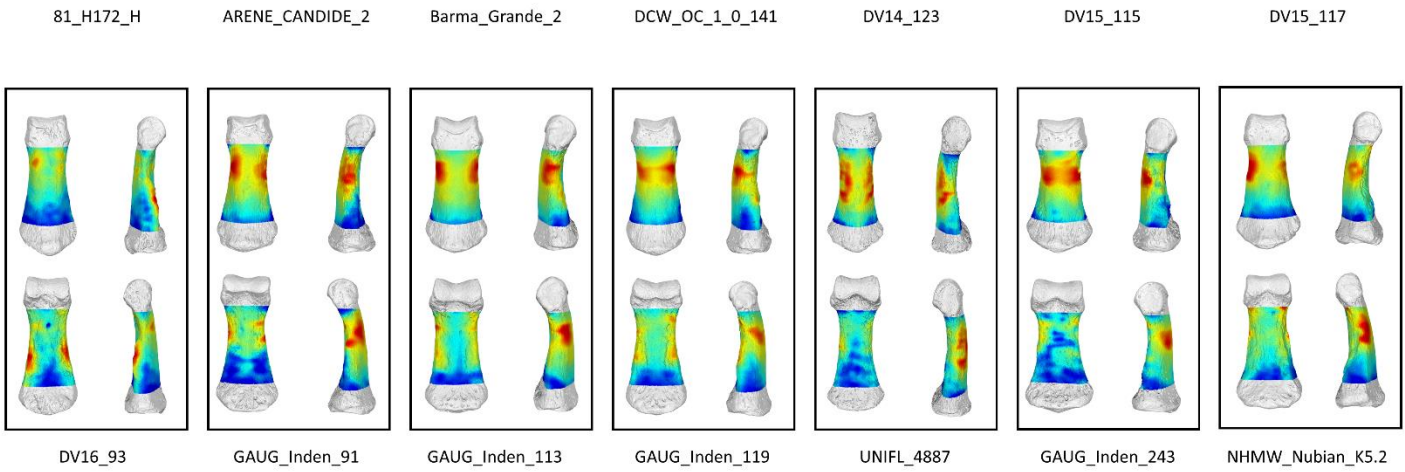
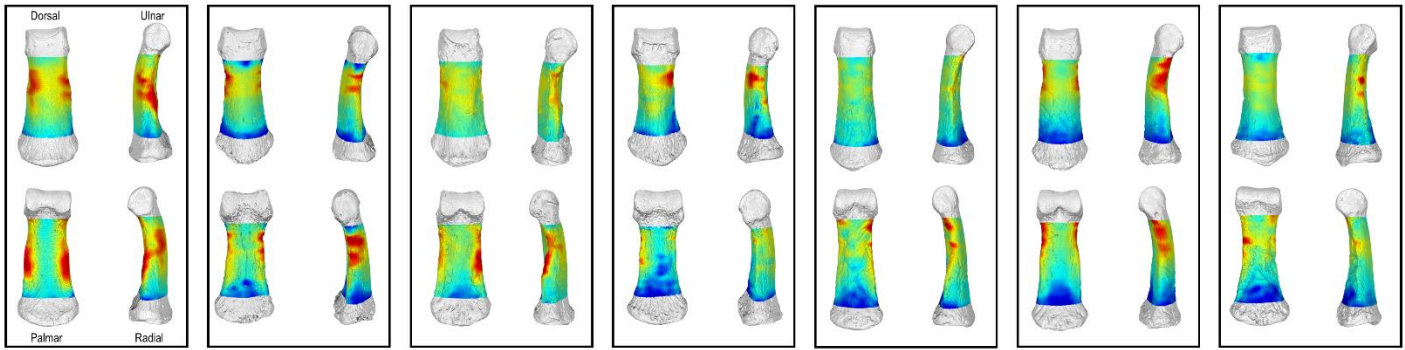
GAUG_Inden_119

NHMW_Nubian_K63

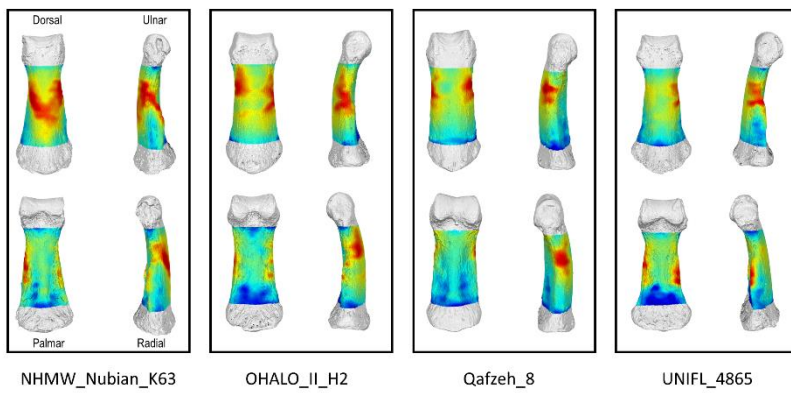
GAUG_Inden_243

NHMW_Nubian_J7

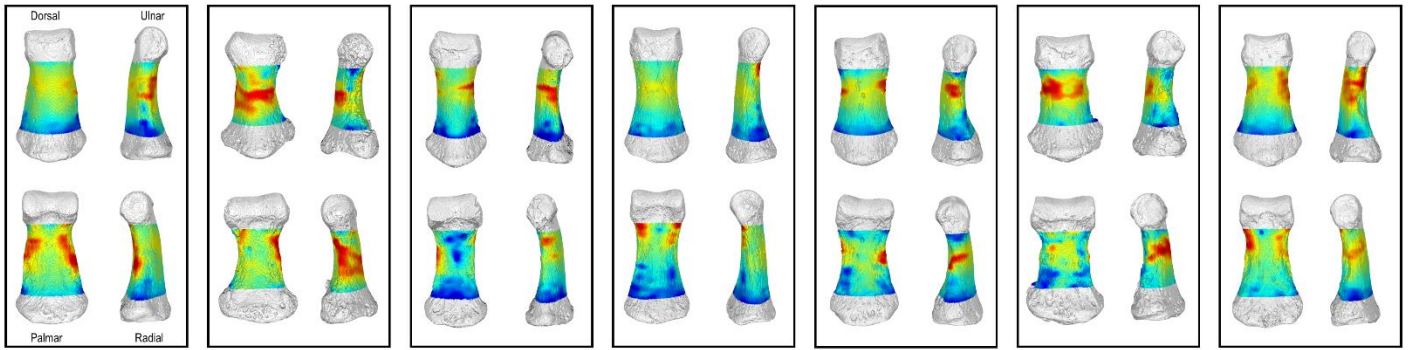
IP4



IP4



IP5



81_H172_H

DCW_AM_3_0_2

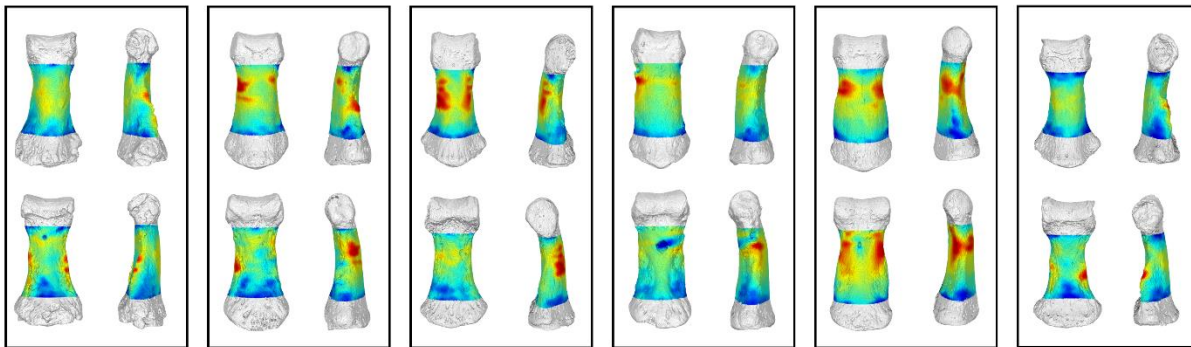
DCW_OC_1_0_141

DV13_98

GAUG_Inden_91

GAUG_Inden_243

NHMW_Nubian_K5.2



NHMW_Nubian_K63

OHALO_II_H2

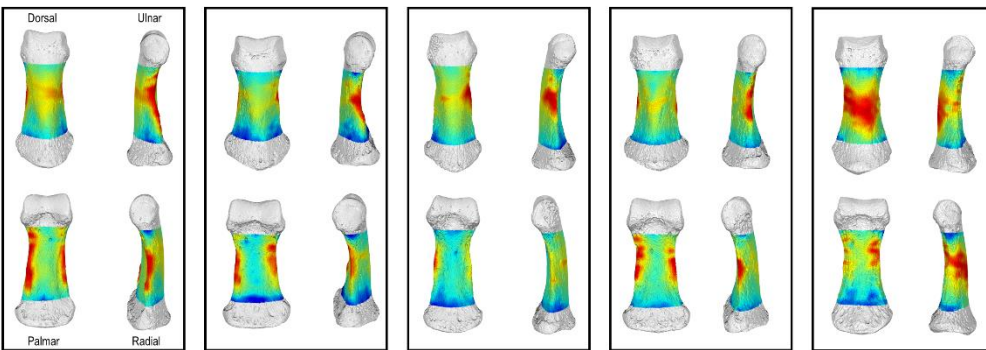
UNIFL_4887

Qafzeh_8

Qafzeh_9

UNIFL_4865

IP2 or IP4



002_DCW_AM_3_0_2

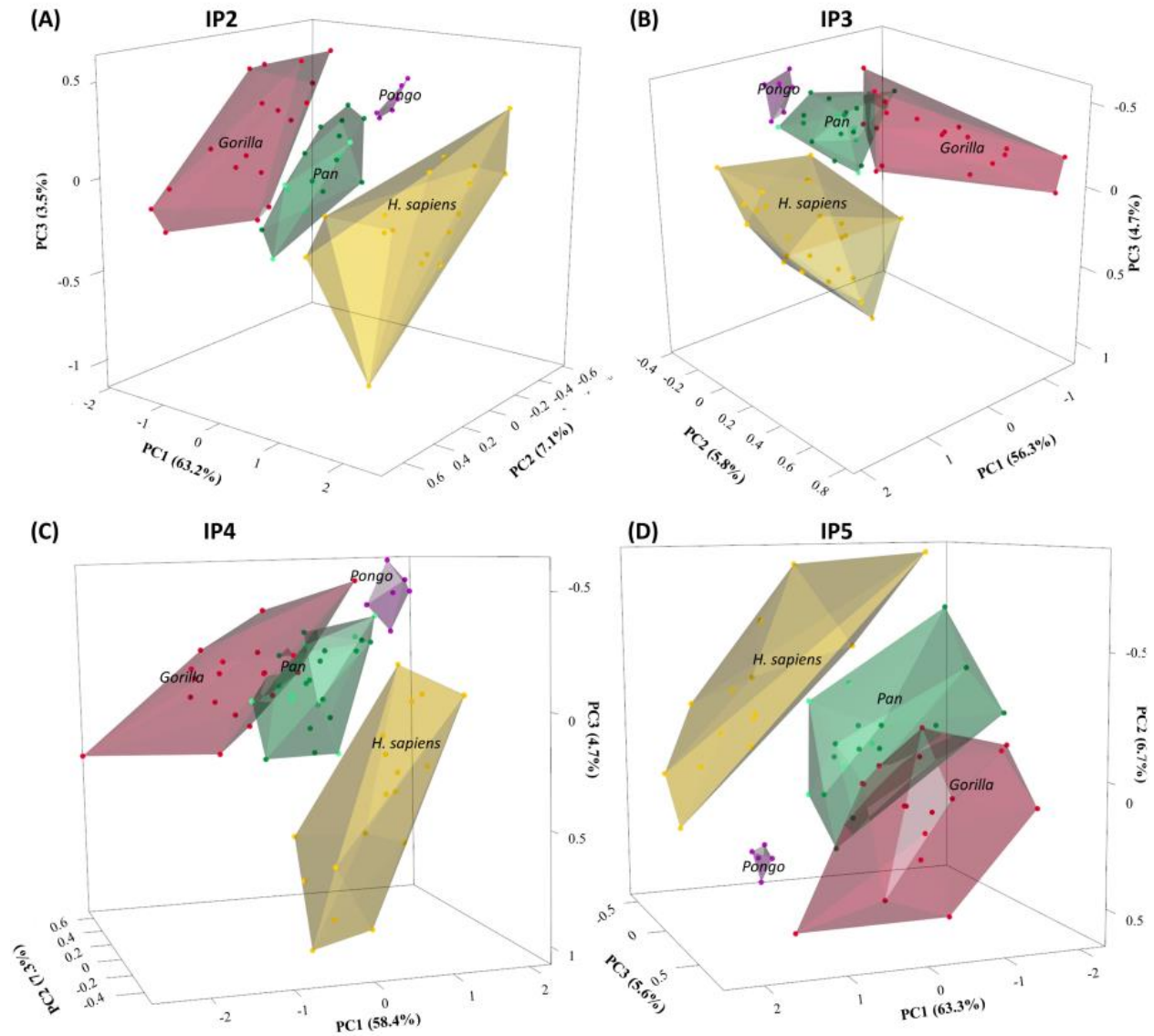
004_DCW_AM_3_0_2

006_DCW_AM_3_0_2

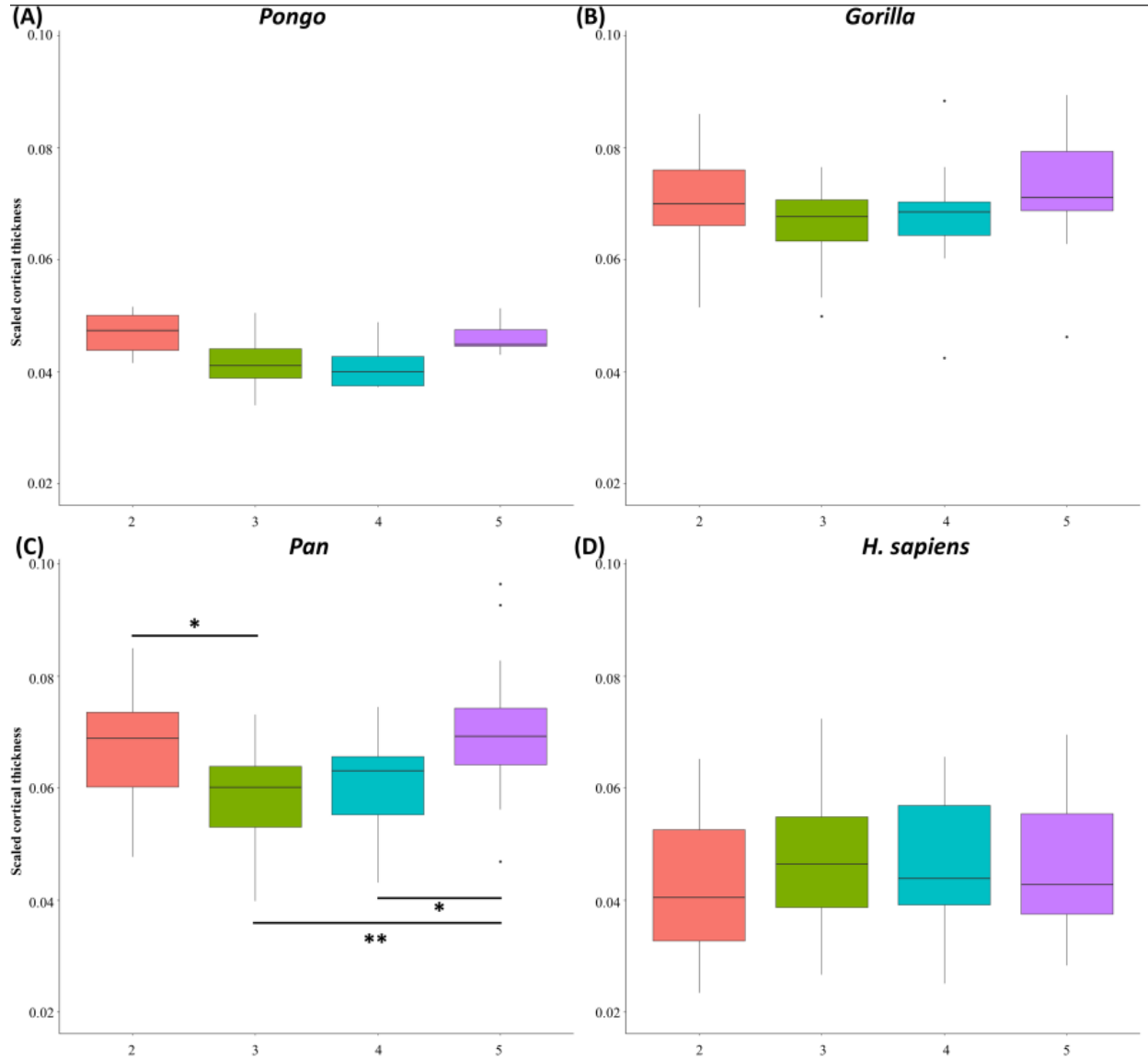
DCW_AM_3_0_2

DCW_OC_1_0_26

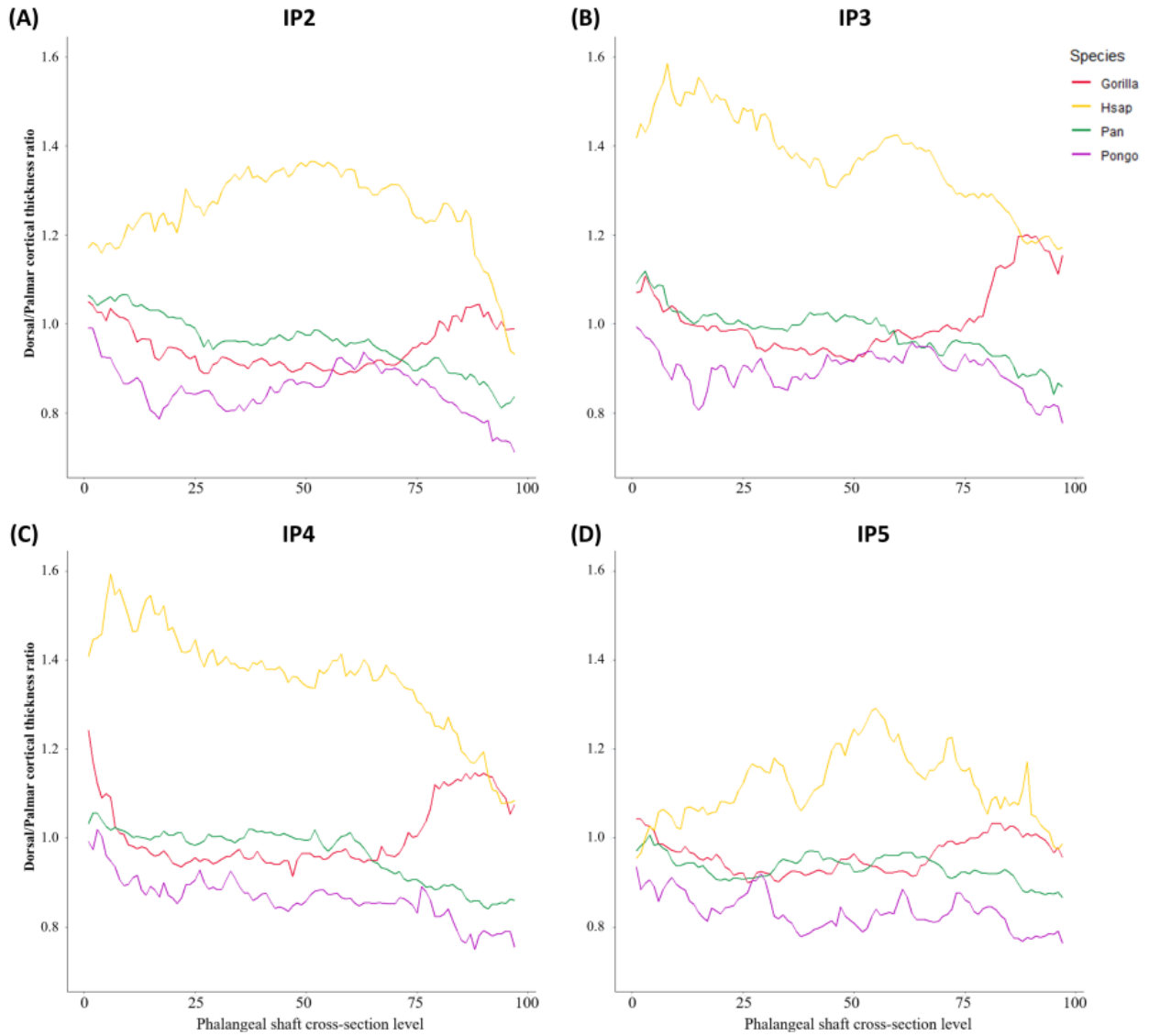
Supplementary Figure 4.2: 3D PCAs of cortical bone distribution of (A) IP2; (B) IP3; (C) IP4; and (D) IP5.



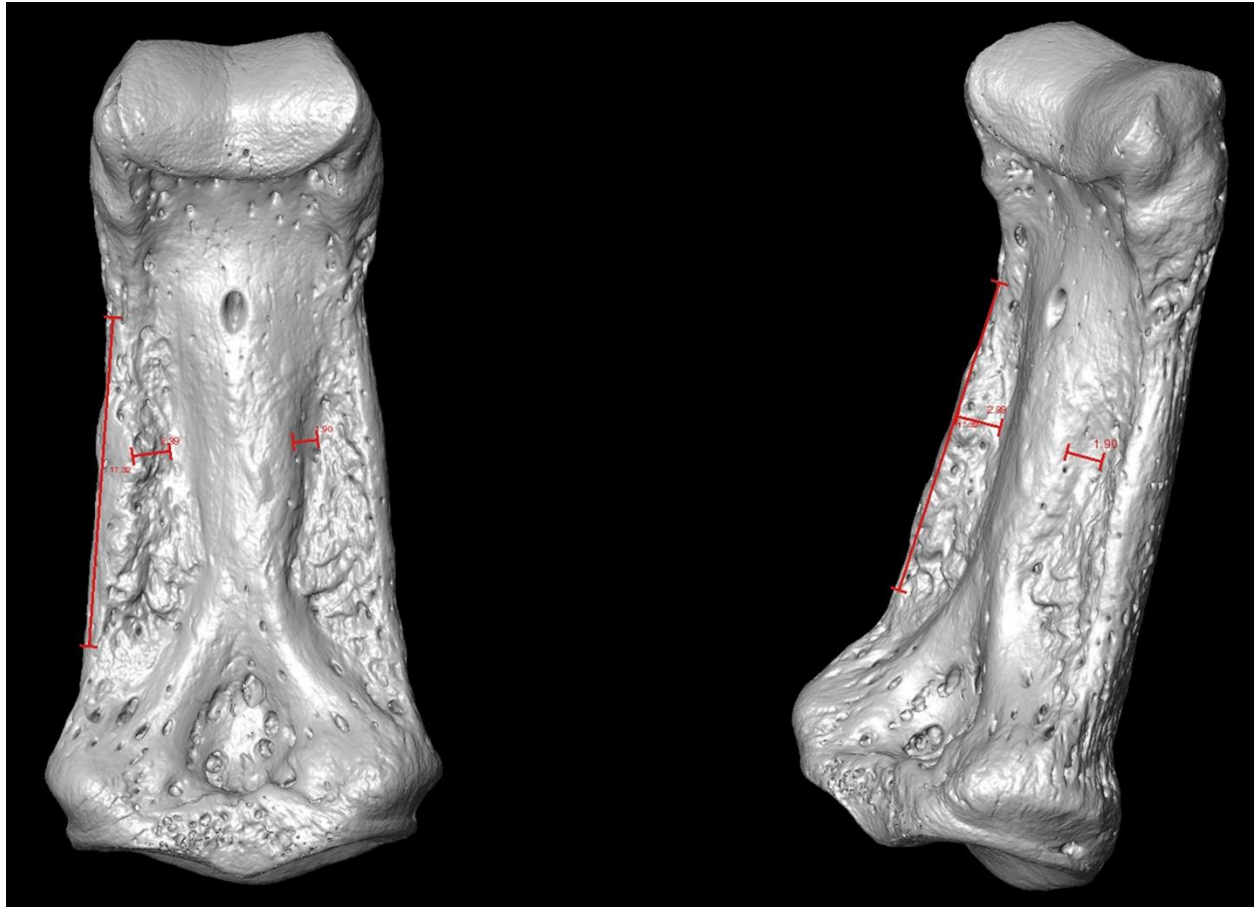
Supplementary Figure 4.3: Mean cortical thickness across the digits of (A) *Pongo*; (B) *Gorilla*; (C) *Pan*; and (D) *H.sapiens*.



Supplementary Figure 4.4: Ratio of dorsal/palmar cortical bone thickness plotted from the proximal end to the distal end of the phalangeal shaft in (A) IP2; (B) IP3; (C) IP4; and (D) IP5. Values greater than 1 represent more dorsal cortex relative to the palmar cortex in the shaft.



Supplementary Figure 4.5: Image depicting 3D measurements quantifying the palmar external features of the intermediate phalanges. Measurements were taken in Avizo 9.0.0.



8.4. SUPPLEMENTARY MATERIALS: Hand use in fossil hominins: reconstruction of manual behaviours via phalangeal cortical bone morphology

Supplementary Table 5.1: Results of permutational Hotelling's T^2 test, which conducts comparisons of fossil taxa to extant species. The test was conducted on the first 3 PCs of cortical bone thickness distribution values of (A) the proximal phalanges and (B) the intermediate phalanges of each extant species and fossil species. Values reported here are Significant F -values with the * indicating significance ($p < 0.05$).

(A)

Proximal phalanges	<i>A. africanus</i>	<i>A. sediba</i>	<i>H. naledi</i>	SKX27431	SKX15468	SKX5018
<i>Pongo</i>	117.89*	52.063*	37.717*	85.816*	115.47*	113.82*
<i>Gorilla</i>	56.628*	118.15*	76.278*	44.688*	83.07*	76.323*
<i>Pan</i>	94.437*	70.352*	59.074*	68.891*	91.815*	90.425*
<i>H. sapiens</i>	122.18*	107.09*	125.5*	140.18*	116.52*	122.76*

(B)

Intermediate phalanges	<i>A. africanus</i>	<i>A. sediba</i>	<i>H. naledi</i>
<i>Pongo</i>	118.31*	269.66*	3.8531
<i>Gorilla</i>	36.962*	44.743*	32.149*
<i>Pan</i>	17.718*	11.146*	11.41*
<i>H. sapiens</i>	98.205*	106.34*	98.76*

8.5. SUPPLEMENTARY MATERIAL: Discussion and conclusion

Supplementary Table 6.1: Summary statistics testing the relationship between phalangeal length and cortical thickness of the phalangeal shaft within species across the digits.

	ρ	p
PP2		
<i>H. sapiens</i>	0.183	0.379
<i>Pan</i>	0.582	0.003
<i>Gorilla</i>	0.852	<0.001
<i>Pongo</i>	0.317	0.410
PP3		
<i>H. sapiens</i>	0.037	0.845
<i>Pan</i>	0.389	0.059
<i>Gorilla</i>	0.786	<0.001
<i>Pongo</i>	0.400	0.291
PP4		
<i>H. sapiens</i>	0.271	0.147
<i>Pan</i>	0.460	0.022
<i>Gorilla</i>	0.684	0.001
<i>Pongo</i>	0.133	0.744
PP5		
<i>H. sapiens</i>	0.291	0.178
<i>Pan</i>	0.461	0.048
<i>Gorilla</i>	0.777	<0.001
<i>Pongo</i>	0.524	0.197
IP2		
<i>H. sapiens</i>	0.314	0.220
<i>Pan</i>	0.162	0.534
<i>Gorilla</i>	0.688	0.002
<i>Pongo</i>	0.486	0.356
IP3		
<i>H. sapiens</i>	0.269	0.204
<i>Pan</i>	0.475	0.041
<i>Gorilla</i>	0.733	<0.001

<i>Pongo</i>	0.600	0.242
IP4		
<i>H. sapiens</i>	0.463	0.047
<i>Pan</i>	0.371	0.083
<i>Gorilla</i>	0.784	<0.001
<i>Pongo</i>	0.657	0.175
IP5		
<i>H. sapiens</i>	0.393	0.165
<i>Pan</i>	0.398	0.092
<i>Gorilla</i>	0.788	<0.001
<i>Pongo</i>	0.900	0.083

8.6. PUBLISHED WORK

Cortical bone distribution of the proximal phalanges in great apes: implications for reconstructing manual behaviours

Samar M. Syeda¹  | Zewdi J. Tsegai²  | Marine Cazenave^{1,3,4}  |
Matthew M. Skinner¹  | Tracy L. Kivell⁵ 

¹Skeletal Biology Research Centre, School of Anthropology and Conservation, University of Kent, Canterbury, UK

²Department of Organismal Biology and Anatomy, University of Chicago, Chicago, Illinois, USA

³Division of Anthropology, American Museum of Natural History, New York, New York, USA

⁴Department of Anatomy, Faculty of Health Sciences, University of Pretoria, Pretoria, South Africa

⁵Department of Human Origins, Max Planck Institute for Evolutionary Anthropology, Leipzig, Germany

Correspondence

Samar M. Syeda, Skeletal Biology Research Centre, School of Anthropology and Conservation, University of Kent, Canterbury, UK.
Email: ss2510@kent.ac.uk

Funding information

H2020 European Research Council, Grant/Award Number: 819960; HORIZON EUROPE Marie Skłodowska-Curie Actions, Grant/Award Number: 101025719

Abstract

Primate fingers are typically in direct contact with the environment during both locomotion and manipulation, and aspects of external phalangeal morphology are known to reflect differences in hand use. Since bone is a living tissue that can adapt in response to loading through life, the internal bone architecture of the manual phalanges should also reflect differences in manual behaviours. Here, we use the R package Morphomap to analyse high-resolution microCT scans of hominid proximal phalanges of digits 2–5 to determine whether cortical bone structure reflects variation in manual behaviours between bipedal (*Homo*), knuckle-walking (*Gorilla*, *Pan*) and suspensory (*Pongo*) taxa. We test the hypothesis that relative cortical bone distribution patterns and cross-sectional geometric properties will differ both among extant great apes and across the four digits due to locomotor and postural differences. Results indicate that cortical bone structure reflects the varied hand postures employed by each taxon. The phalangeal cortices of *Pongo* are significantly thinner and have weaker cross-sectional properties relative to the African apes, yet thick cortical bone under their flexor sheath ridges corresponds with predicted loading during flexed finger grips. Knuckle-walking African apes have even thicker cortical bone under the flexor sheath ridges, as well as in the region proximal to the trochlea, but *Pan* also has thicker diaphyseal cortices than *Gorilla*. Humans display a distinct pattern of distodorsal thickening, as well as relatively thin cortices, which may reflect the lack of phalangeal curvature combined with frequent use of flexed fingered hand grips during manipulation. Within each taxon, digits 2–5 have a similar cortical distribution in *Pongo*, *Gorilla* and, unexpectedly, *Homo*, which suggest similar loading of all fingers during habitual locomotion or hand use. In *Pan*, however, cortical thickness differs between the fingers, potentially reflecting differential loading during knuckle-walking. Inter- and intra-generic variation in phalangeal cortical bone structure reflects differences in manual behaviours, offering a comparative framework for reconstructing hand use in fossil hominins.

This is an open access article under the terms of the [Creative Commons Attribution](https://creativecommons.org/licenses/by/4.0/) License, which permits use, distribution and reproduction in any medium, provided the original work is properly cited.

© 2023 The Authors. *Journal of Anatomy* published by John Wiley & Sons Ltd on behalf of Anatomical Society.

KEYWORDS

cortical bone, functional morphology, internal bone structure, manual behaviour, phalangeal morphology, primates

1 | INTRODUCTION

As the primate hand, and particularly the fingers, interacts directly with the external environment, they have the potential to provide functional information about both locomotion and/or manipulation. Studies exploring phalangeal external morphology (Inouye, 1994; Matarazzo, 2008; Patel & Maiolino, 2016; Rein, 2011; Rein & McCarty, 2012; Susman, 1979), phalangeal curvature (Jungers et al., 1997; Richmond, 2007; Stern et al., 1995) and internal bone architecture of the wrist (Bird et al., 2021, 2022; Tocheri et al., 2007), metacarpals (Dunmore et al., 2019; Stephens et al., 2018; Tsegai et al., 2013; Zeininger et al., 2011) and phalanges (Matarazzo, 2015; Stephens et al., 2018) have demonstrated a functional signal between the external and/or internal morphology of the hand and manual behaviours (Kivell, 2015). The functional link between internal bone structure and locomotor behaviour has been established in several skeletal elements (Arias-Martorell et al., 2021; Cotter et al., 2009; Saers et al., 2016; Scherf et al., 2013; Tsegai, Skinner, et al., 2017), however, the internal architecture of the manual phalanges remains relatively understudied, despite the phalanges of digits 2–5 being involved in grasping during both locomotion and manipulation (Bardo et al., 2017; Byrne & Byrne, 2001; Marzke, 1997; Matarazzo, 2013; Neufuss et al., 2017). Here, we investigate variation in cortical bone structure of the proximal phalanges of digits 2–5 (PP2–PP5) in humans and other extant hominids.

Much of the work to date exploring fossil and extant primate phalangeal morphology has focused on quantifying variation in shaft curvature, as it is considered to be functionally informative about hand use during locomotion and particularly differences in arboreality (Deane & Begun, 2008; Jungers et al., 1997; Matarazzo, 2008; Richmond, 1998; Rein, 2011; Stern et al., 1995; Stern & Susman, 1983; Susman et al., 1984; but see Wallace et al., 2020). During grasping, longitudinally curved phalanges are thought to be more effective than straight phalanges because the curvature helps to reduce bending moments by aligning the bone more closely with the joint reaction force (Oxnard, 1973; Preuschoft, 1973). Finite element (FE) modelling techniques have validated these functional hypotheses regarding phalangeal curvature by testing differences in strain distribution in curved versus mathematically straightened phalanges, revealing curved phalanges experience overall lower strain (Nguyen et al., 2014; Richmond, 2007). Furthermore, the degree of phalangeal curvature changes throughout ontogeny depending on mechanical loading (Richmond, 1998, 2007). For example, juvenile chimpanzees and gorillas have a higher degree of phalangeal curvature than adults (Richmond, 1998; Sarringhaus, 2013), reflecting a decrease in arboreality throughout ontogeny (Doran, 1997). This research suggests a strong functional link between locomotor behaviour and the external morphology of phalanges (but see Wallace et al., 2020).

In contrast to research on phalangeal external shape, the functional relationship between the internal bone morphology of phalanges and locomotor behaviour has yet to be thoroughly explored. Internal bone architecture consists of cortical and trabecular bone, both of which are subject to epigenetic changes that result from loading experienced by the bone during an individual's lifetime; a process known as bone functional adaptation (Currey, 2003; Pearson & Lieberman, 2004; Ruff et al., 2006). Cortical bone adapts to the functional demands placed upon it through adjustments to its mineralization to adapt its stiffness and changes in overall shape to resist loads or by increasing its thickness (Currey, 2003; Ruff et al., 2006). Overall, both cortical and trabecular bone adapt in response to their mechanical environment by removing bone in skeletal areas where stress is low and adding bone where stress is high (Pearson & Lieberman, 2004; Ruff et al., 2006).

Cortical bone is usually studied through analysis of cross-sectional geometric (CSG) properties that offer robust estimations of strength and rigidity of a bone (Ruff et al., 2006; Ruff & Runestad, 1992). Understanding how CSG patterns correlate with loading regimes of an individual is complex and drawing functional interpretations can be challenging, but CSG patterns provide an indirect method to understand potential loading patterns when direct biomechanical data are not available or not possible to measure. Recently, studies of cortical thickness distribution of long bones have also revealed that the cortex varies throughout the shaft across different skeletal elements in ways that relate to locomotor behaviour (Cazenave et al., 2019; Jashashvili et al., 2015; Puymerail, 2013; Tsegai, Stephens, et al., 2017; Wei et al., 2021). Combining the analysis of CSG with cortical bone distribution and thickness can allow inference of bone adaptation in relation to habitual loading (Jashashvili et al., 2015).

Within the hand, only cortical structure of the metacarpals has been studied in extant hominids (Dunmore et al., 2020; Marchi, 2005; Patel et al., 2020), which found cross-sectional properties can distinguish habitual locomotor behaviours of extant great apes. Several studies have also explored the functional morphology of trabecular bone in the carpals and metacarpals (Bird et al., 2021, 2022; Dunmore et al., 2019; Schilling et al., 2014; Tsegai et al., 2013). However, to date, there have only been three studies published to our knowledge that have explored the internal bone structure of proximal phalanges of the fingers (Doden, 1993; Matarazzo, 2015; Stephens et al., 2018). Doden (1993) studied the internal cortical structure of the phalanges in gibbons and humans, noting a functional link between the shape and density of cortical bone and manual behaviours. Matarazzo (2015) analysed the trabecular architecture at the proximal and distal epiphysis of the phalanges of digit 3 in extant non-human hominoids and macaques, with patterns of trabecular orientation differing between

the locomotor modes of the taxa. However, other variables of trabecular bone (e.g., bone volume fraction, degree of anisotropy, isotropy index) in the phalanges failed to distinguish between locomotor behaviours (Matarazzo, 2015). Stephens et al. (2018) documented variation in the structure of trabecular bone in post-Neolithic and foraging human hands, revealing greater trabecular bone volume fraction in foragers that is consistent with higher intensity loading than that experienced by post-Neolithic individuals. Therefore, the analysis of the internal bone structure of manual phalanges of extant great apes holds potential for reconstructing the behaviour of fossil hominin species. However, there has yet to be a detailed analysis of variation in cortical thickness in hominid phalanges, which is important to consider in light of differences in trabecular structure (Matarazzo, 2015; Stephens et al., 2018) and phalangeal curvature (Jungers et al., 1997; Matarazzo, 2008; Rein, 2011; Richmond, 1998; Stern et al., 1995; Wennemann et al., 2022).

Here, we conduct a detailed examination of cortical structure of the proximal phalanges of digits 2–5 in extant hominids. We assume phalangeal cortical bone morphology in non-human hominids will primarily reflect locomotor loading. This is due to the high mechanical loads on the fingers from dynamic loading and body mass that occur during locomotion (Preuschoft, 2019). Although all non-human hominids show enhanced manual dexterity and tool use abilities in the wild (e.g., Byrne & Byrne, 2001; Lesnik et al., 2015; Marzke et al., 2015; Van Schaik et al., 1996) and captivity (e.g., Bardo et al., 2016, 2017; Pouydebat et al., 2005), we assume that loading during manipulation will be lower than that of locomotion. In contrast, we assume human phalangeal cortical structure will reflect loading during manipulation given the rarity with which individuals in our sample likely used their hands for locomotion.

1.1 | Predictions

This study examines the cortical structure of the proximal manual phalanges of digits 2–5 to determine whether variation in manual behaviours associated with locomotion and manipulation correlates with cortical bone properties in *Pongo*, *Gorilla*, *Pan* and *Homo sapiens*, and how potential differences in cortical thickness vary with differences in phalangeal curvature. We quantify both variation in cortical thickness throughout the phalangeal shaft and cross-sectional geometric properties at sections along the shaft (35%, 50% and 65% of bone length). We test three main predictions regarding variation in cortical bone structure based on observations of great ape, including humans, manual behaviour, bone functional adaptation and studies on phalangeal external morphology and biomechanics.

Our first prediction is that relative cortical bone distribution patterns will significantly differ among extant great apes due to locomotor and postural differences. Second, we predict that across the four digits of each species, there will be variation in cortical bone thickness distribution, mean cortical bone thickness and CSG properties. Finally, we predict that mean cortical bone thickness and

cross-sectional properties will significantly differ across the great apes. We discuss these specific predictions for each taxon below.

Pongo is highly arboreal, with torso-orthograde suspension dominating their complex postural and locomotor behaviours (Cant, 1987; Thorpe et al., 2009; Thorpe & Crompton, 2006). During suspension, the hand is positioned like a hook around the substrate, which may mitigate bending stress during suspension, because joint reaction forces load the articular ends of the phalanges dorsally in compression, while the forces from the digital flexor muscles, along with the joint reaction and gravitational forces, pull the phalanges palmarly (Carlson & Patel, 2006; Richmond, 2007; Schmitt et al., 2016). In *Pongo* phalanges, the high degree of longitudinal curvature (Figure 1), combined with flexor sheath ridges (FSRs) located opposite the maximum arc of curvature, are thought to be advantageous for frequent flexed finger grasping (Susman, 1979). Thus, we predict *Pongo* will exhibit a pattern of maximum thickness on the disto-palmar surface of the phalangeal shaft, as the proximal phalanges are most often being loaded in flexed finger grasping during locomotion and are experiencing tensile and compressive forces from the joint reaction forces and substrate reaction forces (Matarazzo, 2015; Nguyen et al., 2014; Preuschoft, 1973; Tsegai et al., 2013). We predict that this cortical distribution pattern, as well as mean cortical bone thickness and CSG properties, will be similar across the four digits, as all four digits are thought to be used in a similar manner during manual behaviours (Rose, 1988 but see McClure et al., 2012). Across the great apes, we expect cortical properties, associated with strength and rigidity against bending and torsional loads, of *Pongo* to be less than that of the African apes as the external phalangeal morphology helps mitigate stress from arboreal locomotion.

Gorilla engage primarily in knuckle-walking (Doran, 1996, 1997; Inouye, 1994; Tuttle & Watts, 1985), during which the dorsal surfaces of the intermediate phalanges are in contact with the substrate and the proximal phalanges, metacarpals and body mass of the animal are elevated above the hand (Preuschoft, 1973; Tuttle, 1967; Wunderlich & Jungers, 2009). Zoo-housed *Gorilla* most often use a palm-back (pronated) position and experience relatively even pressure across digits 2–5 (Matarazzo, 2013; Tuttle, 1969), while wild *Gorilla* have been observed to have more variable hand postures (Thompson et al., 2018). The radio-ulnarly wide, stout and flat phalanges are thought to reflect these frequent knuckle-walking hand postures. The proximal phalanges also have prominent FSRs, indicating forceful grasping during arboreal locomotion and/or food processing (Neufuss et al., 2019; Remis, 1998; Susman, 1979; Tuttle & Watts, 1985). We predict that the cortical thickness pattern of *Gorilla* will be similar palmarly and dorsally due to loading of a flexed proximal interphalangeal (PIP) and hyper-extended metacarpophalangeal (McP) joint (Tsegai et al., 2013). Across digits 2–5, we expect no differences in cortical thickness and cross-sectional properties, due to the similar pressure experienced by digits 2–5 during knuckle-walking (Matarazzo, 2013). Relative to *Pongo* and *H. sapiens*, the phalanges of *Gorilla* are predicted to have thicker cortices and stronger CSG properties, as the phalanges are incurring ground reaction forces from locomotion and joint reaction forces

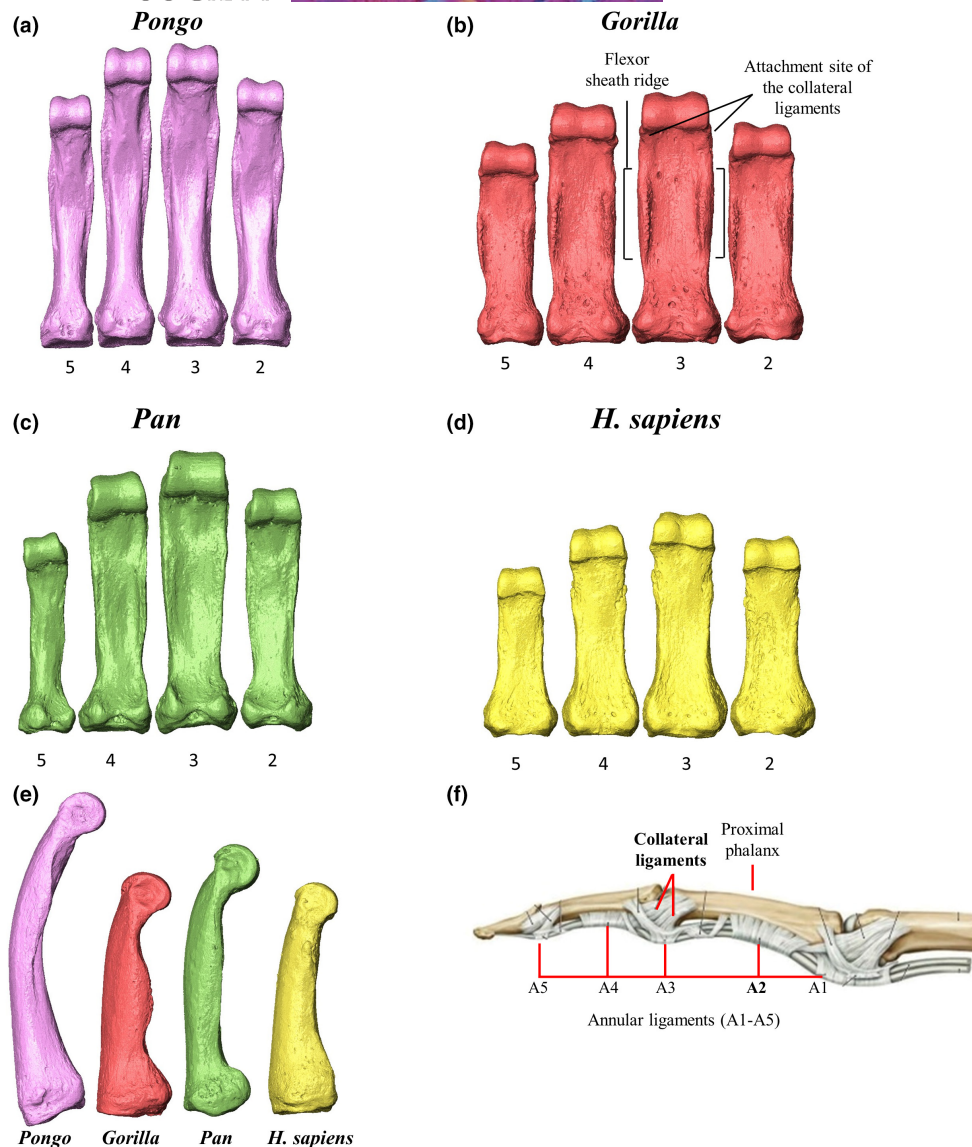


FIGURE 1 Representative 3D surfaces of proximal phalanges of (a) *Pongo pygmaeus*, (b) *Gorilla gorilla*, (c) *Pan troglodytes*, (d) *Homo sapiens*. Digits 2–5 are represented from right to left. The proximal phalanges have been scaled to relative size. (e) Medial surface of the third proximal phalanx of each taxa. Variation in curvature and flexor sheath ridge morphology is evident. (f) Depiction of ligaments of the finger. The second annular pulley (A2) and collateral ligament of the PIP joint are highlighted in subset F (modified from Gilroy & MacPherson, 2016) and the flexor sheath ridges and attachment sites of the collateral ligaments are shown in subset B.

resulting from the contraction of the finger flexor and extensor musculature, along with the gravitational forces supporting the body mass (Jenkins & Fleagle, 1975; Tsegai et al., 2013). However, it is important to acknowledge that wild mountain gorilla (*Gorilla beringei*) knuckle-walking hand postures in their natural habitat are much more variable than those of zoo-housed gorilla and they commonly use non-knuckle walking hand postures (Thompson et al., 2018). These variable hand postures could result in different degrees of flexion/extension of the finger joints and more variable loading of the proximal phalanges (Thompson et al., 2018).

Pan (*Pan troglodytes* and *Pan paniscus*) also engages primarily in terrestrial knuckle-walking but is more variable in its positional behaviour than *Gorilla*, both within and across populations (Doran, 1996; Doran & Hunt, 1996; Hunt, 2020; Sarringhaus et al., 2014). Zoo

studies show that *P. troglodytes* use more variable hand postures than *Gorilla* (Inouye, 1994; Tuttle, 1969). In zoo-housed *Pan*, digits 3 and 4 typically experience the highest loads during knuckle-walking, while in some bouts of knuckle-walking digit 5 does not touch down or experiences significantly less loading than the radial three digits (Matarazzo, 2013; Wunderlich & Jungers, 2009). Arboreal behaviours are more common in *Pan*, compared to *Gorilla*, but the frequency can vary substantially among sexes, communities and (sub)species (Doran, 1996; Doran & Hunt, 1996; Hunt, 2020; Ramos, 2014; Remis, 1998; Sarringhaus et al., 2014). *Pan* proximal phalanges show a greater degree of dorsal curvature than *Gorilla* (Figure 1), which may reflect an increased degree of arboreality in their locomotor repertoire (Susman, 1979; but see Wallace et al., 2020). However, the frequency of habitual knuckle-walking is

greater than arboreal behaviours (Doran & Hunt, 1996; Hunt, 2020) and, as such, knuckle-walking signals will likely be reflected in the internal structure of manual phalanges. Thus, we predict *Pan* and *Gorilla* will share a similar pattern of cortical bone distribution due to their similar locomotor repertoires, along with cortical thickness and CSG properties of strength and rigidity against loads that are greater than those of *Pongo* and *H. sapiens*. Within *Pan*, we expect relative differences in cortical thickness and properties across the digits due to the more variable hand postures employed during their locomotor repertoire (Doran & Hunt, 1996; Matarazzo, 2013; Wunderlich & Jungers, 2009).

Humans are unique among great apes in using their hands mainly for manipulation, rather than locomotion. Forceful precision grips, power squeeze grips and precise in-hand manipulation are important in stone tool making and use and are thought to distinguish modern human manipulatory abilities from other hominids (Marzke, 1997; Williams-Hatala, 2016). Across modern human adults, power grips are employed most frequently during daily activities (Dollar, 2014; Feix et al., 2015). Power grips require the fingers to be in flexion, with experimental studies quantifying the biomechanics of power grips revealing that joint forces increase distally and digit 2 experiences the greatest loads followed by digits 3, 4 and 5 (De Monsabert et al., 2012; Sancho-Bru et al., 2014; Vigouroux et al., 2011). Human proximal phalanges are gracile and lack dorsopalmar curvature and strong muscle markings (Patel & Maiolino, 2016; Susman, 1979), likely reflecting lower loads incurred during manipulation compared with those of locomotion. We predict the pattern in *H. sapiens* will be of maximum thickness in the dorsal aspect of the shaft, as the straight proximal phalanges are typically in a flexed position during manipulation (Marzke, 1997; Rolian et al., 2011) and are experiencing bending stresses (Doden, 1993; Nguyen et al., 2014; Richmond, 2007), which are concentrated on the dorsal surface in straight phalanges. We also predict humans to show greater variability across the digits due to the frequent loading of digits 2 and 3 during daily manipulative activities (De Monsabert et al., 2012; Sancho-Bru et al., 2014). Finally, cortical thickness and CSG properties, associated with strength and rigidity against bending and torsional loads, of *H. sapiens* are predicted to be lower than that of the other great apes as humans most frequently use their hands for manipulation (Marzke, 2013; Tocheri et al., 2008).

2 | METHODS

2.1 | Study sample

The study sample consists of manual proximal phalanges from digit 2 ($n=80$ elements), digit 3 ($n=86$ elements), digit 4 ($n=83$ elements) and digit 5 ($n=70$ elements) of *H. sapiens* ($n=34$ individuals), *Pan* ($n=24$ individuals, including *P. troglodytes* and *P. paniscus*), *Gorilla gorilla* ($n=25$ individuals) and *Pongo* ($n=9$ individuals, including *Pongo abelii* and *Pongo pygmaeus*) (Table 1). Details of the study sample are shown in Table S1 and representative morphology of each taxon is

TABLE 1 Summary of study sample included in the study.

Taxon	N	PP2	PP3	PP4	PP5
<i>Homo sapiens</i>	33	22	26	27	21
<i>Pan paniscus</i>	7	7	7	7	6
<i>Pan troglodytes</i>	17	16	17	17	12
<i>Gorilla gorilla</i>	25	23	23	20	21
<i>Pongo abelii</i>	2	2	2	2	2
<i>Pongo pygmaeus</i>	7	7	7	7	6

depicted in Figure 1. All non-human apes were wild individuals with no obvious signs of pathologies within their hand skeletons or upper limbs. Our human sample originates from diverse post-industrial populations including 20th century Syracuse, Italy ($n=2$ individuals), 18th–19th century Inden, Germany ($n=5$), 16th century males of the Mary Rose shipwreck ($n=7$). It also includes pre-industrial populations including 6th–11th century Nubian Egyptians ($n=4$), 19th century Tierra del Fuego ($n=3$), an indigenous Inuit from Greenland and two Aboriginal Australians. We also included in our *H. sapiens* sample several fossil *H. sapiens* including Qafzeh 8 and 9 ($n=2$ individuals, 80–130 Ka, Qafzeh, Israel; Niewoehner, 2001), Ohalo II H2 ($n=1$, 19 Ka, Sea of Galilee, Israel; Hershkovitz et al., 1995), Barma Grande ($n=1$, 15–17 Ka, Ventimiglia, Italy; Churchill & Formicola, 1997), Arene Candide ($n=1$, 12–11 Ka, Liguria, Italy; Sparacello et al., 2021) and Dolní Věstonice ($n=4$, 31 Ka, Dolní Věstonice, Czech Republic; Fewlass et al., 2019).

2.2 | MicroCT scanning

All phalanges were scanned with high-resolution micro-computed tomography (microCT) using a BIR ACTIS 225/300, Diondo D3 or Skyscan 1172 scanner housed at the Department of Human Evolution, Max Planck Institute for Evolutionary Anthropology (Leipzig, Germany), a Nikon 225/XTH scanner at the Cambridge Biotomography Centre, University of Cambridge (Cambridge, UK) or with a Diondo D1 scanner at the Imaging Centre for Life Sciences University of Kent (Canterbury, UK). The scan parameters included acceleration voltages of 100–160kV and 100–140 μ A using a 0.2–0.5mm copper or brass filter. Scan resolution ranged between 0.018mm and 0.044mm depending on the size of the bone. Images were reconstructed as 16-bit TIFF stacks.

2.3 | Data processing

Non-bone inclusions or remaining soft tissues were removed from the scans and each phalanx was rotated into a standard orientation using Avizo Lite 9.0.0 (Visualization Sciences Group, SAS). Scans were subsequently segmented using the medical image analysis (MIA) clustering method (Dunmore et al., 2018). Once segmented, the outer and inner layers of the cortex were defined using Medtool v 4.5 (www.dr-pahr.at/medtool), following Tsegai

et al. (2013) and Gross et al. (2014). This involves use of a ray-casting method to isolate the external and internal edges of the cortex in 3D and morphological filters to fill the bone, resulting in a mask of the inner and outer regions of the cortex. Smooth external and internal surfaces of these voxel data were created using a custom script in Paraview v 4.4 and Meshlab v 2020.03 (Figure 2). Six *Pan* and five *Gorilla* phalanges were excluded from the study sample (i.e., not included in sample sizes listed earlier) because their cortices were so thickened distally (i.e., almost completely filling the medullary cavity) that it did not allow for the creation of a distal internal surfaces because the rays could not detect a non-bone voxel.

2.4 | Cortical bone analysis

This study quantifies cortical bone distribution patterns and CSG parameters using the R package morphomap (Profico et al., 2021). In brief, morphomap allows the user to divide a 3D mesh of a long bone surface into a certain number of cross-sections and place a desired number of landmarks on the periosteal and endosteal outlines of the bone. The landmark data allow for the quantification and mapping

of cortical bone thickness, while the associated periosteal and endosteal outlines of each slice are used to measure CSG properties.

2.4.1 | Morphomap parameters

Morphomap is designed to produce cross-sections across a certain percentage of the bone defined by the user (Profico et al., 2021). Since this study quantifies cortical thickness of the phalangeal shaft across species of varying morphology, there was not a standardized percentage of phalangeal length that we could consistently define as the shaft across all individuals/taxa. Variation in the shape and size of the proximal phalanx base and the trochlea meant that these features extended onto the diaphysis to differing degrees (Figure 1). Thus, to compare homologous structures, we defined a region of interest (ROI) of the shaft as between the distal most extent of the base and the proximal end of the trochlea individually for each specimen.

The ROI was defined based on the external morphological features outlined earlier, both in palmar and lateral views, to ensure the greatest extent of the trochlea or base was not included in the ROI. The external and internal surfaces were cropped using Avizo Lite



FIGURE 2 Steps taken to create surfaces for cortical thickness analysis. In Medtool 4.5 morphological filters were applied in the following steps: (a) Original microCT data of a *Homo sapiens* fourth proximal phalanx, (b) microCT data after MIA segmentation, (c) creation of outer layer of the cortex, (d) creation of inner layer of the cortex, (e) creation of an external (cortical) 3D surface from step c and an internal 3D surface from step d. Following surface creation, using Avizo Lite 9.0.0 the external and internal surfaces were cut (f and g) to define the shaft of the phalanx and (h) create cut surfaces for cortical bone thickness analysis in morphomap.

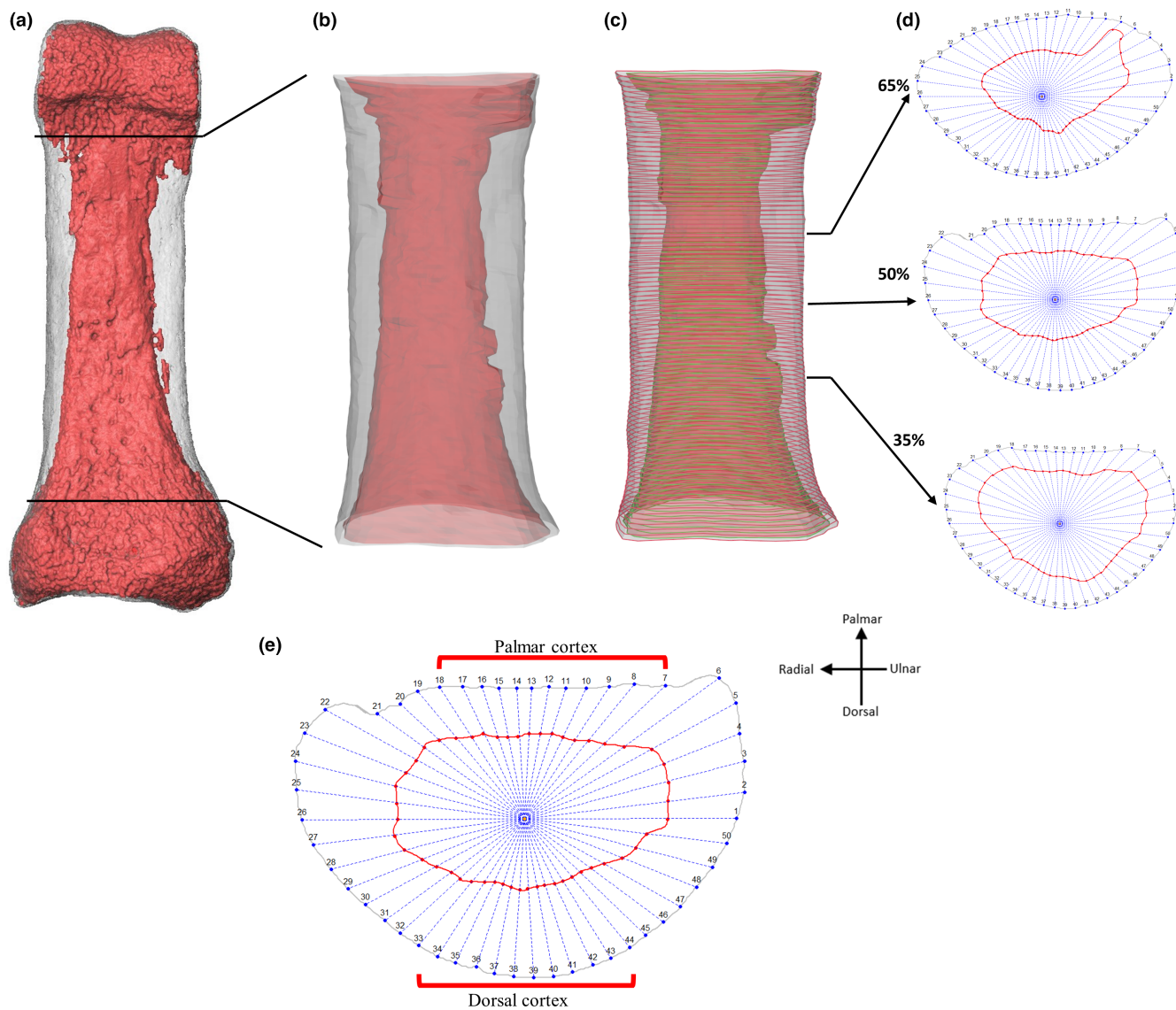


FIGURE 3 Data acquisition in *morphomap*. (a) External (grey) and internal (red) 3D surface models of proximal phalanx of digit 4 in a *Homo sapiens* individual. (b) Cut external and internal 3D surfaces defining the shaft (as defined in text) for cortical thickness quantification in *morphomap*. (c) Cortical bone parameters are measured in 1% cross-sectional increments along the shaft and arrows indicate cross-section locations (35%, 50%, 65%) where CSG parameters were analysed. (d) Cross-sections at 35%, 50% and 65% of the bone length. At each cross-section, 50 semi-landmarks were placed on the external and internal surfaces equiangularly and were used to calculate cortical thickness. (e) Landmarks used to divide the cortex into palmar and dorsal cortex.

9.0.0 (Visualization Sciences Group, SAS), however, as *morphomap* required a slight buffer on either end of the cropped ROI, this crop was at 2% above and below the defined shaft, so cortical thickness could be mapped across the entire ROI (Figures 2f–h and 3a–c). Within *morphomap*, the cut external and internal ROIs were used to extract 97 sections at increments of 1% between 2% and 98% of the ROI length (i.e., the defined shaft length). At each cross-section, 50 paired equiangular semi-landmarks, centred around the cortical area of each cross-section, were placed on the outlines of the external and internal surfaces to accurately capture the complex morphology of the phalangeal shaft. The combination of cross-sections and the landmarks placed on them allow a set of lines to be drawn from the centroid of each slice outwards to the landmarks placed

on the internal and external outlines of the 3D surfaces (Profico et al., 2021). Using these lines, cortical thickness is calculated as the length of the line between the internal and external surface outlines.

Along with measuring cortical thickness along the entire shaft, we also measured cortical thickness of landmark-defined palmar and dorsal surfaces of the shaft, which was assessed as a ratio of palmar/dorsal mean thickness. This allowed comparison of cortical thickness across genera without the influence of variation in size or shape of the FSRs, which are not represented by the dorsal and palmar landmarks. This morphology was defined by selecting an equal number of landmarks on the palmar and dorsal surfaces of the shaft, but excluding the medial or lateral aspects of the bone, where the FSRs are located (Figure 3e). To visualize the pattern of cortical bone

distribution, morphometric maps of cortical thickness for each individual were created using R package morphomap.

2.4.2 | Cross-sectional geometry

Cross-sectional geometric properties were calculated at each slice across the shaft with the R package morphomap. Different CSG properties quantify different aspects of the diaphysis and the most commonly used properties to understand the dynamic loads incurred by locomotion are cortical area (CA; measure of axial strength), polar moment of area (J ; measure of bending and torsional rigidity) and polar section modulus (Z_{pol} ; measure of maximum bending strength) (Lieberman et al., 2004; Marchi, 2005; Patel et al., 2020; Ruff & Runestad, 1992; Schaffler et al., 1985; Trinkaus & Ruff, 2012). We studied these cross-sectional properties at three positions along the shaft (35%, 50% and 65% of the shaft length) of each phalanx to quantify variation in cortical robusticity within the phalangeal shaft. The specific cross-sections were chosen to account for variation in the proximodistal extension of the base and trochlear morphology across our sample and to ensure each cross-section sampled only the diaphysis.

2.5 | Phalangeal curvature

The degree of phalangeal curvature was measured using the included angle (IA) method. The IA (θ) method assumes the curvature of a phalanx in the dorsopalmar direction is represented by an arc length on the perimeter of a circle (Stern et al., 1995). Low values of θ are characteristic of straighter phalanges, commonly associated with quadrupedalism and bipedalism, and higher values of θ are characteristic of increasingly curved phalanges, commonly associated with arboreality (Jungers et al., 1997; Stern et al., 1995). The IA method was chosen as it has been the most prevalent approach to calculate phalangeal curvature and does well to distinguish the locomotor behaviours of species (Jungers et al., 1997; Matarazzo, 2008; Rein, 2011; Stern et al., 1995). However, it is important to note that the IA method is susceptible to measurement errors (Deane & Begun, 2008; Patel & Maiolino, 2016), therefore three repeated measurements were taken to correct for intra-observer measurement error.

2.6 | Statistical analyses

As larger bones and individuals will potentially have higher absolute values of cortical bone and larger cross-sections, we scaled the data by the length of the bone. Phalangeal length was measured digitally on surface models in Avizo 9.0., from the most proximal extent of the base to the most distal extent of the trochlea in dorsal view. All statistical analyses were conducted on the scaled data, as well as on raw data for intra-generic comparisons.

2.6.1 | Cortical thickness distribution pattern

Cortical thickness values were calculated from a measurement between each pair of corresponding landmarks at the inner and outer cortical surfaces on each slice of the defined shaft, resulting in 4850 measurements per phalanx. To explore differences in the distribution of cortical bone thickness between taxa, each of the 4850 measurements were treated as a variable in a principal component analysis (PCA). To test if cortical thickness distribution patterns of each taxon were significantly different from each other, an omnibus permutational multivariate analysis of variance was run on the first three PC scores using the R package Vegan. If this test was statistically significant ($p < 0.05$), it was followed by a pairwise one-way permutational multivariate analysis of variance with a Bonferroni correction to test which groups were significantly different from one another. Permutational multivariate analysis of variance tests were conducted because Shapiro–Wilk tests revealed that not all data were normally distributed.

2.6.2 | Mean cortical thickness

Inter- and intra-generic differences in mean cortical thickness were assessed using Kruskal–Wallis tests, as Shapiro–Wilk tests revealed the data were not normally distributed, followed by a post hoc Dunn test. Inter-generic testing was conducted on each digit separately.

2.6.3 | Cross-sectional geometric properties

Intra-generic differences in cross-sectional properties (CA, Z_{pol} and J) at the three diaphyseal positions (35%, 50%, 65%) across the digits of each taxon were compared using a Kruskal–Wallis test, followed by a post hoc Dunn test separately, along with intra-generic differences in diaphysis position within each digit. Inter-generic differences in cross-sectional geometric properties were assessed for each property at each position for each digit using a Kruskal–Wallis test, followed by a post hoc Dunn test.

2.6.4 | Relationship between curvature and cortical thickness

Regression analyses were used to test the relationship between phalangeal curvature (IA values) and mean cortical thickness for each taxon. For each taxon, all four digits were pooled together to increase the sample size and to produce a more reliable fit of the regression model.

All statistical tests were performed using the R package RVAideMemoire (v 0.9-79 Hervé, 2022), Stats (R Core Team, 2020) and FSA (v 0.9.3 Ogle et al., 2022). Statistical tests were carried out

in R version 4.1.3 and all tests were considered statistically significant with a $p < 0.05$.

3 | RESULTS AND DISCUSSION

This study explored the relationship between expected loading during various locomotor and hand-use behaviours and the cortical structure of non-pollical proximal phalanges in extant hominids. The distribution of cortical bone, as well as its overall thickness and CSG properties differed among genera, and across the digits within genera, in line with some of our predictions. These results support a relationship between cortical morphology of the manual phalanges and loading of the hand among great apes. Figure 4 depicts cortical thickness distribution morphometric maps of the proximal phalanges (digits 2–5) in a representative individual for each taxon, while morphometric maps for all individuals within our sample are presented in Figure S1. Figure 5 depicts average cortical thickness plotted across the shaft for each taxon and Table 2 shows mean values of cortical thickness. Table S2 shows mean values of all cross-sectional properties across the three cross-sections. Variation in cortical bone distribution patterns were assessed via PCA. This is followed by a description of cortical distribution patterns, as well as variation in cortical thickness and cross-sectional properties for each study taxon.

3.1 | Cortical bone thickness distribution

Principal component analysis of scaled cortical thickness values from each phalanx (digits 2–5) was used to assess whether cortical thickness distribution patterns differ among taxa and whether this corresponds with their respective differences in hand use (Figures 6 and S2). PCA was conducted for each digit, however, due to comparable separation among the study taxa across all four digits, as well as similar PC1 and PC2 loadings, we describe the general pattern common to the proximal phalanges of each taxa, but highlight instances where particular digits differed from the general pattern.

PC1 explains 56% to 63% of the total variance in each of the four digits. *Gorilla* is separated from the other taxa by having low PC1 scores, representing more developed FSRs, and *H. sapiens* is characterized by high PC1 scores, reflecting a thicker distodorsal cortex in PP2–PP4. *Pan* and *Pongo* are intermediate and variably overlap with other taxa. The overlap of *Pan* and *Pongo* in PP2–PP4 may be due to the greater frequency of arboreal locomotion in *Pan* relative to *Gorilla* (Doran & Hunt, 1996; Doran, 1996; Tuttle & Watts, 1985) (Figures 6 and S2).

For PP3, low PC1 values separating *Gorilla* from other taxa are related to thickened FSRs with a low-to-intermediately thick dorsal region of the shaft, compared to high PC1 values in *Pongo* and *H. sapiens* reflecting distodorsal thickness and thick cortices on the FSR. The greater overlap between *Gorilla* and *Pan* in PP3 relative to the

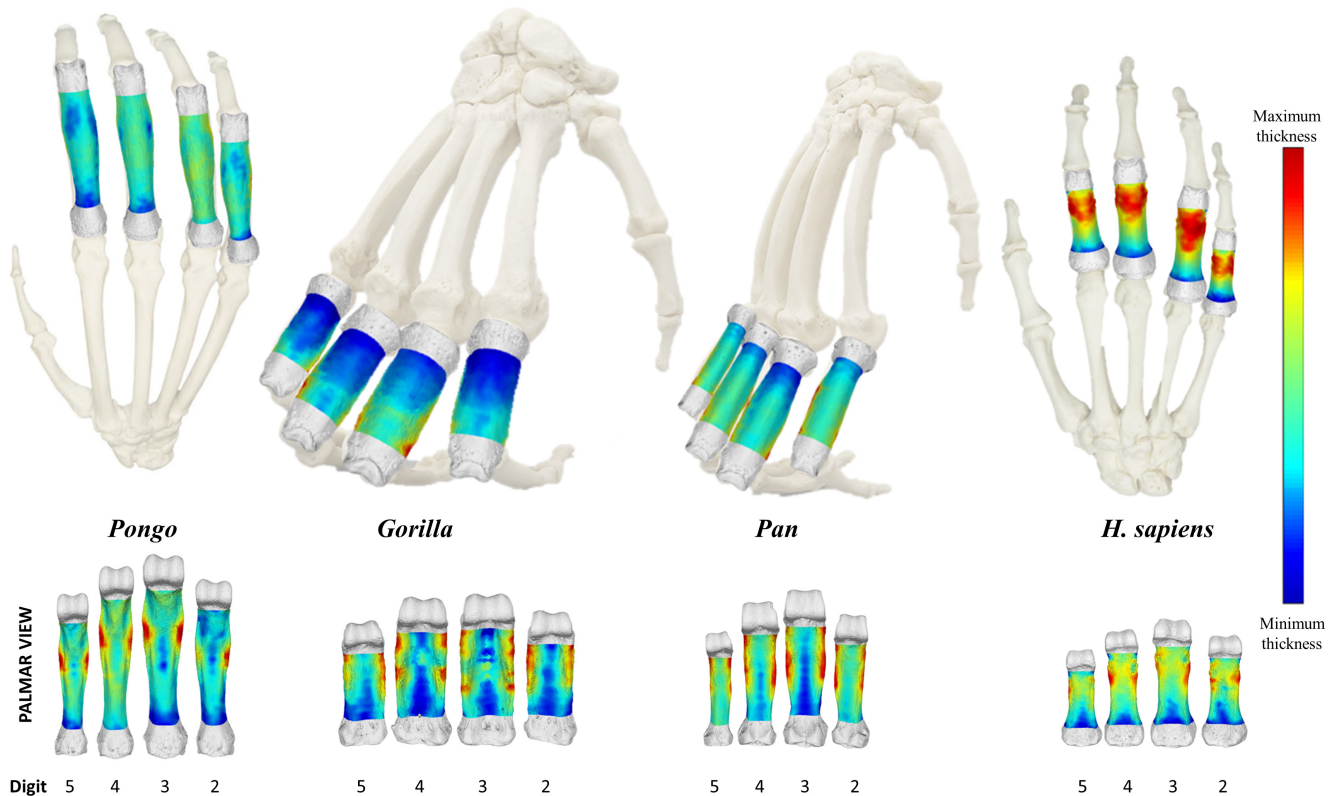


FIGURE 4 Representative 3D maps of cortical bone distribution of proximal phalanges of digits 2–5 of *Pongo pygmaeus*, *Gorilla gorilla*, *Pan troglodytes*, *Homo sapiens* in dorsal (top) and palmar (bottom) view. Thickness maps of each bone are independent of each other. Proximal phalanges are not scaled.

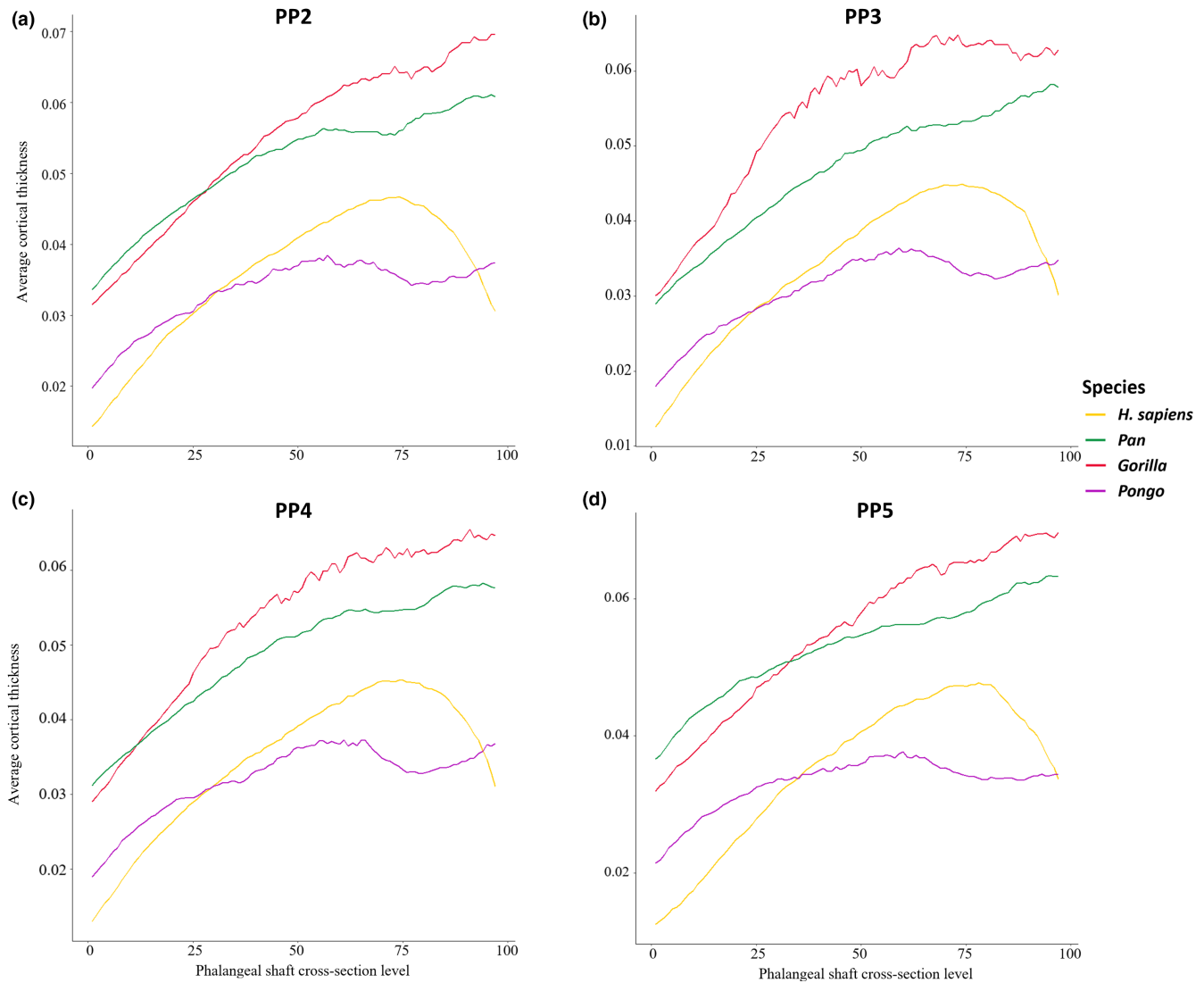


FIGURE 5 Average scaled cortical bone thickness plotted from the proximal end (0) to the distal end (100) of the phalangeal shaft of *Homo sapiens*, *Pan*, *Gorilla* and *Pongo*. (a) PP2; (b) PP3; (c) PP4; (d) PP5.

other digits is due to a few individuals of *Gorilla* displaying an intermediately thick shaft similar to *Pan*.

For PP5, low values of PC1 characterize *Gorilla* and *Pan* with thick FSRs and high values reflect distodorsal and FSR thickness in *Pongo* and *H. sapiens*. The complete overlap of *Pongo* with *H. sapiens* in PP5 is due to a distal thickening of the region under the trochlea in PP5 of both species.

PC2 explains <8% of the variance in the PCAs of all four digits and represents the region of overall maximum cortical thickness. Low values along PC2 are driven by a proximal to distal cortical bone distribution on the palmar surface and high values represent a cortical bone concentration on either the mid-shaft to distal region of the palmar or dorsal surface of the shaft. *Gorilla* and *Pan* are the only taxa to be separated along PC2, reflecting a palmar proximo-distal concentration of cortical bone in *Gorilla* and a mid-shaft to distal concentration in *Gorilla* and *Pan*.

A 3D plot of PC1, PC2 and PC3 (<6%) provides clear separation among taxa, especially for PP5, with only slight overlap in *Pan* and

Pongo in PP2 and PP4 and between *Pan*, *Pongo* and *H. sapiens* in PP3 (Figure S2).

3.2 | Mean cortical thickness

Table 2 shows mean values of cortical thickness. Scaled mean cortical thickness values across the shaft reveal the African apes have significantly thicker cortex than *H. sapiens* and *Pongo* (Table 2; Figure S3).

3.3 | Cross-sectional geometry

Descriptive statistics of the scaled cross-sectional geometric properties at 35%, 50% and 65% of the shaft are presented in Table S2 and depicted in Figures 8–10. Only *Gorilla* has significantly larger values of CA, Z_{pol} and J across all digits and cross-sectional levels

TABLE 2 Summary statistics of raw (mm) and standardized (dimensionless) cortical thickness measurements of the phalangeal shaft.

	<i>Homo sapiens</i>	<i>Pan</i>	<i>Gorilla</i>	<i>Pongo</i>
	Mean (SD)	Mean (SD)	Mean (SD)	Mean (SD)
Raw				
PP2	1.477 (0.290)	2.520 (0.438)	2.862 (0.550)	2.078 (0.328)
PP3	1.561 (0.261)	2.679 (0.481)	3.220 (0.563)	2.187 (0.341)
PP4	1.507 (0.264)	2.605 (0.452)	2.924 (0.512)	2.212 (0.360)
PP5	1.199 (0.262)	2.257 (0.361)	2.556 (0.504)	1.981 (0.298)
Standardized ^a				
PP2	0.036 (0.007)	0.051 (0.007)	0.054 (0.006)	0.033 (0.005)
PP3	0.034 (0.006)	0.048 (0.008)	0.055 (0.006)	0.031 (0.004)
PP4	0.035 (0.006)	0.049 (0.007)	0.053 (0.006)	0.032 (0.005)
PP5	0.035 (0.007)	0.053 (0.008)	0.055 (0.008)	0.033 (0.004)

^aStandardized by bone length.

compared to the other taxa (Table S3). CSG properties differ across the digits in all taxa except *Pongo* (Table S4).

3.4 | *Pongo*

As the hand of *Pongo* is used primarily for grasping, we predicted that *Pongo* would have thicker regions of cortical bone distopalmarly on the shaft, especially close to the FSRs, and that this pattern would be consistent across the hand. In support of this prediction, we find cortical bone in *Pongo* to be thickest at the FSRs in all phalanges (Figures 4 and S1), corresponding with expected loading during grips in which the PIP joint is flexed. The point of maximum thickness within the shaft is at the distal end of the FSR, with cortical thickness reducing just distal to the FSRs and then increasing again proximal to the trochlea (Figure 5). The ratio of cortical thickness of the dorsal and palmar shaft (i.e., removing the influence of the FSRs) demonstrates that the palmar aspect of the shaft is always thicker than the dorsal (Table 3; Figure 7). A biomechanical function of FSRs is to reduce strain on the shaft, such that the taller the ridge, the more strain it experiences and consequently the amount of strain distributed to the palmar shaft is reduced (Nguyen et al., 2014). However, the FSRs in *Pongo* are not particularly prominent (i.e., do not extend far above the palmar surface of the shaft) relative to other taxa, such as *Gorilla* (Syeda et al., 2021). This suggests that the strain resulting from grasping arboreal substrates during suspension is dissipated across the FSRs, without requiring modelling of the cortical structure along the remainder of the shaft.

Comparison of these patterns across the hand shows that, as we predicted, cortical bone distribution is similar across the digits in *Pongo*, with the exception of PP2, where cortical bone is thicker on the radial aspect of the palmar shaft (*Pongo* PP2 in Figure S1). This radial asymmetry could reflect grasping of very thin substrates, during which the second digit is greatly extended relative to the ulnar digits (Napier, 1960). Despite this differing pattern of cortical bone distribution in PP2, there are no significant differences in

mean cortical thickness or CSG properties across the *Pongo* digits (Figure S4). The absence of significant differences in mean cortical thickness or CSG properties between the digits is consistent with relatively equal loading of all fingers during arboreal locomotion in *Pongo* (Rose, 1988; Susman, 1974; Thorpe et al., 2009; Thorpe & Crompton, 2006).

Regarding CSG properties, we predicted that *Pongo* phalanges would have thinner cortices and be less resistant to bending and torsion than those of the African apes. *Pongo* has the thinnest mean relative cortical thickness when scaled by bone length (Table 2; Figure S3), which is significantly thinner than that of African apes, partially supporting our third prediction (Figure S3). Cross-sectional properties of *Pongo* are only significantly lower than those of *Gorilla*. However, while not significantly different from *Pan* and *H. sapiens*, relative mean values of CSG properties are lowest in *Pongo* among our sample. (Figures 8–10; Table S2). This thin cortical structure and low cross-sectional properties of the *Pongo* proximal phalanges may relate to aspects of their external morphology. Among the great apes, *Pongo* phalanges have the greatest degree of curvature and their FSRs are located opposite the point of the maximum arc of this curvature, thus preventing the long tendons of the digital flexor muscles from being pulled into an extreme palmar position (Susman, 1979). This acts to reduce joint reaction forces and also aligns the bone more closely with this joint reaction force, ultimately leading to optimized distribution of load across the phalanx (Nguyen et al., 2014; Richmond, 2007; Susman, 1979). Thus, in *Pongo* a thicker cortex may not be needed due to the functional adaptations of the external shape to minimize strain experienced by the phalanx (Pearson & Lieberman, 2004; Ruff et al., 2006).

3.5 | *Gorilla*

In support of our predictions, morphometric maps of cortical bone thickness distribution reveal the regions of thickest cortex in

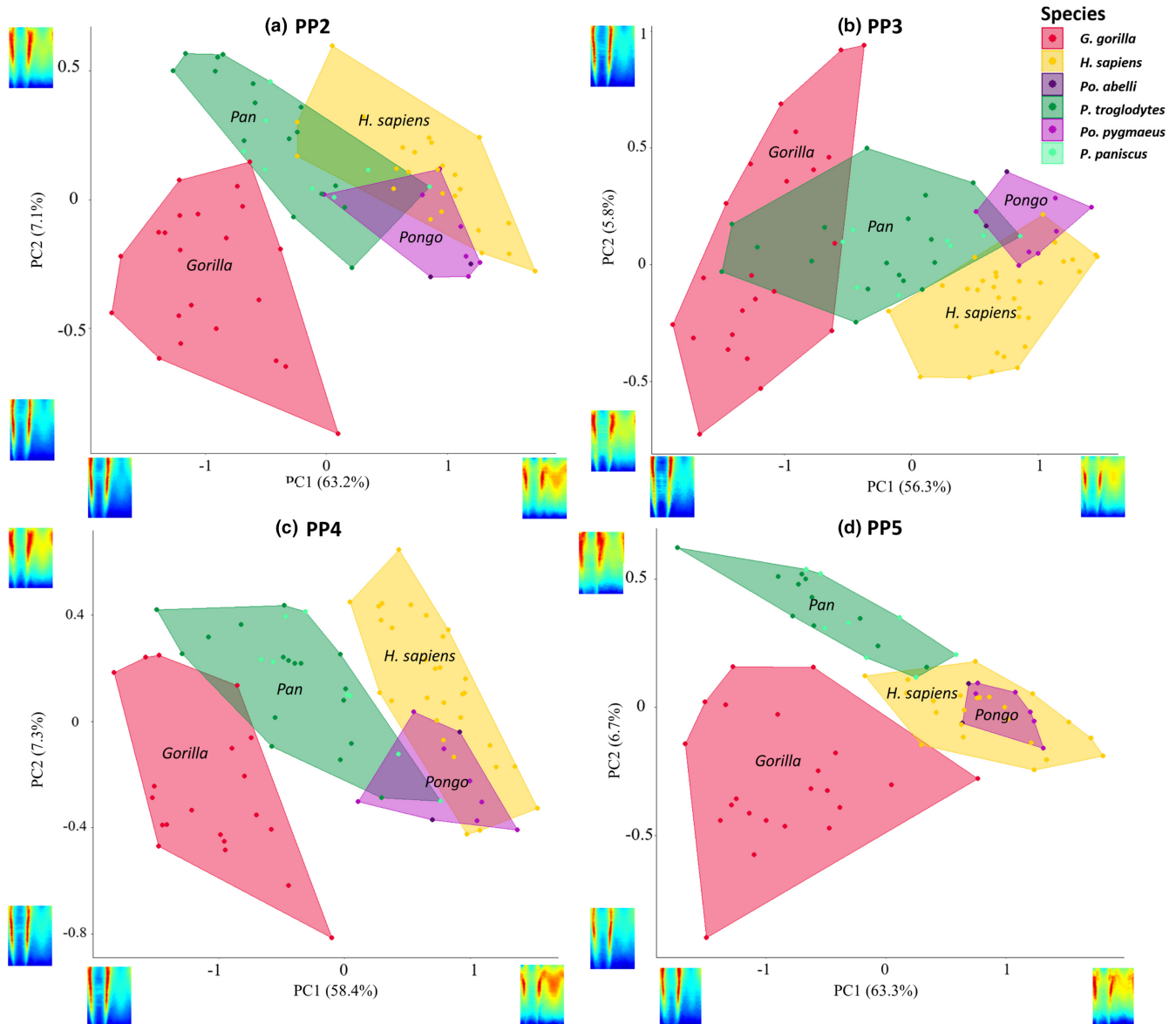


FIGURE 6 PC1 and PC2 for cortical bone distribution of proximal phalanges of (a) PP2, (b) PP3, (c) PP4 and (d) PP5 of *Homo sapiens*, *Pan* sp., *Gorilla* and *Pongo* sp.

Gorilla PP2–PP4 are located in patches along the FSRs, as well as proximal to the trochlea (Figures 4 and S1). The shaft shows low-to-intermediate cortical thickness, with the FSRs being thicker than the remaining aspects of the shaft. Quantitative comparisons of *Gorilla* mean cortical thickness values across the shaft show a distal increase in cortical thickness in all digits (Figure 5). The distinctive regions of thicker palmar cortical bone are located at the attachment points of the soft tissues involved in stabilizing the fingers in flexed positions during knuckle-walking. On the FSR, these locations of thicker cortical bone correspond with the attachment points of the ligaments and pulleys (Figure 4) that provide biomechanical advantage by keeping the flexor tendons close to the bone and in line with the joint axis. This decreases the moment arm and allows for optimal joint function and force transmission during finger flexion (Ayhan & Ayhan, 2020; Doyle, 2001).

During knuckle-walking, the stress in the flexor tendon is concentrated distally on the second annular pulley (A2), at the location where the tendon is maximally bent during knuckle-walking (Leijnse et al., 2021). When the phalangeal joints are in flexion during knuckle-walking, the flexor tendons are pulled palmarly and the digital pulleys are then stretched, which leads to increased strain in the phalanx in the same regions as we find thicker cortical bone (Ayhan & Ayhan, 2020; Leijnse et al., 2021; Ruff et al., 2006). The region of thick cortical bone proximal to the trochlea coincides with the attachment site of the collateral ligaments of the PIP joint. The collateral ligaments arise from the radial and ulnar sides of the distal end of the proximal phalanx and run obliquely to the palmar radial and ulnar surfaces of the intermediate phalanx (Figure 1f), providing lateral stability to the phalangeal joints during flexion and extension (Ayhan & Ayhan, 2020). This stability is

TABLE 3 Paired samples *t* tests on scaled palmar versus dorsal cortical thickness across species.

		<i>Homo sapiens</i>	<i>Pan</i>	<i>Gorilla</i>	<i>Pongo</i>
PP2	Palmar mean	0.031	0.048	0.048	0.033
	Dorsal mean	0.038	0.046	0.044	0.031
	<i>t</i> ratio	-3.489	1.057	2.363	0.904
	<i>p</i>	0.001**	NS	0.023*	NS
PP3	Palmar mean	0.029	0.042	0.043	0.030
	Dorsal mean	0.037	0.044	0.045	0.029
	<i>t</i> ratio	-4.447	-1.178	-0.945	0.516
	<i>p</i>	<0.001***	NS	NS	NS
PP4	Palmar mean	0.029	0.045	0.043	0.031
	Dorsal mean	0.038	0.045	0.044	0.030
	<i>t</i> ratio	-5.682	-0.335	-0.926	0.326
	<i>p</i>	<0.001***	NS	NS	NS
PP5	Palmar mean	0.031	0.052	0.052	0.033
	Dorsal mean	0.035	0.048	0.046	0.030
	<i>t</i> ratio	-2.149	1.583	2.940	1.791
	<i>p</i>	0.037*	NS	0.005**	NS

The bold value significance ($p > 0.05$). * $p < 0.05$, ** $p < 0.01$, *** $p < 0.001$. Abbreviation: NS, not significant.

essential for the intermediate phalanx to accommodate high loads during knuckle-walking.

Contrary to our predictions, the pattern of cortical bone thickness distribution in PP5 is distinct from that of the more radial digits, in that the region of maximum thickness is consistently located between the proximal end of the FSR and the region just proximal to the trochlea (Figure S1). This variation in thickness may be due to lower pressure being placed on the fifth digit during knuckle-walking compared to the other rays (Matarazzo, 2013), such that the pressure is being evenly dissipated from the proximal end of the FSRs to the distal end of the bone. The attachment points of the pulleys and ligaments may not be experiencing enough strain to elicit a biomechanical remodelling response at those regions. There is some asymmetry in the cortical thickness distribution patterns of PP2 and PP5, such that the thickest portion of the shaft in PP2 is on the palmar ulnar surface and in PP5 is on the palmar radial surface (Figure S1). This may reflect the location of pressures experienced during knuckle-walking, which are highest on the third digit (Matarazzo, 2013; Preuschoft, 1973; Samuel et al., 2018).

Furthermore, there is variation in the patterning of palmar and dorsal cortical thickness in the proximal phalanges of *Gorilla*. There is no significant difference in thickness between the palmar and dorsal cortex of PP3 and PP4, but in PP2 ($p = 0.023$) and PP5 ($p = 0.005$) the cortex is significantly thicker palmarly compared to dorsally (Table 3). This could be due to the smaller FSRs of PP2 and PP5 compared to PP3 and PP4, in which the strain on the palmar shaft is reduced due to the tall FSRs (Nguyen et al., 2014; Susman, 1979). While there are nuanced differences in each of the digits in regard to cortical bone distribution pattern and relative palmar and dorsal

cortical thickness, we predicted no overall differences in mean cortical thickness and cross-sectional properties across the *Gorilla* digits. However, PP5 has significantly lower CSG than PP3 (Tables S2 and S4). These results could be due to more neutral position of the *Gorilla* hand during the majority of knuckle-walking hand postures, along with similar lengths of the metacarpus and proximal phalanges, which allows them to consistently touchdown with their fifth digit despite placing significantly less pressure on it relative to the other digits (Matarazzo, 2013; Susman, 1979; Susman & Stern, 1979; Thompson et al., 2018). However, it is important to acknowledge the studies that quantified pressure distribution during locomotion in extant non-human great apes (e.g., Matarazzo, 2013; Samuel et al., 2018; Wunderlich & Jungers, 2009) have, for logistical reasons, focused on animals in captivity in an enclosed space and likely do not fully reflect manual behaviours in the wild.

3.6 | *Pan*

Our expectations for *Pan* were generally supported. The pattern of cortical bone distribution in *Pan* is similar to *Gorilla* in having thicker cortical bone at the FSRs and in the region proximal to the trochlea. However, unlike *Gorilla*, the shaft is relatively intermediate in its thickness compared to the thin proximal region of the bone (Figures 4 and S1). This difference in cortical bone thickness patterning among the knuckle-walking apes could be a reflection of *Pan* participating in arboreal behaviours to a greater extent than *Gorilla* (Doran, 1996, 1997; Hunt, 2020; MacKinnon, 1976; Sarringhaus et al., 2014; Susman, 1984). While the magnitude of loads during knuckle-walking and arboreal locomotion have been shown to be similar (Synek et al., 2020), loads of knuckle-walking may be reflected in the internal morphology more so than the overall forces of infrequent arboreal behaviours. External morphological features may play a role in these differences in internal bone structure. Within the African apes, the higher degree of curvature of the *Pan* phalanges, relative to that of *Gorilla*, should be an advantage for load distribution during arboreal behaviours (Deane & Begun, 2008; Hunt, 1991; Oxnard, 1973; Richmond, 2007; Stern et al., 1995), but the less prominent FSRs would not act to reduce strain experienced by the remainder of the shaft to the same extent as in *Gorilla* (Nguyen et al., 2014). As such, CSG properties, mean cortical bone thickness and distribution patterns may reflect the greater degree of arboreal behaviours in *Pan*.

Our prediction that there will be variation in cortical thickness pattern and properties across the *Pan* digits was not fully supported. Unexpectedly, PP5 has significantly thicker cortex ($p = 0.044$; Figure S4) than PP3, but when compared to PP5, the radial three digits are significantly stronger in resisting axial, bending and torsional loads, along with PP3 being stronger than PP2 (Tables S2 and S4). Overall, these results may reflect low loading of the fifth digit during knuckle-walking, as it is loaded significantly less than the other digits and sometimes does not make contact with the substrate (Matarazzo, 2013; Wunderlich & Jungers, 2009). While

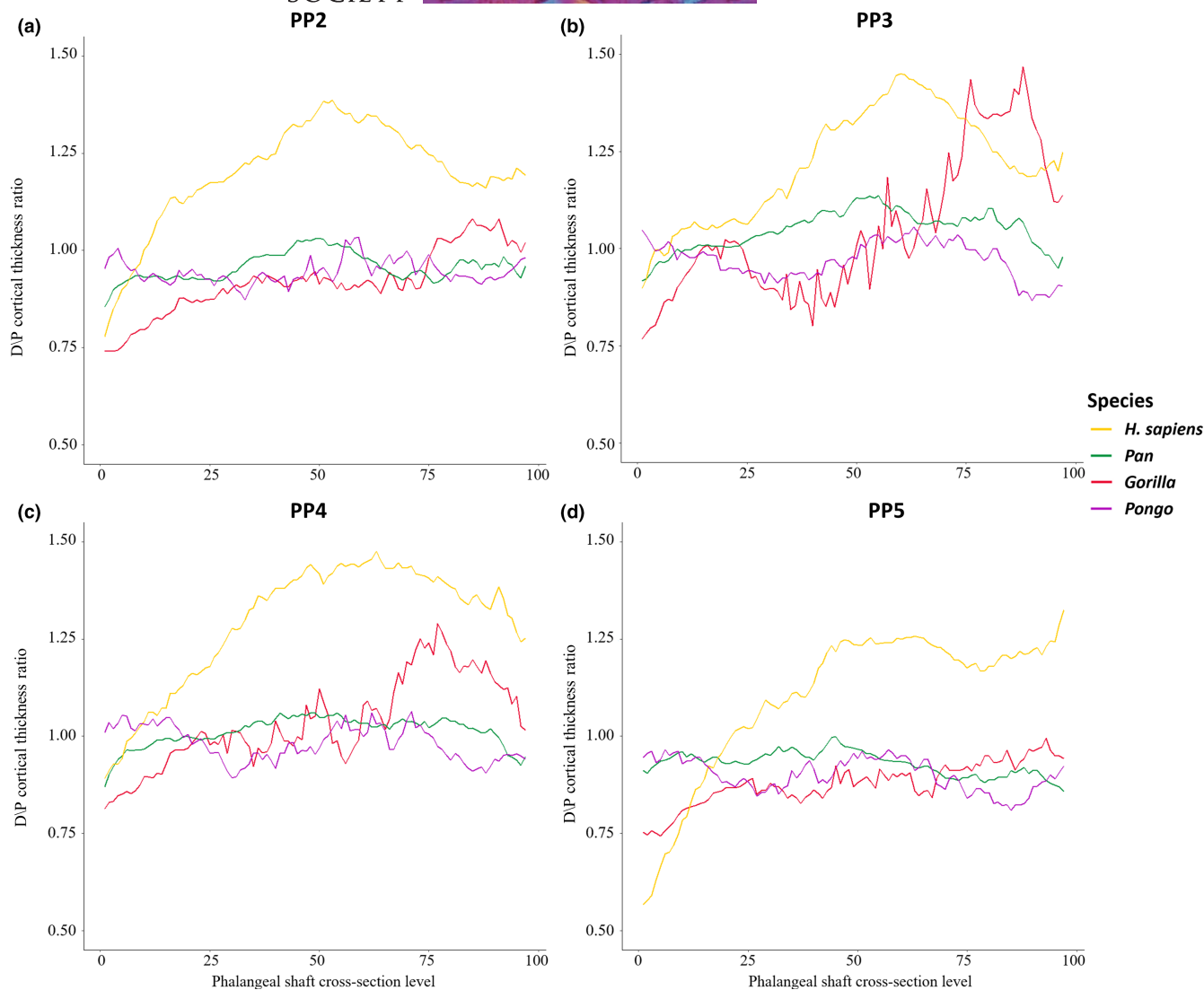


FIGURE 7 Ratio of dorsal/palmar cortical bone thickness plotted from the proximal end to the distal end of the phalangeal shaft of *Homo sapiens*, *Pan*, *Gorilla* and *Pongo*. (a) PP2; (b) PP3; (c) PP4; (d) PP5. Values greater than 1 represent more dorsal cortex relative to the palmar cortex in the shaft.

surprising, the relatively thinner cortex in PP3 may be reflecting the impact of external morphology (taller FSRs, high degree of curvature), which are most prominent in the third digit within the *Pan* hand, on cortical remodelling. The similarity in cortical properties among the radial digits could be explained by the variability of hand postures used by *Pan* (Inouye, 1994; Matarazzo, 2013; Samuel et al., 2018; Tuttle, 1967, 1969; Wunderlich & Jungers, 2009), such that the varying hand positions during locomotion result in differing sequences of digital placement, affecting which digit receives the greatest pressures (Wunderlich & Jungers, 2009). The variation in knuckle-walking hand postures and greater degree of arboreality in the *Pan* locomotor repertoire, may also explain the intermediate thickness of the shaft with no significant difference in palmar and dorsal cortical thickness (Figure 4; Table 3). PP5 is also distinct from the other digits in displaying a radial concentration in its thickness pattern (Figure S1), potentially reflecting peak pressures during locomotion being located around the centre of the hand and lower

pressures under the fifth digit (Matarazzo, 2013; Preuschoft, 1973; Samuel et al., 2018).

3.7 | *H. sapiens*

Our predictions that *H. sapiens* would display the thickest cortex in the distodorsal region of the shaft and that they would be characterized by thick cortical bone where FSRs are present, are generally supported (Figures 4 and S1). Although the distal dorsal and palmar aspects of the phalangeal shaft are thick as predicted, cortical thickness is concentrated on the mid-shaft to distodorsal region of the diaphysis. Cortical thickness of the dorsal surface is significantly greater than the palmar surface (Figure 7; Table 3) and decreases past the distodorsal region of maximum cortical thickness (Figure 5). This could reflect the lack of phalangeal curvature in *H. sapiens* and the frequent use of flexed hand postures during modern human

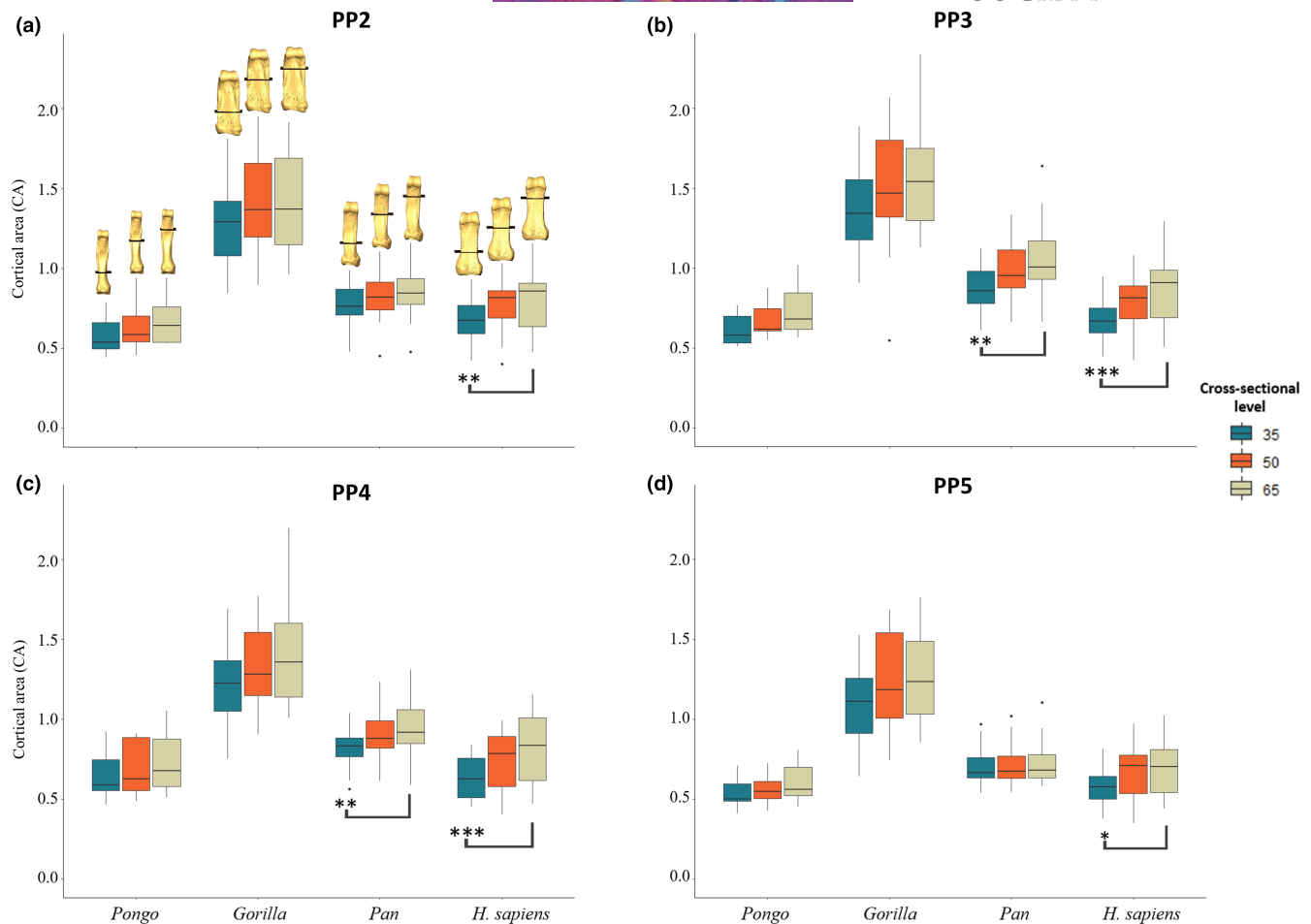


FIGURE 8 Boxplots representing cortical area for (a) PP2, (b) PP3, (c) PP4, and (d) PP5 of *Homo sapiens*, *Pan* sp., *Gorilla* and *Pongo* sp. at 35%, 50% and 65% of the bone length. Section locations are represented on 3D surfaces of PP2 of an individual from each taxon.

manipulation. Hand grips used during manipulation result in bending forces being placed on the phalanges, with the dorsal surface on the bone experiencing higher tensile forces and the palmar surface experiencing compression, and the lack of curvature characteristic of *H. sapiens* phalanges results in higher bending forces experienced by the bone overall (Oxnard, 1973; Preuschoft, 1973; Richmond, 2007).

Across the digits, we predicted PP2 and PP3 would display the thickest cortices and greatest cross-sectional strength, as experimental studies have revealed that the thumb and radial digits experience the highest loads during manipulation (Key, 2016; Rolian et al., 2011; Williams-Hatala et al., 2018). Furthermore, experimental studies testing force distribution of power grips used in modern human daily activities have revealed that, within digits 2–5, digit 2 experiences the greatest loads and the three ulnar digits experience relatively equal loads when grasping larger objects (De Monsabert et al., 2012; Sancho-Bru et al., 2014; Vigouroux et al., 2011). In contrast, loading of the digits is variable when grasping objects with a smaller diameter (<6.4 cm), as positioning of the fingers can be adjusted to maximize endurance without losing hold of the object (Sancho-Bru et al., 2014). Mean cortical thickness and cross-sectional properties are greatest in PP3, followed by PP2, PP4 and PP5, but there were no significant differences in cortical thickness across the

digits (Table 2; Figure S4). Only PP5 was significantly lower in its measure of axial strength (CA), bending strength (Z_{pol}) and bending and torsional rigidity (J) (Tables S2 and S4; Figures 8–10). As our sample includes a diverse range of pre- and post-industrial populations, our results could simply reflect the varied hand postures employed during the daily activities of individuals from these populations, and not necessarily correspond with those employed during stone tool production (see Key et al., 2019).

3.8 | Phalangeal curvature and cortical thickness

The regression analyses showed no relationship between the degree of curvature (IA) and phalangeal cortical thickness in *Pongo*, *Gorilla* and *H. sapiens* (Figure S8). There was a significant ($p=0.001$), but weak ($R^2=0.106$) positive correlation between curvature and cortical thickness in *Pan* proximal phalanges (Table S5). Our results suggest a weak relationship between phalangeal curvature and cortical thickness, despite a curved phalanx having been shown to dissipate load differently than a straight phalanx (Oxnard, 1973; Preuschoft, 1973). These results may also reflect the lack of precision offered by the IA method, which assumes a consistent degree

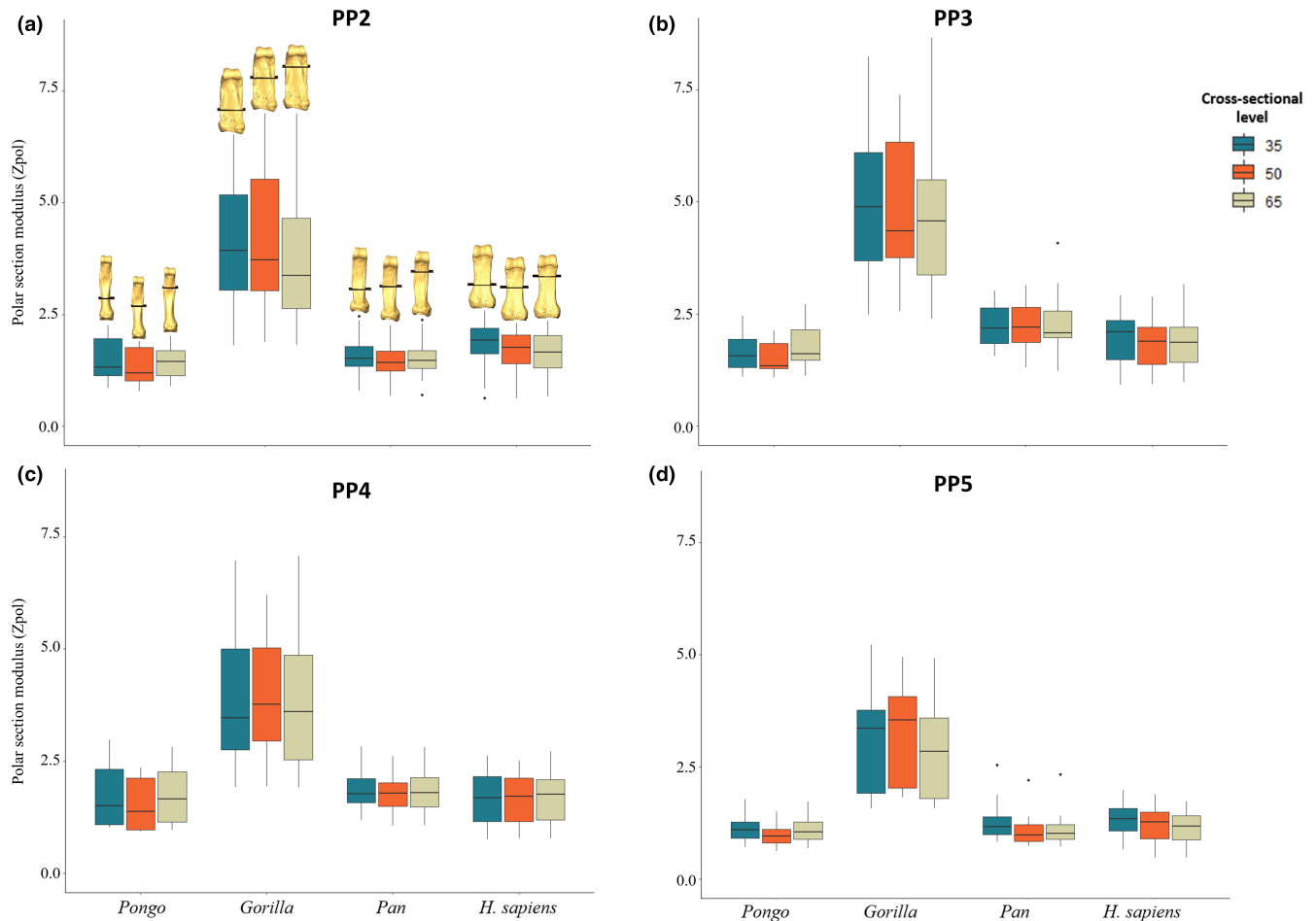


FIGURE 9 Boxplots representing polar section modulus (Z_{pol}) for (a) PP2, (b) PP3, (c) PP4, and (d) PP5 of *Homo sapiens*, *Pan* sp., *Gorilla* and *Pongo* sp. at 35%, 50% and 65% of the bone length. Section locations are represented on 3D surfaces of PP2 of an individual from each taxon.

of curvature throughout the phalanx (see Deane & Begun, 2008; Wennemann et al., 2022).

3.9 | Behavioural signals in the cortex of the proximal phalanges

Great apes use their hands in distinct ways and adopt variable hand postures to accomplish a wide range of locomotor and/or manipulative tasks. Aspects of their external hand bone morphology aid them in successfully participating in these manual behaviours, with associated modelling of internal cortical and trabecular bone morphology (Bird et al., 2022; Dunmore et al., 2019; Kivell, 2015; Marchi, 2005; Matarazzo, 2008; Nguyen et al., 2014; Tsegai et al., 2013). Here, we demonstrate that cortical bone in the proximal phalanges reflects differences in hand use behaviours and external morphology.

While cortical bone properties and distribution patterns differed across the great apes, the functional role of FSRs is clear across all taxa. Within the non-human great apes, the location of maximum cortical thickness always includes the FSRs and in human individuals, where FSRs are present, they are maximally thick as well (Figures 4

and S1). These results, coupled with the pattern in *Gorilla* where phalanges with less prominent FSRs (PP2 and PP5) have thicker palmar cortex than dorsal cortex, while phalanges with more prominent FSRs (PP3 and PP4) show no differences, further suggests that prominent FSRs reduce strain experienced by the palmar shaft (Nguyen et al., 2014). This is also apparent in the cortical thickness distribution pattern of *Pongo* phalanges, where though FSRs are the thickest region of the shaft, the shaft is also intermediately thick because *Pongo* FSRs are not very prominent. While *Pongo* FSRs are small, they are optimally located to resist forces during flexion and are coupled with high phalangeal curvature (Patel & Maiolino, 2016; Susman, 1979; Syeda et al., 2021), such that the external morphology of *Pongo* phalanges and cortical bone distribution pattern may be optimal for the manual loads they experience during flexed finger grasping. We draw this conclusion based on the fact that *Pongo* phalanges have thin cortices and weak cross-sectional properties relative to the other great apes, suggesting that a mechanical modelling response for a thicker cortex might not be needed (Pearson & Lieberman, 2004).

Gorilla and *Pan* have a similar locomotor repertoire (Doran, 1996; Matarazzo, 2013; Samuel et al., 2018; Wunderlich & Jungers, 2009), which is reflected in the cortical bone morphology of their proximal

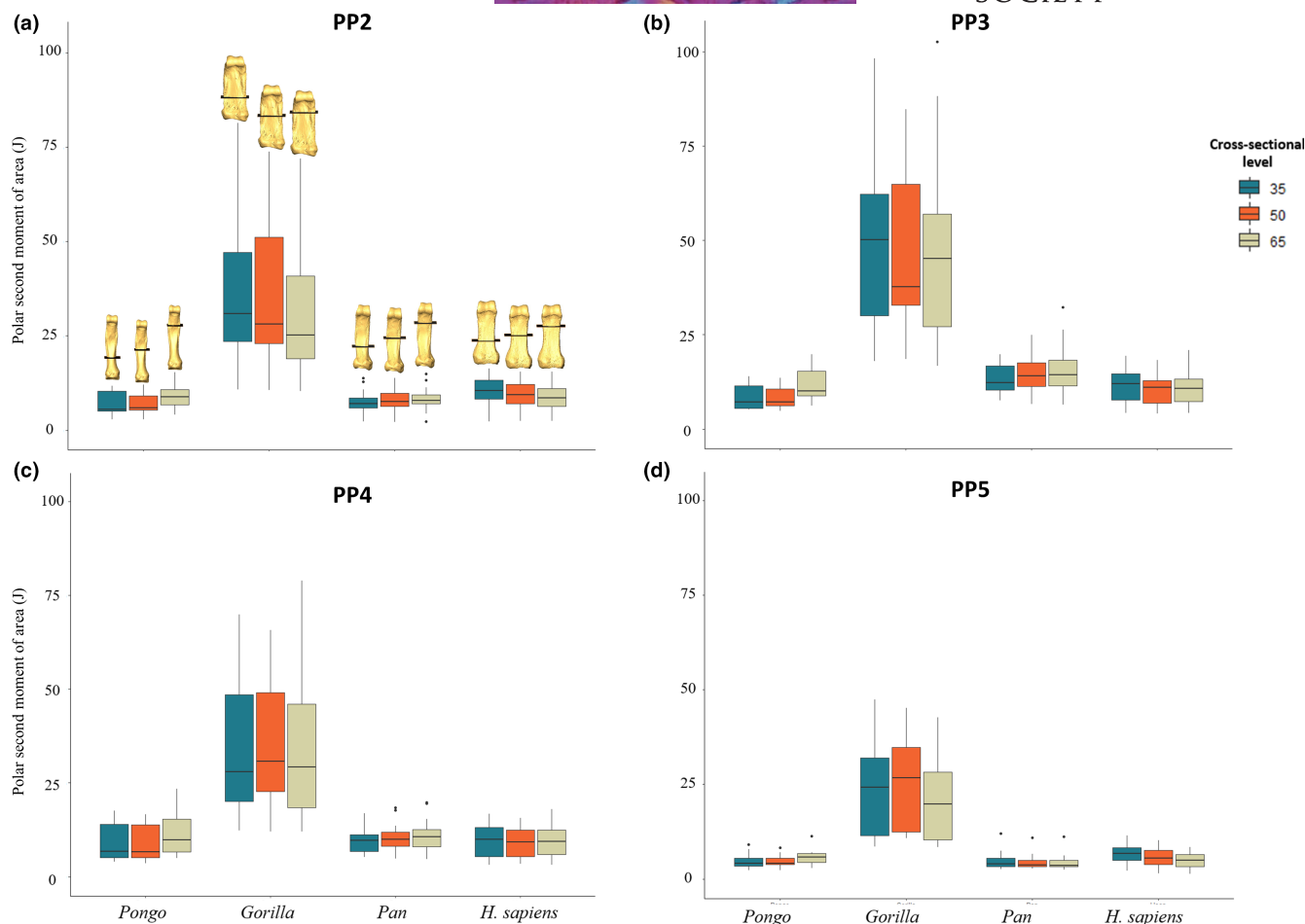


FIGURE 10 Boxplots representing polar second moment of area (J) for (a) PP2, (b) PP3, (c) PP4, and (d) PP5 of *Homo sapiens*, *Pan* sp., *Gorilla* and *Pongo* sp. at 35%, 50% and 65% of the bone length. Section locations are represented on 3D surfaces of PP2 of an individual from each taxon.

phalanges. Specifically, a shared pattern of thick cortex at the FSRs and in the distal region under the trochlea in *Gorilla* and *Pan* is indicative of the loading pattern incurred during knuckle-walking (Matarazzo, 2013; Samuel et al., 2018; Wunderlich & Jungers, 2009). Even though loads experienced by the metacarpals, and possibly the proximal phalanges, during knuckle-walking and arboreal behaviours are similar (Synek et al., 2020), the frequency of knuckle walking is greater (e.g., Doran, 1996, 1997; Hunt, 1991). We assume, therefore, that the cortical patterns we found primarily reflect knuckle-walking, and this is supported by variation in external and internal morphology between African apes and *Pongo*. However, it is important to acknowledge that infrequent behaviours can also result in bone (re-)modelling (Barak et al., 2011; Burr, 1990; Pontzer et al., 2006). For example, the digital flexor muscles are minimally active during knuckle-walking but highly active during arboreal climbing and suspension (Leijnse et al., 2021; Susman & Stern, 1979; Thompson et al., 2019; Tuttle et al., 1972), and thus arboreal behaviours are likely contribute to some of the patterns we observe in *Gorilla* and *Pan* proximal phalanges. As for differences, the variation in hand morphology and postures employed by the two species during locomotion likely leads to differences in the pattern of

loading across the non-pollical digits, and this is also reflected in our results (Inouye, 1994; Tuttle, 1969).

The distinct dorsal thickening of human phalanges is expected for phalanges that are relatively straight and are consistently loaded in a flexed position. We predicted that cortical structure of PP2 and PP3 would reflect their more frequent use during daily manipulative behaviours but instead found a consistent pattern across the digits. This could reflect use of a diverse set of precision and power grips by modern humans (Dollar, 2014; Feix et al., 2015; Sancho-Bru et al., 2014). Furthermore, it is important to acknowledge that studies of recent modern human (often industrialized, Western populations) daily hand use are likely not representative of daily hand use in our geographically and temporally diverse sample. However, PP5 was significantly weaker and had a thinner cortex than the remaining three digits across our sample, which could reflect a general pattern of more limited recruitment of the fifth digit during habitual manual activities (but see Key et al., 2019; Marzke, 1997).

Evaluating bone strength using cross-sectional properties plotted across the shaft showed a distinct pattern in non-human great apes (Figures S5–S7). Specifically, the proximal phalangeal shaft

exhibits a CA that is generally greatest on the distal end of the bone, while the rigidity and resistance to torsion are greatest on the proximal end (Figures 8 and S5–S7; Tables S2). This pattern may reflect the disto-proximal transfer of load across the digit, such that the proximal aspect of the bone needs to be structurally adapted to resist greater loads (Matarazzo, 2015).

While our results support the conclusion that phalangeal cortical bone structure reflects differences in manual behaviours in extant great apes, these interpretations rely on predictions of loading patterns and force transfer that are dependent on the function of muscles, ligaments and other soft tissue structures, about which we know very little. Furthermore, we chose to scale our cortical bone measures by the length of the proximal phalanx, but there are fundamental differences in hand proportions across the great apes (Patel & Maiolino, 2016) that do not show a direct relationship to body mass, and thus a different scaling factor might produce different relative patterns. We tested this potential difference by scaling our data by a geometric mean of phalangeal length, mid-shaft breadth, breadth of the base and breadth of the trochlea, which reflect proximal phalanx size, but found a similar pattern to scaling with phalangeal bone length. Detailed behavioural and kinematic studies on various manual behaviours used by great apes, ideally in natural environments, together with musculoskeletal modelling and cadaveric validation are required (e.g., Leijnse et al., 2021; Lu et al., 2018; Synek et al., 2020). In addition, further investigation of ontogenetic changes in both external morphology (e.g., phalangeal curvature, enthesal morphology) and internal bone structure would also provide insight into the functional interplay between bone shape and bone modelling.

4 | CONCLUSIONS

While, among great apes, cortical bone thickness patterns generally reflect the predicted loading regimes of different locomotor and manual behaviours, more nuanced information about loading during varying hand postures is evident from patterns of cortical bone distribution and cross-sectional properties. Cortical bone and its cross-sectional parameters reflected not just hand postural differences, but also the differences within the hand of each great ape species. More research is needed on phalangeal external and internal forms, however, this study has demonstrated that cortical bone of proximal phalanges of digits 2–5 holds functional signals of hand use and thus, the cortex of proximal phalanges has the potential to aid in reconstruction of manual behaviours of fossil hominids, including hominins.

AUTHOR CONTRIBUTIONS

SMS conceived and designed the experiments, acquire data, analysed and interpreted the data, prepared figures and tables, authored the first draft and reviewed subsequent drafts of the paper, and approved of the final draft. ZJT and MC provided tools for data analysis, provided critical revision of the manuscript, and approved

of the final manuscript. TLK and MMS conceived and designed the experiments, contributed data, assisted with the interpretation of the data, provided critical revision of the manuscript, and approved the final manuscript.

ACKNOWLEDGMENTS

This project has received funding under the European Union's Horizon 2020 research and innovation programme for European Research Council Consolidator Grant #819960 (MMS and TLK) and Marie Skłodowska-Curie Action #101025719 (ZJT). For access to specimens we thank the following individuals/institutions: C. Boesch, Max Planck Institute for Evolutionary Anthropology; J.-J., Hublin, College de France; F. Mayer and C. Funk Museum für Naturkunde—Leibniz Institute for Evolution and Biodiversity Science; I. Livne, Powell-Cotton Museum; E. Gilissen, Royal Museum for Central Africa; J. Moggi-Cecchi and S. Bortoluzzi, University of Florence; B. Grosskopf, Johann-Friedrich-Blumenback-Institute for Zoology and Anthropology, Georg-August University, Goettingen; V. Volpato, Frankfurt Senckenberg Museum; J. Svoboda, Science Academy of the Czech Republic; I. Hershkovitz, Tel Aviv University; M. M. Lahr, the Duckworth Collection, University of Cambridge; A. D. Pascale, Museo Archeologico del Finale; A. Hildred, The Mary Rose Trust. We are grateful to E. Vereecke for her thoughtful review that greatly improved our manuscript. The authors declare no conflict of interest.

DATA AVAILABILITY STATEMENT

Copies of all scans are curated by the relevant curatorial institutions that are responsible for the original specimens and access can be requested through each institution. The authors confirm that the data supporting the findings of this study are available from the corresponding author upon reasonable request.

ORCID

Samar M. Syeda  <https://orcid.org/0000-0003-1514-8086>

Zewdi J. Tsegai  <https://orcid.org/0000-0001-9041-4829>

Marine Cazenave  <https://orcid.org/0000-0001-7194-5958>

Matthew M. Skinner  <https://orcid.org/0000-0001-8321-3543>

Tracy L. Kivell  <https://orcid.org/0000-0001-5087-0897>

REFERENCES

- Ayhan, Ç. & Ayhan, E. (2020) Kinesiology of the wrist and the hand. In: Angin, S. & Simsek, I. (Eds.) *Comparative kinesiology of the human body*. Academic Press, pp. 211–282.
- Arias-Martorell, J., Zeininger, A. & Kivell, T.L. (2021) Trabecular structure of the elbow reveals divergence in knuckle-walking biomechanical strategies of African apes. *Evolution*, 75(11), 2959–2971.
- Barak, M.M., Lieberman, D.E. & Hublin, J.J. (2011) A Wolff in sheep's clothing: trabecular bone adaptation in response to changes in joint loading orientation. *Bone*, 49(6), 1141–1151.
- Bardo, A., Borel, A., Meunier, H., Guéry, J.P. & Pouydebat, E. (2016) Behavioral and functional strategies during tool use tasks in bonobos. *American Journal of Physical Anthropology*, 161(1), 125–140.
- Bardo, A., Cornette, R., Borel, A. & Pouydebat, E. (2017) Manual function and performance in humans, gorillas, and orangutans during

- the same tool use task. *American Journal of Physical Anthropology*, 164(4), 821–836.
- Bird, E.E., Kivell, T.L. & Skinner, M.M. (2021) Cortical and trabecular bone structure of the hominoid capitate. *Journal of Anatomy*, 239(2), 351–373.
- Bird, E.E., Kivell, T.L. & Skinner, M.M. (2022) Patterns of internal bone structure and functional adaptation in the hominoid scaphoid, lunate, and triquetrum. *American Journal of Biological Anthropology*, 177(2), 266–285.
- Burr, D.B. (1990) Experimental overload and bone adaptation. In: Takahashi, H.E. (Ed.) *Bone morphometry*. Japan, Nishimura: Nishimura Co Ltd, pp. 140–148.
- Byrne, R.W. & Byrne, J.M. (2001) Manual dexterity in the gorilla: bimanual and digit role differentiation in a natural task. *Animal Cognition*, 4(3), 347–361.
- Cant, J.G. (1987) Positional behavior of female Bornean orangutans (*Pongo pygmaeus*). *American Journal of Primatology*, 12(1), 71–90.
- Carlson, K.J. & Patel, B.A. (2006) Habitual use of the primate forelimb is reflected in the material properties of subchondral bone in the distal radius. *Journal of Anatomy*, 208(6), 659–670.
- Case, D.T. & Heilman, J. (2006) New siding techniques for the manual phalanges: a blind test. *International Journal of Osteoarchaeology*, 16(4), 338–346.
- Cazenave, M., Braga, J., Oetlé, A., Pickering, T.R., Heaton, J.L., Nakatsukasa, M. et al. (2019) Cortical bone distribution in the femoral neck of *Paranthropus robustus*. *Journal of Human Evolution*, 135, 102666.
- Churchill, S.E. & Formicola, V. (1997) A case of marked bilateral asymmetry in the upper limbs of an upper Palaeolithic male from Barma Grande (Liguria), Italy. *International Journal of Osteoarchaeology*, 7(1), 18–38.
- Cotter, M.M., Simpson, S.W., Latimer, B.M. & Hernandez, C.J. (2009) Trabecular microarchitecture of hominoid thoracic vertebrae. *The Anatomical Record*, 292(8), 1098–1106.
- Currey, J.D. (2003) The many adaptations of bone. *Journal of Biomechanics*, 36(10), 1487–1495.
- De Monsabert, B.G., Rossi, J., Berton, E. & Vigouroux, L. (2012) Quantification of hand and forearm muscle forces during a maximal power grip task. *Medicine and Science in Sports and Exercise*, 44(10), 1906–1916.
- Deane, A.S. & Begun, D.R. (2008) Broken fingers: retesting locomotor hypotheses for fossil hominoids using fragmentary proximal phalanges and high-resolution polynomial curve fitting (HR-PCF). *Journal of Human Evolution*, 55(4), 691–701.
- Dollar, A.M. (2014) Classifying human hand use and the activities of daily living. In: Balasubramanian, R. & Santos, V.J. (Eds.) *The human hand as an inspiration for robot hand development*. Springer, pp. 201–216.
- Doden, E. (1993) The relationship between the function and the inner cortical structure of metacarpal and phalangeal bones. In: Preuschoft, H. & Chivers, D.J. (Eds.) *Hands of primates*. Vienna: Springer, pp. 271–284.
- Doran, D.M. (1996) Comparative positional behavior of the African apes. In: *Great ape societies*. Cambridge: Cambridge University Press, pp. 213–224.
- Doran, D.M. & Hunt, K.D. (1996) Comparative locomotor behavior of chimpanzees and Bonobos: Species and habitat differences. In: Wrangham, R.W., McGrew, W.C., de Waal, F.B.M. & Heltne, P.G. (Eds.) *Chimpanzee cultures*. Harvard University Press, pp. 93–108.
- Doran, D.M. (1997) Ontogeny of locomotion in mountain gorillas and chimpanzees. *Journal of Human Evolution*, 32(4), 323–344.
- Doyle, J.R. (2001) Palmar and digital flexor tendon pulleys. *Clinical Orthopaedics and Related Research*, 383, 84–96.
- Dunmore, C.J., Kivell, T.L., Bardo, A. & Skinner, M.M. (2019) Metacarpal trabecular bone varies with distinct hand-positions used in hominid locomotion. *Journal of Anatomy*, 235(1), 45–66.
- Dunmore, C.J., Skinner, M.M., Bardo, A., Berger, L.R., Hublin, J.J., Pahr, D.H. et al. (2020) The position of *Australopithecus sediba* within fossil hominid hand use diversity. *Nature Ecology & Evolution*, 4(7), 911–918.
- Dunmore, C.J., Wollny, G. & Skinner, M.M. (2018) MIA-clustering: a novel method for segmentation of paleontological material. *PeerJ*, 6, e4374.
- Feix, T., Romero, J., Schmiedmayer, H.B., Dollar, A.M. & Kragic, D. (2015) The grasp taxonomy of human grasp types. *IEEE Transactions on Human-Machine Systems*, 46(1), 66–77.
- Fewlass, H., Talamo, S., Kromer, B., Bard, E., Tuna, T., Fagault, Y. et al. (2019) Direct radiocarbon dates of mid upper Palaeolithic human remains from Dolní Věstonice II and Pavlov I, Czech Republic. *Journal of Archaeological Science: Reports*, 27, 102000.
- Gross, T., Kivell, T.L., Skinner, M.M., Nguyen, N.H. & Pahr, D.H. (2014) A CT-image-based framework for the holistic analysis of cortical and trabecular bone morphology. *Palaeontologia Electronica*, 17(3), 1–13.
- Gilroy, A.M. & MacPherson, B.R. (2016) *Atlas of anatomy*, 3rd edition. Thieme.
- Hunt, K.D. (1991) Mechanical implications of chimpanzee positional behavior. *American Journal of Physical Anthropology*, 86(4), 521–536.
- Hunt, K.D. (2020) *Chimpanzee: lessons from our sister species*. Cambridge: Cambridge University Press.
- Hershkovitz, I., Speirs, M.S., Frayer, D., Nadel, D., Wish-Baratz, S. & Arensburg, B. (1995) Ohalo II H2: A 19,000-year-old skeleton from a water-logged site at the Sea of Galilee, Israel. *American Journal of Physical Anthropology*, 96(3), 215–234.
- Hervé, M. (2022) *RVAideMemoire: Testing and plotting procedures for bio-statistics*. R package version 0.9-81-2. <https://CRAN.R-project.org/package=RVAideMemoire>
- Inouye, S.E. (1994) Ontogeny of knuckle-walking hand postures in African apes. *Journal of Human Evolution*, 26(5–6), 459–485.
- Jashashvili, T., Dowdeswell, M.R., Lebrun, R. & Carlson, K.J. (2015) Cortical structure of hallucal metatarsals and locomotor adaptations in hominoids. *PLoS One*, 10(1), e0117905.
- Jenkins, F.A. & Fleagle, J.G. (1975) Knuckle-walking and the functional anatomy of the wrists in living apes. In: Tuttle, R.H. (Ed.) *Primate functional morphology and evolution*. De Gruyter Mouton, pp. 213–227.
- Jungers, W.L., Godfrey, L.R., Simons, E.L. & Chatrath, P.S. (1997) Phalangeal curvature and positional behavior in extinct sloth lemurs (Primates, Palaeopropithecidae). *Proceedings of the National Academy of Sciences*, 94(22), 11998–12001.
- Key, A. J. (2016) Manual loading distribution during carrying behaviors: implications for the evolution of the hominid hand. *PLoS One*, 11(10), e0163801.
- Key, A.J., Dunmore, C.J. & Marzke, M.W. (2019) The unexpected importance of the fifth digit during stone tool production. *Scientific Reports*, 9(1), 1–8.
- Kivell, T.L. (2015) Evidence in hand: recent discoveries and the early evolution of human manual manipulation. *Philosophical Transactions of the Royal Society B: Biological Sciences*, 370(1682), 20150105.
- Leijnse, J.N., Spoor, C.W., Pullens, P. & Vereecke, E.E. (2021) Kinematic and dynamic aspects of chimpanzee knuckle walking: finger flexors likely do not buffer ground impact forces. *Journal of Experimental Biology*, 224(19), jeb236604.
- Lesnik, J.J., Sanz, C.M. & Morgan, D.B. (2015) The interdigital brace and other grips for termite nest perforation by chimpanzees of the Goulougo Triangle, Republic of Congo. *American Journal of Physical Anthropology*, 157(2), 252–259.
- Lieberman, D.E., Polk, J.D. & Demes, B. (2004) Predicting long bone loading from cross-sectional geometry. *American Journal of Physical Anthropology*, 123(2), 156–171.

- Lu, S.-C., Vereecke, E.E., Synek, A., Pahr, D.H. & Kivell, T.L. (2018) A novel experimental design for the measurement of metacarpal bone loading and deformation and fingertip force. *PeerJ*, 6, e5480.
- MacKinnon, J. (1976) Mountain gorillas and bonobos. *Oryx*, 13(4), 372–382.
- Marchi, D. (2005) The cross-sectional geometry of the hand and foot bones of the Hominoidea and its relationship to locomotor behavior. *Journal of Human Evolution*, 49(6), 743–761.
- Marzke, M.W. (1997) Precision grips, hand morphology, and tools. *American Journal of Physical Anthropology*, 102(1), 91–110.
- Marzke, M.W. (2013) Tool making, hand morphology and fossil hominins. *Philosophical Transactions of the Royal Society B: Biological Sciences*, 368(1630), 20120414.
- Marzke, M.W., Marchant, L.F., McGrew, W.C. & Reece, S.P. (2015) Grips and hand movements of chimpanzees during feeding in Mahale Mountains National Park, Tanzania. *American Journal of Physical Anthropology*, 156(3), 317–326.
- Matarazzo, S. (2008) Knuckle walking signal in the manual digits of *Pan* and *Gorilla*. *American Journal of Physical Anthropology*, 135(1), 27–33.
- Matarazzo, S.A. (2013) *Knuckle-walking signal in the manual phalanges and metacarpals of the great apes (Pan and Gorilla)*, PhD dissertation. Amherst, MA, USA: University of Massachusetts Amherst.
- Matarazzo, S.A. (2015) Trabecular architecture of the manual elements reflects locomotor patterns in primates. *PLoS One*, 10(3), e0120436.
- McClure, N.K., Phillips, A.C., Vogel, E.R. & Tocheri, M.W. (2012) Unexpected pollex and hallux use in wild *Pongo pygmaeus wurmbii*. *American Journal of Physical Anthropology*, 147(S54), S208.
- Napier, J.R. (1960) Studies of the hands of living primates. *Proceedings of the Zoological Society of London*, 134(4), 647–657.
- Neufuss, J., Robbins, M.M., Baeumer, J., Humle, T. & Kivell, T.L. (2017) Comparison of hand use and forelimb posture during vertical climbing in mountain gorillas (*Gorilla beringei beringei*) and chimpanzees (*Pan troglodytes*). *American Journal of Physical Anthropology*, 164(4), 651–664.
- Neufuss, J., Robbins, M.M., Baeumer, J., Humle, T. & Kivell, T.L. (2019) Manual skills for food processing by mountain gorillas (*Gorilla beringei beringei*) in Bwindi Impenetrable National Park, Uganda. *Biological Journal of the Linnean Society*, 127(3), 543–562.
- Nguyen, N.H., Pahr, D.H., Gross, T., Skinner, M.M. & Kivell, T.L. (2014) Micro-finite element (μ FE) modeling of the siamang (*Symphalangus syndactylus*) third proximal phalanx: the functional role of curvature and the flexor sheath ridge. *Journal of Human Evolution*, 67, 60–75.
- Niewoehner, W.A. (2001) Behavioral inferences from the Skhul/Qafzeh early modern human hand remains. *Proceedings of the National Academy of Sciences*, 98(6), 2979–2984.
- Ogle, D. H., Doll, J. C., Wheeler, A. P., & Dinno, A. (2022). FSA: Simple fisheries stock assessment methods. R package version 0.9.4. <https://CRAN.R-project.org/package=FSA>
- Oxnard, C.E. (1973) *Form and pattern in human evolution: some mathematical, physical, and engineering approaches*. Chicago, IL: University of Chicago Press.
- Patel, B.A., Orr, C.M. & Jashashvili, T. (2020) Strength properties of extant hominoid hallucal and pollical metapodials. *Journal of Human Evolution*, 143, 102774.
- Patel, B.A. & Maiolino, S.A. (2016) Morphological diversity in the digital rays of primate hands. In: Kivell, T.L., Lemelin, P., Richmond, B.G. & Schmitt, D. (Eds.) *The evolution of the primate hand*. Springer, pp. 55–100.
- Pearson, O.M. & Lieberman, D.E. (2004) The aging of Wolff's "law": ontogeny and responses to mechanical loading in cortical bone. *American Journal of Physical Anthropology*, 125(S39), 63–99.
- Pontzer, H., Lieberman, D.E., Momin, E., Devlin, M.J., Polk, J.D., Hallgrímsson, B. et al. (2006) Trabecular bone in the bird knee responds with high sensitivity to changes in load orientation. *Journal of Experimental Biology*, 209(1), 57–65.
- Pouydebat, E., Berge, C., Gorce, P. & Coppens, Y. (2005) Use and manufacture of tools to extract food by captive *Gorilla gorilla gorilla*: experimental approach. *Folia Primatologica*, 76(3), 180–183.
- Preuschoft, H. (1973) Functional anatomy of the upper extremity. In: H. Bourne (Ed.), *The chimpanzee*, vol. 6. Atlanta, GA: Krager, pp. 34–120.
- Preuschoft, H. (2019) Power grip or precision handling? What determines hand morphology in primates, including Hominidae? *Biological Journal of the Linnean Society*, 127(3), 694–706.
- Profico, A., Bondioli, L., Raia, P., O'Higgins, P. & Marchi, D. (2021) Morphomap: an R package for long bone landmarking, cortical thickness, and cross-sectional geometry mapping. *American Journal of Physical Anthropology*, 174(1), 129–139.
- Puymeraul, L. (2013) The functionally-related signatures characterizing the endostructural organisation of the femoral shaft in modern humans and chimpanzee. *Comptes Rendus Palevol*, 12(4), 223–231.
- R Core Team. (2020) *R: A language and environment for statistical computing*. R Foundation for Statistical Computing. <https://www.R-project.org/>
- Ramos, G.L., III. (2014) *Positional behavior of Pan paniscus at Lui Kotale, Democratic Republic of Congo*, PhD dissertation. Bloomington, IN, USA: Indiana University.
- Rein, T.R. (2011) The correspondence between proximal phalanx morphology and locomotion: implications for inferring the locomotor behavior of fossil catarrhines. *American Journal of Physical Anthropology*, 146(3), 435–445.
- Rein, T.R. & McCarty, L.A. (2012) Metacarpophalangeal joint orientation in anthropoid manual phalanges. *The Anatomical Record: Advances in Integrative Anatomy and Evolutionary Biology*, 295(12), 2057–2068.
- Richmond, B.G. (1998) *Ontogeny and biomechanics of phalangeal form in primates*, PhD dissertation. Stony Brook, NY, USA: State University of New York at Stony Brook.
- Richmond, B.G. (2007) Biomechanics of phalangeal curvature. *Journal of Human Evolution*, 53(6), 678–690.
- Rolian, C., Lieberman, D.E. & Zermeno, J.P. (2011) Hand biomechanics during simulated stone tool use. *Journal of Human Evolution*, 61(1), 26–41.
- Rose, M.D. (1988) Functional anatomy of the cheiridia. In: Schwartz, J.H. (Ed.) *Orangutan biology*. New York, NY: Oxford University Press, pp. 299–310.
- Remis, M.J. (1998) The gorilla paradox. In: Strasser, E., Fleagle, J., Rosenberger, A. & McHenry, H. (Eds.) *Primate locomotion*. Springer, pp. 95–106.
- Ruff, C., Holt, B. & Trinkaus, E. (2006) Who's afraid of the big bad Wolff?: "Wolff's law" and bone functional adaptation. *American Journal of Physical Anthropology*, 129(4), 484–498.
- Ruff, C.B. & Runestad, J.A. (1992) Primate limb bone structural adaptations. *Annual Review of Anthropology*, 21, 407–433.
- Saers, J.P., Cazorla-Bak, Y., Shaw, C.N., Stock, J.T. & Ryan, T.M. (2016) Trabecular bone structural variation throughout the human lower limb. *Journal of Human Evolution*, 97, 97–108.
- Samuel, D.S., Nauwelaerts, S., Stevens, J.M. & Kivell, T.L. (2018) Hand pressures during arboreal locomotion in captive bonobos (*Pan paniscus*). *Journal of Experimental Biology*, 221(8), jeb170910.
- Sancho-Bru, J.L., Mora, M.C., León, B.E., Pérez-González, A., Iserete, J.L. & Morales, A. (2014) Grasp modelling with a biomechanical model of the hand. *Computer Methods in Biomechanics and Biomedical Engineering*, 17(4), 297–310.
- Sarringhaus, L.A. (2013) *Positional and morphological development of wild chimpanzees, Pan Troglodytes* (PhD dissertation). The University of Michigan.
- Sarringhaus, L.A., MacLatchy, L.M. & Mitani, J.C. (2014) Locomotor and postural development of wild chimpanzees. *Journal of Human Evolution*, 66, 29–38.

- Schaffler, M.B., Burr, D.B., Jungers, W.L. & Ruff, C.B. (1985) Structural and mechanical indicators of limb specialization in primates. *Folia Primatologica*, 45(2), 61–75.
- Scherf, H., Harvati, K. & Hublin, J.J. (2013) A comparison of proximal humeral cancellous bone of great apes and humans. *Journal of Human Evolution*, 65(1), 29–38.
- Schmitt, D., Zeining, A. & Granatosky, M.C. (2016) Patterns, variability, and flexibility of hand posture during locomotion in primates. In: Kivell, T.L., Lemelin, P., Richmond, B.G. & Schmitt, D. (Eds.) *The evolution of the primate hand*. Springer, pp. 345–369.
- Schilling, A.M., Tofanelli, S., Hublin, J.J. & Kivell, T.L. (2014) Trabecular bone structure in the primate wrist. *Journal of Morphology*, 275(5), 572–585.
- Sparacello, V.S., Dori, I., Rossi, S., Varalli, A., Riel-Salvatore, J., Gravel-Miguel, C. et al. (2021) New human remains from the late Epigravettian necropolis of Arene Candide (Liguria, northwestern Italy): direct radiocarbon evidence and inferences on the funerary use of the cave during the younger dryas. *Quaternary Science Reviews*, 268, 107131.
- Stephens, N.B., Kivell, T.L., Pahr, D.H., Hublin, J.J. & Skinner, M.M. (2018) Trabecular bone patterning across the human hand. *Journal of Human Evolution*, 123, 1–23.
- Stern, J.T., Jr., Jungers, W.L. & Susman, R.L. (1995) Quantifying phalangeal curvature: an empirical comparison of alternative methods. *American Journal of Physical Anthropology*, 97(1), 1–10.
- Stern, J.T., Jr. & Susman, R.L. (1983) The locomotor anatomy of *Australopithecus afarensis*. *American Journal of Physical Anthropology*, 60(3), 279–317.
- Susman, R.L. (1974) Facultative terrestrial hand postures in an orangutan (*Pongo pygmaeus*) and pongid evolution. *American Journal of Physical Anthropology*, 40(1), 27–37.
- Susman, R.L. (1979) Comparative and functional morphology of hominoid fingers. *American Journal of Physical Anthropology*, 50(2), 215–236.
- Susman, R.L., Stern, J.T. & Jungers, W.L. (1984) Arboreality and bipedality in the Hadar hominids. *Folia Primatologica*, 43(2–3), 113–156.
- Susman, R.L. & Stern, J.T., Jr. (1979) Telemetered electromyography of flexor digitorum profundus and flexor digitorum superficialis in *Pan troglodytes* and implications for interpretation of the OH 7 hand. *American Journal of Physical Anthropology*, 50(4), 565–574.
- Susman, R.L. (1984) The locomotor behavior of *Pan paniscus* in the Lomako Forest. In: Susman, R.L. (Ed.) *The pygmy chimpanzee*. Springer, pp. 369–393.
- Syeda, S.M., Tsegai, Z.J., Dunmore, C.J., Cazenave, M., Skinner, M.M. & Kivell, T.L. (2021) Inferring hand use in *Australopithecus sediba*: analysis of the external and internal morphology of hominin proximal and intermediate phalanges. *PaleoAnthropology*, 2021(1), 258.
- Synek, A., Lu, S.C., Nauwelaerts, S., Pahr, D.H. & Kivell, T.L. (2020) Metacarpophalangeal joint loads during bonobo locomotion: model predictions versus proxies. *Journal of the Royal Society Interface*, 17(164), 20200032.
- Thompson, N.E., Ostrofsky, K.R., McFarlin, S.C., Robbins, M.M., Rubinstein, D. & Almécija, S. (2018) Preliminary 3-D kinematic data of wild mountain gorilla terrestrial locomotion: using lab-based methods in ape environments. *American Journal of Physical Anthropology*, 165(S66), 274.
- Thompson, N.E., Patel, B.A., Stern, J.T., Jr. & Larson, S.G. (2019) 3-D kinematics, kinetics, and EMG of knuckle-walking in chimpanzees. *American Journal of Physical Anthropology*, 168, 246–247.
- Thorpe, S.K. & Crompton, R.H. (2006) Orangutan positional behavior and the nature of arboreal locomotion in Hominoidea. *American Journal of Physical Anthropology*, 131(3), 384–401.
- Thorpe, S.K., Holder, R. & Crompton, R.H. (2009) Orangutans employ unique strategies to control branch flexibility. *Proceedings of the National Academy of Sciences*, 106(31), 12646–12651.
- Tocheri, M.W., Orr, C.M., Jacofsky, M.C. & Marzke, M.W. (2008) The evolutionary history of the hominin hand since the last common ancestor of *Pan* and *Homo*. *Journal of Anatomy*, 212(4), 544–562.
- Tocheri, M.W., Orr, C.M., Larson, S.G., Sutikna, T., Jatmiko, Saptomo, E.W. et al. (2007) The primitive wrist of *Homo floresiensis* and its implications for hominin evolution. *Science*, 317(5845), 1743–1745.
- Trinkaus, E. & Ruff, C.B. (2012) Femoral and tibial diaphyseal cross-sectional geometry in Pleistocene *Homo*. *PaleoAnthropology*, 2012, 13–62.
- Tsegai, Z.J., Kivell, T.L., Gross, T., Nguyen, N.H., Pahr, D.H., Smaers, J.B. et al. (2013) Trabecular bone structure correlates with hand posture and use in hominoids. *PLoS One*, 8(11), e78781.
- Tsegai, Z.J., Skinner, M.M., Gee, A.H., Pahr, D.H., Treece, G.M., Hublin, J.J. et al. (2017) Trabecular and cortical bone structure of the talus and distal tibia in *Pan* and *Homo*. *American Journal of Physical Anthropology*, 163(4), 784–805.
- Tsegai, Z.J., Stephens, N.B., Treece, G.M., Skinner, M.M., Kivell, T.L. & Gee, A.H. (2017) Cortical bone mapping: an application to hand and foot bones in hominoids. *Comptes Rendus Palevol*, 16(5–6), 690–701.
- Tuttle, R., Basmajian, J.V., Regenos, E. & Shine, G. (1972) Electromyography of knuckle-walking: results of four experiments on the forearm of *Pan gorilla*. *American Journal of Physical Anthropology*, 37(2), 255–265.
- Tuttle, R.H. (1967) Knuckle-walking and the evolution of hominoid hands. *American Journal of Physical Anthropology*, 26(2), 171–206.
- Tuttle, R.H. (1969) Quantitative and functional studies on the hands of the Anthroidea. I. The Hominoidea. *Journal of Morphology*, 128(3), 309–363.
- Tuttle, R.H. & Watts, D.P. (1985) The positional behavior and adaptive complexes of *Pan gorilla*. In: Kondo, S. (Ed.) *Primate morphophysiology: Locomotor analyses and human bipedalism*. University of Tokyo Press, pp. 261–288.
- Van Schaik, C.P., Fox, E.A. & Sitompul, A.F. (1996) Manufacture and use of tools in wild Sumatran orangutans. *Naturwissenschaften*, 83(4), 186–188.
- Vigouroux, L., Rossi, J., Foissac, M., Grélot, L. & Berton, E. (2011) Finger force sharing during an adapted power grip task. *Neuroscience Letters*, 504(3), 290–294.
- Wallace, I.J., Burgess, M.L. & Patel, B.A. (2020) Phalangeal curvature in a chimpanzee raised like a human: implications for inferring arboreality in fossil hominins. *Proceedings of the National Academy of Sciences*, 117(21), 11223–11225.
- Wei, P., Zhao, Y., Walker, C.S., He, J., Lu, X., Hui, J. et al. (2021) Internal structural properties of the humeral diaphyses in an early modern human from Tianyuan Cave, China. *Quaternary International*, 591, 107–118.
- Wennemann, S.E., Lewton, K.L., Orr, C.M., Almécija, S., Tocheri, M.W., Jungers, W.L. et al. (2022) A geometric morphometric approach to investigate primate proximal phalanx diaphysis shape. *American Journal of Biological Anthropology*, 177(3), 581–602.
- Williams-Hatala, E.M. (2016) Biomechanics of the human hand: From stone tools to computer keyboards. In: Kivell, T.L., Lemelin, P., Richmond, B.G. & Schmitt, D. (Eds.) *The evolution of the primate hand*. Springer, pp. 285–312.
- Williams-Hatala, E.M., Hatala, K.G., Gordon, M., Key, A., Kasper, M. & Kivell, T.L. (2018) The manual pressures of stone tool behaviors and their implications for the evolution of the human hand. *Journal of Human Evolution*, 119, 14–26.
- Wunderlich, R.E. & Jungers, W.L. (2009) Manual digital pressures during knuckle-walking in chimpanzees (*Pan troglodytes*). *American Journal of Physical Anthropology*, 139(3), 394–403.

Zeininger, A., Richmond, B.G. & Hartman, G. (2011) Metacarpal head biomechanics: A comparative backscattered electron image analysis of trabecular bone mineral density in *Pan troglodytes*, *Pongo pygmaeus*, and *Homo sapiens*. *Journal of Human Evolution*, 60(6), 703–710.

SUPPORTING INFORMATION

Additional supporting information can be found online in the Supporting Information section at the end of this article.

How to cite this article: Syeda, S.M., Tsegai, Z.J., Cazenave, M., Skinner, M.M. & Kivell, T.L. (2023) Cortical bone distribution of the proximal phalanges in great apes: implications for reconstructing manual behaviours. *Journal of Anatomy*, 243, 707–728. Available from: <https://doi.org/10.1111/joa.13918>

RESEARCH ARTICLE

Cortical bone architecture of hominid intermediate phalanges reveals functional signals of locomotion and manipulation

Samar M. Syeda¹  | Zewdi J. Tsegai²  | Marine Cazenave^{3,4,5}  |
Matthew M. Skinner⁴  | Tracy L. Kivell⁴ 

¹Skeletal Biology Research Centre, School of Anthropology and Conservation, University of Kent, Canterbury, UK

²Department of Organismal Biology and Anatomy, University of Chicago, Chicago, Illinois, USA

³Department of Anatomy, Faculty of Health Sciences, University of Pretoria, Pretoria, South Africa

⁴Department of Human Origins, Max Planck Institute for Evolutionary Anthropology, Leipzig, Germany

⁵Division of Anthropology, American Museum of Natural History (AMNH), New York, USA

Correspondence

Samar M. Syeda, Skeletal Biology Research Centre, School of Anthropology and Conservation, University of Kent, Canterbury, UK.
Email: ss2510@kent.ac.uk

Funding information

H2020 European Research Council, Grant/Award Number: 819960; HORIZON EUROPE Marie Skłodowska-Curie Actions, Grant/Award Number: 101025719

Abstract

Objectives: Reconstruction of fossil hominin manual behaviors often relies on comparative analyses of extant hominid hands to understand the relationship between hand use and skeletal morphology. In this context, the intermediate phalanges remain understudied. Thus, here we investigate cortical bone morphology of the intermediate phalanges of extant hominids and compare it to the cortical structure of the proximal phalanges, to investigate the relationship between cortical bone structure and inferred loading during manual behaviors.

Materials and Methods: Using micro-CT data, we analyze cortical bone structure of the intermediate phalangeal shaft of digits 2–5 in *Pongo pygmaeus* ($n = 6$ individuals), *Gorilla gorilla* ($n = 22$), *Pan spp.* ($n = 23$), and *Homo sapiens* ($n = 23$). The R package morphomap is used to study cortical bone distribution, cortical thickness and cross-sectional properties within and across taxa.

Results: Non-human great apes generally have thick cortical bone on the palmar shaft, with *Pongo* only having thick cortex on the peaks of the flexor sheath ridges, while African apes have thick cortex along the entire flexor sheath ridge and proximal to the trochlea. Humans are distinct in having thicker dorsal shaft cortex as well as thick cortex at the disto-palmar region of the shaft.

Discussion: Variation in cortical bone distribution and properties of the intermediate phalanges is consistent with differences in locomotor and manipulative behaviors in extant great apes. Comparisons between the intermediate and proximal phalanges reveals similar patterns of cortical bone distribution within each taxon but with potentially greater load experienced by the proximal phalanges, even in knuckle-walking African apes. This study provides a comparative context for the reconstruction of habitual hand use in fossil hominins and hominids.

KEYWORDS

cortical bone, functional morphology, hominin manual behaviors, internal bone structure, phalangeal morphology

This is an open access article under the terms of the [Creative Commons Attribution](https://creativecommons.org/licenses/by/4.0/) License, which permits use, distribution and reproduction in any medium, provided the original work is properly cited.

© 2024 The Authors. *American Journal of Biological Anthropology* published by Wiley Periodicals LLC.

1 | INTRODUCTION

Extant great apes and modern humans use a range of hand postures during positional (locomotor and postural) and manipulative behaviors (e.g., Kivell et al., 2020; Schmitt et al., 2016), which have been successfully linked to the morphological variation within great ape hands (Bird et al., 2021, 2022; Dunmore et al., 2019; Dunmore, Bardo, et al., 2020; Dunmore, Skinner, et al., 2020; Marchi, 2005; Matarazzo, 2008, 2015; Tsegai et al., 2013). This form-function link among extant taxa has been used to infer habitual manual activities of fossil taxa, ranging from Miocene apes (Almecija et al., 2009; Almécija et al., 2012; Susman, 2004) to fossil *Homo sapiens* (Bardo et al., 2020; Kivell et al., 2022; Stephens et al., 2018). Recent discoveries of hominin hand fossils have revealed mosaic morphologies suggesting hand use during both arboreal locomotion and dextrous manipulation (Dunmore, Skinner, et al., 2020; Kivell et al., 2015, 2018). Notably, the manual intermediate phalanges within the hominin fossil record show a mix of primitive and derived morphologies that suggest a diverse range of manual behaviors during the evolution of the hominin hand (Alba et al., 2003; Haile-Selassie & WoldeGabriel, 2009; Kivell et al., 2015, 2018, 2020; Larson et al., 2009; Napier, 1962; Susman & Creel, 1979). Functional inferences regarding manual behaviors of these fossil specimens have been made using elements of the carpus (Kivell et al., 2013; Marzke et al., 2010; Tocheri et al., 2007), the metacarpus (Dunmore, Skinner, et al., 2020; Galletta et al., 2019; Skinner et al., 2015) and the phalanges (Almecija et al., 2010; Kivell et al., 2015, 2018, 2022; Syeda et al., 2022), but the intermediate phalanges are relatively understudied. Here we build on our previous work (Syeda et al., 2023) and investigate variation in cortical bone structure of the intermediate phalanges of digits 2–5 (IP2–IP5) within the context of inferred hand use in humans and other extant hominids (*Pongo*, *Gorilla*, and *Pan*). We also conduct intra-digit comparisons of both the proximal and intermediate phalanges and discuss how the combined cortical structure of these two elements may reflect function of the fingers during manual behaviors.

Phalangeal external morphology, as well as the internal bone structure, have been shown to be functionally informative (Jungers et al., 1997; Karakostis et al., 2018; Matarazzo, 2008; Patel & Maiolino, 2016; Susman, 1979; Syeda et al., 2023). The structure of both cortical and trabecular bone can adapt in response to mechanical loading by removing bone in skeletal areas where stress is low and adding bone where stress is high (Barak et al., 2011; Currey, 2013; Pearson & Lieberman, 2004; Ruff et al., 2006) as well as by changing the orientation and alignment of the trabecular struts (Barak et al., 2011; Pontzer et al., 2006). Preserved cortical and trabecular architecture of fossil specimens of different limb elements has been used to infer locomotor behavior and manipulative activities (e.g., Cazenave et al., 2019; Chirchir, 2019; Dunmore, Skinner, et al., 2020; Georgiou et al., 2020; Ruff et al., 2016; Skinner et al., 2015; Su & Carlson, 2017; Zeininger et al., 2016; see also the review in Cazenave & Kivell, 2023). These behavioral reconstructions rely on understanding the relationship between bone structure and known behaviors of extant taxa.

1.1 | External morphology of the intermediate phalanges

Among great apes, external morphology of the intermediate phalanges is variable in the degree of longitudinal curvature, shape of the base, shaft, and trochlea, as well as a suite of morphological features on the palmar surface (Marzke et al., 2007; Patel & Maiolino, 2016; Susman, 1979; Syeda et al., 2021). These palmar morphological features include a median bar, lateral fossae, and the flexor sheath ridges (FSRs) (Figure 1). The median bar typically runs along the length of the palmar shaft with lateral fossae on either side and that are bounded by the FSRs (Marzke et al., 2007; Susman, 2004). The lateral fossae of the intermediate phalanges are traditionally thought to be attachment sites for the flexor digitorum superficialis (FDS) muscle (Marzke et al., 2007) and the size, depth and shape of these are quite variable across great apes (Susman, 1979) and throughout the fossil hominin record (Alba et al., 2003; Bush et al., 1982; Haile-Selassie & WoldeGabriel, 2009; Kivell et al., 2015, 2018, 2020; Larson et al., 2009; Napier, 1962; Pickering et al., 2018; Susman & Creel, 1979; Ward et al., 2012). The relative size and overall morphology of these fossae have been used to make functional inferences regarding the locomotion of fossil hominins (Bush et al., 1982; Day, 1978; Ricklan, 1987; Stern & Susman, 1983; Susman, 1979; Susman & Creel, 1979; Susman & Stern, 1979; Tuttle, 1981). The deep lateral fossae of *Australopithecus afarensis* and *Australopithecus africanus* intermediate phalanges have been interpreted as evidence of efficient power grasping, which would have allowed them to engage in climbing and suspensory locomotion despite having short fingers, with *A. africanus* also potentially participating in tool using activities (Ricklan, 1987; Stern & Susman, 1983; Susman et al., 1984). Similar inferences have been made for the intermediate phalanges of the OH 7 *Homo habilis* hand (Susman & Creel, 1979). While these previous studies have linked FSR morphology to the size and use of the FDS muscles, there is a lack of evidence linking the morphology of muscle attachment sites and the size of the muscle (Shrewsbury et al., 2003; Williams-Hatala et al., 2016; but see Karakostis et al., 2017). Furthermore, as the morphology of the intermediate phalanges is understudied, the functional implications of the variation observed in FSR morphology and the palmar median bar have remained relatively unexplored.

1.2 | Functional morphology of the intermediate phalanges

To date, only two studies, of which we are aware, have directly investigated the biomechanical and behavioral implications of palmar phalangeal morphology (Marzke et al., 2007; Nguyen et al., 2014). In a comparative anatomical study of primate intermediate phalanges, Marzke et al. (2007) showed that the FDS tendon does not exclusively insert onto the lateral fossae and, when it does, it does not occupy the whole fossa. Instead, the FDS tendon mainly inserted onto the FSRs at varying distances from the base, with the fibers running

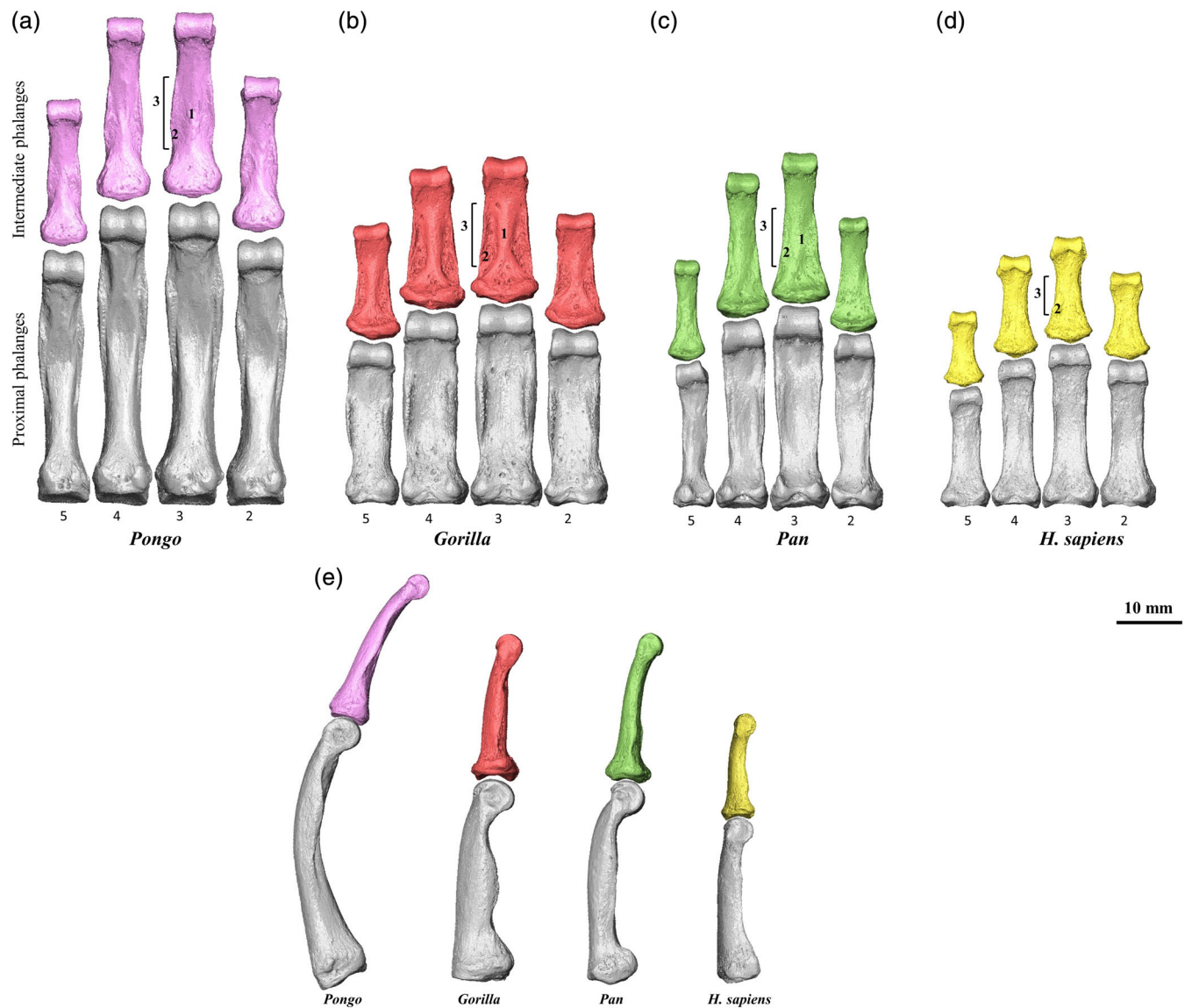


FIGURE 1 Surface models derived from micro-CT scans of proximal and intermediate phalanges of digits 2–5 from (a) *Pongo pygmaeus*, (b) *Gorilla gorilla*, (c) *Pan troglodytes*, and (d) *Homo sapiens* showing variation in external morphology. External morphological features are labelled: 1: Palmar median bar, 2: Lateral fossae, and 3: flexor sheath ridge. (e) Proximal and intermediate phalanges of the third digit in the ulnar view to demonstrate variation in longitudinal curvature across the sample.

towards different aspects of the palmar shaft (Marzke et al., 2007). The length of the lateral fossae also did not predict the cross-sectional area or length of the FDS tendon, concluding that the development of this external morphology cannot be explained by the FDS tendon attachments or the stresses associated with FDS muscle activity (Marzke et al., 2007). An alternative explanation of lateral fossae development proposed by Marzke et al. (2007) is that the lateral fossae could be a by-product of the median bar thickening and developing anteriorly in response to loading. This hypothesis is consistent with Begun et al. (1994) study of the pedal intermediate phalanges of *Proconsul* in which they posited that the palmar median bar reflects dorsopalmarly directed bending stresses that accompany the contraction of the power digital flexor muscles and substrate reaction forces. In contrast, Walker et al. (1993) suggested that the

palmar median bar could form as a result of the lateral fossae excavations, however, this hypothesis requires a functional explanation for the hollowing out of the palmar phalangeal shaft. While Marzke et al. (2007) focused on the shape and size of the lateral fossae, they did not explicitly explain or address the functional role and morphology of the FSRs. The work of Nguyen et al. (2014) sheds light on the biomechanical importance of the FSRs in the proximal phalanx of hylobatids. Using 3D microfinite element modeling, they showed that the larger FSRs experienced higher peak strains and were associated with lower peak strains on the palmar shaft, suggesting that taller FSRs helped to reduce the strain experienced by the palmar shaft (Nguyen et al., 2014). If the same is true for intermediate phalanges, this may help to explain variation in FSR development across hominoid taxa.

Variation in hominoid external intermediate phalangeal shape, especially regarding phalangeal curvature, FSR morphology and soft tissue anatomy, make functional interpretations in extant and fossil phalangeal form challenging. However, exploration of internal bone structure may provide more direct information about finger use. To date, only three studies have investigated the functional relationship between the internal bone morphology of intermediate phalanges and hand use behaviors (Doden, 1993; Matarazzo, 2015; Stephens et al., 2018). Doden (1993) showed that the intermediate phalanges of modern humans have thinner cortical bone towards the distal end, with overall thicker cortical bone on the dorsal surface of the phalanx and the midshaft having the highest density of bone. Matarazzo (2015) and Stephens et al. (2018) studied the trabecular structure of catarrhine and modern human phalanges, respectively, and noted a functional link between manual behaviors and the orientation and volume of trabecular bone.

We previously explored cortical bone distribution patterns and properties in the proximal phalanges of digits 2–5 (PP2–PP5) in extant great apes and showed that the pattern of cortical bone within the non-pollical proximal phalanges is capable of distinguishing varied hand postures employed by each taxon and corresponds with predicted loading during these hand postures (Syeda et al., 2023). Results also indicated that cortical bone patterns and properties reflect the variable digital loading within the hand of each taxon (Syeda et al., 2023). Here, we build upon this research and provide the first detailed, comparative study of the cortical morphology of extant hominid intermediate phalanges in digits 2–5. We examine cortical bone distribution patterns and cortical robusticity via cross-sectional geometry (CSG) in the phalangeal shaft to test whether these cortical properties reflect predicted loading differences during manual behaviors. We then discuss the cortical bone morphology of the intermediate phalanges alongside the proximal phalanges to provide a more holistic insight into the relationship between phalangeal morphology and hominid hand use.

1.3 | Predictions

1.3.1 | Inter-specific comparisons of cortical bone structure

We predict cortical bone distribution patterns will differ among the extant great apes, reflecting the presumed loading associated with the typical hand postures employed by each taxon. *Pongo* locomotor repertoire is dominated by suspensory, arboreal behaviors (Hunt, 1991; Thorpe & Crompton, 2006; but see Sarmiento, 1988; Susman, 1974; Tuttle, 1967) in which the hand wraps around the substrate using flexed-finger postures. We predict that the intermediate phalanges of *Pongo* will display a pattern of thick cortical bone on the midshaft-to-distal palmar surface, as the flexed finger posture of the phalanges will result in joint and substrate reaction forces that will load the phalanx in compression dorsally and tension palmarly, with the FSRs and longitudinal curvature of the phalanx helping reduce

overall strain experienced by the shaft (Nguyen et al., 2014; Preuschoft, 1973; Richmond, 2007).

The African apes (*Gorilla* and *Pan*) most often engage in knuckle-walking (on average ~90% of time spent locomoting, but this can vary substantially across groups and individuals; Hunt, 2020) and, less often, in arboreal behaviors (Doran, 1996, 1997; Hunt, 2020; Remis, 1998; Schaller, 1963; Tuttle & Watts, 1985). During knuckle-walking, the intermediate phalanges contact the substrate with the dorsal surface, the metacarpophalangeal (McP) joint is hyperextended, the PIP joint is hyperflexed, and the DIP joint is flexed (Inouye, 1994; Matarazzo, 2013; Thompson, 2020; Thompson et al., 2018; Tuttle, 1967). We predict *Gorilla* and *Pan* will share a similar pattern of cortical bone distribution, with an overall thick phalangeal shaft due to ground reaction forces being dissipated on the dorsal surface and large compressive forces from supporting body mass during knuckle-walking (Matarazzo, 2015; Wunderlich & Jungers, 2009).

Modern humans primarily use their hands for manipulation, employing power grips frequently, as well as power squeeze grips and precision grips between the finger pads and thumb (Dollar, 2014; Feix et al., 2015; Zheng et al., 2011). These grips most often result in flexion at the fingers, which will result in compressive and bending stresses on the dorsal surface of the relatively straight phalanges (Doden, 1993; Marzke, 1997; Preuschoft, 1973; Zheng et al., 2011). As such, we expect humans to have the thickest cortex on the dorsal surface of the phalanx.

Along with differences in cortical distribution patterns, we predict there will be differences in cortical thickness values across the phalanx and cross-sectional geometric (CSG) properties across the taxa. It is predicted the African apes will have relatively thicker mean cortical thickness and higher cross-sectional properties compared to *Pongo* and *H. sapiens*. *Pongo* will display cortical bone thickness and properties that are intermediate between the African apes and modern humans, as the gravitational forces associated with below-branch manual postures will be distributed across all three phalanges in each digit and thus loads experienced directly by the intermediate phalanx will be lower than those incurred during knuckle-walking. Human intermediate phalanges are predicted to have the thinnest cortices and weakest CSG properties compared to the other taxa, as the lower loads experienced during manipulation are predominant in humans and loading during locomotion is likely to be negligible in the human sample used in this study.

1.3.2 | Intra-specific comparisons of cortical bone structure

Given differences in loading among the digits during habitual hand postures, we also predict that cortical bone distribution, mean thickness and CSG properties will differ across the digits within each taxon. Within the African apes, captive *Gorilla* has been observed to load its digits 2–5 more evenly (but see Thompson et al., 2018) compared to captive *Pan*, which is more variable in its positional behavior (Doran, 1996; Doran & Hunt, 1996; Hunt, 1992; Inouye, 1994;

Matarazzo, 2013; Sarringhaus et al., 2014; Tuttle, 1969). Generally, in *Pan* digits 3 and 4 experience the greatest loads and digit 5 sometimes does not even touch down while knuckle-walking (Matarazzo, 2013; Samuel et al., 2018; Wunderlich & Jungers, 2009). Thus, *Gorilla* is predicted to have similar cortical bone distribution and properties across digits 2–5 while *Pan* is predicted to be more variable with greater cortical bone thickness and properties in the third digit (Samuel et al., 2018; Wunderlich & Jungers, 2009). In *Pongo*, cortical distribution, mean thickness and CSG properties are expected to be similar across the digits since *Pongo* is thought to typically use all four fingers in a similar manner during arboreal grasping (Rose, 1988; but see McClure et al., 2012). Within modern humans, we expect digit 2 and 3 to have thicker cortices and stronger CSG properties than digits 4 and 5 as experimental studies have shown greatest loads are experienced by the radial digits during modern human grasping (Cepriá-Bernal et al., 2017; De Monsabert et al., 2012; Sancho-Bru et al., 2014).

1.3.3 | Comparison of proximal and intermediate phalanges

We expect to observe similar relative patterns and interspecific differences in cortical morphology of the intermediate phalanges that we did in the proximal phalanges (PPs) (Syeda et al., 2023). Specifically, we expect *Pongo* and *H. sapiens* to show similar patterns between their respective IPs and PPs, while African apes will show greater differences between their phalangeal elements due to direct loading of the IPs during knuckle-walking.

2 | METHODS

2.1 | Sample

This study included high resolution micro-CT scans of intermediate phalanges of modern *H. sapiens* ($n = 23$ individuals, including recent and early modern specimens), *Pan* spp. ($n = 23$ individuals), *Gorilla gorilla* ($n = 22$ individuals), and *Pongo pygmaeus* ($n = 6$ individuals) for manual digit 2 ($n = 56$ elements), digit 3 ($n = 62$ elements), digit 4 ($n = 64$ elements), and digit 5 ($n = 53$ elements) (Table 1). Non-human specimens were adult wild-shot individuals with no indication of pathologies and included associated intermediate phalanges (IP) of digits 2–5 from a single hand. The human sample consists of adults

TABLE 1 Summary of the sample included in the study.

Taxon	N	IP2	IP3	IP4	IP5
<i>Homo sapiens</i>	23	15	19	18	1
<i>Pan paniscus</i>	6	6	5	6	5
<i>Pan troglodytes</i>	17	11	13	15	14
<i>Gorilla gorilla</i>	22	18	19	19	16
<i>Pongo pygmaeus</i>	6	6	6	6	5

from pre-industrial ($n = 6$) and post-industrial ($n = 7$) modern human populations, as well as nine fossil *H. sapiens* specimens (further detail on populations and fossil specimens are provided in Table S1). The majority (74%) of our human sample did not have all four associated digits and therefore we assigned phalanges to a digit using morphological characteristics described in Susman (1979) and Case and Heilman (2006). For individuals in our sample that had associated PPs (see Syeda et al., 2023), we compared cortical distribution and properties with the IPs.

2.2 | MicroCT data collection

Specimens were scanned using a BIR ACTIS 225/300, Diondo D3 or Skyscan 1172 scanner housed at the Department of Human Evolution, Max Planck Institute for Evolutionary Anthropology (Leipzig, Germany), a Nikon 225/XTH scanner at the Cambridge Biotomography Centre, University of Cambridge (Cambridge, UK), or with the Diondo D1 scanner at the Imaging Centre for Life Sciences University of Kent (Canterbury, UK). The scan parameters included acceleration voltages of 100–160 kV and 100–140 μ A using a 0.2–0.5 mm copper or brass filter. Scan resolution ranged between 0.018 and 0.044 mm depending on the size of the bone. Images were reconstructed as 16-bit TIFF stacks. All scans were cleaned (i.e., the removal of soft tissue or other non-bone material) and reoriented into a standard anatomical position using Avizo Lite 9.0.0 (Visualization Sciences Group, SAS). These scans were then segmented using medical image analysis (MIA), a clustering algorithm method (Dunmore et al., 2018).

2.3 | Analysis of cortical bone structure

The R package morphomap (Profico et al., 2021) was used to quantify cortical bone structure distribution and CSG properties. To prepare the data for analysis, we used Medtool v 4.5 (www.dr-pahr.at/medtool; Gross et al., 2014; Tsegai et al., 2013) on the original and MIA segmented scans, to define the inner and outer layer of cortical bone in the segmented scans. The protocol identified the external and internal border by casting rays in 3D and used morphological filters to fill the bone, which resulted in masks of the outer and inner region of cortical bone. These masks were converted into smooth external and internal surfaces for processing in morphomap using an in-house script for Paraview v 4.4 and Meshlab v 2020.03.

Prior to analysis, we extracted a region of interest (ROI) from the inner and outer surfaces that defined the phalangeal shaft in all taxa. This ensured that the cortical region analyzed was homologous across the morphologically variable phalangeal shafts of the hominid sample. The ROI was defined distally by the proximal end of the trochlea and proximally by the distal end of the base. Cortical morphology was quantified using the R package morphomap (Profico et al., 2021) and the methodological steps and parameters applied were following Syeda et al. (2023). Briefly, 97 cross sections were extracted between 2% and 98% of the length of the ROI at 1% increments and 50 equian-gular semi-landmarks were placed on each cross-section to capture

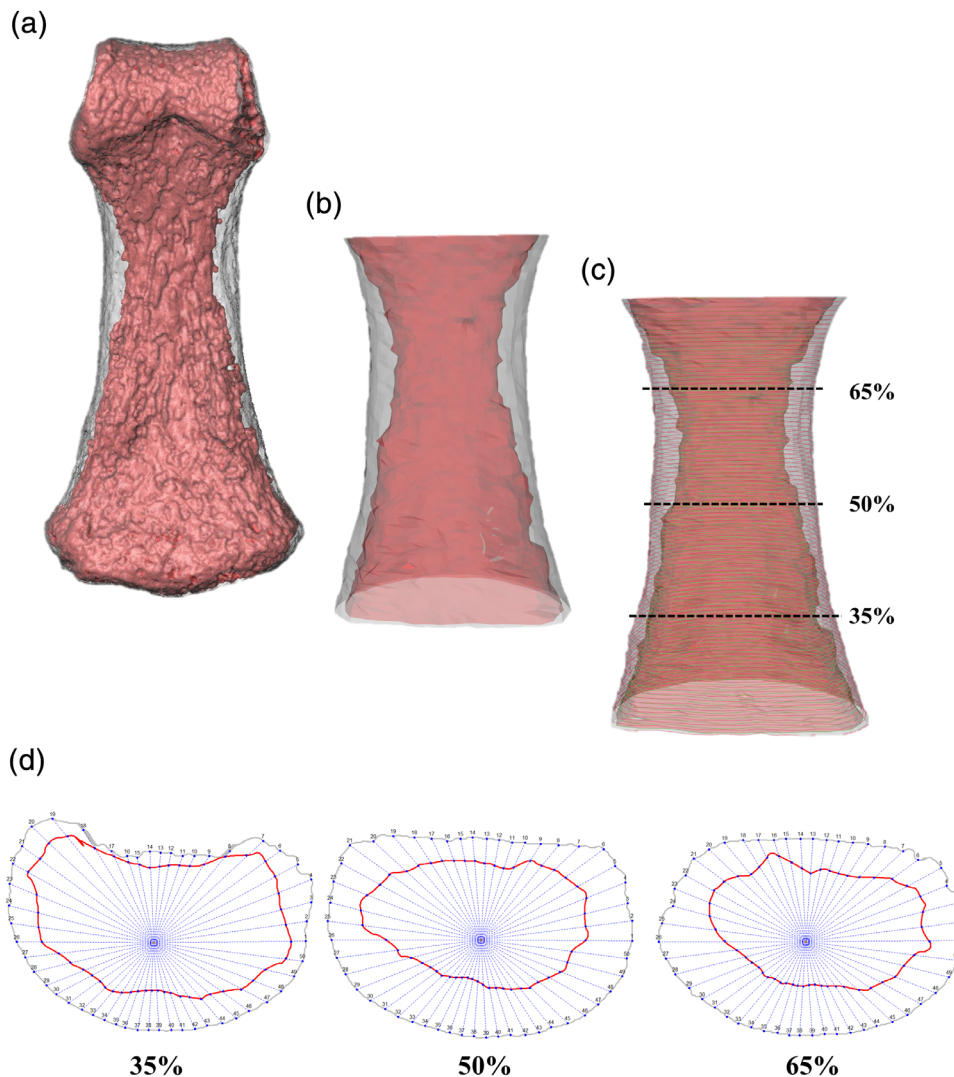


FIGURE 2 Images showing the steps taken in morphomap for cortical bone analysis in a human third intermediate phalanx. (a) External (gray) and internal (red) 3D surface model of the phalanx, (b) cut external and internal surfaces defining the ROI for input into morphomap, (c) cross-sections placed in 1% increments along the shaft to calculate cortical thickness with the dotted black lines indicating the cross-sectional levels at which cross-sectional properties were assessed, and (d) cross-sections at 35%, 50%, and 65% of the phalanx, depicting the landmarks placed on the external and internal outline.

the morphologically complex shape of the phalangeal shaft (Figure 2). To define these landmarks, rays were sent from the centroid of each cross-section outward, with cortical thickness calculated as the length of the segment between the landmarks placed on the internal and external outline. Morphometric maps of cortical bone distribution were used to visualize cortical bone distribution patterns for each individual. Mean morphometric maps were also created to visualize the overall pattern of cortical bone distribution of each digit within each taxon. To compare cortical thickness between the dorsal and palmar shaft, equiangular semi-landmarks were defined that excluded those placed on the flexor sheath ridges, that would bias measurements, and a ratio of dorsal to palmar mean cortical thickness was calculated.

2.4 | External morphological features

External morphological features (i.e., FSRs, median bar and phalangeal curvature depicted in Figure 1) of the intermediate phalanx were quantified to explore the potential relationship between external form and internal cortical architecture. We quantified phalangeal curvature

using the included angle method (Stern et al., 1995). The size of the median bar and FSRs was quantified using 3D metric measurements (Avizo Lite 9.0.0, Visualization Sciences Group, SAS). The size of the median bar was quantified from the palmar most protruding part of the bar to the palmar shaft (Figure S6). The size of the FSRs was quantified by measuring its depth (tallest point of the ridge to the palmar shaft) and its proximodistal length. The relationship between FSR and median bar morphology was only quantified in the IP3s of our sample.

2.5 | Cross-sectional geometry

Cross-sectional geometric properties quantifying the strength and rigidity of the phalangeal shaft of great apes were calculated across the shaft using morphomap (Profico et al., 2021). We analyzed cortical area (CA; measure of compressive and tensile strength), polar section modulus (Z_{pol} ; measure of maximum bending strength), and polar moment of area (J ; a measure of bending and torsional rigidity) at 35%, 50%, and 65% of the phalangeal length (Figure 3) to quantify variation in cortical bone strength properties across the phalangeal shaft.

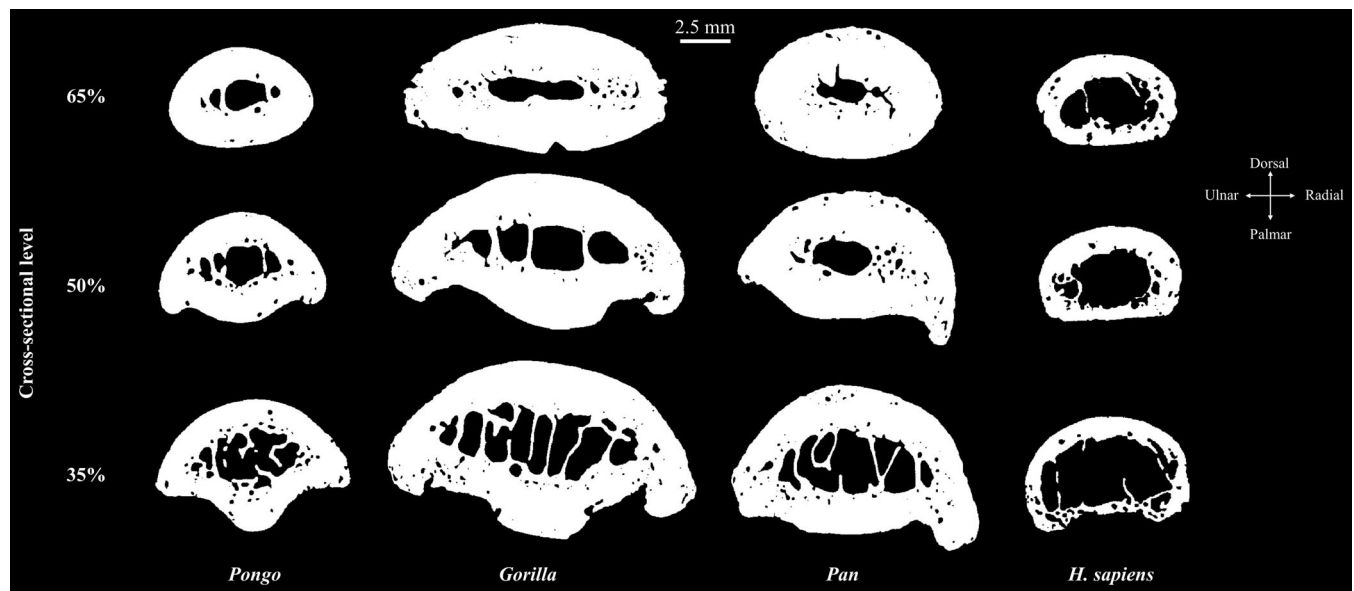


FIGURE 3 Cross-sections at 35%, 50%, and 65% of a third intermediate phalanx for each taxon. Cross-sections are scaled to relative size.

2.6 | Statistical analysis

Cortical bone thickness values, CSG properties, and metric measurements of the palmar shaft morphology were scaled by the inter-articular length of the phalanx. We also scaled our data by a geometric mean of several measurements of phalanx size, which yielded the same overall results. Thus, we chose to use phalangeal length alone to scale our data due to its direct relationship with bending stresses. First, to investigate cortical bone distribution patterns across the taxa, a principal component analysis (PCA) was conducted on the cortical thickness values of the entire shaft using R function *prcomp*. The PCA extremes were calculated from the results of the PCA, with the loadings at ± 2 standard deviations for each PC axis added to the mean morphometric map at each cell. Following the PCA, an omnibus permutational multivariate analysis of variance was conducted on the first three PC scores to test if these cortical bone distribution patterns were significantly different across the taxa. If results were statistically significant ($p < 0.05$), a pairwise one-way permutational multivariate analysis of variance with a Bonferroni correction was used to determine significant differences between the groups.

Second, to test for differences in cortical bone thickness of the shaft, mean differences were compared inter- and intra-generically using Kruskal–Wallis and post hoc Dunn tests. Wilcoxon signed-rank tests were conducted on the mean palmar and dorsal cortical thickness values to test whether they statistically differed. Regression analyses were used to assess whether a statistically significant relationship exists between cortical thickness of the shaft and degree of phalangeal curvature, as well as between cortical thickness and median bar height.

Additionally, each cross-sectional property (CA, Z_{pol} , and J) was analyzed at each cross-section (35%, 50%, and 65%) to test for inter- and intra-generically mean differences using Kruskal–Wallis and post hoc

Dunn tests. Further intra-generically testing evaluated mean differences in cross-sectional properties (CA, Z_{pol} , and J) within a phalanx at the different cross-sectional levels (35%, 50%, and 65%) using a Kruskal–Wallis test, followed by a post hoc Dunn test.

Finally, we compared cortical morphology of the intermediate phalanges with associated proximal phalanges, analyses of which were reported in our previous study (Syeda et al., 2023). The same data collection protocol was used to quantify cortical thickness in both the intermediate and proximal phalanges to ensure comparable results. We used Wilcoxon signed-rank tests to evaluate intra-generically mean differences in cortical thickness and cross-sectional properties between proximal and intermediate phalanges. We tested whether the mean cortical thickness of proximal and intermediate phalanges was significantly different across digits 2–5 of each taxon. The same tests were conducted for each cross-sectional property at each cross-section as well.

All statistical analysis was performed in R (v 4.1.3) and packages RVAideMemoire (v 0.9-79 Hervé, 2022), Stats (R Core Team, 2021), Vegan (v 2.5-7 Oksanen et al., 2020), and FSA (v 0.9.3 Ogle et al., 2022) were used.

3 | RESULTS

3.1 | Cortical bone distribution pattern and thickness

Mean morphometric maps of cortical bone distribution patterns in IP2–5 for each taxon are shown in Figure 4 and mean thickness data are presented in Table 2. Below we describe in detail the cortical bone distribution patterns and variation in scaled mean cortical thickness values for each taxon.

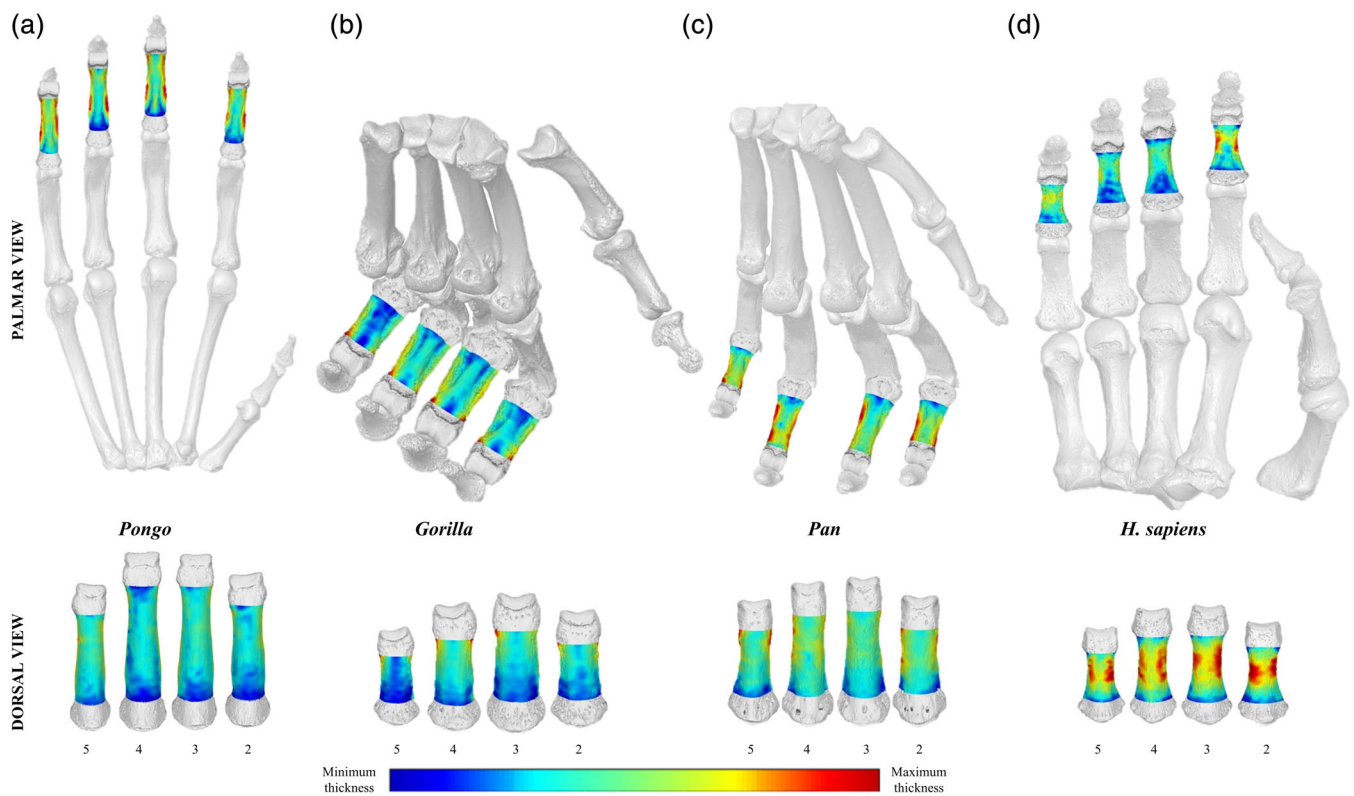


FIGURE 4 3D maps of cortical bone distribution across the intermediate phalanges in a representative individual of each taxon: (a) *Pongo pygmaeus*, (b) *Gorilla gorilla*, (c) *Pan troglodytes*, and (d) *Homo sapiens*. Thickness maps are independent of each other, and images are not to scale.

TABLE 2 Summary statistics of raw (mm) and standardized (dimensionless) cortical thickness measurements of the phalangeal shaft.

	<i>Homo sapiens</i>	<i>Pan</i>	<i>Gorilla</i>	<i>Pongo</i>
	Mean (SD)	Mean (SD)	Mean (SD)	Mean (SD)
Raw				
IP2	1.074 (0.300)	2.147 (0.289)	2.430 (0.361)	1.734 (0.240)
IP3	1.393 (0.383)	2.392 (0.342)	2.820 (0.387)	1.837 (0.300)
IP4	1.359 (0.387)	2.291 (0.293)	2.703 (0.457)	1.818 (0.250)
IP5	0.967 (0.264)	1.923 (0.346)	2.265 (0.428)	1.669 (0.300)
Standardized ^a				
IP2	0.042 (0.011)	0.068 (0.010)	0.070 (0.008)	0.047 (0.004)
IP3	0.047 (0.012)	0.058 (0.008)	0.067 (0.007)	0.042 (0.006)
IP4	0.046 (0.012)	0.061 (0.008)	0.068 (0.009)	0.041 (0.005)
IP5	0.046 (0.012)	0.070 (0.012)	0.073 (0.011)	0.046 (0.003)

^aStandardized by bone length.

3.1.1 | Cortical bone distribution patterns

Suspensory *Pongo* has thicker cortical bone on the peak of the FSRs and the region proximal to the trochlea, with the shaft ranging from

low to intermediate thickness relative to the regions of maximum thickness (Figure 4a). This pattern is generally similar across the four digits, with the exception of IP2 and IP5, where some individuals display cortical bone that is thicker on the ulnar FSR relative to the radial FSR (Figure 4a, Figure S1).

In knuckle-walking apes, thickest cortical bone is typically found from the FSRs up to the region proximal to the trochlea, while the cortical thickness of the shaft ranges from relatively low to intermediately thick (Figure 4b,c). However, compared to *Pan*, distribution of cortex of the *Gorilla* phalangeal shaft is generally low in thickness relative to its thick FSRs. Across *Gorilla* IP2–IP4, individuals that possess thick and prominent FSRs have a shaft relatively low in thickness, while individuals with relatively thinner and smaller FSRs have a shaft that is intermediate in its thickness (Figure 4b, Figure S1). In *Pan* individuals that do not possess prominent FSRs, only the region proximal to the trochlea is maximally thick while the remainder of the phalangeal shaft (including the FSRs) is relatively intermediate in its thickness (Figure 4c, Figure S1). Across the *Pan* hand, some individuals show thicker cortex radially in IP2 and IP3 compared to the ulnar surface.

The human pattern of cortical bone distribution is distinct from the other great apes, with the thickest cortical bone found on the dorsal midshaft-to-distal region as well as the disto-palmar region across the digits (Figure 4d, Figure S1). The FSRs, when present, are maximally thick as well.

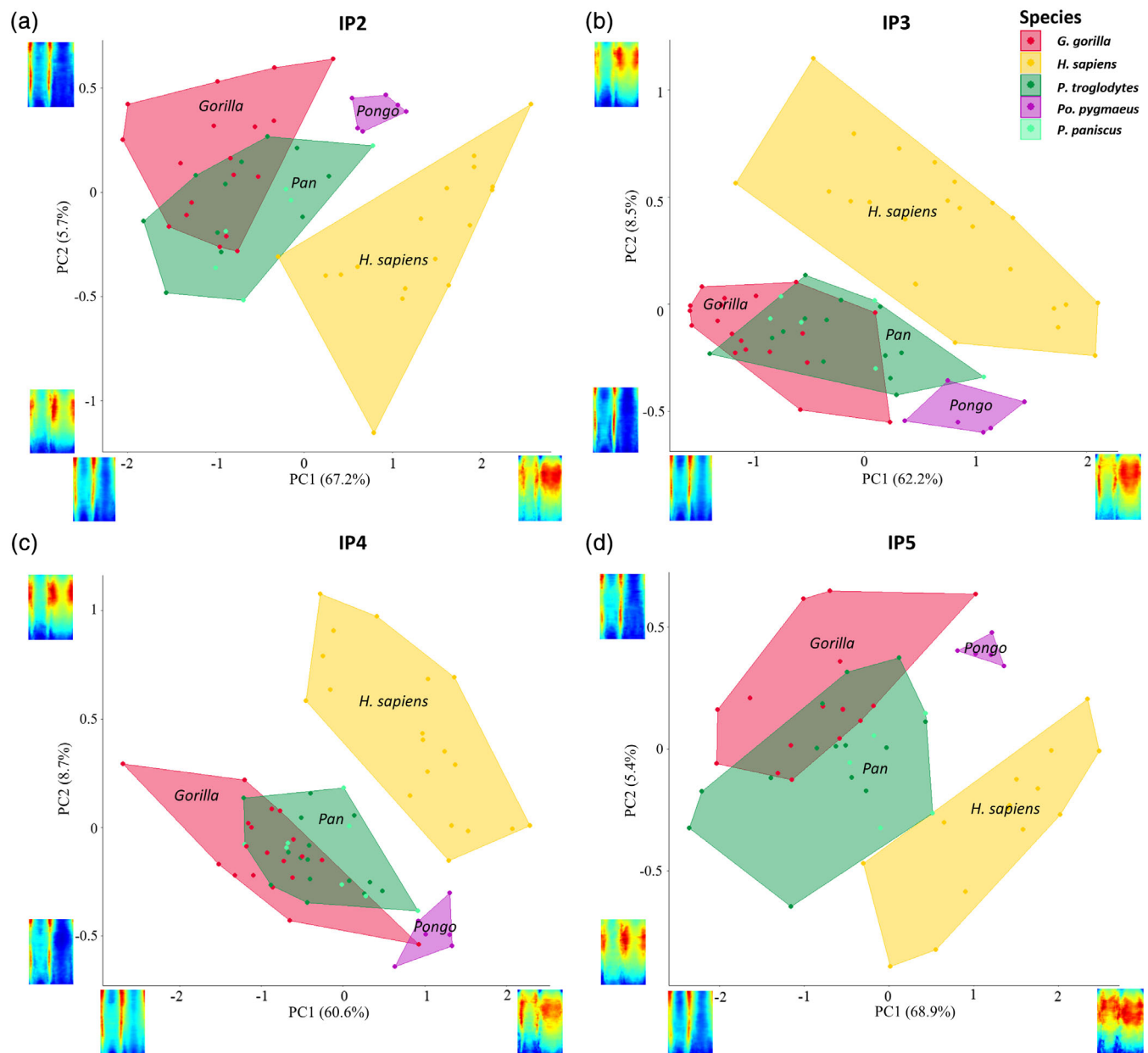


FIGURE 5 PC1 and PC2 for cortical bone distribution of intermediate phalanges of IP2, IP3, IP4, and IP5 of *Pongo*, *Gorilla*, *Pan* spp., and *Homo sapiens*.

3.1.2 | Cortical bone distribution variation across taxa

The PCA distinguishes taxa based on scaled cortical thickness distribution patterns of each phalanx. The results of the PCAs were similar between digits, with similar loadings and separation among the humans and non-human great apes (Figure 5; 3D PCA in Figure S2). PC1 explains between 60% and 69% of the total variance for each of the four digits. Low PC1 scores separate the African apes with relatively thicker FSRs and high PC1 scores distinguish humans with thicker cortex on the dorsal shaft along with thick radial and ulnar palmar cortex in IP2–IP4. IP5 distinguishes the species similarly, with the same loadings on low PC1 values, but high PC1 values represent thick midshaft-to-distal dorsal and palmar shaft thickness. African apes

variably overlap with each other, and *Pongo* is close to the humans and across all digits (Figure 5).

PC2 explains between 5% and 9% of the variance in the PCAs for each of the four digits and represents the region of overall maximum cortical thickness. Within IP2 and IP5, the nonhuman great apes are characterized by high PC2 scores, with maximum cortical thickness located on the palmar radial and ulnar surfaces, while humans have a wide range of PC2 scores with maximum cortical thickness located on the radial and ulnar surface of the mid-to-distal shaft. The PCA of IP3 and IP4 represents the same relative patterns, but the axes are flipped such that low PC2 scores generally characterize nonhuman great apes with thicker palmar radial and ulnar cortex and a wide range of PC2 values generally reflect humans having thicker cortical bone on the radial and ulnar surface of the mid-

TABLE 3 Significance values for post hoc comparisons of cortical thickness among species.

		<i>Pan</i>	<i>Gorilla</i>	<i>Pongo</i>
IP2	<i>Homo sapiens</i>	<0.001	<0.001	NS
	<i>Pan</i>		NS	0.021
	<i>Gorilla</i>			0.004
IP3	<i>Homo sapiens</i>	0.033	<0.001	NS
	<i>Pan</i>		NS	0.035
	<i>Gorilla</i>			<0.001
IP4	<i>Homo sapiens</i>	0.007	<0.001	NS
	<i>Pan</i>		NS	0.010
	<i>Gorilla</i>			<0.001
IP5	<i>Homo sapiens</i>	<0.001	<0.001	NS
	<i>Pan</i>		NS	0.034
	<i>Gorilla</i>			0.008

Note: The bold values are values that are statistically significant given a $p < 0.05$. Abbreviation: NS, not significant ($p > 0.05$).

to-distal shaft. Together, PC1 and PC2 generally separate humans from the other taxa in all rays.

3.1.3 | Mean cortical thickness

In interspecific comparisons, African apes have significantly thicker cortical bone than *Pongo* and *H. sapiens* across all digits (Table 3). No significant differences in cortical thickness were found between *Gorilla* and *Pan* or between *Pongo* and *Homo* in any digit. In comparisons of cortical thickness patterns across the hand, mean cortical thickness between the IPs does not significantly differ ($p > 0.05$) within *Pongo*, *Gorilla*, and *H. sapiens* (Figure S3). In contrast, in *Pan* mean cortical thickness of IP5 was significantly greater than that of IP3 and IP4, with mean cortical thickness of IP2 being significantly greater than IP3 as well (Figure S3).

3.1.4 | Mean cortical thickness across the shaft

Mean cortical thickness of the shaft reveals that all non-human great apes have a shared pattern across each of the four IPs (Figure 6). Mean cortical thickness increases up until the midshaft and from there remains consistent with the thickest cortex located at the distal end of the shaft. In contrast, in humans cortical thickness increases proximo-distally, peaking just distal to the midshaft and then decreases at the distal shaft in IP2–5.

3.1.5 | Palmar versus dorsal cortical thickness

A ratio of palmar and dorsal cortical thickness (Figure S4) reveals that within the *Pongo* digits, cortex on the palmar surface is significantly

thicker than the dorsal surface in all four digits except IP3 (Table 4). *Gorilla* and *Pan* have similar thickness values in the palmar and dorsal shaft, except in the *Gorilla* IP2 ($p = 0.033$) and *Pan* IP5 ($p = 0.045$) where the palmar cortex is significantly thicker. Across the human digits, the dorsal surface of the shaft has significantly thicker cortex than the palmar surface, with the exception of IP5 where there are no significant differences ($p > 0.05$).

3.2 | Cross sectional geometry

Descriptive statistics of the scaled cross-sectional geometric properties (CA, Z_{pol} , and J) at 35%, 50%, and 65% of the shaft are presented in Table S2 and depicted in Figures 7–9. There were differences across species in the different cross-sections in CA, Z_{pol} , and J for all four digits ($p < 0.05$), which are presented in Table S3.

In *Pongo*, CSG properties are similar in all cross-sections (35%, 50%, and 65%) (Figures 7–9), with no significant differences across IP2–IP5. Within *Gorilla*, IP3 is significantly greater than IP5 in all cross-sectional properties with some variation at the different cross-sectional levels (Table S4). At the 35% cross-section, there are no significant differences in CA across the *Gorilla* digits and at the 50% level, J of IP4 is also significantly greater than IP5. In *Pan*, the CSG properties across IP2–IP5 follow a similar pattern to that of *Gorilla*, with IP3 being significantly greater than IP5 in all CSG properties across the different cross-sections, with some variation in values of Z_{pol} and J at specific cross-sections (Table S4). In *H. sapiens* digits, only Z_{pol} of IP3 is significantly greater than IP5 and J of IP3 and IP4 greater than IP5 across all cross-sections (Table S4).

Analysis of intra-taxic differences in CSG properties at the different cross-sectional levels, reveal significant differences in CSG properties within the phalangeal shaft of *Gorilla*, *Pan*, and *H. sapiens* (Table S5). There are no significant differences across the *Pongo* digits. Within the *Gorilla* digits, CA at the midshaft of IP3 is significantly greater than at 65% of the shaft. Z_{pol} and J increase disto-proximally within the shaft, with values at the proximal end (35% of the shaft) being significantly greater than values at the distal end (65% of the shaft) in IP2–IP5 (Table S5). Within IP3, the values at the midshaft (50% of the shaft) are also significantly greater than values at the distal end (65% of the shaft). Mean values of all three CSG properties in *Pan* phalanges increase disto-proximally within the shaft (Table S2). In IP2–IP4, all CSG properties at the proximal end are significantly greater than the distal end the shaft, with values of Z_{pol} and J at the proximal end also being significantly greater than at the midshaft. Within IP5, only Z_{pol} and J at 35% of the shaft is greater than 65% of the shaft (Table S5). Within *H. sapiens*, CA is greatest at the midshaft and Z_{pol} and J increase disto-proximally, similar to *Pongo* and *Gorilla* (Figures 7–9; Table S2). There is little variation within the shaft of each digit such that only J at 35% of the shaft is greater than 65% of the shaft across IP2–4 and CA at 50% is significantly greater than 35% of the shaft only in IP2 (Table S5).

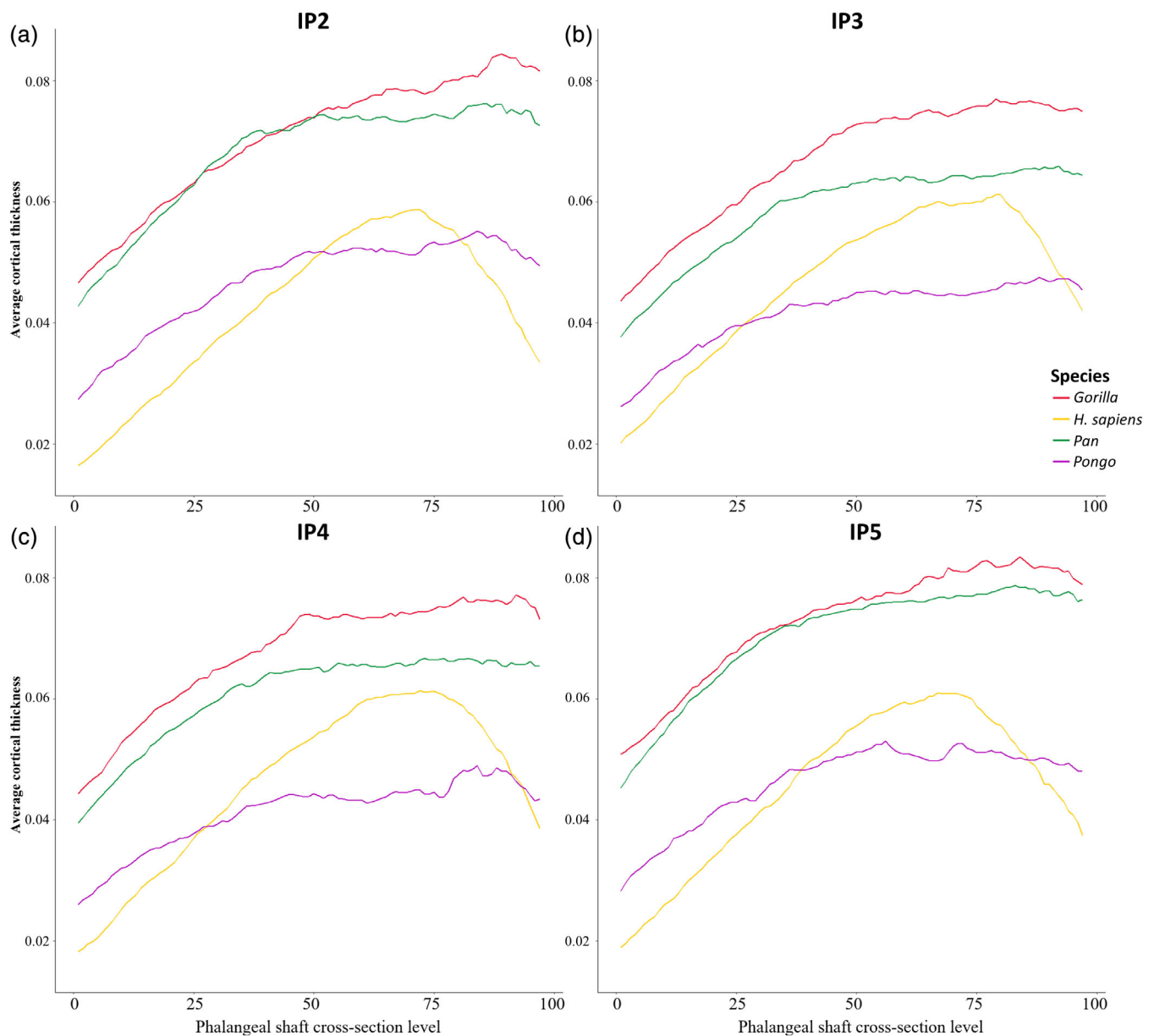


FIGURE 6 Average cortical bone thickness plotted from the proximal end (0) to the distal end (100) of the defined phalangeal shaft of *Pongo*, *Gorilla*, *Pan* spp., and *Homo sapiens*.

3.2.1 | Inter-taxic analysis of cross-sectional properties

Values of scaled cross-sectional properties are greatest in *Gorilla*, followed variably by *Pan* and *H. sapiens*, and are lowest in *Pongo* at the proximal end (35%) of the shaft. Distally (50% and 65% of the shaft) the pattern of CA is similar, but Z_{pol} and J is greatest in *Gorilla*, followed by *H. sapiens*, *Pan*, and *Pongo* (Table S2). Significance tests reveal *Gorilla* has significantly larger values of CA, Z_{pol} , and J across all digits and cross-sectional levels compared to the other taxa, except for Z_{pol} and J in IP5 at 50% cross-section (Table S3). At the 50% level in IP5, *Gorilla* is only greater than *Pan* in Z_{pol} and greater than *Pan* and *H. sapiens* in J . Overall, the remaining taxa, *Pongo*, *Pan*, and *H. sapiens*

are not significantly different from each other in any cross-sectional properties across the different levels, except for CA. Values of CA in the IP2 of *Pan* are significantly greater than that of *H. sapiens* at 35% of the shaft.

3.3 | Cortical thickness and external morphology

3.3.1 | Phalangeal curvature and cortical thickness

Regression analyses testing the relationship between phalangeal cortical thickness and curvature across the extant great apes reveal that there is no relationship between the cortical thickness and degree of

TABLE 4 Paired samples *t*-tests palmar versus dorsal thickness across species.

		<i>Homo sapiens</i>	<i>Pan</i>	<i>Gorilla</i>	<i>Pongo</i>
IP2	Palmar mean	0.035	0.061	0.062	0.046
	Dorsal mean	0.045	0.058	0.058	0.039
	<i>t</i> -ratio	-3.328	1.522	2.170	4.061
	<i>p</i>	<0.001	NS	0.033	<0.001
IP3	Palmar mean	0.037	0.053	0.057	0.040
	Dorsal mean	0.050	0.051	0.057	0.036
	<i>t</i> -ratio	-5.634	0.861	-0.222	2.021
	<i>p</i>	<0.001	NS	NS	NS
IP4	Palmar mean	0.036	0.056	0.058	0.041
	Dorsal mean	0.049	0.053	0.058	0.035
	<i>t</i> -ratio	-5.038	1.531	-0.016	2.757
	<i>p</i>	<0.001	NS	NS	0.013
IP5	Palmar mean	0.042	0.066	0.064	0.046
	Dorsal mean	0.047	0.062	0.062	0.038
	<i>t</i> -ratio	-1.689	2.036	1.158	4.992
	<i>p</i>	NS	0.045	NS	<0.001

Abbreviation: NS, not significant ($p > 0.05$). The bold values in are values that are statistically significant given a $p < 0.05$.

curvature of the intermediate phalanges of *Pan*, IP2 and IP4–IP5 of *Pongo*, IP2–IP4 of *Gorilla*, and IP3–IP5 of humans (Figure S5; Table S6). There is a significant but weak relationship between the curvature and cortical thickness of *Pongo* IP3 ($p = 0.030$ and $R^2 = 0.073$), *Gorilla* IP5 ($p = 0.022$ and $R^2 = 0.321$), and *H. sapiens* IP2 ($p = 0.024$ and $R^2 = 0.295$) (Table S6).

3.3.2 | Palmar surface morphology and cortical thickness

Testing the relationship between phalangeal cortical thickness, median bar height, FSR length, and FSR depth in the IP3 of our sample reveals weak but significant relationships between these variables in *Gorilla*, *Pan*, and *H. sapiens* (Tables S7–S9 and S11). Within these variables, there is no significant relationship between FSR length of median bar of extant hominid IP3s (Table S10).

3.4 | Comparison of proximal and intermediate phalanges

3.4.1 | Mean cortical thickness

Comparing scaled mean cortical thickness values in the proximal and intermediate phalanges of digits 2–5, cortical thickness values of the intermediate phalanges are significantly greater than the proximal phalanges across all taxa (Figure 10). However, the raw values reveal a different pattern for each species (Figure 11). In *Pongo*, there are no

significant differences between the raw cortical thickness of the proximal and intermediate phalanges. Within knuckle-walkers, *Gorilla* cortical thickness of the proximal phalanges is greater in digit 2 and 3, while in *Pan* all proximal phalanges have significantly thicker cortex than the associated intermediate phalanges. In humans, there are no significant differences across the digits except for digit 2 in which the cortical thickness of the proximal phalanx is significantly greater than that of its associated intermediate phalanx.

3.4.2 | Cross-sectional geometry

Analyzing relative CSG properties between the proximal and intermediate phalanges of digits 2–5 reveals greater variation in the mean values of Z_{pol} and J compared to CA. Across the digits and three cross-sections, there are no significant differences in the mean values of CA between the proximal and intermediate phalanges of *Pongo*, *Gorilla*, and *H. sapiens* (Table S12). *Pan* has significantly greater values of CA in the proximal phalanges of digits 2–4 at 35% and 65% of the shaft.

Mean values of Z_{pol} in *Pongo* are significantly greater in the proximal phalanx of digit 2 at 35% and 65% of the shaft ($p = 0.036$ and $p = 0.033$, respectively), and in the proximal phalanx of digit 3 at 50% and 65% of the shaft ($p = 0.035$ and $p = 0.003$, respectively) (Table S13). Within the proximal and intermediate phalanges of *Gorilla*, Z_{pol} values are significantly greater in the proximal phalanges across all digits and cross-sections. Mean Z_{pol} values of *Pan* are significantly greater in the proximal phalanges of digit 3 and 4 at 35% of the shaft, digit 2–4 at 50% of the shaft, and across all digits at 65% of the shaft (Table S13). Within the human proximal and intermediate phalanges, the proximal phalanx of digit 2 has significantly greater values than the intermediate phalanx at 35% and 50% of the shaft and across digits 2–4 at 65% of the shaft.

Across the digits of *Pongo*, relative mean values of J are greater in the proximal phalanx of digit 3 at 50% of the shaft and across digit 2–4 at 65% of the shaft (Table S14). Similar to the Z_{pol} values of *Gorilla*, mean values of J are significantly greater in the proximal phalanges of all four digits across all three cross-sections. Within the proximal and intermediate phalanges of *Pan*, the proximal phalanx of digit 4 has significantly greater values of J than the intermediate phalanx at 35% of the shaft. At 50% and 65% of the shaft, the proximal phalanges of all four digits have significantly greater values of J compared to the intermediate phalanges. The human proximal phalanges have significantly greater values of J for: digit 2 at 35% of the shaft, digit 2 and 3 at 50% of the shaft, and digit 2–4 at 65% of the shaft.

4 | DISCUSSION

Studies of internal structure of the hand have generally focused on the metacarpus and elements of the carpus, with the phalanges being comparatively understudied (e.g., Bird et al., 2022; Dunmore et al., 2019; Marchi, 2005; Skinner et al., 2015). Here, we investigated

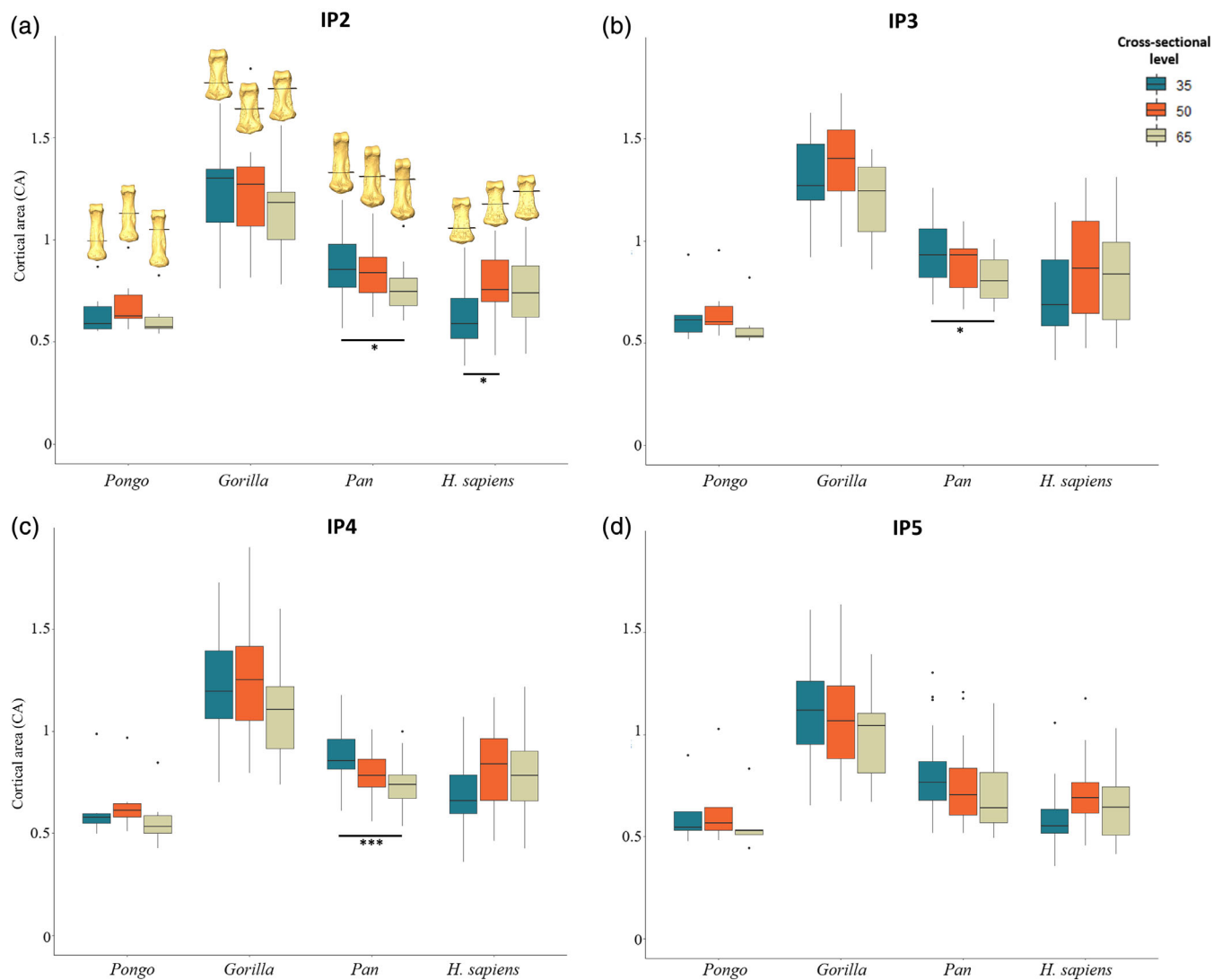


FIGURE 7 Cortical area (CA) for digits 2–5 of *Pongo*, *Gorilla*, *Pan* spp., and *Homo sapiens* at 35%, 50%, and 65% of the bone length. * $p < 0.05$; ** $p < 0.01$; *** $p < 0.001$.

variation in hominoid cortical bone distribution patterns of the intermediate phalanges of digits 2–5 in relation to hand use and postures, building upon our previous study of proximal phalanges in the same taxa (and specimens) (Syeda et al., 2023). Cortical bone distribution patterns, along with overall cortical bone thickness and CSG properties, were consistent with differences in hand use among suspensory *Pongo*, knuckle-walking *Gorilla* and *Pan*, and humans. Comparisons of cortical bone structure between the proximal and intermediate phalanges, provides greater insight into digit loading during manual behaviors.

4.1 | Extant great ape intermediate phalangeal cortical distribution, thickness and cortical properties

We predicted that cortical bone in *Pongo* would be thickest in the midshaft-to-distal palmar surfaces with no significant differences in

cortical structure across the digits, reflecting the flexed-finger, hook grip of all the fingers during suspensory behaviors (Rose, 1988; Sarmiento, 1988). Our predictions were supported. In *Pongo* regions of thickest cortical bone were located proximally on the FSRs and in the region proximal to the trochlea, with the remaining shaft having low to intermediate thickness across all IPs. This pattern reflects the known biomechanical role of the FSRs and phalangeal curvature, which is to reduce strain on the phalangeal shaft (Nguyen et al., 2014; Richmond, 2007). The lack of significant differences in cortical thickness and CSG properties across the digits is consistent with equal use and similar loading of all four digits during suspensory locomotion in *Pongo* (Rose, 1988; Susman, 1974; Thorpe & Crompton, 2006).

Within the African apes, we predicted that *Gorilla* and *Pan* would have a similar pattern of cortical bone distribution but would differ in their cortical bone properties across the digits. Our predictions were not fully supported. The general African ape pattern across the rays was characterized by thick cortical bone at the FSRs and proximal to

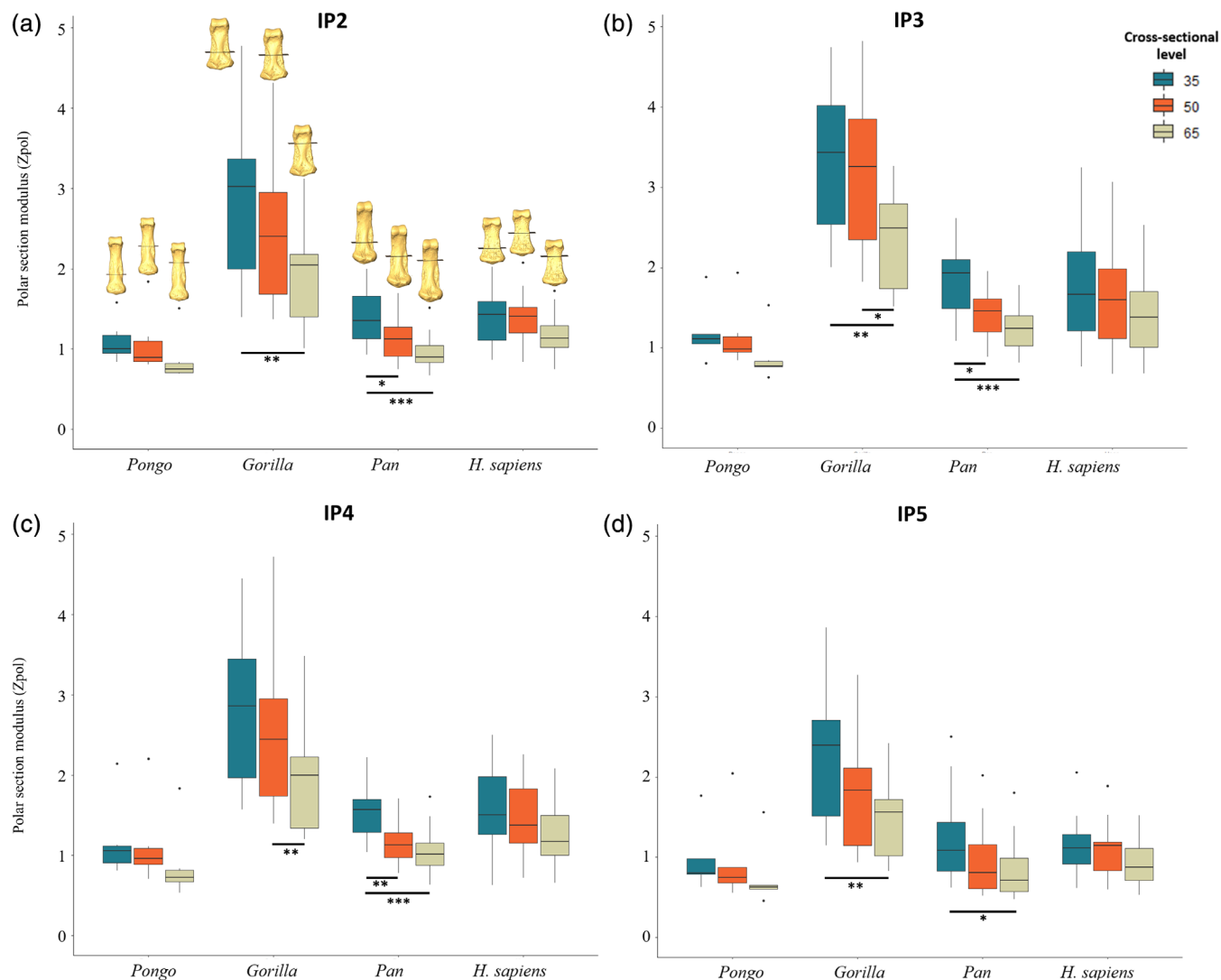


FIGURE 8 Polar section modulus (Z_{pol}) for digits 2–5 of *Pongo*, *Gorilla*, *Pan* spp., and *Homo sapiens* at 35%, 50%, and 65% of the bone length. * $p < 0.05$; ** $p < 0.01$; *** $p < 0.001$.

the trochlea, with a low to intermediately thick cortex along the shaft. This African ape pattern differs from *Pongo* in that the African ape FSRs generally span the majority of the proximodistal length of the phalanx, while in *Pongo* the FSRs are located on the proximal half of the shaft. The African ape pattern is surprising as EMG data on sub-adult chimpanzees has shown minimal to no activation of flexor muscles during knuckle-walking (Susman & Stern, 1979). However, a recent experimental study has shown stress is concentrated on pulleys, which hold the flexor tendon close to the bone during interphalangeal joint flexion (Leijnse et al., 2021). These pulleys arise from the radial and ulnar edges of the palmar surface, with annular pulleys A2 and A4 being the main pulleys within the fingers (Ayhan & Ayhan, 2020). The A4 pulley is located on the intermediate phalanges and Leijnse et al. (2021) have shown that stress is concentrated proximally on the A4 pulley, which coincides with the location of the FSRs. Although Marzke et al. (2007) found no relationship between the size of the FDS tendon and palmar phalangeal morphology, if the regions

of thickest cortex reflect stress related to the adjacent A4 pulley insertions, then cortical bone distribution patterns may be reflecting the role of the flexor muscles during different African ape manual behaviors that are not reflected in external morphology alone. These manual behaviors could include stretching of the flexor tendons during knuckle-walking (Leijnse et al., 2021) or activation of flexor muscles during arboreal grasping (Susman & Stern, 1979). While the overall pattern is generally similar, the majority (82%) of *Pan* individuals had an intermediately thick shaft while the majority (69%) of *Gorilla* individuals had a relatively thin shaft cortex. This difference may reflect the greater frequency of arboreal behaviors in *Pan* and thus flexor muscle activation, as well as differences in the external morphology (Hunt, 2020; Susman, 1979; Susman & Stern, 1979). *Gorilla* has a significantly lower degree of phalangeal curvature than *Pan*, while *Pan* has significantly smaller FSRs than *Gorilla* (Doran, 1996; Hunt, 1992; Sarringhaus et al., 2014; Susman, 1979; Syeda et al., 2021).

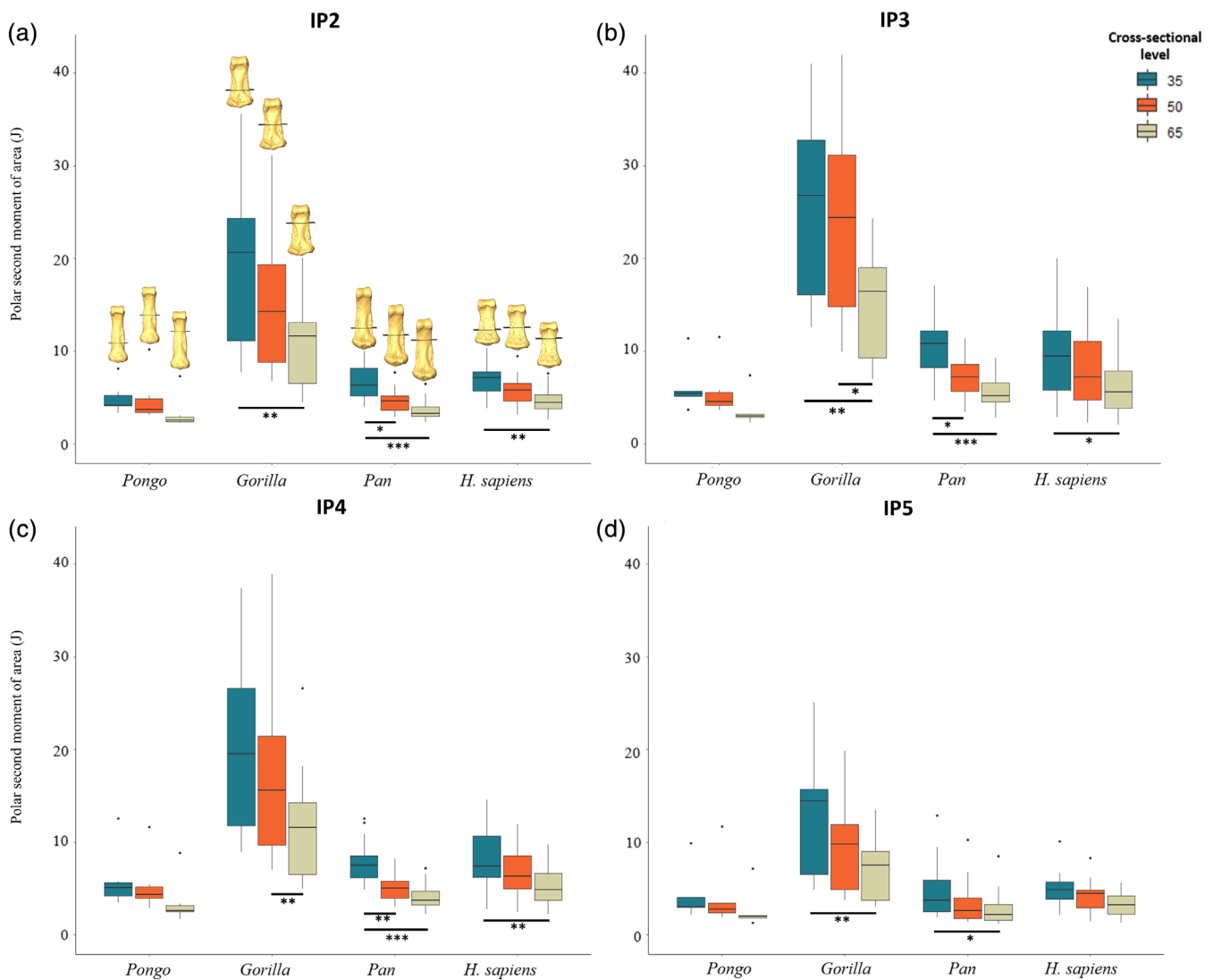


FIGURE 9 Polar second moment of area (J) for digits 2–5 of *Pongo*, *Gorilla*, *Pan* spp., and *H. sapiens* at 35%, 50%, and 65% of the bone length. * $p < 0.05$; ** $p < 0.01$; *** $p < 0.001$.

Along with differences in cortical bone distribution pattern between the African apes, cortical properties of the intermediate phalanges across the digits differ between *Gorilla* and *Pan*. This result is consistent with data from captive individuals showing differences in digit use and loading between these two taxa (Matarazzo, 2013; Samuel et al., 2018; Thompson, 2020; Wunderlich & Jungers, 2009). While recent observations of mountain gorillas in the wild show much greater variation in manual postures than in captivity (Thompson et al., 2018), zoo-housed *Gorilla* loads digits 2–5 more evenly than *Pan* (Matarazzo, 2013; Tuttle, 1969). This is reflected in the variation in cortical properties across the digits of the respective taxa. *Gorilla* mean cortical thickness does not significantly differ across the digits but CSG properties show that IP3 is significantly stronger than IP5, which is consistent with pressure studies that have shown greater loads occurring around the midline of the hand during knuckle-walking (Samuel et al., 2018; Tuttle et al., 1972). Contrary to our prediction, IP5 of *Pan* had significantly thicker cortical bone than IP3 and IP4, which are the digits that experience the highest loading

(Matarazzo, 2013; Samuel et al., 2018; Wunderlich & Jungers, 2009). However, the *Pan* IP3 did have CSG properties reflecting greater strength relative to IP5. The thicker cortex and weaker CSG properties of IP5 relative to IP3 may reflect the role of external morphological features in the modeling of internal bone structure. IP5 has smaller FSRs and a lower degree of phalangeal curvature (Susman, 1979; Syeda et al., 2021) that, all things being equal, would increase strain experienced by the shaft on the IP5 relative to the IP3 (Nguyen et al., 2014).

As predicted, human cortical bone was thickest on the distodorsal region, including in individuals that possess well-developed FSRs. This cortical bone distribution pattern may reflect the role of phalangeal curvature in dissipating forces across the phalanx. Typically, *H. sapiens* manual behaviors involve flexed-finger postures in which the dorsal surfaces of the phalanges experience high compressive forces and the palmar surfaces experience tensile forces. These bending forces dissipated across a relatively straight phalanx result in greater stress experienced by the dorsal surface (Preuschoft, 1973). Along with thick

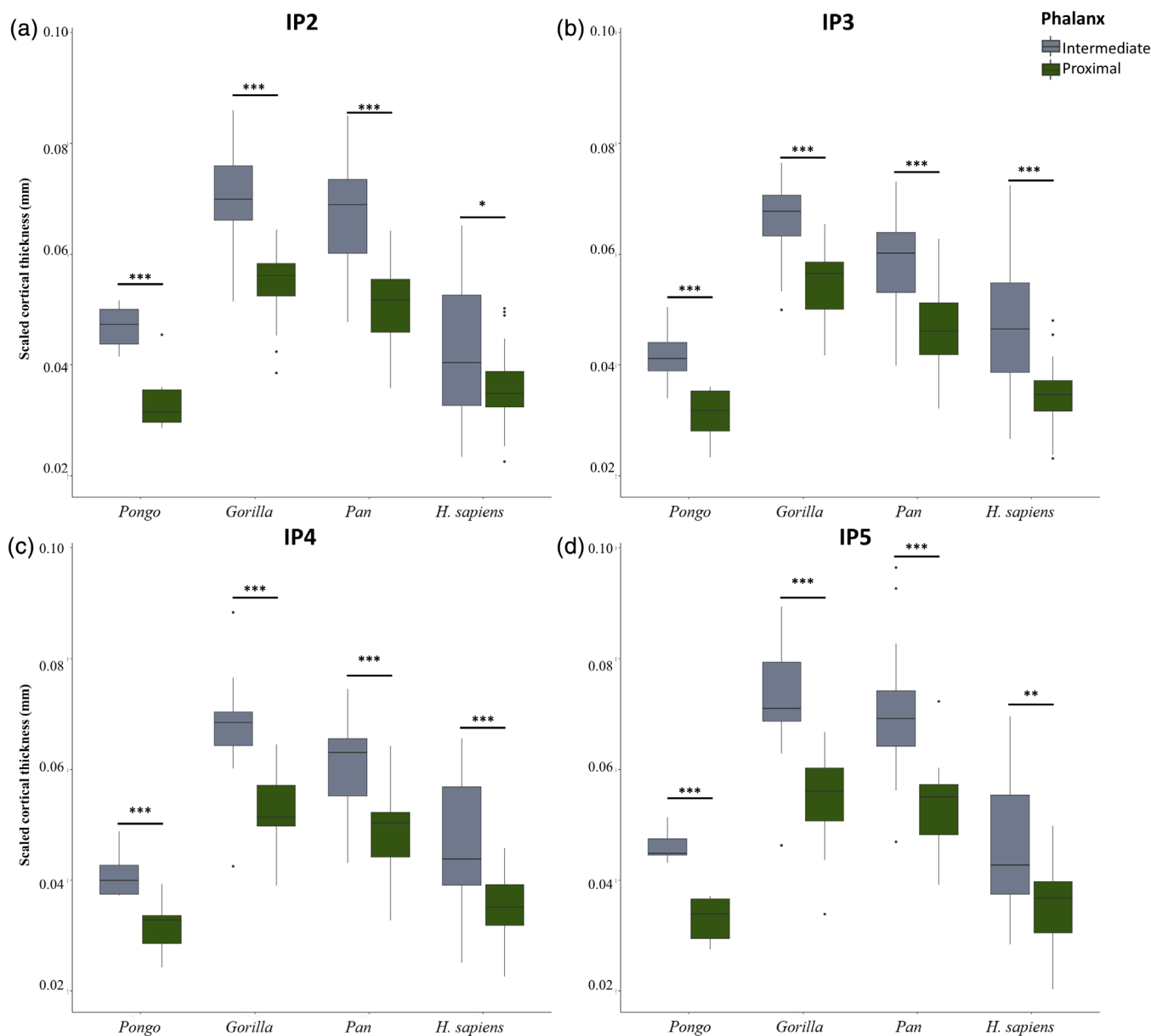


FIGURE 10 Scaled cortical thickness of the proximal and intermediate phalanges across (a) IP2; (b) IP3; (c) IP4; (d) IP5 of *Pongo*, *Gorilla*, *Pan* spp., and *Homo sapiens*. * $p < 0.05$; ** $p < 0.01$; *** $p < 0.001$. Intermediate phalanges have significantly thicker cortex in all taxa across the digits.

distodorsal cortex in humans, cortical bone on the distal palmo-radial and palmo-ulnar surfaces is thick irrespective of the presence of FSRs (Figure S1). In contrast, human proximal phalanges did not show consistently thick cortex at the radial and ulnar edges of the palmar surface (Syeda et al., 2023), suggesting that the pattern found in human IPs reflects the point of insertion of the FDS tendon. Across the hand, we predicted that digits 2 and 3 would have thicker cortices and stronger cortical properties than digits 4 and 5 as experimental studies have shown that greatest loads are experienced by the radial digits and the thumb (Cepriá-Bernal et al., 2017; De Monsabert et al., 2012; Sancho-Bru et al., 2014). However, our prediction is not supported; only IP3 was higher than IP5 in measures of bending strength (Z_{pol}) and only IP3 and IP4 were higher than IP5 in measures of bending

and torsional rigidity (J). The lack of distinct differences across the digits may reflect the presumed varied manual behaviors employed by our *H. sapiens* sample, which ranges from fossil specimens to a diverse range of pre- and post-industrial populations.

4.2 | Intermediate phalangeal pattern of cortical bone distribution compared to proximal phalanges

4.2.1 | *Pongo*

This cortical bone distribution pattern of *Pongo* IPs is similar to that of their PPs, further reflecting similar loading across the digits during

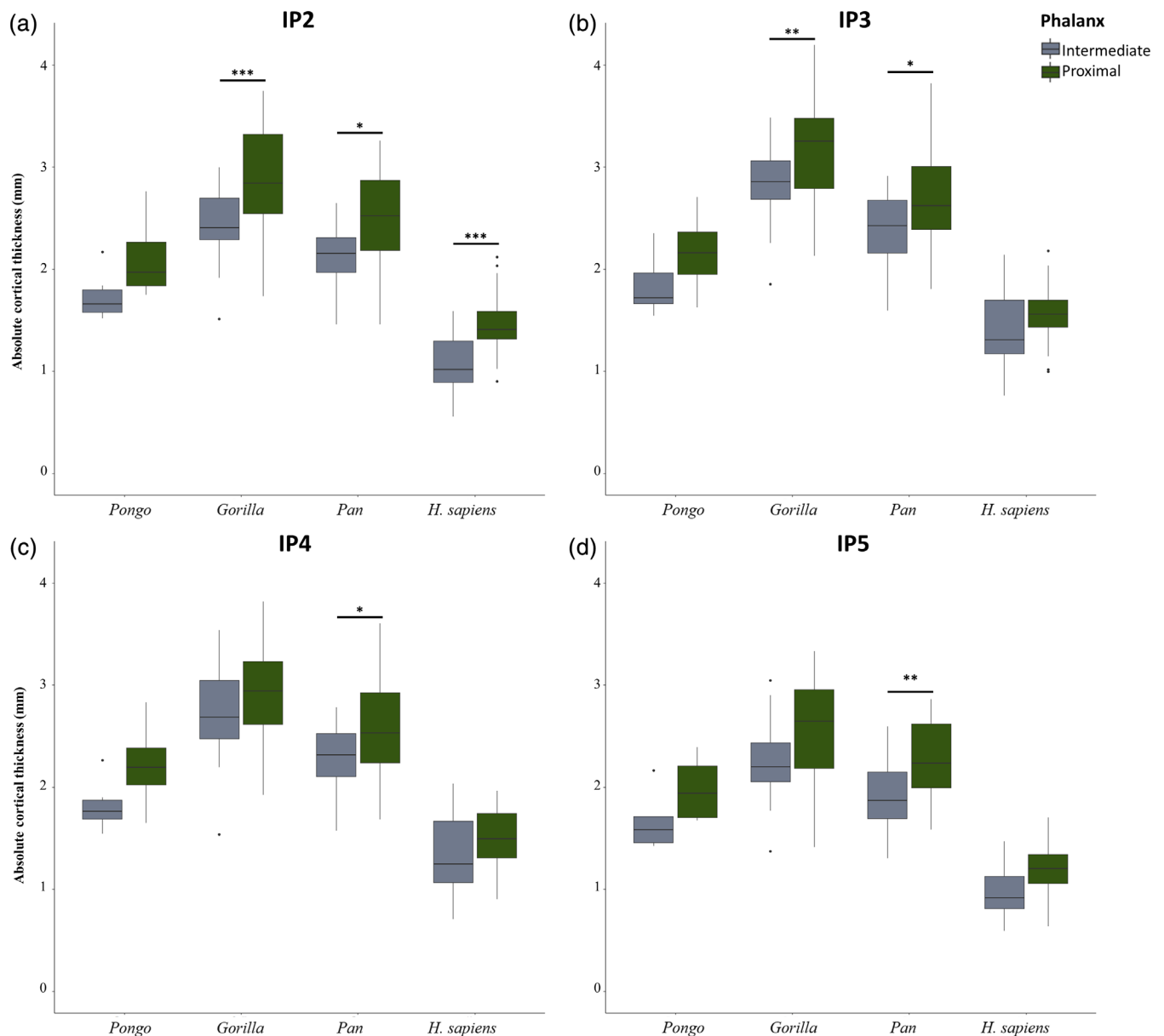


FIGURE 11 Absolute cortical thickness of the proximal and intermediate phalanges across (a) IP2; (b) IP3; (c) IP4; (d) IP5 of *Pongo*, *Gorilla*, *Pan* spp., and *Homo sapiens*. * $p < 0.05$; ** $p < 0.01$; *** $p < 0.001$.

flexed-fingered grips of the hand. It is an oversimplification to classify *Pongo* hand postural behaviors to just hook-like grips, as variation in *Pongo* locomotion and hand use has been increasingly observed (McClure et al., 2012; Thorpe & Crompton, 2006). However, we expect phalangeal cortical structure to reflect the repetitive hand postural behaviors of *Pongo*, which have generally been observed to be flexed-fingered grips (Napier, 1960; Rose, 1988). While the proximal and intermediate phalanges share a general pattern of thickness localized at the FSRs with an intermediately thick shaft, there is a slightly different pattern observed in PP2. The PP2 of some individuals showed thicker palmar radial cortex (Syeda et al., 2023), which was hypothesized to reflect greater extension of the second digit when

grasping thin substrates (Napier, 1960). However, if this hypothesis is correct, we would expect a similar cortical distribution on the IP2, which we did not find. Instead, our sample of IP2s has relatively thicker cortex on the ulnar, rather than radial, edge of the palmar surface in most individuals. However, our sample of intermediate phalanges is constrained to only six individuals and thus these patterns may reflect general variation within this taxon. Deducing more subtle differences in hand postures will require larger sample sizes and detailed observational, and ideally biomechanical, data on hand use during *Pongo* locomotion.

Comparing cortical thickness values and cross-sectional properties of *Pongo* intermediate and proximal phalanges revealed mixed

signals. Scaled average cortical thickness of the IPs was significantly greater than the PPs across all digits. However, bending strength of PP2 and PP3 was significantly higher than their IPs and the bending and torsional rigidity of digit 2–4 PPs was significantly greater than the IPs in the distal region of the shaft (65% cross-section). While the IPs had thicker cortices than the PPs on average, higher CSG values of the PPs relative to the IPs could reflect the disto-proximal increase in load across the digit (Cooney & Chao, 1977), such that the PPs are experiencing greater forces and are better structurally adapted to resist greater loads (Matarazzo, 2015).

4.2.2 | Gorilla

Similar to the pattern previously identified in the *Gorilla* PPs (Syeda et al., 2023), the regions of thickest cortical bone in the IPs coincides with attachment points of soft tissues that stabilize the interphalangeal joints. Cortical bone of the PPs was thickest in patches along the FSRs, while in the IPs thick cortical bone was found across the length of the FSRs. The FSRs of the IPs are located on the proximal half of the phalangeal shaft, and as stress is concentrated proximally at the A4 annular pulley (Leijnse et al., 2021), this thickness of the FSRs in the proximal region of the bone may reflect the stress that occurs when the FDS tendon is bent during knuckle-walking. Similarly, the cortical bone distribution pattern of the PPs may reflect FDS tendon bending that occurs distally at the A2 annular pulley. These similar patterns of thick cortical bone in regions that are thought to be stressed by FDS tendon stretching and phalangeal soft tissue attachment points may provide support for experimental evidence that suggests that, during knuckle-walking, stress is concentrated at the maximum bending point of the tendons and at the pulleys which hold these tendons close to the shaft (Leijnse et al., 2021). Alternatively, these patterns might be a signal of less frequent (relative to knuckle-walking) arboreal behaviors (Hunt, 2020) in which the flexor muscles are highly active (Susman & Stern, 1979).

Across the PPs and IPs of *Gorilla* digits 2–5, the average scaled IP cortical thickness was significantly thicker than the PPs. Along with their thick cortices, there was also greater variation within the CSG properties across phalangeal shaft in the IPs compared to that of the PPs, such that the CSG properties at the proximal end of the bone were significantly greater than at the distal end. However, bending strength and resistance to bending and torsional rigidity is significantly greater in the PPs relative to the IPs. These results could indicate that despite the IPs making the initial contact with the substrate and directly incurring the ground reaction forces during knuckle-walking, the proximal end of the IPs and the PPs, as a whole, are better able to resist the forces generated during manual behaviors. Across the PPs and IPs, digit 2 shows thicker palmar cortex, which may reflect the relatively small FSRs of digit 2 compared to digits 3 and 4 (Susman, 1979), however it does not explain why PP5 has relatively thicker palmar cortex but IP5 does not.

4.2.3 | Pan

The pattern of cortical bone distribution of *Pan* IPs was similar to that reported for the PPs (Syeda et al., 2023), in that the region of thickest cortical bone was located proximodistally along the FSRs. Across our sample, *Pan* was the only taxon that showed differences in mean cortical thickness across the digits within its PPs and IPs. The proximal and intermediate phalanx of digit 5 had significantly thicker cortical bone than the proximal and intermediate phalanx of digit 3. However, the CSG properties of digit 3 were significantly greater than digit 5. This may be because the external morphological features of digit 5 (i.e., tall FSRs, phalangeal curvature) are not as prominent as they are in the other radial digits. Thus, loads may not be dissipated as effectively in digit five, leading to higher strains experienced by the shaft, increased cortical bone modeling and thus thicker cortical bone compared with digit 3, in which external morphological features are most pronounced (Nguyen et al., 2014; Susman, 1979). Average cortical thickness was greater in the IPs while the PPs had significantly stronger CSG properties than the IPs; a pattern similar to that found in *Gorilla*. As the primary mode of locomotion of *Gorilla* and *Pan* is knuckle-walking, these similarities in cortical bone structure of the PPs and IPs are expected.

4.2.4 | Homo sapiens

The cortical bone pattern of *H. sapiens* IPs was similar to that found in their PPs (Syeda et al., 2023) in that the thickest region of cortical bone was concentrated at the distodorsal surface of the phalanges. However, the IPs were distinct in also having thick cortical bone along the distodorsal region of the palmar surface (regardless of the development of the FSRs). There were no significant differences in cortical thickness across the digits in either the PPs or the IPs and the dorsal cortex was consistently thicker than the palmar cortex, except for in IP5. In IP5, similar dorsal and palmar cortical thickness may indicate that IP5 is not being loaded in the same manner as the other phalanges. This has been noted in an experimental study of load distribution during power grips, in which the fifth digit does not remain active throughout the length of a gripping task in contrast to the remaining digits (Sancho-Bru et al., 2014). This is also reflected in the CSG properties of the PPs and IPs, with CSG properties in the PPs of digits 2–4—but not digit 5—being significantly stronger than the IPs. The absence of differences in the CSG properties of the phalanges of digit 5 may reflect overall lower levels of loading for this digit.

4.3 | Relationship between proximal and intermediate cortical bone thickness

While the pattern of cortical bone distribution was similar in the proximal and intermediate phalanges within our study taxa, the scaled values of mean cortical thickness were not. Intermediate phalanges on

average had thicker cortical bone in the phalangeal shaft when scaled to the length of the bone. This could be due to many factors. First, external morphological features that are thought to help resist forces are generally less developed in the IPs compared to the PPs (i.e., degree of curvature; development of FSRs). Therefore, the relative cortical thickness in the intermediate phalanges may need to be greater to withstand higher bone strain experienced by the shaft. Second, the FDS tendons insertion site is located on the intermediate phalanges, whereas they are only passing across the proximal phalanx (with pulleys inhibiting the buckling of the tendon). Therefore, the majority of the internal forces exerted by these muscular tendons are likely incurred by the intermediate phalanges. Finally, it could be that the relationship between bone length and required cortical thickness is not linear such the minimum amount of cortical bone needed when scaled for length is larger than that required for longer proximal phalanges.

Comparing absolute values of PP and IP cortical thickness reveals a unique relationship between the two in each taxon (Figures 10 and 11). Similar values of absolute average cortical thickness across the PPs and IPs of *Pongo*, coupled with their thin cortex and low cross-sectional properties, may further reflect that, due to their external morphology minimizing strain on the phalangeal shaft, cortical modeling and thicker cortex might not be needed (Ruff et al., 2006; Syeda et al., 2023). Within the African apes, *Gorilla* had significantly thicker cortical bone in the PP of digits 2 and 3 while *Pan* had significantly thicker PP cortical structure across all digits. These results provide additional support for our inference that the PPs of African apes might be better adapted to the loads resulting from their manual behaviors compared to their IPs. Across *H. sapiens* digits, only digit 2 had significantly thicker cortical bone in the PP relative to the IP, while the remaining digits showed no differences. The absolutely thicker cortices of the PPs can be attributed to the absolutely larger size compared to the IPs, but the general lack of significant differences in PP and IP absolute cortical thickness of *Pongo*, *Gorilla*, and *H. sapiens* digits indicates phalangeal size is not the only factor impacting phalangeal cortical thickness.

4.4 | Phalangeal curvature

We found significant, but not strong, correlations between cortical thickness and the degree of curvature in the IPs and PPs (Syeda et al., 2023) in our sample. These results might therefore call into question the functional significance or plasticity of phalangeal curvature (see also Wallace et al., 2020). Phalangeal curvature has been shown to change throughout ontogeny based on the frequency of arboreality (Richmond, 1998) and has been experimentally demonstrated to reduce strain experienced by the (proximal) phalanx during suspensory loading (Nguyen et al., 2014; Richmond, 2007). If cortical thickness reflects loads incurred during life (Ruff et al., 2006), one might expect taxa with more curved phalanges to have thinner cortex or for humans to have more curved phalanges if they are habitually using flexed-finger postures. However, our results suggest that the

relationship between cortical bone thickness and curvature is more complex. Overall length of the phalanx and the shape and size of the flexor sheath ridges will also influence how loads are incurred by the phalanx, and the frequency and magnitude of external and internal loads are critical. For example, musculoskeletal modeling of the third digit shows that the ratio of (internal) tendon load relative to (external) fingertip force and bone load magnitude to fingertip force was 42% and 55% higher, respectively, in a bonobo than a human (Synek et al., 2019). Thus, we propose that loads incurred during flexed-finger postures in human manipulative activities are not of sufficient magnitude to stimulate plasticity in curvature, but are sufficient to cause cortical modeling of the dorsum (in comparatively straight phalanges).

4.5 | Flexor sheath ridges

The development of the FSRs has been linked to arboreal behaviors (Nakatsukasa et al., 2003) and our study supports the hypothesized biomechanical role of the FSR in reducing the strain on the phalangeal shaft (Nguyen et al., 2014). It can be called into question that FSRs will always be the thickest region of cortical bone within a phalanx because it is a bony projection. However, individuals with small FSRs, or with no FSRs, have a shaft that is relatively thicker compared with the phalangeal shaft thickness of individuals with larger FSRs (see individual specimens in Figure S1).

While an experimental study has explained the biomechanical function of the FSRs (Nguyen et al., 2014), ontogenetic development of the FSRs has yet to be studied. Currently there is a lack of evidence explaining the variability of the FSRs and the functional implications of this variability. For example, it is not clear as to why *Gorilla* have the most prominent FSRs among the extant great apes when at least mountain gorillas spend considerably less time engaging in arboreal locomotion than *Pan* and *Pongo* (Doran, 1997). We also observed variation in FSR morphology within *Pan*, with some individuals displaying FSRs that project minimally from the palmar shaft while others are quite prominent. This variation is present within both male and female individuals of *P. paniscus* and *P. troglodytes* and therefore sexual dimorphism and systemic differences in the skeleton within or between these two species cannot explain the differences in FSR morphology. Variation in FSR morphology may related to other aspects of external morphology, particularly the degree of phalangeal curvature. For example, large FSRs of *Gorilla* may be explained by their relatively straight phalanges while smaller FSRs in *Pan* reflect greater phalangeal curvature. More prominent FSRs in *Gorilla* relative to *Pan* might also be related to the larger forces external (body mass) and internal (e.g., tendon loads) that the *Gorilla* phalanges must withstand during knuckle-walking with more prominent FSRs providing a greater surface area to dissipate forces. However, such hypotheses would predict strong correlations in the development of FSR morphology and variation in phalangeal curvature and body mass (e.g., sex differences) that were not clear within our study sample. These hypotheses require experimental and developmental validation on larger sample sizes to confirm the functional implications of this bony morphology.

4.6 | Palmar median bar

Along with the FSRs, the functional morphology and the development of the palmar median bar and its (generally) accompanying lateral fossae are not well understood. The median bar is an anterior extension of cortical bone on the palmar surface and is typically assumed to have a biomechanical function (Tocheri et al., 2008). As such, we expected that the palmar cortical thickness of the phalangeal shaft would have been significantly thicker in taxa that possess well-developed median bars (i.e., *Pongo* and *Gorilla*). However, preliminary analyses on the IP3s of our sample, shows no evidence of a relationship between palmar median bar morphology and phalangeal cortical thickness. An alternate explanation for the presence of palmar median bar is that it is simply a by-product of the hollowing out of the lateral fossae. However, this hypothesis would imply thin cortical bone at the lateral fossae, which was not observed in our sample. Cortical thickness of the lateral fossae is similar to the thickness of the palmar shaft (except for FSRs) across our sample. Nonetheless, the palmar median bar morphology will affect the shape, distribution of load, and therefore the CSG and bending rigidity and strength is likely to be different. Ontogenetic and biomechanical analyses (e.g., via micro-finite element modeling) that allows on to test the potential functional role of these palmar features is needed to improve our understanding of the general form-function relationships and “trade-offs” of phalangeal external and internal morphology.

4.7 | Limitations

There are some limitations to our study that should be acknowledged. First, our study is founded upon the concept of bone functional adaptation (i.e., bone modeling occurs in response to loads incurred during life that influence both external shape and internal structure), but many other factors, such as genetics, age, sex, and hormones, can also influence bone structure (see review in Kivell, 2016). Furthermore, as CSG relies on beam theory (Lieberman et al., 2004), functional interpretations resulting from cross-sectional properties of bones that are less cylindrical (such as the IPs) may not be as robust or straightforward to interpret and thus should be interpreted with caution. However, there is evidence that (e.g., Gosman et al., 2013; Rodriguez et al., 2018) CSG properties of non-cylindrical regions of bone can be successfully linked to function. Ultimately, a thorough investigation into the relationship between external and internal morphology, alongside kinematic and musculoskeletal modeling, is needed to provide a holistic understanding of how great ape manual behaviors are reflected in variation in bone structure.

5 | CONCLUSION

Our results provide a detailed analysis of the internal structure of the great ape intermediate phalanges. Cortical bone structure of the

intermediate phalanges across the extant great apes reflected differences in hand postures during manual behaviors across the taxa and within the hand of each taxon. Results of this study coupled with the known cortical structure of the proximal phalanges, revealed a similar pattern of cortical bone distribution across the proximal and intermediate phalanges but greater load resistance by proximal phalanges. This demonstrates the functional signals that can be gleaned from the cortex of the proximal and intermediate phalanges of digits 2–5, which can be applied to the reconstruction of hand use in fossil hominins. It also highlights the importance of considering variation in external morphological features for the interpretation of the biomechanical environment that leads to variation in internal bone structure.

AUTHOR CONTRIBUTIONS

Samar M. Syeda: Conceptualization (equal); data curation (lead); formal analysis (lead); investigation (lead); methodology (lead); project administration (equal); visualization (lead); writing – original draft (lead); writing – review and editing (lead). **Zewdi J. Tsegai:** Funding acquisition (supporting); investigation (supporting); methodology (supporting); writing – review and editing (equal). **Marine Cazenave:** Investigation (supporting); methodology (supporting); writing – review and editing (equal). **Matthew M. Skinner:** Conceptualization (equal); data curation (supporting); funding acquisition (lead); investigation (supporting); methodology (supporting); resources (lead); software (lead); supervision (supporting); writing – review and editing (equal). **Tracy L. Kivell:** Conceptualization (equal); data curation (supporting); funding acquisition (lead); investigation (supporting); methodology (supporting); project administration (equal); resources (lead); software (lead); supervision (lead); writing – review and editing (lead).

ACKNOWLEDGMENTS

This project has received funding under the European Union's Horizon 2020 research and innovation programme for European Research Council Consolidator Grant #819960 (MMS and TLK) and Marie Skłodowska-Curie Action #101025719 (ZJT). For access to specimens we thank the following individuals/institutions: C. Boesch, Max Planck Institute for Evolutionary Anthropology; J.-J., Hublin, College de France; F. Mayer and C. Funk, Museum für Naturkunde – Leibniz Institute for Evolution and Biodiversity Science; I. Livne, Powell-Cotton Museum; E. Gilissen, Royal Museum for Central Africa; J. Moggi-Cecchi and S. Bortoluzzi, University of Florence; B. Grosskopf, Johann-Friedrich-Blumenback-Institute for Zoology and Anthropology, Georg-August University, Goettingen; V. Volpato, Frankfurt Senckenberg Museum; J. Svoboda, Science Academy of the Czech Republic; I. Herskovitz, Tel Aviv University; M. M. Lahr, the Duckworth Collection, University of Cambridge; A. D. Pascale, Museo Archeologico del Finale; A. Hildred, The Mary Rose Trust. Finally, we thank the editors and three anonymous reviewers whose helpful feedback improved previous versions of this manuscript.

CONFLICT OF INTEREST STATEMENT

The authors declare no conflict of interest.

DATA AVAILABILITY STATEMENT

Copies of all scans are curated by the relevant curatorial institutions that are responsible for the original specimens and access can be requested through each institution. The authors confirm that the data supporting the findings of this study are available from the corresponding author upon reasonable request.

ORCID

Samar M. Syeda  <https://orcid.org/0000-0003-1514-8086>

Zewdi J. Tsegai  <https://orcid.org/0000-0001-9041-4829>

Marine Cazenave  <https://orcid.org/0000-0001-7194-5958>

Tracy L. Kivell  <https://orcid.org/0000-0001-5087-0897>

REFERENCES

- Alba, D. M., Moyà-Solà, S., & Köhler, M. (2003). Morphological affinities of the *Australopithecus afarensis* hand on the basis of manual proportions and relative thumb length. *Journal of Human Evolution*, 44(2), 225–254. [https://doi.org/10.1016/S0047-2484\(02\)00207-5](https://doi.org/10.1016/S0047-2484(02)00207-5)
- Almécija, S., Alba, D. M., & Moyà-Solà, S. (2009). Pierolapithecus and the functional morphology of Miocene ape hand phalanges: Paleobiological and evolutionary implications. *Journal of Human Evolution*, 57(3), 284–297. <https://doi.org/10.1016/j.jhevol.2009.02.008>
- Almécija, S., Alba, D. M., & Moyà-Solà, S. (2012). The thumb of Miocene apes: New insights from Castell de Barberà (Catalonia, Spain). *American Journal of Physical Anthropology*, 148(3), 436–450. <https://doi.org/10.1002/ajpa.22071>
- Almécija, S., Moyà-Solà, S., & Alba, D. M. (2010). Early origin for human-like precision grasping: A comparative study of pollical distal phalanges in fossil hominins. *PLoS One*, 5(7), e11727. <https://doi.org/10.1371/journal.pone.0011727>
- Ayhan, Ç., & Ayhan, E. (2020). Kinesiology of the wrist and the hand. In S. Angin & I. Simsek (Eds.), *Comparative kinesiology of the human body* (pp. 211–282). Academic Press.
- Barak, M. M., Lieberman, D. E., & Hublin, J. J. (2011). A Wolff in sheep's clothing: Trabecular bone adaptation in response to changes in joint loading orientation. *Bone*, 49(6), 1141–1151. <https://doi.org/10.1016/j.bone.2011.08.020>
- Bardo, A., Moncel, M. H., Dunmore, C. J., Kivell, T. L., Pouydebat, E., & Cornette, R. (2020). The implications of thumb movements for Neanderthal and modern human manipulation. *Scientific Reports*, 10(1), 1–12. <https://doi.org/10.1038/s41598-020-75694-2>
- Begun, D. R., Teaford, M. F., & Walker, A. (1994). Comparative and functional anatomy of Proconsul phalanges from the Kaswanga primate site, Rusinga Island. *Journal of Human Evolution*, 26(2), 89–165. <https://doi.org/10.1006/jhevol.1994.1008>
- Bird, E. E., Kivell, T. L., & Skinner, M. M. (2021). Cortical and trabecular bone structure of the hominoid capitate. *Journal of Anatomy*, 239(2), 351–373. <https://doi.org/10.1111/joa.13437>
- Bird, E. E., Kivell, T. L., & Skinner, M. M. (2022). Patterns of internal bone structure and functional adaptation in the hominoid scaphoid, lunate, and triquetrum. *American Journal of Biological Anthropology*, 177(2), 266–285. <https://doi.org/10.1002/ajpa.24449>
- Bush, M. E., Lovejoy, C. O., Johanson, D. C., & Coppens, Y. (1982). Hominid carpal, metacarpal, and phalangeal bones recovered from the Hadar Formation: 1974–1977 collections. *American Journal of Physical Anthropology*, 57(4), 651–677. <https://doi.org/10.1002/ajpa.1330570410>
- Case, D. T., & Heilman, J. (2006). New siding techniques for the manual phalanges: A blind test. *International Journal of Osteoarchaeology*, 16(4), 338–346. <https://doi.org/10.1002/oa.826>
- Cazenave, M., Braga, J., Oettlé, A., Pickering, T. R., Heaton, J. L., Nakatsukasa, M., Thackeray, J. F., de Beer, F., Hoffman, J., Dumoncel, J., & Macchiarelli, R. (2019). Cortical bone distribution in the femoral neck of *Paranthropus robustus*. *Journal of Human Evolution*, 135, 102666. <https://doi.org/10.1016/j.jhevol.2019.102666>
- Cazenave, M., & Kivell, T. L. (2023). Challenges and perspectives on functional interpretations of australopith postcrania and the reconstruction of hominin locomotion. *Journal of Human Evolution*, 175, 103304. <https://doi.org/10.1016/j.jhevol.2022.103304>
- Cepriá-Bernal, J., Pérez-González, A., Mora, M. C., & Sancho-Bru, J. L. (2017). Grip force and force sharing in two different manipulation tasks with bottles. *Ergonomics*, 60(7), 957–966. <https://doi.org/10.1080/00140139.2016.1235233>
- Chirchir, H. (2019). Trabecular bone fraction variation in modern humans, fossil hominins and other primates. *The Anatomical Record*, 302(2), 288–305. <https://doi.org/10.1002/ar.23967>
- Cooney, W. P., 3rd, & Chao, E. Y. (1977). Biomechanical analysis of static forces in the thumb during hand function. *The Journal of Bone and Joint Surgery*, 59(1), 27–36.
- Currey, J. D. (2013). In I. Bones (Ed.), *Bones*. Princeton University Press. <https://doi.org/10.1515/9781400849505>
- Day, M. H. (1978). Functional interpretations of the morphology of postcranial remains of early African hominids. In C. J. Jolly (Ed.), *Early hominids of Africa* (pp. 311–345). St Martin's Press.
- De Monsabert, B. G., Rossi, J., Berton, E., & Vigouroux, L. (2012). Quantification of hand and forearm muscle forces during a maximal power grip task. *Medicine and Science in Sports and Exercise*, 44(10), 1906–1916. <https://doi.org/10.1249/MSS.0b013e31825d9612>
- Doden, E. (1993). The relationship between the function and the inner cortical structure of metacarpal and phalangeal bones. In H. Preuschoft & D. J. Chivers (Eds.), *Hands of primates* (pp. 271–284). Springer. https://doi.org/10.1007/978-3-7091-6914-8_19
- Dollar, A. M. (2014). Classifying human hand use and the activities of daily living. In R. Balasubramanian & V. J. Santos (Eds.), *The human hand as an inspiration for robot hand development* (pp. 201–216). Springer. https://doi.org/10.1007/978-3-319-03017-3_10
- Doran, D. M. (1996). Comparative positional behavior of the African apes. In *Great ape societies* (pp. 213–224). Cambridge University Press. <https://doi.org/10.1017/CBO9780511752414.018>
- Doran, D. M. (1997). Ontogeny of locomotion in mountain gorillas and chimpanzees. *Journal of Human Evolution*, 32(4), 323–344. <https://doi.org/10.1006/jhevol.1996.0095>
- Doran, D. M., & Hunt, K. D. (1996). Comparative locomotor behavior of chimpanzees and bonobos: Species and habitat differences. In R. W. Wrangham, W. C. McGrew, F. B. M. de Waal, & P. G. Heltne (Eds.), *Chimpanzee cultures* (pp. 93–108). Harvard University Press.
- Dunmore, C. J., Bardo, A., Skinner, M. M., & Kivell, T. L. (2020). Trabecular variation in the first metacarpal and manipulation in hominids. *American Journal of Physical Anthropology*, 171(2), 219–241. <https://doi.org/10.1002/ajpa.23974>
- Dunmore, C. J., Kivell, T. L., Bardo, A., & Skinner, M. M. (2019). Metacarpal trabecular bone varies with distinct hand-positions used in hominid locomotion. *Journal of Anatomy*, 235(1), 45–66. <https://doi.org/10.1111/joa.12966>
- Dunmore, C. J., Skinner, M. M., Bardo, A., Berger, L. R., Hublin, J. J., Pahr, D. H., Rosas, A., Stephens, N. B., & Kivell, T. L. (2020). The position of *Australopithecus sediba* within fossil hominin hand use diversity. *Nature Ecology & Evolution*, 4(7), 911–918. <https://doi.org/10.1038/s41559-020-1207-5>
- Dunmore, C. J., Wollny, G., & Skinner, M. M. (2018). MIA-clustering: A novel method for segmentation of paleontological material. *PeerJ*, 6, e4374. <https://doi.org/10.7717/peerj.4374>
- Feix, T., Romero, J., Schmiedmayer, H. B., Dollar, A. M., & Kragic, D. (2015). The grasp taxonomy of human grasp types. *IEEE Transactions on Human-Machine Systems*, 46(1), 66–77. <https://doi.org/10.1109/THMS.2015.2470657>
- Galletta, L., Stephens, N. B., Bardo, A., Kivell, T. L., & Marchi, D. (2019). Three-dimensional geometric morphometric analysis of the first

- metacarpal distal articular surface in humans, great apes and fossil hominins. *Journal of Human Evolution*, 132, 119–136. <https://doi.org/10.1016/j.jhevol.2019.04.008>
- Georgiou, L., Dunmore, C. J., Bardo, A., Buck, L. T., Hublin, J. J., Pahr, D. H., Stratford, D., Synek, A., Kivell, T. L., & Skinner, M. M. (2020). Evidence for habitual climbing in a Pleistocene hominin in South Africa. *Proceedings of the National Academy of Sciences of the United States of America*, 117(15), 8416–8423. <https://doi.org/10.1073/pnas.1914481117>
- Gosman, J. H., Hubbell, Z. R., Shaw, C. N., & Ryan, T. M. (2013). Development of cortical bone geometry in the human femoral and tibial diaphysis. *The Anatomical Record*, 296(5), 774–787. <https://doi.org/10.1002/ar.22688>
- Gross, T., Kivell, T. L., Skinner, M. M., Nguyen, N. H., & Pahr, D. H. (2014). A CT-image-based framework for the holistic analysis of cortical and trabecular bone morphology. *Palaeontologia Electronica*, 17(3), 1–13. <https://doi.org/10.26879/438>
- Haile-Selassie, Y., & WoldeGabriel, G. (2009). *Ardipithecus kadabba: Late miocene evidence from the Middle Awash, Ethiopia* (Vol. 2). University of California Press.
- Hervé, M. (2022). *RVAideMemoire: Testing and plotting procedures for bio-statistics*. R package version 0.9-81-2. <https://cran.r-project.org/package=RVAideMemoire>
- Hunt, K. D. (1991). Mechanical implications of chimpanzee positional behavior. *American Journal of Physical Anthropology*, 86(4), 521–536. <https://doi.org/10.1002/ajpa.1330860408>
- Hunt, K. D. (1992). Positional behavior of Pan troglodytes in the Mahale mountains and Gombe stream national parks, Tanzania. *American Journal of Physical Anthropology*, 87(1), 83–105. <https://doi.org/10.1002/ajpa.1330870108>
- Hunt, K. D. (2020). *Chimpanzee: Lessons from our sister species*. Cambridge University Press.
- Inouye, S. E. (1994). Ontogeny of knuckle-walking hand postures in African apes. *Journal of Human Evolution*, 26(5–6), 459–485. <https://doi.org/10.1006/jhev.1994.1028>
- Jungers, W. L., Godfrey, L. R., Simons, E. L., & Chatrath, P. S. (1997). Phalangeal curvature and positional behavior in extinct sloth lemurs (Primates, Palaeopropithecidae). *Proceedings of the National Academy of Sciences of the United States of America*, 94(22), 11998–12001. <https://doi.org/10.1073/pnas.94.22.11998>
- Karakostis, F. A., Hotz, G., Scherf, H., Wahl, J., & Harvati, K. (2017). Occupational manual activity is reflected on the patterns among hand entheses. *American Journal of Physical Anthropology*, 164(1), 30–40. <https://doi.org/10.1002/ajpa.23253>
- Karakostis, F. A., Hotz, G., Tourloukis, V., & Harvati, K. (2018). Evidence for precision grasping in Neandertal daily activities. *Science Advances*, 4(9), eaat2369. <https://doi.org/10.1126/sciadv.aat2369>
- Kivell, T. L. (2016). A review of trabecular bone functional adaptation: what have we learned from trabecular analyses in extant hominoids and what can we apply to fossils?. *Journal of Anatomy*, 228(4), 569–594. <https://doi.org/10.1111/joa.12446>
- Kivell, T. L., Baraki, N., Lockwood, V., Williams-Hatala, E. M., & Wood, B. A. (2022). Form, function and evolution of the human hand. *American Journal of Biological Anthropology*, 181(S76), 6–57. <https://doi.org/10.1002/ajpa.24667>
- Kivell, T. L., Barros, A. P., & Smaers, J. B. (2013). Different evolutionary pathways underlie the morphology of wrist bones in hominoids. *BMC Evolutionary Biology*, 13, 1–12. <https://doi.org/10.1186/1471-2148-13-229>
- Kivell, T. L., Churchill, S. E., Kibii, J. M., Schmid, P., & Berger, L. R. (2018). The hand of *Australopithecus sediba*. *PaleoAnthropology*, 1, 282–333. <https://doi.org/10.4207/PA.2018.ART115>
- Kivell, T. L., Deane, A. S., Tocheri, M. W., Orr, C. M., Schmid, P., Hawks, J., Berger, L. R., & Churchill, S. E. (2015). The hand of *Homo naledi*. *Nature Communications*, 6(1), 1–9. <https://doi.org/10.1038/ncomms9431>
- Kivell, T. L., Ostrofsky, K. R., Richmond, B. G., & Drapeau, M. S. (2020). Metacarpals and manual phalanges. In *Hominin postcranial remains from Sterkfontein, South Africa, 1936-1995* (p. 106). <https://doi.org/10.1093/oso/9780197507667.003.0009>
- Larson, S. G., Jungers, W. L., Tocheri, M. W., Orr, C. M., Morwood, M. J., Sutikna, T., Awe, R. D., & Djubiantono, T. (2009). Descriptions of the upper limb skeleton of *Homo floresiensis*. *Journal of Human Evolution*, 57(5), 555–570. <https://doi.org/10.1016/j.jhevol.2008.06.007>
- Leijnse, J. N., Spoor, C. W., Pullens, P., & Vereecke, E. E. (2021). Kinematic and dynamic aspects of chimpanzee knuckle walking: Finger flexors likely do not buffer ground impact forces. *Journal of Experimental Biology*, 224(19), jeb236604. <https://doi.org/10.1242/jeb.236604>
- Lieberman, D. E., Polk, J. D., & Demes, B. (2004). Predicting long bone loading from cross-sectional geometry. *American Journal of Physical Anthropology*, 123(2), 156–171. <https://doi.org/10.1002/ajpa.10316>
- Marchi, D. (2005). The cross-sectional geometry of the hand and foot bones of the Hominoidea and its relationship to locomotor behavior. *Journal of Human Evolution*, 49(6), 743–761. <https://doi.org/10.1016/j.jhevol.2005.08.002>
- Marzke, M. W. (1997). Precision grips, hand morphology, and tools. *American Journal of Physical Anthropology*, 102(1), 91–110. [https://doi.org/10.1002/\(sici\)1096-8644\(199701\)102:1%3C91::aid-ajpa8%3E3.0.co;2-g](https://doi.org/10.1002/(sici)1096-8644(199701)102:1%3C91::aid-ajpa8%3E3.0.co;2-g)
- Marzke, M. W., Shrewsbury, M. M., & Horner, K. E. (2007). Middle phalanx skeletal morphology in the hand: Can it predict flexor tendon size and attachments? *American Journal of Physical Anthropology*, 134(2), 141–151. <https://doi.org/10.1002/ajpa.20646>
- Marzke, M. W., Tocheri, M. W., Steinberg, B., Femiani, J. D., Reece, S. P., Linscheid, R. L., Orr, C. M., & Marzke, R. F. (2010). Comparative 3D quantitative analyses of trapeziometacarpal joint surface curvatures among living catarrhines and fossil hominins. *American Journal of Physical Anthropology*, 141(1), 38–51. <https://doi.org/10.1002/ajpa.21112>
- Matarazzo, S. A. (2008). Knuckle walking signal in the manual digits of *Pan* and *Gorilla*. *American Journal of Physical Anthropology*, 135(1), 27–33. <https://doi.org/10.1002/ajpa.20701>
- Matarazzo, S. A. (2013). *Knuckle-walking signal in the manual phalanges and metacarpals of the great apes (Pan and Gorilla)*. PhD Dissertation. University of Massachusetts Amherst. <https://doi.org/10.7275/gcet-On48>
- Matarazzo, S. A. (2015). Trabecular architecture of the manual elements reflects locomotor patterns in primates. *PLoS One*, 10(3), e0120436. <https://doi.org/10.1371/journal.pone.0120436>
- McClure, N. K., Phillips, A. C., Vogel, E. R., & Tocheri, M. W. (2012). Unexpected pollex and hallux use in wild *Pongo pygmaeus wurmbii*. *American Journal of Physical Anthropology*, 147(S54), S208.
- Nakatsukasa, M., Kunimatsu, Y., Nakano, Y., Takano, T., & Ishida, H. (2003). Comparative and functional anatomy of phalanges in *Nacholapithecus kerioi*, a Middle Miocene hominoid from northern Kenya. *Primates*, 44, 371–412. <https://doi.org/10.1007/s10329-003-0051-y>
- Napier, J. R. (1960). Studies of the hands of living primates. *Proceedings of the Zoological Society of London*, 134(4), 647–657. <https://doi.org/10.1111/j.1469-7998.1960.tb05606.x>
- Napier, J. R. (1962). Fossil hand bones from Olduvai Gorge. *Nature*, 196, 409–411. <https://doi.org/10.1038/196409a0>
- Nguyen, N. H., Pahr, D. H., Gross, T., Skinner, M. M., & Kivell, T. L. (2014). Micro-finite element (μ FE) modeling of the siamang (*Symphalangus syndactylus*) third proximal phalanx: The functional role of curvature and the flexor sheath ridge. *Journal of Human Evolution*, 67, 60–75. <https://doi.org/10.1016/j.jhevol.2013.12.008>
- Ogle, D. H., Doll, J. C., Wheeler, A. P., & Dinno, A. (2022). *FSA: Simple fisheries stock assessment methods*. R package version 0.9.4. <https://cran.r-project.org/package=FSA>
- Oksanen, J., Blanchet, F. G., Friendly, M., Kindt, R., Legendre, P., McGlinn, D., Minchin, P. R., O'Hara, R. B., Simpson, G. L., Solymos, P., Stevens, M. H. H., Szoecs, E., & Wagner, H. (2020). *Vegan: Community ecology package*. R package version 2.5-7. <https://CRAN.R-project.org/package=vegan>

- Patel, B. A., & Maiolino, S. A. (2016). Morphological diversity in the digital rays of primate hands. In T. L. Kivell, P. Lemelin, B. G. Richmond, & D. Schmitt (Eds.), *The evolution of the primate hand: Anatomical, developmental, functional, and paleontological evidence* (pp. 55–100). Springer. https://doi.org/10.1007/978-1-4939-3646-5_4
- Pearson, O. M., & Lieberman, D. E. (2004). The aging of Wolff's "law": Ontogeny and responses to mechanical loading in cortical bone. *American Journal of Physical Anthropology*, 125(S39), 63–99. <https://doi.org/10.1002/ajpa.20155>
- Pickering, T. R., Heaton, J. L., Clarke, R. J., & Stratford, D. (2018). Hominin hand bone fossils from Sterkfontein Caves, South Africa (1998–2003 excavations). *Journal of Human Evolution*, 118, 89–102. <https://doi.org/10.1016/j.jhevol.2018.02.014>
- Pontzer, H., Lieberman, D. E., Momin, E., Devlin, M. J., Polk, J. D., Hallgrímsson, B., & Cooper, D. M. L. (2006). Trabecular bone in the bird knee responds with high sensitivity to changes in load orientation. *Journal of Experimental Biology*, 209(1), 57–65. <https://doi.org/10.1242/jeb.01971>
- Preuschoft, H. (1973). Functional anatomy of the upper extremity. In *The chimpanzee* (Vol. 6, pp. 34–120). Krager.
- Profico, A., Bondioli, L., Raia, P., O'Higgins, P., & Marchi, D. (2021). Morphomap: An R package for long bone landmarking, cortical thickness, and cross-sectional geometry mapping. *American Journal of Physical Anthropology*, 174(1), 129–139. <https://doi.org/10.1002/ajpa.24140>
- R Core Team (2021). R: A language and environment for statistical computing. R Foundation for Statistical Computing, Vienna, Austria. <https://www.R-project.org/>
- Remis, M. J. (1998). The gorilla paradox. In E. Strasser, J. G. Fleagle, A. L. Rosenberger, & H. M. McHenry (Eds.), *Primate locomotion* (pp. 95–106). Springer. https://doi.org/10.1007/978-1-4899-0092-0_6
- Richmond, B. G. (1998). Ontogeny and biomechanics of phalangeal form in primates. *PhD dissertation*, State University of New York at Stony Brook.
- Richmond, B. G. (2007). Biomechanics of phalangeal curvature. *Journal of Human Evolution*, 53(6), 678–690. <https://doi.org/10.1016/j.jhevol.2007.05.011>
- Ricklan, D. E. (1987). Functional anatomy of the hand of *Australopithecus africanus*. *Journal of Human Evolution*, 16(7–8), 643–664. [https://doi.org/10.1016/0047-2484\(87\)90018-2](https://doi.org/10.1016/0047-2484(87)90018-2)
- Rodríguez, L., Carretero, J. M., García-González, R., & Arsuaga, J. L. (2018). Cross-sectional properties of the lower limb long bones in the Middle Pleistocene Sima de los Huesos sample (Sierra de Atapuerca, Spain). *Journal of Human Evolution*, 117, 1–12. <https://doi.org/10.1016/j.jhevol.2017.11.007>
- Rose, M. D. (1988). Functional anatomy of the cheiridia. In J. H. Schwartz (Ed.), *Orangutan biology* (pp. 299–310). Oxford University Press.
- Ruff, C., Holt, B., & Trinkaus, E. (2006). Who's afraid of the big bad Wolff?: "Wolff's law" and bone functional adaptation. *American Journal of Physical Anthropology*, 129(4), 484–498. <https://doi.org/10.1002/ajpa.20371>
- Ruff, C. B., Burgess, M. L., Ketcham, R. A., & Kappelman, J. (2016). Limb bone structural proportions and locomotor behavior in AL 288-1 ("Lucy"). *PLoS One*, 11(11), e0166095. <https://doi.org/10.1371/journal.pone.0166095>
- Samuel, D. S., Nauwelaerts, S., Stevens, J. M., & Kivell, T. L. (2018). Hand pressures during arboreal locomotion in captive bonobos (*Pan paniscus*). *Journal of Experimental Biology*, 221(8), jeb170910. <https://doi.org/10.1242/jeb.170910>
- Sancho-Bru, J. L., Mora, M. C., León, B. E., Pérez-González, A., Iserte, J. L., & Morales, A. (2014). Grasp modelling with a biomechanical model of the hand. *Computer Methods in Biomechanics and Biomedical Engineering*, 17(4), 297–310. <https://doi.org/10.1080/10255842.2012.682156>
- Sarmiento, E. E. (1988). Anatomy of the hominoid wrist joint: Its evolutionary and functional implications. *International Journal of Primatology*, 9, 281–345. <https://doi.org/10.1007/BF02737381>
- Sarringhaus, L. A., MacLachy, L. M., & Mitani, J. C. (2014). Locomotor and postural development of wild chimpanzees. *Journal of Human Evolution*, 66, 29–38. <https://doi.org/10.1016/j.jhevol.2013.09.006>
- Schaller, G. E. (1963). *The mountain gorilla: Ecology and behavior*. University of Chicago Press.
- Schmitt, D., Zeininger, A., & Granatosky, M. C. (2016). Patterns, variability, and flexibility of hand posture during locomotion in primates. In T. L. Kivell, P. Lemelin, B. G. Richmond, & D. Schmitt (Eds.), *The evolution of the primate hand: Anatomical, developmental, functional, and paleontological evidence* (pp. 345–369). Springer. https://doi.org/10.1007/978-1-4939-3646-5_13
- Shrewsbury, M. M., Marzke, M. W., Linscheid, R. L., & Reece, S. P. (2003). Comparative morphology of the pollical distal phalanx. *American Journal of Physical Anthropology*, 121(1), 30–47. <https://doi.org/10.1002/ajpa.10192>
- Skinner, M. M., Stephens, N. B., Tsegai, Z. J., Foote, A. C., Nguyen, N. H., Gross, T., Pahr, D. H., Hublin, J. J., & Kivell, T. L. (2015). Human-like hand use in *Australopithecus africanus*. *Science*, 347(6220), 395–399. <https://doi.org/10.1126/science.1261735>
- Stephens, N. B., Kivell, T. L., Pahr, D. H., Hublin, J. J., & Skinner, M. M. (2018). Trabecular bone patterning across the human hand. *Journal of Human Evolution*, 123, 1–23. <https://doi.org/10.1016/j.jhevol.2018.05.004>
- Stern, J. T., Jungers, W. L., & Susman, R. L. (1995). Quantifying phalangeal curvature: An empirical comparison of alternative methods. *American Journal of Physical Anthropology*, 97(1), 1–10. <https://doi.org/10.1002/ajpa.1330970102>
- Stern, J. T., & Susman, R. L. (1983). The locomotor anatomy of *Australopithecus afarensis*. *American Journal of Physical Anthropology*, 60(3), 279–317. <https://doi.org/10.1002/ajpa.1330600302>
- Su, A., & Carlson, K. J. (2017). Comparative analysis of trabecular bone structure and orientation in South African hominin tali. *Journal of Human Evolution*, 106, 1–18. <https://doi.org/10.1016/j.jhevol.2016.12.006>
- Susman, R. L. (1974). Facultative terrestrial hand postures in an orangutan (*Pongo pygmaeus*) and pongid evolution. *American Journal of Physical Anthropology*, 40(1), 27–37. <https://doi.org/10.1002/ajpa.1330400104>
- Susman, R. L. (1979). Comparative and functional morphology of hominoid fingers. *American Journal of Physical Anthropology*, 50(2), 215–236. <https://doi.org/10.1002/ajpa.1330500211>
- Susman, R. L. (2004). *Oreopithecus bambolii*: An unlikely case of hominid like grip capability in a Miocene ape. *Journal of Human Evolution*, 46(1), 105–117. <https://doi.org/10.1016/j.jhevol.2003.10.002>
- Susman, R. L., & Creel, N. (1979). Functional and morphological affinities of the subadult hand (OH 7) from Olduvai Gorge. *American Journal of Physical Anthropology*, 51(3), 311–331. <https://doi.org/10.1002/ajpa.1330510303>
- Susman, R. L., & Stern, J. T. (1979). Telemetered electromyography of flexor digitorum profundus and flexor digitorum superficialis in pan troglodytes and implications for interpretation of the OH 7 hand. *American Journal of Physical Anthropology*, 50(4), 565–574. <https://doi.org/10.1002/ajpa.1330500408>
- Susman, R. L., Stern, J. T., & Jungers, W. L. (1984). Arboreality and bipedality in the Hadar hominids. *Folia Primatologica*, 43(2–3), 113–156. <https://doi.org/10.1159/000156176>
- Syeda, S. M., Tsegai, Z. J., Cazenave, M., Dunmore, C. J., Skinner, M. M., & Kivell, T. L. (2022). Reconstructing hand use in *Australopithecus sediba* and *Homo naledi*: Mapping variation in cortical thickness across the proximal and intermediate phalanges. *PaleoAnthropology*, 2, 588. <https://doi.org/10.48738/2022.iss2.809>
- Syeda, S. M., Tsegai, Z. J., Cazenave, M., Skinner, M. M., & Kivell, T. L. (2023). Cortical bone distribution of the proximal phalanges in great apes: Implications for reconstructing manual behaviours. *Journal of Anatomy*, 243, 1–22. <https://doi.org/10.1111/joa.13918>

- Syeda, S. M., Tsegai, Z. J., Dunmore, C. J., Cazenave, M., Skinner, M. M., & Kivell, T. L. (2021). Inferring hand use in *Australopithecus sediba*: Analysis of the external and internal morphology of hominin proximal and intermediate phalanges. *PaleoAnthropology*, 1, 258. <https://doi.org/10.48738/2021.iss1.75>
- Synek, A., Lu, S. C., Vereecke, E. E., Nauwelaerts, S., Kivell, T. L., & Pahr, D. H. (2019). Musculoskeletal models of a human and bonobo finger: Parameter identification and comparison to in vitro experiments. *PeerJ*, 7, e7470. <https://doi.org/10.7717/peerj.7470>
- Thompson, N. E. (2020). The biomechanics of knuckle-walking: 3-D kinematics of the chimpanzee and macaque wrist, hand and fingers. *Journal of Experimental Biology*, 223(14), jeb224360. <https://doi.org/10.1242/jeb.224360>
- Thompson, N. E., Ostrofsky, K. R., McFarlin, S. C., Robbins, M. M., Stoinski, T. S., & Alméjida, S. (2018). Unexpected terrestrial hand posture diversity in wild mountain gorillas. *American Journal of Physical Anthropology*, 166(1), 84–94. <https://doi.org/10.1002/ajpa.23404>
- Thorpe, S. K., & Crompton, R. H. (2006). Orangutan positional behavior and the nature of arboreal locomotion in Hominoidea. *American Journal of Physical Anthropology*, 131(3), 384–401. <https://doi.org/10.1002/ajpa.20422>
- Tocheri, M. W., Orr, C. M., Jacofsky, M. C., & Marzke, M. W. (2008). The evolutionary history of the hominin hand since the last common ancestor of *Pan* and *Homo*. *Journal of Anatomy*, 212, 544–562. <https://doi.org/10.1111/j.1469-7580.2008.00865.x>
- Tocheri, M. W., Orr, C. M., Larson, S. G., Sutikna, T., Jatmiko, Saptomo, E. W., Due, R. A., Djubiantono, T., Morwood, M. J., & Jungers, W. L. (2007). The primitive wrist of *Homo floresiensis* and its implications for hominin evolution. *Science*, 317(5845), 1743–1745. <https://doi.org/10.1126/science.1147143>
- Tsegai, Z. J., Kivell, T. L., Gross, T., Nguyen, N. H., Pahr, D. H., Smaers, J. B., & Skinner, M. M. (2013). Trabecular bone structure correlates with hand posture and use in hominoids. *PLoS One*, 8(11), e78781. <https://doi.org/10.1371/journal.pone.0078781>
- Tuttle, R. H. (1967). Knuckle-walking and the evolution of hominoid hands. *American Journal of Physical Anthropology*, 26(2), 171–206. <https://doi.org/10.1002/ajpa.1330260207>
- Tuttle, R. H. (1969). Quantitative and functional studies on the hands of the Anthropoidea. I. The Hominoidea. *Journal of Morphology*, 128(3), 309–363. <https://doi.org/10.1002/jmor.1051280304>
- Tuttle, R. H. (1981). Evolution of hominid bipedalism and prehensile capabilities. *Philosophical Transactions of the Royal Society of London B*, 292(1057), 89–94. <https://doi.org/10.1098/rstb.1981.0016>
- Tuttle, R. H., Basmajian, J. V., Regenos, E., & Shine, G. (1972). Electromyography of knuckle-walking: Results of four experiments on the forearm of *Pan gorilla*. *American Journal of Physical Anthropology*, 37(2), 255–265. <https://doi.org/10.1002/ajpa.1330370210>
- Tuttle, R. H., & Watts, D. P. (1985). The positional behavior and adaptive complexes of *Pan gorilla*. In *Primate morphophysiology, locomotor analysis and human bipedalism* (pp. 261–288). University of Tokyo Press.
- Walker, A., Leakey, R. E., & Leakey, R. (Eds.). (1993). *The nariokotome Homo erectus skeleton*. Harvard University Press.
- Wallace, I. J., Burgess, M. L., & Patel, B. A. (2020). Phalangeal curvature in a chimpanzee raised like a human: Implications for inferring arboreality in fossil hominins. *Proceedings of the National Academy of Sciences of the United States of America*, 117(21), 11223–11225. <https://doi.org/10.1073/pnas.2004371117>
- Ward, C. V., Kimbel, W. H., Harmon, E. H., & Johanson, D. C. (2012). New postcranial fossils of *Australopithecus afarensis* from Hadar, Ethiopia (1990–2007). *Journal of Human Evolution*, 63(1), 1–51. <https://doi.org/10.1016/j.jhevol.2011.11.012>
- Williams-Hatala, E. M., Hatala, K. G., Hiles, S., & Rabey, K. N. (2016). Morphology of muscle attachment sites in the modern human hand does not reflect muscle architecture. *Scientific Reports*, 6(1), 28353. <https://doi.org/10.1038/srep28353>
- Wunderlich, R. E., & Jungers, W. L. (2009). Manual digital pressures during knuckle-walking in chimpanzees (*Pan troglodytes*). *American Journal of Physical Anthropology*, 139(3), 394–403. <https://doi.org/10.1002/ajpa.20994>
- Zeininger, A., Patel, B. A., Zipfel, B., & Carlson, K. J. (2016). Trabecular architecture in the StW 352 fossil hominin calcaneus. *Journal of Human Evolution*, 97, 145–158. <https://doi.org/10.1016/j.jhevol.2016.05.009>
- Zheng, J. Z., De La Rosa, S., & Dollar, A. M. (2011). An investigation of grasp type and frequency in daily household and machine shop tasks. In *IEEE international conference on robotics and automation* (Vol. 2011, pp. 4169–4175). IEEE. <https://doi.org/10.1109/ICRA.2011.5980366>

SUPPORTING INFORMATION

Additional supporting information can be found online in the Supporting Information section at the end of this article.

How to cite this article: Syeda, S. M., Tsegai, Z. J., Cazenave, M., Skinner, M. M., & Kivell, T. L. (2024). Cortical bone architecture of hominid intermediate phalanges reveals functional signals of locomotion and manipulation. *American Journal of Biological Anthropology*, e24902. <https://doi.org/10.1002/ajpa.24902>